

From pure cultures to particles:
Tracing microbial metabolism through amino
acid $^2\text{H}/^1\text{H}$ ratios

Thesis by
Shaelyn Nicole Silverman

In Partial Fulfillment of the Requirements for the
Degree of
Doctor of Philosophy in Geobiology



CALIFORNIA INSTITUTE OF TECHNOLOGY
Pasadena, California

2025
Defended May 1, 2025

© 2025

Shaelyn Nicole Silverman
ORCID: 0000-0001-9201-6904

All rights reserved

Abstract

Microbial metabolisms exert profound impact on our planet's atmosphere and surface geochemistry. Most available tools to study microbial metabolism in the environment provide only snapshots of activity at the time of sampling. However, holistic understanding of microbial function requires the ability to quantitatively reconstruct their activities prior to sampling, for which tools are currently limited. The overarching research presented in this thesis addresses this challenge through development of a new isotopic tool, amino acid hydrogen isotope ($\delta^2\text{H}_{\text{AA}}$) analysis, into a useful tracer of microbial metabolism in the environment. We begin by solving a major analytical challenge: correcting for contributions of exchangeable amine-bound hydrogen in derivatized amino acids, which unlocks the ability to accurately measure $\delta^2\text{H}_{\text{AA}}$ values in organisms via gas chromatography-pyrolysis-isotope ratio mass spectrometry. We demonstrate in aerobic heterotrophic bacteria and phytoplankton that $\delta^2\text{H}_{\text{AA}}$ values are controlled by metabolism (specifically, carbon flow in cells), and we apply this isotopic tool to natural samples of marine particulate organic matter (POM), demonstrating substantial potential turnover of photoautotrophic proteins into heterotrophic proteins (up to $57 \pm 18\%$) in POM with depth at different ocean sites. We further explore the microscale dynamics of marine bacteria on diatom aggregates to contextualize our understanding of controls on marine POM degradation. In particular, we find that both intra- and interspecies interactions profoundly shape microbial colonization dynamics, which in turn likely affect bulk particle degradation rates. Together, this body of work demonstrates the profound utility of $\delta^2\text{H}_{\text{AA}}$ analysis as a tracer of microbial metabolism—a timely development given the need to trace and quantify the metabolic responses of microbial communities to ongoing environmental perturbations.

Acknowledgements

First and foremost, I would like to extend my deepest gratitude to Alex Sessions, Victoria Orphan, and members of their lab groups, for extensive training and guidance in my development as a scientist. These two groups comprised my scientific 'families' at Caltech and fostered tremendous scientific exchange, intellectual curiosity, and—mostly importantly—immense joy throughout my PhD. I am especially grateful to my thesis advisor Alex, who never ceased supporting, encouraging, or believing in me, even in times when my research progress stagnated to points I thought were irreconcilable. My training in stable isotope biogeochemistry and organic geochemistry comes nearly entirely from his lab, and he inspired in me a particular carefulness and rigor that has made me a better scientist. I am also immensely grateful to my co-advisor Victoria, who supported me in adopting a project (read: second PhD) midway through my graduate tenure to gain skills and experience in microbial ecology, which significantly shaped my future career interests.

I would also like to thank my two other committee members—Dianne Newman and Jared Leadbetter—for mentorship and support in ways that significantly strengthened the quality of my thesis work. Dianne's Microbial Metabolic Diversity course (which I had the pleasure to TA) was particularly helpful to me in making sense of the diverse landscape of microbial metabolisms through their elegant underlying principles. Jared was generous in allowing me to permanently inhabit one of his lab benches to carry out my microbiology work. I am additionally grateful to Woody Fischer for significant use of his laboratory equipment for my projects, and for running the Geobiology reading group, which, along with his Introduction to Geobiology course, was formative in my training as a Geobiologist. I am also deeply grateful to Fenfang Wu, Stephanie Connon, and Michael Mathuri for training and

support in analytical, laboratory, and equipment use in the Sessions and Orphan labs.

I would like to give special acknowledgments to my undergraduate research advisors Sebastian Kopf and Sanjoy Som, who first introduced me to Geobiology and inspired me to pursue a PhD through the immense curiosity and joy they brought to their research every day. I am additionally grateful to Alexis Templeton, Brad Bebout, and other members of the CU Boulder, NASA Ames, and Blue Marble Institute of Science groups, which collectively fostered my early growth as a scientist and scientific communicator. My gratitude is additionally extended to Ruth Barrientos for guiding my first steps in academic science; to my high school teachers Mr. Penner and Ms. Clark for sparking my interest in science and helping me become a better writer, respectively; to my outstanding postdoc mentors Reto Wijker, Fabai Wu, and Jeremy Schreier, who trained me in stable isotope analysis and microbiology at different points in my PhD; and to the excellent department staff who work tirelessly to keep the Caltech GPS division running seamlessly every day.

My scientific horizons were greatly expanded through working with amazing collaborators, mentors, and mentees, who each contributed substantially to the intellectual and/or material development of my work: Reto Wijker, Fabai Wu, Gabriella Weiss, Elise Wilkes, Alexandra Phillips, John Eiler, Elizabeth Niespolo, Juli Panehal, Alessandra Flaherty, Eunice Tsang, Hilary Close, Elizabeth Yanuskiewicz, Jeremy Schreier, Uria Alcolombri, and Julia Schwartzman. My participation in the Simons Foundation PriME collaboration was particularly impactful in my training in marine microbial ecology, and crucially taught me how to interrogate questions in this field through a quantitative lens. I am also indebted to Dan Utter for his generosity in helping me through all my bioinformatics and myriad miscellaneous research questions; and to Elliott Mueller from whom I learned more than

I can articulate. I would like to additionally acknowledge several organizations that were special pillars of my enrichment, both inside and outside of science: the International Geobiology Summer Course, the Caltech Center for Environmental Microbial Interactions (CEMI), and GO-Outdoors (the Caltech GPS outreach program I helped co-found during the COVID-19 pandemic, and which was a true joy to be part of).

Finally, the immense support of my family and friends was critical to my success and well-being at Caltech. In particular, my first year 'pit' cohort (Makayla Betts, Elliott Mueller, Juliet Ryan-Davis, Sergio Parra, Philip Woods, Emily Miao, and Sarah Zeichner); my additional GPS friends (Hannah Dion-Kirschner, Alex Phillips, Miquela Ingalls, and countless others); my office mates (in particular, Hannah and Aditi Narayanan); and my friends outside of Caltech (Susan Evans, Joseph Evans, Tammy Taller, Kate Napier, Nisha Udupa, and many more), served as huge sources of support and joy throughout my PhD. A very special acknowledgment goes to my friends in the Caltech Alpine Club, who introduced me to the world of trail running and helped me stay sane by running more miles than we could count in the San Gabriel Mountains. I want to especially thank my mom, Kim Silverman; my brother, Shawn Silverman; and my future husband, Marshall Yale, for their unconditional love and support throughout my PhD journey, without which this thesis would not have been possible. Finally, I would like to dedicate my thesis to my dad, Mike Silverman, who passed away in 2014. He inspired my initial interest in STEM and my love for the outdoors. Through my avid pursuit of both, I continue to carry his memory with me.

Table of Contents

| | |
|---|----------|
| Abstract | iii |
| Acknowledgements | iv |
| List of Figures | xiii |
| List of Tables | xxii |
| 1 Introduction | 1 |
| 1.1 Interrogating microbial metabolism: A need for quantitative tools | 1 |
| 1.2 Thesis outline | 3 |
| 2 Practical considerations for amino acid isotope analysis | 6 |
| 2.1 Introduction | 7 |
| 2.1.1 Terminology | 9 |
| 2.2 Sample storage and preparation | 10 |
| 2.3 Acid hydrolysis | 11 |
| 2.3.1 Conventional hydrolysis | 14 |
| 2.3.2 Isotopic fractionation | 14 |
| 2.3.3 Alternative hydrolysis methods | 15 |
| 2.4 Analyte clean-up | 18 |
| 2.4.1 Ion exchange | 18 |
| 2.5 Derivatization (for gas chromatography) | 19 |
| 2.5.1 Amine group derivatives | 24 |
| 2.5.1.1 Pivaloyl derivatives | 24 |
| 2.5.1.2 Fluorinated derivatives | 25 |

| | | |
|---------|--|----|
| 2.5.1.3 | Non-fluorinated acetyl derivatives | 26 |
| 2.5.1.4 | Alkoxycarbonyl derivatives | 27 |
| 2.5.2 | Carboxyl group derivatives | 28 |
| 2.5.2.1 | Ester derivatives | 28 |
| 2.5.2.2 | Silyl derivatives | 29 |
| 2.6 | Separations | 29 |
| 2.6.1 | Gas chromatography | 30 |
| 2.6.2 | Liquid chromatography | 32 |
| 2.6.3 | Ion chromatography | 33 |
| 2.6.4 | Capillary electrophoresis | 33 |
| 2.6.5 | Methods of assessing purity | 34 |
| 2.7 | Isotopic analysis | 36 |
| 2.7.1 | Isotope ratio mass spectrometry | 36 |
| 2.7.1.1 | GC-IRMS | 37 |
| 2.7.1.2 | LC-IRMS | 39 |
| 2.7.1.3 | EA-IRMS | 40 |
| 2.7.1.4 | IRMS configurations for position-specific isotope analysis | 41 |
| 2.7.2 | High-resolution mass spectrometry | 42 |
| 2.7.3 | Nuclear magnetic resonance spectroscopy (NMR) | 44 |
| 2.7.4 | Referencing strategies for isotopic analysis | 46 |
| 2.8 | Conclusions and outlook | 47 |
| 3 | Biosynthetic and catabolic pathways control amino acid $\delta^2\text{H}$ values in aerobic heterotrophs | 69 |
| 3.1 | Introduction | 70 |
| 3.2 | Materials and methods | 75 |
| 3.2.1 | Strain and culture conditions | 75 |
| 3.2.2 | Amino acid hydrolysis, derivatization, extraction, and quantification | 76 |
| 3.2.3 | Isotope analysis | 79 |
| 3.2.4 | Hydrolysis and derivatization tests for isotopic alteration | 80 |

| | | |
|-----------|--|-----|
| 3.2.5 | Correction for derivative and exchangeable amine hydrogen | 80 |
| 3.3 | Results | 82 |
| 3.3.1 | Derivative correction | 82 |
| 3.3.2 | Tests for isotopic alteration during sample preparation | 84 |
| 3.3.3 | $^2\text{H}/^1\text{H}$ fractionations and carbon fluxes across wildtype organisms grown on glucose | 85 |
| 3.3.4 | $^2\text{H}/^1\text{H}$ fractionations and carbon fluxes in <i>E. coli</i> knockout mutants grown on glucose | 88 |
| 3.3.5 | $^2\text{H}/^1\text{H}$ fractionations across wildtype organisms grown on different substrates | 89 |
| 3.4 | Discussion | 90 |
| 3.4.1 | Controls on the $^2\varepsilon_{\text{AA}/\text{w}}$ pattern during glucose metabolism | 93 |
| 3.4.1.1 | Proline | 93 |
| 3.4.1.2 | Phenylalanine | 94 |
| 3.4.1.3 | Leucine and valine | 95 |
| 3.4.1.4 | Isoleucine | 96 |
| 3.4.2 | Controls on variations in $^2\varepsilon_{\text{AA}/\text{w}}$ values | 97 |
| 3.4.2.1 | Metabolite pools in activated catabolic pathways | 98 |
| 3.4.2.1.1 | Pyruvate $\delta^2\text{H}$ | 99 |
| 3.4.2.1.2 | NADPH $\delta^2\text{H}$ | 106 |
| 3.4.2.2 | Enzymatic variations in biosynthetic pathways | 109 |
| 3.4.3 | Conclusions and potential applications | 110 |
| 4 | The $\delta^2\text{H}_{\text{AA}}$ signature of phytoplankton | 121 |
| 4.1 | Introduction | 122 |
| 4.2 | Materials and methods | 124 |
| 4.2.1 | Strain and culture conditions | 124 |
| 4.2.2 | Amino acid preparation and isotope analysis | 126 |
| 4.3 | Results | 128 |
| 4.3.1 | Phytoplankton $^2\text{H}/^1\text{H}$ fractionations | 128 |
| 4.3.2 | <i>E. huxleyi</i> $^2\text{H}/^1\text{H}$ fractionations in response to salinity | 132 |
| 4.3.3 | Diatom $^2\text{H}/^1\text{H}$ fractionations in response to irradiance | 134 |

| | | |
|---------|---|-----|
| 4.4 | Discussion | 136 |
| 4.4.1 | Phytoplankton fractionate amino acid hydrogen isotopes more substantially than do heterotrophic bacteria | 136 |
| 4.4.2 | Biochemical mechanisms controlling $^2\text{H}/^1\text{H}$ fractionations of individual amino acids in phytoplankton | 139 |
| 4.4.2.1 | Comparison of amino acid $^2\text{H}/^1\text{H}$ fractionations between phytoplankton and heterotrophic bacteria | 139 |
| 4.4.3 | Effects of environmental parameters on phytoplankton $^2\varepsilon_{\text{AA/w}}$ values | 142 |
| 4.4.3.1 | Response to salinity | 143 |
| 4.4.3.2 | Response to irradiance | 150 |
| 4.5 | Conclusion and potential applications | 154 |
| 5 | Marine particulate organic matter $\delta^2\text{H}_{\text{AA}}$ values reflect substantial heterotrophic turnover with depth | 166 |
| 5.1 | Introduction | 167 |
| 5.2 | Sample site context | 172 |
| 5.2.1 | Porcupine Abyssal Plain Sustained Observatory, Northeast Atlantic Ocean | 172 |
| 5.2.2 | Station ALOHA, North Pacific Subtropical Gyre | 173 |
| 5.3 | Materials and methods | 174 |
| 5.3.1 | Particle sampling and oceanographic context | 174 |
| 5.3.1.1 | Porcupine Abyssal Plain Sustained Observatory | 174 |
| 5.3.1.2 | Station ALOHA | 176 |
| 5.3.1.3 | Filter preparation | 177 |
| 5.3.2 | Amino acid preparation and isotope analysis | 177 |
| 5.3.3 | Bayesian mixing model | 178 |
| 5.4 | Results and discussion | 179 |
| 5.4.1 | Surface POM $\delta^2\text{H}_{\text{AA}}$ values carry a distinct phytoplankton signature | 179 |
| 5.4.2 | $\delta^2\text{H}_{\text{AA}}$ trends with depth in the euphotic zone | 181 |
| 5.4.3 | $\delta^2\text{H}_{\text{AA}}$ trends with depth in the mesopelagic zone | 182 |
| 5.5 | Conclusion and potential applications | 191 |

| | | |
|-------|---|-----|
| 6 | Microscale ecological dynamics of marine bacteria on diatom aggregates | 207 |
| 6.1 | Introduction | 208 |
| 6.2 | Materials and methods | 210 |
| 6.2.1 | Bacterial cultures | 210 |
| 6.2.2 | Particle colonization experiments | 210 |
| 6.2.3 | Visualization and image analysis | 212 |
| 6.2.4 | Annotation of CAZymes and sulfatases | 213 |
| 6.2.5 | Antagonism assay | 214 |
| 6.3 | Results and discussion | 215 |
| 6.3.1 | Particle colonization is not solely driven by metabolic capability | 215 |
| 6.3.2 | Microcolony formation is a consistent feature accompanying strong particle colonization | 220 |
| 6.3.3 | Bacteria/bacteria interactions significantly shape particle colonization dynamics | 228 |
| 6.4 | Conclusion | 232 |
| 7 | Concluding remarks | 242 |

Appendices **245**

| | | |
|-------|---|-----|
| A | Supplementary material for Chapter 2 | 246 |
| A.1 | Mechanisms of amino acid loss during hydrolysis | 246 |
| A.1.1 | Aliphatic amino acids | 246 |
| A.1.2 | Acidic and amidic amino acids | 247 |
| A.1.3 | Hydroxylic amino acids | 248 |
| A.1.4 | Aromatic amino acids | 250 |
| A.1.5 | S-containing amino acids | 253 |
| A.2 | Data correction, isotope effect quantification, and error propagation for derivatives | 257 |
| A.3 | Other IRMS configurations | 260 |

| | | |
|-------|---|-----|
| A.4 | Additional details about PSIA of amino acids by high-resolution mass spectrometry | 261 |
| A.5 | ^1H Isotopic NMR for PSIA of amino acids | 262 |
| B | Supplementary material for Chapter 3 | 268 |
| B.1 | Rationale for amino acids targeted | 268 |
| B.2 | Carbon fluxes | 270 |
| B.3 | Amino acid $\delta^2\text{H}$ values | 273 |
| B.4 | Error associated with improper $\delta^2\text{H}$ corrections for N-bound hydrogen in amino acids | 279 |
| B.5 | Hydrolysis and derivatization tests | 283 |
| B.6 | Controls on variations in $^2\varepsilon_{\text{AA/w}}$ values | 287 |
| B.6.1 | Water fraction factors | 287 |
| B.6.2 | Pyruvate hydrogen | 291 |
| B.6.3 | NADPH hydrogen | 292 |
| B.7 | Biosynthetic pathways | 300 |
| B.7.1 | Proline biosynthesis | 300 |
| B.7.2 | Phenylalanine biosynthesis | 301 |
| B.7.3 | Leucine and valine biosynthesis | 301 |
| B.7.4 | Isoleucine biosynthesis | 303 |
| B.7.5 | Distribution of amino acid biosynthetic enzymes across organisms | 304 |
| C | Supplementary material for Chapter 4 | 311 |
| C.1 | Consistency standards | 311 |
| C.2 | Peak size corrections | 311 |
| C.3 | Phytoplankton $^2\text{H}/^1\text{H}$ fractionations | 316 |
| C.4 | <i>E. huxleyi</i> $^2\text{H}/^1\text{H}$ fractionations in response to salinity | 319 |
| C.5 | Diatom $^2\text{H}/^1\text{H}$ fractionations in response to irradiance | 325 |
| D | Supplementary material for Chapter 6 | 330 |
| E | Supplementary material for Chapter 6 | 332 |

List of Figures

| <i>Number</i> | <i>Page</i> |
|---|-------------|
| 2.1 A typical workflow for amino acid isotope analysis, highlighting the major preparatory and analytical steps examined in this review paper. | 8 |
| 2.2 Structures of 20 common proteinogenic amino acids in zwitterion form at pH 7. | 12 |
| 2.3 Yields of free amino acid standard mixtures (dark gray triangles) and of amino acids from proteins (light gray shapes) after conventional acid hydrolysis (6N HCl, 110°C, 20–24h, anoxic conditions). . . . | 13 |
| 2.4 Summary of stable and unstable residues during common acid hydrolysis procedures. | 17 |
| 2.5 Derivatives commonly used for gas chromatography separation of amino acids. | 24 |
| 2.6 Summarized capabilities of common analytical techniques used for amino acid isotope analysis. | 38 |
| 3.1 Simplified schematic of biosynthetic pathways (showing end-member compounds), central metabolic pathway precursors, and hydrogen sources for the five amino acids investigated in this study (proline, phenylalanine, leucine, valine, isoleucine). | 72 |
| 3.2 Derivatization scheme for amino acids and methods used to measure $\delta^2\text{H}$ values of derivative reagents. | 78 |
| 3.3 Size of derivative $\delta^2\text{H}$ corrections versus native amino acid isotopic compositions. | 83 |

| | | |
|-----|--|-----|
| 3.4 | Summary of $^2\text{H}/^1\text{H}$ fractionations between amino acids and water in wildtype organisms (A) and in <i>E. coli</i> wildtype (WT) and mutant organisms (B) grown on glucose. | 86 |
| 3.5 | $^2\varepsilon_{\text{AA/w}}$ values for leucine (black) and valine (white) in wildtype organisms grown on glucose versus relative carbon flux (i.e., normalized to glucose uptake rates) through pyruvate synthesis-related enzymes in central metabolism. | 87 |
| 3.6 | Summary of $^2\text{H}/^1\text{H}$ fractionations between amino acids and water in wildtype organisms grown on different substrates. | 89 |
| 3.7 | Hypotheses explored for pyruvate and NADPH controls on $\delta^2\text{H}_{\text{AA}}$ variations in organisms grown on different substrates. | 101 |
| 3.8 | Schematic models of hydrogen flow through relevant central metabolic pathways (CMPs), corresponding isotopic fractionations, and relative ^2H -enrichment of leucine and valine upon growth of microbes on different carbon substrates. | 105 |
| 4.1 | Summary of $^2\text{H}/^1\text{H}$ fractionations between amino acids and water in phytoplankton cultured in this study. | 128 |
| 4.2 | Probability distributions (with data from Figure 4.1 overlaid) of amino acid/water $^2\text{H}/^1\text{H}$ fractionations in cyanobacteria, diatoms, and <i>E. huxleyi</i> cultured in this study. | 129 |
| 4.3 | Probability distributions (with data overlaid) of amino acid/water $^2\text{H}/^1\text{H}$ fractionations in 10 species of phytoplankton (this study; Figure 4.2), and in five species of terrestrial bacteria cultured on sugars or organic acids (Silverman et al., 2024). | 130 |
| 4.4 | Amino acid/water $^2\text{H}/^1\text{H}$ fractionations in <i>E. huxleyi</i> cultured in different salinities. | 131 |

| | | |
|-----|---|-----|
| 4.5 | Amino acid abundances (reported as percent abundance in total cell dry weight (CDW)) in <i>E. huxleyi</i> biomass cultured in media with different salinities. | 133 |
| 4.6 | Amino acid/water $^2\text{H}/^1\text{H}$ fractionations in <i>C. muelleri</i> and <i>T. pseudonana</i> grown under different irradiances. | 134 |
| 4.7 | Summary of amino acid/water $^2\text{H}/^1\text{H}$ fractionations, displayed as the means $\pm 1\sigma$ of collective data from each metabolic subgroup. | 140 |
| 4.8 | Slopes of regressions of $^2\varepsilon_{\text{AA/w}}$ versus salinity for each amino acid from Figure 4.4. | 148 |
| 5.1 | Maps of sample sites, with blue shading corresponding to the seafloor depth below sea level. | 172 |
| 5.2 | Comparison of $^2\text{H}/^1\text{H}$ fractionations (versus water) for amino acids from size-fractionated surface POM samples (25–30 m depth) and axenic phytoplankton cultures. | 179 |
| 5.3 | Vertical profiles of $\delta^2\text{H}_{\text{AA}}$ values in size-fractionated POM from Sta. ALOHA and PAP-SO. | 182 |
| 5.4 | Amino acid $\delta^2\text{H}$ values in size-fractionated POM samples from PAP-SO (A) and from Sta. ALOHA (B) , normalized to mean $\delta^2\text{H}_{\text{AA}}$ values within each sample to more easily visualize changes in intermolecular patterns with depth. | 183 |
| 5.5 | ^2H -enrichments of individual amino acids from the euphotic zone (specifically, the euphotic zone base at PAP-SO) through the mid-mesopelagic (~ 300 m) in particles from the larger size class at each site. | 185 |
| 5.6 | Estimated heterotrophic contribution to Sta. ALOHA (3–53 μm) and PAP-SO (>51 μm) particulate amino acids with depth. | 188 |

| | | |
|-----|--|-----|
| 6.1 | Number of CAZymes belonging to the glycoside hydrolase (GH; light blue) and polysaccharide lyase (PL; dark blue) families in each strain. | 217 |
| 6.2 | Fluorescence micrographs of diatom particles (green) with different marine bacterial strains (pink) after up to 8d of continuous colonization. | 218 |
| 6.3 | GH and PL repertoire of select strains examined in this study. . . . | 221 |
| 6.4 | Dynamics of bacterial strains on <i>T. pseudonana</i> aggregates over 140h of continuous colonization. | 224 |
| 6.5 | Distribution of cell patches of individual strains from mono- and co-cultures on <i>T. pseudonana</i> aggregates after 140h of continuous colonization. | 225 |
| 6.6 | Fluorescent micrographs of pairwise combinations of strains on <i>T. pseudonana</i> aggregates after 140h of continuous colonization. . . . | 227 |
| 6.7 | Relative bacterial cell biomass on <i>T. pseudonana</i> aggregates after 140h of continuous colonization by individual or pairs of strains. . . | 228 |
| A.1 | Reversible cyclization of glycine to diketopiperazine. | 247 |
| A.2 | Asparagine is quantitatively deamidated to aspartic acid via an S _N 2 reaction under acidic conditions, as described in Wright (1991). . . | 248 |
| A.3 | Proposed mechanism for dehydration of serine to pyruvic acid. . . . | 249 |
| A.4 | Esterification of serine during acid hydrolysis. | 249 |
| A.5 | Trace amounts of Br ₂ or Cl ₂ in HCl can halogenate tyrosine at the C-6 and/or C-8 position (Sanger & Thompson, 1963). | 251 |
| A.6 | Degradation of tryptophan during acid hydrolysis in the presence of O ₂ and cystine. | 252 |
| A.7 | Degradation of tryptophan during acid hydrolysis in the presence of O ₂ and a sulfoxide compound (e.g., dimethyl sulfoxide (DMSO) or methionine sulfoxide). | 252 |

| | | |
|-----|---|-----|
| A.8 | Progressive oxidation of the S-containing amino acids. | 253 |
| A.9 | Condensation reactions of cysteine with formaldehyde and pyruvic acid, forming ring structures after nucleophilic attack and proton transfer of sulfhydryl groups. | 254 |
| B.1 | Typical chromatogram and isotope ratio trace from GC/P/IRMS analysis of amino acids from microbial biomass. | 269 |
| B.2 | Schematic of enzymatic reactions in central metabolic pathways. | 270 |
| B.3 | Visual summary of ^{13}C -based metabolic fluxes in wildtype organisms grown on glucose. | 273 |
| B.4 | Visual summary of ^{13}C -based metabolic fluxes in <i>E. coli</i> mutant organisms grown on glucose lacking certain dehydrogenase or transhydrogenase genes. | 273 |
| B.5 | $^2\text{H}/^1\text{H}$ fractionations between amino acids and water in from biological replicates of wildtype organisms grown on different carbon substrates. | 276 |
| B.6 | Summary of $^2\text{H}/^1\text{H}$ fractionations between amino acids and water in replicate cultures of wildtype organisms grown on glucose. | 279 |
| B.7 | Theoretical errors in reported $\delta^2\text{H}_{\text{AA}}$ values when (A) no correction for the isotopic contribution by amine-bound hydrogen (F_{NH}) is made (Equation B.1), or (B) when a correction is made with the erroneous assumption that F_{NH} is equivalent to the isotopic composition of water (F_w ; Equation B.2). | 282 |
| B.8 | Theoretical errors in reported $\delta^2\text{H}$ values for proline when our derivative correction is applied (see Equation B.3 and Section 3.2.5 in the main text), as no amine-bound hydrogen remains in proline after derivatization. | 283 |

| | | |
|------|---|-----|
| B.9 | Effect of hydrolysis on amino acid $\delta^2\text{H}$ values from BSA (gray triangles) and a mixture of pure standards (black circles). | 285 |
| B.10 | Effect of derivatization on amino acid $\delta^2\text{H}$ values from BSA (gray triangles) and a mixture of pure standards (black circles). | 286 |
| B.11 | Influence of media $\delta^2\text{H}$ on amino acid $\delta^2\text{H}$ values in wildtype organisms grown on glucose. | 289 |
| B.12 | Regressions of pyruvate-derived hydrogen in amino acids versus shifts in $\delta^2\text{H}_{\text{AA}}$ values in wildtype organisms grown on glucose versus on acetate, pyruvate, and succinate. | 292 |
| B.13 | Regressions of NADPH-derived hydrogen in amino acids versus shifts in $\delta^2\text{H}_{\text{AA}}$ values in wildtype organisms grown on glucose versus on acetate, pyruvate, and succinate. | 293 |
| B.14 | Lack of correlations between amino acid/water fractionations and NADPH metabolism in wildtype organisms grown on glucose. | 298 |
| B.15 | Correlations between amino acid/water fractionations and NADPH metabolism in <i>E. coli</i> wildtype and mutant organisms grown on glucose. | 299 |
| B.16 | General biosynthetic pathway of proline with colors representing tracked hydrogen sources (red for OAA, purple for acetyl-CoA, light blue for water, green for NADPH). | 300 |
| B.17 | General biosynthetic pathway of phenylalanine with colors representing tracked hydrogen sources. | 301 |
| B.18 | General biosynthetic pathways of leucine and valine with colors representing tracked hydrogen sources. | 302 |
| B.19 | General biosynthetic pathway of isoleucine with colors representing tracked hydrogen sources. | 303 |

| | | |
|------|---|-----|
| B.20 | Distribution of enzymes in amino acid biosynthetic pathways across organisms investigated in this study. | 305 |
| C.1 | Summary of measured $\delta^2\text{H}$ values of amino acid standards injected throughout sample analyses carried out in 2022 and 2025 to monitor analytical consistency and ensure cross-experimental data comparability. | 311 |
| C.2 | Effect of peak size on measured $\delta^2\text{H}$ values amino acid standards, plotted with peak size represented by the mass-3 amplitude (A) and by the mass-3 amplitude normalized to that of the hydrogen reference gas peaks within the given analysis (B) | 314 |
| C.3 | Linear regressions of standard amino acid isotopic compositions (in F notation) versus the inverse of the mass-3 amplitudes (relative to hydrogen reference gas peak amplitudes, and normalized to the relative number of hydrogen atoms in each amino acid). | 316 |
| C.4 | Results from residual sum of squares model to correct amino acid isotope data for peak size effects. | 317 |
| C.5 | Distribution of relative mass-3 peak amplitudes of all phytoplankton biomass samples measured in this study. | 318 |
| C.6 | Peak size-dependent $\delta^2\text{H}_{\text{AA}}$ corrections applied to phytoplankton biomass from control and salinity experiments (A) and from irradiance experiments (B) | 319 |
| C.7 | Comparison of phytoplankton amino acid $^2\text{H}/^1\text{H}$ fractionations, with data from Figure 4.2 visualized here as density curves. | 320 |
| C.8 | Comparison of bacteria and phytoplankton amino acid $^2\text{H}/^1\text{H}$ fractionations, with data from Figure 4.3 and visualized here as density curves. | 321 |

| | | |
|------|---|-----|
| C.9 | Growth of <i>E. huxleyi</i> in media with different salinities, plotted as full growth curves measured via OD ₆₀₀ (A) and as the linear portions of the growth curves in logarithmic space (B) | 323 |
| C.10 | Amino acid/water ² H/ ¹ H fractionations in <i>E. huxleyi</i> grown in media with different salinities. | 324 |
| C.11 | <i>C. muelleri</i> cultures grown under varying light intensities. | 325 |
| C.12 | Growth of diatoms under varying light intensities, plotted as full growth curves measured via OD ₇₅₀ (A) and as the linear portions of the growth curves in logarithmic space (B) | 326 |
| C.13 | Amino acid/water ² H/ ¹ H fractionations in <i>C. muelleri</i> and <i>T. pseudonana</i> grown under different irradiances. | 327 |
| C.14 | Amino acid/water ² H/ ¹ H fractionations in <i>C. muelleri</i> (orange) and <i>T. pseudonana</i> (blue) grown under different irradiances, including $I=50\mu\text{mols photons m}^{-2} \text{ s}^{-1}$ | 328 |
| E.1 | Image of <i>T. pseudonana</i> aggregates. | 332 |
| E.2 | Example image segmentation performed for particle-attached bacteria cells. | 333 |
| E.3 | Heatmap showing the number of homologues of glycoside hydrolase (GH) family CAZymes within each strain. | 334 |
| E.4 | Heatmap showing the number of homologues of polysaccharide lyase (PL) family CAZymes within each strain. | 335 |
| E.5 | Increase in relative biomass of pseud3D05 and phaeoC3M10 (each strain in monoculture) on <i>T. pseudonana</i> aggregates after 42h of continuous colonization followed by washing of unattached cells and 98h of continued growth on particles. | 336 |

| | | |
|-----|---|-----|
| E.6 | Distribution of pseud3D05 and phaeoC3M10 cell patches on <i>T. pseudonana</i> aggregates over time in monoculture colonization experiments. | 337 |
|-----|---|-----|

List of Tables

| <i>Number</i> | | <i>Page</i> |
|---------------|--|-------------|
| 2.1 | Common amino acid derivatives for GC separation. | 22 |
| 2.2 | Summary of reaction information for six major derivatization strategies employed for GC analysis of amino acids. | 23 |
| 2.3 | Summary of analytical techniques for isotopic analysis. | 35 |
| 3.1 | Summary of potential biochemical controls on $\delta^2\text{H}_{\text{AA}}$ values. | 92 |
| 4.1 | Summary statistics for regressions shown in Figure 4.4. | 133 |
| 6.1 | Genomic content, physiological information, and predicted trophic functions of focal bacterial strains. | 222 |
| A.1 | Percentage recovery of amino acids from standards and proteins hydrolyzed under conventional acid hydrolysis conditions (6N HCl, 110°C, 20–24h, anoxic conditions). | 255 |
| A.2 | Yields and N isotope fractionations ($\Delta^{15}\text{N} = \delta^{15}\text{N}_{\text{after}} - \delta^{15}\text{N}_{\text{before}}$) of amino acids following cation exchange column desalting with Dowex 50WX8 resin, 100–200 or 200–400 mesh size. | 256 |
| B.1 | Estimated net carbon fluxes of wildtype organisms and <i>E. coli</i> mutants grown on glucose, reproduced from Wijker et al. (2019). | 271 |
| B.2 | Growth rates and measured $\delta^2\text{H}$ values of amino acids (AA), substrates (s), and culture media (w) for each growth condition. | 274 |
| B.3 | $\delta^2\text{H}$ values of amino acids (AA) that were not discussed in the main text. | 277 |
| B.4 | $\delta^2\text{H}$ values and standard deviations (from duplicate or triplicate analyses) of amino acids from bovine serum albumin hydrolyzed under different conditions. | 284 |

| | | |
|-----|--|-----|
| B.5 | Summary of slopes and 95% confidence intervals calculated from regressions of amino acid versus water $\delta^2\text{H}$ values for wildtype organisms grown on glucose (Figure B.11). | 290 |
| B.6 | Estimated isotopic compositions of and shifts in intracellular metabolite pools presented in Supplementary Section B.6.2. | 297 |
| C.1 | Summary of pairwise comparisons of differences between phytoplankton subgroup $^2\varepsilon_{\text{AA/w}}$ distributions (data from Figure 4.2) as determined from the non-parametric Mann-Whitney U test. | 318 |
| C.2 | Summary of pairwise comparisons of differences between phytoplankton and bacteria $^2\varepsilon_{\text{AA/w}}$ distributions (data from Figure 4.3) as determined from the non-parametric Mann-Whitney U test. | 322 |
| C.3 | Growth rates of diatoms grown under different light intensities, measured from the logarithmic OD_{750} data shown in Figure C.12B. | 325 |
| D.1 | Particulate amino acid concentrations from Station ALOHA used to calculate lower bound estimates of POM turnover. Concentrations were measured by H. Close (unpublished data). Those measured at PAP-SO are reported in Yanuskiewicz et al. (unpublished). | 330 |
| D.2 | Estimated contributions of heterotrophic biomass to POM based on Bayesian mixing model results. | 330 |
| E.1 | Isolation details for bacterial strains used in particle colonization experiments. | 332 |

Chapter 1

Introduction

1.1 Interrogating microbial metabolism: A need for quantitative tools

Microbial life is predominant in nearly every corner of Earth's environment. Although invisible to the naked eye, microorganisms exert profound impact on our planet's atmosphere and surface geochemistry—and have been doing so for billions of years—due to their nearly unfathomable numbers in the environment. Indeed, this unseen majority has mediated some of the most significant geochemical transformations throughout Earth history, including, perhaps most famously, the oxygenation of our atmosphere, which unlocked the ability for multicellular life to evolve. Today, microbes mediate all the major biogeochemical cycles on Earth. However, as we are keenly aware, our environment is changing. How microbes are adapting and responding to ongoing environmental perturbations is an open question, but one that carries significant implications for what future Earth will look like. Yet, crucially, we lack predictive understanding of how microbes are responding (and will continue to respond), to these perturbations.

A prime example of this mismatch is the pivotal yet unpredictable role of microbes in the biological pump. In the sunlight surface ocean, phytoplankton fix a substantial burden of atmospheric carbon ($\sim 50 \text{ Pg C yr}^{-1}$, or $\sim 10\%$ of atmospheric CO_2 ; Field et al., 1998). Aggregation of phytoplankton into particles that are exported into the ocean interior comprises the dominant mechanism by which carbon is

sequestered in the deep ocean. However, this vertical carbon flux is substantially attenuated by the collective work of microbial communities, which colonize and degrade the sinking (or slowly settling) particles (e.g., Datta et al., 2016; Giering et al., 2014; Nguyen et al., 2022). The impact of microbial activity on carbon sequestration is not straightforward: microbial activity can both reduce sequestration (via respiratory loss of particulate organic matter as CO₂) or enhance sequestration (via solubilization of particulate organic matter and transformation to recalcitrant dissolved organic matter that can persist in the ocean for millennia; Jiao et al., 2024; Williams and Druffel, 1987). Changes in microbial metabolic functions and activities may directly influence whether our future ocean will continue to serve as a net carbon sink—a first-order question carrying significant global consequences (e.g., Gruber et al., 2023)—yet our ability to accurately forecast these changes is limited by our lack of fundamental understanding of what factors control microbial particulate organic matter turnover rates.

Such limitations in our predictive understanding of how microbes will respond to environmental perturbations stem in part from our limited tools available to quantitatively reconstruct which microbial metabolic activities occurred in the environment based on samples collected at a later time. The overarching goal of my research has sought to address this gap through development of a relatively new isotopic tool, amino acid hydrogen isotope analysis, into a useful tracer of microbial metabolism in the environment. This research was inspired by the seminal work of Marilyn Fogel, who was a visionary leader in the field of stable isotope biogeochemistry and, among countless impactful contributions, first proposed the potential utility of this isotopic tool for tracing microbial metabolism (Fogel et al., 2016). My thesis presents a steady march toward realizing this goal, beginning with crucial methods development to make accurate amino acid hydrogen isotope ($\delta^2\text{H}_{\text{AA}}$) measurements; to pure culture studies for fundamental characterization

of controls on $\delta^2\text{H}_{\text{AA}}$ in organisms; to ultimate application of $\delta^2\text{H}_{\text{AA}}$ analysis to reconstruct microbial turnover of particulate organic matter (POM) in the ocean. An overview of these chapters is presented in Section 1.2. Understanding controls on marine POM turnover is of significant scientific interest to me given the importance of this processes in mediating global carbon cycling (discussed above), thus is the focus of my $\delta^2\text{H}_{\text{AA}}$ application and further work examining microscale dynamics that shape bacterial colonization of marine particles. There are also countless other potential applications of $\delta^2\text{H}_{\text{AA}}$ analysis to quantitatively trace microbial metabolism in environments beyond marine snow.

1.2 Thesis outline

Chapter 2—developed during the COVID-19 pandemic—reviews the literature on preparatory chemistry steps and instrumentation routinely used for isotopic analyses of amino acids, highlighting the breadth of analytical options available and potential for C, N, S, and H isotope fractionation during each stage. Supplementary material for this chapter is provided in Appendix A. This chapter is published in *Organic Geochemistry* (Silverman et al., 2022).

Chapter 3 develops the first method to correct amino acid $\delta^2\text{H}$ values for the exchangeable amine hydrogen (necessary to accurately characterize native isotopic signals) and interrogates the biochemical link between microbial metabolism and $\delta^2\text{H}_{\text{AA}}$ values in model aerobic heterotrophic bacteria grown on different carbon substrates and with measured metabolic fluxes. Supplementary material for this chapter is provided in Appendix B. This chapter is published in *Frontiers in Microbiology* (Silverman et al., 2024).

Chapter 4 investigates controls on hydrogen isotope fractionation of marine phy-

toplankton (including salinity and irradiance) and compares $\delta^2\text{H}_{\text{AA}}$ signals of photoautotrophic metabolism to those of heterotrophic bacterial metabolism (investigated in Chapter 3). In particular, this work provides the first characterization of $\delta^2\text{H}_{\text{AA}}$ values in photosynthetic organisms. Supplementary material for this chapter is provided in Appendix C.

Chapter 5 provides the first characterization of marine POM $\delta^2\text{H}_{\text{AA}}$ values (with POM samples from the Northeast Atlantic Ocean and North Pacific Subtropical Gyre) and applies $\delta^2\text{H}_{\text{AA}}$ analysis to trace and quantify heterotrophic turnover of marine POM with depth at both sites. Supplementary material for this chapter is provided in Appendix D.

Chapter 6 investigates the colonization dynamics and spatial structures of bacteria on diatom particles to test whether principles about microbial assembly and function developed through studies involving synthetic polysaccharide particle systems hold true in a complex substrate context. This work further serves to develop hypotheses regarding how intra- and interspecies interactions shape the single-cell activities of microbes on particles, which will be tested in future work involving nanoscale secondary ion mass spectrometry. Supplementary material for this chapter is provided in Appendix E.

All scientific content presented in my thesis was in some way touched by my excellent collaborators, mentors, and peers, whose names are acknowledged at the start or end of each chapter.

References

Datta, M. S., Sliwerska, E., Gore, J., Polz, M. F., & Cordero, O. X. (2016). Microbial interactions lead to rapid micro-scale successions on model marine

- particles. *Nature Communications*, 7(1), 11965. <https://doi.org/10.1038/ncomms11965>
- Field, C. B., Behrenfeld, M. J., Randerson, J. T., & Falkowski, P. (1998). Primary Production of the Biosphere: Integrating Terrestrial and Oceanic Components. *Science*, 281(5374), 237–240. <https://doi.org/10.1126/science.281.5374.237>
- Fogel, M. L., Griffin, P. L., & Newsome, S. D. (2016). Hydrogen isotopes in individual amino acids reflect differentiated pools of hydrogen from food and water in *Escherichia coli*. *Proceedings of the National Academy of Sciences*, 113(32), E4648–E4653. <https://doi.org/10.1073/pnas.1525703113>
- Giering, S. L. C., Sanders, R., Lampitt, R. S., Anderson, T. R., Tamburini, C., Boutrif, M., Zubkov, M. V., Marsay, C. M., Henson, S. A., Saw, K., Cook, K., & Mayor, D. J. (2014). Reconciliation of the carbon budget in the ocean's twilight zone. *Nature*, 507, 480–483. <https://doi.org/10.1038/nature13123>
- Gruber, N., Bakker, D. C. E., DeVries, T., Gregor, L., Hauck, J., Landschützer, P., McKinley, G. A., & Müller, J. D. (2023). Trends and variability in the ocean carbon sink. *Nature Reviews Earth & Environment*, 4(2), 119–134. <https://doi.org/10.1038/s43017-022-00381-x>
- Jiao, N., Luo, T., Chen, Q., Zhao, Z., Xiao, X., Liu, J., Jian, Z., Xie, S., Thomas, H., Herndl, G. J., Benner, R., Gonsior, M., Chen, F., Cai, W.-J., & Robinson, C. (2024). The microbial carbon pump and climate change. *Nature Reviews Microbiology*, 22(7), 408–419. <https://doi.org/10.1038/s41579-024-01018-0>
- Nguyen, T. T. H., Zakem, E. J., Ebrahimi, A., Schwartzman, J., Caglar, T., Amarnath, K., Alcolombri, U., Peaudecerf, F. J., Hwa, T., Stocker, R., Cordero, O. X., & Levine, N. M. (2022). Microbes contribute to setting the ocean carbon flux by altering the fate of sinking particulates. *Nature Communications*, 13(1), 1657. <https://doi.org/10.1038/s41467-022-29297-2>
- Silverman, S. N., Wijker, R. S., & Sessions, A. L. (2024). Biosynthetic and catabolic pathways control amino acid $\delta^2\text{H}$ values in aerobic heterotrophs. *Frontiers in Microbiology*, 15, 1–20. <https://doi.org/10.3389/fmicb.2024.1338486>
- Silverman, S. N., Phillips, A. A., Weiss, G. M., Wilkes, E. B., Eiler, J. M., & Sessions, A. L. (2022). Practical considerations for amino acid isotope analysis. *Organic Geochemistry*, 164, 104345. <https://doi.org/10.1016/j.orggeochem.2021.104345>
- Williams, P. M., & Druffel, E. R. M. (1987). Radiocarbon in dissolved organic matter in the central North Pacific Ocean. *Nature*, 330(6145), 246–248. <https://doi.org/10.1038/330246a0>

Chapter 2

Practical considerations for amino acid isotope analysis

Silverman, S. N., Phillips, A. A., Weiss, G. M., Wilkes, E. B., Eiler, J. M., & Sessions, A. L. (2022). Practical considerations for amino acid isotope analysis. *Organic Geochemistry*, *164*, 104345. <https://doi.org/https://doi.org/10.1016/j.orggeochem.2021.104345>

This chapter has been modified from its published version in the following way:
Figure 2.3 appears in color here for ease of visualization.

Abstract

Over the last few decades, isotopic analysis of amino acids at the compound- and position-specific levels has been rapidly advancing across diverse fields. As these techniques progress, evaluation of isotopic fractionation associated with sample workup is essential. This critical review of analytical methods through the lens of isotope geochemistry provides a benchmark for researchers across disciplines seeking to make compound- and position- specific amino acid isotope measurements. We focus on preparation, acid hydrolysis, clean-up, derivatization, separation, and C, H, N, and S isotope measurement. Despite substantial customizability across these steps, the following general recommendations should maximize recovery while minimizing isotopic fractionation. Samples should be freeze-dried and stored anoxically at $\leq -20^{\circ}\text{C}$ prior to conventional acid hydrolysis (6N HCl, 110°C , 20–24 h, anoxic), which suffices for many residues. Both gas and liquid chromatographic (GC and LC, respectively) techniques are well-established and separate about 15

amino acids; LC bypasses the need for derivatization, while GC provides higher sensitivity. When derivatization is needed, *n*-acetyl and alkoxy-carbonyl esters provide the most reproducible C isotope ratios. For compound-specific analyses, online GC–IRMS and LC–IRMS systems offer the easiest workflow, but EA–IRMS enables potential multi-element isotope analysis. Emerging techniques like high-resolution mass spectrometry are also promising for multi-element analysis and recover position-specific isotopic information. Looking forward to the next decade of innovation, isotope geochemists and ecologists can improve amino acid isotope analysis by focusing on streamlining multi-element analysis and standardizing calibration practices across laboratories.

2.1 Introduction

Stable isotope ratios ($^{13}\text{C}/^{12}\text{C}$, $^{15}\text{N}/^{14}\text{N}$, $^2\text{H}/^1\text{H}$, and $^{34}\text{S}/^{32}\text{S}$) of amino acids record details of biosynthesis, enabling interrogation of environmental and physiological processes. This review covers common steps within the workflow for amino acid isotope analysis, including protein hydrolysis, derivatization, chromatographic separation, and isotope ratio detection (Figure 2.1). While these steps build on earlier studies quantifying amino acids (e.g., Homer, 1915; Rees, 1946; Tristram, 1939), no review has covered amino acid isotope analysis in full, but rather have provided overviews of C and N isotope analysis that emphasize data interpretation and ecological applications (McMahon & Newsome, 2019; Ohkouchi et al., 2017; Whiteman et al., 2019). Here we review published techniques encompassing sample preparation through isotope ratio measurement for C, N, H, and S (Figure 2.1). We highlight (1) where nonquantitative reactions and/or incomplete separations can fractionate isotopes, and (2) established and emerging analytical options available to isotope geochemists that enable compound-specific and position-specific

isotope analysis of amino acids.

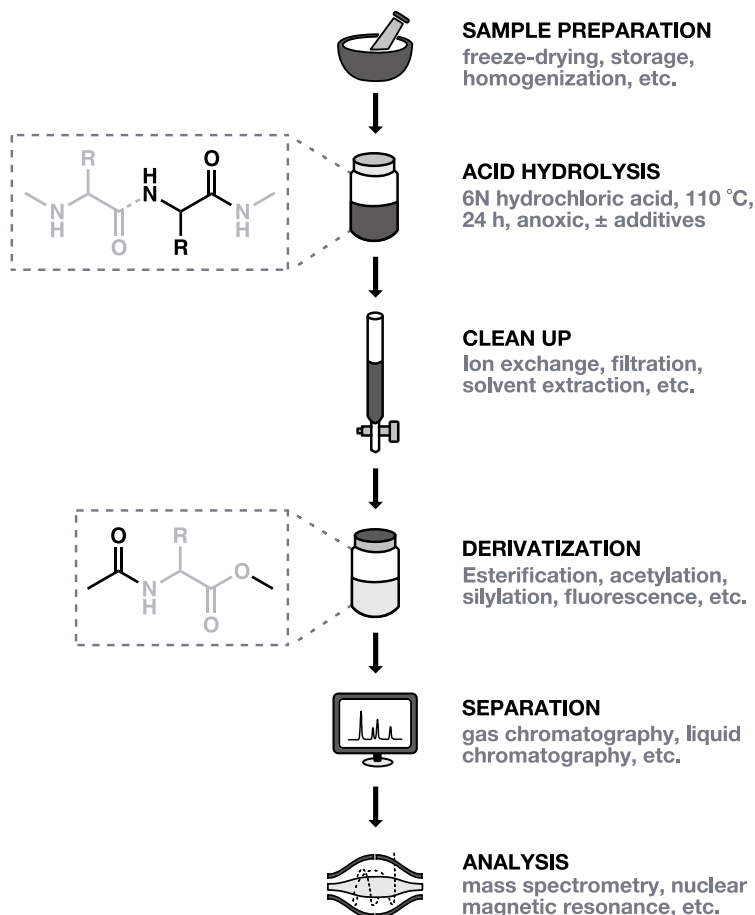


Figure 2.1. A typical workflow for amino acid isotope analysis, highlighting the major preparatory and analytical steps examined in this review paper. We cover sample preparation, acid hydrolysis, clean-up, derivatization, separation, and isotopic analysis. Sample preparation includes drying and homogenization steps, and, less commonly, clean-up steps prior to hydrolysis. Peptide-bound amino acids can be released by acid hydrolysis and are typically followed by additional clean-up steps depending on the sample matrix. Amino acids must be derivatized to decrease their polarity and make them amenable to separation by gas chromatography. Samples can also be separated without derivatization via liquid chromatography. Finally, isotope measurements are achieved via a variety of established and emerging techniques including isotope ratio mass spectrometry (IRMS), high-resolution mass spectrometry (e.g., Orbitrap), or nuclear magnetic resonance (NMR). Insets show peptide bonds cleaved during acid hydrolysis and example derivative groups added during derivatization.

2.1.1 Terminology

Natural-abundance stable isotope compositions are typically reported in delta (δ) notation (McKinney et al., 1950; Urey, 1948) to highlight small variations between samples. A δ value is the relative difference in isotope ratio (R) between a sample and standard (Equation 2.1), commonly expressed in parts per thousand (per mil, ‰). The heavy (i.e., rare) isotope is placed in the numerator of R by convention.

$$\delta = \left(\frac{R_{\text{sample}} - R_{\text{standard}}}{R_{\text{standard}}} \right) = \left(\frac{R_{\text{sample}}}{R_{\text{standard}}} - 1 \right) \quad (2.1)$$

Isotopic substitutions alter the bond energies and physical properties of molecules, causing them to react at different rates or partition differently between phases. These physical phenomena are “isotope effects,” defined as the change in some chemical or physical parameter (kinetic rate constant, equilibrium constant, vapor pressure, etc.) due to isotopic substitution. A kinetic isotope effect (KIE) represents the ratio of reaction rate constants between two isotopologues (versions of molecules with differing isotopic substitutions); a “normal” KIE describes a reaction in which the lighter isotope reacts faster (Hayes, 2002). Isotope effects are considered primary at the reacting atomic position(s), and secondary at non-reacting positions (Hayes, 2002).

Isotope effects result in measurable differences in isotopic composition between products, pools, materials, etc., called “fractionations.” Isotope fractionations are commonly expressed as fractionation factors (α), the ratio of isotope ratios between two pools of interest (Hayes, 2002). For example, given the generic reaction $A \rightarrow B$, the isotopic fractionation would be described as:

$$\alpha_{B-A} = \frac{R_B}{R_A} \quad (2.2)$$

There is no consensus on whether reactant or product belongs in the numerator of α . Throughout this review, we use the convention shown in Equation 2.2, which for a normal KIE results in $\alpha < 1$. For convenience, α is occasionally expressed as an ε value, in ‰ (Equation A.3). For further review on notation and calculations, we refer the readers to Hayes (2002) and Coplen (2011).

$$\varepsilon = (\alpha - 1) \times 10^3 \quad (2.3)$$

2.2 Sample storage and preparation

Sample storage conditions should be selected to minimize amino acid degradation and contamination, ideally achieved by storing freeze-dried or frozen samples in clean plastic or baked glassware with an anoxic headspace. Higher storage temperatures ($>-20^{\circ}\text{C}$) may promote decomposition (Laegeler et al., 1974; Rutherford & Gilani, 2009; Whiteman et al., 2019), while oxic conditions can degrade cysteine, methionine, and tryptophan (Hunt, 1985). There is no consensus on whether plastic or glass containers are better for amino acid recovery. Because dust, fingerprints, sweat, and reagents may introduce contaminant amino acids (Henrichs, 1991; McCoy et al., 2019; Ozols, 1990, and references therein), any glassware, foil, or glass fiber filters that will contact samples should be baked (e.g., at 450°C for 8h; Larsen et al., 2013; Molero et al., 2011; Unger and Holzgrabe, 2018; Whiteman et al., 2019). Most samples should be homogenized – e.g., by mortar and pestle, bead beater, or cryogenic grinding – before or after storage to increase efficiency of acid hydrolysis.

While general storage recommendations can be made, pretreatment is more sample-dependent as geochemists process diverse sample matrices ranging from hard rocks

to soft tissues. The goal of pretreatment is to remove large, non-amino acid components that interfere with measurement (e.g., through co-elutions or column overloading) and cannot be eliminated at a later stage. However, as each additional step may lower recovery or fractionate isotopes, we recommend minimizing pretreatments and monitoring procedural blanks and external standards. Procedural blanks are controls that do not contain the sample matrix and are subjected to the entire workflow, including pretreatment; external standards are well-characterized materials (e.g., proteins like bovine serum albumin or amino acids with known isotope ratios) that are processed alongside samples. Additional pretreatment steps are highly matrix-specific and should be carefully assessed, but could include surface rinsing, mechanical abrasion, or deeper cleaning (e.g., Hare et al., 1991; Johnson et al., 1998; Schiff et al., 2014); solvent extraction to remove lipids from fatty tissues (Bligh & Dyer, 1959; S. D. Newsome et al., 2018; Whiteman et al., 2019); demineralization with hydrofluoric acid (Cheng, 1975; Gélinas et al., 2001; Ingalls et al., 2003; Nunn & Keil, 2006); or decarbonation with hydrochloric acid (e.g., Hare et al., 1991; Johnson et al., 1998; Schiff et al., 2014). Protein extraction prior to hydrolysis, though tempting to avoid interfering components, is not recommended, as this procedure is labor-intensive and introduces bias by preferentially removing hydrophilic or hydrophobic peptides (Nguyen & Harvey, 1998; Niu et al., 2018; Nunn & Keil, 2006; Wang et al., 2003).

2.3 Acid hydrolysis

The goal of acid hydrolysis is to liberate proteinogenic amino acids into their “free” (non-peptide-bound) forms (Figure 2.2) with maximum recovery and minimal isotopic fractionation. Studies have largely converged on heating samples in 6N HCl for 20–24h at 110°C under anoxic conditions (e.g., flushed with N₂

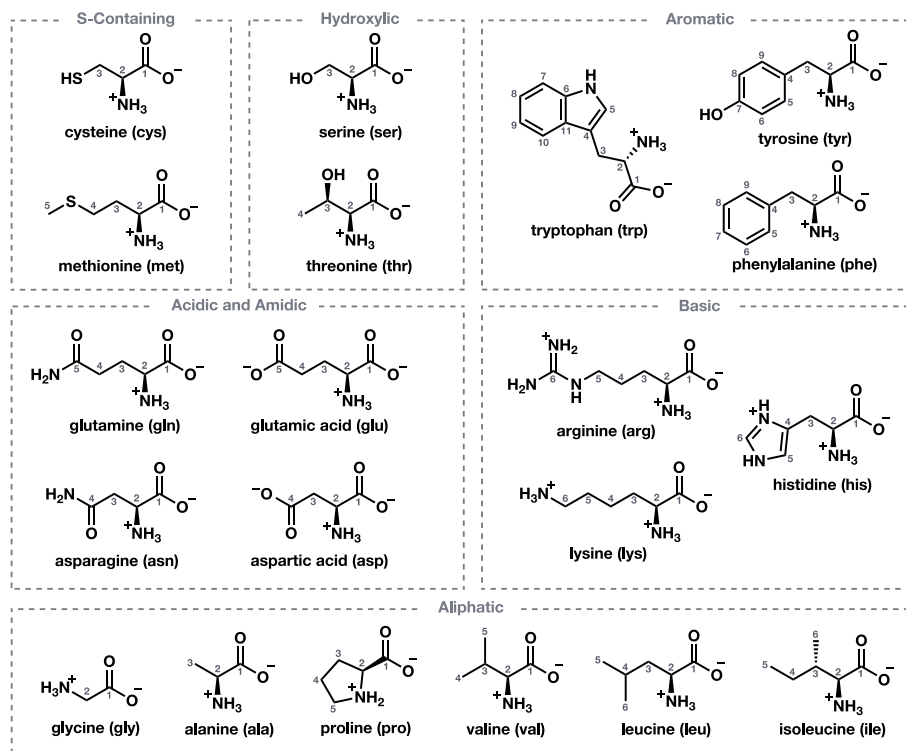


Figure 2.2. Structures of 20 common proteinogenic amino acids in zwitterion form at pH 7. Residues are grouped by side-chain chemistries. Numbering for amino acid sites (e.g., C-1) used throughout this review is shown.

gas; Fogel et al., 2016; Fountoulakis and Lahm, 1998; Moore and Stein, 1963; Rutherford and Gilani, 2009), hereafter referred to as “conventional hydrolysis.” We recommend this method for most applications, as it results in high recoveries and negligible fractionation of many amino acids with minimal additional chemical workups (Figure 2.3). Here we discuss this conventional hydrolysis method and its variations, including different durations and additives that stabilize certain amino acid side-chains. We also discuss fast hydrolysis alternatives, including microwave and vapor-phase methods. It is important to emphasize that no single hydrolysis method recovers all amino acids (Figure 2.4); in particular, no current method prevents quantitative deamidation of asparagine and glutamine to aspartic acid and glutamic acid (Supplementary Figure A.2; Supplementary Section A.1.2; R. L.

Hill, 1965; Rutherford and Gilani, 2009; Wright, 1991). Yields and isotopic compositions are therefore commonly reported as asx (asparagine + aspartic acid) and glx (glutamine + glutamic acid). Loss mechanisms are influenced by amino acid side-chain chemistry (e.g., hydroxyl groups on serine and threonine; see Supplementary Section A.1), protein composition (e.g., the proportion of S-containing amino acids), and hydrolysis method (e.g., duration, temperature). Sample matrix effects also likely influence yields, but studies thus far have focused on loss and isotopic fractionations of pure standards or synthetic polypeptides and cannot account for the complexity of geochemically relevant samples.

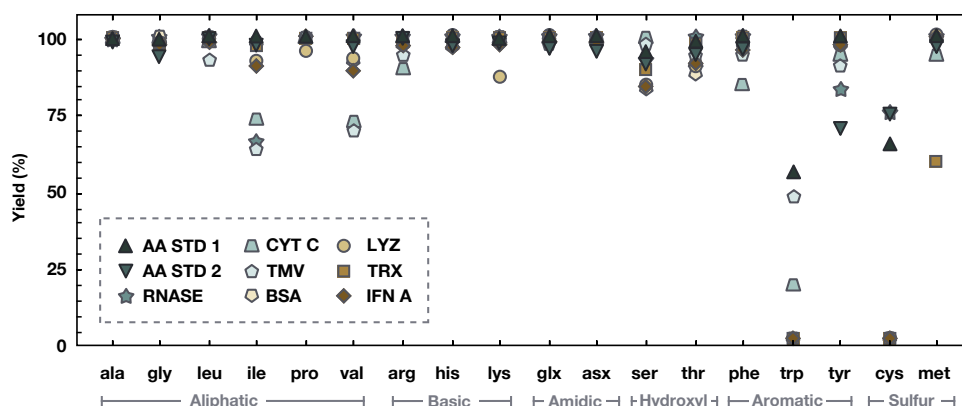


Figure 2.3. Yields of free amino acid standard mixtures (dark gray triangles) and of amino acids from proteins (light gray shapes) after conventional acid hydrolysis (6N HCl, 110°C, 20–24h, anoxic conditions). Corresponding yield data can be found in Supplementary Table A.1. Abbreviations and references: AA STDs, amino acid standard 1 (Mondino & Bongiovanni, 1970) and amino acid standard 2 (Keutmann & Potts, 1969); RNASE, Ribonuclease (Keutmann & Potts, 1969); CYT C, Cytochrome c (Matsubara & Sasaki, 1969); TMV, Tobacco mosaic virus (Matsubara & Sasaki, 1969); BSA, Bovine serum albumin (Manneberg et al., 1995); LYZ, Lysozyme (Manneberg et al., 1995); TRX, Thioredoxin (Manneberg et al., 1995); IFN A, Interferon A (Manneberg et al., 1995).

2.3.1 Conventional hydrolysis

Conventional hydrolysis (6N HCl, 110°C, 20–24h, anoxic conditions) results in consistently high yields for 13 of the 20 amino acids (Figures 2.3 and 2.4; Supplementary Table A.1), including all aliphatic and basic amino acids. Lengthening or shortening hydrolysis duration reduces the total number of stable residues but can maximize yields of particular amino acids (Figure 2.4). For example, extended hydrolyses (>24h) improve recoveries of most aliphatic amino acids, especially valine, leucine, and isoleucine (A. Darragh & Moughan, 2005) at the expense of other amino acids (A. J. Darragh et al., 1996; Hirs et al., 1954; E. L. Smith & Stockell, 1954). Meanwhile, shortened hydrolysis times (<20h) optimize yields of serine and threonine (Albin et al., 2000; Rowan et al., 1992), with maximum recovery between ~10 and 16h (Gardner, 1981; Gehrke et al., 1985; Rutherford, 2009). Although phenylalanine and tyrosine are stable regardless of hydrolysis length, tryptophan has low and variable yields (0–55%; Figure 2.3; Supplementary Table A.1; Hunt, 1985; Keutmann and Potts, 1969; Manneberg et al., 1995; Matsubara and Sasaki, 1969; Mondino and Bongiovanni, 1970; Rutherford and Gilani, 2009). Like tryptophan, sulfur-containing and amidic amino acids are unstable regardless of hydrolysis length (Figure 2.4; Hunt, 1985).

2.3.2 Isotopic fractionation

Each amino acid experiences different mechanisms and magnitudes of loss during conventional hydrolysis, which can lead to isotopic fractionation. We review what is known about isotopic fractionation during hydrolysis and peptide bond cleavage; mechanistic details concerning amino acid losses are presented in Supplementary Section A.1. Studies of pure amino acid standards subjected to hydrolysis condi-

tions revealed minimal C isotope changes (Demmelmair & Schmidt, 1993; Metges & Daenzer, 2000), even for amino acids with significant losses like serine and methionine. This is further supported by Jim et al. (2003), who found no detectable C isotope fractionation upon hydrolysis of synthetic alanine, serine, glutamic acid, phenylalanine, leucine, or proline polypeptides. Nitrogen isotopes may be more susceptible, especially in aliphatic amino acids. Bada et al. (1989) observed $\sim 20\text{‰}$ ^{15}N -enrichment of residual, unhydrolyzed collagen, and Silfer et al. (1992) observed temperature-dependent normal ^{15}N -KIEs of 0.9960–0.9975 for residual diglycine. We also caution interpreting $\delta^{15}\text{N}$ values of asx and glx due to the loss of amide-N from asparagine and glutamine. Although few studies have investigated H isotopes of amino acids, deuterated and tritiated hydrolysis experiments suggest H isotope exchange with the aqueous medium is significant for tyrosine (C-3 atomic site; Figure 2.2), aspartic acid (C-3 site), and glutamic acid (C-4 site; Fogel et al., 2016; J. Hill and Leach, 1964). Studies of S isotopes are also limited but indicate a ^{34}S -KIE of 0.985 associated with oxic degradation of cysteine during conventional hydrolysis (Phillips et al., 2021). Importantly, the lack of geochemically-relevant sample matrices in all the aforementioned studies limits the scope of conclusions that can be drawn. Moving forward, a more comprehensive characterization of isotope fractionations accompanying protein hydrolysis in complex matrices like sediments and soils is needed.

2.3.3 Alternative hydrolysis methods

Variations on conventional hydrolysis offer some specific advantages, including: (1) protection of certain amino acids through chemical additives and/or (2) much faster hydrolysis times via microwave or vapor-phase methods. For additives, the use of β -mercaptoethanol appears most promising, as it increases the number of

stable residues from 13 to 17 (Figure 2.4; Hunt, 1985; Ng et al., 1987). We especially recommend the use of β -mercaptoethanol for studies of tryptophan, as this is the only method that can reproducibly recover this residue. Phenol is another common additive as it mitigates halogenation of aromatic residues, but it does not stabilize other amino acids so is not recommended for general use. Addition of the oxidizing agent performic acid is one of the few hydrolysis methods that recovers cysteine, but it destroys several aromatic and hydroxylic residues (Figure 2.4; Hunt, 1985; Rutherford and Gilani, 2009). Microwave-assisted and vapor-phase methods achieve complete hydrolysis in <90 min and generally recover the same amino acids as conventional hydrolysis (Figure 2.4; Chiou, 1989; Tsugita et al., 1987; Weiss et al., 1998; Yarnes and Herszage, 2017), although with slightly lower yields (Enggrob et al., 2019). Vapor-phase methods have the added benefit of minimizing contact between samples and liquids, reducing potential contamination. These high-temperature, short-duration hydrolyses also limit amino acid racemization (Csapó et al., 1997) and potentially minimize H isotope exchange with the aqueous medium.

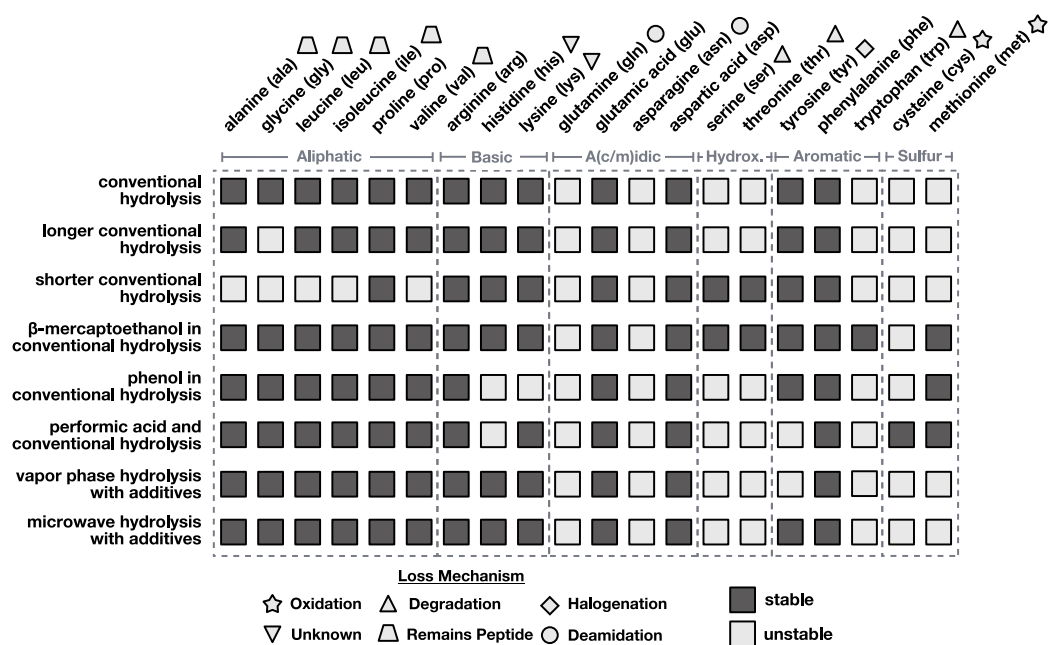


Figure 2.4. Summary of stable and unstable residues during common acid hydrolysis procedures. Primary loss mechanisms are denoted by shapes. Conventional hydrolysis is defined as 20–24h at 110°C in 6N HCl under anoxic conditions. The recommended vapor phase hydrolysis uses 7N HCl, 10% trifluoroacetic acid, and 0.1% phenol for 22 min at 158°C. The recommended microwave assisted hydrolysis uses 6N HCl, 0.02% phenol, 0.2% 3-(2-aminoethyl)-indole for 4 min at 155°C. See text for details and references.

2.4 Analyte clean-up

There are two main goals of clean-up: (1) removing large particles and (2) eliminating extraneous compounds such as lipids, carbohydrates, and salts that are liberated during acid hydrolysis. These components can interfere with derivatization and isotope analysis (e.g., by consuming derivatizing reagents or damaging the gas chromatography- isotope ratio mass spectrometer (GC-IRMS) combustion interfaces; Cheng et al., 1975; Hedges and Stern, 1983; Takano et al., 2010). At a minimum, large particles must be removed. While this can be accomplished via filtration with baked glass fiber filters (Amelung & Zhang, 2001), quartz wool pipette columns (Enggrob et al., 2019), or non- protein binding syringe filters (e.g., PES, PVDF; Larsen et al., 2013; Phillips et al., 2021), we recommend cation exchange chromatography (Section 2.4.1) for most applications because it eliminates both salts and particles. Less commonly, organic/aqueous solvent extraction can complement cation-exchange chromatography to remove excess hydrophobic components (e.g., lipids from fatty tissues). Solvent extraction is recommended for samples with > 2% lipid content (McMahon & Newsome, 2019) and can be performed before or after hydrolysis. Some derivatizing reagents (e.g., BSTFA) require moisture-free reaction conditions so samples must be carefully dried as a final clean-up step. This can be achieved via rotary evaporation, addition of sodium sulfate desiccants, or azeotropically with dichloromethane (DCM).

2.4.1 Ion exchange

Studies have converged on the Dowex 50WX8 hydrogen form resin (200–400 mesh) for cation exchange. Most amino acids are recovered with >90% yield, including from complex matrices like clay minerals (Supplementary Table A.2; Amelung and

Zhang, 2001; Cheng et al., 1975; Moore and Stein, 1951; Takano et al., 2010). Cation exchange also preserves amino acid chirality and introduces no background contaminants when resins are washed (Takano et al., 2010). Additional rinses with 0.1N oxalic acid can be added to remove metal cations from soils, rocks, and sediment samples (Amelung & Zhang, 2001). As cation exchange involves both binding of the amine group and elution with ammonia, potential alteration of $\delta^{15}\text{N}$ values is a concern. However, Takano et al. (2010) observed $<0.3\text{‰}$ differences in $\delta^{15}\text{N}$ values for 12 amino acids before versus after elution on the Dowex 50WX8 resin, despite losses of up to 17% (Supplementary Table A.2). Carbon is not involved in adsorption or elution and is not expected to fractionate. Indeed, Abelson and Hoering (1961) found minimal C isotope fractionation ($<0.6\text{‰}$) of alanine on the Dowex 50WX8 resin.

Anion exchange (Dowex 1X8) is another option for desalting (Cheng et al., 1975), but is far less common, perhaps due to (1) the fact that in geochemical samples, interfering anions (i.e., sugars and organic acids) are present in greater concentrations than cations, (2) evidence of C isotope fractionation during elution (Abelson & Hoering, 1961), and (3) the need to work with corrosive HF to condition some anion exchange resins (Abelson & Hoering, 1961).

2.5 Derivatization (for gas chromatography)

Derivatization is required to make amino acids amenable to separation by GC. Polar functional (carboxyl, amine, hydroxyl, and thiol) groups are modified via the addition of various organic moieties to make amino acids more volatile, with the products termed “derivatives.” For H isotope analysis, derivatization serves the additional purpose of removing exchangeable H atoms, such as on carboxyl and

amine groups, that would otherwise equilibrate with the aqueous medium and alter the original $\delta^2\text{H}$ value.

Derivatization strategies for amine and carboxyl groups can be chosen independently, provided the reactions are compatible, leading to a variety of combinations (Tables 2.1 and 2.2). Amine, hydroxyl, and thiol side-chains are typically derivatized by the same reagent used for the amine group. No single derivatization strategy is optimized for all 20 amino acids (Tables 2.1 and 2.2). In particular, arginine and histidine are incompatible with many reactions (Table 2.1; Hušek and Macek, 1975). Several factors govern the selection of GC derivatives, including reaction time, ease of procedure, product volatility, derivative stability, the number of non-analyte atoms added, reaction yield, byproduct formation, enantiomer preservation (i.e., lack of racemization), combustion or pyrolysis efficiency, and chromatographic resolution. Tradeoffs abound: for example, a less stable derivative may be preferable if the reaction is rapid, as samples can be derivatized immediately before analysis.

Derivatizing reagents should be present in excess to enable reaction completion and avoid isotopic fractionation of amino acids (Docherty et al., 2001). However, even under these conditions, it appears that derivatization reactions are not always quantitative, as N isotope fractionation accompanies formation of many derivative products (Table 2.1; D. Hofmann et al., 2003; Walsh et al., 2014). All derivatizing agents add C and/or H atoms which alter the molecular isotope ratio of derivatized amino acids (Figure 2.5; Tables 2.1 and 2.2) and must be subtracted. Large derivative groups are less suited for isotope analysis, as analytical uncertainty scales with the number of atoms added by the derivative group(s) (Rieley, 1994). For details on this data correction, error propagation, and associated isotope effects, see Supplementary Section A.2.

Numerous derivatives are used in ecological and geochemical studies. For N isotope analysis, we recommend pivaloyl derivatives, while for C and H isotope analysis, *n*-acetyl methyl esters (NACMEs) or methoxycarbonyl (MOC) methyl esters are ideal, as they introduce few exogenous atoms (Ohkouchi et al., [2017](#)). Fluorinated derivatives, though popular, are best reserved for applications that do not rely on combustion or pyrolysis of analytes. We discuss these and other common amino acid derivatives for GC analysis below, with sections separated by targeted functional group (amine versus carboxyl). Reagent toxicity is not individually discussed, but it should be noted that many are acutely toxic (particularly pivaloyl chloride and methyl/ethyl chloroformate; Ohkouchi et al., [2017](#); Walsh et al., [2014](#)).

Table 2.1. Common amino acid derivatives for GC separation.

| Derivative ^a | Added | | Problematic amino acids ^b | Recommended columns | Co-elutions | KIE | | References |
|-------------------------|-------|-------|--------------------------------------|---|--|------------------------------|------------------------------|---|
| | C | H | | | | ¹³ α ^c | ¹⁵ α ^d | |
| NPNP | 8–13 | 16–25 | arg, asn, gln | High polarity: ZB-WAX VF-23 ms | | 0.891–0.982 | | Corr et al. (2007b); Tea and Tcherkez (2017) |
| NPIP | 8–13 | 16–25 | arg, asn, cys, gln, his, trp, val | Low to high polarity: Ultra-2 ZB-WAX ZB-FFAP | | 0.874–1.03 | 0.994–1.002 | Metges et al. (1996); Metges and Daenzer (2000); Hofmann et al. (2003); Chikaraishi et al. (2007); Corr et al. (2007b); Tea and Tcherkez (2017); Ohkouchi et al. (2017) |
| TFA-IP | 5–8 | 7–14 | arg, asn, cys, gln, his, trp | Low polarity: ZB-1 Ultra-2 | | 0.919–0.992 | 0.986–1.008 | Hušek and Macek (1975); Silfer et al. (1991); Docherty et al. (2001); Hofmann et al. (2003); Corr et al. (2007b); Ohkouchi et al. (2017) |
| TFA-ME | 3–5 | 3–6 | arg, asn, gln, his, ser, thr, tyr | Low polarity: ZB-5 | | | | Darbre and Blau (1965); Islam and Darbre (1972); Hušek and Macek (1975); Jim et al. (2006) |
| PFP-IP | 6–9 | 7–14 | arg, cys, his | Low polarity: Ultra-2 | lys/cys/ tyr | | | Frank et al. (1982); Amelung and Zhang (2001); Glaser and Amelung (2002); Kayacelebi et al. (2015); Tea and Tcherkez (2017) |
| HFB-IB | 8–12 | 9–18 | his, met | Low polarity: DB-5 | | | | Engel and Hare (1985); Golan and Wolfe (1979); MacKenzie and Tenaschuk (1979) |
| NANP | 5–8 | 10–17 | arg, asn, cys, gln, his, thr | High polarity: ZB-WAX ZB-FFAP VF-23 ms | pro/thr (VF-23 ms) phe/glx (ZB- WAX) | 0.948–0.997 | | Demmelmair and Schmidt (1993); Metges and Daenzer (2000); Corr et al. (2007b) |
| NAIP | 5–8 | 10–17 | asn, gln | High polarity: VF-23 ms | ile/gly glu/met | 0.946–0.978 | 0.997–1.002 | Adams (1974); Hofmann et al. (2003); Corr et al. (2007b); Yarnes and Herszage (2017) |
| NACME | 3–5 | 6–9 | arg, asn, gln, gly, his, lys, met | Mid to high polarity: DB-225 ms VF-23 ms DB-WAX | leu/ile pro/thr (VF-23 ms) | 0.933–0.981 | | Corr et al. (2007a,b); Dunn et al. (2011) |
| MOC ME | 3–5 | 6–9 | arg, ser, his | High polarity: VF-23 ms | leu/ile | 0.978–1.060 | 0.978–1.002 | Hušek (1991a,b); Walsh et al. (2014) |
| EOC EE | 5–8 | 10–15 | arg | Mid to high polarity: DB-225 ms VF-23 ms DB-WAX | ser/gln (DB- WAX) leu/ile (DB-225 ms) | | | Hušek (1991a,b); Godin et al. (2007) |
| TMS | 3–9 | 9–27 | | Low polarity: DB-5 | | | | Molnár-Perl and Katona (2000); Sobolevsky et al. (2003); Zaikin and Halket (2005); Tea and Tcherkez (2017) |
| <i>t</i> -BDMS | 6–18 | 15–45 | | Low polarity: DB-5 | | | 0.999–1.080 ^e | Molnár-Perl and Katona (2000); Hofmann et al. (2003); Sobolevsky et al. (2003); Tea and Tcherkez (2017) |

^a Abbreviations: NPNP, *n*-pivaloyl *n*-propyl ester; NPIP, *n*-pivaloyl isopropyl ester; TFA-IP, trifluoroacetyl isopropyl ester; TFA-ME, trifluoroacetyl methyl ester; PFP-IP, pentafluoropropionyl isopropyl ester; HFB-IB, heptafluorobutyl isobutyl ester; NANP, *n*-acetyl *n*-propyl ester; NAIP, *n*-acetyl isopropyl ester; NACME, *n*-acetyl methyl ester; MOC ME, methoxycarbonyl methyl ester; EOC EE, ethoxycarbonyl ethyl ester; TMS, trimethylsilyl; *t*-BDMS, *tert*-butyldimethylsilyl.

^b As reported in the specified literature (References column).

^c Range of ¹³α values reported in Corr et al. (2007b), except that for MOC ME, which is calculated from data in Walsh et al. (2014) using Equation 2 in Corr et al. (2007b).

^d ¹⁵α calculated using Equation 2 in Corr et al. (2007b) with data from D. Hofmann et al. (2003) (NPIP, TFA-IP, NAIP, and *t*-BDMS) and from Walsh et al. (2014) (MOC ME).

^e Calculated assuming amine, hydroxyl, and thiol groups are each derivatized by only one *t*-BDMS group, which may not be true (see discussion in main text).

Table 2.2. Summary of reaction information for six major derivatization strategies employed for GC analysis of amino acids. Note that all derivatization methods for the amine group require correction for C isotope fractionation.

| Derivatization strategy ^a | Groups targeted | Atoms per group | Reaction time and temp | | Derivative stability | Pros | Cons | References | |
|--------------------------------------|---------------------------|-------------------------------------|------------------------|---|------------------------|------------------|--|--|--|
| | | | C | H | | | | | |
| Pivaloylation | with pivaloyl chloride | Amine, hydroxyl, thiol | 5 | 9 | 120 mins, 110 °C | Months at -18 °C | Highly stable; products have excellent chromatographic resolution; enantiomers preserved | Generates co-eluting byproducts; adds many C and H atoms; reagent toxic | Metges et al. (1996); Abe et al. (2002); Chikaraishi et al. (2007); Corr et al. (2007b); Tea and Tcherkez (2017) |
| Fluoroacetylation | with TFAA | Amine, hydroxyl, thiol | 2 | 0 | 5 mins to 1 d, 100 °C | Days at -18 °C | Derivatization can be rapid and targets arginine; adds few C and no H atoms; enantiomers preserved; products elute quickly, are well-resolved, and fragment extensively in electron impact ion sources | Moisture- and alcohol-sensitive; $\delta^{13}\text{C}$ and $\delta^{15}\text{N}$ values comprised by CuF_2 , NiF_2 , and CO generation during combustion; $\delta^2\text{H}$ values comprised by HF generation during pyrolysis; products can degrade during elution through some GC columns | Darbre and Blau (1965); Hušek and Macek, (1975); Meier-Augenstein (1999); Jones (2002); McCarthy et al. (2004); Corr et al. (2007b); Hannides et al. (2009); Dunn et al. (2011); McMahon et al. (2011); Kayacelebi et al. (2015); Renpenning et al. (2017) |
| | with HFB | | 4 | 0 | | | | | |
| | with PFP | | 3 | 0 | 10 mins, 110 °C | | | | |
| Non-fluorinated acetylation | with acetic anhydride | Amine, hydroxyl, thiol | 2 | 3 | 10 mins, 60 °C | Months at -5 °C | Products have good chromatographic resolution and are highly stable; adds few C and H atoms | | Adams (1974); Corr et al. (2007a,b); Dunn et al. (2011); Tea and Tcherkez (2017); Enggrob et al. (2019) |
| Alkoxy-carbonylation | with methyl chloroformate | Amine, hydroxyl, thiol ^b | 2 | 3 | <5 mins, 25 °C | Weeks at -20 °C | Derivatization rapid; reaction in aqueous conditions; enantiomers preserved; adds few C and H atoms | Reagent toxic; byproducts may form; certain side-chains not consistently derivatized; amino acids may not react quantitatively | Hušek (1991a,b); Huang et al. (1993); Peláez et al. (2000); Montigon et al. (2001); Meier-Augenstein (2004); Zampolli et al. (2007); Chen et al. (2010); Walsh et al. (2014) |
| | with ethyl chloroformate | | 3 | 5 | | | | | |
| Esterification | with methanol | Carboxyl, hydroxyl ^c | 1 | 3 | 5–60 mins, | Months at -18 °C | Can be coupled with any derivatization strategy; no fractionation correction needed; reactions are rapid and quantitative; adds few C atoms | Can be moisture or alcohol sensitive; <i>n</i> -propanol and isopropanol add many H atoms | Hušek (1991a); Silfer et al. (1991); Chikaraishi et al. (2007); Corr et al. (2007a,b) |
| | with ethanol | | 2 | 5 | 25–70 °C | | | | |
| | with <i>n</i> -propanol | | 3 | 7 | 60 mins, 100 °C | | | | |
| with isopropanol | | | 3 | 7 | | | | | |
| Silylation | with BSTFA with MTBSTFA | Carboxyl, amine, hydroxyl, thiol | 3 | 9 | 15–150 mins, 60–150 °C | Hours at 4 °C | No extraction required; products very volatile; derivatization is quantitative and occurs in a single step | Derivatization inconsistent; $\delta^{13}\text{C}$ values compromised by silicon carbide formation in combustion reactor; adds many C and H atoms; products are moisture-sensitive and unstable | Hušek and Macek (1975); Hofmann et al. (1995); Colombini et al. (1998); Molnár-Perl and Katona (2000); Shinebarger et al. (2002) Sobolevsky et al. (2003); Zaikin and Halket (2005); Tea and Tcherkez (2017) |

^a Abbreviations: TFAA, trifluoroacetic anhydride; HFB, heptafluorobutyric anhydride; PFP, pentafluoropropionic anhydride; BSTFA, bis-(trimethylsilyl)trifluoroacetamide; MTBSTFA, methyltributylsilyl tetrafluoroacetamide.

^b Thiol group of cysteine is derivatized when ethyl chloroformate is used, but not when methyl chloroformate is used.

^c Hydroxyl groups not usually esterified, but serine and threonine can be methylated upon derivatization to MOC methyl esters.

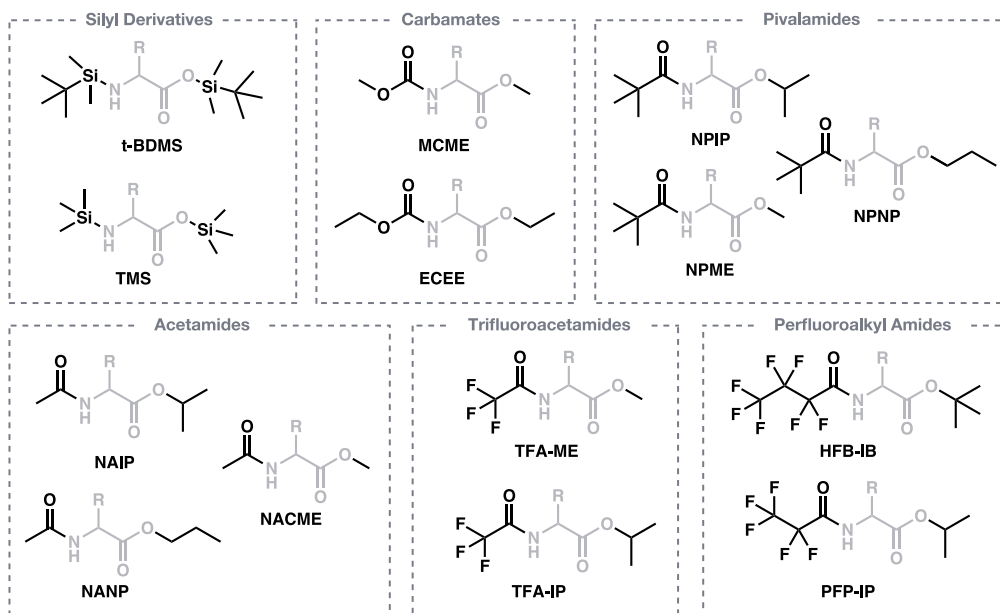


Figure 2.5. Derivatives commonly used for gas chromatography separation of amino acids. Abbreviations: *t*-BDMS, *tert*-butyldimethylsilyl; TMS, trimethylsilyl; MOC, methoxycarbonyl; EOC, ethoxycarbonyl; NPIP, *n*-pivaloyl isopropyl ester; NPMP, *n*-pivaloyl *n*-propyl ester; NPME, *n*-pivaloyl methyl ester; NAIP, *n*-acetyl isopropyl ester; NACME, *n*-acetyl methyl ester; NANP, *n*-acetyl *n*-propyl ester; TFA-ME, trifluoroacetyl methyl ester; TFA-IP, trifluoroacetyl isopropyl ester; HFB-IB, heptafluorobutyryl isobutyl ester; PFP-IP, pentafluoropropionyl isopropyl ester.

2.5.1 Amine group derivatives

2.5.1.1 Pivaloyl derivatives

Pivaloyl esters are optimal for $\delta^{15}\text{N}$ analysis as they are stable, have excellent chromatographic properties, and can be coupled to esterification of the carboxyl group to form a variety of derivatives (Figure 2.5, Tables 2.1 and 2.2; Chikaraishi et al., 2007; Corr et al., 2007b; Metges et al., 1996; Tea and Tcherkez, 2017). Furthermore, enantiomers are preserved and can be separated using chiral stationary phases (Abe et al., 2002; Takano et al., 2009). Pivaloyl esters are not recommended for $\delta^{13}\text{C}$ or $\delta^2\text{H}$ analysis due to their many exogenous C and H

atoms (Tables 2.1 and 2.2; Supplementary Equation A.6; Corr et al., 2007a). Pivaloylation is achieved with pivaloyl chloride and targets amine, hydroxyl, and thiol groups (Table 2.2; Corr et al., 2007b). An isotope effect is known for the carbonyl C of pivaloyl chloride during derivatization (Corr et al., 2007b), and N isotope fractionation accompanying *n*-pivaloyl isopropyl ester formation has been observed (Table 2.1; D. Hofmann et al., 2003).

2.5.1.2 Fluorinated derivatives

Trifluoroacetyl (TFA) esters (and less commonly, pentafluoropropionic (PFP) and heptafluorobutyric (HFB) esters) are popular because they contain minimal exogenous atoms, are resolved with short retention times on standard GC columns and can be synthesized in ~5–10 mins (Figure 2.5; Tables 2.1 and 2.2; Corr et al., 2007b; Kayacelebi et al., 2015; Ohkouchi et al., 2017; Riekenberg et al., 2017; Silfer et al., 1991; Tea and Tcherkez, 2017; Veuger et al., 2005). However, some TFA procedures are lengthier as they include several rounds of purification (Hannides et al., 2009; McMahon et al., 2011). Despite their popularity, fluorinated derivatives have notable limitations when analytes must be combusted or pyrolyzed (i.e., during GC–IRMS analyses). During combustion, Cu and Ni oxides form fluorides, lowering the reactor's oxidizing capacity (Meier-Augenstein, 1999; Tea & Tcherkez, 2017) and potentially leading to incomplete combustion of amino acids. This can compromise both $\delta^{13}\text{C}$ and $\delta^{15}\text{N}$ values (Dunn et al., 2011; Ghashghaie & Tcherkez, 2013; Tea & Tcherkez, 2017). During pyrolysis, HF is formed, which causes fractionation of H isotopes (Renpenning et al., 2017; Sauer et al., 2001) and can potentially corrode metal and silica components downstream of the reactor (Corr et al., 2007b; Dunn et al., 2011; Meier-Augenstein, 1999). TFA derivatives pose additional analytical challenges, including their sensitivity to moisture and alcohol, and low stabilities both in storage and during GC separation (Table 2.2;

Corr et al., 2007b; Darbre and Blau, 1965; Hušek and Macek, 1975).

While TFA derivatives should be avoided for combustion- and pyrolysis-based analyses, their extensive fragmentation in electron impact ion sources (e.g., Jones, 2002) makes them attractive targets for position-specific isotope analysis by high-resolution mass spectrometry (e.g., Orbitrap; see Section 2.7.2). Moreover, enantiomers are preserved and can be separated on chiral columns (Macko et al., 1997; McCarthy et al., 2004; Serban et al., 1988; Silfer et al., 1991; Yamaguchi & McCarthy, 2018), and fluoroacetylation reactions can be adapted for arginine, which is not generally amenable to derivatization (Amelung & Zhang, 2001; Hušek & Macek, 1975; Kayacelebi et al., 2015). TFA derivative $\delta^{13}\text{C}$ values must be corrected for the isotope effect expressed at the TFA carbonyl C atom during derivatization (Table 2.1; Corr et al., 2007b; Silfer et al., 1991). N isotope fractionation during TFA isopropyl ester formation has been observed (Table 2.1; D. Hofmann et al., 2003).

2.5.1.3 Non-fluorinated acetyl derivatives

Reaction with acetic anhydride targets amine, hydroxyl, and thiol groups to form *n*-acetyl-based derivatives such as NACMEs (Figure 2.5; Table 2.2; Corr et al., 2007a, 2007b). For C isotope analyses, these non-fluorinated analogues perform better than, or similarly to, TFA derivatives on several metrics. Dunn et al. (2011) compared amino acid $\delta^{13}\text{C}$ values measured by liquid chromatography (LC)–IRMS and elemental analysis (EA)–IRMS against GC–IRMS and found that the *n*-acetyl derivatives consistently yielded better agreement among complementary measurements than the TFA derivatives. *N*-acetyl derivatives are also more stable, introduce the same number of C atoms, and can be separated on a variety of GC columns (Figure 2.5; Tables 2.1 and 2.2; Adams, 1974; Corr et al., 2007a, 2007b;

Enggrob et al., 2019). Acetylation can cause fractionation for C and N isotopes, but data is easily correctable (Table 2.1; Corr et al., 2007a, 2007b; D. Hofmann et al., 2003).

2.5.1.4 Alkoxy carbonyl derivatives

Methoxycarbonyl (MOC) methyl esters and ethoxycarbonyl (EOC) ethyl esters are favorable for C, N, and H isotope analyses because their reactions are simple and rapid (≤ 5 mins), do not require heating (Hušek, 1991a; Hušek, 1991b), introduce minimal non-analyte C and H (Tables 2.1 and 2.2), and can be carried out in aqueous conditions (e.g., 0.1N HCl), allowing for easy isolation of the products via extraction with organic solvent. Carbamate derivatives do not racemize (Zampolli et al., 2007) and can be baseline-separated on polar GC columns (Hušek, 1991a; Walsh et al., 2014). Alkyl chloroformate derivatizes amine groups (including the side-chains of lysine and histidine), as well as the phenol group of tyrosine (Chen et al., 2010; Huang et al., 1993). The side-chains of serine, threonine, and cysteine are either esterified, acylated, or not derivatized, depending on the derivatizing reagents used (Chen et al., 2010; Huang et al., 1993; Walsh et al., 2014; Zampolli et al., 2007). Carbon and nitrogen isotope fractionation accompany MOC ester formation (Table 2.1; Sacks and Brenna, 2005; Walsh et al., 2014).

Byproduct formation is known to occur during derivatization with alkyl chloroformate, but these products are easily separated from amino acids on the GC column (Chen et al., 2010; Hušek, 1998; Peláez et al., 2000; Walsh et al., 2014). Additionally, a minor product can form in which the carboxyl group is esterified by the alkyl chloroformate rather than the alcohol (Chen et al., 2010; Peláez et al., 2000). Reaction conditions for chloroformate-based derivatization can cause glutamic acid to cyclize (Airaud et al., 1987; Huang et al., 1993; Hušek, 1991a;

Sacks & Brenna, 2005; Walsh et al., 2014), and acidic and amidic amino acid pairs to interconvert (Chen et al., 2010), although amidic residues deamidate anyways during hydrolysis.

2.5.2 Carboxyl group derivatives

2.5.2.1 Ester derivatives

Methyl ester derivatives are attractive because they form rapidly and quantitatively with few non-analyte C and H atoms (Tables 2.1 and 2.2). Ethyl, *n*-propyl, and isopropyl esters introduce more exogenous atoms, but may be selected to improve GC separation. Esterification reactions target carboxyl groups, but when coupled to derivatization with methyl chloroformate they can additionally target the hydroxyl groups of serine and threonine (Table 2.2; Chen et al., 2010; Huang et al., 1993; Walsh et al., 2014; Zampolli et al., 2007). Conditions for esterification are usually acidic, but basic conditions have been used occasionally (e.g., Corr et al., 2007b; Tuckey and Stevenson, 1979). Acidic conditions are created with acetyl chloride, thionyl chloride, or dilute HCl, although comparisons have found that acetyl chloride results in the highest yields of amino acids (Corr et al., 2007b; Peláez et al., 2000). Isopropylation and *n*-propylation require heating and must be performed in moisture-free conditions (e.g., Chikaraishi et al., 2007; Corr et al., 2007b; Silfer et al., 1991), while requirements for methylation and ethylation differ. When coupled to derivatization with alkyl chloroformates, reactions may be performed in aqueous conditions at room temperature (Chen et al., 2010; Hušek, 1991b; Sacks & Brenna, 2005; Walsh et al., 2014), but when combined with other amine group derivatization strategies (e.g., acetylation or pivaloylation) anhydrous conditions and heating are required to avoid expression of isotope effects at carboxyl sites (Corr et al., 2007a, 2007b). When excess reagent is used and reactions

are quantitative, negligible C isotope fractionation is expected, as C sites within the alcohol reagents do not directly participate in bond breakage or formation (Corr et al., 2007a; Rieley, 1994; Silfer et al., 1991).

2.5.2.2 Silyl derivatives

Silylation is not recommended for amino acid isotope analysis despite being a popular GC derivatization strategy for other organic compounds (e.g., Tea and Tcherkez, 2017), as it can add a large number of non-analyte atoms (up to 18 C and 45 H; Table 2.1), products are moisture-sensitive and degrade rapidly (Colombini et al., 1998; Hušek & Macek, 1975), and multiple derivatives may add to amine or hydroxyl groups inconsistently (Colombini et al., 1998; Hušek & Macek, 1975; Molnár-Perl & Katona, 2000; Tea & Tcherkez, 2017; Zaikin & Halket, 2005). Carbon does not participate in silylation, precluding expression of C isotope effects (Rieley, 1994). However, trimethylsilyl (TMS) derivatives may promote silicon carbide formation in GC-IRMS combustion reactors, leading to C isotope fractionation via non-quantitative conversion of analytes to CO₂ (Shinebarger et al., 2002; Tea & Tcherkez, 2017). Nitrogen isotope fractionation can be significant due to non-quantitative derivatization of amino acids and degradation of derivative products (Table 2.1; D. Hofmann et al., 1995, 2003).

2.6 Separations

Amino acids must be separated from complex mixtures prior to isotope analysis, without inadvertently fractionating isotopes. Separation can be achieved using a variety of chromatographic techniques, stationary phases, and mobile phases, but to date no combination sufficiently separates all 20 proteinogenic amino acids.

Separation is commonly achieved by GC coupled directly to an IRMS (i.e., 'on-line' measurement) without intermediate analyte collection. This method requires derivatization and an associated correction for added C or H atoms. Less commonly, LC is used for preparatory (i.e., 'offline') separation of underivatized amino acids, which are recovered using a fraction collector, sometimes assessed for purity, then analyzed on a separate instrument (e.g., EA-IRMS). New LC-IRMS systems enable LC separation online prior to isotope ratio measurement (Section 2.7.1.2). Considerations for optimizing GC and LC separations are beyond the scope of this review, but the reader is referred to Rood (2007) and Snyder et al. (2010) for excellent guides.

For many LC separations the lighter isotopologues elute from the column first (Broek et al., 2013; McCullagh et al., 2006), whereas for GC separations on nonpolar columns the heavier isotopologues typically elute first. Separation of isotopologues leads to isotopic fractionation across the width of a chromatographic peak. For example, differences between the front and tail halves of a peak separated using LC were 8.3‰ and 4.2‰ for $\delta^{15}\text{N}$ and $\delta^{13}\text{C}$ values, respectively (Broek et al., 2013). Thus, peaks must be completely collected or integrated to avoid altering the apparent isotope ratio of the sample (Meier-Augenstein, 1999; Sessions, 2006).

In the following sections, we compare GC and LC techniques for amino acid separation, examine the potential of IC and CE to be coupled to amino acid isotope analyses, and highlight several methods for determining sample purity.

2.6.1 Gas chromatography

GC is currently the most popular choice for separating amino acids for isotope analysis, yet there is no consensus on the best combination of stationary phase,

derivative, and instrument settings. Many published approaches separate at least 10–15 amino acids (Table 2.1) in an hour or less. These separations commonly use 50m or 60m columns, carrier gas flow rates of 1–2 mL/min, and GC oven temperature programs from ~40°C to 300°C. While most separations are on non-polar or low-polarity stationary phases (e.g., Ultra-2, DB-5 ms), high-polarity columns (VF-23 ms, ZB-FFAP, and ZB-WAX) substantially improve peak shapes of *n*-acetyl and alkoxycarbonyl ester derivatives, have higher analyte capacities, and are compatible with other common derivatives (Corr et al., 2007b; Walsh et al., 2014).

The main advantage of using GC to separate amino acids is the ability to couple directly to an IRMS, thus increasing analysis speed and sensitivity. The main drawbacks are: (1) low analyte capacity on GC columns – i.e., only a small amount of analyte can be introduced without degrading peak shape – especially for H and N isotope analyses where more sample is needed; (2) low temperature limits for polar columns (resulting in long runs and high background signals from degradation of the stationary phase); (3) poor suitability for four amino acids (arginine, histidine, asparagine, and glutamine are challenging to derivatize); and (4) mandatory derivatization (introducing exogenous atoms, additional sample workup, and possible isotopic fractionations — see Section 2.5).

Comprehensive GC × GC (Tobias et al., 2008, 2011) is a promising advancement that uses two columns with different stationary phases to improve separation of complex mixtures and reduce preparatory steps. This method has been successfully coupled to online isotope measurements of other organic compounds (Tobias et al., 2008, 2011) and may expand to amino acid isotope analysis.

2.6.2 Liquid chromatography

High performance liquid chromatography (HPLC or, more generally, LC) is widely used for offline separation and quantification of amino acids, but subsequent isotope analysis requires specialized equipment (fraction collectors) or instrumentation (LC–IRMS). LC provides some advantages over GC: derivatization is not needed for amino acids, and column capacity is substantially higher. However, purifying and collecting fractions offline may necessitate larger sample sizes, especially if an EA–IRMS is used for isotope analysis. Certain amino acids, like isoleucine and leucine, are difficult to separate when underivatized.

Amino acid separation by LC typically uses nonpolar stationary phases and polar mobile phases (e.g., water, acetonitrile, methanol). The SIELC Primesep A is the most popular column for online $\delta^{13}\text{C}$ (Dunn et al., 2011; McCullagh et al., 2006; C. I. Smith et al., 2009; Tripp et al., 2006) and offline $\delta^{15}\text{N}$ and $\delta^{13}\text{C}$ measurements (Broek & McCarthy, 2014; Broek et al., 2013; Sun et al., 2020). Primesep A columns can separate 14 amino acids with run times of 105 mins (Broek et al., 2013). An alternative is “hydrophilic interaction liquid chromatography” (HILIC). HILIC initially employs a mobile phase with high organic and low aqueous content, allowing a small water layer to form between the stationary and mobile phases, which provides good separation of amino acids – particularly aspartic acid and serine which cannot be separated using other LC stationary phases (Park et al., 2019). Finally, while not currently common instrumentation, the LC–IRMS system (discussed further in Section 2.7.1.2) enables online C isotope analysis, has similar sensitivity to some GC–IRMS applications (Table 2.3), and may become more popular in future amino acid isotope research.

2.6.3 Ion chromatography

Ion chromatography (IC) is primarily used to quantify amino acids, but has also been used for online (Morrison et al., 2010) and offline (L. Zhang et al., 2021) IRMS analyses. IC separation can be coupled to an IRMS for online C isotope analysis via an Isoprime Liquiface system (Morrison et al., 2010). Abaye et al. (2011) used this system to measure the $\delta^{13}\text{C}$ values of 11 amino acids, including arginine, lysine, and some aliphatic amino acids, which were quickly resolved (70 mins) with adequate precisions (SD <1‰; Abaye et al., 2011). IC has also been used to separate 9 amino acids offline prior to N isotope analysis using a purge-and-trap continuous-flow IRMS (L. Zhang et al., 2021). Advantages of separating amino acids by IC are that neither pre- nor post-column derivatization is required, and other matrix components (carbohydrates, glycols, and sugar alcohols) can be simultaneously separated (Larson et al., 2002), minimizing the sample workup steps needed (see Sections 2.2 and 2.4). A major disadvantage is lengthy run times (180 mins or longer; L. Zhang et al., 2021).

2.6.4 Capillary electrophoresis

Capillary electrophoresis (CE) separates compounds based on mobility in an electric field (Ewing et al., 1989) but has not yet been coupled to isotope measurements. Although CE currently lacks selectivity compared to other separation methods, its speed, simplicity, and low cost hold potential for future applications involving online amino acid isotope analysis. As with LC, samples do not require derivatization or conversion to gases and CE can be coupled to numerous detectors. Chiral buffers can be used to change the mobility of D- vs L-amino acids to separate enantiomers (Hutt et al., 1999). Miniaturized versions of CE systems (microchip

electrophoresis) have been explored for inclusion on extraterrestrial sampling missions that investigate amino acids to distinguish between biotic and abiotic sources (Creamer et al., 2017; Hutt et al., 1999) and may prove useful when combined with sensitive techniques (e.g., high-resolution mass spectrometry – Section 2.7.2).

2.6.5 Methods of assessing purity

Most compound-specific isotope analyses require purified samples. For example, isotope ratio monitoring by nuclear magnetic resonance spectroscopy (NMR; Section 2.7.3) requires > 98% analyte. Other methods, such as EA-IRMS (Section 2.7.1.3), lack online separation so geochemists must first purify amino acids offline for compound-specific applications and ensure no contaminants are present. Numerous options exist for assessing sample purity. LC-MS or GC-MS can be used to identify contaminants (Hare et al., 1991; Phillips et al., 2021), but some contaminants may avoid detection if their mass falls outside of the analytical window selected. Proton (^1H) NMR is an attractive option for purity verification as it is non-destructive, rapid (≤ 5 min), and commonly available at user facilities. Elemental composition determined using an EA system can be used to indirectly assess purity because pure amino acids have a narrow range of elemental ratios ($\text{C/N} = 1.5\text{--}9.0$, $\text{C/S} = 3.0\text{--}5.0$). We recommend verifying sample purity in studies using offline separations that are decoupled from the final isotopic analyses.

Table 2.3. Summary of analytical techniques for isotopic analysis. Many of these methods have yet to be applied to amino acids from the environment, although some have been used to measure amino acid standards.

| Analytical technique ^a | | Isotopes | Measured species | Specificity | Typical precision (1 σ , ‰) | Typical sensitivity (nmol) | References ^{b,c} |
|-----------------------------------|----------------------|----------------|--|--------------------------------------|------------------------------------|---|---|
| IRMS | Conventional GC-IRMS | C | CO ₂ | Compound-specific | ~0.6–2.3 | 0.1–10 | McCarthy et al. (2004) ^c ; Sessions (2006); Corr et al. (2007b) ^b ; Baczynski et al. (2018) |
| | | N | N ₂ | Compound-specific | 0.5–1 | 1–10 | McClelland and Montoya (2002) ^{b,c} ; Sessions (2006); Rieckenberg et al. (2020) ^{b,c} |
| | Optimized GC-IRMS | H | H ₂ | Compound-specific | ~10 | 10–50 | Sessions (2006); Fogel et al. (2016) ^{b,c} |
| | | C | CO ₂ | Compound-specific | 0.9–1.5 | 0.05–0.6 | Baczynski et al. (2018) |
| | Pyrolysis-GC-IRMS | C | CO ₂ (from pyrolytic fragments) | Position-specific | ~1 | ~100s | Wolyniak et al. (2005) ^b ; Gilbert et al. (2016a,b) |
| | LC-IRMS | C | CO ₂ | Compound-specific | 0.1–1.4 | 7–55 | Smith et al. (2009) ^{b,c} ; Dunn et al. (2011) ^{b,c} |
| | PT-CF-IRMS | N | N ₂ O | Compound-specific | 0.3–0.7 | <15 | Zhang et al. (2021) ^{b,c} |
| | FIA-NR-IRMS | C | CO ₂ (from carboxyl group) | Position-specific | 0.1 | 15 | Fry et al. (2018) ^b ; Fry and Carter (2019) ^{b,c} |
| | SWiM-IRMS | C | CO ₂ | Bulk | 0.6 | 1–10 | Sessions et al. (2005) ^b ; Eek et al. (2007) |
| | Conventional EA-IRMS | C | CO ₂ | Bulk | 0.1–0.5 | 2000–8500 | Polissar et al. (2009); Ogawa et al. (2010) ^b ; Sun et al. (2020) ^{b,c} |
| | | N | N ₂ | Bulk | 0.1–0.5 | 1500–3500 | Ogawa et al. (2010) ^b ; Broek et al. (2013) ^{b,c} ; Rieckenberg et al. (2020) ^{b,c} |
| | TCEA-IRMS | S | SO ₂ | Bulk | 0.3 | 500–3000 | Giesemann et al. (1994) |
| | | H | H ₂ | Bulk | 0.3–3 | 300,000 | Gehre et al. (2015) ^b ; Fogel et al. (2016) ^b ; Newsome et al. (2020) ^b |
| | Optimized EA-IRMS | C | CO ₂ | Bulk | 0.2–0.5 | 40–60 | Polissar et al. (2009) |
| N | | N ₂ | Bulk | 0.1–0.5 | 10–25 | Polissar et al. (2009); Ogawa et al. (2010) ^b ; Broek and McCarthy (2014) ^{b,c} ; Swalethorp et al. (2020) ^{b,c} | |
| | | S | SO ₂ | Bulk | 0.1–0.3 | 50–150 | Phillips et al. (2021); Sayle et al. (2019) ^{b,c} |
| High-resolution MS | Orbitrap | C, N, S, H | Molecular ion, fragment ions | Compound-specific, position-specific | ≤1 | ~0.1–10 | Eiler et al. (2017); Neubauer et al. (2018) ^b ; Chimiak et al. (2021) ^{b,c} |
| NMR | ¹³ C NMR | C | Molecule | Position-specific | ~1 | ~1,000,000 | Romek et al. (2017) ^b |
| | ¹ H NMR | C | Molecule | Position-specific | 0.5–3.5 | 50,000–300,000 | Rasmussen and Hoffman (2020) ^b |

^a Abbreviations: IRMS, isotope ratio mass spectrometry; GC-IRMS, gas chromatography-IRMS; LC-IRMS, liquid chromatography-IRMS; PT-CF-IRMS, purge-and-trap continuous-flow IRMS; FIA-NR-IRMS, flow injection analysis reaction with ninhydrin-IRMS; SWiM-IRMS, spooling wire micro-combustion-IRMS; EA-IRMS, elemental analysis-IRMS; TCEA-IRMS, thermal conversion-EA-IRMS; NMR, nuclear magnetic resonance.

^b Method applied to pure amino acid standards.

^c Method applied to amino acids in natural (terrestrial or extraterrestrial) materials.

2.7 Isotopic analysis

Potential goals of amino acid isotopic analysis include characterizing the stable isotope ratios of one or more elements ($^{13}\text{C}/^{12}\text{C}$, $^{15}\text{N}/^{14}\text{N}$, $^{34}\text{S}/^{32}\text{S}$, and/or $^2\text{H}/^1\text{H}$), either averaged across each amino acid molecule (“compound-specific” or “molecular-average”) or characterized at individual atomic positions (“position-specific” or “intramolecular”). Established techniques for characterizing isotopic compositions of amino acids from natural samples use IRMS paired with offline or online separation strategies (Section 2.6) and combustion or pyrolysis of separated analytes. Additional techniques are in early stages of development — especially for position-specific isotope analysis of amino acids — but have not yet been applied to terrestrial materials. We describe the isotopic analysis techniques that are currently useful to organic geochemists, as well as possible future advancements (e.g., high-resolution mass spectrometry), summarizing figures of merit, required preparatory steps, and key advantages and disadvantages. Methodological improvements will continue to combine different online separation and isotope detection strategies in novel ways.

2.7.1 Isotope ratio mass spectrometry

IRMS achieves high levels of precision and accuracy (Table 2.3) via simultaneous comparison of two or more isotopes (i.e., the isotope ratio). Isotope ratios are further compared between the sample and a standard of known composition on an international scale (e.g., VPDB) and reported as δ values (Equation 2.1). Amino acids must be quantitatively converted to CO_2 (for $^{13}\text{C}/^{12}\text{C}$ analysis), N_2 ($^{15}\text{N}/^{14}\text{N}$ analysis), H_2 ($^2\text{H}/^1\text{H}$ analysis) or SO_2 ($^{34}\text{S}/^{32}\text{S}$ analysis; Table 2.3) for IRMS measurements. This goal was originally achieved by combusting pre-purified amino

acids in sealed tubes offline, then isolating the resulting CO₂ and N₂ for isotope analysis (Abelson & Hoering, 1961; Macko et al., 1983; Tuross et al., 1988). Today, this is typically achieved via online methods in which analytes are carried by an inert gas through a chemical conversion interface on their way to the IRMS. The most common interfaces employ combustion or pyrolysis, but other techniques such as chemical oxidation or high-temperature combustion-desolvation have also been reported (Tea & Tcherkez, 2017). Here we cover GC-IRMS, LC-IRMS, and EA-IRMS instrumentation, and summarize capabilities of these methods in Figure 2.6. For more detailed reviews of IRMS principles, analytical considerations, and historical context, see Brenna (1994), Brand (1996), Brenna et al. (1997), Meier-Augenstein (1999), and Sessions (2006).

2.7.1.1 GC-IRMS

GC-IRMS is routinely used to measure compound-specific $\delta^{13}\text{C}$ and $\delta^{15}\text{N}$ values of amino acids (Close, 2019; Ohkouchi et al., 2017), and, less commonly, $\delta^2\text{H}$ values (Fogel et al., 2016; S. Newsome et al., 2020). The GC is typically coupled to the IRMS via a combustion (for CO₂ or N₂) or pyrolysis (for H₂) interface. Amino acid samples must be derivatized for GC separation and free of water, particles, elemental S, and salts to avoid damage to the GC column and chemical conversion interface.

GC-IRMS can achieve instrumental precision of $\leq 0.1\text{‰}$ for C, $< 1\text{‰}$ for N, and 2‰ for H in other common analytes (Table 2.3; Sessions, 2006). Amino acids have larger propagated uncertainties of 0.6‰ to over 2‰ for C (e.g., Corr et al., 2007a; Dunn et al., 2011; C. I. Smith et al., 2009) and up to $\sim 10\text{‰}$ for H (Table 2.3; Fogel et al., 2016) because the added C or H derivative atoms increase the uncertainty on the final amino acid isotope ratio (see Section 2.5). Measurements typically

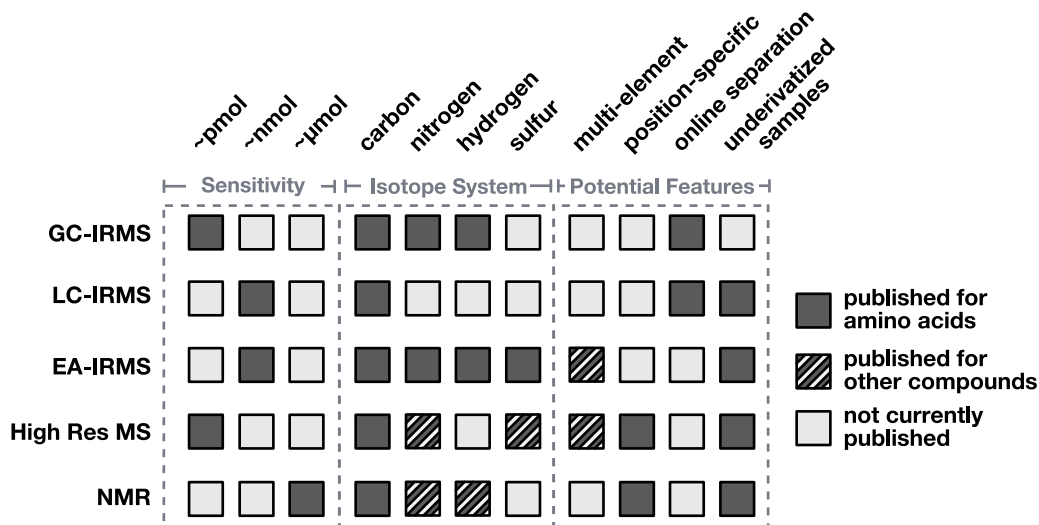


Figure 2.6. Summarized capabilities of common analytical techniques used for amino acid isotope analysis. Sensitivities given are lower limits. “Multi-element” refers to simultaneous measurement of different isotopic systems (i.e. $^{13}\text{C}/^{12}\text{C}$ and $^{15}\text{N}/^{14}\text{N}$) in a single analysis. “Online separation” refers to the ability to measure multiple compounds from a mixture online. A “position-specific” measurement encompasses the ability to extract isotopic information from individual sites within a compound. We do not consider bulk or compound-specific isotope measurements on molecules containing single elements (e.g., N or S in amino acids), nor chemical approaches to site-specific measurements (e.g., decarboxylation reactions) as “position-specific” capabilities of the instrument. For more details and references, see Table 2.3 and Section 2.7.

require ~ 0.1 to 10s of nmol C or N, and one to two orders of magnitude more H (Table 2.3). Specific advantages of GC-IRMS for amino acid isotope analysis are its high sensitivity and high throughput. GC-IRMS is especially appropriate for small samples and for researchers seeking concurrent isotopic data on as many amino acids as possible. Disadvantages include difficulty of use, added sample workup steps, and larger uncertainties associated with derivatization. Recent work couples narrow-diameter column (“fast”) GC to IRMS (Baczynski et al., 2018; Sacks et al., 2007), paving the way for future amino acid isotope analyses with sharper chromatographic peaks, faster run times, and enhanced sensitivity for $\delta^{13}\text{C}$ analyses.

2.7.1.2 LC-IRMS

A recent development, the Finnigan LC IsoLink system (LC-IRMS), provides the ability to measure $^{13}\text{C}/^{12}\text{C}$ isotope ratios of underivatized amino acids separated online by liquid chromatography (Juchelka & Krumpal, 2008; McCullagh et al., 2006). Samples are introduced in dissolved form, separated by LC, and chemically oxidized to CO_2 (at 100°C) before introduction into the IRMS (Godin & McCullagh, 2011; Juchelka & Krumpal, 2008). Several studies demonstrate that quantitative conversion to CO_2 can be achieved across environmentally relevant sample sizes. Leucine samples with concentrations of $\sim 50\text{--}300\text{ ng }\mu\text{L}^{-1}$ had $\delta^{13}\text{C}$ precisions $\leq 0.15\text{‰}$ (Juchelka & Krumpal, 2008), although standard deviations were higher (0.35‰) for a mixture of four amino acids at concentrations of $\sim 50\text{--}400\text{ ng }\mu\text{L}^{-1}$ (Juchelka & Krumpal, 2008).

A significant drawback to current LC-IRMS systems is that they must use acidic, organic-free mobile phases, as any organic solvents would be oxidized to CO_2 along with the analytes. Typical concentrations of organic solvents used in mobile phases for LC separations would saturate the IRMS detector (Godin et al., 2005). Additionally, LC-IRMS is generally less sensitive than GC-IRMS and can only measure C isotopes, not N or H (Figure 2.6). For information on LC-IRMS technical challenges and solutions, we refer the reader to a review by Godin and McCullagh (2011). Thus far, LC-IRMS systems have successfully measured amino acids from peptides and archaeological samples (Godin et al., 2005; McCullagh et al., 2006), but methods are still in development for complex materials like marine sediments (Close, 2019).

2.7.1.3 EA-IRMS

EA-IRMS instruments are most commonly used to measure the bulk isotopic compositions of complex, solid samples, but can also be coupled with offline preparatory techniques such as LC with fraction collection to provide isotopic measurements of individual amino acids or proteins (e.g., Broek et al., 2013; Dong et al., 2017). Isolated amino acids are packed into metal foil capsules, combusted to CO₂, N₂, H₂O, and/or SO₂, then dried and separated using a short GC column for isotope ratio measurement.

Although three orders of magnitude less sensitive than GC-IRMS (requiring μmol of C or N; Figure 2.6; Table 2.3) and requiring time-consuming offline separations, EA-IRMS systems may be the ideal choice for certain specialized applications (e.g., $\delta^{34}\text{S}$ measurements of pre-isolated cysteine or methionine or high-precision $\delta^{15}\text{N}$ measurements) or when sample size is not limiting. Additionally, EA-IRMS instruments are more widely available, achieve better precisions ($\sim 0.1\text{--}0.5\text{‰}$; Table 2.3), and are simpler to operate than GC-IRMS or LC-IRMS. Perhaps most importantly, EA-IRMS offers the ability to simultaneously analyze the isotope ratios of multiple elements in the same acquisition (e.g., C and N, with or without S; Brodie and Kracht, 2016; Broek and McCarthy, 2014; Fourel et al., 2014; Fry, 2007; Sayle et al., 2019)—although this strategy is not yet established for amino acids (Figure 2.6).

Recent optimizations have enhanced the sensitivity of EA-IRMS (Table 2.3). The nano-EA-IRMS system (Polissar et al., 2009) improved sensitivities by 100–500-fold for $\delta^{13}\text{C}$ and $\delta^{15}\text{N}$ measurements of pre-purified amino acids, while achieving similar precisions (Broek & McCarthy, 2014; Swalethorp et al., 2020). Optimizations for S isotope analysis by EA-IRMS (Fourel et al., 2014; Fry, 2007) enabled the first compound-specific $\delta^{34}\text{S}$ measurements of cysteine and methionine (Phillips

et al., 2021). Furthermore, H isotope analysis by pyrolysis EA (also known as thermal conversion EA, or TCEA), has been demonstrated for ~ 0.3 mmol analyte (Table 2.3; Gehre et al., 2015) but has only been applied thus far to pure amino acid standards (Fogel et al., 2016; S. Newsome et al., 2020).

We see optimized EA–IRMS systems (in combination with automated, offline preparatory techniques) as an area of potential for amino acid isotope studies, especially when leveraged for analyzing multiple isotope systems simultaneously. We recommend optimized EA–IRMS configurations for measuring amino acid $\delta^{34}\text{S}$ values, as S cannot be measured by GC–IRMS or LC–IRMS systems, and we emphasize that EA–IRMS can achieve more precise and accurate $\delta^{15}\text{N}$ measurements than GC–IRMS (Table 2.3; Broek and McCarthy, 2014; Swalethorp et al., 2020). For individual applications, these advantages must be weighed against the need for offline sample separation and large sample sizes, and/or the availability of optimized instrumentation like the nano-EA–IRMS.

Finally, we note that a variety of other promising IRMS configurations have been applied to isotope analysis of individual amino acids or proteins by initially isolating analytes offline using preparatory techniques. These approaches include “spooling wire micro-combustion IRMS” (SWiM–IRMS; Eek et al., 2007; Sessions et al., 2005, and purge-and-trap continuous-flow IRMS (PT-CF–IRMS; L. Zhang et al., 2021). These configurations are not yet widely available but achieve sensitivities and precisions similar to GC–IRMS without requiring derivatization (see Supplementary Section A.3).

2.7.1.4 IRMS configurations for position-specific isotope analysis

Other IRMS-coupled techniques are in development for position-specific isotope analysis. The approach is to introduce an initial chemical/thermal degradation

step that isolates different atomic positions of the analyte prior to isotope ratio measurement. One example is “flow injection analysis reaction with ninhydrin IRMS” (FIA-NR-IRMS), which uses a chemical reaction to decarboxylate amino acids and measure the position-specific $\delta^{13}\text{C}$ value of the carboxyl-C position with $\sim 0.3\text{--}0.5\text{‰}$ precision (Table 2.3; Fry et al., 2018; $\delta^{34}\text{Fry}$ and Carter, 2019). Another is a method for the preparatory isolation and chemical work-up of free glutamine for position-specific $\delta^{15}\text{N}$ measurement by PT-CF-IRMS (Table 2.3; Lee et al., 2021). Glutamine is split into two fractions: (1) the amino-N is oxidized to nitrite, and (2) the amide-N is converted into ammonium by acid hydrolysis, then oxidized to nitrite. Both nitrite pools are reduced to N_2O and analyzed separately, recovering isotope ratios for the amino-N and amide-N, respectively. Finally, several variations of online-pyrolysis-GC-IRMS systems have been developed and applied to position-specific $^{13}\text{C}/^{12}\text{C}$ analysis of amino acid standards. Analytes are thermally converted (pyrolyzed) into fragments that encompass different carbon positions from the original amino acid molecule. These fragments are then separated by GC, individually combusted, and measured by IRMS to recover position-specific signatures (for reviews, see Gauchotte-Lindsay and Turnbull (2016) and Gilbert (2021)). Published precisions range from $<0.2\text{‰}$ for directly measured positions of alanine and phenylalanine standards to $0.9\text{--}6.5\text{‰}$ for calculated position-specific $\delta^{13}\text{C}$ values due to error propagation (Table 2.3; Wolyniak et al., 2005). Application of these techniques to amino acids in geochemical samples has not yet been realized.

2.7.2 High-resolution mass spectrometry

Directly converting amino acids to CO_2 , N_2 , and H_2 destroys information recorded in the position-specific distributions of isotopes. For example, ^{13}C -enrichment at

the C-1 versus C-2 position in alanine has different implications for its origins (Chimiak et al., 2021), but cannot be discerned from the ratio of $^{13}\text{C}/^{12}\text{C}$ in CO_2 produced by whole-molecule combustion (e.g., as in GC-IRMS). High-resolution mass spectrometry of intact analyte ions (as opposed to whole combustion or pyrolysis products) provides an avenue for analyzing position-specific isotope distributions in amino acids. This approach is still in development for natural materials relevant to organic geochemists (e.g., plant biomass – Wilkes et al., 2019), but represents a promising future direction.

Position-specific isotope ratios can be accessed by measuring fragments of an amino acid molecule, which form spontaneously during ionization and/or collision in an ion trap. Constraining position-specific isotopic differences is accomplished by measuring and comparing isotope ratios of two or more fragments of an amino acid in a mass spectrometer. These measurements require that the spectrometer can distinguish molecular fragments containing different rare isotopes, e.g., ^{13}C vs ^2H or ^{15}N (Supplementary Section A.4). Several mass spectrometers achieve mass resolutions that can distinguish these different rare isotope substitutions, but only OrbitrapTM-based instruments have been studied in detail (e.g., Eiler et al., 2017; Hilbert et al., 2021; A. E. Hofmann et al., 2020; Neubauer et al., 2020). Orbitrap mass analyzers may be coupled to GC or LC for online isolation of amino acids; thus, required sample preparation (e.g., derivatization) and clean-up steps would reflect the choice of instrumentation. In addition, Orbitrap instruments hold the potential to measure clumped-isotope compositions of amino acids (i.e., containing two or more rare isotopes).

Orbitrap analysis of pure amino acid standards indicates minimal sample sizes are required to obtain $\delta^{13}\text{C}$ precisions $\leq 1\text{‰}$ for fragments of amino acids (Table 2.3; Eiler et al., 2017; Neubauer et al., 2018). An initial application to samples of the Murchison meteorite revealed substantial differences in $\delta^{13}\text{C}$ values between dif-

ferent atomic sites within meteoritic alanine (Chimiak et al., 2021), but had large propagated uncertainties for individual C positions. Limitations of this measurement approach for amino acids may include insufficient fragmentation or the lack of available position-specific isotopic reference materials for reporting results. For example, while Neubauer et al. (2018) calculated isotope ratios for most positions of pure methionine samples, not all amino acids fragment as easily (Piraud et al., 2003; P. Zhang et al., 2019). Accurately identifying the atomic positions from the original amino acid that ends up in each fragment is crucial but may present a bottleneck, as isotope labeling experiments may be required to resolve ambiguities. Further, standardization requires a separate working standard for each amino acid analyzed, which must then be characterized by a different position-specific isotopic technique (e.g., NMR) to anchor results to an international reference frame (e.g., VPDB).

2.7.3 Nuclear magnetic resonance spectroscopy (NMR)

Isotopic NMR (or SNIF-NMR[®], hereafter simply NMR) provides stable C and H isotope ratios for individual atomic positions within an amino acid by ¹³C NMR or ²H NMR, respectively (Romek et al., 2017; Vallet et al., 1991). Because of its large sample size requirements (Table 2.3), NMR is best suited for characterizing pure standards but provides a path for establishing position-specific isotope standards anchored to the international scale that may be used with a more sensitive technique (e.g., Orbitrap). A separate radio frequency signal is produced by each chemically distinct ¹³C or ²H atom within a molecule. These NMR signals are quantified through peak integration and used to calculate position-specific isotope distributions by comparison with the average isotope ratio for the entire molecule (measured separately by IRMS; reviewed by Jézéquel et al., 2017). However, ¹³C

NMR and ^2H NMR typically require hundreds of milligrams (~ 1 mmol) of pure analyte to achieve precisions of $\sim 1\text{‰}$ and 5‰ , respectively (Table 2.3; Gilbert, 2021; Romek et al., 2017). Such sample size requirements are prohibitive for applications to amino acids from natural samples and all published NMR analyses of amino acids to date have targeted pure standards (Rasmussen & Hoffman, 2020; Romek et al., 2017; Vallet et al., 1991)). An alternative NMR approach for position-specific $^{13}\text{C}/^{12}\text{C}$ analysis was recently applied to amino acid standards using ^1H NMR (Rasmussen & Hoffman, 2020; Supplementary Section A.5). This technique has at least two advantages over direct ^{13}C NMR, while achieving similar precisions ($\sim 1\text{‰}$; Table 2.3) and accuracies: (1) it uses more commonly available equipment, and (2) it is an order of magnitude more sensitive (Table 2.3; Hoffman and Rasmussen, 2019). One challenge of using ^1H NMR to study C isotopes is that not all C positions in amino acids are visible.

All of the above NMR techniques are non-destructive and can be readily calibrated to internationally recognized scales, yet NMR has significant drawbacks compared to other isotopic measurements – notably, poor sensitivity and precision (requiring up to six orders of magnitude more C than IRMS for $0.5\text{--}3.5\text{‰}$ precision; Table 2.3). NMR requires analytes to be purified ($>98\%$) offline prior to measurement, followed by several hours of analysis (Remaud et al., 2018). While analytical advances are ongoing (Hoffman & Rasmussen, 2019; Jézéquel et al., 2017), we anticipate NMR will remain most useful as a complementary technique for calibrating standards rather than a primary tool for measuring isotope ratios in (bio)geochemical samples.

2.7.4 Referencing strategies for isotopic analysis

Making accurate and precise isotope ratio measurements are major challenges in the stable isotope community. As compound-specific (and emerging position-specific) isotope applications expand across fields, the need for inter-laboratory comparability of data becomes more urgent. In addition to variable sample preparation strategies, protocols used across laboratories to calibrate and quality-check isotope ratio measurements are inconsistent, which hampers data reproducibility between studies (Carter & Fry, 2013; Yarnes & Herszage, 2017). Inter-laboratory comparisons of amino acid $\delta^{13}\text{C}$ values recovered from the same samples are not commonly published, but when done so, often show disagreement (e.g., Arthur et al., 2014; Ayayee et al., 2015) comparisons for N isotope analyses are even less common. Following recommendations by Carter and Fry (2013) and Yarnes and Herszage (2017), we urge widespread adoption of the following standardization practices: (1) calibration of data based on internal standards (synthetic amino acids like norleucine that are co-injected with samples) and/or multipoint amino acid isotope standards (i.e., spanning a range of isotopic compositions outside those of samples) to account for scale compression effects by instruments (e.g., Riekenberg et al., 2020; Yarnes and Herszage, 2017; L. Zhang et al., 2021), (2) use of quality assessment materials, such as an external standard measured repeatedly throughout sample analysis (e.g., Styring et al., 2015), to verify measurement accuracy, and (3) increased comparisons of isotopic data between laboratories and publication of results.

Several internationally recognized amino acid reference materials are available for compound-specific isotope analysis: glycine, L-valine, and L-glutamate standards with known values of $\delta^{13}\text{C}$ and $\delta^{15}\text{N}$ have been calibrated through interlaboratory ring tests and are distributed by the USGS, IAEA, and Indiana University (Qi

et al., 2003; Qi et al., 2016; Schimmelmann et al., 2016). Comparability of isotope ratio measurements would be greatly improved by the development of: (1) additional amino acid standards encompassing a wider range of $\delta^{13}\text{C}$ and $\delta^{15}\text{N}$ values, (2) amino acid $\delta^2\text{H}$ and $\delta^{34}\text{S}$ reference materials (the former effort is currently challenged by lack of a reliable method to correct for exchangeable hydrogen (Schimmelmann et al., 2016), (3) internationally-recognized protein standards with calibrated amino acid isotopic compositions (Yarnes & Herszage, 2017), and (4) position-specific reference materials anchored to international scales.

2.8 Conclusions and outlook

We have synthesized the extensive literature on amino acid isotope analysis from preparation to measurement, highlighting established techniques and emerging technologies that may offer future benefits to geochemists. We emphasize that there is no “one size fits all” method for amino acid isotopic analysis: researchers have multiple options and choices will be guided by sample type, individual applications, and available resources. Over the next decade, attention to standardizing referencing strategies and developing reference materials is needed for data generated across laboratories to be reproducible. A second beneficial area of attention is measuring H and S isotope ratios in amino acids, which would expand environmental and ecological applications. For example, $^2\text{H}/^1\text{H}$ ratios could provide information on migration and energy flow (e.g., Bowen et al., 2005; Fogel et al., 2016; Rubenstein and Hobson, 2004), and $^{34}\text{S}/^{32}\text{S}$ ratios could track dietary protein sources (e.g., Richards et al., 2001). To date, the $\delta^2\text{H}$ and $\delta^{34}\text{S}$ values of amino acids have been characterized in relatively few published studies (Fogel et al., 2016; S. Newsome et al., 2020; Phillips et al., 2021), so the full potential of these measurements is only beginning to be explored.

Finally, we see three areas of amino acid isotope research where methodologic innovation will have the most impact. First, there are numerous opportunities for method automation. In addition to the substantial improvements stemming from online LC–IRMS and GC–IRMS techniques, further coupling (e.g., combining protein hydrolysis with high pressure ion-exchange clean-up) would increase throughput. A second area for innovation is simultaneous analysis of multiple isotope systems on the same sample and instrument. Because preparing amino acids for isotope measurement is tedious, measuring H, C, N, and S concurrently offers greater reward and is increasingly possible with techniques like optimized EA–IRMS and high-resolution mass spectrometry. Multi-element analysis of amino acids will be especially helpful for ecological and forensics studies that reconstruct modern and paleo diets, food webs, animal and human movement, and behaviors of ancient civilizations. Third, we see a renaissance in position-specific isotope analysis via high-resolution mass spectrometry and/or pyrolysis-GC–IRMS. Specific intramolecular information, such as C–S bond clumping in methionine or C–H bond clumping in aliphatic residues, could inform targeted questions about synthesis. Further, the ability to measure position-specific isotope ratios at natural abundance may complement or replace isotope labelling methods in metabolomics studies. None of these advancements will be possible without the analytical expertise of isotope geochemists and ecologists, whose experiments and observations will inform these promising frontiers.

Acknowledgments

The authors would like to thank Kate Freeman, Sarah Zeichner, and Phillip M. Riekenberg for their helpful feedback on early versions of this review. The authors also acknowledge Karli Holman for her expertise in reviewing proposed acid hy-

drololysis reactions and thank members of the Sessions and Eiler labs at Caltech and of the Freeman lab at Penn State for their informative discussions with authors, as well as the two anonymous reviewers and the Associate Editor for their constructive comments. This work was supported in part by grants from the NSF GRFP (to SNS, Fellow ID 2018259065), NASA Astrobiology Institute (grant number 80NSSC18M094 to ALS and JME), NSF Geobiology (grant number EAR-1921330 to ALS), the Agouon Institute (grant number AI-F-GB54.19.2 to EBW) and the Simons Foundation (to JME, award number 626103) and DOE (to JME, award number DESC0016561). Any opinions, findings, or recommendations expressed in this material are those of the authors and do not necessarily reflect the views of the funding agencies.

References

- Abaye, D., Morrison, D., & Preston, T. (2011). Strong anion exchange liquid chromatographic separation of protein amino acids for natural ^{13}C -abundance determination by isotope ratio mass spectrometry. *Rapid Communications in Mass Spectrometry*, *25*, 429–435.
- Abe, I., Minami, H., Nakao, Y., & Nakahara, T. (2002). *N*-pivaloyl methyl ester derivatives of amino acids for separation of enantiomers by chiral-phase capillary gas chromatography. *Journal of Separation Science*, *25*, 661–664.
- Abelson, P. H., & Hoering, T. C. (1961). Carbon isotope fractionation in the formation of amino acids by photosynthetic organisms. *Proceedings of the National Academy of Sciences*, *47*(5), 623–632. <https://doi.org/10.1093/arclin/acr023>
- Adams, R. F. (1974). Determination of amino acid profiles in biological samples by gas chromatography. *Journal of Chromatography*, *95*, 189–212.
- Airaudo, C. B., Gayte-Sorbier, A., & Armand, P. (1987). Stability of glutamine and pyroglutamic acid under model system conditions: influence of physical and technological factors. *Journal of Food Science*, *52*(6), 1750–1752. <https://doi.org/10.1016/j.cossms.2010.07.001>

- Albin, D. M., Wubben, J. E., & Gabert, V. M. (2000). Effect of hydrolysis time on the determination of amino acids in samples of soybean products with ion-exchange chromatography or precolumn derivatization with phenyl isothiocyanate. *Journal of Agricultural and Food Chemistry*, *48*(5), 1684–1691. <https://doi.org/10.1021/jf990599q>
- Amelung, W., & Zhang, X. (2001). Determination of amino acid enantiomers in soils. *Soil Biology and Biochemistry*, *33*, 553–562. www.elsevier.com/locate/soilbio
- Arthur, K., Kelez, S., Larsen, T., Choy, C., & Popp, B. (2014). Tracing the biosynthetic source of essential amino acids in marine turtles using $\delta^{13}\text{C}$ fingerprints. *Ecology*, *95*, 1285–1293.
- Ayayee, P., Larsen, T., Rosa, C., Felton, G., Ferry, J., & Hoover, K. (2015). Essential amino acid supplementation by gut microbes of a wood-feeding Cerambycid. *Environmental Entomology*, *45*, 66–73.
- Baczynski, A. A., Polissar, P. J., Juchelka, D., Schwieters, J., Hilkert, A., Summons, R. E., & Freeman, K. H. (2018). Picomolar-scale compound-specific isotope analyses. *Rapid Communications in Mass Spectrometry*, *32*(9), 730–738. <https://doi.org/10.1002/rcm.8084>
- Bada, J. L., Schoeninger, M. J., & Schimmelmann, A. (1989). Isotopic fractionation during peptide bond hydrolysis. *Geochimica et Cosmochimica Acta*, *53*(12), 3337–3341. [https://doi.org/10.1016/0016-7037\(89\)90114-2](https://doi.org/10.1016/0016-7037(89)90114-2)
- Bligh, E. G., & Dyer, W. J. (1959). A rapid method of total lipid extraction and purification. *Canadian Journal of Biochemistry and Physiology*, *37*(8), 911–917. <https://doi.org/10.1139/o59-099>
- Bowen, G., Wassenaar, L., & Hobson, K. (2005). Global application of stable hydrogen and oxygen isotopes to wildlife forensics. *Oecologia*, *143*, 337–348.
- Brand, W. A. (1996). High precision isotope ratio monitoring techniques in mass spectrometry. *Journal of Mass Spectrometry*, *31*(3), 225–235. [https://doi.org/10.1002/\(SICI\)1096-9888\(199603\)31:3<225::AID-JMS319>3.0.CO;2-L](https://doi.org/10.1002/(SICI)1096-9888(199603)31:3<225::AID-JMS319>3.0.CO;2-L)
- Brenna, J. (1994). High-precision gas isotope ratio mass spectrometry: recent advances in instrumentation and biomedical applications. *Accounts of Chemical Research*, *27*, 340–346.
- Brenna, J., Corso, T., Tobias, H., & Caimi, R. (1997). High-precision continuous flow isotope ratio mass spectrometry. *Mass Spectrometry Reviews*, *16*, 227–258.
- Brodie, C., & Kracht, O. (2016). EA – IRMS : Simultaneous NCS Isotope Analysis. *Thermo Scientific Application Note*.

- Broek, T. A., & McCarthy, M. D. (2014). A new approach to $\delta^{15}\text{N}$ compound-specific amino acid trophic position measurements: Preparative high pressure liquid chromatography technique for purifying underivatized amino acids for stable isotope analysis. *Limnology and Oceanography: Methods*, *12*, 840–852. <https://doi.org/10.4319/lom.2014.12.840>
- Broek, T. A., Walker, B. D., Andreasen, D. H., & McCarthy, M. D. (2013). High-precision measurement of phenylalanine $\delta^{15}\text{N}$ values for environmental samples: A new approach coupling high-pressure liquid chromatography purification and elemental analyzer isotope ratio mass spectrometry. *Rapid Communications in Mass Spectrometry*, *27*, 2327–2337. <https://doi.org/10.1002/rcm.6695>
- Carter, J. F., & Fry, B. (2013). Ensuring the reliability of stable isotope ratio data - Beyond the principle of identical treatment. *Analytical and Bioanalytical Chemistry*, *405*(9), 2799–2814. <https://doi.org/10.1007/s00216-012-6551-0>
- Chen, W. P., Yang, X. Y., Hegeman, A. D., Gray, W. M., & Cohen, J. D. (2010). Microscale analysis of amino acids using gas chromatography-mass spectrometry after methyl chloroformate derivatization. *Journal of Chromatography B: Analytical Technologies in the Biomedical and Life Sciences*, *878*(24), 2199–2208. <https://doi.org/10.1016/j.jchromb.2010.06.027>
- Cheng, C. N. (1975). Extracting and desalting amino acids from soils and sediments: Evaluation of methods. *Soil Biology and Biochemistry*, *7*, 319–322. [https://doi.org/10.1016/0038-0717\(75\)90074-7](https://doi.org/10.1016/0038-0717(75)90074-7)
- Cheng, C. N., Shufeldt, R. C., & Stevenson, F. J. (1975). Amino acid analysis of soils and sediments: Extraction and desalting. *Soil Biology and Biochemistry*, *7*, 143–151. [https://doi.org/10.1016/0038-0717\(75\)90012-7](https://doi.org/10.1016/0038-0717(75)90012-7)
- Chikaraishi, Y., Kashiyama, Y., Ogawa, N. O., Kitazato, H., & Ohkouchi, N. (2007). Metabolic control of nitrogen isotope composition of amino acids in macroalgae and gastropods: Implications for aquatic food web studies. *Marine Ecology Progress Series*, *342*(July), 85–90. <https://doi.org/10.3354/meps342085>
- Chimiak, L., Elsila, J., Dallas, B., Dworkin, J., Aponte, J., Sessions, A., & Eiler, J. (2021). Carbon isotope evidence for the substrates and mechanisms of prebiotic synthesis in the early solar system. *Geochimica et Cosmochimica Acta*, *292*, 188–202.
- Chiou, S.-h. (1989). Rapid protein hydrolysis by microwave irradiation using heat-resistant teflon-pyrex tubes. *Journal of the Chinese Chemical Society*, *36*, 435–442.
- Close, H. G. (2019). Compound-specific isotope geochemistry in the ocean. *Annual Review of Marine Science*, *11*, 27–56. <https://doi.org/10.1146/annurev-marine-121916-063634>

- Colombini, M. P., Fuoco, R., Giacomelli, A., & Muscatello, B. (1998). Characterization of proteinaceous binders in wall painting samples by microwave-assisted acid hydrolysis and GC-MS determination of amino acids. *Studies in Conservation*, 43(1), 33–41.
- Coplen, T. (2011). Guidelines and recommended terms for expression of stable-isotope-ratio and gas-ratio measurement results. *Rapid Communications in Mass Spectrometry*, 25, 2538–2560.
- Corr, L. T., Berstan, R., & Evershed, R. P. (2007a). Development of *N*-acetyl methyl ester derivatives for the determination of $\delta^{13}\text{C}$ values of amino acids using gas chromatography-combustion-isotope ratio mass spectrometry. *Analytical Chemistry*, 79(23), 9082–9090. <https://doi.org/10.1021/ac071223b>
- Corr, L. T., Berstan, R., & Evershed, R. P. (2007b). Optimisation of derivatization procedures for the determination of $\delta^{13}\text{C}$ values of amino acids by gas chromatography-combustion-isotope ratio mass spectrometry. *Rapid Communications in Mass Spectrometry*, 21, 3759–3771. <https://doi.org/10.1002/rcm.3252>
- Creamer, J. S., Mora, M. F., & Willis, P. A. (2017). Enhanced resolution of chiral amino acids with capillary electrophoresis for biosignature detection in extraterrestrial samples. *Analytical Chemistry*, 89(2), 1329–1337. <https://doi.org/10.1021/acs.analchem.6b04338>
- Csapó, J., Csapó-Kiss, Z., Wágner, L., Tálos, T., Martin, T. G., Folestad, S., Tivesten, A., & Némethy, S. (1997). Hydrolysis of proteins performed at high temperatures and for short times with reduced racemization, in order to determine the enantiomers of D- and L-amino acids. *Analytica Chimica Acta*, 339(1-2), 99–107. [https://doi.org/10.1016/S0003-2670\(96\)00452-7](https://doi.org/10.1016/S0003-2670(96)00452-7)
- Darbre, A., & Blau, K. (1965). Trifluoroacetylated amino acid esters: The stability of the derivatives of cysteine, hydroxyproline, serine, threonine, and tyrosine. *Biochim. Biophys. Acta*, 100, 298–300.
- Darragh, A., & Moughan, P. (2005). The effect of hydrolysis time on amino acid analysis. *Journal of AOAC International*, 88, 888–893.
- Darragh, A. J., Garrick, D. J., Moughan, P. J., & Hendriks, W. H. (1996). Correction for amino acid loss during acid hydrolysis of a purified protein. *Analytical Biochemistry*, 236, 199–207. <https://doi.org/10.1006/abio.1996.0157>
- Demmelair, H., & Schmidt, H.-L. (1993). Precise $\delta^{13}\text{C}$ -determination in the range of natural abundance on amino acids from protein hydrolysates by gas chromatography-isotope ratio mass spectrometry. *Isotopenpraxis Isotopes in Environmental and Health Studies*, 29(3), 237–250. <https://doi.org/10.1080/00211919308046690>

- Docherty, G., Jones, V., & Evershed, R. P. (2001). Practical and theoretical considerations in the gas chromatography-combustion-isotope ratio mass spectrometry $\delta^{13}\text{C}$ analysis of small polyfunctional compounds. *Rapid Communications in Mass Spectrometry*, *15*, 730–738. <https://doi.org/10.1002/rcm.270>
- Dong, H., Xiao, K., & Luo, D. (2017). Stability of carbon and nitrogen isotopic compositions of the protein extracted from milk and their potential as "fingerprints" of geographical origin. *RSC Advances*, *7*(31), 18946–18952. <https://doi.org/10.1039/c7ra00722a>
- Dunn, P. J., Honch, N. V., & Evershed, R. P. (2011). Comparison of liquid chromatography-isotope ratio mass spectrometry (LC-IRMS) and gas chromatography-combustion-isotope ratio mass spectrometry (GC-C-IRMS) for the determination of collagen amino acid $\delta^{13}\text{C}$ values for palaeodietary and palaeoecological reconstruction. *Rapid Communications in Mass Spectrometry*. <https://doi.org/10.1002/rcm.5174>
- Eek, K., Sessions, A., & Lies, D. (2007). Carbon-isotopic analysis of microbial cells sorted by flow cytometry. *Geobiology*, *5*, 85–95.
- Eiler, J., Cesar, J., Chimiak, L., Dallas, B., Grice, K., Griep-Raming, J., Juchelka, D., Kitchen, N., Lloyd, M., Makarov, A., Robins, R., & Schwieters, J. (2017). Analysis of molecular isotopic structures at high precision and accuracy by Orbitrap mass spectrometry. *International Journal of Mass Spectrometry*, *422*, 126–142. <https://doi.org/10.1016/j.ijms.2017.10.002>
- Engel, M. H., & Hare, P. E. (1985). Gas-liquid chromatographic separation of amino acids and their derivatives. In G. Barrett (Ed.), *Chemistry and Biochemistry of the Amino Acids* (pp. 462–479). Springer. https://doi.org/10.1007/978-94-009-4832-7_16
- Enggrob, K. L., Larsen, T., Larsen, M., Elsgaard, L., & Rasmussen, J. (2019). The influence of hydrolysis and derivatization on the determination of amino acid content and isotopic ratios in dual-labeled (^{13}C , ^{15}N) white clover. *Rapid Communications in Mass Spectrometry*, *33*(1), 21–30. <https://doi.org/10.1002/rcm.8300>
- Ewing, A. G., Wallingford, R. A., & Olefirowicz, T. M. (1989). Capillary Electrophoresis. *Analytical Chemistry*, *61*(4). <https://doi.org/10.1021/ac00179a002>
- Fogel, M. L., Griffin, P. L., & Newsome, S. D. (2016). Hydrogen isotopes in individual amino acids reflect differentiated pools of hydrogen from food and water in *Escherichia coli*. *Proceedings of the National Academy of Sciences*, *113*(32), E4648–E4653. <https://doi.org/10.1073/pnas.1525703113>
- Fountoulakis, M., & Lahm, H.-W. (1998). Hydrolysis and amino acid composition analysis of proteins. *Journal of Chromatography A*, *826*(2), 109–134. [https://doi.org/10.1016/S0021-9673\(98\)00721-3](https://doi.org/10.1016/S0021-9673(98)00721-3)

- Fourel, F., Martineau, F., Seris, M., & Lecuyer, C. (2014). Simultaneous N, C, S stable isotope analyses using a new purge and trap elemental analyzer and an isotope ratio mass spectrometer. *Rapid Communications in Mass Spectrometry*, *28*, 2587–2594.
- Frank, H., Rettenmeler, A., Welcker, H., Nicholson, G. J., & Bayer, E. (1982). Determination of enantiomer-labeled amino acids in small volumes of blood by gas chromatography. *Analytical Chemistry*, *54*(4), 715–719. <https://doi.org/10.1021/ac00241a027>
- Fry, B. (2007). Coupled N, C and S stable isotope measurements using a dual-column gas chromatography system. *Rapid Communications in Mass Spectrometry*, *21*(5), 750–756.
- Fry, B., & Carter, J. (2019). Stable carbon isotope diagnostics of mammalian metabolism, a high-resolution isotomics approach using amino acid carboxyl groups. *PLoS ONE*, *14*, e0224297.
- Fry, B., Carter, J. F., Yamada, K., Yoshida, N., & Juchelka, D. (2018). Position-specific $^{13}\text{C}/^{12}\text{C}$ analysis of amino acid carboxyl groups – automated flow-injection analysis based on reaction with ninhydrin. *Rapid Communications in Mass Spectrometry*, *32*(12), 992–1000. <https://doi.org/10.1002/rcm.8126>
- Gardner, M. L. G. (1981). Amino acid analysis in the study of protein digestion and absorption. In J. M. Rattenbury (Ed.), *Amino Acid Analysis* (p. 172). Ellis Horwood.
- Gauchotte-Lindsay, C., & Turnbull, S. M. (2016, February). On-line high-precision carbon position-specific stable isotope analysis: A review. <https://doi.org/10.1016/j.trac.2015.07.010>
- Gehre, M., Renpenning, J., Gilevska, T., Qi, H., Coplen, T. B., Meijer, H. A., Brand, W. A., & Schimmelmann, A. (2015). On-Line hydrogen-isotope measurements of organic samples using elemental chromium: An extension for high temperature elemental-analyzer techniques. *Analytical Chemistry*, *87*(10), 5198–5205. <https://doi.org/10.1021/acs.analchem.5b00085>
- Gehrke, C. W., Wall, L. L., & Absheer, J. S. (1985). Sample preparation for chromatography of amino acids: Acid hydrolysis of proteins. *Journal of the Association of Official Analytical Chemists*, *68*(5), 811–821. <https://doi.org/10.1093/jaoac/68.5.811>
- Gélinas, Y., Baldock, J. A., & Hedges, J. I. (2001). Demineralization of marine and freshwater sediments for CP/MAS ^{13}C NMR analysis. *Organic Geochemistry*, *32*(5), 677–693. [https://doi.org/10.1016/S0146-6380\(01\)00018-3](https://doi.org/10.1016/S0146-6380(01)00018-3)
- Ghashghaie, J., & Tcherkez, G. (2013). *Isotope ratio mass spectrometry technique to follow plant metabolism. Principles and applications of $^{13}\text{C}/^{12}\text{C}$ isotopes* (1st ed., Vol. 67). Elsevier Ltd. <https://doi.org/10.1016/B978-0-12-397922-3.00008-3>

- Giesemann, A., Jäger, H.-J., Norman, A., Krouse, H., & Brand, W. (1994). On-line sulfur-isotope determination using an elemental analyzer coupled to a mass spectrometer. *Analytical Chemistry*, *66*, 2816–2819.
- Gilbert, A. (2021). The organic isotopologue frontier. *Annual Review of Earth and Planetary Sciences*, *49*, 435–464.
- Gilbert, A., Suda, K., Yamada, K., Ueno, Y., & Yoshida, N. (2016). Position-specific isotope analysis by on-line pyrolysis coupled to IRMS. *AGU Fall Meeting Abstracts, 2016*, Article V33G-05, V33G-05.
- Gilbert, A., Yamada, K., Suda, K., Ueno, Y., & Yoshida, N. (2016). Measurement of position-specific ^{13}C isotopic composition of propane at the nanomole level. *Geochimica et Cosmochimica Acta*, *177*, 205–216. <https://doi.org/10.1016/j.gca.2016.01.017>
- Glaser, B., & Amelung, W. (2002). Determination of ^{13}C natural abundance of amino acid enantiomers in soil: Methodological considerations and first results. *Rapid Communications in Mass Spectrometry*, *16*(9), 891–898. <https://doi.org/10.1002/rcm.650>
- Godin, J. P., Faure, M., Breuille, D., Hopfgartner, G., & Fay, L. B. (2007). Determination of ^{13}C isotopic enrichment of valine and threonine by GC-C-IRMS after formation of the N(O,S)-ethoxycarbonyl ethyl ester derivatives of the amino acids. *Analytical and Bioanalytical Chemistry*, *388*(4), 909–918. <https://doi.org/10.1007/s00216-007-1275-2>
- Godin, J. P., Hau, J., Fay, L. B., & Hopfgartner, G. (2005). Isotope ratio monitoring of small molecules and macromolecules by liquid chromatography coupled to isotope ratio mass spectrometry. *Rapid Communications in Mass Spectrometry*, *19*(18), 2689–2698. <https://doi.org/10.1002/rcm.2117>
- Godin, J. P., & McCullagh, J. S. (2011). Review: Current applications and challenges for liquid chromatography coupled to isotope ratio mass spectrometry (LC/IRMS). *Rapid Communications in Mass Spectrometry*, *25*(20), 3019–3028. <https://doi.org/10.1002/rcm.5167>
- Golan, A., & Wolfe, F. H. (1979). Gas chromatographic analysis of protein amino acid *N*-heptafluorobutyryl-isopropyl esters. *Canadian Institute of Food Science and Technology Journal*, *12*(3), 123–127. [https://doi.org/10.1016/s0315-5463\(79\)73097-5](https://doi.org/10.1016/s0315-5463(79)73097-5)
- Hannides, C. C., Popp, B. N., Landry, M. R., & Graham, B. S. (2009). Quantification of zooplankton trophic position in the North Pacific Subtropical Gyre using stable nitrogen isotopes. *Limnology and Oceanography*, *54*(1), 50–61. <https://doi.org/10.4319/lo.2009.54.1.0050>
- Hare, P. E., Fogel, M. L., Stafford, T. W., Mitchell, A. D., & Hoering, T. C. (1991). The isotopic composition of carbon and nitrogen in individual amino acids isolated from modern and fossil proteins. *Journal of Archaeological Science*, *18*(3), 277–292. [https://doi.org/10.1016/0305-4403\(91\)90066-X](https://doi.org/10.1016/0305-4403(91)90066-X)

- Hayes, J. M. (2002). Practice and Principles of Isotopic Measurements in Organic Geochemistry. *Society*, (August).
- Hedges, J., & Stern, J. (1983). Carbon and nitrogen determinations of carbonate-containing solids. *Limnology and Oceanography*, *29*, 657–663.
- Henrichs, S. M. (1991). Methods of sample handling and analysis for dissolved and particulate amino acids and carbohydrates in seawater. In D. Hurd & D. Spencer (Eds.), *Marine Particles: Analysis and Characterization* (Geophys. M, pp. 139–149). AGU. <https://doi.org/10.1029/gm063p0139>
- Hilkert, A., Böhlke, J., Mroczkowski, S., Fort, K., Aizikov, K., Wang, X., Kopf, S., & Neubauer, C. (2021). Exploring the potential of electrospray-Orbitrap for stable isotope analysis using nitrate as a model. *Analytical Chemistry*, *93*, 9139–9148.
- Hill, J., & Leach, S. J. (1964). Hydrogen exchange at carbon-hydrogen sites during acid or alkaline treatment of proteins. *Biochemistry*, *3*(12), 1814–1818. <https://doi.org/10.1021/bi00900a003>
- Hill, R. L. (1965). Hydrolysis of proteins. *Advances in Protein Chemistry*, *20*, 37–107. [https://doi.org/https://doi.org/10.1016/S0065-3233\(08\)60388-5](https://doi.org/https://doi.org/10.1016/S0065-3233(08)60388-5)
- Hirs, C. H. W., Stein, W. H., & Moore, S. (1954). The amino acid composition of ribonuclease. *Journal of Biological Chemistry*, *211*, 941–950.
- Hoffman, D. W., & Rasmussen, C. (2019). Position-specific carbon stable isotope ratios by proton NMR spectroscopy. *Analytical Chemistry*, *91*(24), 15661–15669. <https://doi.org/10.1021/acs.analchem.9b03776>
- Hofmann, A. E., Chimiak, L., Dallas, B., Griep-Raming, J., Juchelka, D., Makarov, A., Schwieters, J., & Eiler, J. M. (2020). Using Orbitrap mass spectrometry to assess the isotopic compositions of individual compounds in mixtures. *International Journal of Mass Spectrometry*, *457*, 116410. <https://doi.org/10.1016/j.ijms.2020.116410>
- Hofmann, D., Gehre, M., & Jung, K. (2003). Sample preparation techniques for the determination of natural $^{15}\text{N}/^{14}\text{N}$ variations in amino acids by gas chromatography-combustion-isotope ratio mass spectrometry (GC-C-IRMS). *Isotopes in Environmental and Health Studies*, *39*, 233–244.
- Hofmann, D., Jung, K., Segschneider, H. J., Gehre, M., & Schüürmann, G. (1995). $^{15}\text{N}/^{14}\text{N}$ analysis of amino acids with GC-C-IRMS - Methodical investigations and ecotoxicological applications. *Isotopes in Environmental and Health Studies*, *31*(3-4), 367–375. <https://doi.org/10.1080/10256019508036284>
- Homer, A. (1915). A method for the estimation of the tryptophane content of proteins, involving the use of baryta as a hydrolyzing agent. *The Journal of Biological Chemistry*, *22*, 369–389.

- Huang, Z. H., Wang, J., Gage, D. A., Throck Watson, J., Sweeley, C. C., & Hušek, P. (1993). Characterization of *N*-ethoxycarbonyl ethyl esters of amino acids by mass spectrometry. *Journal of Chromatography A*, 635(2), 271–281. [https://doi.org/10.1016/0021-9673\(93\)80370-N](https://doi.org/10.1016/0021-9673(93)80370-N)
- Hunt, S. (1985). Degradation of amino acids accompanying *in vitro* protein hydrolysis. In G. C. Barrett (Ed.), *Chemistry and Biochemistry of the Amino Acids* (pp. 376–398). Springer Netherlands. https://doi.org/10.1007/978-94-009-4832-7_12
- Hušek, P. (1991a). Rapid derivatization and gas chromatographic determination of amino acids. *Journal of Chromatography A*, 552(100), 289–299. [https://doi.org/10.1016/S0021-9673\(01\)95945-X](https://doi.org/10.1016/S0021-9673(01)95945-X)
- Hušek, P. (1991b). Amino acid derivatization and analysis in five minutes. *FEBS Letters*, 280(2), 354–356. [https://doi.org/10.1016/0014-5793\(91\)80330-6](https://doi.org/10.1016/0014-5793(91)80330-6)
- Hušek, P. (1998). Chloroformates in gas chromatography as general purpose derivatizing agents. *Journal of Chromatography B*, 717, 57–91.
- Hušek, P., & Macek, K. (1975). Gas chromatography of amino acids. *Journal of Chromatography A*, 113(2), 139–230. [https://doi.org/10.1016/S0021-9673\(00\)86962-9](https://doi.org/10.1016/S0021-9673(00)86962-9)
- Hutt, L. D., Glavin, D. P., Bada, J. L., & Mathies, R. A. (1999). Microfabricated capillary electrophoresis amino acid chirality analyzer for extraterrestrial exploration. *Analytical Chemistry*, 71(18), 4000–4006. <https://doi.org/10.1021/ac9903959>
- Ingalls, A. E., Lee, C., Wakeham, S. G., & Hedges, J. I. (2003). The role of biominerals in the sinking flux and preservation of amino acids in the Southern Ocean along 170°W. *Deep-Sea Research Part II: Topical Studies in Oceanography*, 50(3-4), 713–738. [https://doi.org/10.1016/S0967-0645\(02\)00592-1](https://doi.org/10.1016/S0967-0645(02)00592-1)
- Islam, A., & Darbre, A. (1972). Gas-liquid chromatography of trifluoroacetylated amino acid methyl esters: Determination of their molar responses with the flame ionization detector. *Journal of Chromatography*, 71, 223–232.
- Jézéquel, T., Joubert, V., Giraudeau, P., Remaud, G. S., & Akoka, S. (2017). The new face of isotopic NMR at natural abundance. *Magnetic Resonance in Chemistry*, 55(2), 77–90. <https://doi.org/10.1002/mrc.4548>
- Jim, S., Jones, V., Ambrose, S. H., & Evershed, R. P. (2006). Quantifying dietary macronutrient sources of carbon for bone collagen biosynthesis using natural abundance stable carbon isotope analysis. *British Journal of Nutrition*, 95(6), 1055–1062. <https://doi.org/10.1079/bjn20051685>

- Jim, S., Jones, V., Copley, M. S., Ambrose, S. H., & Evershed, R. P. (2003). Effects of hydrolysis on the $\delta^{13}\text{C}$ values of individual amino acids derived from polypeptides and proteins. *Rapid Communications in Mass Spectrometry*, *17*(20), 2283–2289. <https://doi.org/10.1002/rcm.1177>
- Johnson, B., Fogel, M., & Miller, G. (1998). Stable isotopes in modern ostrich eggshell: a calibration for paleoenvironmental applications in semi-arid regions of southern Africa. *Geochimica et Cosmochimica Acta*, *62*, 2451–2461.
- Jones, V. (2002). *Investigating the routing and synthesis of amino acids between diet and bone collagen via feeding experiments and applications to palaeodietary reconstruction* [Doctoral dissertation, University of Bristol].
- Juchelka, D., & Krummen, M. (2008). *irm-LC/MS: $\delta^{13}\text{C}$ analysis of underivatized amino acids*. *Thermo Scientific Application Note*, 30065.
- Kayacelebi, A. A., Knöfel, A. K., Beckmann, B., Hanff, E., Warnecke, G., & Tsikas, D. (2015). Measurement of unlabeled and stable isotope-labeled homoarginine, arginine and their metabolites in biological samples by GC-MS and GC-MS/MS. *Amino Acids*, *47*(9), 2023–2034. <https://doi.org/10.1007/s00726-015-1984-3>
- Keutmann, H. T., & Potts, J. T. (1969). Improved recovery of methionine after acid hydrolysis using mercaptoethanol. *Analytical Biochemistry*, *29*, 175–185.
- Laegeler, W., Tio, J. M., & Blake, M. I. (1974). Stability of certain amino acids in a parenteral nutrition solution. *American Journal of Hospital Pharmacy*, *31*, 776–779. <https://doi.org/10.1093/ajhp/31.3.296>
- Larsen, T., Ventura, M., Andersen, N., O'Brien, D. M., Piatkowski, U., & McCarthy, M. D. (2013). Tracing carbon sources through aquatic and terrestrial food webs using amino acid stable isotope fingerprinting. *PLoS ONE*, *8*(9), 1–9. <https://doi.org/10.1371/journal.pone.0073441>
- Larson, T. M., Gawlitzek, M., Evans, H., Albers, U., & Cacia, J. (2002). Chemometric evaluation of on-line high-pressure liquid chromatography in mammalian cell cultures: Analysis of amino acids and glucose. *Biotechnology and Bioengineering*, *77*(5), 553–563. <https://doi.org/10.1002/bit.10116>
- Lee, C., Hayes, L., Kreider-Mueller, A., Kuhnel, E., Baca, J., Shaw, C., Glibert, P., Altabet, M., & Zhang, L. (2021). Position-specific N isotope analysis of glutamine extracted from culture phytoplankton. *Goldschmidt Virtual Meetings*.
- MacKenzie, S. L., & Tenaschuk, D. (1979). Quantitative formation of N(O,S)-heptafluorobutyryl isobutyl amino acids for gas chromatographic analysis. *Journal of Chromatography*, *173*, 53–63.

- Macko, S. A., Estep, M. L., Hare, P. E., & Hoering, T. C. (1983). Stable nitrogen and carbon isotopic composition of individual amino acids isolated from cultured microorganisms. *Carnegie Institution of Washington Year Book*, 82(1905), 404–410.
- Macko, S. A., Uhle, M. E., Engel, M. H., & Andrusevich, V. (1997). Stable nitrogen isotope analysis of amino acid enantiomers by gas chromatography/combustion/isotope ratio mass spectrometry. *Analytical Chemistry*, 69(5), 926–929. <https://doi.org/10.1021/ac960956l>
- Manneberg, M., Lahm, H.-W., & Fountoulakis, M. (1995). Quantification of cysteine residues following oxidation to cysteic acid in the presence of sodium azide. *Analytical Biochemistry*, 231, 349–353.
- Matsubara, H., & Sasaki, R. M. (1969). High recovery of tryptophan from acid hydrolysates of proteins. *Biochemical and Biophysical Research Communications*, 35(2), 175–181. [https://doi.org/10.1016/0006-291X\(69\)90263-0](https://doi.org/10.1016/0006-291X(69)90263-0)
- McCarthy, M., Benner, R., Lee, C., Hedges, J., & Fogel, M. (2004). Amino acid carbon isotopic fractionation patterns in oceanic dissolved organic matter: an unaltered photoautotrophic source for dissolved organic nitrogen in the ocean? *Marine Chemistry*, 92, 123–134.
- McClelland, J., & Montoya, J. (2002). Trophic relationships and the nitrogen isotopic composition of amino acids in plankton. *Ecology*, 83, 2173–2180.
- McCoy, V. E., Gabbott, S. E., Penkman, K., Collins, M. J., Presslee, S., Holt, J., Grossman, H., Wang, B., Solórzano Kraemer, M. M., Delclòs, X., & Peñalver, E. (2019). Ancient amino acids from fossil feathers in amber. *Scientific Reports*, 9(1), 1–8. <https://doi.org/10.1038/s41598-019-42938-9>
- McCullagh, J., Juchelka, D., & Hedges, R. (2006). Analysis of amino acid ^{13}C abundance from human and faunal bone collagen using liquid chromatography/isotope ratio mass spectrometry. *Rapid Communications in Mass Spectrometry*, 20, 2761–2768. <https://doi.org/10.1002/rcm.2651>
- McKinney, C. R., McRea, I., Epstein, S., Allen, H., & Urey, H. (1950). Improvements in mass spectrometers for measurement of small differences in isotope abundance ratios. *Review of Scientific Instruments*, 21, 724–730.
- McMahon, K. W., & Newsome, S. D. (2019). Amino acid isotope analysis: a new frontier in animal migration and foraging ecology. In K. A. Hobson & L. I. Wassenaar (Eds.), *Tracking Animal Migration with Stable Isotopes* (pp. 173–190). Elsevier.
- McMahon, K., Fogel, M., Johnson, B., Houghton, L., & Thorrold, S. (2011). A new method to reconstruct fish diet and movement patterns from $\delta^{13}\text{C}$ values in otolith amino acids. *Canadian Journal of Fisheries and Aquatic Sciences*, 68, 1330–1340.

- Meier-Augenstein, W. (1999). Applied gas chromatography coupled to isotope ratio mass spectrometry. *Journal of Chromatography A*, 842(1-2), 351–371. [https://doi.org/10.1016/S0021-9673\(98\)01057-7](https://doi.org/10.1016/S0021-9673(98)01057-7)
- Meier-Augenstein, W. (2004). GC and IRMS technology for ^{13}C and ^{15}N analysis on organic compounds and related gases. In *Handbook of Stable Isotope Analytical Techniques* (pp. 153–176). Elsevier.
- Metges, C. C., & Daenzer, M. (2000). ^{13}C gas chromatography-combustion isotope ratio mass spectrometry analysis of *N*-pivaloyl amino acid esters of tissue and plasma samples. *Analytical Biochemistry*, 278(2), 156–164. <https://doi.org/10.1006/abio.1999.4426>
- Metges, C. C., Petzke, K. J., & Hennig, U. (1996). Gas chromatography/combustion/isotope ratio mass spectrometric comparison of *N*-acetyl- and *N*-pivaloyl amino acid esters to measure ^{15}N isotopic abundances in physiological samples: A pilot study on amino acid synthesis in the upper gastro-intestinal tract. *Journal of Mass Spectrometry*, 31(4), 367–376. [https://doi.org/10.1002/\(SICI\)1096-9888\(199604\)31:4<367::AID-JMS310>3.0.CO;2-V](https://doi.org/10.1002/(SICI)1096-9888(199604)31:4<367::AID-JMS310>3.0.CO;2-V)
- Molero, G., Aranjuelo, I., Teixidor, P., Araus, J. L., & Nogués, S. (2011). Measurement of ^{13}C and ^{15}N isotope labeling by gas chromatography/combustion/isotope ratio mass spectrometry to study amino acid fluxes in a plant-microbe symbiotic association. *Rapid Communications in Mass Spectrometry*, 25(5), 599–607. <https://doi.org/10.1002/rcm.4895>
- Molnár-Perl, I., & Katona, Z. F. (2000). GC-MS of amino acids as their trimethylsilyl/*t*-butyldimethylsilyl derivatives: In model solutions III. *Chromatographia*, 51(1). <https://doi.org/10.1007/bf02492811>
- Mondino, A., & Bongiovanni, G. (1970). An experimental study of amino acid degradation under open flask hydrolytic conditions. *Journal of Chromatography*, 52, 405–413.
- Montigon, F., Boza, J. J., & Fay, L. B. (2001). Determination of ^{13}C - and ^{15}N -enrichment of glutamine by gas chromatography/mass spectrometry and gas chromatography/combustion/isotope ratio mass spectrometry after N(O,S)-ethoxycarbonyl ethyl ester derivatisation. *Rapid Communications in Mass Spectrometry*, 15(2), 116–123. [https://doi.org/10.1002/1097-0231\(20010130\)15:2<116::aid-rcm202>3.3.co;2-v](https://doi.org/10.1002/1097-0231(20010130)15:2<116::aid-rcm202>3.3.co;2-v)
- Moore, S., & Stein, W. H. (1951). Chromatography of amino acids on sulfonated polystyrene resins. *Journal of Biological Chemistry*, 192, 663–681. <http://www.jbc.org/>
- Moore, S., & Stein, W. H. (1963). Chromatographic determination of amino acids by the use of automatic recording equipment. *Methods in Enzymology*, 6(100), 819–831. [https://doi.org/10.1016/0076-6879\(63\)06257-1](https://doi.org/10.1016/0076-6879(63)06257-1)

- Morrison, D., Taylor, K., & Preston, T. (2010). Strong anion-exchange liquid chromatography coupled with isotope ratio mass spectrometry using a Liquiface interface. *Rapid Communications in Mass Spectrometry*, *24*, 1755–1762.
- Neubauer, C., Crémière, A., Wang, X. T., Thiagarajan, N., Sessions, A. L., Adkins, J. F., Dalleska, N. F., Turchyn, A. V., Clegg, J. A., Moradian, A., Sweredoski, M. J., Garbis, S. D., & Eiler, J. M. (2020). Stable isotope analysis of intact oxyanions using electrospray quadrupole-Orbitrap mass spectrometry. *Analytical Chemistry*, *92*(4), 3077–3085. <https://doi.org/10.1021/acs.analchem.9b04486>
- Neubauer, C., Sweredoski, M. J., Moradian, A., Newman, D. K., Robins, R. J., & Eiler, J. M. (2018). Scanning the isotopic structure of molecules by tandem mass spectrometry. *International Journal of Mass Spectrometry*, *434*, 276–286. <https://doi.org/10.1016/j.ijms.2018.08.001>
- Newsome, S., Nakamoto, B., Curras, M., & Fogel, M. (2020). Compound-specific $\delta^2\text{H}$ analysis highlights the relationship between direct assimilation and de novo synthesis of amino acids from food and water in a terrestrial mammalian omnivore. *Oecologia*, *193*, 827–842.
- Newsome, S. D., Chivers, S. J., & Kowalewski, M. B. (2018). The influence of lipid-extraction and long-term DMSO preservation on carbon ($\delta^{13}\text{C}$) and nitrogen ($\delta^{15}\text{N}$) isotope values in cetacean skin. *Marine Mammal Science*, *34*(2), 277–293. <https://doi.org/10.1111/mms.12454>
- Ng, L. T., Pascaud, A., & Pascaud, M. (1987). Hydrochloric acid hydrolysis of proteins and determination of tryptophan by reversed-phase high-performance liquid chromatography. *Analytical Biochemistry*, *167*(1), 47–52. [https://doi.org/10.1016/0003-2697\(87\)90132-1](https://doi.org/10.1016/0003-2697(87)90132-1)
- Nguyen, R. T., & Harvey, H. R. (1998). Protein preservation during early diagenesis in marine waters and sediments. In B. A. Stankiewicz & P. F. van Bergen (Eds.), *Nitrogen-Containing Macromolecules in the Bio- and Geosphere ACS Symposium Series* (pp. 88–112, Vol. 707). American Chemical Society. <https://doi.org/10.1021/bk-1998-0707.ch007>
- Niu, L., Zhang, H., Wu, Z., Wang, Y., Liu, H., Wu, X., & Wang, W. (2018). Modified TCA/acetone precipitation of plant proteins for proteomic analysis (T. Chardot, Ed.). *PLOS ONE*, *13*(12), e0202238. <https://doi.org/10.1371/journal.pone.0202238>
- Nunn, B. L., & Keil, R. G. (2006). A comparison of non-hydrolytic methods for extracting amino acids and proteins from coastal marine sediments. *Marine Chemistry*, *98*(1), 31–42. <https://doi.org/10.1016/j.marchem.2005.06.005>
- Ogawa, N. O., Nagata, T., Kitazato, H., & Ohkouchi, N. (2010). Ultrasensitive elemental analyzer/isotope ratio mass spectrometer for stable nitrogen and carbon isotope analyses. *Earth, Life and Isotopes, Kyoto Univ. Press*, (January 2010), 339–353.

- Ohkouchi, N., Chikaraishi, Y., Close, H. G., Fry, B., Larsen, T., Madigan, D. J., McCarthy, M. D., McMahon, K. W., Nagata, T., Naito, Y. I., Ogawa, N. O., Popp, B. N., Steffan, S., Takano, Y., Tayasu, I., Wyatt, A. S., Yamaguchi, Y. T., & Yokoyama, Y. (2017). Advances in the application of amino acid nitrogen isotopic analysis in ecological and biogeochemical studies. *Organic Geochemistry*, *113*, 150–174. <https://doi.org/10.1016/j.orggeochem.2017.07.009>
- Ozols, J. (1990). Amino acid analysis. *Methods in Enzymology*, *182*(100), 587–601. [https://doi.org/10.1016/0076-6879\(90\)82046-5](https://doi.org/10.1016/0076-6879(90)82046-5)
- Park, S. H., Lovejoy, K., Grosse, S., De Pra, M., Meding, S., & Steiner, F. (2019). Underivatized amino acid analysis in wine by HILIC separation and mass detection. *Thermo Scientific Application Note*, 73151.
- Peláez, M. V., Bayón, M. M., Alonso, J. I. G., & Sanz-Medel, A. (2000). Comparison of different derivatization approaches for the determination of selenomethionine by GC-ICP-MS. *Journal of Analytical Atomic Spectrometry*, *15*(9), 1217–1222. <https://doi.org/10.1039/b000505n>
- Phillips, A., Wu, F., & Sessions, A. (2021). Compound-specific sulfur isotope analysis of cysteine and methionine via preparatory liquid chromatography and elemental analyzer isotope-ratio mass spectrometry. *Rapid Communications in Mass Spectrometry*.
- Piraud, M., Vianey-Saban, C., Petritis, K., Elfakir, C., Steghens, J. P., Morla, A., & Bouchu, D. (2003). ESI-MS/MS analysis of underivatized amino acids: A new tool for the diagnosis of inherited disorders of amino acid metabolism. Fragmentation study of 79 molecules of biological interest in positive and negative ionisation mode. *Rapid Communications in Mass Spectrometry*, *17*(12), 1297–1311. <https://doi.org/10.1002/rcm.1054>
- Polissar, P. J., Fulton, J. M., Junium, C. K., Turich, C. C., & Freeman, K. H. (2009). Measurement of ^{13}C and ^{15}N isotopic composition on nanomolar quantities of C and N. *Analytical Chemistry*, *81*(2), 755–763. <https://doi.org/10.1021/ac801370c>
- Qi, H., Coplen, T., Geilmann, H., Brand, W., & Böhlke, J. (2003). Two new organic reference materials for $\delta^{13}\text{C}$ and $\delta^{15}\text{N}$ measurements and a new value for the $\delta^{13}\text{C}$ of NBS 22 oil. *Rapid Communications in Mass Spectrometry*, *17*, 2483–2487.
- Qi, H., Coplen, T. B., Mroczkowski, S. J., Brand, W. A., Brandes, L., Geilmann, H., & Schimmelmann, A. (2016). A new organic reference material, L-glutamic acid, USGS41a, for $\delta^{13}\text{C}$ and $\delta^{15}\text{N}$ measurements - a replacement for USGS41. *Rapid Communications in Mass Spectrometry*, *30*(7), 859–866. <https://doi.org/10.1002/rcm.7510>

- Rasmussen, C., & Hoffman, D. W. (2020). Intramolecular distribution of $^{13}\text{C}/^{12}\text{C}$ isotopes in amino acids of diverse origins. *Amino Acids*, 52, 955–964. <https://doi.org/10.1016/j.cossms.2010.07.001>
- Rees, M. W. (1946). The estimation of threonine and serine in proteins. *Biochemical Journal*, 40(5-6), 632–640. <https://doi.org/10.1042/bj0400632>
- Remaud, G., Giraudeau, P., Lesot, P., & Akoka, S. (2018). Isotope ratio monitoring by NMR: Part 1 – recent advances. In G. Webb (Ed.), *Modern Magnetic Resonance* (pp. 1353–1378). Springer, Cham.
- Renpenning, J., Schimmelmann, A., & Gehre, M. (2017). Compound-specific hydrogen isotope analysis of fluorine-, chlorine-, bromine- and iodine-bearing organics using gas chromatography-chromium-based high-temperature conversion (Cr/HTC)-isotope ratio mass spectrometry. *Rapid Communications in Mass Spectrometry*, 31(13), 1095–1102. <https://doi.org/10.1002/rcm.7872>
- Richards, M., Fuller, B., & Hedges, R. (2001). Sulphur isotopic variation in ancient bone collagen from Europe: implications for human palaeodiet, residence mobility, and modern pollutant studies. *Earth and Planetary Science Letters*, 191, 185–190.
- Riekenberg, P. M., Oakes, J. M., & Eyre, B. D. (2017). Uptake of dissolved organic and inorganic nitrogen in microalgae-dominated sediment: Comparing dark and light in situ and ex situ additions of ^{15}N . *Marine Ecology Progress Series*, 571(May), 29–42. <https://doi.org/10.3354/meps12127>
- Riekenberg, P. M., van der Meer, M., & Schouten, S. (2020). Practical considerations for improved reliability and precision during determination of $\delta^{15}\text{N}$ values in amino acids using a single combined oxidation-reduction reactor. *Rapid Communications in Mass Spectrometry*, 34(14), e8797. <https://doi.org/10.1002/rcm.8797>
- Rieley, G. (1994). Derivatization of organic compounds prior to gas chromatographic-combustion-isotope ratio mass spectrometric analysis: identification of isotope fractionation processes. *Analyst*, 119, 915–919.
- Romek, K. M., Krzemińska, A., Remaud, G. S., Julien, M., Paneth, P., & Robins, R. J. (2017). Insights into the role of methionine synthase in the universal ^{13}C depletion in *O*- and *N*-methyl groups of natural products. *Archives of Biochemistry and Biophysics*, 635(September), 60–65. <https://doi.org/10.1016/j.abb.2017.10.012>
- Rood, D. (2007). In *The Troubleshooting and Maintenance Guide for Gas Chromatographers* (4th ed., pp. 3–88). Wiley-VCH, Weinheim.
- Rowan, A. M., Wilson, M. N., & Moughan, P. J. (1992). Effect of hydrolysis time on the determination of the amino acid composition of diet, ileal digesta, and feces samples and on the determination of dietary amino acid digestibil-

- ity coefficients. *Journal of Agricultural and Food Chemistry*, 40(6), 981–985. <https://doi.org/10.1021/jf00018a013>
- Rubenstein, D., & Hobson, K. (2004). From birds to butterflies: animal movement patterns and stable isotopes. *Trends in Ecology and Evolution*, 19, 256–263.
- Rutherford, S. M. (2009). Accurate determination of the amino acid content of selected feedstuffs. *International Journal of Food Sciences and Nutrition*, 60(SUPPL. 7), 53–62. <https://doi.org/10.1080/09637480802269957>
- Rutherford, S. M., & Gilani, G. S. (2009). Amino acid analysis. *Current Protocols in Protein Science*, 58, 11.9.1–11.9.37. <https://doi.org/10.1002/0471140864.ps1109s58>
- Sacks, G. L., & Brenna, J. T. (2005). $^{15}\text{N}/^{14}\text{N}$ position-specific isotopic analyses of polynitrogenous amino acids. *Analytical Chemistry*, 77(4), 1013–1019. <https://doi.org/10.1021/ac048903o>
- Sacks, G. L., Zhang, Y., & Brenna, J. T. (2007). Fast gas chromatography combustion isotope ratio mass spectrometry. *Analytical Chemistry*, 79(16), 6348–6358. <https://doi.org/10.1021/ac0706325>
- Sauer, P. E., Eglinton, T. I., Hayes, J. M., Schimmelmann, A., & Sessions, A. L. (2001). Compound-specific D/H ratios of lipid biomarkers from sediments as a proxy for environmental and climatic conditions. *Geochimica et Cosmochimica Acta*, 65(2), 213–222. [https://doi.org/10.1016/S0016-7037\(00\)00520-2](https://doi.org/10.1016/S0016-7037(00)00520-2)
- Sayle, K. L., Brodie, C. R., Cook, G. T., & Hamilton, W. D. (2019). Sequential measurement of $\delta^{15}\text{N}$, $\delta^{13}\text{C}$ and $\delta^{34}\text{S}$ values in archaeological bone collagen at the Scottish Universities Environmental Research Centre (SUERC): A new analytical frontier. *Rapid Communications in Mass Spectrometry*, 33(15), 1258–1266. <https://doi.org/10.1002/rcm.8462>
- Schiff, J., Batista, F., Sherwood, O., Guilderson, T., Hill, T., Ravelo, A., McMahon, K., & McCarthy, M. (2014). Compound specific amino acid $\delta^{13}\text{C}$ patterns in a deep-sea proteinaceous coral: Implications for reconstructing detailed $\delta^{13}\text{C}$ records of exported primary production. *Marine Chemistry*, 166, 82–91.
- Schimmelmann, A., Qi, H., Coplen, T. B., Brand, W. A., Fong, J., Meier-Augenstein, W., Kemp, H. F., Toman, B., Ackermann, A., Assonov, S., Aerts-Bijma, A. T., Brejcha, R., Chikaraishi, Y., Darwish, T., Elsner, M., Gehre, M., Geilmann, H., Gröning, M., Hélie, J. F., . . . Werner, R. A. (2016). Organic reference materials for hydrogen, carbon, and nitrogen stable isotope-ratio measurements: caffeine, *n*-alkanes, fatty acid methyl esters, glycines, L-valines, polyethylenes, and oils. *Analytical Chemistry*, 88(8), 4294–4302. <https://doi.org/10.1021/acs.analchem.5b04392>

- Serban, A., Engel, M. H., & Macko, S. A. (1988). The distribution, stereochemistry and stable isotopic composition of amino acid constituents of fossil and modern mollusk shells. *Organic Geochemistry*, *13*(4-6), 1123–1129. [https://doi.org/10.1016/0146-6380\(88\)90298-7](https://doi.org/10.1016/0146-6380(88)90298-7)
- Sessions, A. L. (2006). Isotope-ratio detection for gas chromatography. *Journal of Separation Science*, *29*(12), 1946–1961. <https://doi.org/10.1002/jssc.200600002>
- Sessions, A. L., Sylva, S. P., & Hayes, J. M. (2005). Moving-wire device for carbon isotopic analyses of nanogram quantities of nonvolatile organic carbon. *Analytical Chemistry*, *77*(20), 6519–6527. <https://doi.org/10.1021/ac051251z>
- Shinebarger, S. R., Haisch, M., & Matthews, D. E. (2002). Retention of carbon and alteration of expected ^{13}C -tracer enrichments by silylated derivatives using continuous-flow combustion-isotope ratio mass spectrometry. *Analytical Chemistry*, *74*(24), 6244–6251. <https://doi.org/10.1021/ac026061s>
- Silfer, J. A., Engel, M. H., & Macko, S. A. (1992). Kinetic fractionation of stable carbon and nitrogen isotopes during peptide bond hydrolysis: experimental evidence and geochemical implications. *Chemical Geology*, *101*(3-4), 211–221. [https://doi.org/10.1016/0009-2541\(92\)90003-N](https://doi.org/10.1016/0009-2541(92)90003-N)
- Silfer, J. A., Engel, M. H., Macko, S. A., & Jumeau, E. J. (1991). Stable carbon isotope analysis of amino acid enantiomers by conventional isotope ratio mass spectrometry and combined gas chromatography/isotope ratio mass spectrometry. *Analytical Chemistry*, *63*(4), 370–374. <https://doi.org/10.1021/ac00004a014>
- Smith, C. I., Fuller, B. T., Choy, K., & Richards, M. P. (2009). A three-phase liquid chromatographic method for $\delta^{13}\text{C}$ analysis of amino acids from biological protein hydrolysates using liquid chromatography-isotope ratio mass spectrometry. *Analytical Biochemistry*, *390*(2), 165–172. <https://doi.org/10.1016/j.ab.2009.04.014>
- Smith, E. L., & Stockell, A. (1954). Amino acid composition of crystalline carboxypeptidase. *Journal of Biological Chemistry*, *207*, 501–514.
- Snyder, L., Kirkland, J., & Dolan, J. (2010). Basic concepts and the control of separation. In L. Snyder, J. Kirkland, & J. Dolan (Eds.), *Introduction to Modern Liquid Chromatography* (pp. 19–86). John Wiley Sons Inc.
- Sobolevsky, T. G., Revelsky, A. I., Miller, B., Oriedo, V., Chernetsova, E. S., & Revelsky, I. A. (2003). Comparison of silylation and esterification/acetylation procedures in GC-MS analysis of amino acids. *Journal of Separation Science*, *26*(17), 1474–1478. <https://doi.org/10.1002/jssc.200301492>

- Styring, A., Fraser, R., Arbogast, R., Halstead, P., Isaakidou, V., Pearson, J., Schäfer, M., Triantaphyllou, S., Valamoti, S., Wallace, M., Bogaard, A., & Evershed, R. (2015). Refining human palaeodietary reconstruction using amino acid $\delta^{15}\text{N}$ values of plants, animals and humans. *Journal of Archaeological Science*, *53*, 504–515.
- Sun, Y., Ishikawa, N., Ogawa, N., Kawahata, H., Takano, Y., & Naohiko, O. (2020). A method for stable carbon isotope measurement of underivatized individual amino acids by multi-dimensional high-performance liquid chromatography and elemental analyzer/isotope ratio mass spectrometry. *Rapid Communications in Mass Spectrometry*, *34*, e8885.
- Swailethorp, R., Aluwihare, L., Thompson, A., Ohman, M., & Landry, M. (2020). Errors associated with compound-specific $\delta^{15}\text{N}$ analysis of amino acids in preserved fish samples purified by high-pressure liquid chromatography. *Limnology and Oceanography: Methods*, *18*, 259–270.
- Takano, Y., Chikaraishi, Y., Ogawa, N., Kitazato, H., & Ohkouchi, N. (2009). Compound-specific nitrogen isotope analysis of D-alanine, L-alanine, and valine: application of diastereomer separation to $\delta^{15}\text{N}$ and microbial peptidoglycan studies. *Analytical Chemistry*, *81*, 394–399.
- Takano, Y., Kashiya, Y., Ogawa, N. O., Chikaraishi, Y., & Ohkouchi, N. (2010). Isolation and desalting with cation-exchange chromatography for compound-specific nitrogen isotope analysis of amino acids: application to biogeochemical samples. *Rapid Communications in Mass Spectrometry*, *24*, 2317–2323. <https://doi.org/10.1002/rcm.4651>
- Tea, I., & Tcherkez, G. (2017). Natural isotope abundance in metabolites: techniques and kinetic isotope effect measurement in plant, animal, and human tissues. In M. E. Harris & V. E. Anderson (Eds.), *Measurement and Analysis of Kinetic Isotope Effects* (1st ed., pp. 113–147, Vol. 596). Elsevier Inc. <https://doi.org/10.1016/bs.mie.2017.07.020>
- Tobias, H. J., Sacks, G. L., Zhang, Y., & Brenna, J. T. (2008). Comprehensive two-dimensional gas chromatography combustion isotope ratio mass spectrometry. *Analytical Chemistry*, *80*(22), 8613–8621. <https://doi.org/10.1021/ac801511d>
- Tobias, H. J., Zhang, Y., Auchus, R. J., & Brenna, J. T. (2011). Detection of synthetic testosterone use by novel comprehensive two-dimensional gas chromatography combustion-isotope ratio mass spectrometry. *Analytical Chemistry*, *83*(18), 7158–7165. <https://doi.org/10.1021/ac2015849>
- Tripp, J. A., McCullagh, J. S., & Hedges, R. E. (2006). Preparative separation of underivatized amino acids for compound-specific stable isotope analysis and radiocarbon dating of hydrolyzed bone collagen. *Journal of Separation Science*, *29*(1), 41–48. <https://doi.org/10.1002/jssc.200500247>

- Tristram, G. R. (1939). The basic amino-acids of leaf proteins. With a discussion of various methods of analysis. *Biochemical Journal*, 33(8), 1271–1283. <https://doi.org/10.1042/bj0331271>
- Tsugita, A., Uchida, T., Mewes, H. W., & Ataka, T. (1987). A rapid vapor-phase acid (hydrochloric acid and trifluoroacetic acid) hydrolysis of peptide and protein. *Journal of Biochemistry*, 102, 1593–1597. <https://academic.oup.com/jb/article-abstract/102/6/1593/818176>
- Tuckey, R., & Stevenson, P. (1979). Methanolysis of cholesteryl esters: conditions for quantitative preparation of methyl esters. *Analytical Biochemistry*, 94, 402–408.
- Tuross, N., Fogel, M. L., & Hare, P. E. (1988). Variability in the preservation of the isotopic composition of collagen from fossil bone. *Geochimica et Cosmochimica Acta*, 52(4), 929–935. [https://doi.org/10.1016/0016-7037\(88\)90364-X](https://doi.org/10.1016/0016-7037(88)90364-X)
- Unger, N., & Holzgrabe, U. (2018). Stability and assessment of amino acids in parenteral nutrition solutions. *Journal of Pharmaceutical and Biomedical Analysis*, 147, 125–139. <https://doi.org/10.1016/j.jpba.2017.07.064>
- Urey, H. C. (1948). Oxygen isotopes in nature in the laboratory. *Science*, 108, 489–496.
- Vallet, C., Arendt, M., Mabon, F., Naulet, N., & Martin, G. J. (1991). Combination of mass spectrometry and site-specific NMR isotope analyses in the characterisation of amino acids. *Journal of the Science of Food and Agriculture*, 56(2), 167–185. <https://doi.org/10.1002/jsfa.2740560207>
- Veuger, B., Middelburg, J. J., Boschker, H. T., & Houtekamer, M. (2005). Analysis of ¹⁵N incorporation into D-alanine: A new method for tracing nitrogen uptake by bacteria. *Limnology and Oceanography: Methods*, 3(5), 230–240. <https://doi.org/10.4319/lom.2005.3.230>
- Walsh, R. G., He, S., & Yarnes, C. T. (2014). Compound-specific $\delta^{13}\text{C}$ and $\delta^{15}\text{N}$ analysis of amino acids: a rapid, chloroformate-based method for ecological studies. *Rapid Communications in Mass Spectrometry*, 28(1), 96–108. <https://doi.org/10.1002/rcm.6761>
- Wang, W., Scali, M., Vignani, R., Spadafora, A., Sensi, E., Mazzuca, S., & Cresti, M. (2003). Protein extraction for two-dimensional electrophoresis from olive leaf, a plant tissue containing high levels of interfering compounds. *Electrophoresis*, 24(14), 2369–2375. <https://doi.org/10.1002/elps.200305500>
- Weiss, M., Manneberg, M., Juranville, J.-F., Lahm, H.-W., & Fountoulakis, M. (1998). Effect of the hydrolysis method on the determination of the amino acid composition of proteins. *Journal of Chromatography A*, 795, 263–275.

- Whiteman, J. P., Smith, E. A., Besser, A. C., & Newsome, S. D. (2019). A guide to using compound-specific stable isotope analysis to study the fates of molecules in organisms and ecosystems. *Diversity*, *11*(1), 8. <https://doi.org/10.3390/d11010008>
- Wilkes, E., Sessions, A. L., Dallas, B., Yashiro, H., & Eiler, J. M. (2019). Position-specific isotope analysis of serine by GC Orbitrap mass spectrometry. *Abstract B43D-04. American Geophysical Union Fall Meeting, San Francisco.*
- Wolyniak, C., Sacks, G., Pan, B., & Brenna, J. (2005). Carbon position-specific isotope analysis of alanine and phenylalanine analogues exhibiting nonideal pyrolytic fragmentation. *Analytical Chemistry*, *77*, 1746–1752.
- Wright, H. T. (1991). Nonenzymatic deamidation of asparaginy and glutaminy residues in proteins. *Critical Reviews in Biochemistry and Molecular Biology*, *26*(1), 1–52.
- Yamaguchi, Y., & McCarthy, M. (2018). Sources and transformation of dissolved and particulate organic nitrogen in the North Pacific Subtropical Gyre indicated by compound-specific $\delta^{15}\text{N}$ analysis of amino acids. *Geochimica et Cosmochimica Acta*, *220*, 329–347.
- Yarnes, C. T., & Herszage, J. (2017). The relative influence of derivatization and normalization procedures on the compound-specific stable isotope analysis of nitrogen in amino acids. *Rapid Communications in Mass Spectrometry*, *31*(8), 693–704. <https://doi.org/10.1002/rcm.7832>
- Zaikin, V. G., & Halket, J. M. (2005). Derivatization in mass spectrometry - 6. Formation of mixed derivatives of polyfunctional compounds. *European Journal of Mass Spectrometry*, *11*(6), 611–636. <https://doi.org/10.1255/ejms.773>
- Zampolli, M. G., Basaglia, G., Dondi, F., Sternberg, R., Szopa, C., & Pietrogrande, M. C. (2007). Gas chromatography-mass spectrometry analysis of amino acid enantiomers as methyl chloroformate derivatives: application to space analysis. *Journal of Chromatography A*, *1150*(1-2), 162–172. <https://doi.org/10.1016/j.chroma.2006.12.033>
- Zhang, L., Lee, W.-m., Kreider-Mueller, A., Kuhnelt, E., Baca, J., Ji, C., & Altabet, M. (2021). High-precision measurement of phenylalanine and glutamic acid $\delta^{15}\text{N}$ by coupling ion-exchange chromatography and purge-and-trap continuous-flow isotope ratio mass spectrometry. *Rapid Communications in Mass Spectrometry*, *35*, e9085.
- Zhang, P., Chan, W., Ang, I. L., Wei, R., Lam, M. M., Lei, K. M., & Poon, T. C. (2019). Revisiting Fragmentation Reactions of Protonated α -Amino Acids by High-Resolution Electrospray Ionization Tandem Mass Spectrometry with Collision-Induced Dissociation. *Scientific Reports*, *9*(1), 1–10. <https://doi.org/10.1038/s41598-019-42777-8>

Chapter 3

Biosynthetic and catabolic pathways control amino acid $\delta^2\text{H}$ values in aerobic heterotrophs

Silverman, S. N., Wijker, R. S., & Sessions, A. L. (2024). Biosynthetic and catabolic pathways control amino acid $\delta^2\text{H}$ values in aerobic heterotrophs. *Frontiers in Microbiology*, 15, 1–20. <https://doi.org/10.3389/fmicb.2024.1338486>

Abstract

The hydrogen isotope ratios ($\delta^2\text{H}_{\text{AA}}$ values) of amino acids in all organisms are substantially fractionated relative to growth water. In addition, they exhibit large variations within microbial biomass, animals, and human tissues, hinting at rich biochemical information encoded in such signals. In lipids, such $\delta^2\text{H}$ variations are thought to primarily reflect NADPH metabolism. Analogous biochemical controls for amino acids remain largely unknown, but must be elucidated to inform the interpretation of these measurements. Here, we measured the $\delta^2\text{H}$ values of amino acids from five aerobic, heterotrophic microbes grown on different carbon substrates, as well as five *Escherichia coli* mutant organisms with perturbed NADPH metabolisms. We observed similar $\delta^2\text{H}_{\text{AA}}$ patterns across all organisms and growth conditions, which—consistent with previous hypotheses—suggests a first-order control by biosynthetic pathways. Moreover, $\delta^2\text{H}_{\text{AA}}$ values varied systematically with the catabolic pathways activated for substrate degradation, with variations explainable by the isotopic compositions of important cellular metabolites, including pyruvate and NADPH, during growth on each substrate. As such, amino acid $\delta^2\text{H}$

values may be useful for interrogating organismal physiology and metabolism in the environment, provided we can further elucidate the mechanisms underpinning these signals.

3.1 Introduction

Stable hydrogen isotope analysis of amino acids ($\delta^2\text{H}_{\text{AA}}$) is receiving growing attention due to its potential utility as a tracer of ecological and/or physiological processes, as well as the extreme fractionations recorded in laboratory-grown and natural organisms. In the first published study on terrestrial $\delta^2\text{H}_{\text{AA}}$ values, Fogel et al. (2016) discovered large ($>100\%$) variations in $\delta^2\text{H}_{\text{AA}}$ values in *Escherichia coli* cultured on glucose or tryptone (a complex protein source) in different growth waters, with two key insights emerging from their study: (1) patterns of $\delta^2\text{H}_{\text{AA}}$ values may be driven by ubiquitous biochemical mechanisms associated with amino acid synthesis in organisms, and (2) hydrogen can be directly routed from organic substrates, or incorporated from water via *de novo* amino acid synthesis, to variable extents depending on the protein content of the medium. Expanding this work to an animal model, Newsome et al. (2020) observed that hydrogen sources of amino acids in mouse muscle tissue are driven by similar metabolic factors as *E. coli*, but that carbohydrates and amino acids from both the diet and gut microbiome are particularly important hydrogen sources. Recently, Gharibi, Chernobrovkin, Eriksson, et al. (2022) reported extreme ^2H -enrichments in proline and hydroxyproline ($\delta^2\text{H}$ values $>1,000\%$) from seal bone collagen, although the cause of these extreme $\delta^2\text{H}$ values was not identified. (D. A. Smith et al., 2022) ruled out growth rate as a primary control on $\delta^2\text{H}_{\text{AA}}$ values in *E. coli* and revealed that carbon and hydrogen isotope compositions of amino acids are governed by different biochemical factors. Drawing on the well-known spatial variations in precipitation

isotope ratios (Craig, 1961; Dansgaard, 1964; Kendall & Coplen, 2001; Poage & Chamberlain, 2001; Rozanski et al., 1993), Mancuso et al. (2023) revealed the first systematic link between $\delta^2\text{H}_{\text{AA}}$ values in human tissue (scalp hair) and local water $\delta^2\text{H}$, supporting the utility of this compound-specific tool as a potential tracer of geographical origin (Bowen et al., 2005; Rubenstein & Hobson, 2004). Together, these results encourage a variety of potential exciting applications of $\delta^2\text{H}_{\text{AA}}$ analysis across diverse fields such as ecology, archaeology, microbiology, biogeochemistry, and forensics. However, these applications are limited by our lack of fundamental understanding of which biochemical controls set $\delta^2\text{H}_{\text{AA}}$ values in terrestrial organisms.

Here we seek to elucidate some of the mechanistic controls on biological $\delta^2\text{H}_{\text{AA}}$ values. We focus on microbes, which are simpler systems than animals because most microbes are unicellular, can synthesize all 20 amino acids (Price et al., 2018), and can be grown in defined media. Furthermore, microbes are the major drivers of biogeochemical processes such as energy and nutrient cycling in the environment (Falkowski et al., 2008), so understanding how their $\delta^2\text{H}_{\text{AA}}$ values relate to their metabolic activities may render $\delta^2\text{H}_{\text{AA}}$ analysis a useful tool for interrogating the critical microbial-driven changes to our planet's surface geochemistry. Amino acids are formed via biosynthetic pathways that are ubiquitous across most forms of life. Their carbon skeleton precursors are the intermediates of central metabolic pathways (Figure 3.1), and the hydrogen on each amino acid is derived from different combinations of sources, including the organic precursors, water, and NAD(P)H. As such, $\delta^2\text{H}_{\text{AA}}$ values are complicated to interpret, but may contain multiple layers of useful biochemical information.

In this study, we investigated the $\delta^2\text{H}$ values of amino acids from the biomass of five aerobic, heterotrophic bacteria that was previously generated for lipid $\delta^2\text{H}$ analysis (Wijker et al., 2019). The organisms included *E. coli*, *Bacillus subtilis*,

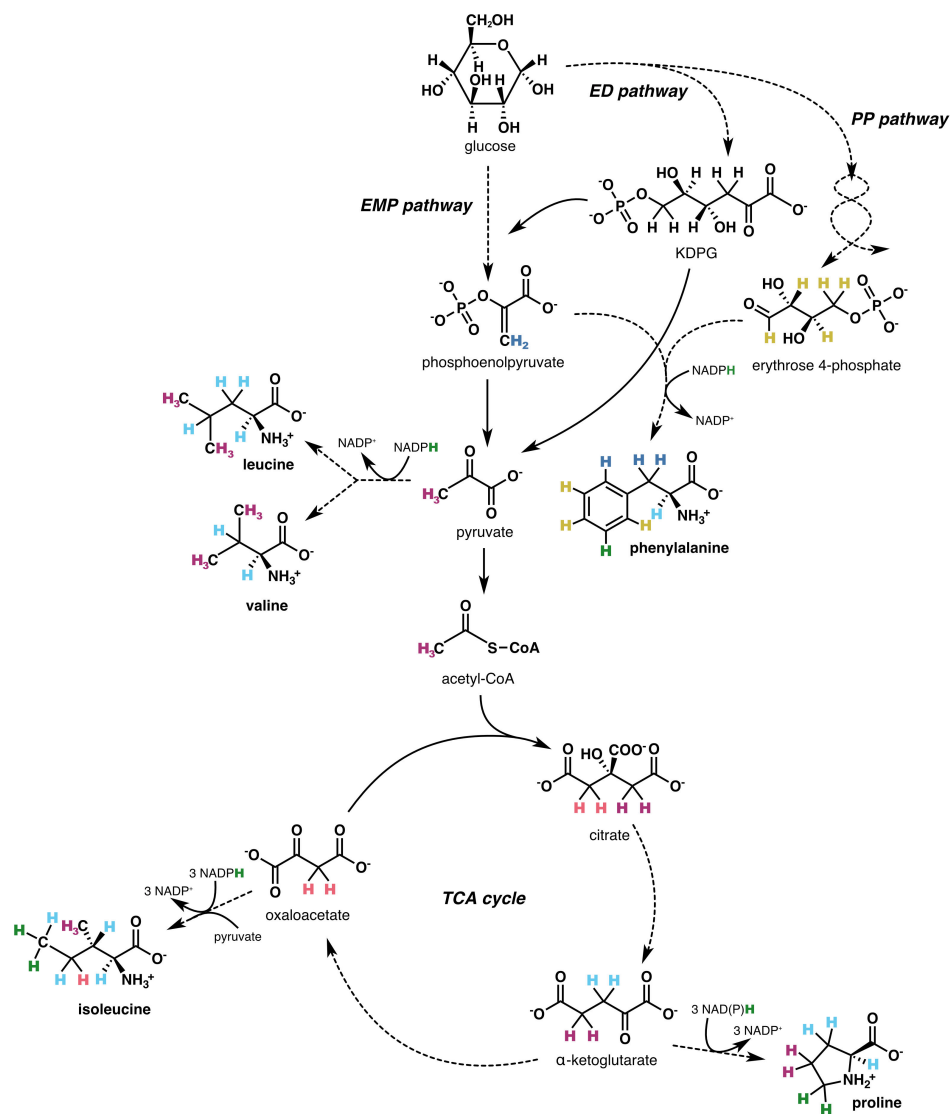


Figure 3.1. Simplified schematic of biosynthetic pathways (showing end-member compounds), central metabolic pathway precursors, and hydrogen sources for the five amino acids investigated in this study (proline, phenylalanine, leucine, valine, isoleucine). Hydrogen atoms are visually tracked from source to amino acid through colors: green indicates hydrogen from NAD(P)H, light blue from water, and the remaining colors correspond to hydrogen from organic precursors. Solid arrows denote single metabolic reactions; dashed arrows encompass multiple steps. Although NAD(P)H is used to reduce substrates in all amino acid biosynthetic pathways, some NAD(P)H-derived hydrogen is subsequently lost due to elimination or equilibration with water (see detailed biosynthetic pathways in Supplementary Figures B.16–B.19). EMP, Embden-Meyerhof-Parnas; ED, Entner-Doudoroff; PP, pentose phosphate; TCA, tricarboxylic acid.

Ensifer meliloti, *Pseudomonas fluorescens*, and *Rhizobium radiobacter*, as well as five mutant *E. coli* organisms lacking specific dehydrogenase or transhydrogenase enzymes. These organisms were grown on different carbon substrates, including on glucose for which their metabolic fluxes were characterized (Wijker et al., 2019), enabling investigation of the mechanistic link between $\delta^2\text{H}_{\text{AA}}$ values and microbial metabolism. This experimental system provides the opportunity to test a number of hypotheses about the mechanisms that govern amino acid $\delta^2\text{H}$ values, including whether NADPH metabolism is a primary control (the case for lipids; Wijker et al., 2019; Zhang et al., 2009), and how varied fluxes through specific enzymes in central metabolism affect $\delta^2\text{H}_{\text{AA}}$ values. We targeted five amino acids—proline, phenylalanine, leucine, valine, and isoleucine—which were selected because (1) they span different parts of central metabolism (Figure 3.1), and (2) their hydrogen isotope compositions are among the most reliable to interpret, as these amino acids exhibit consistent baseline chromatographic separation (Supplementary Figure B.1), have relatively high ionization efficiencies, and maintain stable hydrogen isotope compositions through hydrolysis and derivatization (Supplementary Figures B.9, B.10; Supplementary Table B.4; Silverman et al., 2022; for further details, see Supplementary Section B.1). We provide hypotheses for the observed $\delta^2\text{H}_{\text{AA}}$ patterns within and across organisms cultured under different conditions. As such, we aim to elucidate the underlying mechanisms that control $^2\text{H}/^1\text{H}$ fractionation in these five amino acids.

Additionally, $\delta^2\text{H}_{\text{AA}}$ analyses to-date have been hampered by the presence of “labile” organic hydrogen in the amine ($-\text{NH}_2$) and carboxyl ($-\text{COOH}$) groups, which readily exchange with hydrogen in both water and ambient water vapor. Derivatization of amino acids removes the carboxyl- and one amine-bound hydrogen, but the remaining amine hydrogen cannot be excluded from the measured isotopic composition, and may dilute or obscure biological signals (i.e., those of

non-exchangeable, C- bound hydrogen in the amino acids) and furthermore lead to incomparable results across laboratories. Previous studies (Fogel et al., 2016; Mancuso et al., 2023; Newsome et al., 2020; D. A. Smith et al., 2022) have attempted to correct for the contribution of derivative and exchangeable hydrogen to measured $\delta^2\text{H}_{\text{AA}}$ values through the use of amino acid standards, whereby the $\delta^2\text{H}$ values of underivatized amino acid powders pre-equilibrated with ambient water vapor (following the comparative equilibration method; Wassenaar and Hobson, 2003) are measured via a high-temperature conversion elemental analyzer coupled to an isotope ratio mass spectrometer, then subtracted via mass balance from the $\delta^2\text{H}$ values of corresponding derivatized amino acids. The central issue with this approach is that hydrogen in the derivative reagents, derivatized amino acids, and underivatized amino acids cannot be mass balanced, as (1) the isotopic fractionations between the exchangeable hydrogen and water (or ambient moisture) are unknown, thus the $\delta^2\text{H}$ values of the carboxyl and amine hydrogen atoms removed during derivatization cannot be properly accounted for, and (2) the isotopic fractionation between the amine-bound hydrogen and water likely differs when amino acids are in derivatized (possessing a secondary amine) versus underivatized (primary amine) form, so knowledge of the amine hydrogen $\delta^2\text{H}$ value in the latter case may not help correct for exchangeable hydrogen in the former case. Independent measurements of the derivative reagent $\delta^2\text{H}$ values are possible in some cases, but without accompanying correction for the amine-bound hydrogen in derivatized amino acids, errors in the reported $\delta^2\text{H}$ values of amino acid carbon-bound hydrogen may be significant (on the order of 10 to 100‰; Supplementary Figure B.7; Supplementary Section B.4). Here we have developed a new, simple procedure for controlling this exchangeable amine-bound hydrogen based on separate oxidation and derivatization of a diamine compound to obtain the combined $\delta^2\text{H}$ value of our amine group derivative and the exchangeable hydrogen. By subtracting the iso-

topic contribution of both the derivative hydrogen and exchangeable amine-bound hydrogen, we are able to accurately calculate the $\delta^2\text{H}$ value of pure carbon-bound hydrogen in amino acids.

3.2 Materials and methods

3.2.1 Strain and culture conditions

The microbial biomass measured here was generated in a prior study targeting lipid $\delta^2\text{H}$ analysis (Wijker et al., 2019); all relevant culturing details are recapitulated here. Five wildtype aerobic heterotrophic microbes (*Escherichia coli* MG1655, *Bacillus subtilis* PY79, *Ensifer meliloti* Young 2003, *Pseudomonas fluorescens* 2-79, and *Rhizobium radiobacter* C58) and five mutant *E. coli* organisms carrying specific deletions of dehydrogenase or transhydrogenase genes (glucose 6-phosphate dehydrogenase deleted in JW1841, phosphoglucose isomerase deleted in JW3985, membrane-bound transhydrogenase deleted in PntAB, soluble transhydrogenase deleted in UdhA, and both transhydrogenases deleted in UdhA- PntAB) were cultured on unlabeled glucose for hydrogen isotope analysis, and on ^{13}C -labeled glucose (100% 1- ^{13}C -glucose and a mixture of 20% (wt/wt) U- $^{13}\text{C}_6$ -glucose + 80% (wt/wt) unlabeled glucose) for metabolic flux analysis. The relative metabolic fluxes were calculated based on the ^{13}C -labeling pattern of proteinogenic amino acids—see Wijker et al. (2019) for more details. Wild-type organisms were additionally cultured on acetate, citrate, fructose, pyruvate, and/or succinate in an isotopically constant growth water; as well as on glucose in growth waters with different isotopic compositions, which were manipulated by adding specific volumes of 99.9% purity D_2O to distilled, deionized water. Each organism was grown with 4 g/L of carbon source in M9 minimal medium (pre-

pared as described in Fuhrer et al., 2005) in batch culture on a rotary shaker at 200 rpm, thereby ensuring aerobic conditions were maintained and fermentation was avoided throughout the course of the experiments. The carbon source served as the limiting nutrient in each culture, causing cells to transition to stationary growth phase upon depletion. *B. subtilis* and *R. radiobacter* cultures were supplemented with a vitamin mixture, while strains JW1841 and JW3985 were given 50 µg/mL of kanamycin. *B. subtilis* and *E. coli* cultures were incubated at 37°C; all other organisms were incubated at 30°C. All wildtype cultures were prepared in duplicate except for organisms grown in D₂O-spiked media (for growth water experiments) and for *E. coli*, which was grown on pyruvate and acetate in single cultures, and on glucose in two non-replicate cultures: culture 1 was grown along with the rest of the wildtype organisms, *E. coli* mutants, and growth water experiments for non-*E. coli* organisms; culture 2 was grown at a later date as one of four cultures in *E. coli* growth water experiments. Although culturing conditions were identical between *E. coli* cultures 1 and 2 grown on glucose, the different timing of culturing, and different methods used to process the biomass (see Section 3.2.2), renders culture 2 a repeat experiment, but not true biological replicate, to culture 1. Culture growth was monitored by measuring optical density at 600 nm (OD₆₀₀), and cells were harvested in late-exponential phase, lyophilized, and stored at -80°C until further processing for lipid and amino acid $\delta^2\text{H}$ analysis (Wijker et al., 2019 and this study, respectively).

3.2.2 Amino acid hydrolysis, derivatization, extraction, and quantification

A 10–20 mg of dry biomass from each sample was hydrolyzed anoxically in 6N HCl at 110°C for 24h in tightly capped VOA vials. Following hydrolysis, samples were

uncapped and left on the hot plates until the 6N HCl was completely evaporated, then samples were resuspended in 0.5 ml of 0.1N HCl. Amino acids in all samples except *E. coli* culture 2 were derivatized with 7:6:3 (v/v/v) anhydrous methanol (MeOH), pyridine, and methyl chloroformate (MCF); reagents were added at room temperature, then samples were immediately capped and sonicated for ~5 min (procedure adapted from Hušek, 1991a, 1991b and Zampolli et al., 2007). *E. coli* culture 2 was derivatized with the same reagent bottles and reaction procedure as the other samples, but was placed on dry ice while derivative reagents were added to slow the derivatization reaction. Note that in contrast to most published $\delta^2\text{H}_{\text{AA}}$ studies (Fogel et al., 2016; Mancuso et al., 2023; Newsome et al., 2020; D. A. Smith et al., 2022), we avoid using fluorinated derivative reagents, as hydrofluoric acid can form during pyrolysis in the gas chromatograph/isotope ratio mass spectrometer (GC/IRMS), leading to potential hydrogen isotope fractionation (Renpenning et al., 2017; P. E. Sauer et al., 2001; Silverman et al., 2022).

The resulting methoxycarbonyl (MOC) esters (Figure 3.2A) were extracted twice with methyl *tert*-butyl ether (MTBE) and filtered through a sodium sulfate column to adsorb any water present. Samples were concentrated to ~0.25–0.5 ml under N_2 . MOC ester peaks were identified via gas chromatography/mass spectrometry (GC/MS) on a Thermo-Scientific Trace ISQ equipped with a Zebron ZB-5 ms column (30-m \times 0.25-mm i.d., 0.25 μm film thickness) and programmable temperature vaporizing (PTV) injector operated in splitless mode, using He as a carrier gas (flow rate = 1.4 ml/min). The GC oven was held at 80°C for 1 min, ramped at 5°C/min to 280°C with no hold, then ramped at 20°C/min to 310°C with a final 5 min temperature hold. Peaks were identified by comparing the relative retention times and mass spectra to those of known MOC ester standards, as well as to mass spectra in the NIST MS Library database.

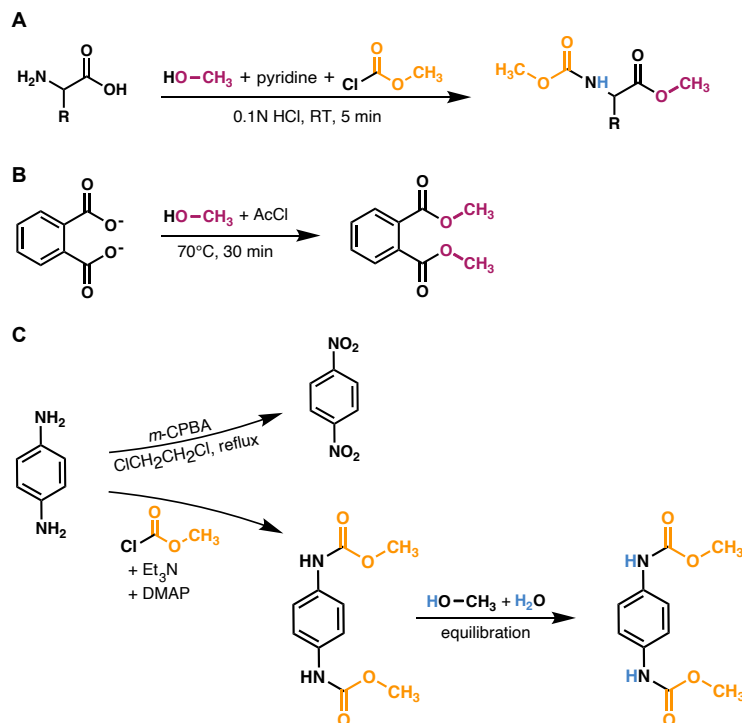


Figure 3.2. Derivatization scheme for amino acids and methods used to measure $\delta^2\text{H}$ values of derivative reagents. **(A)** Amino acids were derivatized with anhydrous methanol, pyridine, and methyl chloroformate in 0.1N HCl; see Section 3.2.2 for details. The exchangeable amine hydrogen atom (blue in derivatized product) was equilibrated in the solvent (0.1N HCl), which was prepared using the same water supply as that used to equilibrate the N-bound hydrogen in the dimethyl 1,4-phenylenedicarbamate product [DCP; depicted in **C**]. **(B)** The $\delta^2\text{H}$ value of anhydrous methanol was measured by derivatizing disodium phthalate with known isotopic composition (Sessions et al., 2002) with anhydrous methanol in acetyl chloride (AcCl); see Section 3.2.5 for details. **(C)** The $\delta^2\text{H}$ value of methyl chloroformate was measured by first oxidizing *p*-phenylenediamine (PPD) to dinitrobenzene (DNB) to obtain the aromatic hydrogen $\delta^2\text{H}$ value (top reaction), then separately derivatizing PPD with methyl chloroformate to produce the DCP (bottom reaction). DCP was purified, then dissolved in a 1:1 (v/v) mixture of anhydrous methanol:water to equilibrate the N-bound hydrogen atoms before extraction and measurement via GC/P/IRMS. See Section 3.2.5 for details.

3.2.3 Isotope analysis

The $\delta^2\text{H}$ values of MOC esters were measured by a gas chromatograph coupled to an isotope ratio mass spectrometer (Thermo Finnigan Delta⁺XP) using a pyrolysis interface (i.e., GC/P/IRMS). Chromatographic separation was achieved on a thick-film Zebron ZB-5ms column (30-m \times 0.25-mm i.d., 1.00 μm film thickness) with a nearly identical chromatographic method as used in GC/MS analysis [exceptions included a higher carrier gas flow rate (1.7 ml/min) and slight modifications to the temperature program to optimize MOC ester separation] so peaks could be identified by retention order and relative height. Measured isotope ratios were calibrated using hydrogen gas of known isotopic composition and are reported in δ notation (in units of ‰, or parts per thousand; McKinney et al., 1950; Urey, 1948) relative to the Vienna Standard Mean Ocean Water (VSMOW) international standard ($\delta^2\text{H} = R_{\text{AA}}/R_{\text{VSMOW}} - 1$), where $R = {}^2\text{H}/{}^1\text{H}$. Additionally, an eight-compound fatty acid methyl ester standard mixture was analyzed between every 5–6 samples to verify instrument accuracy and precision. Samples were analyzed in triplicate, and the MOC ester $\delta^2\text{H}$ values were corrected for the addition of methyl hydrogen from the derivative reagents, as well as for the remaining exchangeable amine hydrogen (see Section 3.2.5). The standard deviation of triplicate analyses for individual amino acids was typically $\leq 6\text{‰}$. The average root-mean-square error of the external FAME standard was 3.2‰ across all analyses. $\delta^2\text{H}$ values of the culture media ($\delta^2\text{H}_w$) were measured previously using a Los Gatos Research DLT-100 liquid water isotope analyzer and calibrated against up to four working standards with $\delta^2\text{H}$ values ranging from -73 to $+458\text{‰}$ (Wijker et al., 2019). Data are reported as apparent fractionations between amino acids (AA) and culture medium water (w) according to the equation ${}^2\varepsilon_{\text{AA}/w} = (\delta^2\text{H}_{\text{AA}} + 1)/(\delta^2\text{H}_w + 1) - 1$, with uncertainty propagated as Equation 3.1

$$\sigma_{\varepsilon} = \left(\frac{\delta^2\text{H}_{\text{AA}} + 1}{\delta^2\text{H}_w + 1} \right) \sqrt{\left(\frac{\sigma_{\text{AA}}}{\delta^2\text{H}_{\text{AA}} + 1} \right)^2 + \left(\frac{\sigma_w}{\delta^2\text{H}_w + 1} \right)^2} \quad (3.1)$$

3.2.4 Hydrolysis and derivatization tests for isotopic alteration

Potential changes in amino acid isotopic compositions during acid hydrolysis were investigated by varying the hydrolysis conditions used (temperature, duration, and O₂ presence). For a control treatment, standard bovine serum albumin (BSA) was hydrolyzed in 6N HCl for 24h at 110°C under anoxic conditions (achieved by sparging samples with N₂ for 2 min with vigorous shaking). Variations on these conditions were achieved by either hydrolyzing BSA (1) without sparging with N₂ (oxic hydrolysis), (2) at 105°C, or (3) for 20 or 48h. All conditions were prepared in duplicate. Amino acids were derivatized to MOC esters, extracted, and analyzed via GC/P/IRMS using methods described in Sections 3.2.2, 3.2.3.

Additionally, to test for hydrogen isotope exchange with aqueous medium during hydrolysis and derivatization (Fogel et al., 2016; Hill & Leach, 1964; Silverman et al., 2022), BSA and a mixture of pure amino acid standards were separately hydrolyzed (6N HCl, 24h, 110°C, oxic) and derivatized (0.1N HCl, 7:2:3 v/v/v anhydrous MeOH, pyridine, MCF) in aqueous solvent with different hydrogen isotope compositions.

3.2.5 Correction for derivative and exchangeable amine hydrogen

To determine the $\delta^2\text{H}$ value of MeOH, 100 μg of disodium phthalate with known isotopic composition (Sessions et al., 2002) was derivatized in 2 ml of 20:1

(v/v) anhydrous MeOH:acetyl chloride (70°C, 30 min; Figure 3.2B). The derivatized product was extracted with 4 ml of 1:1 water:hexane, then measured by GC/P/IRMS, and contribution of disodium phthalate hydrogen was subtracted by mass balance.

The combined $\delta^2\text{H}$ value of MCF and the remaining exchangeable amine hydrogen was characterized via derivatization of *p*-phenylenediamine (PPD)—a compound with two primary amine groups—with MCF and separate oxidation of PPD to dinitrobenzene (DNB), which has no nitrogen-bound hydrogen. One hundred mM of PPD was dissolved in 5 ml of anoxic dichloromethane with 3 Equation triethylamine (pre-distilled with CaH_2 to remove any HCl generated in the reaction) and 0.1 Equation 4-dimethylamino pyridine, and was subsequently derivatized via an overnight reaction with 2.5 Equation MCF to yield dimethyl 1,4- phenylenedicarbamate (hereafter, “dicarbamate product”, or DCP in Equation 3.2; Figure 3.2C). The DCP was purified via flash column chromatography with silica gel. Five mg of DCP was dissolved in 2 ml of anhydrous MeOH, then 2 ml of distilled, deionized water was slowly added. The solution was mixed on a shaker for 2h to ensure complete equilibration of the two amine hydrogen atoms with water, then the DCP was extracted once with 4 ml MTBE, filtered through a sodium sulfate column, and analyzed by GC/P/IRMS. In a separate reaction, PPD was oxidized to DNB using 8 Equation of *m*-chloroperbenzoic acid added under refluxing 1,2-dichloroethane in a procedure adapted from Liu et al. (2014) (Figure 3.2C). DNB was purified via flash column chromatography with silica gel, then 3 mg of DNB was dissolved in MTBE and analyzed via GC/P/IRMS. The $\delta^2\text{H}$ value of MCF and the exchangeable nitrogen-bound hydrogen (MCF+NH) was obtained by solving for $F_{\text{MCF+NH}}$ in the mass balance equation

$$12F_{\text{DCP}} = 8F_{\text{MCF+NH}} + 4F_{\text{DNB}} \quad (3.2)$$

where F is the fractional abundance (i.e., mole fraction) of ^2H in each compound. PPD was chosen for these reactions (1) because of the favorable 8/4 ratio of (MCF + amine)/aromatic hydrogen in the dicarbamate product, and (2) because the exchangeable amine hydrogen atoms on the dicarbamate product and on MOC esters should have similar hydrogen isotope compositions when equilibrated in the same water supply, as the amine hydrogen in the dicarbamate product and in MOC esters share similar intramolecular bonding environments so should be controlled by similar equilibrium $^2\text{H}/^1\text{H}$ fractionation factors at a constant temperature (Wang et al., 2009).

3.3 Results

3.3.1 Derivative correction

Hydrogen atoms on amine and carboxyl groups rapidly exchange with water so do not contribute information about native $\delta^2\text{H}_{\text{AA}}$ values. Derivatization of the carboxyl group removes the exchangeable hydrogen, but derivatization of the amine group removes only one of the two exchangeable hydrogen atoms (Figure 3.2A). In order to determine the isotope compositions of the native, non-exchangeable (i.e., carbon-bound) hydrogen on the amino acids, it is necessary to correct $\delta^2\text{H}_{\text{AA}}$ values not only for the added derivative (MeOH and MCF) hydrogen, but also for the exchangeable amine hydrogen atom remaining after derivatization. A suitable method for this latter correction has eluded prior studies of $\delta^2\text{H}_{\text{AA}}$ thus far, yet is imperative, as errors in reported $\delta^2\text{H}_{\text{AA}}$ values can be on the order of 10 to 100‰ when the amine-bound hydrogen is improperly accounted for (Supplementary Figure B.7; Supplementary Section B.4). Here we developed a method to characterize the combined $\delta^2\text{H}$ values of MCF and the exchangeable amine hy-

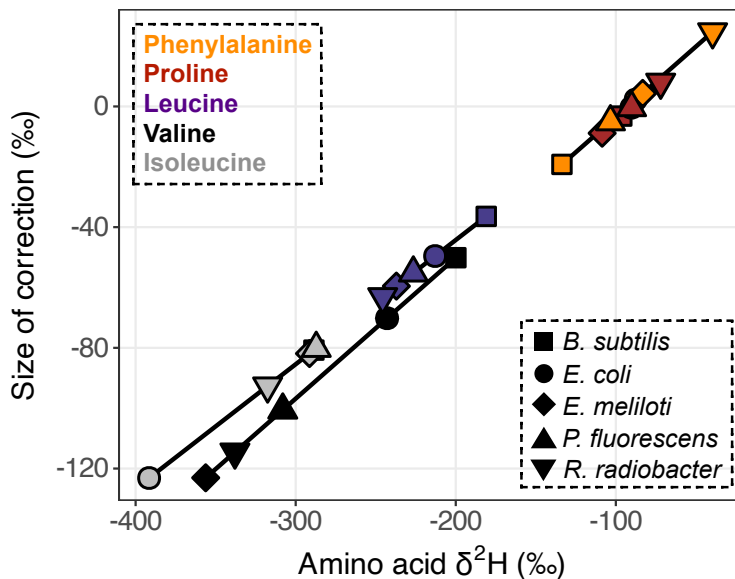


Figure 3.3. Size of derivative $\delta^2\text{H}$ corrections versus native amino acid isotopic compositions. Measured $\delta^2\text{H}_{\text{AA}}$ values were corrected for derivative and exchangeable amine hydrogen contributions ($\delta^2\text{H}_{\text{MeOH}} = -67.27 \pm 1.78\text{‰}$, $\delta^2\text{H}_{\text{MCF+NH}} = -111.43 \pm 1.96\text{‰}$). Data displayed are from one replicate of wildtype organisms grown on glucose (shapes denote organisms as defined in the lower right legend). Amino acids are denoted by colors (upper left legend) and corresponding symbols are connected to highlight compound-specific magnitudes of correction effects. Horizontal error bars (indicating the propagated uncertainties ($\pm 1\sigma$) from the amino acid and derivative measurements) are smaller than symbols.

drogen by derivatizing PPD with MCF, separately oxidizing PPD to DNB (which removes all four of the nitrogen-bound hydrogens; Figure 3.2C), and analyzing both resulting products using GC/P/IRMS. Importantly, this approach requires derivatizing samples with the same reagents and water as those used to measure PPD.

The $\delta^2\text{H}$ value of the MCF + amine hydrogen was $-111.43 \pm 1.96\text{‰}$ when equilibrated with water of $\delta^2\text{H} = -86.50 \pm 0.36\text{‰}$. The $\delta^2\text{H}$ value of MeOH was $-67.27 \pm 1.78\text{‰}$. Correction for these non-biological contributions generally shifted $\delta^2\text{H}_{\text{AA}}$ values lower (Figure 3.3). For the relatively ^2H -depleted amino acids (leucine, valine, and isoleucine), changes in $\delta^2\text{H}$ values were substantial, reaching up to 123‰

for wildtype organisms grown on glucose. For the relatively ^2H -enriched amino acids (proline and phenylalanine), this correction resulted in small or negligible changes, but in some cases resulted in higher $\delta^2\text{H}$ values. However, note that correction of proline $\delta^2\text{H}$ values using this approach may introduce small ($<20\text{‰}$) errors, as proline does not contain amine-bound hydrogen after derivatization, but the isotopic composition of MCF cannot be isolated from our measured $\delta^2\text{H}$ value for MCF + amine hydrogen (see Supplementary Section B.4). For other researchers to adopt our correction method, they will need to re-analyze PPD of known $\delta^2\text{H}$ (available by request) with their own reagents and water.

3.3.2 Tests for isotopic alteration during sample preparation

Certain preparatory steps can alter the isotopic compositions of amino acids (reviewed in Silverman et al., 2022). In particular, degradation or non-quantitative recovery of amino acids during acid hydrolysis can lead to isotopic fractionation (e.g., Bada et al., 1989; Phillips et al., 2021). To assess the isotopic consequences of different hydrolysis conditions on $\delta^2\text{H}_{\text{AA}}$ values, standard BSA protein was hydrolyzed at different temperatures (105 or 110°C), for different durations (20, 24, or 48h), anoxically or with O_2 present. Compared to conventional hydrolysis conditions (6N HCl, 110°C, 20-24h, anoxic; Silverman et al., 2022), no treatment significantly altered the hydrogen isotope composition of amino acids (Supplementary Table B.4).

To investigate whether carbon-bound hydrogen in amino acids exchanges with aqueous medium during hydrolysis or derivatization, BSA and a mixture of amino acid standards were separately hydrolyzed (6N HCl, 110°C, 24h) and derivatized to MOC esters in solvents with different isotopic compositions. Slopes of regressions of amino acid versus water $\delta^2\text{H}$ values (Supplementary Figures B.9, B.10)

represent the equilibrium fractionation factor (α_{eq}) between organic hydrogen and water, multiplied by the fraction of hydrogen exchanged in the amino acid. To estimate the maximum percent of carbon-bound hydrogen exchanged, each slope was divided by $\alpha_{eq} = 0.9$, an estimate based on fractionation factors for a variety of hydrogen positions in linear and cyclic organic molecules (Wang et al., 2009, 2013).

These calculations indicate that ten amino acids experienced negligible (<2%) hydrogen exchange with aqueous medium during hydrolysis, while tryptophan experienced significant exchange (~27%; Supplementary Figure B.9). Asparagine + aspartic acid (Asx), glutamine + glutamic acid (Glx), and tyrosine experienced moderate exchange (4%–10%); this effect has been previously demonstrated through deuterated and tritiated hydrolysis experiments (Fogel et al., 2016; Hill & Leach, 1964) and is likely due to the increased lability of hydrogen adjacent to the polar—R groups. Hydrogen exchange in tryptophan may have occurred through a reversible reaction with sulfur-containing amino acids in the presence of oxygen (common tryptophan degradation mechanisms summarized in Silverman et al., 2022). All amino acids experienced low (<2%) hydrogen exchange during derivatization (Supplementary Figure B.10).

3.3.3 $^2\text{H}/^1\text{H}$ fractionations and carbon fluxes across wild-type organisms grown on glucose

The substantial variations in $^2\varepsilon_{AA/w}$ values within wildtype organisms grown on glucose are summarized in Figure 3.4A and Supplementary Table B.2 for the five amino acids analyzed, and in Supplementary Figure B.6 and Supplementary Table B.3 for the other amino acids measured in this study. All organisms produced similar $^2\varepsilon_{AA/w}$ patterns, where phenylalanine and proline were the most ^2H -enriched,

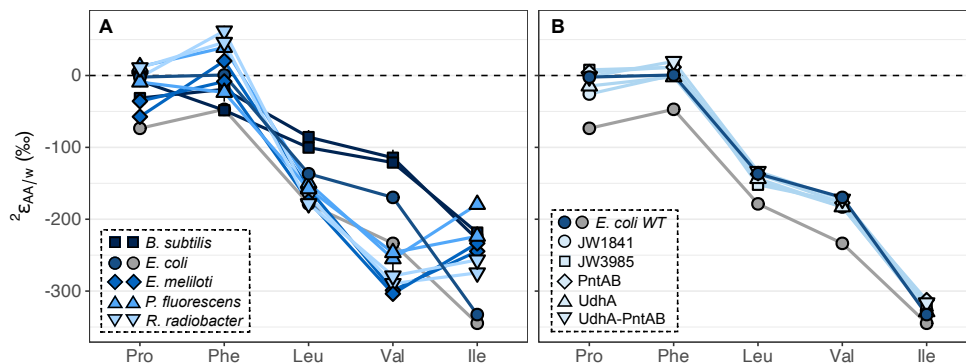


Figure 3.4. Summary of ${}^2\text{H}/{}^1\text{H}$ fractionations between amino acids and water in wildtype organisms (**A**) and in *E. coli* wildtype (WT) and mutant organisms (**B**) grown on glucose. Wildtype cultures were grown in biological duplicate, except for *E. coli*, which was grown in two non-replicate cultures (see Sections 3.2.1, 3.2.2) distinguished by blue and gray symbols for cultures 1 and 2, respectively. Error bars indicate the propagated uncertainties (± 1) from the amino acid, derivative, and water measurements and are smaller than symbols. Amino acids are proline (Pro), phenylalanine (Phe), leucine (Leu), valine (Val), and isoleucine (Ile).

while isoleucine and valine were the most ${}^2\text{H}$ -depleted. This pattern mirrors that previously observed for *E. coli* (Fogel et al., 2016), with the exception of phenylalanine, which in our study was significantly more ${}^2\text{H}$ -enriched relative to the average. Within a single organism, the five ${}^2\epsilon_{AA/w}$ values spanned large ranges (220‰–352‰). Valine exhibited the largest variation across organisms (190‰) while proline and leucine ${}^2\epsilon_{AA/w}$ values varied the least (86‰–93‰). ${}^2\epsilon_{AA/w}$ values from biological replicates of wildtype organisms grown on glucose were generally reproducible (within 30‰) except for phenylalanine and isoleucine from *P. fluorescens* cultures (Supplementary Figure B.5; Supplementary Table B.2), which differed between replicates for unknown reasons. ${}^2\epsilon_{AA/w}$ values in *E. coli* cultures grown on glucose also differed by $>30\%$ for four of the amino acids, but these cultures are not considered biological replicates due to differences in sample preparation (see Section 3.2.1).

Metabolic flux analysis carried out in a previous study (Wijker et al., 2019) revealed

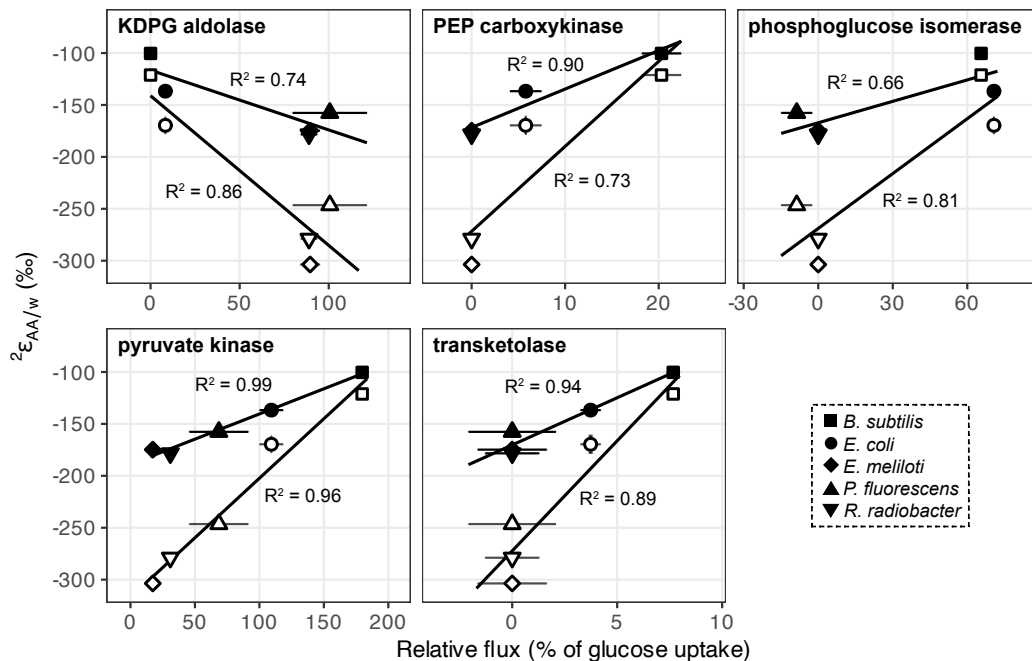


Figure 3.5. ${}^2\epsilon_{AA/w}$ values for leucine (black) and valine (white) in wildtype organisms grown on glucose versus relative carbon flux (i.e., normalized to glucose uptake rates) through pyruvate synthesis-related enzymes in central metabolism: KDPG aldolase (ED pathway), PEP carboxykinase (anaplerotic pathway), phosphoglucose isomerase (EMP pathway), pyruvate kinase (EMP + ED pathways), and fructose 6-phosphate-forming transketolase (PP pathway). Error bars represent ± 1 . Regression analyses were performed using ${}^2\epsilon_{AA/w}$ values from the first of each biological replicate condition (see Supplementary Table B.2).

substantial differences in pathways used for glucose breakdown and in carbon fluxes through central metabolic enzymes (Supplementary Figure B.3; Supplementary Table B.1; Wijker et al., 2019). *E. coli* and *B. subtilis* primarily used the EMP pathway for glucose catabolism and excreted high fluxes of acetate. In contrast, *E. meliloti* and *R. radiobacter* mainly relied on the ED pathway to metabolize glucose and exhibited moderate fluxes through the TCA cycle. *P. fluorescens* exhibited high fluxes through the ED pathway and TCA cycle, as well as periplasmic conversion of glucose to gluconate and 2-ketogluconate, and cyclic flux through the EDEMP pathway (Nikel et al., 2015; Wijker et al., 2019). ${}^2\epsilon_{AA/w}$ values for leucine and valine correlated with carbon fluxes through enzymes related to pyru-

vate synthesis: KDPG aldolase (ED pathway), PEP carboxykinase (anaplerotic pathway), phosphoglucose isomerase (EMP pathway), pyruvate kinase (EMP + ED pathways), and transketolase (PP pathway; Figure 3.5). Directions of correlations between ${}^2\epsilon_{AA/w}$ values and carbon flux through EMP and ED pathways opposed those observed for lipid/water fractionations (${}^2\epsilon_{L/w}$, presented in Wijker et al., 2019), although these relationships may not be directly comparable, as ${}^2\epsilon_{L/w}$ values are primarily controlled by NADPH metabolism (Wijker et al., 2019; Zhang et al., 2009) while leucine and valine do not inherit hydrogen from NADPH. ${}^2\epsilon_{AA/w}$ values for other amino acids did not correlate with carbon flux through any central metabolic enzyme in wildtype organisms.

3.3.4 ${}^2\text{H}/{}^1\text{H}$ fractionations and carbon fluxes in *E. coli* knock-out mutants grown on glucose

Specific dehydrogenase and transhydrogenase genes were deleted in *E. coli* organisms in a previous study (Wijker et al., 2019) to interrogate the influence of NADPH on lipid $\delta^2\text{H}$ values. Deletion of these genes forced carbon flux through alternative central metabolic enzymes to accomplish glucose catabolism and NADPH balance (Supplementary Figure B.4; Table B.1). Despite drastic differences in the magnitudes of carbon fluxes, *E. coli* mutant organisms produced similar ${}^2\epsilon_{AA/w}$ values compared to wildtype *E. coli* culture 1, differing by $<40\%$ for any given amino acid (Figure 3.4B; Supplementary Table B.2; see note about *E. coli* culture 2 in Section 3.3: ' ${}^2\text{H}/{}^1\text{H}$ fractionations and carbon fluxes across wildtype organisms grown on glucose'). Lipid $\delta^2\text{H}$ values showed a similar response in these organisms (Wijker et al., 2019), as did $\delta^2\text{H}_{AA}$ values in *E. coli* mutants with inhibited glycolysis or oxidative pentose phosphate pathways in a previous study (D. A. Smith et al., 2022). Nevertheless, variations in isotopic compositions

hint at some control by NADPH, as $\delta^2\text{H}_{\text{AA}}$ values correlated with carbon fluxes through all NADPH-related enzymes (Supplementary Figure B.15), with proline exhibiting the strongest correlations ($R^2 = 0.70\text{--}0.86$), followed by phenylalanine ($R^2 = 0.58\text{--}0.71$), then isoleucine ($R^2 = 0.36\text{--}0.49$). The PGI knockout mutant, JW3985, had a severely perturbed metabolism and fell off the regressions in most cases so was excluded from the regression analyses.

3.3.5 $^2\text{H}/^1\text{H}$ fractionations across wildtype organisms grown on different substrates

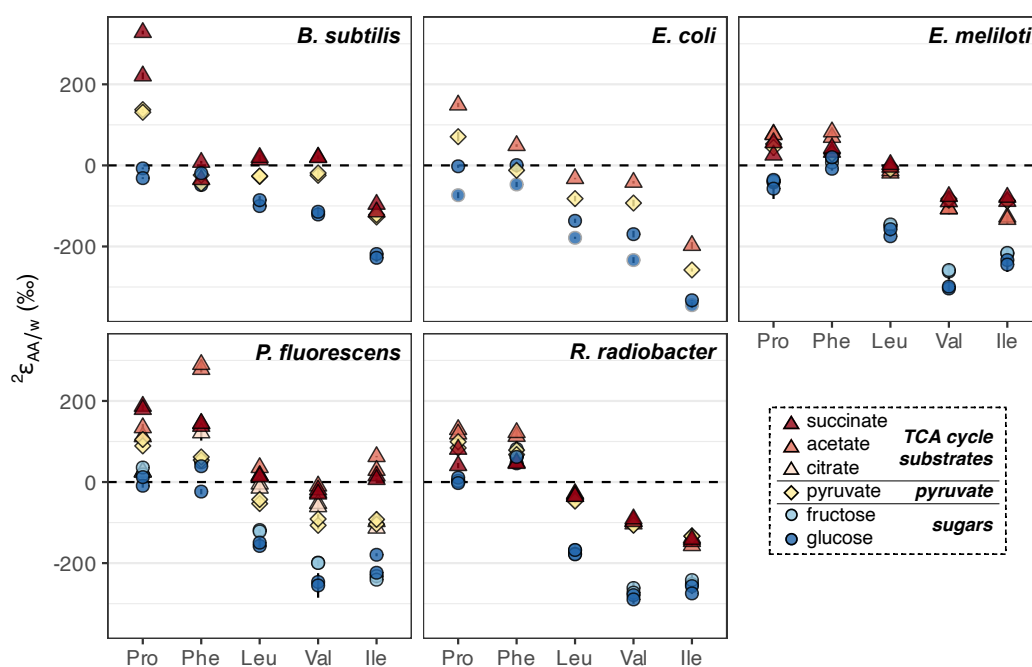


Figure 3.6. Summary of $^2\text{H}/^1\text{H}$ fractionations between amino acids and water in wild-type organisms grown on different substrates (denoted by colors) spanning metabolically distinct classes (denoted by shapes). Error bars indicate the propagated uncertainties (± 1) from the amino acid, derivative, and water measurements, and are smaller than symbols. Duplicate cultures were set up for all organisms and conditions except *E. coli*, which was grown on acetate and pyruvate in a single replicate, and on glucose in two different (non-replicate) experiments (with cultures 1 and 2 distinguished by dark blue circles with black and gray borders, respectively; see Sections 3.2.1, 3.2.2).

In addition to glucose, wildtype organisms were cultured on acetate, citrate, fructose, pyruvate, and/or succinate, which enter central metabolism at different nodes and activate different catabolic pathways for substrate breakdown. ${}^2\varepsilon_{AA/w}$ values from biological replicates of wildtype organisms grown on each substrate were generally reproducible (within 30‰) except for proline and phenylalanine in *B. subtilis* grown on succinate, and proline in *R. radiobacter* grown on succinate, which differed between replicates for unclear reasons (Figure 3.6, Supplementary Figure B.5, Supplementary Table B.2). Fructose led to similar ${}^2\varepsilon_{AA/w}$ values as glucose-based growth, while pyruvate and TCA cycle substrates (acetate, citrate, and succinate) led to ${}^2\text{H}$ -enrichment of all amino acids (Figure 3.6), mirroring phenomena observed for lipids (Osburn et al., 2016; Wijker et al., 2019; Zhang et al., 2009). The amount of ${}^2\text{H}$ -enrichment varied widely for each amino acid. Proline in *B. subtilis* grown on succinate, and isoleucine and phenylalanine in *P. fluorescens* grown on acetate, exhibited the largest singular ${}^2\text{H}$ -enrichments (286‰–360‰ higher ${}^2\varepsilon_{AA/w}$ values relative to those during glucose-based growth). However, phenylalanine was generally ${}^2\text{H}$ -enriched by the least amount (<100‰ difference between ${}^2\varepsilon_{Phe/w}$ values upon growth on TCA cycle substrates relative to on glucose for all organisms except *P. fluorescens*), while valine was generally ${}^2\text{H}$ -enriched by the greatest amount (142–245‰). These differences were significantly greater than those between growth water (<15‰) or substrate $\delta^2\text{H}$ values (<85‰; Supplementary Table B.2).

3.4 Discussion

Consistencies in ${}^2\varepsilon_{AA/w}$ patterns (i.e., the relative ordering of ${}^2\varepsilon_{AA/w}$ values) within each growth condition, coupled with the substantial shifts in ${}^2\varepsilon_{AA/w}$ values across growth conditions, underscore the existence of systematic controls on $\delta^2\text{H}_{AA}$ val-

ues. Initial investigations (Fogel et al., 2016; Gharibi, Chernobrovkin, Eriksson, et al., 2022; Mancuso et al., 2023; Newsome et al., 2020; D. A. Smith et al., 2022) have begun to explore the complicated factors driving $\delta^2\text{H}_{\text{AA}}$ signals in heterotrophic microbes, mammals, and humans, but we are still far from mechanistic understanding of these controls. In the following sections we interrogate several biochemical controls on the patterns and variations in microbial $\delta^2\text{H}_{\text{AA}}$ values in an attempt to elucidate how these signals can be used as tracers for microbial or ecological studies in the environment (summarized in Table 3.1). Our data allow us to provide a mechanistic explanation for some, though not all, of the observed $^2\varepsilon_{\text{AA/w}}$ patterns. As numerous enzymes in central metabolism are referenced throughout the discussion, a schematic of the central metabolic pathways with all enzymes annotated is provided for reference (Supplementary Figure B.2).

Table 3.1. Summary of potential biochemical controls on $\delta^2\text{H}_{\text{AA}}$ values.

| AA(s) | Biochemical control hypothesized | Effect on $\delta^2\text{H}_{\text{AA}}$ values | Data where effect is observed/explored | Potential application of $\delta^2\text{H}_{\text{AA}}$ analysis |
|---------------|---|--|--|---|
| Pro | Citrate synthase: KIE leads to ^2H -enrichment of α -ketoglutarate (proline precursor in TCA cycle). | Stimulates high proline $\delta^2\text{H}$ values, i.e., small proline/water fractionations. | High proline $\delta^2\text{H}$ values across all carbon substrate conditions (Figure 6). Large slopes in regressions of proline vs. water $\delta^2\text{H}$ (growth water experiments; Supplementary Figure S11), implying small proline/water fractionations (Supplementary Section 6.1). | |
| Phe | High fraction of water-derived hydrogen in precursors PEP and erythrose-4-phosphate, with water-derived hydrogen having equilibrated with water. | Leads to small but positive phenylalanine/water fractionations, with phenylalanine $\delta^2\text{H}$ values relatively insensitive to diet. | Supported by small phenylalanine/water fractionations across all substrate conditions (except in <i>P. fluorescens</i> grown on TCA cycle substrates; Figure 6). | Proxy for environmental water $\delta^2\text{H}$. Bio-thermometer if organic hydrogen/water equilibration is temperature-dependent. |
| Pro, Phe, Ile | NADPH metabolism: KIEs of dehydrogenases and transhydrogenases control the $\delta^2\text{H}$ value of the NADPH pool. | Contributes to some variations in $\delta^2\text{H}$ values of amino acids with NADPH-derived hydrogen. | Correlations between $\delta^2\text{H}_{\text{AA}}$ values and carbon flux through NADPH-related enzymes, and between $\delta^2\text{H}_{\text{AA}}$ values and NADPH imbalance fluxes in <i>E. coli</i> organisms (Supplementary Figure S15; Section 4.2.1.2). Correlations between $\delta^2\text{H}_{\text{AA}}$ shifts in organisms grown on glucose \rightarrow TCA cycle substrates and fraction of NADPH-derived amino acid hydrogen (Figure 7B, Supplementary Figure S13). Substrate ordering of estimated NADPH-related ^2H -enrichment of proline with measured and published NADPH imbalance fluxes in <i>E. coli</i> and <i>B. subtilis</i> (Figure 7C; Section 4.2.1.2). | Elucidate NADPH balance and redox metabolism in cells. |
| All AAs | Catabolic pathways activated: control $\delta^2\text{H}$ values of central metabolites (e.g., pyruvate) through differential activation of catabolic pathways and associated enzymes. | Contributes to systematic variations in $\delta^2\text{H}_{\text{AA}}$ values, with lowest $\delta^2\text{H}$ values upon growth on sugars, moderate upon growth on pyruvate, and highest upon growth on TCA cycle substrates. | Correlations between leucine and valine $\delta^2\text{H}$ values and carbon flux through pyruvate synthesis-related enzymes in organisms grown on glucose (Figure 5). Correlations between $\delta^2\text{H}_{\text{AA}}$ shifts in organisms grown on glucose \rightarrow TCA cycle substrates and fraction of pyruvate-derived amino acid hydrogen (Figure 7B, Supplementary Figure S12). Systematic variations in $\delta^2\text{H}_{\text{AA}}$ values (Figure 7A) explainable by considering relative ^2H -enrichment of cellular pyruvate in different carbon substrate conditions (Figure 8; Section 4.2.1.1). | Interrogate an organism's diet and/or metabolic lifestyle. |
| | Enzymes in biosynthetic pathways. | Set the overall pattern of $\delta^2\text{H}_{\text{AA}}$ values, but variations in enzymes and isotope effects across organisms may contribute to variations in $\delta^2\text{H}_{\text{AA}}$ values. | Similar $\delta^2\text{H}_{\text{AA}}$ patterns across organisms and substrate conditions (Figure 6). Similar $\delta^2\text{H}_{\text{AA}}$ values across <i>E. coli</i> organisms grown on glucose, despite different fluxes through catabolic pathways (Figure 4B). Diversity in isozymes employed in each amino acid biosynthetic step across organisms (Supplementary Figure S20). | Fingerprinting method to trace origins of amino acids in organic matter, if $\delta^2\text{H}_{\text{AA}}$ patterns within different taxonomic groups are unique. |

3.4.1 Controls on the ${}^2\varepsilon_{AA/w}$ pattern during glucose metabolism

${}^2\varepsilon_{AA/w}$ patterns were strikingly similar across wildtype organisms and *E. coli* mutants grown on all carbon substrates (Figures 3.4, 3.6), indicating that biosynthetic pathways (as opposed to catabolic pathways) serve as first-order controls on δ^2H_{AA} values. Our interpretation is consistent with Fogel et al. (2016), who observed similar δ^2H_{AA} patterns in *E. coli* cultured on glucose or tryptone in different growth waters. In this section, we investigate the biochemical factors that set the general ${}^2\varepsilon_{AA/w}$ pattern in glucose-grown cultures, focusing our interpretation on hydrogen sources and mechanisms of hydrogen exchange, as well as relevant isotope effects associated with enzymes in central metabolic and biosynthetic pathways. Based on these interpretations, we speculate on the most prominent types of biological information that can be obtained from δ^2H_{AA} measurements. Amino acids are discussed in order from most to least 2H -enriched. As these microbes share the same biosynthetic pathways, variations in ${}^2\varepsilon$ values of a given amino acid across organisms (e.g., Figure 3.4A) hint at the importance of additional, second-order controls, which are examined in Section 3.4.2.

3.4.1.1 Proline

The high δ^2H values of proline are likely due in large part to the 2H -enriching kinetic isotope effect (KIE) of citrate synthase in the TCA cycle. Proline is mainly synthesized from the TCA cycle intermediate α -ketoglutarate and inherits four hydrogen atoms from α -ketoglutarate, two from NAD(P)H, and one from water (Figure 3.1, Supplementary Figure B.16). In the first step of the TCA cycle, citrate synthase combines acetyl-CoA with oxaloacetate to form citrate, abstracting a proton from acetyl-CoA's methyl group with a large KIE (1.94 measured in vitro; Lenz et al., 1971). The resulting 2H -enriched hydrogen in citrate is retained

through formation of α -ketoglutarate (and ultimately, synthesis of proline), as aconitase and isocitrate dehydrogenase stereospecifically remove the oxaloacetate-derived hydrogen from citrate and isocitrate, respectively (Supplementary Figure B.16; Csonka and Fraenkel, 1977; Lowenstein, 1967; Ochs and Talele, 2020; W. G. Smith and York, 1970). As proline inherits 30% of its hydrogen from NAD(P)H through this synthesis pathway, and its $\delta^2\text{H}$ value appears to be controlled to some extent by NADPH metabolism (see Section 3.4.2.1.2), proline may be a sensitive indicator of redox balance in cells. Some microbial species within the families Rhizobiaceae and Pseudomonadaceae can additionally synthesize proline from ornithine, which in turn is synthesized from arginine (Schindler et al., 1989; Stalon et al., 1987). The prevalence of this pathway in the *P. fluorescens* and *R. radiobacter* strains examined in this study is unclear, but its operation would presumably reduce the fraction of NAD(P)H-derived hydrogen in proline.

3.4.1.2 Phenylalanine

The source of phenylalanine's high $\delta^2\text{H}$ values is unclear, but may be due to relatively large fractions of water-derived hydrogen in phenylalanine's organic precursors (phosphoenolpyruvate and erythrose-4-phosphate; Figure 3.1, Supplementary Figure B.17). During glucose metabolism, phosphoenolpyruvate (PEP) is primarily synthesized through the EMP or ED pathway, and its hydrogen can be directly routed from glucose or partially exchanged with water (e.g., at the triose phosphate level; Reynolds et al., 1971; Rose and O'Connell, 1961; Russell and Young, 1990; Saur et al., 1968). Erythrose-4-phosphate is synthesized through the PP pathway, which includes numerous isomerizations and reversible reactions that exchange organic hydrogen with water (Russell & Young, 1990). As these equilibrations are presumably controlled by equilibrium rather than kinetic isotope effects, the resulting fractionations are unlikely to be strongly negative (in con-

trast to the potentially large normal KIEs expressed during water incorporation into pyruvate; Section 3.4.1.3). Indeed, theoretical calculations predict slightly negative to relatively positive equilibrium fractionations for the hydrogen sites susceptible to equilibration with water in the organic intermediates (Wang et al., 2009). The relatively small isotopic fractionation of phenylalanine across carbon substrate conditions (Figure 3.6) further supports a large fraction of water-derived hydrogen, which may render phenylalanine a useful proxy for environmental water $\delta^2\text{H}$, and potentially a bio-thermometer if equilibration with water is temperature-dependent.

3.4.1.3 Leucine and valine

The low $\delta^2\text{H}$ values of leucine and valine, as well as the consistent ^2H -depletion of valine relative to leucine in glucose-grown organisms, may be attributed in part to low pyruvate $\delta^2\text{H}$ values. Leucine and valine are formed through overlapping biosynthetic pathways, initiated by condensation of two pyruvate molecules to form 2-acetolactate. Both pyruvate methyl groups remain intact through this and subsequent steps, ultimately becoming part of the isopropyl groups of these amino acids (Figure 3.1, Supplementary Figure B.18). During glucose metabolism, pyruvate's methyl hydrogen is likely to become ^2H -depleted relative to the methylene hydrogen in its central metabolite precursors (PEP, KDPG, and malate), as all pyruvate synthesis reactions incorporate solvent hydrogen with potentially large isotope effects, ranging from -141‰ for equilibrium-controlled incorporation (Wang et al., 2009) to presumably larger fractionations for kinetically-controlled transfers. For example, solvent isotope effects measured *in vitro* for pyruvate kinase and KDPG aldolase were 1,700 and 3,250‰, respectively (Bollenbach et al., 1999; Meloche, 1975), although note that the applicability of such measurements to *in vivo* studies is untested, and enzyme reversibility (such as with KDPG aldolase; Jacobson et al.,

2019) as well as keto-enol tautomerization of pyruvate (Chiang et al., 1992) would drive pyruvate $\delta^2\text{H}$ values toward equilibrium. As valine inherits a larger proportion of pyruvate hydrogen (Figure 3.1, Supplementary Figure B.18), variations in the isotopic composition of pyruvate would result in more pronounced changes in the $\delta^2\text{H}$ value of valine compared to leucine, as observed here (Figure 3.5). All additional carbon-bound hydrogen in leucine and valine are likely transferred from water, and the isotope compositions of these hydrogen atoms may reflect equilibrium and/or kinetic control. Pyruvate occupies a crucial node at the intersection of many branches of central metabolism. The isotope composition of its methyl hydrogen should therefore be sensitive to the central metabolic pathways activated (see Section 3.4.2.1.1), and consequently to the types of carbon substrates consumed by an organism. As leucine and valine inherit unaltered pyruvate methyl hydrogen (in addition to isotopically invariant water hydrogen), these amino acids should also be sensitive to organisms' diet if they are synthesized *de novo*.

3.4.1.4 Isoleucine

As with leucine and valine, low isoleucine $\delta^2\text{H}$ values in organisms grown on glucose may be the result of relatively ^2H -depleted hydrogen sources (pyruvate and NADPH) and large normal KIEs associated with hydrogen transfer from water. Isoleucine is formed from oxaloacetate, which in turn is synthesized from malate in the TCA cycle, or from PEP or pyruvate through anaplerotic pathways (Figure 3.1, Supplementary Figure B.2, B.19). The pro-*S* position of oxaloacetate's methylene group is retained through biosynthesis of isoleucine (Supplementary Figure B.19); depending on the extent to which oxaloacetate undergoes keto-enol tautomerization (i.e., interconverts between a ketone and enol(ate) structure; Bruice and Bruice, 1978; Kosicki, 1962) and/or is synthesized by malate dehydrogenase (thereby incorporating solvent hydrogen into oxaloacetate's pro-*S* methylene po-

sition; Gawron and Fondy, 1959; Omi et al., 2003), the hydrogen atom retained may originate from water (see details in Supplementary Figure B.19 caption). Together, this hydrogen, along with the water-derived fraction in pyruvate's methyl group (Section 3.4.1.3) and those transferred from or equilibrated with water during isoleucine biosynthesis, contribute to a potentially large ($\geq 60\%$) fraction of carbon-bound hydrogen in isoleucine sourced from water (Supplementary Figure B.19) — an estimate consistent with model predictions by Fogel et al. (2016). In contrast to phenylalanine, whose water-derived hydrogen may be predominantly acquired through equilibrium exchange reactions, isoleucine's water-derived hydrogen may be primarily transferred from water by enzymatic reactions with large KIEs, contributing to very low isoleucine $\delta^2\text{H}$ values. Despite its high water fraction, the $\delta^2\text{H}$ value of isoleucine remains sensitive to the metabolic programming of cells (i.e., both redox balance and central metabolic pathways activated) through its pyruvate and NADPH hydrogen, as evident through the large $\delta^2\text{H}$ variations across growth conditions (Figure 3.6). This sensitivity may be enhanced by the different origins of oxaloacetate-sourced hydrogen in isoleucine (water versus organic hydrogen), which vary depending on which carbon substrates are being catabolized.

3.4.2 Controls on variations in ${}^2\varepsilon_{\text{AA}/\text{w}}$ values

While the similar patterns of ${}^2\varepsilon_{\text{AA}/\text{w}}$ values across glucose-grown organisms reveals remarkable consistencies in net isotopic fractionations of central metabolic and biosynthetic pathways, the variations in ${}^2\varepsilon_{\text{AA}/\text{w}}$ values hint at subtle physiological differences in the organisms. Culturing experiments in which the $\delta^2\text{H}$ value of an organism's growth water is manipulated can provide some constraints on the biochemical causes of these differences (presented in Supplementary Section

B.6.1). The substantial systematic shifts in ${}^2\varepsilon_{AA/w}$ values upon growth on different carbon substrates provide further insight into biochemical controls on these isotopic signals, including the differential activation of enzymes across catabolic pathways (Section 3.4.2.1). Finally, potential differences in ${}^2\varepsilon_{AA/w}$ values due to enzymatic variations in biosynthetic pathways are considered (Section 3.4.2.2).

3.4.2.1 Metabolite pools in activated catabolic pathways

Growth of organisms on carbon substrates that activated different catabolic pathways led to substantial shifts in δ^2H_{AA} values (Figures 3.6, 3.7A). In general, growth on sugars (glucose and fructose) led to the most 2H -depleted amino acids, followed by growth on pyruvate, then TCA cycle substrates (acetate, citrate, and succinate). The overall pattern is similar to that observed in lipids (Wijker et al., 2019; Zhang et al., 2009). Moreover, patterns of 2H -enrichment relative to δ^2H_{AA} values in glucose-grown cells were similar within pairs of metabolically-related organisms (*B. subtilis* + *E. coli* and *E. meliloti* + *R. radiobacter*), highlighting organismal physiology as an important control on δ^2H_{AA} values. The altered metabolic programming in organisms grown on different substrates undoubtedly alters the hydrogen isotope composition of central metabolites that feed into amino acid biosynthesis. In particular, pyruvate occupies a crucial node in central metabolism and contributes hydrogen to all amino acids either directly (the case for leucine, valine, and isoleucine), or indirectly (for proline and phenylalanine; see Supplementary Section B.6.2), so likely controls some of the variation in the δ^2H_{AA} values. Furthermore, some amino acids inherit hydrogen from NADPH (29% in proline, 20% in isoleucine, and 13% in phenylalanine; Figure 3.1, Supplementary Figures B.16–B.19). NADPH serves as a hydride carrier in organisms, both providing reducing power for anabolic reactions and transmitting isotopic information to products. As lipid δ^2H variations are thought to be primarily controlled by the hy-

drogen isotope composition of the NADPH pool (Wijker et al., 2019; Zhang et al., 2009), amino acid $\delta^2\text{H}$ values may be similarly influenced by NADPH metabolism. Together, changes in the isotopic composition of the pyruvate-related and NADPH fractions of hydrogen in the amino acids explain 29%–70% of the shifts in $\delta^2\text{H}_{\text{AA}}$ values between pairs of substrate conditions (e.g., when *E. coli* is grown on acetate versus glucose; Figure 3.7B; Supplementary Section B.6.2). Stated a different way, $\delta^2\text{H}_{\text{AA}}$ values may vary with the inverse of the fraction of water-derived hydrogen in amino acids, however further work is required to quantify these fractions under different metabolic conditions. In the following two sections we separately explore the influences of pyruvate and NADPH on $\delta^2\text{H}_{\text{AA}}$ variations, with mechanisms affecting pyruvate $\delta^2\text{H}$ summarized in Figure 3.8.

3.4.2.1.1 Pyruvate $\delta^2\text{H}$

The substrate-driven ordering of amino acid ^2H -enrichment (TCA cycle substrates > pyruvate > sugars) can be explained by the flow of hydrogen and activated enzymes in the different conditions. Growth on sugars that activate upper EMP/ED pathways should fuel an overall ^2H -depleted pyruvate pool, as pyruvate is predominantly synthesized by enzymes that transfer hydrogen from water with potentially large normal isotope effects (e.g., pyruvate kinase and KDPG aldolase; Figure 3.8; Bollenbach et al., 1999; Meloche, 1975; Wang et al., 2009; although note that the expression of such isotope effects may be diluted by any enzyme reversibility). The influence of pyruvate on $^2\varepsilon_{\text{AA}/\text{w}}$ values in glucose-grown organisms is visible through the correlations between leucine or valine $^2\varepsilon_{\text{AA}/\text{w}}$ values (which should only reflect pyruvate and water hydrogen) and carbon flux through enzymes related to pyruvate synthesis (Figure 3.5). In particular, the ED pathway appears to have a more ^2H -depleting effect on pyruvate $\delta^2\text{H}$ than does the EMP pathway,

as increased flux through KDPG aldolase leads to net ^2H -depletion of leucine and valine, while increased flux through both phosphoglucose isomerase and pyruvate kinase stimulate ^2H -enrichment of the amino acids (Figure 3.5). These trends are consistent with the magnitudes of solvent isotope effects observed for enzymes in the respective pathways (1,700‰ for pyruvate kinase and 3,250‰ for KDPG aldolase; Bollenbach et al., 1999; Meloche, 1975). ^2H -enrichment by PEP carboxykinase (anaplerotic pathway) may be due to the ^2H -enriched hydrogen transferred from the TCA cycle into pyruvate through PEP. Transketolase influences the hydrogen isotope composition of pyruvate by combining PP pathway intermediates to produce fructose 6-phosphate and glyceraldehyde 3-phosphate, which feed into glycolysis (Supplementary Figure B.2). In contrast to the wild-type microbes, mutant *E. coli* organisms mainly synthesized pyruvate via glycolysis (Supplementary Figure B.4, Supplementary Table B.1), resulting in similar $\delta^2\text{H}_{\text{AA}}$ values as wildtype *E. coli*. This particular result highlights how variations in amino acid hydrogen isotope compositions are driven by differences in hydrogen routing through central metabolism rather than merely by changes in the magnitude of flux through a given enzyme.

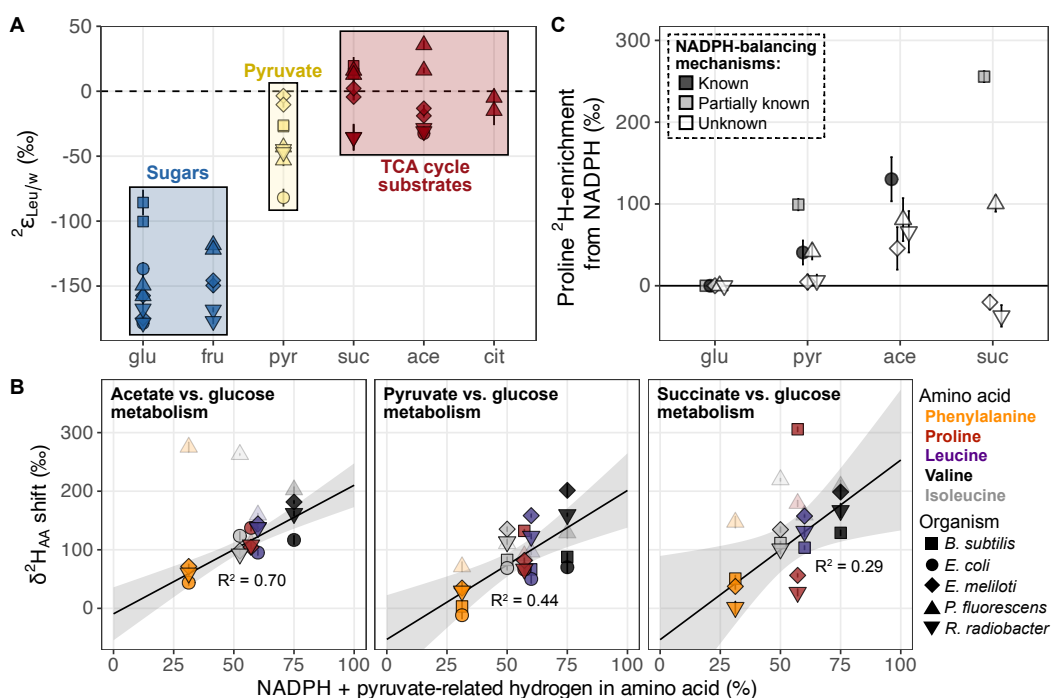


Figure 3.7. Hypotheses explored for pyruvate and NADPH controls on δ^2H_{AA} variations in organisms grown on different substrates. (A) Example of systematic shifts in ${}^2\varepsilon_{Leu/w}$ values for one amino acid (leucine) in wildtype organisms grown on metabolically distinct classes of carbon substrates (denoted by colors). All ${}^2\varepsilon_{AA/w}$ values from Figure 3.6 are plotted. Error bars indicate the propagated uncertainties (± 1) from the amino acid, derivative, and water measurements, and are smaller than symbols. (B) Estimated influence of NADPH- and pyruvate-derived hydrogen on shifts in δ^2H_{AA} values across growth conditions. See Section 3.4.2.1 and Supplementary Section B.6.2 for details on accounting estimates. (Caption continued on next page).

Figure 3.7. (cont.) $\delta^2\text{H}_{\text{AA}}$ shifts were calculated as the difference in $\delta^2\text{H}$ value of a given amino acid between the two substrate conditions compared within each panel (using data from replicate culture 1 for each condition). Error bars on individual data points are the propagated uncertainties (± 1) from each pair of $\delta^2\text{H}_{\text{AA}}$ values measured and are smaller than symbols. The shaded gray region indicates the 95% confidence interval of the coefficients from the linear regression fit; R^2 values are adjusted for the number of predictors in the model. *P. fluorescens* data are shown as transparent symbols but excluded from the regressions due to multiple instances as extreme outliers. When *P. fluorescens* data are included in the regressions, adjusted R^2 values are 0.02, 0.43, and 0.21 for shifts from glucose to acetate, pyruvate, and succinate metabolism, respectively. Colors denote amino acids as shown in the legend to the right of the plot. (C) NADPH-driven ^2H -enrichment of proline (i.e., that beyond ^2H -enrichment due to acetyl-CoA alone) estimated in wildtype organisms cultured on the indicated substrate compared to during growth on glucose (data from replicate 1 cultures used). See Section 3.4.2.1.2 and Supplementary Section B.6.3 for calculation details. Error bars indicate combined uncertainties in measured proline $\delta^2\text{H}$ values (Supplementary Table B.2), estimated shifts in pyruvate $\delta^2\text{H}$ values (Supplementary Table B.6), and/or measured acetate and pyruvate $\delta^2\text{H}$ values (reported in Zhang et al., 2009). Data are slightly spread about the x-axis to increase ease of visualization. In all three figures, shapes denote the organism as shown in the bottom right legend. Growth substrates are glu, glucose; fru, fructose; pyr, pyruvate; suc, succinate; ace, acetate; and cit, citrate.

Compared to glucose metabolism, the cellular pyruvate pool should be more ^2H -enriched when organisms are grown on pyruvate (Figure 3.8), as pyruvate is directly assimilated with presumably minimal isotopic alteration, so the resulting cellular pyruvate $\delta^2\text{H}$ value should be close to that of the starting substrate (-12‰ as measured by Zhang et al., 2009; Supplementary Table B.2). Even higher cellular pyruvate $\delta^2\text{H}$ values are likely produced in organisms grown on TCA cycle substrates (succinate, citrate, and acetate) due to the large KIEs of three differentially activated enzymes: succinate dehydrogenase, citrate synthase, and malate synthase. These enzymes abstract hydrogen from their respective substrates, leading to strong ^2H -enrichment of residual hydrogen in the organic products (Figure 3.8). Succinate dehydrogenase removes one hydrogen from each methylene group in succinate with a large isotope effect (in vitro KIE = 5.4; Rétey et al., 1970), producing highly ^2H -enriched fumarate. Succinate metabolism stimulates high flux through malic enzyme (Gerosa et al., 2015), which carries the ^2H -enriched fumarate hydrogen through malate into pyruvate (although with isotopic dilution via solvent hydrogen incorporation by fumarase and malic enzyme; Figure 3.8), contributing to among the highest $\delta^2\text{H}_{\text{AA}}$ values across growth conditions, including a 228‰–360‰ ^2H -enrichment of proline in *B. subtilis* grown on succinate versus glucose (Figure 3.6). This contrasts with low $\delta^2\text{H}_{\text{AA}}$ values produced during sugar metabolism, whereby malate is predominantly routed around the TCA cycle through oxaloacetate, so the ^2H -enriched hydrogen does not end up in pyruvate, nor in α -ketoglutarate due to stereospecific abstraction by aconitase and isocitrate dehydrogenase (Figure 3.8; Gerosa et al., 2015; Ochs and Talele, 2020; W. G. Smith and York, 1970). During acetate metabolism, acetyl-CoA is either routed around the TCA cycle through citrate synthase, or through the glyoxylate shunt by malate synthase, which conserves carbon by bypassing the decarboxylating steps of the TCA cycle (Gerosa et al., 2015; Zhao & Shimizu, 2003). Both

citrate synthase and malate synthase abstract a hydrogen from the methyl group of acetyl-CoA with large KIEs (in vitro KIEs = 1.94 and 3.8, respectively; Lenz et al., 1971; O'Leary, 1989, leading to ^2H -enriched methylene hydrogen in citrate and malate that are routed into pyruvate through malic enzyme (Figure 3.8). The enzymatic reactions comprising the glyoxylate shunt do not introduce water hydrogen into organic intermediates, thus ^2H -enrichment of malate when the glyoxylate shunt is activated is likely more significant than when malate is synthesized by fumarase. Phenylalanine in *P. fluorescens* experienced the most ^2H -enrichment from glucose to acetate metabolism (239‰–313‰), potentially in part due to transfer of ^2H -enriched TCA cycle hydrogen into PEP through PEP carboxykinase (Dolan et al., 2020; Gerosa et al., 2015). However, in other organisms, the $\delta^2\text{H}$ value of phenylalanine shifted by much smaller amounts. Citrate metabolism bypasses the ^2H -enriching citrate synthase step, leading to significantly lower proline $\delta^2\text{H}$ values in *P. fluorescens* compared to pyruvate, acetate, or succinate metabolism (Figure 3.6). However, flux through succinate dehydrogenase and malic enzyme still carries ^2H -enriched hydrogen into pyruvate, likely contributing to the strong ^2H -enrichment of the other four amino acids during citrate metabolism compared to glucose metabolism. Note that reversibility of any central metabolic enzymatic reaction contributing to equilibration of organic hydrogen with water could dilute any of the aforementioned signals.

Overall, pyruvate appears to exert an important influence on the $\delta^2\text{H}$ values of all amino acids. The $\delta^2\text{H}$ value of pyruvate is likely sensitive to the catabolic pathways activated for substrate degradation, which contributes to some of the variations in $\delta^2\text{H}_{\text{AA}}$ values across substrate conditions. Thus, the hydrogen isotope compositions of amino acids — particularly leucine and valine — may be useful for identifying the types of substrates consumed, and thus metabolic pathways used, by an organism. In other words, $\delta^2\text{H}_{\text{AA}}$ values may provide insight into how

organisms process carbon from their environment. Future work should explore the mechanistic link between pyruvate (and other important central metabolites) and amino acid $\delta^2\text{H}$ values under different metabolic conditions.

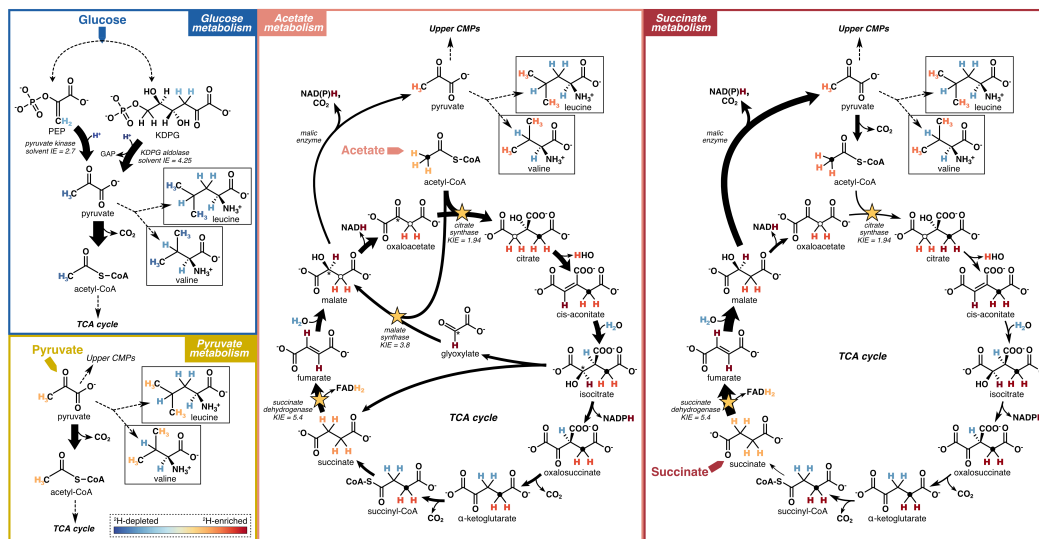


Figure 3.8. Schematic models of hydrogen flow through relevant central metabolic pathways (CMPs), corresponding isotopic fractionations, and relative ^2H -enrichment of leucine and valine upon growth of microbes on different carbon substrates. Reactions potentially having a strong influence on the hydrogen isotope compositions of pyruvate and acetyl-CoA, and thus on the amino acids investigated in this study, are highlighted. Arrow widths indicate flux magnitudes estimated based on ^{13}C -based metabolic flux maps reported in Gerosa et al. (2015). Dashed lines summarize a series of reactions not shown. Filled circles in the TCA cycle metabolites trace the methyl group of acetyl-CoA through succinyl-CoA. Open circles trace the methyl group of acetyl-CoA into malate and through citrate via the glyoxylate shunt (acetate metabolism) and the methylene group of oxaloacetate into citrate (succinate metabolism). The asterisk traces the alcohol carbon position in isocitrate to oxaloacetate via the glyoxylate shunt (acetate metabolism). The color gradient representing the relative ^2H -enrichments or ^2H -depletions of hydrogen within biomolecules is shown as an inset in the “Pyruvate metabolism” box. Isotope effects (KIEs and solvent IEs) shown are reported from Bollenbach et al. (1999), Lenz et al. (1971), Meloche (1975), O’Leary (1989), and Rétey et al. (1970).

3.4.2.1.2 NADPH $\delta^2\text{H}$

Proline, phenylalanine, and isoleucine derive hydrogen from NADPH (Figure 3.1, Supplementary Figures B.16–B.19). The isotopic composition of NADPH is thought to be primarily driven by the relative fluxes through dehydrogenases (which produce NADPH) in central metabolism, and through transhydrogenases that interconvert NADH and NADPH to maintain NADPH balance between catabolic and anabolic processes (Wijker et al., 2019; Zhang et al., 2009). The dehydrogenase and transhydrogenase enzymes have different KIEs (Bizouarn et al., 1995; Fjellström et al., 1999; O’Leary, 1989; Venning et al., 1998), and their fluxes vary across organisms and substrate conditions, leading to large variations in the isotopic composition of NADPH (Wijker et al., 2019). In wildtype organisms grown on glucose, these effects are visible through correlations between lipid $\delta^2\text{H}$ values and fluxes through dehydrogenases (6PGDH, ICDH) or enzymes that directly compete with dehydrogenases (PGI, KDPG aldolase; Wijker et al., 2019). However, amino acid $\delta^2\text{H}$ values across the same organisms grown on glucose showed no correlation with carbon flux through any NADPH-related enzyme, nor with overall NADPH imbalance flux (calculated as the difference between all NADPH-producing and -consuming fluxes; Supplementary Figure B.14). In fact, despite nearly identical carbon fluxes in *E. meliloti* and *R. radiobacter* grown on glucose (Supplementary Figure B.3; Supplementary Table B.1), these organisms exhibited the largest differences in $\delta^2\text{H}$ values for proline (Figure 3.6; Supplementary Table B.2), whose hydrogen is derived from the same sources as lipids: NAD(P)H, acetyl-CoA, and water. Lack of clear control by NADPH on $\delta^2\text{H}_{\text{AA}}$ values during glucose metabolism may be due to the fact that amino acids inherit only a small fraction of hydrogen from NADPH (13–30%) relative to other sources (e.g., ~75% of hydrogen in phenylalanine derived from PEP + erythrose 4-phosphate), so any control by NADPH

may be obscured by variations in isotope compositions of the other sources. Alternatively, these results could be due to different cofactor specificities (i.e., use of NADH versus NADPH; Fuhrer and Sauer, 2009) of biosynthetic enzymes, different isotope effects within amino acid biosynthetic pathways (Section 3.4.2.2), downstream processing of amino acids after synthesis, or an outsized influence of other unknown factors on $\delta^2\text{H}_{\text{AA}}$ values in wildtype organisms. While the extent of NADPH influence on $\delta^2\text{H}_{\text{AA}}$ values in wildtype organisms is unclear when comparing different organisms grown under the same condition, it is more apparent when physiological variability is controlled for—i.e., by comparing single organisms grown under different conditions. In *E. coli* wildtype and mutant organisms with perturbed NADPH metabolisms, $\delta^2\text{H}$ values for proline, phenylalanine, and isoleucine were weakly to moderately correlated with carbon flux through NADPH-related enzymes, and $\delta^2\text{H}$ values for isoleucine and phenylalanine positively correlated with NADPH imbalance fluxes in the cells (Supplementary Figure B.15). This latter result is presumably due to increased activity of soluble transhydrogenase UdhA, which corrects NADPH overproduction by converting NADPH to NADH with an accompanying normal KIE, leading to ^2H -enrichment of the residual NADPH pool. Surprisingly, NADPH imbalance was not correlated with proline $\delta^2\text{H}$ values in *E. coli* organisms, possibly because these modest effects were overprinted by changes in the $\delta^2\text{H}$ value of acetyl-CoA—the other major hydrogen source of proline. We attempted to disentangle these influences by isolating the contribution of NADPH to proline $\delta^2\text{H}$ variations in wildtype organisms. We subtracted the relative contribution of acetyl-CoA $\delta^2\text{H}$ variations ($12\text{H}_{\text{AcCoA}}$) from total shifts in proline $\delta^2\text{H}$ values (12H_{Pro}) between pairs of glucose and non-glucose substrate conditions:

$$\Delta^2\text{H}_{\text{NADPH}} = 7/2\Delta^2\text{H}_{\text{Pro}} - \Delta^2\text{H}_{\text{AcCoA}} \quad (3.3)$$

where $12\text{H}_{\text{NADPH}}$ is the NADPH-driven variation in proline $\delta^2\text{H}$. In turn, $12\text{H}_{\text{AcCoA}}$ can be estimated based on assumptions about how hydrogen is routed through the catabolic pathways. During glucose, pyruvate, and succinate metabolism, the majority of acetyl-CoA is produced from pyruvate via pyruvate dehydrogenase (Gerosa et al., 2015), and as the methyl group remains intact, no hydrogen isotope alteration is presumed to occur (Figure 3.8). Thus, $12\text{H}_{\text{AcCoA}}$ from glucose to pyruvate or succinate metabolism can be approximated as equal to shifts in cellular pyruvate $\delta^2\text{H}$ (12H_{Pyr} ; Supplementary Equation B.6), which in turn can be estimated through shifts in leucine or valine $\delta^2\text{H}$ (see Supplementary Section B.6.3 for details). During acetate metabolism, pyruvate hydrogen does not route into proline (Figure 3.8; Dolan et al., 2020; Gerosa et al., 2015, so individual cellular acetyl-CoA $\delta^2\text{H}$ values upon growth on acetate and glucose were estimated based on measured substrate $\delta^2\text{H}$ values and assumptions about hydrogen routing from substrates into acetyl-CoA (see Supplementary Section B.6.3 for details). The magnitudes of estimated NADPH-driven ^2H -enrichment of proline varied widely across organisms (Figure 3.7C). Interestingly, for *E. coli* and *B. subtilis* in particular, the magnitudes of NADPH imbalances in our glucose-grown cultures (-32 and -11%, respectively, measured in Wijker et al., 2019), as well as those from published work on *E. coli* grown on pyruvate (13%), acetate (50%), and succinate (72%; Gerosa et al., 2015; Haverkorn van Rijsewijk et al., 2016, appear to scale with the substrate ordering of NADPH-driven ^2H -enrichment of proline (Figure 3.7C). In *E. coli* and *B. subtilis*, significant soluble transhydrogenase activity has been demonstrated in association with NADPH overproduction (Fuhrer & Sauer, 2009; Haverkorn van Rijsewijk et al., 2016; U. Sauer et al., 2004), so the potentially progressive increase in ^2H -enrichment of the NADPH pool across growth on glucose, pyruvate, acetate, and succinate, may be contributing to the associated increase in proline (and other amino acid) $\delta^2\text{H}$ values. Control on $\delta^2\text{H}_{\text{AA}}$ values by

NADPH metabolism may also be important in *E. meliloti*, *P. fluorescens*, and *R. radiobacter*, but the extent of this control is unclear due to uncertainty in NADPH balancing mechanisms in these organisms.

Overall, the isotope composition of the NADPH pool appears to exert some control on the $\delta^2\text{H}$ values of amino acids that inherit NADPH hydrogen. Unlike for lipids, the influence of NADPH may be difficult to observe across different organisms, but more readily apparent when considering a given organism grown under different physiological conditions. In this way, primary controls on amino acid $\delta^2\text{H}$ values are different from those for lipids, yet amino acids may offer the unique advantage of isolating the isotopic influence of NADPH—i.e., by comparing the $\delta^2\text{H}$ values of amino acids containing versus lacking NADPH-derived hydrogen—which may enable researchers to probe NADPH-related metabolic phenomena such as redox balance in cells.

3.4.2.2 Enzymatic variations in biosynthetic pathways

Variations in $\delta^2\text{H}_{\text{AA}}$ values across organisms grown on the same substrate (e.g., Figure 3.4) may be driven not only by differences in the organisms' catabolic fluxes and pathways employed for substrate degradation, but also by species-specific differences in the amino acid biosynthetic enzymes and their isotope effects. Throughout the evolution of amino acid biosynthetic pathways, events such as gene duplication, functional convergence, and emergence of alternative pathways have contributed to a diversity in the enzymes and mechanisms of amino acid synthesis employed across different clades and species (Hernández-Montes et al., 2008). These enzymatic variations may contribute to different isotope effects expressed at each biosynthetic step, and consequently, different net fractionations expressed for the overall biosynthetic pathways. The five microbes investigated in this study largely employ

the same enzymatic reactions to synthesize their amino acids, but exhibit large variations in isozymes expressed for each step (Supplementary Figure B.20). For example, *B. subtilis* expresses three isozymes of pyrroline-5-carboxylate reductase (ProG, ProH, and ProI; EC 1.5.1.2)—which transfers hydrogen from NAD(P)H to catalyze the final step of proline biosynthesis (Supplementary Figure B.16)—while the other four organisms express the same single enzyme (ProC). These differences may contribute to some of the variations in $\delta^2\text{H}_{\text{AA}}$ values across the five organisms; however, a general lack of data on isotope effects in these pathways challenges interrogation of this hypothesis in our study. Future studies that elucidate the net hydrogen isotope fractionations in each amino acid biosynthetic pathway will be invaluable in facilitating a more comprehensive, mechanistic understanding of $\delta^2\text{H}_{\text{AA}}$ controls and variations.

3.4.3 Conclusions and potential applications

Here we have explored several hypotheses regarding biochemical controls on $\delta^2\text{H}_{\text{AA}}$ values in aerobic heterotrophic microbes. Our results demonstrate that the overall pattern of amino acid/water fractionations is highly correlated with the individual biosynthetic pathways in organisms, while magnitudes of fractionations are likely controlled by the organic precursor and NADPH isotope compositions. In turn, the $\delta^2\text{H}$ values of organic precursors and the NADPH pool are driven by the relative fluxes through different central metabolic pathways, which vary depending on the catabolic pathways activated for substrate degradation. Together, these results suggest that $\delta^2\text{H}_{\text{AA}}$ values may be useful tracers for carbon processing within organisms and the environment. As the 20 biological amino acids are ubiquitous across the tree of life, and organisms that share similar biosynthetic pathways should produce similar patterns of amino acid/water fractionations, we may expect

the $\delta^2\text{H}$ values of amino acids synthesized *de novo* across microbial and metazoan taxa to be governed by the same controls. Quantitative interrogations of the hypotheses presented in this study will likely require modeling work (e.g., Mueller et al., 2022), but are needed in order to fully understand the information encoded in these signals.

While controls on $\delta^2\text{H}_{\text{AA}}$ values are clearly nuanced and it may not be possible to uniquely relate all $\delta^2\text{H}_{\text{AA}}$ values to simple biological or environmental properties, the different combinations of hydrogen sources in amino acids leads to rich variability in $\delta^2\text{H}_{\text{AA}}$ signals, thus numerous potential applications of $\delta^2\text{H}_{\text{AA}}$ analysis. For example, $\delta^2\text{H}_{\text{AA}}$ values may provide insight into the metabolic strategies that microbes employ for carbon and energy acquisition. Microbes are the major drivers of nutrient and energy cycling in the environment, thereby playing substantial roles in shaping the geochemistry of our planet. While we observed large systematic variations in amino acid/water fractionations across heterotrophic microbes grown on different carbon substrates, we predict that even larger variations should exist between organisms of different metabolic classes (e.g., heterotrophs versus autotrophs), as is the case for lipids (Osburn et al., 2016; Zhang et al., 2009). If true, $\delta^2\text{H}_{\text{AA}}$ values and patterns may be used to decipher the metabolisms of unculturable organisms, to distinguish contributions by metabolically distinct organisms to geochemical processes in nature (e.g., in largely inaccessible environments such as deep subsurface biospheres), and/or to quantify contributions by different metabolisms to bulk organic matter in the environment (including by mixotrophic organisms that operate on a continuum of carbon and energy acquisition strategies, or across diverse taxa such as plants, algae, bacteria, and fungi). While lipid $\delta^2\text{H}$ values have been suggested as a potential tool for this latter application (Cormier et al., 2022), amino acids may offer distinct advantages, as their $\delta^2\text{H}$ values can be linked to host organisms through the isolation and sequencing of proteins (Gharibi,

Chernobrovkin, Saei, et al., 2022), and their different combinations of hydrogen sources capture a more diverse suite of information than is encoded in lipids (which inherit hydrogen from essentially the same three sources: acetyl-CoA, NADPH, and water). However, we view amino acid and lipid $\delta^2\text{H}$ analyses as complementary, as each can help inform interpretations from the other. Leucine and valine $\delta^2\text{H}$ may provide the most direct information about the metabolic 'state' or lifestyle of an organism, as the positioning of pyruvate as a central node in metabolism makes it relatively sensitive to the molecular wiring of central metabolic pathways in cells. In turn, accounting for these metabolic signals may help isolate the NADPH-driven signals in proline and lipid $\delta^2\text{H}$ values, thereby increasing their sensitivity as redox indicators in cells. Moreover, if the majority of phenylalanine hydrogen is indeed equilibrated with water at the level of metabolic intermediates, the $\delta^2\text{H}$ value of phenylalanine may provide insight into water $\delta^2\text{H}$ in places where water sources are unclear (e.g., in environments with intermittent wet/dry cycles), and if such equilibrium is temperature-dependent, phenylalanine could additionally serve as a potential bio-thermometer.

In addition to geomicrobiology-based applications, $\delta^2\text{H}_{\text{AA}}$ analyses may provide useful information about eukaryotic organisms, including their stressors, diets, and migration patterns. The application of $\delta^2\text{H}_{\text{AA}}$ values to human and wildlife forensics is in the early stages of exploration, with links between mammal diet, drinking water, and $\delta^2\text{H}_{\text{AA}}$ values beginning to emerge (Mancuso et al., 2023; Newsome et al., 2020). The biochemical controls discussed here may only be relevant for interpreting $\delta^2\text{H}$ values of non-essential amino acids (e.g., proline) as well as those with relatively high contributions from the gut microbiome (e.g., phenylalanine; Newsome et al., 2020). However, the differentiated tissues in animals, variable residence times of proteins in cells, and integration of numerous dietary hydrogen sources significantly increase the complexity of information encoded in mammalian

$\delta^2\text{H}_{\text{AA}}$ signals, which will require detailed investigations to disentangle. $\delta^2\text{H}_{\text{AA}}$ signals in plants likely carry important physiological information as well. Like microbes, plants can synthesize all 20 proteinogenic amino acids, yet their hydrogen metabolism may be simpler to interpret, as plants derive their organic hydrogen exclusively from water. Amino acids are involved in numerous mechanisms of stress alleviation in plants (e.g., Batista-Silva et al., 2019), so their $\delta^2\text{H}_{\text{AA}}$ values may encode information about their physiological status. For example, synthesis and degradation of proline helps maintain redox balance (i.e., the NADP/NADPH ratio) in plants and appears to facilitate drought tolerance (Batista-Silva et al., 2019; Bhaskara et al., 2015; Sharma et al., 2011). In the first step of proline catabolism, proline dehydrogenase removes a carbon-bound hydrogen atom, which should lead to ^2H -enrichment of the residual proline pool. Consequently, proline $\delta^2\text{H}$ values may serve as a sensitive indicator of oxidative and drought stress in plants, which are highly important aspects of crop health. This mechanism may additionally play a role in the extreme ^2H -enrichment of proline observed in gray seals (Gharibi, Chernobrovkin, Eriksson, et al., 2022), which endure significant periods of oxidative stress while diving. Overall, $\delta^2\text{H}_{\text{AA}}$ analysis has potential to become a highly useful isotopic tool for a variety of diverse applications, which will undoubtedly emerge as we continue to unravel the biochemical mechanisms underpinning $\delta^2\text{H}_{\text{AA}}$ signals in organisms.

Acknowledgments

The authors would like to thank Tyler Fulton and Dr. Brian Stoltz for assistance with the chemical reactions used to measure the isotope composition of methyl chloroformate, as well as Fenfang Wu, Patrick Almhjell, and Elliott Mueller for informative discussions. We would also like to thank both reviewers for their

constructive comments. This work was supported by an NSF GRFP and CEMI (Center for Environmental Microbial Interactions) award to SNS and an NSF award OCE-2023687 and NSF Geobiology and Low-Temperature Geochemistry Program award (#1921330) to ALS.

References

- Bada, J. L., Schoeninger, M. J., & Schimmelmann, A. (1989). Isotopic fractionation during peptide bond hydrolysis. *Geochimica et Cosmochimica Acta*, 53, 3337–3341. [https://doi.org/10.1016/0016-7037\(89\)90114-2](https://doi.org/10.1016/0016-7037(89)90114-2)
- Batista-Silva, W., Heinemann, B., Rugen, N., Nunes-Nesi, A., Araújo, W. L., Braun, H., & Hildebrandt, T. M. (2019). The role of amino acid metabolism during abiotic stress release. *Plant, Cell & Environment*, 42(5), 1630–1644. <https://doi.org/10.1111/pce.13518>
- Bhaskara, G. B., Yang, T.-H., & Verslues, P. E. (2015). Dynamic proline metabolism: Importance and regulation in water limited environments. *Frontiers in Plant Science*, 6. <https://doi.org/10.3389/fpls.2015.00484>
- Bizouarn, T., Grimley, R. L., Cotton, N. P., Stilwell, S. N., Hutton, M., & Jackson, J. B. (1995). The involvement of NADP(H) binding and release in energy transduction by proton-translocating nicotinamide nucleotide transhydrogenase from *Escherichia coli*. *Biochimica et Biophysica Acta*, 1229(1), 49–58. [https://doi.org/10.1016/0005-2728\(94\)00186-9](https://doi.org/10.1016/0005-2728(94)00186-9)
- Bollenbach, T. J., Mesecar, A. D., & Nowak, T. (1999). Role of lysine 240 in the mechanism of yeast pyruvate kinase catalysis. *Biochemistry*, 38(28), 9137–9145. <https://doi.org/10.1021/bi990690n>
- Bowen, G. J., Wassenaar, L. I., & Hobson, K. A. (2005). Global application of stable hydrogen and oxygen isotopes to wildlife forensics. *Oecologia*, 143(3), 337–348. <https://doi.org/10.1007/s00442-004-1813-y>
- Bruice, P. Y., & Bruice, T. C. (1978). Lack of concertedness in the catalysis of the enolization of oxaloacetic acid by general acids and bases. Formation of a carbinolamine intermediate in the tertiary amine catalyzed enolization reaction. *Journal of the American Chemical Society*, 100(15), 4793–4801. <https://doi.org/10.1021/ja00483a027>

- Chiang, Y., Kresge, A. J., & Pruszynski, P. (1992). Keto-enol equilibria in the pyruvic acid system: Determination of the keto-enol equilibrium constants of pyruvic acid and pyruvate anion and the acidity constant of pyruvate enol in aqueous solution. *Journal of the American Chemical Society*, *114*(8), 3103–3107. <https://doi.org/10.1021/ja00034a053>
- Cormier, M.-A., Berard, J.-B., Bougaran, G., Trueman, C. N., Mayor, D. J., Lampitt, R. S., Kruger, N. J., Flynn, K. J., & Rickaby, R. E. M. (2022). Deuterium in marine organic biomarkers: Toward a new tool for quantifying aquatic mixotrophy. *New Phytologist*, *234*(3), 776–782. <https://doi.org/10.1111/nph.18023>
- Craig, H. (1961). Isotopic Variations in Meteoric Waters. *Science*, *133*(3465), 1702–1703. <https://doi.org/10.1126/science.133.3465.1702>
- Csonka, L. N., & Fraenkel, D. G. (1977). Pathways of NADPH formation in *Escherichia coli*. *The Journal of Biological Chemistry*, *252*, 3382–3391.
- Dansgaard, W. (1964). Stable isotopes in precipitation. *Tellus*, *16*(4), 436–468. <https://doi.org/10.1111/j.2153-3490.1964.tb00181.x>
- Dolan, S. K., Kohlstedt, M., Trigg, S., Ramirez, P. V., Kaminski, C. F., Wittmann, C., & Welch, M. (2020). Contextual flexibility in *Pseudomonas aeruginosa* central carbon metabolism during growth in single carbon sources. *American Society for Microbiology*, *11*(2), e02684–19. <https://doi.org/https://doi.org/10.1128/mBio.02684-19>
- Falkowski, P. G., Fenchel, T., & Delong, E. F. (2008). The microbial engines that drive Earth's biogeochemical cycles. *Science*, *320*(5879), 1034–1039. <https://doi.org/10.1126/science.1153213>
- Fjellström, O., Bizouarn, T., Zhang, J.-W., Rydström, J., Venning, J. D., & Jackson, J. B. (1999). Catalytic properties of hybrid complexes of the NAD(H)-binding and NADP(H)-binding domains of the proton-translocating transhydrogenases from *Escherichia coli* and *Rhodospirillum rubrum*. *Biochemistry*, *38*(1), 415–422. <https://doi.org/10.1021/bi9817111>
- Fogel, M. L., Griffin, P. L., & Newsome, S. D. (2016). Hydrogen isotopes in individual amino acids reflect differentiated pools of hydrogen from food and water in *Escherichia coli*. *Proceedings of the National Academy of Sciences*, *113*(32), E4648–E4653. <https://doi.org/10.1073/pnas.1525703113>
- Fuhrer, T., Fischer, E., & Sauer, U. (2005). Experimental identification and quantification of glucose metabolism in seven bacterial species. *Journal of Bacteriology*, *187*(5), 1581–1590. <https://doi.org/10.1128/JB.187.5.1581-1590.2005>
- Fuhrer, T., & Sauer, U. (2009). Different biochemical mechanisms ensure network-wide balancing of reducing equivalents in microbial metabolism. *Journal of Bacteriology*, *191*(7), 2112–2121. <https://doi.org/10.1128/JB.01523-08>

- Gawron, O., & Fondy, T. P. (1959). Stereochemistry of the fumarase and aspartase catalyzed reactions and of the krebs cycle from fumaric acid to *d*-isocitric acid. *Journal of the American Chemical Society*, *81*, 6333–6334.
- Gerosa, L., Haverkorn van Rijsewijk, B. R., Christodoulou, D., Kochanowski, K., Schmidt, T. S., Noor, E., & Sauer, U. (2015). Pseudo-transition analysis identifies the key regulators of dynamic metabolic adaptations from steady-state data. *Cell Systems*, *1*(4), 270–282. <https://doi.org/10.1016/j.cels.2015.09.008>
- Gharibi, H., Chernobrovkin, A. L., Eriksson, G., Saei, A. A., Timmons, Z., Kitchener, A., Kalthoff, D. C., Lidén, K., Makarov, A. A., & Zubarev, R. A. (2022). Abnormal (hydroxy)proline deuterium content redefines hydrogen chemical mass. *Journal of the American Chemical Society*, *144*(6), 2484–2487. <https://doi.org/10.1021/jacs.1c12512>
- Gharibi, H., Chernobrovkin, A. L., Saei, A. A., Zhang, X., Gaetani, M., Makarov, A. A., & Zubarev, R. A. (2022). Proteomics-compatible Fourier transform isotopic ratio mass spectrometry of polypeptides. *Analytical Chemistry*, *94*, 15048–15056. <https://doi.org/10.1021/acs.analchem.2c03119>
- Haverkorn van Rijsewijk, B. R. B., Kochanowski, K., Heinemann, M., & Sauer, U. (2016). Distinct transcriptional regulation of the two *Escherichia coli* transhydrogenases PntAB and UdhA. *Microbiology*, *162*(9), 1672–1679. <https://doi.org/10.1099/mic.0.000346>
- Hernández-Montes, G., Díaz-Mejía, J. J., Pérez-Rueda, E., & Segovia, L. (2008). The hidden universal distribution of amino acids biosynthetic networks: A genomic perspective on its origins and evolution. *Genome Biology*, *9*(6), R95. <https://doi.org/10.1186/gb-2008-9-6-r95>
- Hill, J., & Leach, S. J. (1964). Hydrogen exchange at carbon-hydrogen sites during acid or alkaline treatment of proteins. *Biochemistry*, *3*(12), 1814–1818. <https://doi.org/10.1021/bi00900a003>
- Hušek, P. (1991a). Amino acid derivatization and analysis in five minutes. *Federation of European Biochemical Societies*, *280*(2), 354–356.
- Hušek, P. (1991b). Rapid derivatization and gas chromatographic determination of amino acids. *Journal of Chromatography A*, *552*, 289–299. [https://doi.org/10.1016/S0021-9673\(01\)95945-X](https://doi.org/10.1016/S0021-9673(01)95945-X)
- Jacobson, T. B., Adamczyk, P. A., Stevenson, D. M., Regner, M., Ralph, J., Reed, J. L., & Amador-Noguez, D. (2019). ²H and ¹³C metabolic flux analysis elucidates in vivo thermodynamics of the ED pathway in *Zymomonas mobilis*. *Metabolic Engineering*, *54*, 301–316. <https://doi.org/10.1016/j.ymben.2019.05.006>
- Kendall, C., & Coplen, T. B. (2001). Distribution of oxygen-18 and deuterium in river waters across the United States. *Hydrological Processes*, *15*(7), 1363–1393. <https://doi.org/10.1002/hyp.217>

- Kosicki, G. W. (1962). Isotope rate effects in the enolization of oxalacetic acid. *Canadian Journal of Chemistry*, 40(7), 1280–1284. <https://doi.org/10.1139/v62-196>
- Lenz, H., Buckel, W., Wunderwald, P., Biedermann, G., Buschmeier, V., Eggerer, H., Cornforth, J. W., Redmond, J. W., & Mallaby, R. (1971). Stereochemistry of *si*-citrate synthase and ATP-citrate-lyase reactions. *European Journal of Biochemistry*, 24(2), 207–215. <https://doi.org/10.1111/j.1432-1033.1971.tb19672.x>
- Liu, J., Li, J., Ren, J., & Zeng, B.-B. (2014). Oxidation of aromatic amines into nitroarenes with *m*-CPBA. *Tetrahedron Letters*, 55(9), 1581–1584. <https://doi.org/10.1016/j.tetlet.2014.01.073>
- Lowenstein, J. M. (1967). The tricarboxylic acid cycle. In D. M. Greenberg (Ed.), *Metabolic Pathways* (pp. 146–270, Vol. 1). Academic Press.
- Mancuso, C. J., Ehleringer, J. R., & Newsome, S. D. (2023). Examination of amino acid hydrogen isotope measurements of scalp hair for region-of-origin studies. *Rapid Communications in Mass Spectrometry*, 37(4), e9442. <https://doi.org/10.1002/rcm.9442>
- McKinney, C. R., McRea, I. M., Epstein, S., Allen, H. A., & Urey, H. C. (1950). Improvements in mass spectrometers for measurement of small differences in isotope abundance ratios. *Review of Scientific Instruments*, 21, 724–730.
- Meloche, H. P. (1975). An enzymic synthesis yielding crystalline sodium pyruvate labeled with isotopic hydrogen. *Methods in Enzymology*, 41, 106–110.
- Mueller, E. P., Wu, F., & Sessions, A. L. (2022). Quantifying Isotopologue Reaction Networks (QIRN): A modelling tool for predicting stable isotope fractionations in complex networks. *Chemical Geology*, 610, 121098. <https://doi.org/10.1016/j.chemgeo.2022.121098>
- Newsome, S. D., Nakamoto, B. J., Curras, M. R., & Fogel, M. L. (2020). Compound-specific $\delta^2\text{H}$ analysis highlights the relationship between direct assimilation and de novo synthesis of amino acids from food and water in a terrestrial mammalian omnivore. *Oecologia*, 193(4), 827–842. <https://doi.org/10.1007/s00442-020-04730-9>
- Nikel, P. I., Chavarría, M., Fuhrer, T., Sauer, U., & de Lorenzo, V. (2015). *Pseudomonas putida* KT2440 strain metabolizes glucose through a cycle formed by enzymes of the Entner-Doudoroff, Embden-Meyerhof-Parnas, and pentose phosphate pathways. *The Journal of Biological Chemistry*, 290, 25920–25932. <https://linkinghub.elsevier.com/retrieve/pii/S0021925820495730>
- Ochs, R. S., & Talele, T. T. (2020). Revisiting prochirality. *Biochimie*, 170, 65–72. <https://doi.org/10.1016/j.biochi.2019.12.009>
- O'Leary, M. H. (1989). Multiple isotope effects on enzyme-catalyzed reactions. *Annual Review of Biochemistry*, 58, 377–401.

- Omi, R., Goto, M., Miyahara, I., Mizuguchi, H., Hayashi, H., Kagamiyama, H., & Hirotsu, K. (2003). Crystal structures of threonine synthase from *Thermus thermophilus* HB8. *The Journal of Biological Chemistry*, *278*, 46035–46045.
- Osburn, M. R., Dawson, K. S., Fogel, M. L., & Sessions, A. L. (2016). Fractionation of hydrogen isotopes by sulfate- and nitrate-reducing bacteria. *Frontiers in Microbiology*, *7*. <https://doi.org/10.3389/fmicb.2016.01166>
- Phillips, A. A., Wu, F., & Sessions, A. L. (2021). Sulfur isotope analysis of cysteine and methionine via preparatory liquid chromatography and elemental analyzer isotope ratio mass spectrometry. *Rapid Communications in Mass Spectrometry*, *35*, e9007. <https://doi.org/10.1002/rcm.9007>
- Poage, M. A., & Chamberlain, C. P. (2001). Empirical relationships between elevation and the stable isotope composition of precipitation and surface waters: Considerations for studies of paleoelevation change. *American Journal of Science*, *301*(1), 1–15. <https://doi.org/10.2475/ajs.301.1.1>
- Price, M. N., Zane, G. M., Kuehl, J. V., Melnyk, R. A., Wall, J. D., Deutschbauer, A. M., & Arkin, A. P. (2018). Filling gaps in bacterial amino acid biosynthesis pathways with high-throughput genetics. *PLOS Genetics*, *14*(1), e1007147. <https://doi.org/10.1371/journal.pgen.1007147>
- Renpenning, J., Schimmelmann, A., & Gehre, M. (2017). Compound-specific hydrogen isotope analysis of fluorine-, chlorine-, bromine- and iodine-bearing organics using gas chromatography-chromium-based high-temperature conversion (Cr/HTC) isotope ratio mass spectrometry. *Rapid Communications in Mass Spectrometry*, *31*, 1095–1102. <https://doi.org/10.1002/rcm.7872>
- Rétey, J., Seibl, J., Arigoni, D., Cornforth, J. W., Ryback, G., Zeylemaker, W. P., & Veeger, C. (1970). Stereochemical studies of the exchange and abstraction of succinate hydrogen on succinate dehydrogenase. *European Journal of Biochemistry*, *14*(2), 232–242. <https://doi.org/10.1111/j.1432-1033.1970.tb00282.x>
- Reynolds, S. J., Yates, D. W., & Pogson, C. I. (1971). Dihydroxyacetone Phosphate: Its structure and reactivity with α -glycerophosphate dehydrogenase, aldolase and triose phosphate isomerase and some possible metabolic implications. *Biochemical Journal*, *122*, 285–297.
- Rose, I. A., & O'Connell, E. L. (1961). Intramolecular hydrogen transfer in the phosphoglucose isomerase reaction. *Journal of Biological Chemistry*, *236*(12), 3086–3092. [https://doi.org/10.1016/S0021-9258\(18\)93975-X](https://doi.org/10.1016/S0021-9258(18)93975-X)
- Rozanski, K., Araguás-Araguás, L., & Gonfiantini, R. (1993). Isotopic patterns in modern global precipitation. In P. K. Swart, K. C. Lohmann, J. Mckenzie, & S. Savin (Eds.), *Climate Change in Continental Isotopic Records* (pp. 1–36). American Geophysical Union. <https://doi.org/10.1029/GM078p0001>

- Rubenstein, D. R., & Hobson, K. A. (2004). From birds to butterflies: Animal movement patterns and stable isotopes. *Trends in Ecology & Evolution*, *19*(5), 256–263. <https://doi.org/10.1016/j.tree.2004.03.017>
- Russell, R. W., & Young, J. W. (1990). A review of metabolism of labeled glucoses for use in measuring glucose recycling. *Journal of Dairy Science*, *73*(4), 1005–1016. [https://doi.org/10.3168/jds.S0022-0302\(90\)78759-0](https://doi.org/10.3168/jds.S0022-0302(90)78759-0)
- Sauer, P. E., Eglinton, T. I., Hayes, J. M., Schimmelmann, A., & Sessions, A. L. (2001). Compound-specific D/H ratios of lipid biomarkers from sediments as a proxy for environmental and climatic conditions. *Geochimica et Cosmochimica Acta*, *65*(2), 213–222. [https://doi.org/10.1016/S0016-7037\(00\)00520-2](https://doi.org/10.1016/S0016-7037(00)00520-2)
- Sauer, U., Canonaco, F., Heri, S., Perrenoud, A., & Fischer, E. (2004). The soluble and membrane-bound transhydrogenases UdhA and PntAB have divergent functions in NADPH metabolism of *Escherichia coli*. *Journal of Biological Chemistry*, *279*(8), 6613–6619. <https://doi.org/10.1074/jbc.M311657200>
- Saur, W. K., Crespi, H. L., Halevi, E. A., & Katz, J. J. (1968). Deuterium isotope effects in the fermentation of hexoses to ethanol by *Saccharomyces cerevisiae*. I. Hydrogen exchange in the glycolytic pathway. *Biochemistry*, *7*(10), 3529–3536. <https://doi.org/10.1021/bi00850a030>
- Schindler, U., Sans, N., & Schröder, J. (1989). Ornithine cyclodeaminase from octopine Ti plasmid Ach5: Identification, DNA sequence, enzyme properties, and comparison with gene and enzyme from nopaline Ti plasmid C58. *Journal of Bacteriology*, *171*, 847–854.
- Sessions, A. L., Jahnke, L. L., Schimmelmann, A., & Hayes, J. M. (2002). Hydrogen isotope fractionation in lipids of the methane-oxidizing bacterium *Methylococcus capsulatus*. *Geochimica et Cosmochimica Acta*, *66*(22), 3955–3969. [https://doi.org/10.1016/S0016-7037\(02\)00981-X](https://doi.org/10.1016/S0016-7037(02)00981-X)
- Sharma, S., Villamor, J. G., & Verslues, P. E. (2011). Essential role of tissue-specific proline synthesis and catabolism in growth and redox balance at low water potential. *Plant Physiology*, *157*, 292–304.
- Silverman, S. N., Phillips, A. A., Weiss, G. M., Wilkes, E. B., Eiler, J. M., & Sessions, A. L. (2022). Practical considerations for amino acid isotope analysis. *Organic Geochemistry*, *164*, 104345. <https://doi.org/10.1016/j.orggeochem.2021.104345>
- Smith, D. A., Nakamoto, B. J., Suess, M. K., & Fogel, M. L. (2022). Central metabolism and growth rate impacts on hydrogen and carbon isotope fractionation during amino acid synthesis in *E. coli*. *Frontiers in Microbiology*, *13*, 840167. <https://doi.org/10.3389/fmicb.2022.840167>
- Smith, W. G., & York, J. L. (1970). Stereochemistry of the citric acid cycle. *Journal of Chemical Education*, *47*(8), 588. <https://doi.org/10.1021/ed047p588>

- Stalon, V., Vander Wauven, C., Momin, P., & Legrain, C. (1987). Catabolism of arginine, citrulline and ornithine by *Pseudomonas* and related bacteria. *Journal of General Microbiology*, *133*, 2487–2495.
- Urey, H. C. (1948). Oxygen isotopes in nature and in the laboratory. *Science*, *108*, 489–496.
- Venning, J. D., Bizouarn, T., Cotton, N. P. J., Quirk, P. G., & Jackson, J. B. (1998). Stopped-flow kinetics of hydride transfer between nucleotides by recombinant domains of proton-translocating transhydrogenase. *European Journal of Biochemistry*, *257*(1), 202–209. <https://doi.org/10.1046/j.1432-1327.1998.2570202.x>
- Wang, Y., Sessions, A. L., Nielsen, R. J., & Goddard, W. A. (2009). Equilibrium $^2\text{H}/^1\text{H}$ fractionations in organic molecules. II: Linear alkanes, alkenes, ketones, carboxylic acids, esters, alcohols and ethers. *Geochimica et Cosmochimica Acta*, *73*(23), 7076–7086. <https://doi.org/10.1016/j.gca.2009.08.018>
- Wang, Y., Sessions, A. L., Nielsen, R. J., & Goddard, W. A. (2013). Equilibrium $^2\text{H}/^1\text{H}$ fractionation in organic molecules: III. Cyclic ketones and hydrocarbons. *Geochimica et Cosmochimica Acta*, *107*, 82–95. <https://doi.org/10.1016/j.gca.2013.01.001>
- Wassenaar, L. I., & Hobson, K. A. (2003). Comparative equilibration and on-line technique for determination of non-exchangeable hydrogen of keratins for use in animal migration studies. *Isotopes in Environmental and Health Studies*, *39*, 211–217.
- Wijker, R. S., Sessions, A. L., Fuhrer, T., & Phan, M. (2019). $^2\text{H}/^1\text{H}$ variation in microbial lipids is controlled by NADPH metabolism. *Proceedings of the National Academy of Sciences*, *116*(25), 12173–12182.
- Zampolli, M., Basaglia, G., Dondi, F., Sternberg, R., Szopa, C., & Pietrogrande, M. (2007). Gas chromatography-mass spectrometry analysis of amino acid enantiomers as methyl chloroformate derivatives: Application to space analysis. *Journal of Chromatography A*, *1150*(1-2), 162–172. <https://doi.org/10.1016/j.chroma.2006.12.033>
- Zhang, X., Gillespie, A. L., & Sessions, A. L. (2009). Large D/H variations in bacterial lipids reflect central metabolic pathways. *Proceedings of the National Academy of Sciences*, *106*(31), 12580–12586. <https://doi.org/10.1073/pnas.0903030106>
- Zhao, J., & Shimizu, K. (2003). Metabolic flux analysis of *Escherichia coli* K12 grown on ^{13}C -labeled acetate and glucose using GC-MS and powerful flux calculation method. *Journal of Biotechnology*, *101*(2), 101–117. [https://doi.org/10.1016/S0168-1656\(02\)00316-4](https://doi.org/10.1016/S0168-1656(02)00316-4)

Chapter 4

The $\delta^2\text{H}_{\text{AA}}$ signature of phytoplankton

Coauthors: Gabriella M. Weiss, Juli Panehal, Alessandra Flaherty, and Alex L. Sessions

Abstract

Growing evidence suggests the hydrogen isotope compositions of amino acids ($\delta^2\text{H}_{\text{AA}}$) are useful tracers of carbon flow in cells. Such a proxy is invaluable for more broadly tracing carbon flux in the environment; however, culture-based studies have thus far focused on the impact of aerobic heterotrophic metabolisms on $\delta^2\text{H}_{\text{AA}}$ values. Primary producers fix a substantial amount of atmospheric carbon annually. These organisms dominate our planet's biomass, and their organic matter provides the initial input into terrestrial and marine ecosystems, fueling downstream metabolisms and global biogeochemical cycling of nutrients. As such, characterizing the $\delta^2\text{H}_{\text{AA}}$ values of primary producers as a baseline signal, and understanding the factors that control these signals, are necessary to trace further trophic processing of organic matter in the environment. Here, we explore these aspects in cultures of marine phytoplankton (diatoms, cyanobacteria, and a coccolithophore), and find that photoautotrophic metabolism fractionates amino acid hydrogen isotopes (relative to water) more substantially compared with heterotrophic metabolism, but general patterns in $\delta^2\text{H}_{\text{AA}}$ values are similar between these two metabolic groups. Moreover, variations in salinity and irradiance led to changes in the magnitudes of amino acid $^2\text{H}/^1\text{H}$ fractionations in phytoplankton,

but these effects were secondary when compared to the apparent primary control of biosynthetic and metabolic pathways on $\delta^2\text{H}_{\text{AA}}$ values. Together, these results suggest that organic matter produced by photoautotrophic versus heterotrophic metabolisms in the environment may be distinguishable through $\delta^2\text{H}_{\text{AA}}$ analysis, further strengthening the potential utility of this tool for tracing carbon flow through natural ecosystems.

4.1 Introduction

In the last decade, scientists have begun exploring the final major frontier of compound-specific stable isotope analysis: that of amino acid hydrogen isotopes. Evidence is now mounting that amino acid $\delta^2\text{H}$ values record rich, nuanced information about cellular metabolism (Fogel et al., 2016; Gharibi et al., 2022; Newsome et al., 2020; Silverman et al., 2024; D. A. Smith et al., 2022), rendering these signals potentially highly useful proxies for cellular activity in the environment. In particular, we have shown that $\delta^2\text{H}_{\text{AA}}$ values provide information about the type of carbon substrate metabolized by aerobic, enteric bacteria (with sugar metabolism yielding relatively ^2H -depleted amino acids, and organic acid metabolism stimulating systematic ^2H -enrichments; Silverman et al., 2024). When applied to the environment, hydrogen isotope analysis of amino acids may provide powerful information about carbon cycling in environmental microbial communities. However, much still remains unknown about the metabolic and environmental factors controlling $\delta^2\text{H}_{\text{AA}}$ values in cells.

To date, $\delta^2\text{H}_{\text{AA}}$ studies have been limited to aerobic heterotrophic metabolisms. While such metabolisms play an undeniably important role in driving carbon cycling in many environmental locales, virtually all organic matter production in the biosphere starts with oxygenic photoautotrophy, whose $\delta^2\text{H}_{\text{AA}}$ signatures have yet

to be examined. Global carbon fixation is carried out in nearly equal proportions between terrestrial plants (which are long lived and dominate global biomass; Bar-On et al., 2018) and marine phytoplankton (which, despite exhibiting more rapid biomass turnover, facilitate substantial carbon storage in the deep ocean; Boyd et al., 2019; Field et al., 1998). Primary producer biomass provides the main organic carbon input to terrestrial and marine ecosystems, and its degradation by micro- and macro-organisms fuels important biogeochemical cycling of nutrients. As such, understanding controls on the $\delta^2\text{H}_{\text{AA}}$ values of both terrestrial and marine photoautotrophic organisms will (i) help characterize the baseline $\delta^2\text{H}_{\text{AA}}$ values of the organic matter input into these ecosystems, (ii) potentially enable development of this isotopic tool into a useful tracer for monitoring the physiological status of primary producers (e.g., signs of physiological stress that reduce their primary productivity), and (iii) further our fundamental understanding of metabolic information that can be extracted from general organismal $\delta^2\text{H}_{\text{AA}}$ values.

Here, we explore the above three points by focusing on marine phytoplankton, which are relatively easier to study than higher plants due to their faster growth rates and simpler physiologies. However, conclusions drawn from cyanobacteria and eukaryotic phytoplankton $\delta^2\text{H}_{\text{AA}}$ studies are likely still relevant for terrestrial plant studies, as amino acid biosynthetic pathways in these organisms are largely similar to those in higher plants (Bromke, 2013). We cultured members from three major taxonomic groups, including six strains of the cyanobacteria *Synechococcus*, three species of diatoms (*Chaetoceros muelleri*, *Phaeodactylum tricorutum*, and *Thalassiosira pseudonana*), and the coccolithophore *Emiliania huxleyi*. We characterized their general patterns of amino acid $^2\text{H}/^1\text{H}$ fractionations (both comparisons across phytoplankton groups, and against known $^2\text{H}/^1\text{H}$ fractionations by bacteria) and, furthermore, investigated whether variations in environmentally-relevant physiological conditions—salinity and irradiance—induce

variations in phytoplankton $^2\text{H}/^1\text{H}$ fractionations. Together, our phytoplankton data strengthens conclusions from our earlier work (Silverman et al., 2024) that $\delta^2\text{H}_{\text{AA}}$ values record valuable information about carbon and energy metabolism in cells. As such, $\delta^2\text{H}_{\text{AA}}$ analysis may be a highly useful tool for tracing biogeochemical processes in cells and the environment.

4.2 Materials and methods

4.2.1 Strain and culture conditions

All phytoplankton investigated in this chapter were grown photoautotrophically in batch culture in Thermo Scientific MaxQ 6000 refrigerated shakers. Light levels were controlled with cool white LED light strips and measured with a PHOTOBIO Advanced Quantum PAR meter. Seawater salinity was measured with a YSI conductivity meter. pH was measured using a Beckman Coulter Φ 350 pH meter equipped with a sealed, Tris-compatible Beckman electrode (VWR no. BKA51705).

Emiliana huxleyi CCMP371 (Bigelow NCMA) was cultured in medium prepared using filtered natural seawater from the Kerckhoff Marine Laboratory with added nutrients and trace metals (K/2 recipe; Keller and Guillard, 1985; Keller et al., 1987) and vitamins (f/2 recipe; Guillard, 1975; Guillard and Ryther, 1962). The medium was adjusted to pH = 8.1, then filter sterilized through a 0.2 μm PES filter and stored at 4°C. *E. huxleyi* was cultured in four different salinities (24, 27, 31, and 36 ppt) at 20°C under 16h:8h light:dark cycles, with irradiance = 200 $\mu\text{mol photons m}^{-2} \text{ s}^{-1}$ during the light phase. Prior to starting the experiment, cultures were transferred to new medium to adapt cells to the experimental conditions. Cultures were gently shaken (80rpm) to keep cells and nutrients well-

mixed, and culture growth was monitored by measuring optical density at 600 nm (OD_{600}). At the end of the experiment, cells were harvested via centrifugation during mid-exponential phase, lyophilized, and stored at -20°C until further processing. Aliquots of media were collected following biomass collection to determine the growth water $\delta^2\text{H}$ values.

Six strains of *Synechococcus* sp. (RCC2673, RCC555, WH7803, WH8020, WH8102, and WH8109) were obtained as gifts from the Mackey lab (University of California, Irvine), and cultured in medium prepared using filtered natural seawater from the Kerckhoff Marine Laboratory with added nutrients, trace metals, and vitamins (SN recipe; Waterbury et al., 1986). The medium salinity was 35 ppt, and pH was adjusted to 8.1. The medium was filter sterilized through a $0.2\mu\text{m}$ PES filter and stored at 4°C . All *Synechococcus* cultures were grown under conditions to which they were acclimated in the Mackey lab: 22°C under continuous illumination of $15\mu\text{mol photons m}^{-2} \text{s}^{-1}$. Culture growth was monitored by measuring OD_{600} , and cells were harvested via centrifugation during mid-exponential phase, lyophilized, and stored at -20°C until further processing. Aliquots of media were collected following biomass collection to determine the growth water $\delta^2\text{H}$ values.

Three diatom species (*Chaetoceros muelleri* CCMP1316, *Phaeodactylum tricorutum* CCMP2561, and *Thalassiosira pseudonana* CCMP1335) were obtained as gifts from the Allen lab (Scripps Institution of Oceanography) and cultured in medium prepared using artificial seawater (Aquil salt recipe; Price et al., 1989; Sunda et al., 2005) with added nutrients, trace metals, and vitamins (f/2 recipe; Guillard, 1975; Guillard and Ryther, 1962). The medium salinity was 35 ppt, and pH was adjusted to 8.1. The medium was filter sterilized through a $0.2\mu\text{m}$ PES filter and stored at 4°C . *C. muelleri* was maintained at 24°C , while *P. tricorutum* and *T. pseudonana* were maintained at 18°C . In a control experiment, all three diatoms were cultured in duplicate under 16h:8h light:dark cycles, with irradiance

= 100 $\mu\text{mol photons m}^{-2} \text{ s}^{-1}$ during the light phase. In a separate experiment, *C. muelleri* and *T. pseudonana* were cultured in triplicate under 16h:8h light:dark cycles with different light intensities (50, 100, 400, and 800 $\mu\text{mol photons m}^{-2} \text{ s}^{-1}$). The lowest irradiance (50 $\mu\text{mol photons m}^{-2} \text{ s}^{-1}$) was achieved by covering flasks with Kimwipes, as irradiance measurements with Kimwipe-wrapped glass beakers confirmed reduced light penetration. The other irradiances were achieved by positioning cultures at fixed distances away from the lights. Cells were acclimated to experimental conditions over the course of three transfers to fresh medium. Irradiance levels were verified with the PAR meter. All diatom cultures were grown with shaking at 80rpm. Culture growth was monitored via OD₇₅₀ measurements. Cells were harvested during mid-exponential phase via filtration onto 0.7 μm GF/F filters. Filters were stored at -20°C until further processing. Aliquots of media were collected following filtration to determine the growth water $\delta^2\text{H}$ values.

4.2.2 Amino acid preparation and isotope analysis

Up to 15mg of biomass from each sample was hydrolyzed under N₂ to liberate proteinogenic amino acids, which were subsequently derivatized and extracted following the procedure outlined in Silverman et al. [2024](#). The derivative products (methoxycarbonyl esters) were identified and quantified via gas chromatography/mass spectrometry (GC/MS), with quantification achieved via a six-point calibration curve of amino acid standards injected at known amounts. The hydrogen isotope ratios of the derivatized amino acids were measured via gas chromatography/pyrolysis/isotope ratio mass spectrometry (GC/P/IRMS) using a Thermo Finnigan Delta⁺XP or Thermo Scientific 253 Plus IRMS. The GC columns and methods were identical to those used by Silverman et al. ([2024](#)) (with supplemental use of a thick-film Agilent DB-XLB column—30-m \times 0.25-mm i.d., 1.00 μm

film thickness—to separate alanine and glycine derived from diatom biomass from irradiance experiments), as well as the methods used to calibrate the measured isotope ratios, verify instrument accuracy and precision, and correct for the addition of methyl hydrogen from the derivative reagents and exchangeable amine hydrogen (see also Section 3.2.5 in Chapter 3). A mixture of amino acid standards was additionally analyzed every 6–10 samples to monitor instrument consistency throughout sample runs and across experiments (Figure C.1). Moreover, amino acid peak sizes varied substantially across individual chromatograms, sample injections, and experiments (Figure C.5). As analysis of small peaks can introduce significant measurement artefacts (Figure C.2), $\delta^2\text{H}_{\text{AA}}$ values were corrected for peak size effects based on standard calibration curves generated during each round of sample analysis (see Section C.2 for details).

The standard deviation of triplicate analyses for individual amino acids was typically $\leq 7\text{‰}$. The average root-mean-square error (RMSE) of the external FAME standard was 3.5‰ across all analyses. $\delta^2\text{H}$ values of the culture media ($\delta^2\text{H}_w$) were measured using a Picarro L2140-*i* liquid water isotope analyzer and calibrated against five working standards with $\delta^2\text{H}$ values ranging from -155 to $+4\text{‰}$. Data are reported as apparent fractionations between amino acids (AA) and culture medium water (w) according to the equation ${}^2\varepsilon_{\text{AA/w}} = (\delta^2\text{H}_{\text{AA}} + 1) / (\delta^2\text{H}_w + 1) - 1$, with uncertainty propagated as Equation 3.1, with σ_{AA} representing the combination of uncertainty from the sample analysis (i.e., measurement precision), derivative correction, and peak size correction.

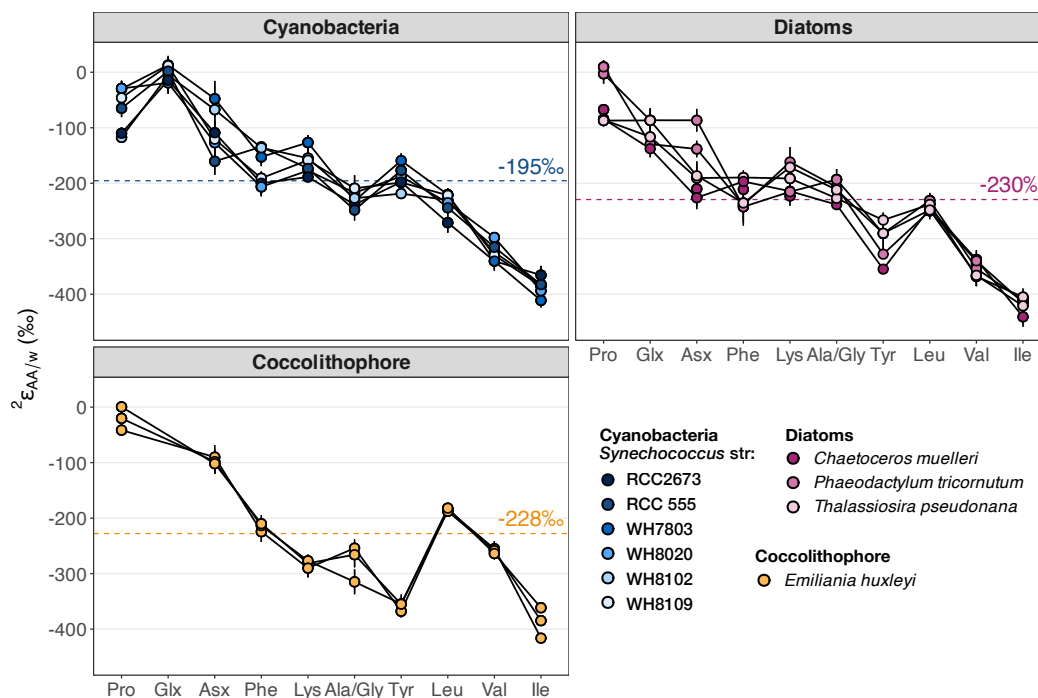


Figure 4.1. Summary of $^2\text{H}/^1\text{H}$ fractionations between amino acids and water in phytoplankton cultured in this study. Error bars indicate the propagated uncertainties ($\pm 1\sigma$) from the amino acid (measurement + peak size correction uncertainty), derivative, and water measurements. The average across all amino acids and cultures for each subgroup of organisms is denoted by the dashed line and colored $^2\epsilon_{\text{AA}/\text{w}}$ value in each panel. Organisms include six strains of *Synechococcus* sp. (cyanobacteria) grown as single replicates (irradiance (I) = $15\mu\text{mol photons m}^{-2} \text{s}^{-1}$; salinity (S) = 35 ppt), three diatoms grown in duplicate (I = $100\mu\text{mol photons m}^{-2} \text{s}^{-1}$; S = 35 ppt), and *E. huxleyi* (coccolithophore) grown as single replicates (I = $200\mu\text{mol photons m}^{-2} \text{s}^{-1}$; S = 27-36 ppt). Amino acids are proline (Pro), glutamic acid + glutamine (Glx), aspartic acid + asparagine (Asx), phenylalanine (Phe), lysine (Lys), alanine + glycine (Ala/Gly), tyrosine (Tyr), leucine (Leu), valine (Val), and isoleucine (Ile).

4.3 Results

4.3.1 Phytoplankton $^2\text{H}/^1\text{H}$ fractionations

The 10 phytoplankton strains cultured photoautotrophically in this study produced amino acids that span a strikingly large range of $\delta^2\text{H}$ values ($\sim 400\text{‰}$ in each

culture). Moreover, the different taxonomic groups produced similar $\delta^2\text{H}$ patterns, with proline, Glx (glutamic acid + glutamine), and Asx (aspartic acid + asparagine) the most ^2H -enriched, and isoleucine the most ^2H -depleted (Figures 4.1 and 4.2). Phenylalanine, lysine, alanine + glycine (combined due to co-elutions on the GC), and leucine generally had $\delta^2\text{H}$ values close to the average across all amino acids in each culture. Moreover, $\delta^2\text{H}$ values of leucine, valine, and isoleucine—synthesized in the same branched chain amino acid biosynthetic pathway—exhibited a fixed ordering across all organisms. In the cyanobacteria, tyrosine $\delta^2\text{H}$ values were higher than those of leucine, whereas in the eukaryotic microalgae (diatoms and *E. huxleyi*), the opposite was observed. The six *Synechococcus* strains yielded $^2\epsilon_{\text{AA/w}}$ values typically within $\pm 30\%$ of each amino acid-specific group average, while the three diatom species yielded $^2\epsilon_{\text{AA/w}}$ values typically within $\pm 40\%$ of each amino acid-specific group average.

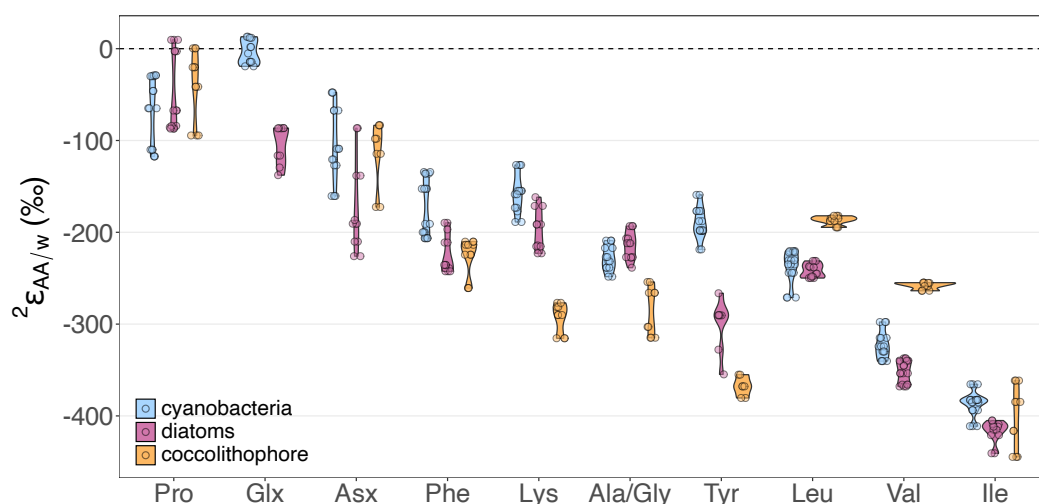


Figure 4.2. Probability distributions (with data from Figure 4.1 overlaid) of amino acid/water $^2\text{H}/^1\text{H}$ fractionations in cyanobacteria, diatoms, and *E. huxleyi* cultured in this study.

Despite the similar general patterns in $^2\epsilon_{\text{AA/w}}$ values observed across all phytoplankton species, systematic differences were observed between bulk taxonomic groups. Diatoms generally produced amino acids with lower $\delta^2\text{H}$ values compared

to cyanobacteria (except for proline, alanine + glycine, and leucine), whereas amino acids synthesized by *E. huxleyi* were generally variably ^2H -enriched or ^2H -depleted relative to the other taxonomic groups (Figure 4.2). Distributions of $^2\epsilon$ values for all amino acids except leucine and proline were significantly different between cyanobacteria and diatoms (p -value < 0.01 from Mann-Whitney U test; Table C.1). In contrast, distributions for only six amino acids were significantly different between *E. huxleyi* and cyanobacteria, and between *E. huxleyi* and diatoms, respectively (p -value < 0.01 ; Table C.1). Pooled $\delta^2\text{H}_{\text{AA}}$ values from all phytoplankton were significantly lower than those from terrestrial bacteria cultured on different sugar or organic acid substrates (measured in Silverman et al., 2024; Figure 4.3; Table C.2). These differences were most pronounced for Asx, phenylalanine, lysine, and tyrosine.

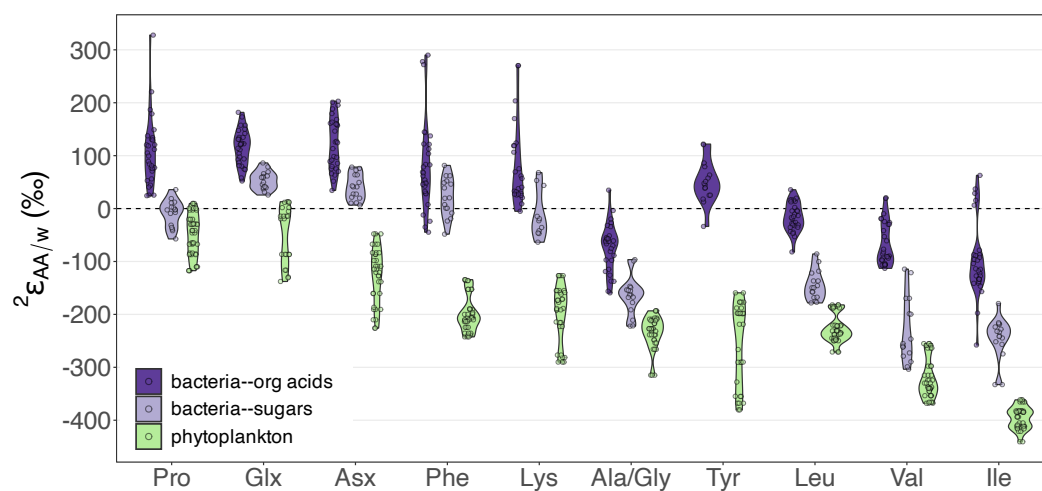


Figure 4.3. Probability distributions (with data overlaid) of amino acid/water $^2\text{H}/^1\text{H}$ fractionations in 10 species of phytoplankton (this study; Figure 4.2), and in five species of terrestrial bacteria cultured on sugars or organic acids (Silverman et al., 2024). Tyrosine was not measured in biomass from sugar-fed bacteria, as the GC method did not properly capture its elution window.

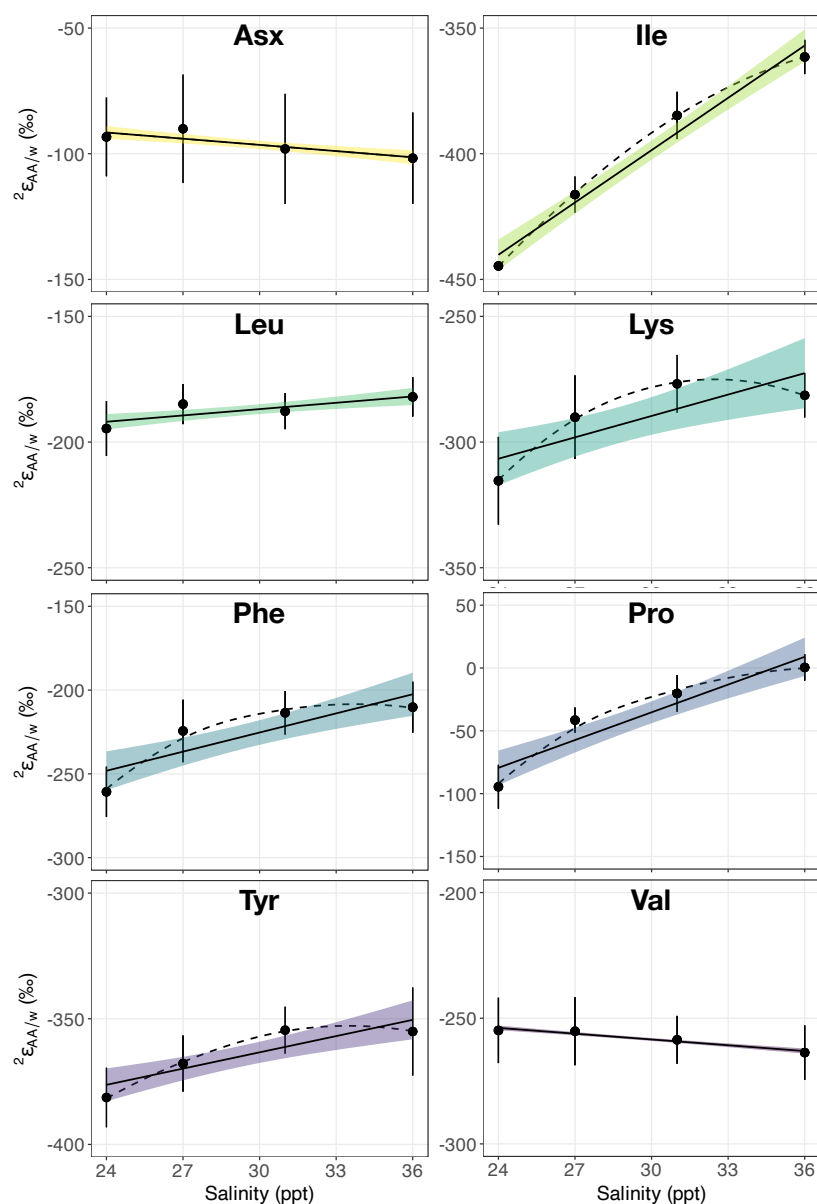


Figure 4.4. Amino acid/water $^2\text{H}/^1\text{H}$ fractionations in *E. huxleyi* cultured in different salinities. Data for all amino acids were fit with linear regressions (solid lines, with standard errors represented by colored shaded regions). Changes in fractionations for five amino acids appeared to plateau after 31 ppt; these data were additionally fit with nonlinear regressions (dashed curves). Slopes accompanying the regressions are provided in Table 4.1.

4.3.2 *E. huxleyi* $^2\text{H}/^1\text{H}$ fractionations in response to salinity

E. huxleyi was cultured in media with different salinity levels in order to test whether, like lipids, amino acid hydrogen isotope fractionations in phytoplankton vary in response to salinity. With increasing salinity (from 24 to 36 ppt), proline and isoleucine became most strongly ^2H -enriched (i.e., decreasing hydrogen isotope fractionation), with average $^2\varepsilon_{\text{AA/w}}$ shifts equal to 7.4 and 6.9‰ per unit salinity, respectively (Figure 4.4; Table 4.1). Fractionations of hydrogen isotopes in lysine, phenylalanine, and tyrosine also decreased strongly with increasing salinity (by averages of 2.2–3.8‰ per unit salinity; Figure 4.4; Table 4.1), falling within the range typically observed for lipids in *E. huxleyi* (1–4‰ per unit salinity; M'Boule et al., 2014; Sachs et al., 2016; Schouten et al., 2006; Weiss et al., 2017). After 31 ppt, changes in $^2\varepsilon_{\text{AA/w}}$ values of isoleucine, lysine, phenylalanine, proline, and tyrosine appeared to plateau. However, error bars on all $^2\varepsilon_{\text{AA/w}}$ measurements for these five amino acids fell within the standard errors accompanying each linear regression (Figure 4.4). As such, both linear and nonlinear fits to the data are reported (Table 4.1). Leucine was ^2H -enriched with salinity, but with a lower magnitude compared to the aforementioned amino acids, whereas Asx and valine appeared to become slightly ^2H -depleted with salinity. Five amino acids were quantified, and all increased in relative abundance with salinity (Figure 4.5).

Relative to the 31 ppt salinity condition, *E. huxleyi* cultures grown in 27 and 36 ppt salinity exhibited slightly longer lag times and lower growth rates. The culture grown in 24 ppt salinity was most dramatically affected, with a nearly two-week lag time and growth rate nearly half of that in the 31 ppt condition (Figure C.9). However, growth of these cultures was tracked by OD_{600} measurements, which may not be a reliable quantitative metric for phytoplankton growth, as chlorophyll can absorb light at 600nm (e.g., Granata et al., 2019). Thus, we avoid overinterpreting

Table 4.1. Summary statistics for regressions shown in Figure 4.4. Slopes and R^2 values are given for linear fits across the entire range of data (Total regression), and across the initial portion of the nonlinear curves (salinity ≤ 31 ppt; Initial regression). Here, slopes represent the average change in $^2\varepsilon_{AA/w}$ per unit salinity ($\text{‰}/\text{ppt}$).

| Compound | Total regression | | Initial regression | |
|----------|------------------|-------|--------------------|-------|
| | slope | R^2 | slope | R^2 |
| Asx | -0.9 | 0.76 | -0.8 | 0.43 |
| Ile | 6.9 | 0.98 | 8.5 | 0.99 |
| Leu | 0.8 | 0.65 | 0.9 | 0.39 |
| Lys | 2.7 | 0.65 | 5.4 | 0.93 |
| Phe | 3.8 | 0.73 | 6.5 | 0.86 |
| Pro | 7.4 | 0.88 | 10.3 | 0.90 |
| Tyr | 2.2 | 0.80 | 3.8 | 0.99 |
| Val | -0.8 | 0.95 | -0.6 | 0.87 |

the growth dynamics captured here.

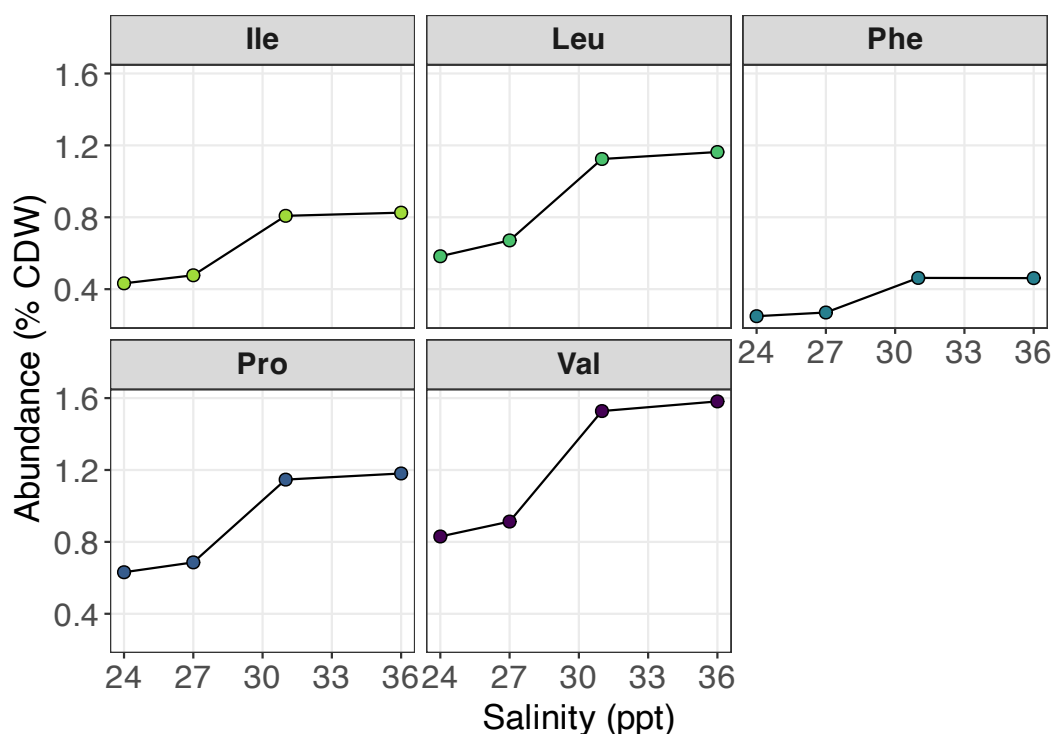


Figure 4.5. Amino acid abundances (reported as percent abundance in total cell dry weight (CDW)) in *E. huxleyi* biomass cultured in media with different salinities. Amino acids were quantified via GC/MS analysis using a six-point calibration curve of amino acid standards injected across a range of known amounts.

4.3.3 Diatom $^2\text{H}/^1\text{H}$ fractionations in response to irradiance

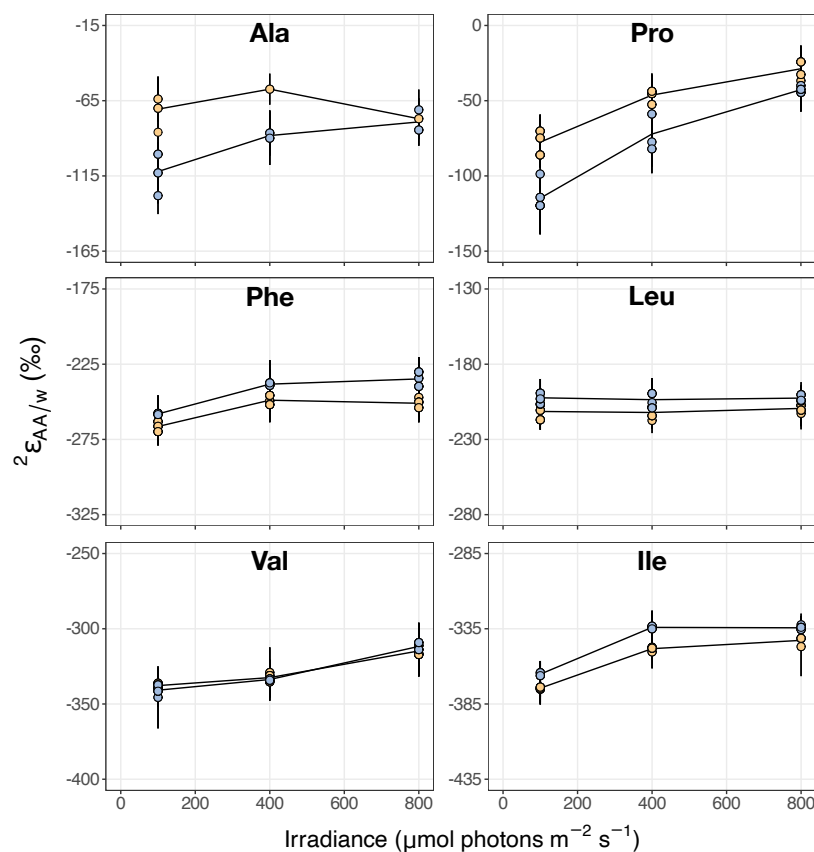


Figure 4.6. Amino acid/water $^2\text{H}/^1\text{H}$ fractionations in *C. muelleri* (orange) and *T. pseudonana* (blue) grown under different irradiances. Data from biological triplicates are displayed, except in cases where amino acid $\delta^2\text{H}$ values were not reliably measurable due to chromatography issues. Lines are plotted through the average of each set of culture replicates. Note that, unlike most of our GC/IRMS analyses which used a ZB-5ms column (on which alanine + glycine co-elute), here, we were able to isolate alanine using a DB-XLB column.

Two diatoms (*C. muelleri* and *T. pseudonana*) were cultured in biological triplicate under a range of light intensities to interrogate whether physiological responses to irradiance are recorded in amino acid $^2\text{H}/^1\text{H}$ fractionations. Six amino acids were analyzed in detail. In both organisms, proline $^2\text{H}/^1\text{H}$ fractionations varied most strongly with irradiance, decreasing by $\sim 50\text{‰}$ and $\sim 70\text{‰}$ from 100 to $800\mu\text{mol photons m}^{-2} \text{s}^{-1}$ in *C. muelleri* and *T. pseudonana*, respectively. Hydrogen isotope

fractionations of phenylalanine and isoleucine in both organisms decreased by 15-20‰, and by ~30‰, respectively, from $I=100$ to $400\mu\text{mol photons m}^{-2} \text{ s}^{-1}$; at $I > 400\mu\text{mol photons m}^{-2} \text{ s}^{-1}$, fractionations of these two amino acids remained constant (Figure 4.6). Isotope fractionations of valine were within error from $I=100$ to $400\mu\text{mol photons m}^{-2} \text{ s}^{-1}$, but slightly increased from $I=400$ to $800\mu\text{mol photons m}^{-2} \text{ s}^{-1}$. Leucine $^2\text{H}/^1\text{H}$ fractionations did not appear to vary with irradiance. Alanine $^2\text{H}/^1\text{H}$ fractionations at 400 and $800\mu\text{mol photons m}^{-2} \text{ s}^{-1}$ were within the large spread of values at $100\mu\text{mol photons m}^{-2} \text{ s}^{-1}$; thus it does not appear that alanine $^2\text{H}/^1\text{H}$ fractionations varied with salinity in these cultures. Many amino acids from cultures grown under $50\mu\text{mol photons m}^{-2} \text{ s}^{-1}$ were ^2H -enriched relative to the $100\mu\text{mol photons m}^{-2} \text{ s}^{-1}$ cultures (Figure C.14), falling off the systematic trend of increasing hydrogen isotope fractionation with decreasing irradiance. This was initially surprising; however, further investigations revealed that the Kimwipes, when wrapped around the Erlenmeyer flasks in which cultures were grown, may have actually induced a light scattering effect that enhanced the apparent irradiance available to the cells. This effect contradicted our observations of reduced irradiance in Kimwipe-wrapped glass beakers, which were used to test the efficacy of using Kimwipes to reduce light penetration through glassware. Given the potential inadvertent increase in light availability, we do not further interpret the observed fractionations of our ' $50\mu\text{mol photons m}^{-2} \text{ s}^{-1}$ ' culture here.

For both diatoms, increased light intensities led to higher growth rates, as monitored via OD_{750} measurements (Figure C.12; Table C.3), following expected trends (Dubinsky & Stambler, 2009; Thompson, 1999; van der Meer et al., 2015). Moreover, at low light levels, diatom cells were visibly darker (shown for *C. muelleri* in Figure C.11), likely due to increased content of chlorophyll, fucoxanthin, and other light harvesting pigments (Dubinsky & Stambler, 2009; Falkowski et al., 1985; Truong et al., 2022).

4.4 Discussion

Our rich dataset provides the first measurements of $\delta^2\text{H}_{\text{AA/w}}$ values in photoautotrophic organisms, expanding the scope of metabolic information captured through $\delta^2\text{H}_{\text{AA/w}}$ analysis. Here we compare photoautotrophic $\delta^2\text{H}_{\text{AA/w}}$ values to those of heterotrophic bacteria (data from Chapter 3) and explore mechanisms driving these signals under the varied physiological conditions tested in this study. Overall, our data here further supports our conclusion that the hydrogen isotope compositions of amino acids robustly capture the metabolic activities of the host organisms. As such, use of $\delta^2\text{H}_{\text{AA/w}}$ values to quantitatively interrogate microbial metabolism in the environment may be a promising application in the future.

4.4.1 Phytoplankton fractionate amino acid hydrogen isotopes more substantially than do heterotrophic bacteria

When $\delta^2\text{H}$ values of amino acids from all cultured heterotrophic bacteria (Chapter 3; Silverman et al., 2024) and phytoplankton (this study) are pooled together, the first-order observation is that amino acids produced photoautotrophically are substantially ^2H -depleted compared to those produced heterotrophically (Figure 4.3). This result mirrors the phenomenon that has been robustly observed for other organic molecules generated from autotrophic versus heterotrophic metabolism (e.g., Estep and Hoering, 1980, 1981; Yakir and DeNiro, 1990; X. Zhang et al., 2009), and is generally linked to larger isotope fractionation associated with photosynthesis. Seminal work by Yakir and DeNiro (1990) estimated this photosynthetic fractionation to be -171‰ (relative to leaf water) for triose phosphates produced photosynthetically in the Calvin-Benson-Bassham (CBB) cycle, based on variations

in cellulose hydrogen and oxygen isotope compositions in the aquatic plant *Lemna gibba* grown under heterotrophic, photoheterotrophic, and photoautotrophic conditions.

The biochemical origin of substantially ^2H -depleted organic compounds produced photosynthetically has been commonly attributed to NADPH, which in turn is produced during the light reactions of photosynthesis and used to reduce 1,3-bisphosphoglycerate to glyceraldehyde 3-phosphate in the CBB cycle. This hypothesis was first proposed by W. G. Smith and York (1970) and has been supported by both direct evidence for ^2H -depleted NADPH produced by cyanobacteria (-600‰ relative to intracellular water; Luo et al., 1991), and observations that fatty acids, which inherit half of their hydrogen from NADPH, are also substantially ^2H -depleted in plants (e.g., Yakir, 1992). However, several independent lines of evidence (summarized by Holloway-Phillips et al., 2025) have challenged the notion that NADPH is the primary driver of low biomolecule $\delta^2\text{H}$ values, including observations that (i) a greater percent of NADPH hydrogen incorporated into organic molecules in photosynthetic organisms does not necessarily translate to lower $\delta^2\text{H}$ values (e.g., Lehmann et al., 2024), and (ii) that the NADPH-derived hydrogen in glucose (i.e., C-4 hydrogen) is surprisingly ^2H -enriched relative to the molecular averages in C_3 plants (Holloway-Phillips et al., 2025; B.-L. Zhang et al., 2002). These do not necessarily rule out production of ^2H -depleted NADPH by photosynthesis, but suggest that the hydrogen atom incorporated into NADPH during photosynthesis (catalyzed by ferredoxin-NADP⁺ reductase, i.e., FNR) may not be transferred to specific biomolecules. In the case of glyceraldehyde 3-phosphate in the CBB cycle, this may result from the incongruent stereospecificities of the NADPH-producing and -consuming enzymes in these reactions (i.e., FNR with *pro-R* stereospecificity, and glyceraldehyde 3-phosphate dehydrogenase with *pro-S*; Holloway-Phillips et al., 2025; Krakow et al., 1965; Levy and Betts, 1989).

However, if the NADPH-consuming enzymes involved in amino acid biosynthesis have both *pro-R* stereospecificity and access to the photosynthetic NADPH pool, the ^2H -depleted photosynthetic hydrogen may be directly incorporated into amino acids. In support of this, shikimate dehydrogenase transfers hydrogen from the *Re* face of NADPH to 3-dehydroshikimate to form shikimate (i.e., with *pro-R* stereospecificity; Davies et al., 1972)—an intermediate in the aromatic amino acid biosynthetic pathway—and the NADPH-derived hydrogen position in phenylalanine derivatives is strongly ^2H -depleted in C_3 plants (Schmidt et al., 2003).

Additionally or alternatively, low $\delta^2\text{H}$ values of photosynthetically-produced amino acids may be directly related to the ^2H -depleted C-6 positions in glucose (B.-L. Zhang et al., 2002), which originate from the C-3 position of glyceraldehyde 3-phosphate produced in the CBB cycle (Holloway-Phillips et al., 2025). This hydrogen may be retained through the production of pyruvate, whose hydrogen is directly or indirectly incorporated into nearly all amino acids (Chapter 3; Silverman et al., 2024), as well as into lipids via acetyl-CoA. The origin of the ^2H -depleted hydrogen at C-3 in glyceraldehyde 3-phosphate is not currently known. Nevertheless, this mechanism would explain why all amino acids—even those that do not directly inherit hydrogen from NADPH (Chapter 3; Silverman et al., 2024)—are relatively ^2H -depleted in the phytoplankton compared to heterotrophs. Finally, larger $^2\text{H}/^1\text{H}$ fractionations by photosynthetic organisms relative to heterotrophs may be driven by different relative pathway fluxes, which could result in different enzyme commitments to reaction directions and, thus, significant differences in expressed isotope effects (Cleland, 1987; Holloway-Phillips et al., 2025). This explanation is attractive, as it does not invoke differences in $\delta^2\text{H}$ values of NADPH-derived hydrogen between photoautotrophic and heterotrophic metabolisms. Wijker et al. (2019) estimated kinetic isotope effects associated with NADPH dehydrogenases and transhydrogenases in the heterotrophic bacteria examined in Chapter 3, and

found them generally comparable to fractionations associated with photosynthesis (e.g., -663‰ for glyceraldehyde-6-phosphate dehydrogenase). The exact mechanism driving substantially ^2H -depleted amino acids in phytoplankton is clearly still an open question. Nevertheless, our study corroborates for yet another class of compounds the substantially larger $^2\text{H}/^1\text{H}$ fractionations expressed by photoautotrophs compared to heterotrophs. As such, $^2\epsilon_{\text{AA/w}}$ values may provide reliable proxies for organismal metabolism in the environment.

4.4.2 Biochemical mechanisms controlling $^2\text{H}/^1\text{H}$ fractionations of individual amino acids in phytoplankton

Across three taxonomically diverse groups of phytoplankton, the patterns of $^2\epsilon_{\text{AA/w}}$ values were largely consistent, with notable exception of tyrosine (Figure 4.1; discussed below). Nevertheless, as these organisms were all cultured photoautotrophically, and their individual $^2\epsilon_{\text{AA/w}}$ patterns were upheld through varied physiological growth conditions (salinity and irradiance; Figures C.10 and C.13), this data further supports the notion that $^2\epsilon_{\text{AA/w}}$ values are primarily set by metabolism (building on conclusions presented in Chapter 3 and Silverman et al., 2024).

4.4.2.1 Comparison of amino acid $^2\text{H}/^1\text{H}$ fractionations between phytoplankton and heterotrophic bacteria

The phytoplankton $^2\epsilon_{\text{AA/w}}$ patterns can be compared to those of heterotrophic bacteria to gain further insight into biochemical controls on these signals. By summarizing the data from Figure 4.3 as the mean $^2\epsilon_{\text{AA/w}}$ value ($\pm 1\sigma$) for each amino acid in each metabolic subgroup, the general $^2\epsilon_{\text{AA/w}}$ patterns can be more easily compared. Despite significant differences in the magnitudes of $^2\text{H}/^1\text{H}$ fractionations (Section 4.4.1), patterns of phytoplankton $^2\epsilon_{\text{AA/w}}$ values generally followed

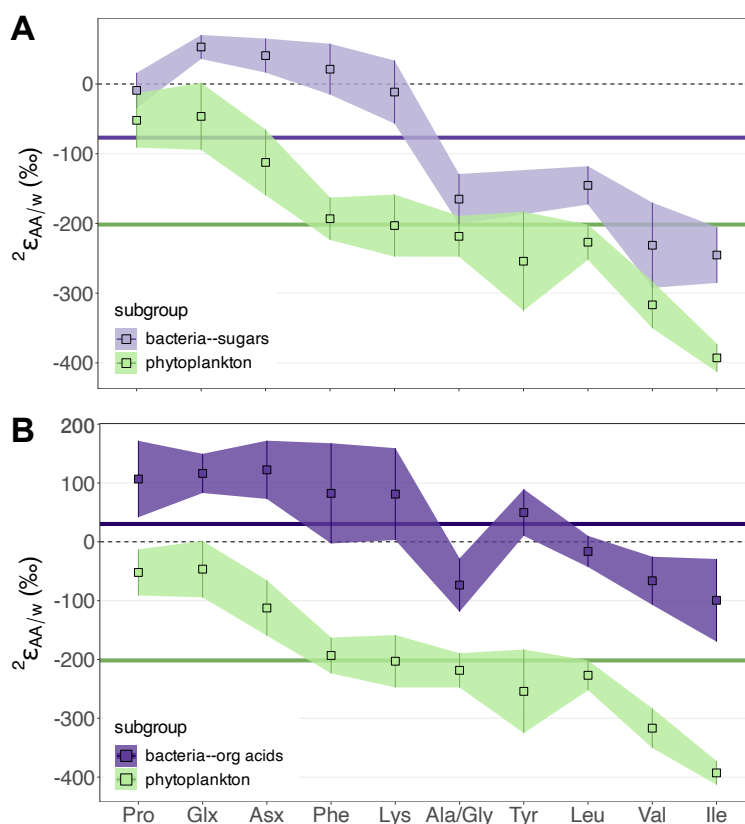


Figure 4.7. Summary of amino acid/water $^2\text{H}/^1\text{H}$ fractionations, displayed as the means $\pm 1\sigma$ of collective data from each metabolic subgroup. General $^2\epsilon_{\text{AA/w}}$ patterns in phytoplankton are compared to those in heterotrophic bacteria grown on sugars (**A**) and on organic acids (**B**), respectively. The thick colored lines in each panel represent the average of all $^2\epsilon_{\text{AA/w}}$ values within the corresponding metabolic subgroup.

those of heterotrophic bacteria, with the same amino acids ^2H -enriched or ^2H -depleted relative to each subgroup average (Figure 4.7; although note exceptions discussed below). This suggests that net isotope fractionations involved in amino acid biosynthesis are largely conserved across the organisms and control the relative pattern of $^2\epsilon_{\text{AA/w}}$ values, while the overall magnitudes of $^2\epsilon_{\text{AA/w}}$ values are driven by the metabolic wiring of pathway fluxes and activated enzymes, which in turn set the isotopic compositions of central metabolic pathway intermediates. This interpretation is consistent with arguments presented in Chapter 3 and Silverman et al. (2024).

Two notable exceptions to the consistent ${}^2\epsilon_{AA/w}$ patterns are alanine + glycine and tyrosine, which are respectively ${}^2\text{H}$ -depleted and ${}^2\text{H}$ -enriched in heterotrophic bacteria compared to phytoplankton (although note that tyrosine was unfortunately not measured in bacteria grown on sugars). These discrepancies may result from differences in the biosynthetic pathways involved. Most of the amino acid biosynthetic pathways are identical across the organisms investigated, with notable exceptions for glycine and tyrosine (e.g., Bromke, 2013; Karp et al., 2019; Moore, Caspi, Campbell, et al., 2024; Umbarger, 1978). In the heterotrophic bacteria, glycine is synthesized from serine (Moore, Caspi, Boyd, et al., 2024; Umbarger, 1978). This pathway is present in the phytoplankton, but glycine (along with serine) are additionally synthesized via the photorespiratory glycolate pathway to salvage carbon upon erroneous fixation of O_2 by ribulose-1,5-bisphosphate carboxylase oxygenase (Rubisco; Bromke, 2013; Karp et al., 2019; Moore, Caspi, Campbell, et al., 2024). Alanine is predominantly synthesized from pyruvate in both the heterotrophic bacteria and phytoplankton, so is unlikely to be the major driver of the relative differences in the net fractionations of the combined alanine + glycine peak between these two groups of organisms. If the major driver is indeed glycine, it is possible that glycine synthesized via photorespiration is more ${}^2\text{H}$ -enriched than glycine synthesized from serine, but further investigation into the isotope effects of the involved enzymes is needed. Alternatively, these differences may be driven by different relative proportions of alanine and glycine in bacteria versus algae.

In the heterotrophic bacteria, tyrosine is synthesized from 4-hydroxyphenylpyruvate in the aromatic amino acid superpathway (Karp et al., 2019; Umbarger, 1978). Interestingly, this also appears to be the predominant biosynthetic pathway for tyrosine in *Synechococcus* sp. (Moore, Caspi, Campbell, et al., 2024), while the eukaryotic phytoplankton synthesize tyrosine from either aroenate or phenylalanine

(Bromke, 2013; Karp et al., 2019). Both groups of bacteria synthesize relatively ^2H -enriched tyrosine compared to the eukaryotic phytoplankton (Figures 4.1 and 4.2). These isotopic differences may thus be related to the different biosynthetic pathways used, but the mechanisms and isotope effects responsible remain to be determined.

Finally, nuanced differences in average isotopic fractionations also exist between the broad metabolic subgroups, including Asx, phenylalanine, and lysine, which are relatively more ^2H -depleted in phytoplankton compared to heterotrophic bacteria (Figure 4.7). This may be driven by the relatively ^2H -depleted hydrogen fixed into intermediates of the CBB cycle, which are retained through synthesis of the amino acids (e.g., phenylalanine is synthesized from erythrose 4-phosphate and phosphoenolpyruvate, of which the former is directly produced in the CBB cycle, and the latter is only two steps removed from the CBB intermediate 3-phosphoglycerate). In contrast, erythrose 4-phosphate and phosphoenolpyruvate synthesized via heterotrophic metabolism are likely more ^2H -enriched, as their hydrogen is largely derived from the carbon substrate and/or incorporated from/exchanged with water (Silverman et al., 2024). Additionally, relatively ^2H -depleted phenylalanine and lysine in phytoplankton (compared to heterotrophic bacteria) may be driven by a more ^2H -depleted, photosynthetically-produced pool of NADPH (see discussion in Section 4.4.1).

4.4.3 Effects of environmental parameters on phytoplankton $^2\epsilon_{\text{AA/w}}$ values

In the surface ocean, phytoplankton experience a range of environmental conditions that vary with their geographical location and depth in the water column, as well as with dynamic temporal fluctuations. The physiological mechanisms that

phytoplankton use to cope with these variations may imprint signals in their $^2\epsilon_{AA/w}$ values. Here, we interrogated these potential effects for two relevant parameters—salinity and irradiance—that vary significantly for phytoplankton in the ocean.

4.4.3.1 Response to salinity

E. huxleyi is near-globally distributed in the marine environment (Thierstein & Young, 2004), spanning both open ocean and coastal settings, which each exhibit wide variations in salinity. Coastal environments can experience large, dynamic fluctuations in sea surface salinity, while salinities in open ocean environments are more temporally stable but exhibit strong spatial variations across a typical range of 29–38 ppt (Zweng et al., 2013). Changes in salinity are well known to drive shifts in the hydrogen isotope fractionation of lipids by *E. huxleyi* and other marine algae (Chivall et al., 2014; Heinzemann et al., 2015; Maloney et al., 2016; M'Boule et al., 2014; Nelson & Sachs, 2014; Sachs et al., 2016; Sachse & Sachs, 2008; Schouten et al., 2006; Schwab & Sachs, 2011; Weiss et al., 2017). Preservation of lipids on geologic timescales renders this isotopic signal a potentially useful proxy for reconstructing paleosalinities of sea surface and lacustrine environments (e.g., Paul, 2002), yet the mechanism driving this phenomenon is not well understood.

Acetogenic lipids (fatty acids, alkenones, etc.) predominantly inherit hydrogen from three sources: acetyl-CoA, NADPH, and water (Robins et al., 2003; Saito et al., 1980). In contrast, the 20 biological amino acids each inherit hydrogen from different sources and in different proportions (Silverman et al., 2024), rendering their $\delta^2\text{H}$ values potentially useful for diagnosing the mechanism(s) responsible for salinity-driven variations in the hydrogen isotope fractionation of biomolecules in marine algae. Indeed, in our *E. huxleyi* cultures, isotope fractionation of all amino acids changed in response to salinity, but the directions and magnitudes of

changes varied for each amino acid (Figure 4.4). Most amino acids became less isotopically fractionated (more ^2H -enriched) at higher salinities, consistent with the effect observed for lipids (see references in preceding paragraph). However, we note that this effect may be nonlinear for some of the amino acids, whereas the effect for lipids is generally described as linear (discussed further below). Several mechanisms have been invoked to explain decreasing fractionation of lipid hydrogen isotopes with salinity, including (i) an increase in the $\delta^2\text{H}$ value of intracellular water; (ii) an increasing relative flux of NADPH produced from less isotopically fractionating enzymes; (iii) a drawdown of ^2H -depleted hydrogen to fuel production of osmolytes; and (iv) a decrease in growth rate of *E. huxleyi* (Maloney et al., 2016; Sachs et al., 2016; Schwab & Sachs, 2011). Continuous culturing experiments ruled out growth rate as the major driver of fractionation changes with salinity in *E. huxleyi* and *T. pseudonana* (Maloney et al., 2016; Sachs et al., 2016; Weiss et al., 2017). The amino acid data generated in this study provides potential constraints on the relative importance of mechanisms *i* and *ii*, with the assumption that the same primary mechanism is responsible for changes in amino acid and lipid hydrogen isotope fractionation with salinity. However, we note that synthesis of amino acids and lipids in different compartments of eukaryotic algae is possible, which could abolish overlap in the primary mechanisms responsible for these isotopic variations.

Mechanism *i*: Variations in intracellular water $\delta^2\text{H}$. The hydrogen isotope composition of intracellular water has been shown to differ from that of extracellular water in metabolically active cells of both prokaryotes and eukaryotes (Kreuzer et al., 2012; Kreuzer-Martin et al., 2006). This effect may occur when transport of extracellular water into cells is reduced and recycling of intracellular water is increased, and has been hypothesized to contribute to diminished lipid hydrogen isotope fractionation at higher salinities (Heinzelmann et al., 2015; Sachs et al.,

2016; Sachse & Sachs, 2008; Schwab & Sachs, 2011). We can attempt to constrain the significance of this effect using our data on leucine and valine, which both inherit hydrogen from two sources: pyruvate and water (Silverman et al., 2024). If changes in the $\delta^2\text{H}$ value of intracellular water drive the primary signals, we would at least expect to see effect magnitudes that scale with the proportion of hydrogen directly incorporated from water into each amino acid (40% and 25% for leucine and valine, respectively). We instead observe only a small decrease in hydrogen isotope fractionation of leucine with salinity (relative to the effect magnitudes for the other amino acids), and the opposite effect for valine (Figure 4.4). It is possible that changes in the $\delta^2\text{H}$ value of pyruvate overprint any signals from intracellular water $\delta^2\text{H}$ variations; however, even if true, these results imply that intracellular water $\delta^2\text{H}$ is not the primary driver of the large changes in hydrogen isotope fractionation of amino acids.

Mechanism ii: Variations in intracellular NADPH $\delta^2\text{H}$. A more promising explanation for significant decreases in amino acid hydrogen isotope fractionation with salinity is changes in the isotope composition of the intracellular NADPH pool. Numerous studies point to the fact that phytoplankton require more reducing power when coping with salinity stress. FNR is a major source of NADPH generation in photoautotrophs, but glucose-6-phosphate dehydrogenase and 6-phosphogluconate dehydrogenase in the oxidative pentose phosphate (OPP) pathway can also supply significant quantities of NADPH (Schmidt et al., 2003; Wamelink et al., 2008). OPP and other NADPH-producing enzymes are upregulated in response to high salinity in numerous photoautotrophs, including diatoms (Cheng et al., 2014), green algae (Liska, 2004), cyanobacteria (Rai et al., 2013, 2014), macroalgae (Huan et al., 2014), and higher plants (Gao et al., 2016; Huang et al., 2003; Nemoto & Sasakuma, 2000; Wang et al., 2008; Yang et al., 2014; Yu et al., 2011). This response has also been observed in marine heterotrophic

bacteria (Danevčič & Stopar, 2011), and may be related to increased NADPH demand to fuel osmolyte production.

Fluctuations in environmental salinity can disrupt the internal osmotic balance and turgor of a cell, which can in turn affect the cell's ability to grow and divide. To maintain osmotic equilibrium, many organisms increase their intracellular concentrations of compatible solutes, which carry neutral charge at physiological pH and thus can accumulate to high concentrations in cells without disrupting vital cellular processes (Record et al., 1998a, 1998b; Strøm & Kaasen, 1993; Yancey, 1994). The major compatible solute in *E. huxleyi* is dimethylsulfoniopropionate (DMSP; Gebser and Pohnert, 2013), whose synthesis in marine algae requires NADPH (Gage et al., 1997; Stefels, 2000). While a portion of the substantial increase in intracellular DMSP (and other osmolytes) at high salinity in *E. huxleyi* can be attributed to its cell volume shrinkage (Gebser & Pohnert, 2013), any increase in actual DMSP synthesis requires a stoichiometric increase in NADPH production. If NADPH production via photosynthesis is insufficient to meet this increased demand, other pathways for NADPH production, such as the OPP pathway, may be upregulated. Indeed, significant upregulation of the OPP pathway (and concomitant NADPH production) in the marine heterotrophic bacterium *Vibrio* sp. DSM14379 in response to high salinity was presumed to accommodate the ~10-fold increase in synthesis of its major compatible solute, proline (Danevčič & Stopar, 2011).

If NADPH produced photosynthetically (via FNR) is more ^2H -depleted than NADPH produced metabolically (via OPP or other central metabolic pathway enzymes), a relative increase in metabolic NADPH production via OPP pathway upregulation could drive the apparent smaller fractionations of biomolecules at high salinities. This mechanism is commonly invoked to explain trends for lipids and is further supported by our amino acid data, as the five amino acids that inherit hydrogen

from NADPH (isoleucine, lysine, phenylalanine, proline, and tyrosine) exhibited strongly decreasing fractionation with salinity, whereas the remaining three amino acids exhibited either the opposite trend (Asx and valine), or the same trend but with a smaller magnitude (leucine; Figure 4.4). However, whether OPP-produced NADPH is more ^2H -depleted than FNR-produced NADPH remains an open question, but is belied by data from Wijker et al. (2019) indicating that large hydrogen isotope fractionations accompany NADPH production by OPP enzymes: -663‰ for glucose-6-phosphate dehydrogenase, and -379‰ for 6-phosphogluconate dehydrogenase, compared to -600‰ for FNR (Luo et al., 1991). Nevertheless, it is possible that changes in the $\delta^2\text{H}$ value of the intracellular NADPH pool may be driving the major signal in both amino acids and lipids.

To investigate potential control by NADPH more quantitatively, we compared the magnitude of response of each amino acid to the relative proportion of NADPH hydrogen in that amino acid. This exercise is complicated by the fact that changes in hydrogen isotope fractionation for amino acids containing NADPH hydrogen appeared convex rather than linear (although we note that error bars on all $^2\epsilon_{\text{AA/w}}$ measurements were within the standard errors accompanying linear regressions). As this experiment was performed with only one biological replicate, follow-up experiments are needed to verify the shape of the response of $^2\epsilon_{\text{AA/w}}$ with salinity. A linear response is not necessarily expected, as metabolic responses to increasing salinity, such as OPP pathway stimulation, can also be nonlinear (e.g., Danevčič and Stopar, 2011). Furthermore, it is possible that the biological mechanism contributing to ^2H -enrichment saturates at higher salinities. Alternatively, multiple mechanisms with overprinting effects may be at play (e.g., variations in both NADPH metabolism and growth rate). All prior studies on lipid hydrogen isotope fractionation have characterized the response to salinity as linear; however, within the range of salinities tested here (24–36 ppt), a similar curvature in response

can be seen in lipid data from some prior studies (e.g., Maloney et al., 2016; M'Boule et al., 2014; Weiss et al., 2017). Nevertheless, as the mechanism contributing to this potential curvature (if real) is not known at this time, we follow the approach of all prior lipid studies by quantifying the magnitudes of observed effects—i.e., changes in ${}^2\varepsilon_{AA/w}$ per unit salinity, or $\Delta^2\varepsilon_{AA/w}S^{-1}$ —via linear regressions (Figure 4.4). We calculate the slopes of regressions between ${}^2\varepsilon_{AA/w}$ values and salinity ($=\Delta^2\varepsilon_{AA/w}S^{-1}$) across all data (total regression), and the initial portion of the curve prior to saturation (salinity ≤ 31 ppt; initial regression). Plotting $\Delta^2\varepsilon_{AA/w}S^{-1}$ for each amino acid against the fraction of NADPH-derived hydrogen in that amino acid yields linear regressions with excellent fits ($R^2=0.89\text{--}0.95$; Figure 4.8), suggesting that NADPH could well be a significant driver of changes in amino acid hydrogen isotope fractionations.

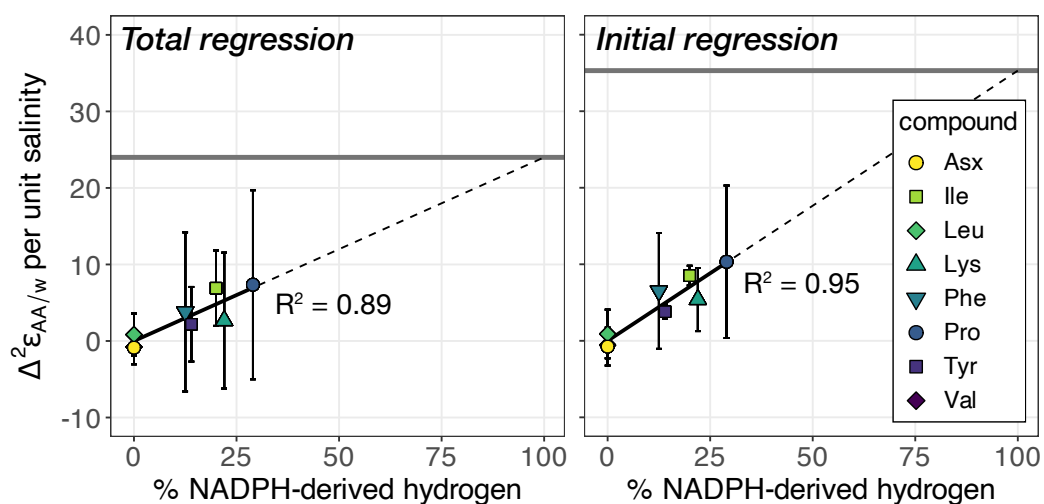


Figure 4.8. Slopes of regressions of ${}^2\varepsilon_{AA/w}$ versus salinity for each amino acid from Figure 4.4, calculated using data across all four salinities (Total regression) and the initial portion of the curve prior to saturation (salinity ≤ 31 ppt; Initial regression). Error bars on slopes represent the RMSE of residuals from the linear fits.

In theory, assuming that any change in the hydrogen isotope composition of the intracellular NADPH pool used for amino biosynthesis is directly (and proportionally) imparted in ${}^2\varepsilon_{AA/w}$ shifts, extrapolation of the slopes in Figure 4.8 to

100% NADPH-derived hydrogen yields the estimated change in the $\delta^2\text{H}$ value of this NADPH pool (gray bars in Figure 4.8 for demonstration). Given the large uncertainties in the calculated slopes for each amino acid (due to the nonlinear changes in isotope fractionation with salinity), estimates for $\Delta^2\varepsilon_{AA/w}S^{-1}$ at 100% NADPH-derived hydrogen via Monte Carlo simulations have accompanying uncertainties significantly larger than the estimates themselves (e.g., $34 \pm 150\%$). Our approach must clearly be refined before useful information can be extrapolated, but could ultimately enable direct quantification of changes in intracellular NADPH $\delta^2\text{H}$ (or other biochemical parameters) with salinity. Such isotopic information can be coupled with flux models to estimate relative NADPH production from different metabolic pathways (i.e., following the approach of Wijker et al., 2019) for holistic understanding of changes in NADPH metabolism and its isotopic consequences in response to salinity.

Based on the regressions in Figure 4.8, we would expect lipids, which inherit 50% of their hydrogen from NADPH, to exhibit a 12–18‰ decrease in fractionation per unit salinity (range given to encompass estimates from both regressions). However, typical decreases in lipid fractionations by *E. huxleyi* are only 1–4‰ per unit salinity (M’Boule et al., 2014; Sachs et al., 2016; Schouten et al., 2006; Weiss et al., 2017), far below this expectation. This discrepancy implies that changes in amino acid hydrogen isotope fractionations with salinity may not be entirely attributed to NADPH. Alternatively, it is possible that lipids and amino acids are not synthesized from the same biochemical pools, or that these two compound classes are processed differently in cells after synthesis. These discrepancies warrant further investigation.

Finally, we investigated whether potential changes in NADPH metabolism and hydrogen isotope composition might be driven, in part, by increased production of proline as a major compatible solute in our *E. huxleyi* cultures. Osmolytes can

reach high concentrations in cells (e.g., reaching up to 10–20% of cell dry weight in some hypersaline bacteria; Ventosa et al., 1998), thereby consuming a substantial fraction of intracellular hydrogen. Proline serves as an important osmolyte in many species of terrestrial and marine microbes, including phytoplankton (Brill et al., 2011; Burg & Ferraris, 2008; Cayley et al., 1992; Danevčič & Stopar, 2011; Dawson, Heal, Boysen, et al., 2020; Dawson, Heal, Torstensson, et al., 2020; Götz et al., 2018; Krell et al., 2007; Lyon et al., 2011; McParland et al., 2021). In the diatom *Nitzschia lecointei*, intracellular proline concentrations increased by 142% with a salinity increase from 32 to 41 ppt (Dawson, Heal, Boysen, et al., 2020). We investigated whether proline concentrations similarly substantially increased in our *E. huxleyi* cultures at high salinity by quantifying proline and four other amino acids via GC/MS as percent mass of the cell dry weight (Figure 4.5). The increase in proline's abundance was comparable to those of the other amino acids, implying proline did not serve as a major compatible osmolyte in our cultures. The increased relative abundances of all amino acids may be attributed to decreases in cell volume, which *E. huxleyi* employs as one mechanism to help increase intracellular osmolyte concentrations in response to high salinity (Gebser & Pohnert, 2013).

4.4.3.2 Response to irradiance

Phytoplankton in the surface ocean must adapt to strong variations in irradiance with depth and on daily and seasonal cycles. PAR near the atmosphere-water interface can exceed $1000 \mu\text{mol photons m}^{-2} \text{ s}^{-1}$, but rapidly attenuates with depth (Dubinsky & Stambler, 2009; R. C. Smith & Mobley, 2008). Changes in irradiance are known to trigger systematic changes in hydrogen isotope fractionations of microalgal lipids (Sachs et al., 2017; van der Meer et al., 2015), although the mechanism(s) driving this response is/are currently unknown. Here, we interro-

gated whether amino acid hydrogen isotope fractionation also changes in response to irradiance, which, in addition to furthering our fundamental characterization of factors controlling photoautotrophic ${}^2\epsilon_{AA/w}$ variations, could potentially shed light on the biochemical mechanisms responsible for irradiance-driven changes in macromolecule ${}^2\text{H}/{}^1\text{H}$ fractionation.

Hydrogen isotope fractionations of the amino acids examined exhibited a range of responses to irradiance. Proline ${}^2\text{H}/{}^1\text{H}$ fractionations were most strongly affected across the range of irradiances tested (Figure 4.6). In comparison, phenylalanine and isoleucine exhibited less pronounced decreases in hydrogen isotope fractionation from 100–400 $\mu\text{mol photons m}^{-2} \text{ s}^{-1}$, and constant fractionations thereafter. Similarly to phenylalanine and isoleucine, van der Meer et al. (2015) observed decreasing alkenone ${}^2\text{H}/{}^1\text{H}$ fractionation through $\sim 300 \mu\text{mol photons m}^{-2} \text{ s}^{-1}$, but increasing fractionation thereafter. Sachs et al. (2017) observed decreasing fractionation of hydrogen isotopes in phytol and C14:0 fatty acids in *T. pseudonana*, but the opposite trend for sterols, and no change with irradiance for C16:0 and C16:1 fatty acids. Similar to the C16 fatty acids, leucine ${}^2\epsilon_{AA/w}$ values did not vary with irradiance (Figure 4.6). In the proceeding discussion, we explore potential mechanisms contributing to the observed ${}^2\epsilon_{AA/w}$ variations, but no single mechanism can satisfactorily explain the different responses of all six amino acids. As such, further studies interrogating these effects in amino acids are needed. Moreover, in eukaryotic microalgae, interpretations incorporating context about where each amino acid is synthesized (i.e., the plastid, mitochondria, or cytosol), and thus how the isotopic compositions of the relevant biochemical pools are varying, may be necessary.

To explain the decreasing alkenone ${}^2\text{H}/{}^1\text{H}$ fractionation through $\sim 300 \mu\text{mol photons m}^{-2} \text{ s}^{-1}$ and increasing fractionation thereafter, van der Meer et al. (2015) argue that the effect is related to photosynthetic activity, which similarly increases

linearly with irradiance until saturating light intensity ($200\text{--}400\mu\text{mol photons m}^{-2}\text{ s}^{-1}$ in *E. huxleyi*; Feng et al., 2008; Flaming and Kromkamp, 1988; Harris et al., 2005) and decays thereafter (Eilers & Peeters, 1988). Moreover, van der Meer et al. (2015) hypothesize that the changes in isotope fractionation might be specifically driven by NADPH, whose synthesis from photosynthetic versus metabolic pathways likely varies with irradiance. This hypothesis invokes differences in the $\delta^2\text{H}$ value of NADPH produced by photosynthetic versus other metabolic pathway enzymes, which may not be true—see Mechanism *ii* discussion in Section 4.4.3.1. Additionally, if photosynthetic NADPH production is maximal at saturating irradiance, one might expect fractionation of lipid hydrogen isotopes to be greatest at $\sim 200\mu\text{mol photons m}^{-2}\text{ s}^{-1}$ —opposite of the trend observed for alkenone hydrogen isotope fractionation (van der Meer et al., 2015). Furthermore, fractionations of C16 fatty acids would be expected to vary with irradiance given their direct inheritance of $\sim 50\%$ hydrogen from NADPH, but this was not the case (Sachs et al., 2017; although these authors hypothesize that post-synthetic enzymatic reprocessing steps may overprint primary $\delta^2\text{H}$ signals in C16 fatty acids). Moreover, our amino acid data does not support NADPH $\delta^2\text{H}$ being the primary driver of irradiance-induced changes in isotope fractionation, as $^2\text{H}/^1\text{H}$ fractionations of valine (which does not inherit NADPH hydrogen) varied with irradiance, albeit only minimally (Figure 4.6). Alanine similarly does not inherit hydrogen from NADPH, but its $^2\text{H}/^1\text{H}$ fractionations at 400 and $800\mu\text{mol photons m}^{-2}\text{ s}^{-1}$ were largely within the range observed at $100\mu\text{mol photons m}^{-2}\text{ s}^{-1}$. Based on several arguments outlined in Holloway-Phillips et al. (2025) and summarized in Section 4.4.1, it does not appear likely that NADPH $\delta^2\text{H}$ influences the hydrogen isotope composition of amino acids and lipids at the level of CBB cycle intermediates (specifically glyceraldehyde 3-phosphate). Moreover, if NADPH were driving these responses, it is puzzling why proline $^2\text{H}/^1\text{H}$ fractionations would continue to decrease after

400 $\mu\text{mol photons m}^{-2} \text{ s}^{-1}$, while those of phenylalanine and isoleucine plateau. Taken together, it appears that a mechanism unrelated to NADPH metabolism is responsible for irradiance-driven changes in amino acid (and potentially lipid) hydrogen isotope fractionation, suggesting salinity and irradiance alter amino acid $\delta^2\text{H}$ values through different mechanisms.

An alternative hypothesis, proposed by Sachs et al. (2017), is that different light levels could alter the relative proportion of pyruvate synthesized in the plastid (i.e., the site of photosynthesis in eukaryotic microalgae) versus in the cytosol or mitochondrion. In turn, the authors propose that pyruvate $\delta^2\text{H}$ could be lower in plastids due to (i) greater incorporation of photosynthetic NADPH or (ii) reduced exchange of organic hydrogen with water, in turn due to shorter residence times and/or less biochemical transformations. Option *i* would again conflict with the argument by Holloway-Phillips et al. (2025) that photosynthetic NADPH hydrogen is not directly transferred to central metabolic intermediates. Option *ii* seems possible; however, both leucine and valine $\delta^2\text{H}$ values should be sensitive to changes in pyruvate $\delta^2\text{H}$, which does not appear to be the case (Figure 4.6). The differing responses of leucine and valine hydrogen isotope fractionation with irradiance may be attributed to different localization of their synthesis (e.g., in the plastid versus cytosol), although given that these amino acids share a common biosynthetic pathway (Bromke, 2013), this seems less likely. Alternatively, it is possible that valine and leucine are processed differently after synthesis in ways that promote ^2H -enrichment of valine or overprinting of any primary signals in leucine $\delta^2\text{H}$.

Overall, it is clear that, as for lipids, the hydrogen isotope fractionations of amino acids vary in response to light intensity. However, numerous factors related to this response are unknown, including whether there is one primary biochemical mechanism driving all such effects, or whether different mechanisms are at play depending on where each amino acid (or lipid) is synthesized in diatom cells.

It seems possible that the confluence of multiple mechanisms is contributing to these varied responses (particularly given the different responses to proline versus phenylalanine and isoleucine after $400\mu\text{mol photons m}^{-2} \text{ s}^{-1}$). Clearly, further work is needed to interrogate the mechanisms driving these signals.

4.5 Conclusion and potential applications

In the introduction of this chapter, we noted three valuable potential outcomes of interrogating photoautotrophic amino acid $^2\text{H}/^1\text{H}$ fractionations, which can be recapitulated as: (i) understanding the baseline amino acid hydrogen isotope compositions in the primary producer organic matter input into all ecosystems, (ii) investigating whether the $^2\varepsilon$ values of certain amino acids can be used as proxies for monitoring primary producer health and physiological stress, and (iii) furthering our understanding of both controls on amino acid $^2\text{H}/^1\text{H}$ fractionations in organisms, and how these signals can be most effectively leveraged to extract quantitative metabolic information about organisms in the environment. Through our detailed examination of marine phytoplankton, we can provide commentary on all three of these points.

Despite some variations in specific amino acid $^2\text{H}/^1\text{H}$ fractionations, it is clear that the general pattern of $^2\varepsilon_{\text{AA/w}}$ values is largely consistent across heterotrophic and photoautotrophic organisms. As such, the net fractionation of each biosynthetic pathway must be similar across the organisms, which in turn can be linked to the exceptional conservation of these pathways. This supports our earlier predictions (Chapter 3; Silverman et al., 2024), and we anticipate that this trend will continue to hold across more metabolically diverse organisms examined as long as their amino acid biosynthetic pathways are similar. Any strong deviations in

$^2\epsilon_{AA/w}$ patterns detected in organisms may lead to exciting discoveries of novel biosynthetic pathways being used.

While heterotrophic and photoautotrophic organisms produce similar $^2\epsilon_{AA/w}$ patterns, photoautotrophic metabolism imparts substantially larger fractionations for nearly every amino acid, leading to clear separations in the distributions of $^2\epsilon_{AA/w}$ values between these broad metabolic regimes. This sets up a number of valuable applications, including quantifying organic matter contributions by photoautotrophy versus heterotrophy to particular environmental locales, and tracing heterotrophic degradation of organic matter from primary producers. A concrete example of the former could be to quantify the prevalence of mixotrophy in marine phytoplankton, which exerts a potentially significant impact on global carbon cycling, but is not quantifiable with most existing tools (Cormier et al., 2022). The ability to trace and quantify heterotrophic degradation of primary producer biomass is especially relevant in the marine environment, where microbial and animal heterotrophic degradation of primary algal biomass exerts significant control on carbon sequestration timescales in the deep ocean (Boyd et al., 2019). The information accessible from amino acid hydrogen isotope analyses is complementary to that gained from lipid $^2\text{H}/^1\text{H}$ and amino acid $^{15}\text{N}/^{14}\text{N}$ analyses, but can be advantageous in environmental applications over the former when protein is substantially more abundant than lipids (e.g., in the case of marine particulate organic matter (POM); Wakeham et al., 1997), and over the latter when multiple mechanisms with different isotopic consequences overprint the metabolic signals (e.g., in the case of marine POM degradation, microbial growth on and hydrolysis of the primary material both alter POM $\delta^{15}\text{N}$ values, so quantitative isolation of just one of these processes is not possible; Wojtal et al., 2023).

Variations in salinity and irradiance led to shifts in many phytoplankton $^2\epsilon_{AA/w}$ values; however, the general pattern of $^2\epsilon_{AA/w}$ values remained consistent (Figures

C.10 and C.13). Given that the total range in $^2\text{H}/^1\text{H}$ fractionations for each amino acid in each condition was still within that encompassed by the cyanobacteria and diatoms grown under constant parameters, it would be difficult to use amino acid $^2\text{H}/^1\text{H}$ ratios as reliable proxies for phytoplankton physiological stress. However, the robustness of the first-order metabolic signals in $^2\varepsilon_{\text{AA/w}}$ values through varying environmental parameters is advantageous for applications described in the preceding paragraph. To move toward such quantitative applications, future studies should continue to interrogate how and why these isotopic signals vary (*i*) across metabolically diverse organisms and (*ii*) with different environmental parameters (with explorations focused on species and variables relevant to the target environment/question).

Acknowledgments

We would like to acknowledge Victoria Orphan, Woody Fischer, Jared Leadbetter for their provision of laboratory space and equipment that made this work possible; John Magyar and Stephanie Connon for their assistance with our equipment use; Michael Mathuri for assistance with the mass spectrometry measurements; Kelly Luis for assistance with the irradiance measurements; and the staff of the Kerckhoff Marine Laboratory for assistance with collection of the seawater used for our culturing work. We would also like to gratefully acknowledge the Mackey (University of California, Irvine) and Allen (Scripps Institution of Oceanography) laboratories, with special acknowledgments to Ashton Bandy and Rob Lampe, for their generous provision of phytoplankton cultures and guidance with the culturing work. This work was supported by an NSF award OCE-2023687 to ALS, and an NSF GRFP fellowship to SNS.

References

- Bar-On, Y. M., Phillips, R., & Milo, R. (2018). The biomass distribution on earth. *Proceedings of the National Academy of Sciences of the United States of America*, *115*, 6506–6511.
- Boyd, P. W., Claustre, H., Levy, M., Siegel, D. A., & Weber, T. (2019). Multi-faceted particle pumps drive carbon sequestration in the ocean. *Nature*, *568*, 327–335.
- Brill, J., Hoffmann, T., Bleisteiner, M., & Bremer, E. (2011). Osmotically controlled synthesis of the compatible solute proline is critical for cellular defense of *Bacillus subtilis* against high osmolarity. *Journal of Bacteriology*, *193*, 5335–5346. <https://doi.org/10.1128/JB.05490-11>
- Bromke, M. A. (2013). Amino acid biosynthesis pathways in diatoms. *Metabolites*, *3*, 294–311.
- Burg, M. B., & Ferraris, J. D. (2008). Intracellular organic osmolytes: Function and regulation. *Journal of Biological Chemistry*, *283*, 7309–7313. <https://doi.org/10.1074/jbc.R700042200>
- Cayley, S., Lewis, B. A., & Record, M. T. (1992). Origins of the osmoprotective properties of betaine and proline in *Escherichia coli* K-12. *Journal of Bacteriology*, *174*(5), 1586–1595. <https://doi.org/10.1128/jb.174.5.1586-1595.1992>
- Cheng, R., Feng, J., Zhang, B.-X., Huang, Y., Cheng, J., & Zhang, C.-X. (2014). Transcriptome and gene expression analysis of an oleaginous diatom under different salinity conditions. *BioEnergy Research*, *7*, 192–205.
- Chivall, D., M'Boule, D., Sinke-Schoen, D., Sinninghe Damsté, J. S., Schouten, S., & van der Meer, M. T. J. (2014). The effects of growth phase and salinity on the hydrogen isotopic composition of alkenones produced by coastal haptophyte algae. *Geochimica et Cosmochimica Acta*, *140*, 381–390.
- Cleland, W. W. (1987). The use of isotope effects in the detailed analysis of catalytic mechanisms of enzymes. *Bioorganic Chemistry*, *15*(3), 283–302. [https://doi.org/10.1016/0045-2068\(87\)90026-5](https://doi.org/10.1016/0045-2068(87)90026-5)
- Cormier, M.-A., Berard, J.-B., Bougaran, G., Trueman, C. N., Mayor, D. J., Lampitt, R. S., Kruger, N. J., Flynn, K. J., & Rickaby, R. E. M. (2022). Deuterium in marine organic biomarkers: Toward a new tool for quantifying aquatic mixotrophy. *New Phytologist*, *234*(3), 776–782. <https://doi.org/10.1111/nph.18023>

- Danevčič, T., & Stopar, D. (2011). Asymmetric Response of Carbon Metabolism at High and Low Salt Stress in *Vibrio* sp. DSM14379. *Microbial Ecology*, 62(1), 198–204. <https://doi.org/10.1007/s00248-011-9870-3>
- Davies, D. D., Teixeira, A., & Kenworthy, P. (1972). The stereospecificity of nicotinamide–adenine dinucleotide-dependent oxidoreductases from plants. *Biochemical Journal*, 127, 335–343. <https://doi.org/10.1042/bj1270335>
- Dawson, H. M., Heal, K. R., Boysen, A. K., Carlson, L. T., Ingalls, A. E., & Young, J. N. (2020). Potential of temperature- and salinity-driven shifts in diatom compatible solute concentrations to impact biogeochemical cycling within sea ice. *Elementa*, 8(25), 1–17. <https://doi.org/10.1525/elementa.421>
- Dawson, H. M., Heal, K. R., Torstensson, A., Carlson, L. T., Ingalls, A. E., & Young, J. N. (2020). Large diversity in nitrogen- and sulfur-containing compatible solute profiles in polar and temperate diatoms. *Integrative and Comparative Biology*, 60, 1401–1413. <https://doi.org/10.1093/icb/icaa133>
- Dubinsky, Z., & Stambler, N. (2009). Photoacclimation processes in phytoplankton: Mechanisms, consequences, and applications. *Aquatic microbial ecology*, 56, 163–176.
- Eilers, P. H. C., & Peeters, J. C. H. (1988). A model for the relationship between light intensity and the rate of photosynthesis in phytoplankton. *Ecological Modelling*, 42, 199–215.
- Estep, M. F., & Hoering, T. C. (1980). Biogeochemistry of the stable hydrogen isotopes. *Geochimica et Cosmochimica Acta*, 44, 1197–1206.
- Estep, M. F., & Hoering, T. C. (1981). Stable hydrogen isotope fractionations during autotrophic and mixotrophic growth of microalgae. *Plant Physiology*, 67, 474–477.
- Falkowski, P. G., Dubinsky, Z., & Wyman, K. (1985). Growth-irradiance relationships in phytoplankton. *Limnology and Oceanography*, 30, 311–321.
- Feng, Y., Warner, M. E., Zhang, Y., Sun, J., Fu, F.-X., Rose, J. M., & Hutchins, D. A. (2008). Interactive effects of increased pCO₂, temperature and irradiance on the marine coccolithophore *Emiliana huxleyi* (Prymnesiophyceae). *European Journal of Phycology*, 43, 87–98.
- Field, C. B., Behrenfeld, M. J., Randerson, J. T., & Falkowski, P. (1998). Primary production of the biosphere: Integrating terrestrial and oceanic components. *Science*, 281, 237–240.
- Flameling, I. A., & Kromkamp, J. (1988). Light dependence of quantum yields for PSII charge separation and oxygen evolution in eucaryotic algae. *Limnology and Oceanography*, 43, 284–297.

- Fogel, M. L., Griffin, P. L., & Newsome, S. D. (2016). Hydrogen isotopes in individual amino acids reflect differentiated pools of hydrogen from food and water in *Escherichia coli*. *Proceedings of the National Academy of Sciences*, *113*(32), E4648–E4653. <https://doi.org/10.1073/pnas.1525703113>
- Gage, D. A., Rhodes, D., Nolte, K., Hicks, W. A., Leustek, T., Cooper, A. J. L., & Hanson, A. D. (1997). A new route for synthesis of dimethylsulphoniopropionate in marine algae. *Nature*, *387*, 891–894.
- Gao, S., Zheng, Z., Huan, L., & Wang, G. (2016). G6PDH activity highlights the operation of the cyclic electron flow around PSI in *Physcomitrella patens* during salt stress. *Scientific Reports*, *6*, 21245. <https://doi.org/10.1038/srep21245>
- Gebser, B., & Pohnert, G. (2013). Synchronized Regulation of Different Zwitterionic Metabolites in the Osmoadaptation of Phytoplankton. *Marine Drugs*, *11*(6), 2168–2182. <https://doi.org/10.3390/md11062168>
- Gharibi, H., Chernobrovkin, A. L., Eriksson, G., Saei, A. A., Timmons, Z., Kitchener, A., Kalthoff, D. C., Lidén, K., Makarov, A. A., & Zubarev, R. A. (2022). Abnormal (hydroxy)proline deuterium content redefines hydrogen chemical mass. *Journal of the American Chemical Society*, *144*(6), 2484–2487. <https://doi.org/10.1021/jacs.1c12512>
- Götz, F., Longnecker, K., Soule, M. C. K., Becker, K. W., McNichol, J., Kujawinski, E. B., & Sievert, S. M. (2018). Targeted metabolomics reveals proline as a major osmolyte in the chemolithoautotroph *Sulfurimonas denitrificans*. *MicrobiologyOpen*, *7*, e00586. <https://doi.org/10.1002/mbo3.586>
- Granata, T., Habermacher, P., Härrä, V., & Egli, M. (2019). The influence of bio-optical properties of *Emiliana huxleyi* and *Tetraselmis* sp. on biomass and lipid production when exposed to different light spectra and intensities of an adjustable LED array and standard light sources. *SN Applied Sciences*, *1*, 524.
- Guillard, R. R. L. (1975). Culture of phytoplankton for feeding marine invertebrates. In W. L. Smith & M. H. Chanley (Eds.), *Culture of Marine Invertebrate Animals* (pp. 26–60). Plenum Press.
- Guillard, R. R. L., & Ryther, J. H. (1962). Studies of marine planktonic diatoms. I. *Cyclotella nana* Hustedt and *Detonula confervacea* Cleve. *Canadian Journal of Microbiology*, *8*, 229–239.
- Harris, G. N., Scanlan, D. J., & Geider, R. J. (2005). Acclimation of *Emiliana huxleyi* (Prymnesiophyceae) to photon flux density. *Journal of Phycology*, *41*, 851–862.
- Heinzelmann, S. M., Chivall, D., M'Boule, D., Sinke-Schoen, D., Villanueva, L., Sininghe Damsté, J. S., Schouten, S., & van der Meer, M. T. J. (2015). Comparison of the effect of salinity on the D/H ratio of fatty acids of

- heterotrophic and photoautotrophic microorganisms. *FEMS Microbiology Letters*, 362, fnv065. <https://doi.org/10.1093/femsle/fnv065>
- Holloway-Phillips, M., Tcherkez, G., Wieloch, T., Lehmann, M. M., & Werner, R. A. (2025). Is photosynthesis-derived NADPH really a source of ^2H -depleted hydrogen in plant compounds? *Plant, Cell & Environment*, 1–16. <https://doi.org/10.1111/pce.15403>
- Huan, L., Xie, X., Zheng, Z., Sun, F., Wu, S., Li, M., Gao, S., Gu, W., & Wang, G. (2014). Positive correlation between PSI response and oxidative pentose phosphate pathway activity during salt stress in an intertidal macroalga. *Plant and Cell Physiology*, 55, 1395–1403.
- Huang, J., Zhang, H., Wang, J., & Yang, J. (2003). Molecular cloning and characterization of rice 6-phosphogluconate dehydrogenase gene that is up-regulated by salt stress. *Molecular Biology Reports*, 30, 223–227.
- Karp, P. D., Billington, R., Caspi, R., Fulcher, C. A., Latendresse, M., Kothari, A., Keseler, I. M., Krummenacker, M., Midford, P. E., Ong, Q., Ong, W. K., Paley, S. M., & Subhraveti, P. (2019). The BioCyc collection of microbial genomes and metabolic pathways. *Briefings in Bioinformatics*, 20, 1085–1093.
- Keller, M. D., & Guillard, R. R. L. (1985). Factors significant to marine diatom culture. In D. M. Anderson, A. W. White, & D. G. Baden (Eds.), *Toxic Dinoflagellates* (pp. 113–116). Elsevier.
- Keller, M. D., Selvin, R. C., Claus, W., & Guillard, R. R. L. (1987). Media for the culture of oceanic ultraphytoplankton. *Journal of Phycology*, 23, 633–638.
- Krakow, G., Ammeraal, R. N., & Vennesland, B. (1965). The stereospecificity of the Hill reaction with triphosphopyridine nucleotide. *Journal of Biological Chemistry*, 240, 1820–1823.
- Krell, A., Funck, D., Plettner, I., John, U., & Dieckmann, G. (2007). Regulation of proline metabolism under salt stress in the psychrophilic diatom *Fragilaria cylindrus* (bacillariophyceae). *Integrative and Comparative Biology*, 43, 753–762.
- Kreuzer, H. W., Quaroni, L., Podlesak, D. W., Zlateva, T., Bollinger, N., McAllister, A., Lott, M. J., & Hegg, E. L. (2012). Detection of metabolic fluxes of O and H atoms into intracellular water in mammalian cells. *PLoS One*, 7, e39685.
- Kreuzer-Martin, H. W., Lott, M. J., Ehleringer, J. R., & Hegg, E. L. (2006). Metabolic Processes Account for the Majority of the Intracellular Water in Log-Phase *Escherichia coli* Cells As Revealed by Hydrogen Isotopes. *Biochemistry*, 45(45), 13622–13630. <https://doi.org/10.1021/bi0609164>

- Lehmann, M. M., Schuler, P., Werner, R. A., Saurer, M., Wiesenberg, G. L. B., & Cormier, M.-A. (2024). Biochemical and biophysical drivers of the hydrogen isotopic composition of carbohydrates and acetogenic lipids. *Science Advances*, *10*(28), eadl3591. <https://doi.org/10.1126/sciadv.adl3591>
- Levy, L. M., & Betts, G. F. (1989). Stereospecificity of C₄ nicotinamide hydrogen transfer of the NADP-dependent glyceraldehyde 3-phosphate dehydrogenase. *Biochimica et Biophysica Acta (BBA) – Protein Structure and Molecular Enzymology*, *997*, 331–333.
- Liska, A. J. (2004). Enhanced photosynthesis and redox energy production contribute to salinity tolerance in *Dunaliella* as revealed by homology-based proteomics. *Plant Physiology*, *136*, 2806–2817.
- Luo, Y.-H., Steinberg, L., Suda, S., Kumazawa, S., & Mitsui, A. (1991). Extremely low D/H ratios of photoproduced hydrogen by cyanobacteria. *Plant and Cell Physiology*, *32*(6), 897–900.
- Lyon, B. R., Lee, P. A., Bennett, J. M., DiTullio, G. R., & Janech, M. G. (2011). Proteomic analysis of a sea-ice diatom: Salinity acclimation provides new insight into the dimethylsulfoniopropionate production pathway. *Plant Physiology*, *157*, 1926–1941. <https://doi.org/10.1104/pp.111.185025>
- Maloney, A. E., Shinneman, A. L., Hemeon, K., & Sachs, J. P. (2016). Exploring lipid ²H/¹H fractionation mechanisms in response to salinity with continuous cultures of the diatom *Thalassiosira pseudonana*. *Organic Geochemistry*, *101*, 154–165. <https://doi.org/10.1016/j.orggeochem.2016.08.015>
- M'Boule, D., Chivall, D., Sinke-Schoen, D., Sinninghe Damsté, J. S., Schouten, S., & van der Meer, M. T. J. (2014). Salinity dependent hydrogen isotope fractionation in alkenones produced by coastal and open ocean haptophyte algae. *Geochimica et Cosmochimica Acta*, *130*, 126–135.
- McParland, E. L., Alexander, H., & Johnson, W. M. (2021). The osmolyte ties that bind: Genomic insights into synthesis and breakdown of organic osmolytes in marine microbes. *Frontiers in Marine Science*, *8*, 689306.
- Moore, L. R., Caspi, R., Boyd, D., Berkmen, M., Mackie, A., Paley, S. M., & Karp, P. D. (2024). Revisiting the y-ome of *Escherichia coli*. *Nucleic Acids Research*, *52*, 12201–12207.
- Moore, L. R., Caspi, R., Campbell, D. A., Casey, J. R., Crevecoeur, S., Lea-Smith, D. J., Long, B., Omar, N. M., Paley, S. M., Schmelling, N. M., Torrado, A., Zehr, J. P., & Karp, P. D. (2024). CyanoCyc cyanobacterial web portal. *Frontiers in Microbiology*, *15*, 1340413.
- Nelson, D. B., & Sachs, J. P. (2014). The influence of salinity on D/H fractionation in alkenones from saline and hypersaline lakes in continental North America. *Organic Geochemistry*, *66*, 38–47. <https://doi.org/10.1016/j.orggeochem.2013.10.013>

- Nemoto, Y., & Sasakuma, T. (2000). Specific expression of glucose-6-phosphate dehydrogenase (G6PDH) gene by salt stress in wheat (*Triticum aestivum* L.) *Plant Science*, *158*, 53–60.
- Newsome, S. D., Nakamoto, B. J., Curras, M. R., & Fogel, M. L. (2020). Compound-specific $\delta^2\text{H}$ analysis highlights the relationship between direct assimilation and de novo synthesis of amino acids from food and water in a terrestrial mammalian omnivore. *Oecologia*, *193*(4), 827–842. <https://doi.org/10.1007/s00442-020-04730-9>
- Paul, H. A. (2002). *Application of novel stable isotope methods to reconstruct paleoenvironments: Compound specific hydrogen isotopes and pore-water oxygen isotopes* [Doctoral dissertation, Swiss Federal Institute of Technology Zürich].
- Price, N. M., Harrison, G. I., Hering, J. G., Hudson, R. J., Nirel, P. M. V., Palenik, B., & Morel, F. M. M. (1989). Preparation and chemistry of the artificial algal culture medium Aquil. *Biological Oceanography*, *6*, 443–461.
- Rai, S., Agrawal, C., Shrivastava, A. K., Singh, P. K., & Rai, L. C. (2014). Comparative proteomics unveils cross species variations in *Anabaena* under salt stress. *Journal of Proteomics*, *98*, 254–270.
- Rai, S., Singh, S., Shrivastava, A. K., & Rai, L. C. (2013). Salt and UV-B induced changes in *Anabaena* PCC 7120: Physiological, proteomic and bioinformatic perspectives. *Photosynthesis Research*, *118*, 105–114.
- Record, M. T. J., Courtenay, E. S., Cayley, D. S., & Guttman, H. J. (1998a). Biophysical compensation mechanisms buffering *Escherichia coli* protein nucleic acid interactions against changing environments. *Trends in Biochemical Sciences*, *23*, 190–194.
- Record, M. T. J., Courtenay, E. S., Cayley, D. S., & Guttman, H. J. (1998b). Responses of *Escherichia coli* to osmotic stress: Large changes in amounts of cytoplasmic solutes and water. *Trends in Biochemical Sciences*, *23*, 143–148.
- Robins, R. J., Billault, J.-R., I. Duan, Guet, S., & Pionnier, B.-L., S. Zhang. (2003). Measurement of ^2H distribution in natural products by quantitative ^2H NMR: An approach to understanding metabolism and enzyme mechanism? *Phytochemistry Reviews*, *2*, 87–102.
- Sachs, J. P., Maloney, A. E., & Gregersen, J. (2017). Effect of light on $^2\text{H}/^1\text{H}$ fractionation in lipids from continuous cultures of the diatom *Thalassiosira pseudonana*. *Geochimica et Cosmochimica Acta*, *209*, 204–215.
- Sachs, J. P., Maloney, A. P., Gregersen, J., & Paschall, C. (2016). Effect of salinity on $^2\text{H}/^1\text{H}$ fractionation in lipids from continuous cultures of the coccolithophorid *Emiliana huxleyi*. *Geochimica et Cosmochimica Acta*, *189*, 96–109.

- Sachse, D., & Sachs, J. P. (2008). Inverse relationship between D/H fractionation in cyanobacterial lipids and salinity in Christmas Island saline ponds. *Geochimica et Cosmochimica Acta*, 72(3), 793–806. <https://doi.org/10.1016/j.gca.2007.11.022>
- Saito, K., Kawaguchi, A., Okuda, S., Seyama, Y., & Yamakawa, T. (1980). Incorporation of hydrogen atoms from deuterated water and stereospecifically deuterium-labeled nicotinamide nucleotides into fatty acids with the *Escherichia coli* fatty acid synthetase system. *Biochimica et Biophysica Acta (BBA) - Lipids and Lipid Metabolism*, 618, 202–213.
- Schmidt, H. L., Werner, R. A., & Eisenreich, W. (2003). Systematics of ^2H patterns in natural compounds and its importance for the elucidation of biosynthetic pathways. *Phytochemistry Reviews*, 2, 61–85.
- Schouten, S., Ossebaar, J., Schreiber, K., Kienhuis, M. V. M., Langer, G., Benthien, A., & Bijma, J. (2006). The effect of temperature, salinity and growth rate on the stable hydrogen isotopic composition of long chain alkenones produced by *Emiliania huxleyi* and *Gephyrocapsa oceanica*. *Biogeosciences*, 3(1), 113–119. <https://doi.org/10.5194/bg-3-113-2006>
- Schwab, V. F., & Sachs, J. P. (2011). Hydrogen isotopes in individual alkenones from the Chesapeake Bay estuary. *Geochimica et Cosmochimica Acta*, 75(23), 7552–7565. <https://doi.org/10.1016/j.gca.2011.09.031>
- Silverman, S. N., Wijker, R. S., & Sessions, A. L. (2024). Biosynthetic and catabolic pathways control amino acid $\delta^2\text{H}$ values in aerobic heterotrophs. *Frontiers in Microbiology*, 15, 1–20. <https://doi.org/10.3389/fmicb.2024.1338486>
- Smith, D. A., Nakamoto, B. J., Suess, M. K., & Fogel, M. L. (2022). Central metabolism and growth rate impacts on hydrogen and carbon isotope fractionation during amino acid synthesis in *E. coli*. *Frontiers in Microbiology*, 13, 840167. <https://doi.org/10.3389/fmicb.2022.840167>
- Smith, R. C., & Mobley, C. D. (2008). Underwater light. In L. O. Björn (Ed.), *Photobiology: The Science of Life and Light* (2nd ed., pp. 131–138). Springer.
- Smith, W. G., & York, J. L. (1970). Stereochemistry of the citric acid cycle. *Journal of Chemical Education*, 47(8), 588. <https://doi.org/10.1021/ed047p588>
- Stefels, J. (2000). Physiological aspects of the production and conversion of DMSP in marine algae and higher plants. *Journal of Sea Research*, 43, 183–197.
- Strøm, A. R., & Kaasen, I. (1993). Trehalose metabolism in *Escherichia coli*: Stress protection and stress regulation of gene expression. *Molecular Microbiology*, 8, 205–210.
- Sunda, W. G., Price, N. M., & Morel, F. M. M. (2005). Trace metal ion buffers and their use in culture studies. In R. A. Andersen (Ed.), *Algal Culturing Techniques* (pp. 35–63). Academic Press/Elsevier.

- Thierstein, H. R., & Young, J. R. (2004). In *Coccolithophores*. Springer-Verlag.
- Thompson, P. (1999). The response of growth and biochemical composition to variations in daylength, temperature, and irradiance in the marine diatom *Thalassiosira pseudonana* (Bacillariophyceae). *Journal of Phycology*, *35*, 1215–1223.
- Truong, T. Q., Park, Y. J., Koo, S. Y., Choi, J.-H., Enkhbayar, A., Song, D.-G., & Kim, S. M. (2022). Interdependence of fucoxanthin biosynthesis and fucoxanthin-chlorophyll a/c binding proteins in *Phaeodactylum tricornutum* under different light intensities. *Journal of Applied Phycology*, *35*, 25–42.
- Umbarger, H. E. (1978). Amino acid biosynthesis and its regulation. *Annual Review of Biochemistry*, *47*, 533–606.
- van der Meer, M. T. J., Benthien, A., French, K. L., Epping, E., Zondervan, I., Reichart, G.-J., Bijma, J., Sinninghe Damsté, J. S., & Schouten, S. (2015). Large effect of irradiance on hydrogen isotope fractionation of alkenones in *Emiliana huxleyi*. *Geochimica et Cosmochimica Acta*, *160*, 16–24.
- Ventosa, A., Nieto, J. J., & Oren, A. (1998). Biology of moderately halophilic aerobic bacteria. *Microbiology and Molecular Biology Reviews*, *62*, 504–544.
- Wakeham, S. G., Lee, C., Hedges, J. I., Hernes, P. J., & Peterson, M. J. (1997). Molecular indicators of diagenetic status in marine organic matter. *Geochimica et Cosmochimica Acta*, *61*(24), 5363–5369. [https://doi.org/10.1016/S0016-7037\(97\)00312-8](https://doi.org/10.1016/S0016-7037(97)00312-8)
- Wamelink, M. M., Struys, E. A., & Jakobs, C. (2008). The biochemistry, metabolism and inherited defects of the pentose phosphate pathway: A review. *Journal of Inherited Metabolic Disease*, *31*, 703–717.
- Wang, X., Ma, Y., Huang, C., Wan, Q., Li, N., & Bi, Y. (2008). Glucose-6-phosphate dehydrogenase plays a central role in modulating reduced glutathione levels in reed callus under salt stress. *Planta*, *227*, 611–623.
- Waterbury, J. B., Watson, S. W., Valois, F. W., & Franks, D. G. (1986). Biological and ecological characterization of the marine unicellular cyanobacterium *Synechococcus*. In T. Platt & W. K. I. Li (Eds.), *Photosynthetic Picoplankton* (pp. 71–120, Vol. 214). Canadian Bulletin of Fisheries; Aquatic Sciences.
- Weiss, G. M., Pfannerstill, E. Y., Schouten, S., Sinninghe Damsté, J. S., & van der Meer, M. T. J. (2017). Effects of alkalinity and salinity at low and high light intensity on hydrogen isotope fractionation of long-chain alkenones produced by *Emiliana huxleyi*. *Biogeosciences*, *14*(24), 5693–5704. <https://doi.org/10.5194/bg-14-5693-2017>
- Wijker, R. S., Sessions, A. L., Fuhrer, T., & Phan, M. (2019). $^2\text{H}/^1\text{H}$ variation in microbial lipids is controlled by NADPH metabolism. *Proceedings of the National Academy of Sciences*, *116*(25), 12173–12182.

- Wojtal, P. K., Doherty, S. C., Shea, C. H., Popp, B. N., Benitez-Nelson, C. R., Buesseler, K. O., Estapa, M. L., Roca-Martí, M., & Close, H. G. (2023). Deconvolving mechanisms of particle flux attenuation using nitrogen isotope analyses of amino acids. *Limnology and Oceanography*, *1no.12398*. <https://doi.org/10.1002/lno.12398>
- Yakir, D. (1992). Variations in the natural abundance of oxygen-18 and deuterium in plant carbohydrates. *Plant, Cell & Environment*, *15*(9), 1005–1020. <https://doi.org/10.1111/j.1365-3040.1992.tb01652.x>
- Yakir, D., & DeNiro, M. J. (1990). Oxygen and hydrogen isotope fractionation during cellulose metabolism in *Lemna gibba* L. *Plant Physiology*, *93*, 325–332.
- Yancey, P. H. (1994). Compatible and counteracting solutes. In K. Strange (Ed.), *Cellular and Molecular Physiology of Cell Volume Regulation* (pp. 81–82). CRC Press.
- Yang, Y., Fu, Z., Su, Y., Zhang, X., Li, G., Guo, J., Que, Y., & Xu, L. (2014). A cytosolic glucose-6-phosphate dehydrogenase gene, ScG6PDH, plays a positive role in response to various abiotic stresses in sugarcane. *Scientific Reports*, *4*, 7090. <https://doi.org/10.1038/srep07090>
- Yu, J., Chen, S., Zhao, Q., Wang, T., Yang, C., Diaz, C., Sun, G., & Dai, S. (2011). Physiological and proteomic analysis of salinity tolerance in *Puccinellia tenuiflora*. *Journal of Proteome Research*, *10*, 3852–3870.
- Zhang, B.-L., Billault, I., Li, X., Mabon, F., Remaud, G., & Martin, M. L. (2002). Hydrogen isotopic profile in the characterization of sugars. Influence of the metabolic pathway. *Journal of Agricultural and Food Chemistry*, *50*(6), 1574–1580. <https://doi.org/10.1021/jf010776z>
- Zhang, X., Gillespie, A. L., & Sessions, A. L. (2009). Large D/H variations in bacterial lipids reflect central metabolic pathways. *Proceedings of the National Academy of Sciences*, *106*(31), 12580–12586. <https://doi.org/10.1073/pnas.0903030106>
- Zweng, M. M., Reagan, J. R., Antonov, J. I., Locarnini, R. A., Mishonov, A. V., Boyer, T. P., Garcia, H. E., Baranova, O. K., Johnson, D. R., Seidov, D., & Biddle, M. M. (2013). World Ocean Atlas 2013. In *NOAA Atlas NESDIS 74* (pp. 1–39, Vol. 2).

Chapter 5

Marine particulate organic matter $\delta^2\text{H}_{\text{AA}}$ values reflect substantial heterotrophic turnover with depth

Coauthors: Hilary G. Close, Elizabeth A. Yanuskiewicz, Eunice P. Y. Tsang, and
Alex L. Sessions

Abstract

The downward flux of particulate organic matter (POM) is the primary conduit for transport of carbon to the deep ocean, where it can be sequestered on geologic timescales. However, this downward flux is counteracted by numerous degradative mechanisms that significantly affect global carbon cycling, yet remain poorly constrained in different ocean basins. One mechanism in particular—heterotrophic bacterial turnover of POM—has been difficult to quantify with available tools. Here, we introduce amino acid hydrogen isotope ($\delta^2\text{H}_{\text{AA}}$) analysis as a tool to quantify the extent of POM turnover into heterotrophic biomass, building on our prior work showing that $\delta^2\text{H}_{\text{AA}}$ values of heterotrophic bacteria are distinguishable from those of phytoplankton. We measured multiple depth records of size-fractionated POM from distinct sites and observed signatures that reflect a transition from phytoplankton-dominated biomass in surface POM to substantial increases in heterotrophic biomass through the mesopelagic zone. Quantitative estimates indicate generally high extents of POM turnover into heterotrophic biomass, which would carry important implications for carbon flow and storage in the ocean.

5.1 Introduction

The vertical flux of particulate organic matter (POM) is the dominant process by which carbon and nutrients are transported to depth in the ocean, leading to both sequestration of CO₂ away from the atmosphere and input of nutrients into deep sea ecosystems. A substantial fraction of POM originates from marine phytoplankton, which annually fix ~50 Pg C (roughly 10% of atmospheric carbon; Field et al., 1998) into their cellular biomass via photosynthesis, then aggregate into particles that can sink into the abyssal ocean through a process known as the biological pump (Boyd et al., 2019). Approximately 5–20% of primary production is annually exported to the deep sea (DeVries & Weber, 2017; Henson et al., 2011; Laws et al., 2000), and an even smaller fraction reaches the seafloor (~1%; H. Ducklow et al., 2001). This strong vertical attenuation in carbon flux is well documented (e.g., Berelson, 2001; Buesseler et al., 2020; Martin et al., 1987) and generally understood to result from several key processes, including microbial alteration (extracellular hydrolysis, secondary heterotrophic production, etc.; Giering et al., 2014; Herndl and Reinthaler, 2013), metazoan heterotrophy (e.g., repackaging of phytoplankton aggregates into zooplankton fecal pellets; S. E. Wilson et al., 2008), and physical disaggregation (e.g., via zooplankton swimming or ocean turbulence; Dilling and Alldredge, 2000; Siegel et al., [EarthArXiv Eprints](#)). However, the specific mechanisms and extents of particle degradation in different ocean basins are poorly constrained, in large part due to the rapid and dynamic nature of particle transformation, as well as the generally low concentrations of particles in the water column (Close et al., 2021). Overcoming this challenge and developing tools to accurately trace the origin and fate of POM is a central endeavor in marine geochemistry, given the need to improve models that forecast how global carbon fluxes will change with future climate perturbations (Kharbush

et al., 2020). Indeed, a major limitation to such predictions is our fundamental lack of understanding of the primary factors that control the mechanisms and rates of POM degradation in different oceanic regimes.

POM is defined operationally as material retained on filters with pore sizes ranging from 0.2-1 μm , excluding living metazoans (Kharbush et al., 2020). However, its composition is generally complex in nature, resulting from the multitude of processes that transform POM during its vertical transit through the twilight zone. Major constituents of POM typically include living cells (phytoplankton and heterotrophic microbes) and detritus (phytodetritus, dead microbial cells, and metazoan waste and carcasses; A. L. Alldredge and Gotschalk, 1990; Thornton, 2002). Particles in the ocean span a large size spectrum, ranging from 0.1 μm to a few mm in diameter (Laurenceau-Cornec et al., 2020). The size of a particle does not directly govern its sinking speed (Cael et al., 2021); nevertheless, large and dense particles (typically $>50 \mu\text{m}$ in diameter and/or with mineral ballast) generally sink quickly—up to hundreds of meters per day (Iversen & Ploug, 2010; Lam et al., 2011)—and contribute substantially to the sinking mass flux of carbon (Lam et al., 2011; Wakeham & Lee, 1993). In contrast, small particles (typically $<50 \mu\text{m}$ in diameter) settle slowly—generally on the order of 1–10 meters per day (Iversen & Ploug, 2010)—and dominate the total mass flux of POM (Alonso-González et al., 2010; Bach et al., 2012; Wakeham & Lee, 1993). However, these size divisions are not static: small particles can aggregate into larger particles that sink more quickly (Abramson et al., 2010; Richardson & Jackson, 2007; Siegel et al., [EarthArXiv Eprints](#)), while large particles can disaggregate into smaller particles (Dilling & Alldredge, 2000; Siegel et al., [EarthArXiv Eprints](#)). Both particle size classes are thus important conduits for vertical carbon transport in the ocean. Moreover, degradative mechanisms can vary for different size classes at the same ocean site (e.g., Wojtal et al., 2023), rendering investigation of size-fractionated particles

important for holistic understanding of controls on particle alteration in the water column.

A variety of tools have been employed in an effort to trace the origins and degradative fate of POM. Macromolecular analyses indicate that particles exhibit an exponential loss of phytoplankton-like biomass throughout the water column, which is accompanied by a concomitant increase (in both relative and absolute terms) in molecularly uncharacterized organic carbon (e.g., Wakeham et al., 1997). The characterizable particulate organic carbon, although diminishing with depth, is dominated by hydrolyzable amino acids throughout the water column (Hedges et al., 2001; Wakeham et al., 1997). Compound-specific stable carbon isotope analyses, sometimes employed in tandem with radiocarbon measurements, have enabled reconstruction of the origins of certain POM constituents (Close et al., 2013; Hwang & Druffel, 2003). Additionally, stable nitrogen isotope analysis of amino acids is an emerging tool with significant utility in deconvolving specific mechanisms of POM alteration (e.g., Choi et al., 2022; Golombek et al., 2024; Hannides et al., 2013; McCarthy et al., 2007; Ohkouchi et al., 2017; Sabadel et al., 2019; Wojtal et al., 2023; Yamaguchi and McCarthy, 2018). In particular, the intermolecular patterns of $\delta^{15}\text{N}_{\text{AA}}$ values have been helpful in distinguishing the relative proportions of phytoplankton biomass, metazoan waste, and microbially altered fractions within POM (Doherty et al., 2021; Wojtal et al., 2023). However, with respect to "microbial alteration", $\delta^{15}\text{N}_{\text{AA}}$ analyses are not able to distinguish between two important mechanisms—namely microbial hydrolysis of the detrital material versus secondary production of heterotrophic microbial biomass—which each contribute to shifts in $\delta^{15}\text{N}_{\text{AA}}$ values. These mechanisms carry different implications for carbon storage in the ocean. Particle hydrolysis via the activity of extracellular enzymes (secreted by microbes) converts POM to DOM (Arnosti, 2011; Cho & Azam, 1988; Smith et al., 1992), of which a fraction can persist

as recalcitrant DOM for millennia before being remineralized back to CO₂ (Jiao et al., 2010; P. M. Williams & Druffel, 1987). In contrast, bacterial turnover of POM encompasses both respiratory loss of POM as CO₂ (which is generally stored in the deep ocean for $\leq 1,000$ years) and retention of POM in bacterial biomass (which, if buried in marine sediments, can be sequestered for hundreds of millions of years; Jiao et al., 2014). These scenarios contrast with direct burial of primary production in which all fixed carbon is retained and sequestered on geologic timescales. The relative balance between POM export and turnover, production of recalcitrant DOM, and respiratory CO₂ loss regulates the timescale of carbon storage in the ocean; thus, tracing the fate of carbon through the water column is crucial for predictive understanding of modern and future marine carbon fluxes (e.g., Giering et al., 2014).

Several approaches aim to specifically quantify bacterial production on POM (i.e., turnover), but are limited in their utility. Incorporation rates of ³H-leucine or ³H-thymidine can provide estimates of microbial protein synthesis rates (thus biomass production; Kirchman et al., 1985), but require sample incubation, which can disrupt *in situ* microbial processes that would otherwise naturally occur. D-enantiomers of amino acids have also been used to quantify bacterial biomass in POM (Kaiser & Benner, 2008; Kawasaki et al., 2011; Shen et al., 2023; Tremblay et al., 2015), as these biomarkers are largely bacterially produced. However, they are not unequivocal proxies for bacterial secondary production, as they are present in varying proportions in both cyanobacteria and heterotrophic bacteria (Kaiser & Benner, 2008) and are mainly components of the resistant cell wall biopolymer peptidoglycan (Schleifer & Kandler, 1972), which has different degradative (or preservation) potential than other POM constituents. As such, the ability to quantitatively distinguish phytoplankton from heterotrophic microbial biomass in POM remains a challenge.

Here, we explore the use of amino acid hydrogen isotope analysis as a tool to quantify microbial (or more generally, "heterotrophic") turnover of marine POM. We hypothesize that microbial hydrolysis of POM does not fractionate the hydrogen isotopes of residual particulate amino acids, as no H-bonds are broken during peptide bond cleavage. In contrast, based on our data presented in Figure 4.3 (Chapter 4) showing that amino acids produced by heterotrophic bacteria are significantly ^2H -enriched relative to those of marine phytoplankton, we hypothesize that production of new bacterial biomass on particles (i.e., turnover of phytoplankton proteins into bacterial proteins) will result in ^2H -enrichment of all amino acids in POM, which will become more pronounced with depth in the water column. Here we tested these hypotheses on two POM sample sets provided by H. Close. The POM samples were collected as multiple size fractions from two distinct sites (the Northeast Atlantic Ocean and North Pacific Subtropical Gyre; Figure 5.1), which featured starkly contrasting trophic regimes (Section 5.2). Moreover, parallel $\delta^{15}\text{N}_{\text{AA}}$ analyses were made on splits of the samples by members of the Close lab (Close et al., unpublished; Yanuskiewicz et al., unpublished), enabling broad comparisons of data interpretations. Overall, we observe $\delta^2\text{H}_{\text{AA}}$ patterns that reflect a transition from phytoplankton-dominated biomass in surface POM to substantial increases in heterotrophic biomass through the mesopelagic zone, with potentially significant extents of turnover into heterotrophic biomass. If true, these results carry important implications for carbon flow and storage in the ocean.

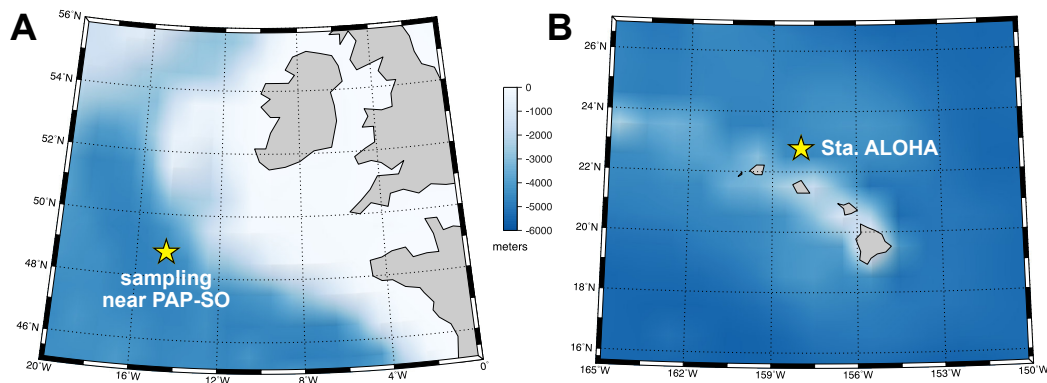


Figure 5.1. Maps of sample sites, with blue shading corresponding to the seafloor depth below sea level. **(A)** Porcupine Abyssal Plain Sustained Observatory (PAP-SO) located in the NE Atlantic Ocean at 48°50'N 16°30'W, 4850 m water depth. The star symbol denotes the location where sampling was conducted (at 49°N, 15°W; 170 km east of PAP-SO). **(B)** Station ALOHA located in the NPSG at 22°45'N, 158°W (denoted by the star symbol), 4740 m water depth.

5.2 Sample site context

5.2.1 Porcupine Abyssal Plain Sustained Observatory, Northeast Atlantic Ocean

The Porcupine Abyssal Plain Sustained Observatory (PAP-SO) is located in the Northeast (NE) Atlantic Ocean (48°50'N 16°30'W, 4850 m water depth; Figure 5.1A). Since its establishment over three decades ago through the North Atlantic Bloom Experiment program within the Joint Global Ocean Flux Study (JGOFS), this long-term open-ocean time series site has provided substantial insight into the nutrient-based connectivity between the surface ocean and seafloor (Hartman et al., 2021). Spring stratification in the North Atlantic drives pronounced phytoplankton blooms (with chlorophyll *a* concentrations ≥ 1.5 mg m⁻³ and primary production rates of 500–1500 mg C m⁻² d⁻¹; Bury et al., 2001; Henson et al., 2009; Savidge et al., 1995). These bloom events are initially dominated by di-

atoms, which grow until surface silica concentrations are depleted, then aggregate and sink into the abyssal ocean, thereby facilitating substantial carbon export (Honjo & Manganini, 1993; Lampitt, 1985). Indeed, of the estimated ~ 9 Pg C yr^{-1} exported out of the euphotic zone in the global ocean, ~ 6 – 22% occurs in the North Atlantic (DeVries & Weber, 2017), and roughly half of this is due to the activity of the annual spring phytoplankton bloom (Sanders et al., 2014; Siegel et al., 2016). After the demise of the diatom bloom, there is a community shift to non-silicifying phytoplankton and other organisms (Leblanc et al., 2009; Lochte et al., 1993; Sieracki et al., 1993).

5.2.2 Station ALOHA, North Pacific Subtropical Gyre

Station ALOHA (A Long-term Oligotrophic Habitat Assessment) is located in the North Pacific Subtropical Gyre (NPSG) ($22^{\circ}45'N$, $158^{\circ}W$, 4740 m water depth; Figure 5.1B). Its establishment in 1988 accompanied the establishment of the Hawaii Ocean Timeseries (HOT) program by the Joint Global Ocean Flux Study (JGOFS). This long-term open-ocean time series site has helped elucidate key aspects of microbial community contributions to marine carbon cycling, and the sensitivities of these communities to the ongoing natural and anthropogenic global-scale perturbations (Karl & Church, 2014). Thermal stratification at Sta. ALOHA prevents winter mixing. The upper mixed layer is effectively isolated from the rest of the water column, starting around 40m, due to warm surface waters ($>24^{\circ}C$) throughout the year, leading to chronic nutrient-depletion in the mixed layer (Karl & Church, 2014). These conditions fuel extreme oligotrophy, with typical chlorophyll *a* concentrations <100 ng l^{-1} and low overall microbial biomass (<2 $\mu\text{g C } l^{-1}$) (Karl & Church, 2014). Nevertheless, microbial activity, production, and growth rates in the NPSG can still be substantial (Hayward, 1991; Laws et al.,

1984; P. J. I. B. Williams et al., 1983), and episodic phytoplankton blooms occur (Dore et al., 2008; Fong et al., 2008; Villareal et al., 2012)—potentially linked to mesoscale eddies and Rossby waves (Guidi et al., 2012; Letelier et al., 2000; Sakamoto et al., 2004; White et al., 2007)—which can be exported well into the mid-mesopelagic (Lukas & Santiago-Mandujano, 2001). Diatoms and diazotrophs can comprise these blooms as well (S. T. Wilson et al., 2015). Microbial growth demands are largely met by highly efficient recycling of energy and nutrients; annual export of primary production is at most a few percent of global primary production (Karl & Church, 2014; Quay et al., 2010). Numerically dominant members of the microbial community within the NPSG surface waters are *Prochlorococcus* spp., members of the alphaproteobacterial order Pelagibacterales (SAR11 clade), and archaea (Campbell et al., 1994, 1997; Eiler et al., 2009; Karl & Church, 2014; Ottesen et al., 2014; Schmidt et al., 1991). The former two bacterial groups, along with members of the Rhodobacterales (Roseobacter clade), dominate the 0.2–1.0 μm particle size class. Moreover, different depth-stratified ecotypes of *Prochlorococcus* spp. exist, including high- and low-light adapted (Malmstrom et al., 2010).

5.3 Materials and methods

5.3.1 Particle sampling and oceanographic context

5.3.1.1 Porcupine Abyssal Plain Sustained Observatory

The PAP-SO POM samples measured in this study were collected during the 2021 NASA EXPORTS (EXport Processes in the Ocean from RemoTe Sensing; Siegel et al., 2015) field campaign, which was conducted from May 4–29, 2021 with the

expressed purpose to "develop a predictive understanding of the export and fate of global ocean net primary production (NPP) and its implications for present and future climates" (Siegel et al., 2016). Samples were specifically collected within an anticyclonic eddy (located at 49°N, 15°W, 170 km east of PAP-SO) to minimize influences from advection (Johnson et al., 2024). Low silicate concentrations coupled with relatively high non-diatom pigment biomarkers in the surface core water at the start of sampling indicated that the diatom bloom had already occurred and terminated, with ~70% estimated to have been already exported from the mixed layer (Johnson et al., 2024; Siegel et al., [EarthArXiv Eprints](#)). The field campaign thus started during the second phase of the spring bloom, during which the phytoplankton community shifted to haptophytes, dinoflagellates, and microphytoplankton (Johnson et al., 2024; Meyer et al., 2024; Siegel et al., [EarthArXiv Eprints](#)). Moreover, the campaign was punctuated by four large storm events, which divided the campaign into three discrete sampling epochs (May 4–10, 11–20, and 21–29) and caused repeated mixed layer deepening, followed by rapid shoaling (Johnson et al., 2024). The average depths of the euphotic zone base (defined as 1% of surface photosynthetically active radiation, i.e., PAR) and mixed layer throughout the sampling campaign were 48.0 and 46.1 m, respectively (Yanusiewicz et al., [unpublished](#)).

The POM samples specifically measured in this study were collected at the start of the third epoch (on May 21) via *in situ* pumps (WTS-LV upright, McLane Research Laboratories, Inc.) onboard the *RRS Discovery* research vessel. Pumps were equipped with different combinations of 142 mm-diameter sequential filters with different pore sizes to separate particles of different size classes: 0.8–51 μm (Supor polyethersulfone); 1–6 μm (combusted quartz fiber filter); 6–51, 51–335, and >335 μm (acid-washed Nitex mesh); and >51 μm (acid-washed polyester mesh). Filters were mounted on tiered mini-MULVFS filter holders (Bishop et

al., 2012). Pumps were deployed at depths of 30, 50, 75, 125, and 340 m and filtered approximately 200–1200 L of seawater. Particles ≤ 51 μm in diameter are considered "small", while those > 51 μm in diameter are considered "large". Following sampling, filters were packed in combusted foil and/or polystyrene petri dishes and stored at -80°C until further processing. POM $\delta^2\text{H}_{\text{AA}}$ measurements reported include all size fractions for surface POM (30 m depth), and only the 0.8–51 and > 51 μm size fractions for POM at depths of > 30 m.

5.3.1.2 Station ALOHA

POM samples from Station ALOHA were collected during the first of a two-part sampling campaign conducted through the C-MORE (Center for Microbial Oceanography: Research and Education) HOE-PhoR (Hawaii Ocean Experiment - Phosphorus Rally) program, which overall sought to "observe and interpret the fundamental role of phosphorus (P) in the sea" (<https://hahana.soest.hawaii.edu/hoephor/hoephor.html>). The HOE-PhoR I campaign took place during the spring of 2013; the POM samples specifically measured in this study were collected on May 24, 2013 via *in situ* pumps (WTS-LV standard, McLane Research Laboratories, Inc.) onboard the R/V *Kilo Moana*. During sample collection, the mixed layer was at a depth of 34 ± 10 m (Diaz et al., 2016), and the deep chlorophyll maximum was located around 100–150 m depth, with a peak at ~ 130 m (Hawaii Ocean Time-Series, 2013). The base of the euphotic zone was at ~ 150 m depth (Close et al., unpublished).

Particle pumps were equipped with 142 mm-diameter, sequential filters with pore sizes of 0.3–3 μm (sterile-packed polyethersulfone filters) and 3–53 μm (pre-combusted quartz fiber filters). Only particles in the 3–53 μm division are discussed here. Filters were mounted on tiered mini-MULVFS filter holders (Bishop

et al., 2012). Pumps were deployed at depths of 25, 72, and 296 m and filtered approximately 800–1300 L of seawater. Following sampling, filters were packed in combusted foil and stored at -80°C until further processing. POM $\delta^2\text{H}_{\text{AA}}$ measurements reported include both size fractions for surface POM (25 m depth), and only the 3–53 μm size fraction for POM at depths of >25 m.

5.3.1.3 Filter preparation

In an on-shore laboratory, filters containing large particles were processed as described by Wojtal et al. (2023) and Yanuskiewicz et al. (unpublished). All filters were lyophilized for ~ 24 h. Dried filters were inspected under a dissecting microscope, and materials such as whole zooplankton that are not expected to be present in passively sinking POM were removed (Doherty et al., 2021).

5.3.2 Amino acid preparation and isotope analysis

Filter samples were hydrolyzed under N_2 to liberate proteinogenic amino acids, then dried and reconstituted in 0.01N HCl. The hydrolysate was purified from the filter pulp by expelling samples through 10 ml syringes containing combusted quartz wool for coarse filtration, and equipped with low protein-binding 0.22 μm PES membrane disc filters for finer filtration. Amino acids were purified via cation exchange chromatography, reprotonated via reconstitution in 0.1N HCl, then derivatized and extracted following methods outlined in Silverman et al. (2024). The derivative products (methoxycarbonyl esters) were identified via gas chromatography/mass spectrometry (GC/MS) by comparison of mass spectra and retention time to those of known derivatized amino acid standards. The hydrogen isotope ratios of the derivatized amino acids were measured via gas chromatography/pyrolysis/isotope ratio mass spectrometry (GC/P/IRMS) using a Thermo Finnigan Delta⁺XP or

Thermo Scientific 253 Plus IRMS. The GC columns and methods were identical to those used by Silverman et al. (2024), as well as the methods used to calibrate the measured isotope ratios, verify instrument accuracy and precision, and correct for the addition of methyl hydrogen from the derivative reagents and exchangeable amine hydrogen (see also Section 3.2.5 in Chapter 3). A mixture of amino acid standards was analyzed every 6–10 samples to monitor instrument consistency throughout sample runs and across experiments. Additionally, $\delta^2\text{H}_{\text{AA}}$ values were corrected for peak size effects following the approach outlined in Section C.2 (Chapter 4 appendix) using standard calibration curves generated during each round of sample analysis. Each amino acid was measured via triplicate injection. Standard deviations accompanying $\delta^2\text{H}_{\text{AA}}$ values reported in this chapter reflect the combination of uncertainty from the sample analysis (i.e., measurement precision), derivative correction, and peak size correction, and were typically $\leq 12\text{‰}$. The average root-mean-square error (RMSE) of the external FAME standard was 4.3‰ across all analyses. Amino acid concentrations were measured on parallel sample splits by members of the Close lab; those used for POM turnover estimates are reported in Table D.1 for Sta. ALOHA samples, and in Yanuskiewicz et al. (unpublished) for PAP-SO samples.

5.3.3 Bayesian mixing model

A Bayesian mixing model was applied to estimate the biomass contributions from two end member metabolisms (photoautotrophy (i.e., phytoplankton) and heterotrophy) to POM samples. $^2\varepsilon_{\text{AA}/\text{w}}$ values used for end member contributions were taken from data on cultures of axenic phytoplankton and bacteria grown on sugars (shown in Figure 4.3, Chapter 4). The mixing model was applied using the SIMMR package in R (Govan & Parnell, 2019). POM $\delta^2\text{H}_{\text{AA}}$ values were con-

verted to ${}^2\varepsilon_{AA/w}$ values using an estimated $\delta^2\text{H}$ value of 5‰ for surface seawater at each site based on prior measurements at Sta. ALOHA and in the Northeast Atlantic Ocean, respectively (Chan et al., 2023; Voelker et al., 2015).

5.4 Results and discussion

5.4.1 Surface POM $\delta^2\text{H}_{AA}$ values carry a distinct phytoplankton signature

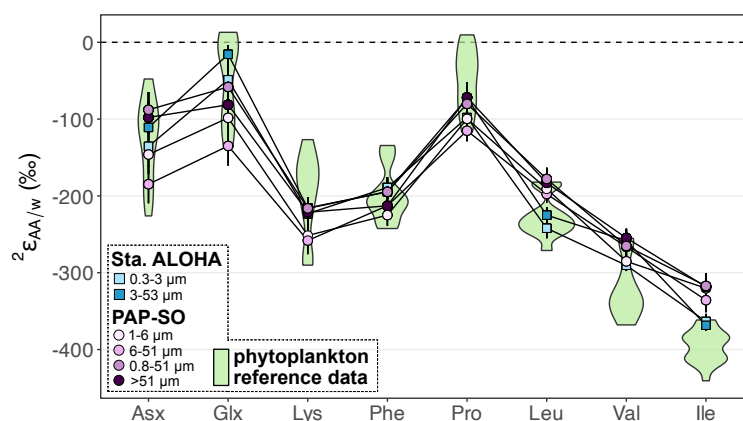


Figure 5.2. Comparison of ${}^2\text{H}/{}^1\text{H}$ fractionations (versus water) for amino acids from size-fractionated surface POM samples (25–30 m depth) and axenic phytoplankton cultures. POM ${}^2\varepsilon_{AA/w}$ values are calculated using an estimated $\delta^2\text{H}$ value of 5‰ for surface seawater at each site (Chan et al., 2023; Voelker et al., 2015). Phytoplankton culture ${}^2\varepsilon_{AA/w}$ values are represented as probability distributions based on data on diatoms, cyanobacteria, and a coccolithophore presented in Chapter 4.

$\delta^2\text{H}_{AA}$ values of surface POM samples (25–30 m depth) from both sites were remarkably similar to those of pure marine phytoplankton cultures (Figure 5.2). In particular, both the magnitudes and overall pattern of most POM amino acid/water ${}^2\text{H}/{}^1\text{H}$ fractionations plotted directly within the ranges captured for axenically cultured diatoms, cyanobacteria, and a coccolithophore (phytoplankton data from Chapter 4; see Figure 5.2 caption for information on conversion of POM $\delta^2\text{H}_{AA}$ to

${}^2\varepsilon_{AA/w}$ values). Compared to phytoplankton δ^2H_{AA} values, those of heterotrophic bacteria are generally significantly higher^a (Figure 4.3 in Chapter 4). Moreover, in heterotrophic bacteria, phenylalanine and lysine are notably 2H -enriched (relative to metabolic subgroup-specific average δ^2H_{AA} values) compared to patterns in marine phytoplankton (Figure 4.7 in Chapter 4). Here, we see this distinct phytoplankton signature in the relatively low phenylalanine and lysine δ^2H_{AA} values (Figure 5.2). Isoleucine was the only amino acid in surface POM whose δ^2H value generally fell outside the range of phytoplankton δ^2H_{AA} values, while those of valine were relatively high but still plotted within the culture reference data. The reason for these deviations is presently unknown. Nevertheless, the general consistency of surface POM- δ^2H_{AA} values with those of phytoplankton confirms that surface POM signatures carry a distinct and dominant signature of phytoplankton biomass. Our results are also consistent with $\delta^{15}N$ -based interpretations of "fresh" phytoplankton-dominated signatures in splits of the same surface POM samples from Sta. ALOHA (Close et al., unpublished) and PAP-SO (Yanusiewicz et al., unpublished). Such phytoplankton-dominated signatures are perhaps surprising given the high proportions of bacteria in the euphotic zones at both sites ($\sim 50\%$ at Sta. ALOHA, and a potentially higher percent during the demise of the North Atlantic spring bloom; Bolaños et al., 2021; Close et al., unpublished; Hawaii Ocean Time-Series, 2013). To explain their nitrogen-isotope-based data at Sta. ALOHA (specifically, trophic positions of all size-fractionated surface POM

^a Although these comparisons involve terrestrial bacteria (data from Silverman et al., 2024), we anticipate that the relative ${}^2\varepsilon_{AA/w}$ patterns in marine heterotrophic bacteria will be consistent with those of our terrestrial organisms when grown under the same metabolic conditions. This assumption stems from the fact that ${}^2\varepsilon_{AA/w}$ values in heterotrophic organisms are primarily controlled by both the catabolic pathways activated during carbon substrate degradation (which should be similar in bacteria consuming the same substrate) and the net ${}^2H/{}^1H$ fractionations of individual amino acid biosynthetic pathways (which are largely ubiquitous across organisms) (Silverman et al., 2024). Additionally, prior culturing work (X. Zhang, L. Zhang, and A. L. Sessions, unpublished) showed similar magnitudes and patterns of lipid/water ${}^2H/{}^1H$ fractionations for *E. coli* and the marine heterotrophic bacterium *Vibrio fischerii* when grown on different substrates, further supporting the likelihood that terrestrial and marine heterotrophic bacteria fractionate amino acid hydrogen isotopes similarly. However, this should be directly tested in future work.

samples resembling those of primary producers), Close et al. hypothesize that heterotrophic bacteria in the surface ocean may either be synthesizing amino acids *de novo* using dissolved inorganic nitrogen (DIN), or directly taking up and incorporating amino acids into their biomass via "salvage incorporation" (McCarthy et al., 2007; Ohkouchi et al., 2017), with low DIN concentrations suggesting the latter strategy may be more likely (Casey et al., 2015; Goldman et al., 1987). Our data supports this interpretation and further hints that bacteria may be preferentially using salvage incorporation (which should not isotopically fractionate amino acids), given that any *de novo* synthesis by heterotrophs would presumably shift lysine and phenylalanine $\delta^2\text{H}$ values substantially higher relative to the baseline average.

5.4.2 $\delta^2\text{H}_{\text{AA}}$ trends with depth in the euphotic zone

POM- $\delta^2\text{H}$ values of many amino acids exhibited slight decreases with depth from the surface ocean through the euphotic zone. In particular, Asx and phenylalanine in 3-53 μm POM from Sta. ALOHA; and lysine, valine, leucine, and phenylalanine in 0.8-51 μm POM from PAP-SO exhibited minima in $\delta^2\text{H}$ values around 75 m (Figure 5.3). These shifts of -16 to -63‰ at Sta. ALOHA, and -7 to -20‰ at PAP-SO, could reflect distinct phytoplankton populations with lower $\delta^2\text{H}_{\text{AA}}$ values at 75 m compared to surface populations. Alternatively, in the case of Sta. ALOHA, these shifts could reflect a relatively stronger phytoplankton signature with less contributions from heterotrophic bacteria, given the proximity of 75 m to the deep chlorophyll maxima at ~ 130 m (Hawaii Ocean Time-Series, 2013). Lower POM $\delta^2\text{H}_{\text{AA}}$ values with depth in the euphotic zone may also be partly linked to the decreased PAR, which we have shown in diatoms contributes to lower $\delta^2\text{H}$ values of several amino acids (Figure 4.6, Chapter 4). Variations in light intensity

and phytoplankton community composition are consistent with interpretations of bulk POM- $\delta^{13}\text{C}$ shifts in the subtropical North Atlantic ocean (Henderson et al., 2024).

5.4.3 $\delta^2\text{H}_{\text{AA}}$ trends with depth in the mesopelagic zone

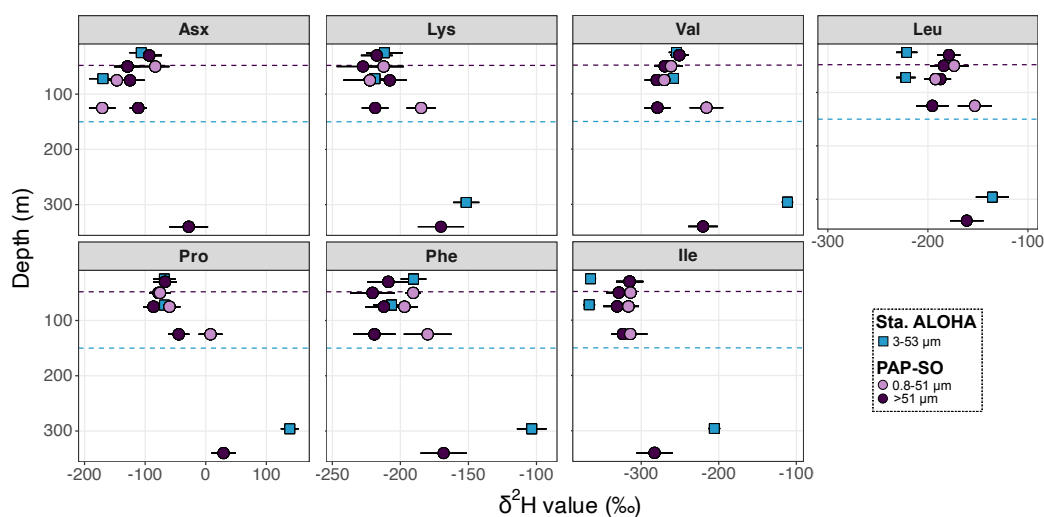


Figure 5.3. Vertical profiles of $\delta^2\text{H}_{\text{AA}}$ values in size-fractionated POM from Sta. ALOHA and PAP-SO. Horizontal dashed lines indicate the euphotic zone base depths at Sta. ALOHA (150 m; blue) and PAP-SO (48 m; purple) during sampling.

The first-order trend in vertical profiles of POM $\delta^2\text{H}_{\text{AA}}$ values is an increase of ~ 50 – 200 ‰ with depth over ~ 300 m at both sites (Figure 5.3), but with preservation of the overall intermolecular $\delta^2\text{H}_{\text{AA}}$ pattern (Figure 5.4). These $\delta^2\text{H}$ shifts are likely not due to alteration of the detrital POM itself, as C-bound H is not involved in peptide bond hydrolysis. Rather, we hypothesize these shifts specifically reflect POM turnover into heterotrophic biomass (discussed below). If true, $\delta^2\text{H}_{\text{AA}}$ is revealing a unique aspect of POM alteration that is not currently accessible by other techniques.

The depth where we observe substantial isotopic alteration of POM beginning to take place is consistent with interpretations of nitrogen isotope-based indicators,

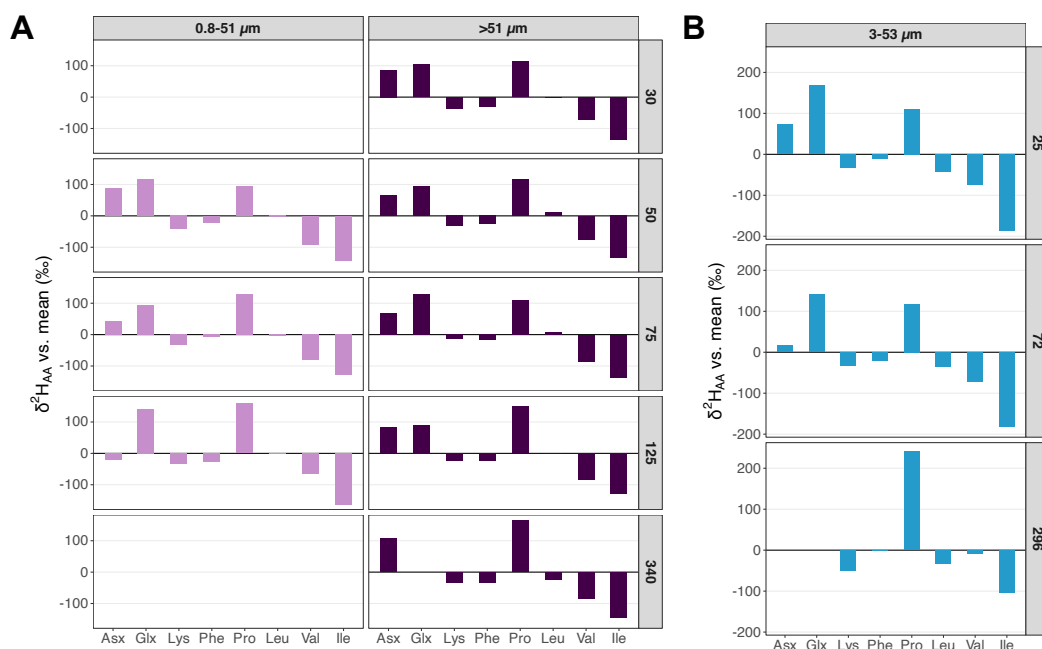


Figure 5.4. Amino acid $\delta^2\text{H}$ values in size-fractionated POM samples from PAP-SO **(A)** and from Sta. ALOHA **(B)**, normalized to mean $\delta^2\text{H}_{\text{AA}}$ values within each sample to more easily visualize changes in intermolecular patterns with depth.

which suggest significant alteration starts when POM reaches the base of the euphotic zone (Close et al., unpublished; Wojtal et al., 2023; Yanuskiewicz et al., unpublished). As noted by Close et al. (unpublished), this depth corresponds to a transition toward increasing expression of extracellular hydrolytic mechanisms by particle-attached microbes (Hoppe et al., 1993; Mende et al., 2017). Particulate amino acid concentrations decrease sharply through the euphotic zone (Aluwihare & Meador, 2008; Wakeham et al., 1997). In the surface ocean where concentrations of phytoplankton-derived amino acids are high, heterotrophic bacteria may preferentially assimilate amino acids into their proteins to conserve energy, which would lead to $\delta^2\text{H}_{\text{AA}}$ values similar to those of phytoplankton (Section 5.4.1; McCarthy et al., 2007; Ohkouchi et al., 2017). With depth, as particulate amino acid concentrations decrease and the distribution in available amino acids departs from that of bacterial biomass, heterotrophic bacteria may increasingly resort to resynthesis and/or *de novo* synthesis for amino acid acquisition. These modes of

amino acid metabolism may become more prominent as particles are increasingly degraded while sinking through the mesopelagic zone. In turn, we predict that this increased turnover of phytoplankton proteins into heterotrophic bacterial proteins is—at least in part—driving the substantial ^2H -enrichments of particulate amino acids through the mesopelagic, given that the $\delta^2\text{H}$ values of amino acids synthesized *de novo* by heterotrophic bacteria are significantly higher than those of phytoplankton, even in the case of bacteria metabolizing sugars (Figure 4.3 in Chapter 4). Moreover, a net shift in bacterial community metabolism from sugar to organic acid degradation is predicted to occur as primary degraders consume the initial phytoplankton-based exopolysaccharide matrix in particles and are gradually replaced by cross-feeders that consume the organic acids released by the degraders (Datta et al., 2016; Enke et al., 2019; Pontrelli et al., 2022). We hypothesize that this metabolic succession would lead to further ^2H -enrichment of amino acids in the particle-attached bacteria given our observations in pure cultures (Silverman et al., 2024, and additionally summarized in Figure 4.3, Chapter 4), resulting in continued increases in POM- $\delta^2\text{H}_{\text{AA}}$ values with depth. Particularly noteworthy is the substantial ^2H -enrichment of proline with depth (by 100-200‰ at both sites; Figure 5.5), as this amino acid was among the most significantly ^2H -enriched in our cultures of bacteria grown on organic acids, including a $>200\%$ ^2H -enrichment in *Bacillus subtilis* grown on succinate (Figure 3.6, Chapter 3).

Metazoan heterotrophic activity (e.g., fecal pellet production) does not appear to significantly contribute to alteration of $\leq 53 \mu\text{m}$ particles at Sta. ALOHA (Close et al., unpublished); however, at PAP-SO, this process appeared to contribute to some of the observed POM- $\delta^{15}\text{N}_{\text{AA}}$ shifts (Yanusiewicz et al., unpublished). No study has yet examined hydrogen isotope fractionation in metazoan fecal matter relative to food, so the effects on POM- $\delta^2\text{H}_{\text{AA}}$ are unknown. However, we hypothesize that metazoan heterotrophic metabolism may produce amino acids

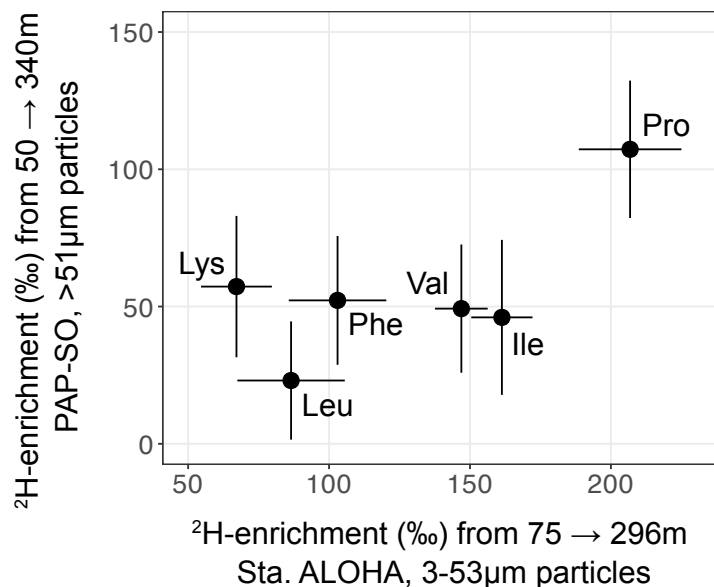


Figure 5.5. ^{2}H -enrichments of individual amino acids from the euphotic zone (specifically, the euphotic zone base at PAP-SO) through the mid-mesopelagic (~ 300 m) in particles from the larger size class at each site. Error bars indicate propagated uncertainties on each pair of $\delta^{2}\text{H}_{\text{AA}}$ values used to calculate the corresponding shift.

with higher values relative to those of phytoplankton (i.e., a similar effect to heterotrophic bacterial metabolism), given our expectation that the general mode of metabolism (here, heterotrophy) controls $\delta^{2}\text{H}_{\text{AA}}$ values. Metazoan heterotrophy would most directly contribute to $\delta^{2}\text{H}_{\text{AA}}$ signatures of non-essential amino acids, but $\delta^{2}\text{H}_{\text{AA}}$ signatures of essential amino acids may additionally be affected through the gut microbiome of host animals (e.g., Newsome et al., 2020). If our general hypothesis is correct, contribution of copepod fecal pellets may additionally be driving some of the observed ^{2}H -enrichments of POM at PAP-SO, which would render POM- $\delta^{2}\text{H}_{\text{AA}}$ increases with depth a more general signature of heterotrophic turnover, and would highlight the complementarity of paired $\delta^{2}\text{H}_{\text{AA}}$ and $\delta^{15}\text{N}_{\text{AA}}$ analyses for investigating POM degradation, as the latter can specifically identify signatures of metazoan heterotrophy (Doherty et al., 2021; Wojtal et al., 2023). Lack of quantitative estimates of fecal pellet contributions to POM at PAP-SO versus Sta. ALOHA challenges our ability to directly compare the potential influence

of microbial versus metazoan heterotrophy on POM- $\delta^2\text{H}_{\text{AA}}$ shifts. Nevertheless, our data suggests that heterotrophic alteration—metazoan or microbial—is lower in the $>51\ \mu\text{m}$ particles at PAP-SO compared to the 3–53 μm particles at Sta. ALOHA (Figure 5.5), discussed further below.

Comparison of $\delta^2\text{H}_{\text{AA}}$ shifts between particle size fractions and sites reveal interesting dynamics that hint at different extents of POM alteration. On average, amino acids in smaller particles at Sta. ALOHA (3–53 μm) were twice as isotopically altered than those in large particles at PAP-SO ($>51\ \mu\text{m}$) from the euphotic zone to the mid-mesopelagic (128‰ versus 62‰, respectively; Figure 5.5). Additionally, at PAP-SO, amino acids in smaller particles became substantially more ^2H -enriched than those in larger particles (31‰ versus 5‰, respectively) from the base of the euphotic zone to the upper mesopelagic (48 to 125 m; Figure 5.3). This general feature is consistent with observations by Close et al. (unpublished), Wojtal et al. (2023), and Yanuskiewicz et al. (unpublished) that small particles are more extensively degraded—particularly by microbial processes (hydrolysis and/or secondary heterotrophic production)—compared to large particles. This may in part be linked to the longer residence times of smaller particles in the water column, which enable more extensive degradation and turnover of POM. At PAP-SO in particular, particles $<100\ \mu\text{m}$ in diameter sank more than four times slower than particles $>100\ \mu\text{m}$ in diameter, with average sinking speeds of $\sim 18\ \text{m d}^{-1}$ versus $>75\ \text{m d}^{-1}$, respectively (Romanelli et al., 2024). Moreover, compositional differences in POM of different size classes may facilitate different particle-specific rates of microbial respiration, as these rates have been shown to vary proportionally with particulate organic carbon concentrations, which in turn often correlate inversely with particle size (A. Alldredge, 1998; Ploug et al., 1999). Additionally, the compositions of particles in the euphotic zone at PAP-SO varied based on size fraction, with smaller particles ($\leq 51\ \mu\text{m}$) containing more phytoplankton cells, versus larger

particles ($>51 \mu\text{m}$) containing more zooplankton waste (Yanusiewicz et al., unpublished). These different starting compositions of particles prior to export into the mesopelagic likely facilitated differences in both the taxonomic composition of, and degradation rates by, the microbial communities that colonized during particle sinking/settling (e.g., Pelve et al., 2017; Simon et al., 1990). Our $\delta^2\text{H}_{\text{AA}}$ data suggests that, not only were smaller particles more extensively hydrolyzed by microbes (as suggested by nitrogen isotope analyses), but that this hydrolysis may have been linked with more extensive turnover into heterotrophic biomass retained within the POM.

To explore this more quantitatively, we estimated the relative contributions of phytoplankton versus bacteria biomass to POM using a Bayesian mixing model with two end-member $^2\varepsilon_{\text{AA}/w}$ value inputs—those of phytoplankton and of bacteria grown on sugars, respectively (data from Figure 5.2, Chapter 4). Using combined data for six amino acids (i.e., those displayed in Figure 5.6A), mixing model estimates corroborate a greater proportion of heterotrophic biomass in smaller mid-mesopelagic particles ($\leq 53 \mu\text{m}$) at Sta. ALOHA compared with larger mid-mesopelagic particles ($>51 \mu\text{m}$) at PAP-SO (Figure 5.6; Table D.2). Interestingly, a bimodal distribution in amino acid-based estimates of heterotrophic contributions was observed, with Asx, isoleucine, leucine, and valine indicating very high contributions of heterotrophic biomass to mesopelagic POM ($85 \pm 5\%$ for $\leq 53 \mu\text{m}$ Sta. ALOHA particles, and $64 \pm 8\%$ for $>51 \mu\text{m}$ PAP-SO particles; Figure 5.6B), and lysine and phenylalanine indicating lower contributions of heterotrophic biomass to mesopelagic POM ($36 \pm 8\%$ for $\leq 53 \mu\text{m}$ Sta. ALOHA particles, and $21 \pm 5\%$ for $>51 \mu\text{m}$ PAP-SO particles; Figure 5.6C). This bimodal distribution may indicate different turnover rates for the two amino acid groups (see below), which in turn may be partly linked to the energetics of amino acid biosynthesis. Phenylalanine is one of the most metabolically costly amino acids to synthesize (Akashi

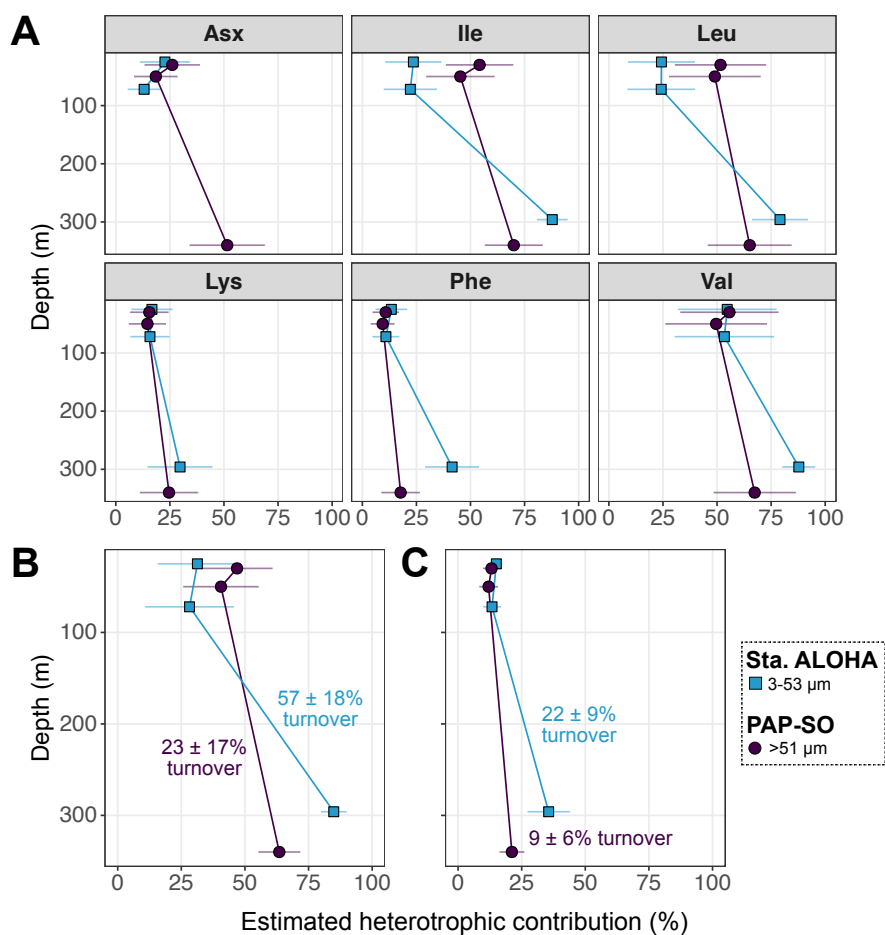


Figure 5.6. Estimated heterotrophic contribution to Sta. ALOHA (3–53 μm) and PAP-SO (>51 μm) particulate amino acids with depth. **(A)** Estimates based on individual amino acid $\delta^2\text{H}$ values. Results are also provided in Table D.2. **(B)** Average estimates based on data for Asx, isoleucine, leucine, and valine. The maximum percent of POM turnover is quantified as the relative increase in heterotrophic biomass from euphotic zone (50–75 m) to the mid-mesopelagic (~ 300 m) for each sample set, and is shown on the plot. **(C)** Average estimates based on data for lysine and phenylalanine, with maximum POM turnover quantified as described for (B). Heterotrophic biomass estimates are derived from a Bayesian mixing model with end member inputs of phytoplankton and sugar-metabolizing bacteria $\delta^2\text{H}_{\text{AA}}$ values (see Section 5.3.3), where the latter is representative of general heterotrophic metabolism, given potentially similar effects of microbial and metazoan heterotrophy on POM- $\delta^2\text{H}_{\text{AA}}$ values. Proline was not included in the model because its $\delta^2\text{H}_{\text{AA}}$ value is similar in phytoplankton and bacteria.

& Gojbori, 2002; Kaleta et al., 2013). It is thus possible that, upon POM peptide hydrolysis, bacteria preferentially assimilate phenylalanine directly into their

proteins rather than synthesizing this amino acid *de novo*, which would result in its lower apparent turnover. However, a lower turnover of lysine is surprising in this framework given that biosynthetic costs of lysine synthesis are comparable to those of leucine and isoleucine (Akashi & Gojobori, 2002; Kaleta et al., 2013). Nevertheless, the amino acid groupings here are consistent with $\delta^{15}\text{N}$ -based groupings of source (phenylalanine and lysine) and trophic (Asx, isoleucine, leucine, and valine) amino acids, indicating potentially similar mechanisms of trophic processing. Future studies should investigate the mechanisms underlying the differential processing of the hydrogen isotope compositions of amino acids between these two groups.

The high estimates of heterotrophic (bacterial) biomass derived from our mixing model are surprising given the generally low estimates of bacterial biomass in sinking particles (<5%; H. W. Ducklow et al., 1985; Turley and Mackie, 1994). However, these studies relied on cell counts, which is likely prone to underestimation. A recent study quantified amino acid D-enantiomers to estimate bacterial biomass in sinking marine particles collected at 1200 m depth at Monterey Bay and found that ~2–27% of the POC was bacterially-derived (Shen et al., 2023). Although we did not measure POM collected in sediment traps, our >51 μm size fraction from PAP-SO contains POM large enough to potentially sink, and our lower-bound estimate of $21 \pm 5\%$ heterotrophic biomass is within the range estimated by Shen et al. (2023). Moreover, we observe a greater potential proportion of heterotrophic biomass in the smaller (i.e., likely more slowly settling) particles compared with the larger particles, consistent with observations by Shen et al. (2023) that the proportion of bacterial biomass varies inversely with POC flux.

When heterotrophic contributions to POM (%) are multiplied by particulate amino acid concentrations (Tables D.1 and D.2), all estimated concentrations of heterotrophically-produced amino acids in the mesopelagic (~300 m depth) are found to be lower

than those in the euphotic zone (50–72 m depth). The same was true for estimated concentrations of photoautotrophically-produced amino acids. These results, together with the apparent increase in heterotrophic contributions to POM protein with depth, may be explained by differential loss of photoautotrophic and heterotrophic proteins with depth (i.e., greater loss of the former), which could result from bacterial respiration of phytoplankton proteins without secondary production, and increased bacterial lysis and/or detachment from particles with depth.

Alternatively, if we assume that the relative increase in heterotrophic biomass is solely due to turnover of photoautotrophic into heterotrophic proteins, we can estimate an upper limit on the relative extent of POM turnover. We quantified the % increase in heterotrophic biomass from the euphotic zone to the mesopelagic, and found that in both groupings of amino acids discussed above, the smaller particles experienced a ~ 2.5 -fold greater turnover compared to large particles, but that turnover estimates for both size classes were generally high: up to as much as $57 \pm 18\%$ turnover of $\leq 53 \mu\text{m}$ particles at Sta. ALOHA, and $23 \pm 17\%$ turnover of $> 51 \mu\text{m}$ particles at PAP-SO (Figure 5.6B–C). Importantly, these estimates encompass the bulk change in 'heterotrophic' signature in the POM, as heterotrophic bacteria that attach to particles but do not contribute to their turnover may still contribute to an apparent increase in POM- $\delta^2\text{H}_{\text{AA}}$ values. Moreover, this approach specifically captures the initial turnover of phytoplankton proteins into bacterial proteins; any secondary turnover of bacterial proteins may not be reflected by POM- $\delta^2\text{H}_{\text{AA}}$ values if turnover is facilitated by metabolically-similar organisms. These calculations thus represent a first pass at estimating POM turnover through $\delta^2\text{H}_{\text{AA}}$ analysis, but this approach should be tested and refined in future studies. In particular, additional measurements should be obtained to disentangle new synthesis from selective preservation of heterotrophic proteins.

Quantifying POM turnover in marine systems may greatly improve our under-

standing of controls on and the dynamics of global carbon cycling. In particular, a high turnover of POM into heterotrophic biomass could carry significant implications with respect to particle degradation and carbon sequestration. Bacterial organic matter has been observed to be more recalcitrant to degradation than algal organic matter (Amon et al., 2001; Lehmann et al., 2020; Nagata et al., 2003); thus, turnover of primary production into bacterial biomass could alter the kinetics of POM degradation and promote carbon sequestration, as proposed by Shen et al. (2023). Moreover, our calculations show that heterotrophic biomass in POM becomes rapidly dominant—by the mid-mesopelagic zone—suggesting that the majority of POM transiting the water column is comprised of heterotrophic material. If true, this would fundamentally change our understanding of the controls on POM degradation rates. In turn, such insight is important for predictive understanding of how the marine carbon cycle will change with ongoing environmental perturbations. Future work should further interrogate the mechanisms driving POM- $\delta^2\text{H}_{\text{AA}}$ variations and examine the utility of this isotopic tool in helping trace the composition and turnover of marine POM.

5.5 Conclusion and potential applications

We introduce $\delta^2\text{H}_{\text{AA}}$ analysis as a potential tool to quantify heterotrophic turnover of marine POM. In pilot samples of size-fractionated POM from Station ALOHA and the North Atlantic spring bloom, we observed $\delta^2\text{H}_{\text{AA}}$ signatures consistent with relatively high proportions of "fresh" phytoplankton biomass in the surface ocean, and substantial increases in POM- $\delta^2\text{H}_{\text{AA}}$ values with depth that may be indicative of heterotrophic replacement of phytoplankton biomass. Isotopic signatures of smaller particles indicated substantially greater rates of turnover, which is consistent with potentially longer residence times in the water column. However,

isotopic signatures for individual amino acids indicated that lysine and phenylalanine in particular may be turned over at a slower rate than Asx, isoleucine, leucine, and valine. This observation cannot solely be explained by energetics of amino acid biosynthesis; thus, which mechanisms are driving the potentially different amino acid-specific turnover rates is an outstanding question from our study. Additionally, we hypothesize that microbial and metazoan heterotrophic metabolisms fractionate amino acid hydrogen isotopes similarly. This should be directly tested in future investigations, with emphasis on using marine heterotrophic bacteria for more relevant calibrations of POM signatures than the terrestrial bacteria reference cultures used in our study. Our hypothesis that amino acid ^2H -enrichment with depth should specifically reflect heterotrophic turnover of POM is based on theoretical consideration of processes involved in hydrogen isotope fractionation. The direct mechanisms controlling POM $\delta^2\text{H}_{\text{AA}}$ alteration with depth remains untested. Finally, future sampling and measurement schemes should endeavor to disentangle new synthesis versus selective preservation of heterotrophic proteins with depth in POM.

As further information regarding the mechanisms controlling amino acid hydrogen isotope fractionation is unveiled, we envision significant utility of $\delta^2\text{H}_{\text{AA}}$ analysis in the field of marine geochemistry beyond tracing POM turnover. For example, as highlighted at the end of Chapter 4, $\delta^2\text{H}_{\text{AA}}$ analysis could be useful for quantifying the prevalence of mixotrophy in marine phytoplankton. This non-strictly autotrophic lifestyle may significantly impact on global carbon cycling, but is not quantifiable with most available tools (Cormier et al., 2022). Moreover, $\delta^2\text{H}_{\text{AA}}$ analysis may help trace bacterial metabolic successions during phytoplankton blooms to better understand the 'mode' and 'tempo' of carbon flow during these events, or more generally trace the types of DOM utilized by free-living microbial communities. Overall, there is significant potential of $\delta^2\text{H}_{\text{AA}}$ analysis in

broadly tracing carbon flow through different ecosystems. As studies employing this isotopic tool continue to expand, so too will the potential applications continue to crystallize.

Acknowledgments

We would like to acknowledge Paul Wojtal and Lillian Henderson for their guidance on the methods used in this study; as well as all members of the Close lab who contributed to the initial filter preparation and processing. We also gratefully acknowledge all individuals who contributed to collection of the POM. For collection of the PAP-SO samples, these include: Steve Pike and Wokil Bam (EXPORTS 2021 pump team); Colleen Durkin, Pat Kelly, and Sean O'Neill (EXPORTS 2021 trap team); Phoebe Lam and lab members for sample handling; and the captain, crew, and science party of the *RRS Discovery*. For collection of the Sta. ALOHA samples, these include: the captains and crew of the R/V *Kilo Moana*; the University of Hawaii School of Ocean and Earth Science and Technology (SOEST) Dean Brian Taylor; Cassie A. Kaapu-Lyons, Blaire Umhau, and Laura Motta Medina for particle collection assistance; Whitney Ko for laboratory assistance, and Craig Glenn for dissecting microscope use. This work was made possible by awards from NSF-OCE, NASA, and NOAA to ALS and HGC. I am additionally grateful to Kim and Ginger Caldwell for their support through the 2022 CEMI Caldwell Fellowship.

References

- Abramson, L., Lee, C., Liu, Z., Wakeham, S. G., & Szlosek, J. (2010). Exchange between suspended and sinking particles in the northwest Mediterranean as inferred from the organic composition of in situ pump and sediment trap samples. *Limnology and Oceanography*, 55(2), 725–739.

- Akashi, H., & Gojobori, T. (2002). Metabolic efficiency and amino acid composition in the proteomes of *Escherichia coli* and *Bacillus subtilis*. *Proceedings of the National Academy of Sciences*, 99(6), 3695–3700. <https://doi.org/10.1073/pnas.062526999>
- Allredge, A. (1998). The carbon, nitrogen and mass content of marine snow as a function of aggregate size. *Deep Sea Research Part I: Oceanographic Research Papers*, 45(4-5), 529–541. [https://doi.org/10.1016/S0967-0637\(97\)00048-4](https://doi.org/10.1016/S0967-0637(97)00048-4)
- Allredge, A. L., & Gotschalk, C. C. (1990). The relative contribution of marine snow of different origins to biological processes in coastal waters. *Continental Shelf Research*, 10(1), 41–58. [https://doi.org/10.1016/0278-4343\(90\)90034-J](https://doi.org/10.1016/0278-4343(90)90034-J)
- Alonso-González, I. J., Arístegui, J., Lee, C., Sanchez-Vidal, A., Calafat, A., Fabrés, J., Sangrá, P., Masqué, P., Hernández-Guerra, A., & Benítez-Barrios, V. (2010). Role of slowly settling particles in the ocean carbon cycle. *Geophysical Research Letters*, 37(13), L13608. <https://doi.org/10.1029/2010GL043827>
- Aluwihare, L. I., & Meador, T. (2008). Chemical Composition of Marine Dissolved Organic Nitrogen. In *Nitrogen in the Marine Environment* (pp. 95–140). Elsevier. <https://doi.org/10.1016/B978-0-12-372522-6.00003-7>
- Amon, R. M. W., Fitznar, H. P., & Benner, R. (2001). Linkages among the bioreactivity, chemical composition, and diagenetic state of marine dissolved organic matter. *Limnology and Oceanography*, 46, 287–297. <https://doi.org/10.4319/lo.2001.46.2.0287>
- Arnosti, C. (2011). Microbial Extracellular Enzymes and the Marine Carbon Cycle. *Annual Review of Marine Science*, 3(1), 401–425. <https://doi.org/10.1146/annurev-marine-120709-142731>
- Bach, L. T., Riebesell, U., Sett, S., Febiri, S., Rzepka, P., & Schulz, K. G. (2012). An approach for particle sinking velocity measurements in the 3–400 μm size range and considerations on the effect of temperature on sinking rates. *Marine Biology*, 159(8), 1853–1864. <https://doi.org/10.1007/s00227-012-1945-2>
- Berelson, W. M. (2001). The flux of particulate organic carbon into the ocean interior: A comparison of four U.S. JGOFS Regional Studies. *Oceanography*, 14(4), 59–67.
- Bishop, J. K. B., Lam, P. J., & Wood, T. J. (2012). Getting good particles: Accurate sampling of particles by large volume in-situ filtration. *Limnology and Oceanography: Methods*, 10, 681–710. <https://doi.org/10.4319/lom.2012.10.681>

- Bolaños, L. M., Choi, C. J., Worden, A. Z., Baetge, N., Carlson, C. A., & Giovannoni, S. (2021). Seasonality of the Microbial Community Composition in the North Atlantic. *Frontiers in Marine Science*, *8*, 624164. <https://doi.org/10.3389/fmars.2021.624164>
- Boyd, P. W., Claustre, H., Levy, M., Siegel, D. A., & Weber, T. (2019). Multifaceted particle pumps drive carbon sequestration in the ocean. *Nature*, *568*, 327–335.
- Buesseler, K. O., Boyd, P. W., Black, E. E., & Siegel, D. A. (2020). Metrics that matter for assessing the ocean biological carbon pump. *Proceedings of the National Academy of Sciences*, *117*(18), 9679–9687. <https://doi.org/10.1073/pnas.1918114117>
- Bury, S. J., Boyd, P. W., Preston, T., Savidge, G., & Owens, N. J. P. (2001). Size-fractionated primary production and nitrogen uptake during a north atlantic phytoplankton bloom: Implications for carbon export estimates. *Deep-Sea Research Part I—Oceanographic Research Papers*, *48*(3), 689–720.
- Cael, B. B., Cavan, E. L., & Britten, G. L. (2021). Reconciling the Size-Dependence of Marine Particle Sinking Speed. *Geophysical Research Letters*, *48*(5), e2020GL091771. <https://doi.org/10.1029/2020GL091771>
- Campbell, L., Liu, H. B., Nolla, H. A., & Vaultot, D. (1997). Annual variability of phytoplankton and bacteria in the subtropical North Pacific Ocean at Station ALOHA during the 1991–1994 ENSO event. *Deep Sea Research Part I: Oceanographic Research Papers*, *44*, 167–192.
- Campbell, L., Nolla, H. A., & Vaultot, D. (1994). The importance of *Prochlorococcus* to community structure in the central North Pacific Ocean. *Limnology and Oceanography*, *39*, 954–961.
- Casey, J. R., Falkowski, P. G., & Karl, D. M. (2015). Substrate selection for heterotrophic bacterial growth in the sea. *Marine Chemistry*, *177*, 349–356.
- Chan, E. W., Alanis, B. A., German, C. R., Lim, D. S., & Breier, J. A. (2023). Oxygen and hydrogen isotopic evidence that Kama’ehuakanaloa (Lō’ihi) Seamount hydrothermal systems are recharged by deep Pacific seawater. *Deep Sea Research Part I: Oceanographic Research Papers*, *197*, 104049. <https://doi.org/10.1016/j.dsr.2023.104049>
- Cho, B. C., & Azam, F. (1988). Major role of bacteria in biogeochemical fluxes in the ocean’s interior. *Nature*, *332*(6163), 441–443. <https://doi.org/10.1038/332441a0>
- Choi, H., Hwang, J., Ryu, Y., Kim, G., & Shin, K.-H. (2022). Seasonal trophic dynamics of sinking particles in the Ulleung Basin of the East Sea (Japan Sea): An approach employing nitrogen isotopes of amino acids. *Frontiers in Marine Science*, *9*. <https://doi.org/10.3389/fmars.2022.824479>

- Close, H. G., Grabb, K. C., Wallsgrove, N., Hannides, C. C. S., Bour, A. L., Doherty, S. C., McCarthy, M. D., Drazen, J. C., & Popp, B. N. (unpublished). *Microbial and metazoan metabolisms leave distinct isotopic traces on marine particles.*
- Close, H. G., Shah, S. R., Ingalls, A. E., Diefendorf, A. F., Brodie, E. L., Hansman, R. L., Freeman, K. H., Aluwihare, L. I., & Pearson, A. (2013). Export of submicron particulate organic matter to mesopelagic depth in an oligotrophic gyre. *Proceedings of the National Academy of Sciences*, *110*(31), 12565–12570. <https://doi.org/10.1073/pnas.1217514110>
- Close, H. G., Lam, P. J., & Popp, B. N. (2021). Marine Particle Chemistry: Influence on Biogeochemical Cycles and Particle Export. *ACS Earth and Space Chemistry*, *5*(5), 1210–1211. <https://doi.org/10.1021/acsearthspacechem.1c00091>
- Cormier, M.-A., Berard, J.-B., Bougaran, G., Trueman, C. N., Mayor, D. J., Lampitt, R. S., Kruger, N. J., Flynn, K. J., & Rickaby, R. E. M. (2022). Deuterium in marine organic biomarkers: Toward a new tool for quantifying aquatic mixotrophy. *New Phytologist*, *234*(3), 776–782. <https://doi.org/10.1111/nph.18023>
- Datta, M. S., Sliwerska, E., Gore, J., Polz, M. F., & Cordero, O. X. (2016). Microbial interactions lead to rapid micro-scale successions on model marine particles. *Nature Communications*, *7*(1), 11965. <https://doi.org/10.1038/ncomms11965>
- DeVries, T., & Weber, T. (2017). The export and fate of organic matter in the ocean: New constraints from combining satellite and oceanographic tracer observations. *Global Biogeochemical Cycles*, *31*(3), 535–555. <https://doi.org/10.1002/2016GB005551>
- Diaz, J. M., Björkman, K. M., Haley, S. T., Ingall, E. D., M., K. D., Longo, A. F., & Dyrman, S. T. (2016). Polyphosphate dynamics at Station ALOHA, North Pacific subtropical gyre. *Limnology and Oceanography*, *61*, 227–239. <https://doi.org/10.1002/lno.10206>
- Dilling, L., & Alldredge, A. L. (2000). Fragmentation of marine snow by swimming macrozooplankton: A new process impacting carbon cycling in the sea. *Deep Sea Research Part I: Oceanographic Research Papers*, *47*, 1227–1245. [https://doi.org/10.1016/S0967-0637\(99\)00105-3](https://doi.org/10.1016/S0967-0637(99)00105-3)
- Doherty, S. C., Maas, A. E., Steinberg, D. K., Popp, B. N., & Close, H. G. (2021). Distinguishing zooplankton fecal pellets as a component of the biological pump using compound-specific isotope analysis of amino acids. *Limnology and Oceanography*, *66*(7), 2827–2841. <https://doi.org/10.1002/lno.11793>
- Dore, J. E., Letelier, R. M., Church, M. J., Lukas, R., & Karl, D. M. (2008). Summer phytoplankton blooms in the oligotrophic North Pacific Subtropical

- Gyre: Historical perspective and recent observations. *Progress in Oceanography*, 76, 2–38.
- Ducklow, H., Steinberg, D., & Buesseler, K. (2001). Upper Ocean Carbon Export and the Biological Pump. *Oceanography*, 14(4), 50–58. <https://doi.org/10.5670/oceanog.2001.06>
- Ducklow, H. W., Hill, S. M., & Gardner, W. D. (1985). Bacterial growth and the decomposition of particulate organic carbon collected in sediment traps. *Continental Shelf Research*, 4(4), 445–464. [https://doi.org/10.1016/0278-4343\(85\)90004-4](https://doi.org/10.1016/0278-4343(85)90004-4)
- Eiler, A., Hayakawa, D. H., Church, M. J., Karl, D. M., & Rappé, M. S. (2009). Dynamics of the SAR11 bacterioplankton lineage in relation to environmental conditions in the oligotrophic North Pacific subtropical gyre. *Environmental Microbiology*, 11, 2291–2300.
- Enke, T. N., Datta, M. S., Schwartzman, J., Cermak, N., Schmitz, D., Barrere, J., Pascual-García, A., & Cordero, O. X. (2019). Modular Assembly of Polysaccharide-Degrading Marine Microbial Communities. *Current Biology*, 29(9), 1528–1535.e6. <https://doi.org/10.1016/j.cub.2019.03.047>
- Field, C. B., Behrenfeld, M. J., Randerson, J. T., & Falkowski, P. (1998). Primary Production of the Biosphere: Integrating Terrestrial and Oceanic Components. *Science*, 281(5374), 237–240. <https://doi.org/10.1126/science.281.5374.237>
- Hawaii Ocean Time-Series. (2013). Data obtained via the Hawaii Ocean Time-series HOT-DOGS application; University of Hawai'i at Mānoa. National Science Foundation Award #2241005.
- Fong, A. A., Karl, D. M., Lukas, R., Letelier, R. M., Zehr, J. P., & Church, M. J. (2008). Nitrogen fixation in an anticyclonic eddy in the oligotrophic North Pacific Ocean. *The ISME Journal*, 2, 663–676.
- Giering, S. L. C., Sanders, R., Lampitt, R. S., Anderson, T. R., Tamburini, C., Boutrif, M., Zubkov, M. V., Marsay, C. M., Henson, S. A., Saw, K., Cook, K., & Mayor, D. J. (2014). Reconciliation of the carbon budget in the ocean's twilight zone. *Nature*, 507, 480–483. <https://doi.org/10.1038/nature13123>
- Goldman, J. C., Caron, D. A., & Dennett, M. R. (1987). Regulation of gross growth efficiency and ammonium regeneration in bacteria by substrate C:N ratio. *Limnology and Oceanography*, 32, 1239–1252.
- Golombek, N. Y., Kienast, M., Pilskaln, C. H., Algar, C., & Sherwood, O. (2024). Origin and alteration of sinking and resuspended organic matter on a benthic nepheloid layer influenced continental shelf. *Geochimica et Cosmochimica Acta*, 366, 31–47. <https://doi.org/10.1016/j.gca.2023.12.008>

- Govan, E., & Parnell, A. (2019). Simmr: A stable isotope mixing model. R package version 0.5.1.216. <https://doi.org/https://CRAN.R-project.org/package=simmr>
- Guidi, L., Calil, P. H. R., Duhamel, S., Björkman, K. M., Doney, S. C., Jackson, G. A., Li, B., Church, M. J., Tozzi, S., Kolber, Z. S., Richards, K. J., Fong, A. A., Letelier, R. M., Gorsky, G., Stemann, L., & Karl, D. M. (2012). Does eddy–eddy interaction control surface phytoplankton distribution and carbon export in the North Pacific Subtropical Gyre? *Journal of Geophysical Research*, *117*, G02024.
- Hannides, C. C. S., Popp, B. N., Choy, C. A., & Drazen, J. C. (2013). Midwater zooplankton and suspended particle dynamics in the North Pacific Subtropical Gyre: A stable isotope perspective. *Limnology and Oceanography*, *58*(6), 1931–1946. <https://doi.org/10.4319/lo.2013.58.6.1931>
- Hartman, S. E., Bett, B. J., Durden, J. M., Henson, S. A., Iversen, M., Jeffreys, R. M., Horton, T., Lampitt, R., & Gates, A. R. (2021). Enduring science: Three decades of observing the Northeast Atlantic from the Porcupine Abyssal Plain Sustained Observatory (PAP-SO). *Progress in Oceanography*, *191*, 102508. <https://doi.org/10.1016/j.pocean.2020.102508>
- Hayward, T. L. (1991). Primary production in the North Pacific Central Gyre: A controversy with important implications. *Trends in Ecology Evolution*, *6*, 281–284.
- Hedges, J. I., Baldock, J. A., Gélinas, Y., Lee, C., Peterson, M., & Wakeham, S. G. (2001). Evidence for non-selective preservation of organic matter in sinking marine particles. *Nature*, *409*(6822), 801–804. <https://doi.org/10.1038/35057247>
- Henderson, L. C., Wittmers, F., Carlson, C. A., Worden, A. Z., & Close, H. G. (2024). Variable carbon isotope fractionation of photosynthetic communities over depth in an open-ocean euphotic zone. *Proceedings of the National Academy of Sciences*, *121*(10), e2304613121. <https://doi.org/10.1073/pnas.2304613121>
- Henson, S. A., Dunne, J. P., & Sarmiento, J. L. (2009). Decadal variability in North Atlantic phytoplankton blooms. *Journal of Geophysical Research—Oceans*, *114*. <https://doi.org/10.1029/2008JC005139>
- Henson, S. A., Sanders, R., Madsen, E., Morris, P. J., Le Moigne, F., & Quartly, G. D. (2011). A reduced estimate of the strength of the ocean's biological carbon pump. *Geophysical Research Letters*, *38*(4), L04606. <https://doi.org/10.1029/2011GL046735>
- Herndl, G. J., & Reinthaler, T. (2013). Microbial control of the dark end of the biological pump. *Nature Geoscience*, *6*(9), 718–724. <https://doi.org/10.1038/ngeo1921>

- Honjo, S., & Manganini, S. J. (1993). Annual biogenic particle fluxes to the interior of the North Atlantic Ocean studied at 34-Degrees-N 21-Degrees-W and 48 Degrees-N 21-Degrees-W. *Deep-Sea Research Part II—Topical Studies in Oceanography*, 40(1-2), 587–607.
- Hoppe, H.-G., Ducklow, H. W., & Karrasch, B. (1993). Evidence for dependency of bacterial growth on enzymatic hydrolysis of particulate organic matter in the mesopelagic ocean. *Marine Ecology Progress Series*, 93, 277–283.
- Hwang, J., & Druffel, E. R. M. (2003). Lipid-Like Material as the Source of the Uncharacterized Organic Carbon in the Ocean? *Science*, 299(5608), 881–884. <https://doi.org/10.1126/science.1078508>
- Iversen, M. H., & Ploug, H. (2010). Ballast minerals and the sinking carbon flux in the ocean: Carbon-specific respiration rates and sinking velocity of marine snow aggregates. *Biogeosciences*, 7(9), 2613–2624. <https://doi.org/10.5194/bg-7-2613-2010>
- Jiao, N., Robinson, C., Azam, F., Thomas, H., Baltar, F., Dang, H., Hardman-Mountford, N. J., Johnson, M., Kirchman, D. L., Koch, B. P., Legendre, L., Li, C., Liu, J., Luo, T., Luo, Y.-W., Mitra, A., Romanou, A., Tang, K., Wang, X., ... Zhang, R. (2014). Mechanisms of microbial carbon sequestration in the ocean – future research directions. *Biogeosciences*, 11(19), 5285–5306. <https://doi.org/10.5194/bg-11-5285-2014>
- Jiao, N., Herndl, G. J., Hansell, D. A., Benner, R., Kattner, G., Wilhelm, S. W., Kirchman, D. L., Weinbauer, M. G., Luo, T., Chen, F., & Azam, F. (2010). Microbial production of recalcitrant dissolved organic matter: Long-term carbon storage in the global ocean. *Nature Reviews Microbiology*, 8(8), 593–599. <https://doi.org/10.1038/nrmicro2386>
- Johnson, L., Siegel, D. A., Thompson, A. F., Fields, E., Erickson, Z. K., Cetinic, I., Lee, C. M., D'Asaro, E. A., Nelson, N. B., Omand, M. M., Sten, M., Traylor, S., Nicholson, D. P., Graff, J. R., Steinberg, D. K., Sosik, H. M., Buesseler, K. O., Brzezinski, M. A., Ramos, I. S., ... Henson, S. A. (2024). Assessment of oceanographic conditions during the North Atlantic EXport processes in the ocean from RemoTe sensing (EXPORTS) field campaign. *Progress in Oceanography*, 220, 103170. <https://doi.org/10.1016/j.pcean.2023.103170>
- Kaiser, K., & Benner, R. (2008). Major bacterial contribution to the ocean reservoir of detrital organic carbon and nitrogen. *Limnology and Oceanography*, 53(1), 99–112. <https://doi.org/10.4319/lo.2008.53.1.0099>
- Kaleta, C., Schäuble, S., Rinas, U., & Schuster, S. (2013). Metabolic costs of amino acid and protein production in *Escherichia coli*. *Biotechnology Journal*, 8(9), 1105–1114. <https://doi.org/10.1002/biot.201200267>

- Karl, D. M., & Church, M. J. (2014). Microbial oceanography and the Hawaii Ocean Time-series programme. *Nature Reviews Microbiology*, *12*, 699–713. <https://doi.org/10.1038/nrmicro3333>
- Kawasaki, N., Sohrin, R., Ogawa, H., Nagata, T., & Benner, R. (2011). Bacterial carbon content and the living and detrital bacterial contributions to suspended particulate organic carbon in the North Pacific Ocean. *Aquatic Microbial Ecology*, *62*(2), 165–176. <https://doi.org/10.3354/ame01462>
- Kharbush, J. J., Close, H. G., Van Mooy, B. A. S., Arnosti, C., Smittenberg, R. H., Le Moigne, F. A. C., Mollenhauer, G., Scholz-Böttcher, B., Obreht, I., Koch, B. P., Becker, K. W., Iversen, M. H., & Mohr, W. (2020). Particulate Organic Carbon Deconstructed: Molecular and Chemical Composition of Particulate Organic Carbon in the Ocean. *Frontiers in Marine Science*, *7*, 518. <https://doi.org/10.3389/fmars.2020.00518>
- Kirchman, D., K'nees, E., & Hodson, R. (1985). Leucine incorporation and its potential as a measure of protein synthesis by bacteria in natural aquatic systems. *Applied and Environmental Microbiology*, *49*(3), 599–607. <https://doi.org/10.1128/aem.49.3.599-607.1985>
- Lam, P. J., Doney, S. C., & Bishop, J. K. B. (2011). The dynamic ocean biological pump: Insights from a global compilation of particulate organic carbon, CaCO₃, and opal concentration profiles from the mesopelagic. *Global Biogeochemical Cycles*, *25*(3), GB3009. <https://doi.org/10.1029/2010GB003868>
- Lampitt, R. S. (1985). Evidence for the seasonal deposition of detritus to the deep-sea floor and its subsequent resuspension. *Deep-Sea Research Part A—Oceanographic Research Papers*, *32*(8), 885–897.
- Laurenceau-Cornec, E. C., Le Moigne, F. A. C., Gallinari, M., Moriceau, B., Toullec, J., Iversen, M. H., Engel, A., & De La Rocha, C. L. (2020). New guidelines for the application of Stokes' models to the sinking velocity of marine aggregates. *Limnology and Oceanography*, *65*(6), 1264–1285. <https://doi.org/10.1002/lno.11388>
- Laws, E. A., Redalje, D. G., Haas, L. W., Bienfang, P. K., Eppley, R. W., Harrison, W. G., Karl, D. M., & Marra, J. (1984). High phytoplankton growth and production rates in oligotrophic Hawaiian coastal waters. *Limnology and Oceanography*, *29*, 1161–1169.
- Laws, E. A., Falkowski, P. G., Smith, W. O., Ducklow, H., & McCarthy, J. J. (2000). Temperature effects on export production in the open ocean. *Global Biogeochemical Cycles*, *14*(4), 1231–1246. <https://doi.org/10.1029/1999GB001229>
- Leblanc, K., Hare, C. E., Feng, Y., Berg, G. M., DiTullio, G. R., Neeley, A., Benner, I., Sprengel, C., Beck, A., Sanudo-Wilhelmy, S. A., Passow, U., Klinck, K., Rowe, J. M., Wilhelm, S. W., Brown, C. W., & Hutchins, D. A.

- (2009). Distribution of calcifying and silicifying phytoplankton in relation to environmental and biogeochemical parameters during the late stages of the 2005 North East Atlantic Spring Bloom. *Biogeosciences*, 6(10), 2155–2179.
- Lehmann, M. F., Carstens, D., Deek, A., McCarthy, M., Schubert, C. J., & Zopfi, J. (2020). Amino acid and amino sugar compositional changes during in vitro degradation of algal organic matter indicate rapid bacterial re-synthesis. *Geochimica et Cosmochimica Acta*, 283, 67–84. <https://doi.org/10.1016/j.gca.2020.05.025>
- Letelier, R. M., Karl, D. M., Abbott, M. R., Flament, P., Freilich, M., Lukas, R., & Strub, T. (2000). Role of late winter mesoscale events in the biogeochemical variability of the upper water column of the North Pacific Subtropical Gyre. *Journal of Geophysical Research*, 105, 28723–28739.
- Lochte, K., Ducklow, H. W., Fasham, M. J. R., & Stienen, C. (1993). Plankton succession and carbon cycling at 47-Degrees-N–20-Degrees-W during the JGOFS North Atlantic Bloom Experiment. *Deep-Sea Research Part II—Topical Studies in Oceanography*, 40(1-2), 91–114.
- Lukas, R., & Santiago-Mandujano, F. (2001). Extreme water mass anomaly observed in the Hawaii Ocean Time Series. *Geophysical Research Letters*, 28, 2931–2934.
- Malmstrom, R. R., Coe, A., Kettler, G. C., Martiny, A. C., Frias-Lopez, J., Zinser, E. R., & Chisholm, S. W. (2010). Temporal dynamics of *Prochlorococcus* ecotypes in the Atlantic and Pacific Oceans. *The ISME Journal*, 4, 1252–1264.
- Martin, J. H., Knauer, G. A., Karl, D. M., & Broenkow, W. W. (1987). VERTEX: Carbon cycling in the northeast Pacific. *Deep Sea Research Part A. Oceanographic Research Papers*, 34(2), 267–285. [https://doi.org/10.1016/0198-0149\(87\)90086-0](https://doi.org/10.1016/0198-0149(87)90086-0)
- McCarthy, M. D., Benner, R., Lee, C., & Fogel, M. L. (2007). Amino acid nitrogen isotopic fractionation patterns as indicators of heterotrophy in plankton, particulate, and dissolved organic matter. *Geochimica et Cosmochimica Acta*, 71(19), 4727–4744. <https://doi.org/10.1016/j.gca.2007.06.061>
- Mende, D. R., Bryant, J. A., Aylward, F. O., Eppley, J. M., Nielsen, T., Karl, D. M., & DeLong, E. F. (2017). Environmental drivers of a microbial genomic transition zone in the ocean's interior. *Nature Microbiology*, 2(10), 1367–1373. <https://doi.org/10.1038/s41564-017-0008-3>
- Meyer, M. G., Brzezinski, M. A., Cohn, M. R., Kramer, S. J., Paul, N., Sharpe, G., Niebergall, A. K., Gifford, S., Cassar, N., & Marchetti, A. (2024). Size-Fractionated Primary Production Dynamics During the Decline Phase of the North Atlantic Spring Bloom. *Global Biogeochemical Cycles*, 38(7), e2023GB008019. <https://doi.org/10.1029/2023GB008019>

- Nagata, T., Meon, B., & Kirchman, D. L. (2003). Microbial degradation of peptidoglycan in seawater. *Limnology and Oceanography*, *48*, 745–754. <https://doi.org/10.4319/lo.2003.48.2.0745>
- Newsome, S. D., Nakamoto, B. J., Curras, M. R., & Fogel, M. L. (2020). Compound-specific $\delta^2\text{H}$ analysis highlights the relationship between direct assimilation and de novo synthesis of amino acids from food and water in a terrestrial mammalian omnivore. *Oecologia*, *193*(4), 827–842. <https://doi.org/10.1007/s00442-020-04730-9>
- Ohkouchi, N., Chikaraishi, Y., Close, H. G., Fry, B., Larsen, T., Madigan, D. J., McCarthy, M. D., McMahon, K. W., Nagata, T., Naito, Y. I., Ogawa, N. O., Popp, B. N., Steffan, S., Takano, Y., Tayasu, I., Wyatt, A. S., Yamaguchi, Y. T., & Yokoyama, Y. (2017). Advances in the application of amino acid nitrogen isotopic analysis in ecological and biogeochemical studies. *Organic Geochemistry*, *113*, 150–174. <https://doi.org/10.1016/j.orggeochem.2017.07.009>
- Ottesen, E. A., Young, C. R., Gifford, S. M., Eppley, J. M., Marin, R., Schuster, S. C., Scholin, C. A., & Delong, E. F. (2014). Multispecies diel transcriptional oscillations in open ocean heterotrophic bacterial assemblages. *Science*, *345*, 207–212.
- Pelve, E. A., Fontanez, K. M., & DeLong, E. F. (2017). Bacterial Succession on Sinking Particles in the Ocean's Interior. *Frontiers in Microbiology*, *8*, 2269. <https://doi.org/10.3389/fmicb.2017.02269>
- Ploug, H., Grossart, H. P., Azam, F., & Jørgensen, B. B. (1999). Photosynthesis, respiration, and carbon turnover in sinking marine snow from surface waters of Southern California Bight: Implications for the carbon cycle in the ocean. *Marine Ecology Progress Series*, *179*, 1–11. <https://doi.org/10.3354/meps179001>
- Pontrelli, S., Szabo, R., Pollak, S., Schwartzman, J., Ledezma-Tejeida, D., Cordero, O. X., & Sauer, U. (2022). Metabolic cross-feeding structures the assembly of polysaccharide degrading communities. *Science Advances*, *8*(8), eabk3076. <https://doi.org/10.1126/sciadv.abk3076>
- Quay, P. D., Peacock, C., Björkman, K., & Karl, D. M. (2010). Measuring primary production rates in the ocean: Enigmatic results between incubation and non-incubation methods at Station ALOHA. *Global Biogeochemical Cycles*, *24*(3), 2009GB003665. <https://doi.org/10.1029/2009GB003665>
- Richardson, T. L., & Jackson, G. A. (2007). Small Phytoplankton and Carbon Export from the Surface Ocean. *Science*, *315*(5813), 838–840. <https://doi.org/10.1126/science.1133471>
- Romanelli, E., Giering, S. L. C., Estapa, M., Siegel, D. A., & Passow, U. (2024). Can intense storms affect sinking particle dynamics after the North Atlantic

- spring bloom? *Limnology and Oceanography*, 69(12), 2963–2974. <https://doi.org/10.1002/lno.12723>
- Sabadel, A., Van Oostende, N., Ward, B., S.Woodward, E., Van Hale, R., & Frew, R. (2019). Characterization of particulate organic matter cycling during a summer North Atlantic phytoplankton bloom using amino acid C and N stable isotopes. *Marine Chemistry*, 214, 103670. <https://doi.org/10.1016/j.marchem.2019.103670>
- Sakamoto, C. M., Karl, D. M., Jannasch, H. W., Bidigare, R. R., Letelier, R. M., Walz, P. M., Ryan, J. P., Polito, P. S., & Johnson, K. S. (2004). Influence of Rossby waves on nutrient dynamics and the plankton community structure in the North Pacific subtropical gyre. *Journal of Geophysical Research*, 109, C05032.
- Sanders, R., Henson, S. A., Koski, M., De La Rocha, C. L., Painter, S. C., Poulton, A. J., Riley, J., Salihoglu, B., Visser, A., Yool, A., Bellerby, R., & P., M. A. (2014). The biological carbon pump in the North Atlantic. *Progress in Oceanography*, 129, 200–218. <https://doi.org/10.1016/j.pocean.2014.05.005>
- Savidge, G., Boyd, P., Pomroy, A., Harbour, D., & Joint, I. (1995). Phytoplankton production and biomass estimates in the Northeast Atlantic Ocean, May to June 1990. *Deep-Sea Research Part I—Oceanographic Research Papers*, 42(5), 599–617.
- Schleifer, K. H., & Kandler, O. (1972). Peptidoglycan types of bacterial cell walls and their taxonomic implications. *Bacteriological Reviews*, 36(4), 407–477. <https://doi.org/10.1128/br.36.4.407-477.1972>
- Schmidt, T. M., DeLong, E. F., & Pace, N. R. (1991). Analysis of a marine picoplankton community by 16S ribosomal RNA cloning and sequencing. *Journal of Bacteriology*, 173, 4371–4378.
- Shen, Y., Guilderson, T. P., Chavez, F. P., & McCarthy, M. D. (2023). Important Contribution of Bacterial Carbon and Nitrogen to Sinking Particle Export. *Geophysical Research Letters*, 50(11), e2022GL102485. <https://doi.org/10.1029/2022GL102485>
- Siegel, D. A., Buesseler, K. O., Behrenfeld, M. J., Benitez-Nelson, C. R., Boss, E., Brzezinski, M. A., Burd, A., Carlson, C. A., D'Asaro, E. A., Doney, S. C., Perry, M. J., Stanley, R. H. R., & Steinberg, D. K. (2015). EXport Processes in the Ocean from RemoTe Sensing (EXPORTS): A Science Plan for a NASA Field Campaign.
- Siegel, D. A., Buesseler, K. O., Behrenfeld, M. J., Benitez-Nelson, C. R., Boss, E., Brzezinski, M. A., Burd, A., Carlson, C. A., D'Asaro, E. A., Doney, S. C., Perry, M. J., Stanley, R. H. R., & Steinberg, D. K. (2016). Prediction of the export and fate of global ocean net primary production: The EXPORTS

- science plan. *Frontiers in Marine Science*, 3(22). <https://doi.org/10.3389/fmar.2016.00022>
- Siegel, D. A., Burd, A. B., Estapa, M., Fields, E., Johnson, L., Romanelli, E., Brzezinski, M. A., Buesseler, K. O., Clevenger, S., Cetinić, I., Drago, L., Durkin, C. A., Kiko, R., Kramer, S. J., Maas, A., Omand, M., Passow, U., & Steinberg, D. K. (EarthArXiv Eprints). *Dynamics of Aggregates and Sinking Carbon Fluxes in a Turbulent Ocean*. <https://doi.org/10.31223/X58709>
- Sieracki, M. E., Verity, P. G., & Stoecker, D. K. (1993). Plankton community response to sequential silicate and nitrate depletion during the 1989 North Atlantic Spring Bloom. *Deep-Sea Research Part II—Topical Studies in Oceanography*, 40(1-2), 213–225.
- Silverman, S. N., Wijker, R. S., & Sessions, A. L. (2024). Biosynthetic and catabolic pathways control amino acid $\delta^2\text{H}$ values in aerobic heterotrophs. *Frontiers in Microbiology*, 15, 1–20. <https://doi.org/10.3389/fmicb.2024.1338486>
- Simon, M., Alldredge, A., & Azam, F. (1990). Bacterial carbon dynamics on marine snow. *Marine Ecology Progress Series*, 65, 205–211. <https://doi.org/10.3354/meps065205>
- Smith, D. C., Simon, M., Alldredge, A. L., & Azam, F. (1992). Intense hydrolytic enzyme activity on marine aggregates and implications for rapid particle dissolution. *Nature*, 359, 139–142. <https://doi.org/10.1038/359139a0>
- Thornton, D., C. O. (2002). Diatom aggregation in the sea: Mechanisms and ecological implications. *European Journal of Phycology*, 37(2), 149–161.
- Tremblay, L., Caparros, J., Leblanc, K., & Obernosterer, I. (2015). Origin and fate of particulate and dissolved organic matter in a naturally iron-fertilized region of the Southern Ocean. *Biogeosciences*, 12(2), 607–621. <https://doi.org/10.5194/bg-12-607-2015>
- Turley, C., & Mackie, P. (1994). Biogeochemical significance of attached and free-living bacteria and the flux of particles in the NE Atlantic Ocean. *Marine Ecology Progress Series*, 115, 191–203. <https://doi.org/10.3354/meps115191>
- Villareal, T. A., Brown, C. G., Brzezinski, M. A., Krause, J. W., & Wilson, C. (2012). Summer diatom blooms in the North Pacific subtropical gyre: 2008–2009. *PLoS ONE*, 7, e33109.
- Voelker, A. H., Colman, A., Olack, G., Waniek, J. J., & Hodell, D. (2015). Oxygen and hydrogen isotope signatures of Northeast Atlantic water masses. *Deep Sea Research Part II: Topical Studies in Oceanography*, 116, 89–106. <https://doi.org/10.1016/j.dsr2.2014.11.006>

- Wakeham, S. G., & Lee, C. (1993). Production, Transport, and Alteration of Particulate Organic Matter in the Marine Water Column [Series Title: Topics in Geobiology]. In F. G. Stehli, D. S. Jones, M. H. Engel, & S. A. Macko (Eds.), *Organic Geochemistry* (pp. 145–169, Vol. 11). Springer US. https://doi.org/10.1007/978-1-4615-2890-6_6
- Wakeham, S. G., Lee, C., Hedges, J. I., Hernes, P. J., & Peterson, M. J. (1997). Molecular indicators of diagenetic status in marine organic matter. *Geochimica et Cosmochimica Acta*, *61*(24), 5363–5369. [https://doi.org/10.1016/S0016-7037\(97\)00312-8](https://doi.org/10.1016/S0016-7037(97)00312-8)
- White, A. E., Spitz, Y. H., & Letelier, R. M. (2007). What factors are driving summer phytoplankton blooms in the North Pacific Subtropical Gyre? *Journal of Geophysical Research*, *112*, C12006.
- Williams, P. J. I. B., Heinemann, K. R., Marra, J., & Purdie, D. A. (1983). Comparison of ^{14}C and O_2 measurements of phytoplankton production in oligotrophic waters. *Nature*, *305*, 49–50.
- Williams, P. M., & Druffel, E. R. M. (1987). Radiocarbon in dissolved organic matter in the central North Pacific Ocean. *Nature*, *330*(6145), 246–248. <https://doi.org/10.1038/330246a0>
- Wilson, S. E., Steinberg, D. K., & Buesseler, K. O. (2008). Changes in fecal pellet characteristics with depth as indicators of zooplankton repackaging of particles in the mesopelagic zone of the subtropical and subarctic North Pacific Ocean. *Deep Sea Research Part II: Topical Studies in Oceanography*, *55*, 1636–1647. <https://doi.org/10.1016/j.dsr2.2008.04.019>
- Wilson, S. T., Barone, B., Ascani, F., Bidigare, R. R., Church, M. J., Del Valle, D. A., Dyrman, S. T., Ferrón, S., Fitzsimmons, J. N., Juranek, L. W., Kolber, Z. S., Letelier, R. M., Martínez-García, S., Nicholson, D. P., Richards, K. J., Rii, Y. M., Rouco, M., Viviani, D. A., White, A. E., . . . Karl, D. M. (2015). Short-term variability in euphotic zone biogeochemistry and primary productivity at Station ALOHA: A case study of summer 2012. *Global Biogeochemical Cycles*, *29*(8), 1145–1164. <https://doi.org/10.1002/2015GB005141>
- Wojtal, P. K., Doherty, S. C., Shea, C. H., Popp, B. N., Benitez-Nelson, C. R., Buesseler, K. O., Estapa, M. L., Roca-Martí, M., & Close, H. G. (2023). Deconvolving mechanisms of particle flux attenuation using nitrogen isotope analyses of amino acids. *Limnology and Oceanography*, Ino.12398. <https://doi.org/10.1002/lno.12398>
- Yamaguchi, Y. T., & McCarthy, M. D. (2018). Sources and transformation of dissolved and particulate organic nitrogen in the North Pacific Subtropical Gyre indicated by compound-specific $\delta^{15}\text{N}$ analysis of amino acids. *Geochimica et Cosmochimica Acta*, *220*, 329–347. <https://doi.org/10.1016/j.gca.2017.07.036>

Yanusiewicz, E. A., Wojtal, P. K., Shea, C. H., Benitez-Nelson, C. R., Buesseler, K., Estapa, M., Roca-Mart, M., Popp, B. N., & Close, H. G. (unpublished). *Organic indicators for the alteration of exported phytodetritus during the North Atlantic spring bloom, Part I: Nitrogen isotopic patterns of amino acids.*

Chapter 6

Microscale ecological dynamics of marine bacteria on diatom aggregates

Coauthors: Jeremy E. Schreier, Uria Alcolombri, Roman Stocker, and Victoria Orphan

Abstract

Marine particulate organic matter degradation plays a key role in driving the global carbon cycle, and in turn is largely driven by bacterial communities that assemble on particle surfaces. Understanding the ecophysiological controls on the degradation rates by these communities is critical for understanding and predicting how carbon cycling in the ocean may change in the future. Model bacteria/particle systems have revealed important aspects of some of the mechanisms driving microbial community assembly and function on particles, but these systems have largely employed synthetic polysaccharides as the particle substrates, which are far from the complex reality of marine snow. To test whether some of the principles extrapolated from these systems hold true during microbial degradation of more compositionally complex particles, we investigated the colonization dynamics, spatial structures, and interactions of model marine bacteria on living diatom particles. We find that microcolony formation is a common feature of particle colonization, with potential implications for intraspecific cooperative interactions facilitating degradation of complex substrates. Trophic interactions are additionally prevalent and substantially impact the colonization dynamics and spatial structures of

the individual bacterial species. However, trophic niches on complex substrates appear more flexible and context-dependent compared to those on single polysaccharides. The potential intra- and interspecies interactions we observed likely shape the single-cell metabolic activities of the particle-attached bacteria, which in turn govern bulk particle degradation rates. We will quantify these effects in future work using stable isotope tracing coupled with nanoscale secondary ion mass spectrometry, enabling direct testing of many of the hypotheses generated in this study. Together, this work will expand our insight into the microscale ecological dynamics that govern the rates of carbon turnover in the ocean.

6.1 Introduction

Heterotrophic bacteria drive a substantial fraction of particulate organic matter turnover in the marine environment, thereby exerting a key control on the amount of carbon exported to, and sequestered in, deep sea ecosystems. As such, understanding the principle factors governing the colonization and degradation dynamics of particle-associated bacteria is critical for accurately forecasting future changes to the global carbon cycle. Numerous approaches have been used to interrogate these dynamics, ranging from environmentally relevant investigations of natural particle-attached community compositions (e.g., Fontanez et al., 2015; Li et al., 2023; Mestre et al., 2018; Roth Rosenberg et al., 2021; Valencia et al., 2022) to experimentally tractable investigations of model marine bacteria degrading hydrogel-based or dissolved polysaccharides (e.g., Alcolombri et al., 2021; G. G. D'Souza et al., 2021; Ebrahimi et al., 2019; Enke et al., 2018; Pontrelli et al., 2022).

From these studies, several key observations have emerged, including: (i) particle association is selective and niche-specific (Fontanez et al., 2015; Valencia et al., 2022), (ii) the substrate composition of particles can influence the resulting spatial

structures of attached microbes (G. G. D'Souza et al., 2021; Ebrahimi et al., 2019), and (iii) both inter- and intra-species interactions can significantly shape microbial community structures and bulk particle degradation rates (Ebrahimi et al., 2019; Enke et al., 2018; Pontrelli et al., 2022). Despite the growing body of literature examining the underlying drivers of microbial community structure and function on marine particles, much remains poorly understood, including what ecological factors govern the specificity of particle colonization, as well as whether many of the principles discovered using synthetic polysaccharide particles hold true when particle complexity approaches environmental realism.

Here, we interrogate these dynamics using a model system with well-characterized marine bacterial isolates coupled with living particles comprised of the diatom *Thalassiosira pseudonana*. Diatoms are common constituents of marine snow (Alldredge & Gotschalk, 1990; Thornton, 2002), and their macromolecular compositions are complex (Gügi et al., 2015; Huang et al., 2021; Vidal-Melgosa et al., 2021). We chose bacterial strains that spanned a range of functional potentials with respect to these particle compositions, and investigated how the bacterial functions contribute to their colonization behaviors, spatial structures, and interactions on the diatom aggregates. Each of these aspects can have significant consequences for particle organic carbon degradation. Although we did not measure particle degradation rates in this study, our observations presented in this chapter have informed a number of specific hypotheses that we will test in a future experiment involving stable isotope tracers coupled with nanoscale secondary ion mass spectrometry (nanoSIMS) to interrogate the single-cell activities of bacteria in their spatial contexts on diatom particles, and the overall impacts of bacterial spatial structures and interactions on bulk particle degradation rates. Ultimately, understanding the major ecological drivers of particle degradation at this single-cell level will help us better understand and predict large-scale carbon cycling in the

ocean.

6.2 Materials and methods

6.2.1 Bacterial cultures

Wildtype strains of all marine bacterial species were received from the Cordero lab (Massachusetts Institute of Technology) and were originally isolated from hydrogel polysaccharide particles incubated with natural seawater (Table E.1; Canoe Beach, Nahant, MA, USA; 42°25'11.5" N, 70°54'26.0" W; Datta et al., 2016; Enke et al., 2019). Fluorescently-labeled versions of all strains except for the Flavobacteria were generated via insertion of plasmids containing E2-Crimson or mNeonGreen fluorescent proteins by Drs. Julia Schwartzman (University of Southern California) and Jeremy Schreier (California Institute of Technology). Species were stored in -80°C glycerol stocks and streaked onto Marine Broth 2216 (BD Difco, no. 279110) plates containing 1.5% agar (BD Difco, no. 214010) before use. Individual colonies were selected and grown in liquid Marine Broth 2216 for 48h prior to the start of particle colonization experiments to allow fluorescent proteins to mature sufficiently for visualization. Plasmid selection during growth was performed using spectinomycin (50 $\mu\text{g ml}^{-1}$; Sigma-Aldrich) or chloramphenicol (12.5 $\mu\text{g ml}^{-1}$; Sigma-Aldrich).

6.2.2 Particle colonization experiments

T. pseudonana CCMP1335 was cultured at 18°C under 16h:8h light:dark cycles in L1 medium prepared using artificial seawater (Guillard & Hargraves, 1993). At the start of the particle colonization experiments, 14d-old diatom cultures were

transferred to replicate 5 ml roller tanks. Bacterial cultures pre-grown in Marine Broth 2216 were washed twice with artificial seawater, then inoculated with the diatoms into the roller tanks, which were rotated continuously at 5 rpm (at room temperature) to induce aggregation of the diatom cells into particles (Figure E.1). In all experiments, light/dark cycles were maintained for the first 2d of colonization to simulate initial conditions of particle formation in the surface ocean. Thereafter, lights were turned off and particle colonization proceeded in darkness to more closely approximate conditions of particle sinking and minimize activity of *T. pseudonana*.

In the first set of colonization experiments, eight individual bacterial strains were inoculated at starting densities of 5×10^7 cells ml⁻¹ and allowed to continuously colonize particles for 8d to assess general colonization behaviors. A subset of particles in each roller tank was sampled at different time points (24, 48, 72, 96, and 192h) using a Pasteur pipette and washed twice with artificial seawater to remove unattached cells. Particles were then fixed by overnight incubation at 4°C in artificial seawater containing 4% paraformaldehyde (PFA). Within 24h of fixation, particles were transferred to poly-L-lysine coated microscope slides (Tekdon) glass slides and kept in darkness at room temperature until particles were dry. 15 min prior to imaging, particles were DAPI-stained.

In the second set of colonization experiments, three strains were inoculated as individuals or in pairwise combinations at starting densities of 5×10^6 cells ml⁻¹ (per strain) for more detailed investigation of colonization dynamics. After 42h, one set of roller tanks were set upright to allow particles to sink, and unattached bacterial cells were removed by washing particles twice with L1 medium in order to interrogate bacterial growth on particles without *de novo* attachment. Removal of planktonic cells was visually confirmed by sampling the final supernatant. The other set of roller tanks were not manipulated, thus colonization from both *de novo*

attachment and growth was investigated. Each strain condition (i.e., each unique set of 1–2 bacterial strains in each experiment) was set up in duplicate. A subset of particles in each roller tank was sampled at different time points (24, 40, 66, 86, 120, and 140h) using a Pasteur pipette and fixed by overnight incubation at 4°C in artificial seawater containing 4% PFA. Within 24h of fixation, particles were transferred to 8 µm polycarbonate membrane filters, washed to remove unattached cells, and kept in darkness at room temperature until filters were dry. 15 min prior to imaging, particles were DAPI-stained.

6.2.3 Visualization and image analysis

Particle-attached bacteria from the first set of colonization experiments were imaged using an Olympus BX51 fluorescence microscope equipped with a 6.0-megapixel QImaging Retiga R6 CCD Camera, an X-Cite 120Q lamp, and the following fluorescence filters: TRITC (545/30 nm excitation, 620/60 nm emission, 570 Beam Splitter), FITC (480/40 nm excitation, 535/50 nm emission, 510 Beam Splitter), and DAPI (350/50 nm excitation, 460/50 nm emission, 400 Beam Splitter). Use of the different fluorescence channels enabled visual distinction of fluorescently-labeled/DAPI-stained bacteria and autofluorescent diatom particles. Images were acquired with a 60X 1.42 NA oil immersion objective. At least 10 particles were imaged per time point for each strain condition. For each particle, a single plane was imaged.

Particle-attached bacteria from the second set of colonization experiments were imaged using an Andor Dragonfly spinning disk confocal microscope equipped with a Nikon TI2 body, a 4.2-megapixel Zyla sCMOS camera, an Andor Dragonfly confocal unit, and an Andor Integrated Laser Engine. All images were acquired with a 60X 1.42 NA oil immersion objective. E2-Crimson images were acquired using 561

nm laser excitation and a 594/43 nm emission filter (RFP channel); mNeonGreen images were acquired using 488 nm laser excitation and a 521/38 nm emission filter (GFP channel); DAPI images were acquired with a 405 nm laser excitation and a 445/46 nm emission filter (DAPI channel). Particle autofluorescence was captured in the RFP and GFP channels, as well as in the CY5 channel (637 nm laser excitation with a 698/77 nm emission filter). At least 8 (but typically 10–14) particles were imaged per time point for each strain condition. Each particle was imaged by taking a z-scan at 0.3 μm intervals. Using Fiji, maximum intensity projections for each particle were obtained from all corresponding z-scans. Fluorescent channel subsets that maximized contrast between the bacteria cells and particles were chosen for each strain condition. Image segmentation was performed on maximum intensity projections in Ilastik, and image analysis was performed in Python (custom script developed), whereby the surface areas of individual cells and cell patches (cells of a given strain within 0.5 μm from one another) were quantified in both absolute units of μm^2 and as percentages relative to particle surface areas.

6.2.4 Annotation of CAZymes and sulfatases

The genomes of the bacteria used in this study were sequenced and annotated upon original isolation (Datta et al., 2016; Enke et al., 2019), and were deposited in NCBI databases. The latest versions of complete genomes were downloaded in January 2024. The carbohydrate active enzyme (CAZyme) contents of these genomes were identified in order to gain insight into the potential degradative capabilities of the strains on diatom particles, which are largely comprised of polysaccharides. CAZymes were annotated using a standard dbCAN annotation workflow (Zheng et al., 2023). Briefly, proteins were annotated upon significant alignment

against those in the dbCAN (family level) and dbCAN-sub (subfamily level) hidden Markov model databases using HMMER (e values $<10^{-15}$), and against those in the CAZy database using DIAMOND (e value $<10^{-102}$). Only annotations converged upon by more than one tool were kept. Substrates were predicted at the CAZyme subfamily level using enzyme Classification And Motif Identification (eCAMI), and are based on proteins that have been experimentally characterized.

All proteins were additionally blasted against a database of classified sulfatases (<https://sulfatlas.sb-roscoff.fr>, version 2.3.1) using an e -value cutoff of 10^{-10} (Stam et al., 2023).

6.2.5 Antagonism assay

Chemical antagonism between pairs of pseud3D05, marib6B07, and phaeoC3M10 was assessed via two different agar plate assays. In the first, pairs of strains were cross-streaked, and evidence for colony clearing at the point of intersection was examined. In the second, each strain was grown in two large, discrete colonies on base agar plates, and slush agar containing a well-mixed culture of each strain (one strain per slush agar mix) was gently poured over the base agar plate. Signs of colony clearing were again assessed for evidence of chemical antagonism. Assays were performed in duplicate. All regular and base agar plates contained Marine Broth 2216 and 1.5% agar. The slush agar was made of Marine Broth 2216 and 0.7% agar.

6.3 Results and discussion

6.3.1 Particle colonization is not solely driven by metabolic capability

The taxonomic composition of particle-attached microbial assemblages is often distinct from that of free-living communities (e.g., Crespo et al., 2013; DeLong et al., 1993; Ghiglione et al., 2009; Roth Rosenberg et al., 2021; Valencia et al., 2022), suggesting that a particle-associated lifestyle is a selective trait among marine bacteria. Members of Alteromonadales (including *Pseudoalteromonas* and *Alteromonas*), Flavobacteriales, Vibrionales, and Rhodobacterales (particularly Roseobacters) are commonly enriched in particle-attached communities (Church et al., 2021; Fontanez et al., 2015; LeCleir et al., 2014; Mestre et al., 2018; Valencia et al., 2022), owing, in part, to (i) their ability to grow rapidly and (ii) their frequent association with surfaces of, and utilization of carbon from, phytoplankton and other eukaryotic marine snow constituents. Moreover, natural marine snow is comprised of a complex mixture of phytoplankton cells, heterotrophic microbes, and detritus (including from copepod carcasses and fecal pellets), and the abundances of the individual constituents can vary widely depending on environmental locality and ecological dynamics (Alldredge & Gotschalk, 1990). This variation in composition can further shape the composition of particle-attached communities due to niche-specific adaptations of individual members (e.g., Pelve et al., 2017). Here, we investigated the extent to which metabolic potential alone drives microbial colonization of particles comprised of living diatoms. We used eight marine bacterial species previously isolated from polysaccharide particles (Table E.1; Datta et al., 2016; Enke et al., 2019). These included two representatives of Alteromonadales (*Pseudoalteromonas* sp. 3D05 and *Alteromonas* sp. C1M14)

and two representatives of Vibrionales (*Vibrio* sp. 1A01 and *Vibrio* sp. C3R12) within the Gammaproteobacteria class, two members of Flavobacteria within the Bacteroidia class (*Maribacter* sp. 6B07 and *Zobellia* sp. A2M03), and two members of the Roseobacter clade belonging to the order Rhodobacterales within the Alphaproteobacteria class (*Phaeobacter* sp. C3M10 and *Ruegeria* sp. A3M17). Hereafter, these strains will be referred to as the concatenated name of their abbreviated genus and strain designation—e.g., *Pseudoalteromonas* sp. 3D05 is "pseud3D05".

Despite the fact that the diatoms in our system are living, our overarching hypothesis was that the particles would behave as abiotic substrates, thus bacterial colonization would be exclusively driven by the potential degradation abilities of the strains with respect to the particle compositions. Diatom-sourced particles are largely comprised of polysaccharides (e.g., Gügi et al., 2015; Huang et al., 2021), which are depolymerized by CAZymes that are specific to not only the type of polysaccharide, but also the specific linkages within the polysaccharide backbone. Thus, knowledge of the diversity of glycosidic linkages encompassed within diatom particles is critical to inform genomic predictions about the potential degradation abilities of the associated bacteria. The polysaccharide composition of diatom particles is poorly characterized (contrasting sharply with our significantly better characterizations of macroalgal polysaccharides; Kloareg and Quatrano, 1988); nevertheless, several important constituents have been elucidated (reviewed by Gügi et al., 2015). Laminarin (i.e., β -1,3- and β -1,6-linked chain of glucose monomers) is the major carbon storage polymer in diatoms (Chiovitti et al., 2004; Myklestad, 1974; Waterkeyn & Bienfait, 1987) and is additionally released as an exometabolite, which has been shown to stimulate bacterial heterotrophy (Ferrer-González et al., 2021; Olofsson et al., 2022). *T. pseudonana* produces β -chitin as both extracellular fibrils and components of its silica frustule

(Frischkorn et al., 2013; Tesson et al., 2008). β -chitin fibers exhibit distinct chain packing from that of α -chitin in crustaceans, but both are degradable by the same chitinases (Kaya et al., 2017). Additional polysaccharides that have been identified in diatom particles, including those of *Thalassiosira* spp., are β -1,4-mannan, β -1,4-xylan, xyloglucan, alginate, and fucose-containing sulfated polysaccharides (FCSP; Huang et al., 2021; Vidal-Melgosa et al., 2021). The bacterial strains we chose exhibited a large diversity in their CAZyme repertoires, with large differences in both number and type of CAZymes encoded in each of the strains' genomes (Figures 6.1, E.3, and E.4), and all have demonstrated particle attachment capabilities given their isolation on synthetic polysaccharide particles. We specifically hypothesized that in bacterial monocultures with diatom particles, the two Roseobacters would colonize particles the least strongly due to their limited CAZyme repertoire, while the other six strains would colonize particles strongly.

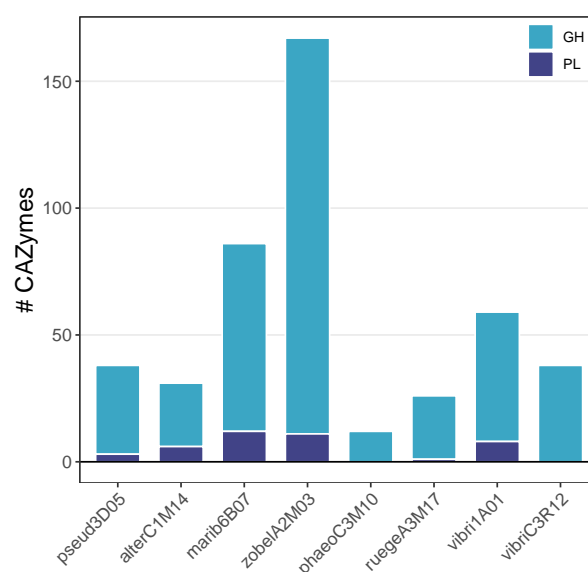


Figure 6.1. Number of CAZymes belonging to the glycoside hydrolase (GH; light blue) and polysaccharide lyase (PL; dark blue) families in each strain. The counts include both unique CAZyme homologues (e.g., porphyran-targeting GH16_e61 and agarose-targeting GH16_e249), as well as multiple copies of the same homologue.

To investigate the colonization behaviors of our bacterial strains, we inoculated

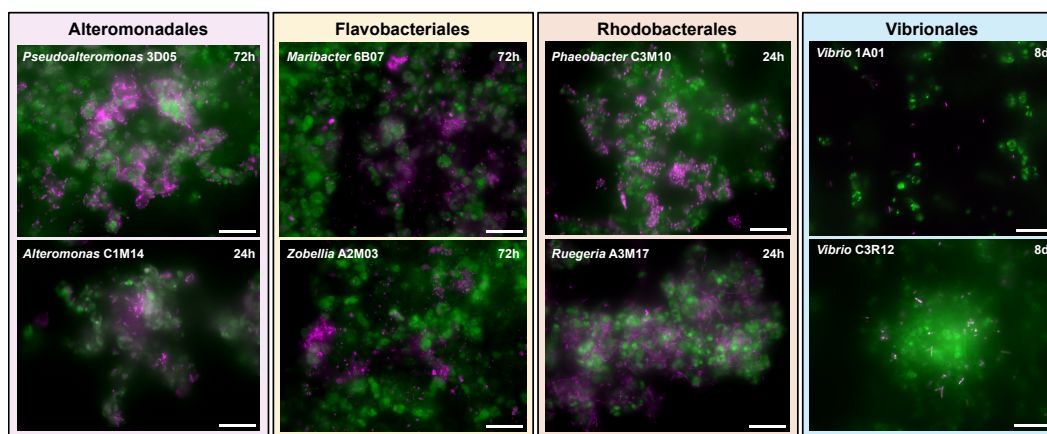


Figure 6.2. Fluorescence micrographs of diatom particles (green) with different marine bacterial strains (pink) after up to 8d of continuous colonization. Representative images highlighting time points when particle colonization and microcolony formation first became pronounced are displayed for species within Alteromonadales, Flavobacteriales, and Rhodobacterales. Neither *Vibrio* species strongly colonized the diatom aggregates. Scale bars, 20 μm .

each strain individually with *T. pseudonana* in roller tanks (which facilitate phytoplankton aggregation; Shanks and Edmondson, 1989) and allowed the bacteria to continuously colonize the diatom aggregates over eight days. Counter to our hypothesis, phaeoC3M10 and ruegeA3M17 colonized particles quickly and prolifically, forming dense clusters of cells throughout the aggregates within the first 24h of colonization (Figure 6.2). Pseud3D05, alterC1M14, marib6B07, and zobela2M03 strongly colonized the particles and formed visible microcolonies within the first three days of the experiment (consistent with our predictions); however, the two *Vibrio* strains were poor colonizers, as they either did not attach to the particles, even after eight days (vibri1A01) or colonized the particles weakly relative to the other strains (vibriC3R12). Lack of any particle colonization by vibri1A01 was particularly surprising, as prior studies have demonstrated that this strain can grow on laminarin and chitin (Datta et al., 2016; Enke et al., 2018; Gralka et al., 2023; Pontrelli et al., 2022), and encodes a diverse suite of CAZymes (including alginate lyases for alginate degradation; Figure E.4). This suggests that either

there are key substrates in the diatom particles that the *Vibrios* are unable to degrade and which we are overlooking, or that colonization is influenced by the interaction between multiple factors beyond metabolic potential alone. This latter possibility is consistent with conclusions by Datta et al. (2016) and Enke et al. (2018) that chemotaxis and bacteria-particle interactions are additionally important drivers of particle colonization. The particles used in our study are not only complex in their compositions, but the living nature of the diatoms undoubtedly adds an additional algal/bacterial interaction dynamic that likely contributes to the resulting colonization dynamics observed. In nature, Roseobacters, Flavobacteria, and Gammaproteobacteria (particularly members of Alteromonadales) are among the clades most commonly associated with phytoplankton (Buchan et al., 2014), and in particular with diatoms (Amin et al., 2012; Grossart et al., 2005; Kaczmarska et al., 2005; Rooney-Varga et al., 2005; Sapp, Schwaderer, et al., 2007; Sapp, Wichels, & Gerdts, 2007; Sapp, Wichels, Wiltshire, & Gerdts, 2007; Teeling et al., 2012, 2016). Although bacteria/algal associations have also been documented for different *Vibrio* spp. (Frischkorn et al., 2013; Rao et al., 2007), interactions and ecological niches can be species- and strain-specific (e.g., Pelve et al., 2017). As such, lack of particle colonization by the two *Vibrio* strains in our study may be related to niche specificity for other host surfaces, such as those of copepods (Sampaio et al., 2022; Takemura et al., 2014), or specific interactions between *T. pseudonana* and our *Vibrio* strains that mitigate strong colonization. If true, our null model of the diatom particles behaving as abiotic polysaccharide particles to the bacteria is not correct, suggesting these complex dynamics are shaped by factors along multiple physical and ecological axes.

6.3.2 Microcolony formation is a consistent feature accompanying strong particle colonization

We chose three strains (pseud3D05, marib6B07, and phaeoC3M10) to further investigate bacterial spatial structures that develop during particle colonization, as well as to quantitatively interrogate how different bacteria/bacteria interactions shape the overall colonization dynamics. These ecological aspects can each exert significant influence on bulk community-level particle degradation rates, as demonstrated by Ebrahimi et al. (2019), Enke et al. (2018), and Nguyen et al. (2022). From our qualitative and quantitative observations here, we develop specific hypotheses regarding impacts of these dynamics on cell-specific particle degradation rates, which will be tested in our future nanoSIMS experiment (presented in the Introduction). Our three focal strains were chosen for their strong colonization behaviors observed during our initial screening (Figure 6.2), as well as for their diverse metabolic capabilities (both predicted and characterized; with CAZyme repertoires summarized in Figure 6.3, and other important metabolic traits summarized in Table 6.1). Given their metabolic repertoires, we predicted that these strains would fulfill distinct trophic niches on aggregates of *T. pseudonana*. Below, we discuss these traits and interpret the strains' individual spatial colonization dynamics through this metabolic lens. In Section 6.3.3, we examine the potential interactions that occurred when the strains colonized the particles in co-culture.

Consistent with the common trophic niche of Alteromonadales and Flavobacteriales members as algal organic matter specialists (Arandia-Gorostidi et al., 2022; Buchan et al., 2014; B. Francis et al., 2021; T. B. Francis et al., 2021; Krüger et al., 2019; Teeling et al., 2012; Vidal-Melgosa et al., 2021), both pseud3D05 and marib6B07 encode a diverse array of CAZymes in their genomes (Figure 6.3), as well as TonB-dependent receptors (TBDR), which facilitate the uptake of

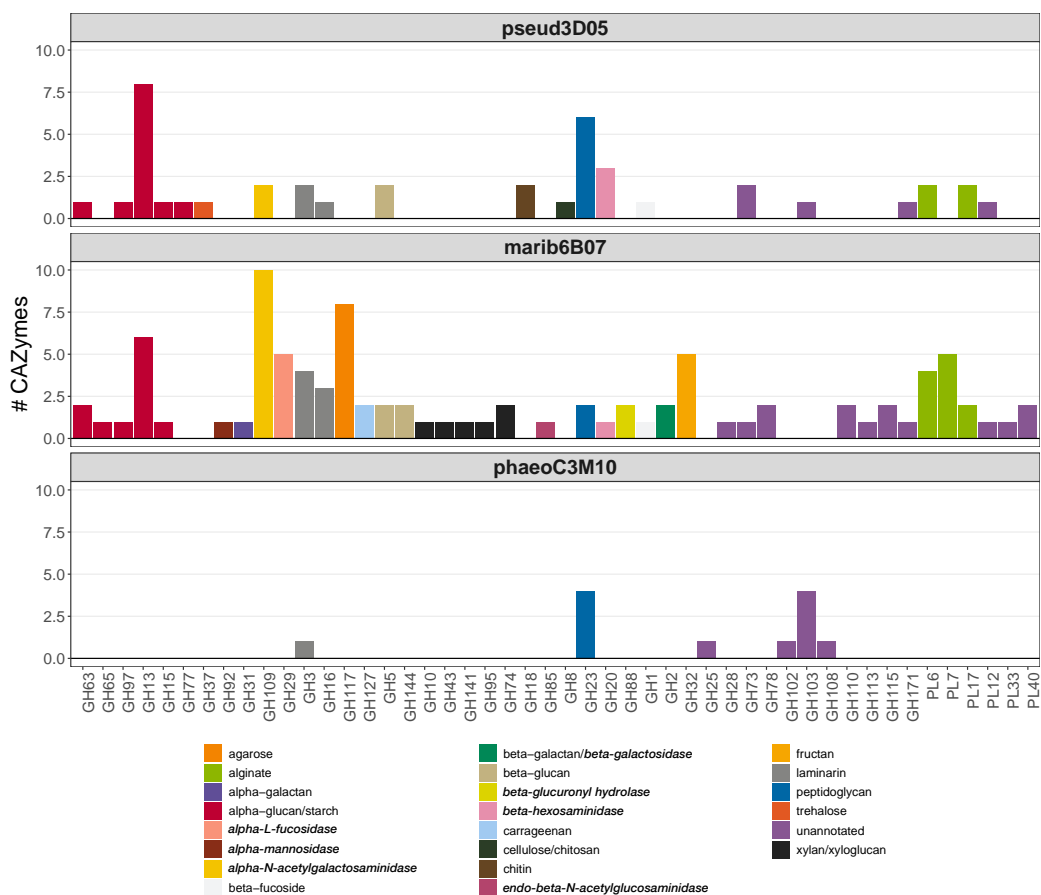


Figure 6.3. GH and PL repertoire of select strains examined in this study. Bar heights represent the number and copy of unique homologues belonging to each CAZyme family, and are colored based on the target substrate(s) of homologues within the family. In cases where the target substrate has not been experimentally characterized, the name of the CAZyme is included instead (denoted in *italics*). Those in which neither the enzyme nor the target substrate has been characterized are represented in purple as unannotated.

high molecular weight compounds (Noinaj et al., 2010). Moreover, many diatom polysaccharide backbones are decorated with sulfate groups (Gügi et al., 2015), necessitating bacterial expression of sulfatases to remove the sulfate esters before the rest of the backbone can be accessed by exo- and endo-acting CAZymes. The genomes of pseud3D05 and marib6B07 encode a variety of sulfatases, some of which may facilitate degradation of *T. pseudonana* polysaccharides (although the substrate specificities of the sulfatases were not characterized in detail here).

Table 6.1. Genomic content, physiological information, and predicted trophic functions of focal bacterial strains.

| | pseud3D05 | marib6B07 | phaeoC3M10 |
|--|---------------------------|------------------|--------------------------------|
| Predicted trophic niche | primary degrader | primary degrader | cross-feeder |
| Potential metabolic preference | peptides, polysaccharides | polysaccharides | small molecules, organic acids |
| Large polymer uptake (TBDR) ^a | 57 | 41 | 3 |
| Small molecule uptake (ABC, TRAP) ^a | 59 | 42 | 215 |
| Sulfatases | yes | yes | yes |
| Proteases ^a | 44 | 27 | 24 |
| Sugar/acid preference ^b | -0.09 | 0.82 | N/A |

^a Numbers given for TBDRs, ABC and TRAP transporters, and proteases include all annotated proteins encoded in the genomes.

^b Sugar/acid preferences were determined by Gralka et al. (2023) for pseud3D05 and marib6B07, and quantify the degree to which each strain is able to consume more sugars than organic acids (or vice versa), with the scale ranging from +1 (for extreme sugar specialists) to -1 (for extreme acid specialists).

Taken together, pseud3D05 and marib6B07 appear well poised to depolymerize, uptake, and grow on the variety of complex *T. pseudonana* polysaccharides and, thus, may generally serve as primary polysaccharide degraders on these particles. Diatom cells are additionally comprised of protein (Gügi et al., 2015). In addition to its polysaccharide-degrading potential, pseud3D05 possesses a diverse set of proteases and has demonstrated a slight growth preference for organic acids over sugars (Table 6.1; Gralka et al., 2023), so may serve an equally or more prominent role as a primary protein degrader. This is consistent with the known ecological role of *Pseudoalteromonas* spp. as abundant protease producers (Chen et al., 2020), and would render the trophic niche of pseud3D05 potentially distinct from that of marib6B07. Nevertheless, we generalize the predicted trophic niches of pseud3D05 and marib6B07 here as primary degraders. In contrast, phaeoC3M10 encodes relatively few CAZymes and only two TBDRs (both of which are anno-

tated for siderophore transport; Figure 6.3; Table 6.1), but a significantly larger and more diverse array of transporters within the ATP-binding cassette (ABC) and tripartite ATP-independent periplasmic (TRAP) families. These transporters are specific for low molecular weight compounds such as free amino acids, sugars, and monocarboxylic or dicarboxylic acids. As such, we predicted that phaeoC3M10 preferentially utilizes small metabolites released by the diatoms over polysaccharides that require depolymerization. This trophic prediction is consistent with prior characterizations of phaeoC3M10 as a cross-feeder in other polysaccharide-degrading communities (Enke et al., 2019), and with general characterizations of Roseobacters as low molecular weight algal organic matter specialists (Buchan et al., 2014).

We first investigated whether each bacterial strain could grow on *T. pseudonana* particles when alone in monoculture. We seeded the particles by allowing each bacterial strain to colonize the particles for 42h, then washed unattached bacterial cells and tracked changes in the residual bacterial biomass over time by subsampling and imaging particles every ~24h. During the 98h following washing, we observed an increase in the relative biomass of pseud3D05 and phaeoC3M10 on particles over time (Figure E.5), suggesting the bacteria were indeed growing on the diatom particles. Biomass increase was visually confirmed for marib6B07, but was not quantified here.

After confirming that each strain could likely grow on the diatom particles, we next interrogated the spatial colonization dynamics of the individual strains to assess whether the resulting spatial structures might be correlated with their potential trophic functions on the particles. Over the course of 140h of continuous colonization, each strain became numerically abundant on particles and formed spatially structured microcolonies that increased in size over time (Figures 6.4, 6.5, and E.6). Here, microcolonies are defined as all cells of a given strain situated within

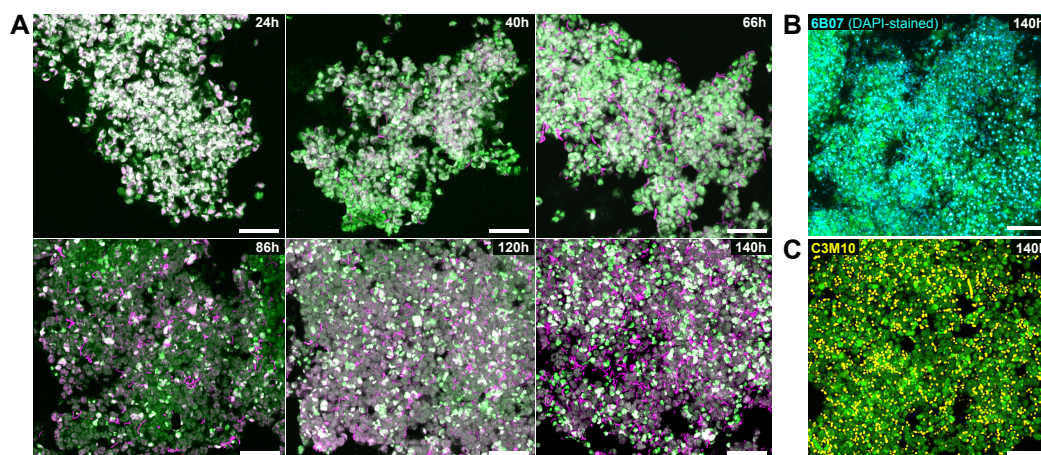


Figure 6.4. Dynamics of bacterial strains on *T. pseudonana* aggregates over 140h of continuous colonization. **(A)** Fluorescent micrographs of colonization time series of pseud3D05. Images were acquired with the RFP channel (which targets E2-Crimson in pseud3D05 and autofluorescence of diatom cells) and the GFP channel (which only captures diatom cell autofluorescence). **(B)** Endpoint micrograph of marib6B07 on particles. Images were acquired with the DAPI channel (cyan; targeting DAPI-stained marib6B07 and diatom cells) and RFP channel (green; targeting diatom autofluorescence alone). **(C)** Endpoint micrograph of phaeoC3M10 on particles. Images were acquired with the GFP channel (yellow; targeting mNeonGreen in phaeoC3M10 and diatom autofluorescence) and RFP channel (green; targeting diatom autofluorescence alone). Scale bars, 20 μm .

0.5 μm from one another—a conservative estimate for an interaction length scale, which can be up to the order of a few cell lengths (Dal Co et al., 2020). Clonal microcolonies can arise from division of single progenitor cells growing on surfaces (e.g., G. G. D'Souza et al., 2021; Nadell et al., 2016), which can be triggered by the presence of complex nutrients that cue cells to remain aggregated (as opposed to dispersing) following division (G. G. D'Souza et al., 2021). Alternatively, microcolonies can form through secondary aggregation of planktonic cells—either via direct attachment of pre-formed bacterial aggregates to particles, or via attachment/detachment dynamics that concentrate bacteria into localized regions on particles. Microcolony formation can be an advantageous growth strategy for bacteria that broadcast extracellular enzymes to degrade complex polymers, as

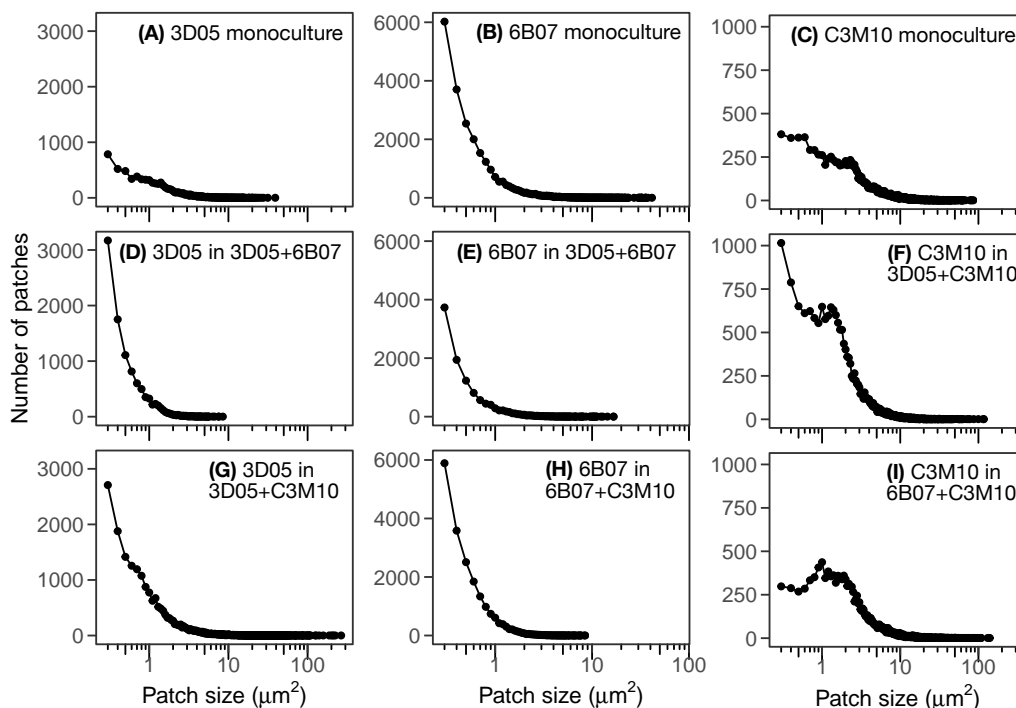


Figure 6.5. Distribution of cell patches of individual strains from mono- and co-cultures on *T. pseudonana* aggregates after 140h of continuous colonization. A cell patch is defined as all cells of a given strain within 0.5 μm from one another, and include isolated single cells. Distributions were compiled using data from 10 randomly sampled particles to facilitate comparisons across experiments.

the localized concentration of cells enables them to benefit from the hydrolytic activities of their immediate neighbors, in turn enabling the collective to grow and degrade polymers more quickly (Dal Co et al., 2020; Drescher et al., 2014; G. G. D'Souza et al., 2021; Ebrahimi et al., 2019; Momeni et al., 2013). As such, it was initially surprising to observe prominent microcolony formation by the putative cross-feeder phaeoC3M10, which we predicted was not growing on *T. pseudonana* particles via degradation of surface-associated polymers. However, in separate experiments, we observed strong aggregation of phaeoC3M10 growing planktonically in spent medium of *T. pseudonana* (in contrast to minimal aggregation of pseud3D05 and marib6B07), indicating aggregation of phaeoC3M10 is not necessarily driven by surface-associated polysaccharide degradation. Indeed,

phaeoC3M10 may subsist off the low molecular weight organics released by *T. pseudonana*, and its aggregation behavior may not be linked to this carbon acquisition strategy. Alternatively, it is possible that phaeoC3M10 is broadcasting enzymes to degrade the particle-associated polymers, as this strain does possess some CAZymes and several proteases (Figure 6.3; Table 6.1), and prior studies have demonstrated that some *Roseobacter* strains can serve as important phytoplankton biopolymer degraders (Christie-Oleza et al., 2015). Moreover, G. D'Souza, Ebrahimi, et al. (2023) demonstrated that the extent to which bacteria aggregate varies inversely with exo-enzyme secretion strength (i.e., low secretors formed larger clusters, and vice versa)—presumably a compensation mechanism for cells to achieve maximal growth rates amidst variations in secretion capabilities. Indeed, phaeoC3M10 formed larger microcolonies than either pseud3D05 or marib6B07 (Figures 6.5A–C), consistent with the possibility that phaeoC3M10 may secrete exo-enzymes, but that the number of unique exo-enzymes secreted and/or the cell-specific rate of enzyme secretion may be lower compared to those of the putative degraders. Microcolony formation may alternatively be mediated by the exchange of resources other than carbon degradation products (e.g., siderophores; Julou et al., 2013). Understanding which mechanism and associated ecological cues are driving microcolony formation here can provide insight into how bacteria sense, respond to, and degrade complex organic matter, and will be specifically tested through our future nanoSIMS work (i.e., by interrogating the spatial distributions of single-cell activities within each microcolony). Alternatively, visual tracking of particle colonization and spatial structure development via microfluidics (following the approach of G. G. D'Souza et al., 2021) could help elucidate the mechanisms driving microcolony formation of each strain.

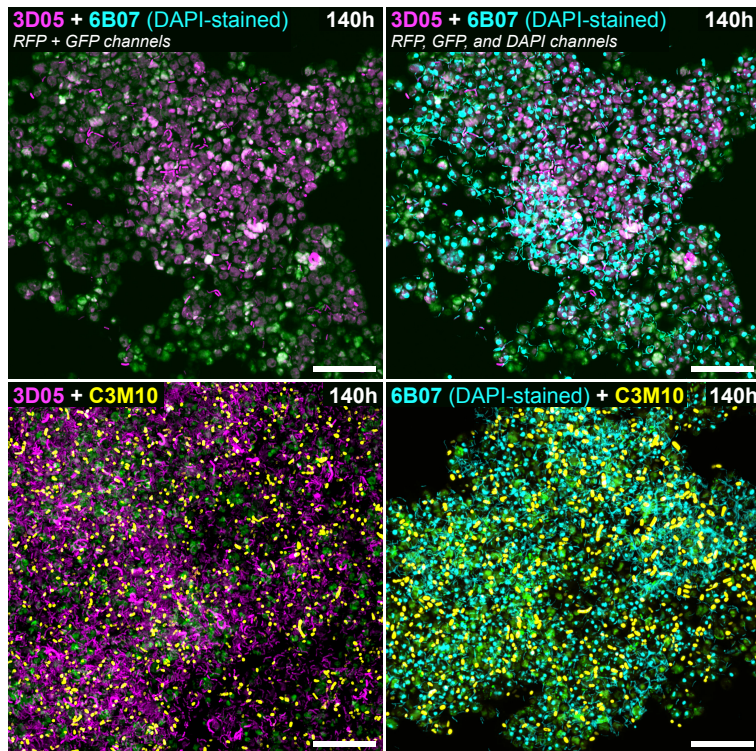


Figure 6.6. Fluorescent micrographs of pairwise combinations of strains on *T. pseudonana* aggregates after 140h of continuous colonization. The top two images correspond to the same particle containing pseud3D05 + marib6B07 but are shown with two different combinations of fluorescent channel overlays to ease visualization of pseud3D05. The bottom two images correspond to particles containing pseud3D05 + phaeoC3M10, and marib6B07 + phaeoC3M10, respectively. Images were acquired using a combination of CY5, RFP, GFP, and DAPI channels, with the following channel overlays: **(top left)** for pseud3D05 + marib6B07, the RFP channel (pink; targeting E2-Crimson in pseud3D05 and diatom autofluorescence) and GFP channel (green; targeting diatom autofluorescence alone) and **(top right)** additionally the DAPI channel (cyan; targeting all DAPI-stained bacteria and diatom cells); **(bottom left)** for pseud3D05 + phaeoC3M10, the RFP channel (pink; targeting E2-Crimson in pseud3D05 and diatom autofluorescence), GFP channel (yellow; targeting mNeonGreen in phaeoC3M10 and diatom autofluorescence), and CY5 channel (green; targeting diatom autofluorescence alone); **(bottom right)** for marib6B07 + phaeoC3M10, the DAPI channel (cyan; targeting DAPI-stained bacteria and diatom cells), GFP channel (yellow; targeting mNeonGreen in phaeoC3M10 and diatom autofluorescence), and CY5 channel (green; targeting diatom autofluorescence alone). Scale bars, 20 μm .

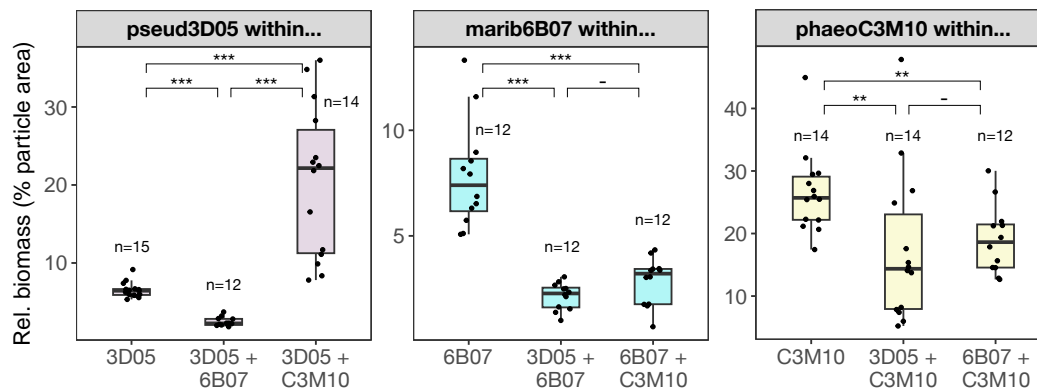


Figure 6.7. Relative bacterial cell biomass on *T. pseudonana* aggregates after 140h of continuous colonization by individual or pairs of strains. Bacterial abundances are quantified as the percent of particle surface area occupied by the biomass of each strain. Each panel title denotes the strain whose quantified biomass is represented in the barplots within that panel. The x-axis labels denote the strain(s) added to the aggregates. The number of particles imaged in each strain condition is shown above each barplot. Significant differences in relative abundance distributions for a given strain between pairs of strain conditions were assessed using the non-parametric Mann-Whitney U test. Asterisks denote statistically significant differences in distributions, with p-values < 0.001 (***), 0.001 < p-value < 0.01 (**), 0.01 < p-value < 0.05 (*), and p-value > 0.05 (-).

6.3.3 Bacteria/bacteria interactions significantly shape particle colonization dynamics

We next investigated whether interactions between the bacteria alter their individual colonization dynamics. We predicted that the two primary degraders, pseud3D05 and marib6B07, would each negatively impact colonization by the other due to competition fueled by their largely overlapping trophic niches (Figure 6.3; Table 6.1). We further predicted that the putative cross-feeder phaeoC3M10 would benefit from the labor of each primary degrader (resulting in higher yields of phaeoC3M10 in co-culture relative to monocultures) at the expense of each primary degrader's yield. This latter hypothesis was formulated based on prior observations of this degrader/cross-feeder dynamic in spatially structured environ-

ments with synthetic polysaccharides (G. D'Souza, Schwartzman, et al., 2023; Enke et al., 2018).

Consistent with our first hypothesis, the final biomass of pseud3D05 and marib6B07 was each significantly reduced when the two degraders colonized particles in co-culture compared to their monoculture dynamics (Figures 6.6 and 6.7). Moreover, their maximum microcolony sizes decreased in co-culture, and the distribution of pseud3D05 clusters shifted toward many more smaller microcolonies and single cells (Figures 6.5A versus D, and B versus E). A negative effect of marib6B07 on colonization and degradation by pseud3D05 has been previously observed in a chitin particle system (Enke et al., 2018)—although marib6B07 served as a secondary consumer in this context—and was interpreted as a function of competition for space rather than due to chemical antagonism. Similarly, in our study, no evidence of antagonistic interactions was observed in agar plate assays designed to detect secreted inhibitory factors. However, it is possible that these strains secrete antibiotics when competing in a diatom particle environment where resources (space and nutrients) are heterogeneous and limited. Our future nanoSIMS work will enable us to quantify the length scale of this interaction with respect to the single-cell activities of each degrader for insight into how these spatial interactions shape larger-scale particulate organic matter degradation rates.

We next investigated the interaction between the putative degrader pseud3D05 and cross-feeder phaeoC3M10. Counter to our second hypothesis, the presence of phaeoC3M10 significantly enhanced the final yields of pseud3D05 (Figures 6.6 and 6.7), as well as both its maximum microcolony size and number of smaller microcolonies that developed (Figures 6.5A versus G). We hypothesize that this positive interaction is driven by phaeoC3M10's drawdown of polymer degradation products or metabolic intermediates released by pseud3D05, which can otherwise accumulate to high concentrations and thermodynamically inhibit degradation.

The enhanced growth of pseud3D05 suggests particle degradation was also enhanced; this will be directly tested in our future nanoSIMS work. However, this potential cross-feeding interaction did not increase the final yield of phaeoC3M10; rather, its final yield was lower in co-culture compared to monoculture (Figure 6.7; with additionally significant impacts on its distribution of microcolony sizes; Figure 6.5C versus F), contrasting with prior studies that have shown a beneficial impact of degrader/cross-feeder interactions on the cross-feeder (G. D'Souza, Schwartzman, et al., 2023; Enke et al., 2018). It is possible that the growth rate of phaeoC3M0 in co-culture is limited by the type or rate of product release by pseud3D05—e.g., pseud3D05 may be depolymerizing and using multiple complex substrates with a high amount of total carbon release, but the concentration of individual metabolites that phaeoC3M10 can uptake could be relatively low. Nevertheless, cross-feeding may still be a beneficial strategy for phaeoC3M10 to conserve energy and resources by not producing exo-enzymes (Huelsmann et al., 2024). An additional possible explanation for its reduced growth in co-culture is that in monoculture, phaeoC3M10 may primarily subsist on exudates released by *T. pseudonana*, but the presence of pseud3D05 could reduce this exudate release either via direct consumption of the exudates, or via a negative interaction between *T. pseudonana* and pseud3D05. Our future nanoSIMS work will enable us to directly quantify the effects of this interaction on each species' single-cell activities, the resulting consequences on community-level particle degradation rates. Moreover, whether the mechanism benefiting pseud3D05 is indeed linked to removal of its degradation/metabolic products can be directly tested in a flow regime with monoculture of pseud3D05 on particles (e.g., Alcolombri et al., 2021).

Given the observed degrader/cross-feeder interaction for pseud3D05 + phaeoC3M10, we hypothesized that in co-culture, marib6B07 would gain a growth benefit from the activity of phaeoC3M10, but the latter might again exhibit lower final yields.

Interestingly, counter to this hypothesis, the final yields and maximum microcolony size of marib6B07 were significantly reduced in the presence of phaeoC3M10, suggesting a different interaction dynamic than observed for pseud3D05 + phaeoC3M10 (Figures 6.6, 6.7, and 6.5B versus H). A possible explanation for this difference is that marib6B07 may primarily degrade polysaccharides through a "selfish uptake mechanism" (rather than through exo-enzyme secretion) in which polysaccharides are bound to the outer membrane and hydrolyzed to larger oligosaccharides that are directly transported into the periplasm for further depolymerization (Cuskin et al., 2015; Reintjes et al., 2017). This strategy appears to be specific to members of Bacteroidetes, and relies on the unique functional coupling of SusD-like TBDRs to SusC-like TonB-dependent porins (Sonnenburg et al., 2010). Through this mode of degradation, marib6B07 would not release oligosaccharide products, which would reduce the growth benefit marib6B07 would gain from phaeoC3M10's drawdown of these products. Although phaeoC3M10 could still be cross-feeding on metabolic intermediates released by marib6B07, the overall metabolic coupling between these two strains would be lower than that between pseud3D05 and phaeoC3M10. In future work, the mode of carbon degradation by marib6B07 can be verified through the use of fluorescently-labeled polysaccharides to trace direct uptake of oligosaccharides (Reintjes et al., 2017) and through enzyme broadcasting assays to investigate the extent of exo-enzyme secretion (e.g., Datta et al., 2016). As in the case of pseud3D05 + phaeoC3M10 co-cultures, final yields of phaeoC3M10 were reduced in the presence of marib6B07 (Figure 6.7). Whether the yields of any of these strains are modulated by product release from the particles can be interrogated by adding various exo-enzymes in different concentrations to particles with bacteria monocultures and assessing whether the bacteria yields are proportionally stimulated. Finally, it is possible that all the potential trophic interactions discussed here are not mediated by carbon, but an alternative nutrient.

Our future nanoSIMS work will additionally capture trophic dynamics involving nitrogen and sulfur, in addition to carbon.

6.4 Conclusion

Substantial insight about the drivers of microbial community assembly and function on particles has been gained from model systems involving bacteria and synthetic polysaccharide particles. Whether many of the extrapolated fundamental principles apply to microbial degradation of more compositionally complex particles is an open question. Here, we have shown using a model diatom particle system that some of these principles do indeed hold true. In particular, microcolony formation (and potentially intraspecific cooperative interactions) appears to be a common property of growth on complex particle substrates. Trophic interactions appear to be prevalent and substantially impact the colonization dynamics and spatial structures of taxa within different trophic niches; however, on complex substrates, trophic niches are not as narrowly-defined as they are on single polysaccharides, and may vary depending on the context of other community member functions (e.g., phaeoC3M10 may switch between modes of (an inefficient) degrader versus scavenger depending on its mono- or co-culture context). Context dependencies appear to underlie many of the interactions here: e.g., degrader/cross-feeder interactions may depend on the mode of carbon acquisition of the degrader, or other trophic or interspecific dynamics. In our experiments, strain pairs were simultaneously inoculated with particles, but the order of colonization may further mediate the types of interactions that occur (Grossart et al., 2003). Moreover, we largely ignored the role that *T. pseudonana* played in mediating the observed colonization dynamics, but this aspect is undoubtedly important and should be the focus of future investigations of this type of model bacteria/particle system.

Our future nanoSIMS work will enable us to directly test whether the single-cell metabolic activities of particle-attached bacteria are shaped by the different intra- and interspecies interactions observed in our system. Variations in these single-cell activities can scale up to emergent community-level properties with profound consequences for particle degradation and global carbon cycling (Nguyen et al., 2022). As such, future studies should continue to investigate these dynamics using complex particles approaching environmental realism, with particular aspiration toward extracting generalizable principles—to the extent possible—about the primary ecophysiological factors that govern community-level POM degradation rates.

Acknowledgments

We would like to acknowledge Julia Schwartzman for tremendously helpful discussions throughout this project, as well as provision of many of the fluorescent bacterial strains used; Andreas Sichert and Ella Case for analysis of the mono- and polysaccharide compositions of our diatom particles; Marshall Yale and Gabriel Vercelli for assistance with development of the image analysis pipeline; Nate Glasser, Georgia Squyres, and the Caltech EBEF Facility for confocal microscopy use and assistance; Rob Lampe and the Allen lab (Scripps Institution of Oceanography) for diatom culture provision and guidance; and members of the Cordero lab (Massachusetts Institute of Technology) for provision of the marine bacterial isolate collection. Additionally, we are grateful to all members of the Simons PriME (Principles of Microbial Ecosystems) collaboration for helpful discussions, and to the Simons Foundation for funding this work. I am additionally grateful to the Caltech CEMI program for conference travel support to share my work.

References

- Alcolombri, U., Peaudecerf, F. J., Fernandez, V. I., Behrendt, L., Lee, K. S., & Stocker, R. (2021). Sinking enhances the degradation of organic particles by marine bacteria. *Nature Geoscience*, *14*(10), 775–780. <https://doi.org/10.1038/s41561-021-00817-x>
- Allredge, A. L., & Gotschalk, C. C. (1990). The relative contribution of marine snow of different origins to biological processes in coastal waters. *Continental Shelf Research*, *10*(1), 41–58. [https://doi.org/10.1016/0278-4343\(90\)90034-J](https://doi.org/10.1016/0278-4343(90)90034-J)
- Amin, S. A., Parker, M. S., & Armbrust, E. V. (2012). Interactions between Diatoms and Bacteria. *Microbiology and Molecular Biology Reviews*, *76*(3), 667–684. <https://doi.org/10.1128/MMBR.00007-12>
- Arandia-Gorostidi, N., Berthelot, H., Calabrese, F., Stryhanyuk, H., Klawonn, I., Iversen, M., Nahar, N., Grossart, H.-P., Ploug, H., & Musat, N. (2022). Efficient carbon and nitrogen transfer from marine diatom aggregates to colonizing bacterial groups. *Scientific Reports*, *12*(1), 14949. <https://doi.org/10.1038/s41598-022-18915-0>
- Buchan, A., LeClerc, G. R., Gulvik, C. A., & González, J. M. (2014). Master recyclers: Features and functions of bacteria associated with phytoplankton blooms. *Nature Reviews Microbiology*, *12*(10), 686–698. <https://doi.org/10.1038/nrmicro3326>
- Chen, X.-L., Wang, Y., Wang, P., & Zhang, Y.-Z. (2020). Proteases from the marine bacteria in the genus *Pseudoalteromonas*: Diversity, characteristics, ecological roles, and application potentials. *Marine Life Science & Technology*, *2*(4), 309–323. <https://doi.org/10.1007/s42995-020-00058-8>
- Chiovitti, A., Molino, P., Crawford, S. A., Teng, R., Spurck, T., & Wetherbee, R. (2004). The glucans extracted with warm water from diatoms are mainly derived from intracellular chrysolaminaran and not extracellular polysaccharides. *European Journal of Phycology*, *39*(2), 117–128. <https://doi.org/10.1080/0967026042000201885>
- Christie-Oleza, J. A., Scanlan, D. J., & Armengaud, J. (2015). "You produce while I clean up", a strategy revealed by exoproteomics during *Synechococcus-Roseobacter* interactions. *PROTEOMICS*, *15*(20), 3454–3462. <https://doi.org/10.1002/pmic.201400562>
- Church, M. J., Kyi, E., Hall, R. O., Karl, D. M., Lindh, M., Nelson, A., & Wear, E. K. (2021). Production and diversity of microorganisms associated with sinking particles in the subtropical North Pacific Ocean. *Limnology and Oceanography*, *66*(9), 3255–3270. <https://doi.org/10.1002/lno.11877>

- Crespo, B. G., Pommier, T., Fernández-Gómez, B., & Pedrós-Alió, C. (2013). Taxonomic composition of the particle-attached and free-living bacterial assemblages in the Northwest Mediterranean Sea analyzed by pyrosequencing of the 16S rRNA. *MicrobiologyOpen*, 2(4), 541–552. <https://doi.org/10.1002/mbo3.92>
- Cuskin, F., Lowe, E., Temple, M., & et al. (2015). Human gut bacteroidetes can utilize yeast mannan through a selfish mechanism. *Nature*, 517, 165–169. <https://doi.org/10.1038/nature13995>
- Dal Co, A., Van Vliet, S., Kiviet, D. J., Schlegel, S., & Ackermann, M. (2020). Short-range interactions govern the dynamics and functions of microbial communities. *Nature Ecology & Evolution*, 4(3), 366–375. <https://doi.org/10.1038/s41559-019-1080-2>
- Datta, M. S., Sliwerska, E., Gore, J., Polz, M. F., & Cordero, O. X. (2016). Microbial interactions lead to rapid micro-scale successions on model marine particles. *Nature Communications*, 7(1), 11965. <https://doi.org/10.1038/ncomms11965>
- DeLong, E. F., Franks, D. G., & Alldredge, A. L. (1993). Phylogenetic diversity of aggregate-attached vs. free-living marine bacterial assemblages. *Limnology and Oceanography*, 38(5), 924–934. <https://doi.org/10.4319/lo.1993.38.5.0924>
- Drescher, K., Nadell, D., Carey, Stone, A., Howard, Wingreen, N. S., & Bassler, B. L. (2014). Solutions to the Public Goods Dilemma in Bacterial Biofilms. *Current Biology*, 24(1), 50–55. <https://doi.org/10.1016/j.cub.2013.10.030>
- D'Souza, G., Ebrahimi, A., Stubbusch, A., Daniels, M., Keegstra, J., Stocker, R., Cordero, O., & Ackermann, M. (2023). Cell aggregation is associated with enzyme secretion strategies in marine polysaccharide-degrading bacteria. *The ISME Journal*, 17(5), 703–711. <https://doi.org/10.1038/s41396-023-01385-1>
- D'Souza, G., Schwartzman, J., Keegstra, J., Schreier, J. E., Daniels, M., Cordero, O. X., Stocker, R., & Ackermann, M. (2023). Interspecies interactions determine growth dynamics of biopolymer-degrading populations in microbial communities. *Proceedings of the National Academy of Sciences*, 120(44). <https://doi.org/10.1016/j.cub.2008.08.019>
- D'Souza, G. G., Povolo, V. R., Keegstra, J. M., Stocker, R., & Ackermann, M. (2021). Nutrient complexity triggers transitions between solitary and colonial growth in bacterial populations. *The ISME Journal*, 15(9), 2614–2626. <https://doi.org/10.1038/s41396-021-00953-7>
- Ebrahimi, A., Schwartzman, J., & Cordero, O. X. (2019). Cooperation and spatial self-organization determine rate and efficiency of particulate organic matter degradation in marine bacteria. *Proceedings of the National Academy*

- of Sciences*, 116(46), 23309–23316. <https://doi.org/10.1073/pnas.1908512116>
- Enke, T. N., Datta, M. S., Schwartzman, J., Cermak, N., Schmitz, D., Barrere, J., Pascual-García, A., & Cordero, O. X. (2019). Modular Assembly of Polysaccharide-Degrading Marine Microbial Communities. *Current Biology*, 29(9), 1528–1535.e6. <https://doi.org/10.1016/j.cub.2019.03.047>
- Enke, T. N., Leventhal, G. E., Metzger, M., Saavedra, J. T., & Cordero, O. X. (2018). Microscale ecology regulates particulate organic matter turnover in model marine microbial communities. *Nature Communications*, 9(1), 2743. <https://doi.org/10.1038/s41467-018-05159-8>
- Ferrer-González, F. X., Widner, B., Holderman, N. R., Glushka, J., Edison, A. S., Kujawinski, E. B., & Moran, M. A. (2021). Resource partitioning of phytoplankton metabolites that support bacterial heterotrophy. *The ISME Journal*, 15(3), 762–773. <https://doi.org/10.1038/s41396-020-00811-y>
- Fontanez, K. M., Eppley, J. M., Samo, T. J., Karl, D. M., & DeLong, E. F. (2015). Microbial community structure and function on sinking particles in the North Pacific Subtropical Gyre. *Frontiers in Microbiology*, 6. <https://doi.org/10.3389/fmicb.2015.00469>
- Francis, B., Urich, T., Mikolasch, A., Teeling, H., & Amann, R. (2021). North sea spring bloom-associated Gammaproteobacteria fill diverse heterotrophic niches. *Environmental Microbiomes*, 16, 15.
- Francis, T. B., Bartosik, D., Sura, T., Sichert, A., Hehemann, J.-H., Markert, S., Schweder, T., Fuchs, B. M., Teeling, H., Amann, R. I., & Becher, D. (2021). Changing expression patterns of TonB-dependent transporters suggest shifts in polysaccharide consumption over the course of a spring phytoplankton bloom. *The ISME Journal*, 15, 2336–2350.
- Frischkorn, K. R., Stojanovski, A., & Paranjpye, R. (2013). *Vibrio parahaemolyticus* type IV pili mediate interactions with diatom-derived chitin and point to an unexplored mechanism of environmental persistence. *Environmental Microbiology*, 15(5), 1416–1427. <https://doi.org/10.1111/1462-2920.12093>
- Ghiglione, J.-F., Conan, P., & Pujo-Pay, M. (2009). Diversity of total and active free-living vs. particle-attached bacteria in the euphotic zone of the NW Mediterranean Sea. *FEMS Microbiology Letters*, 299(1), 9–21. <https://doi.org/10.1111/j.1574-6968.2009.01694.x>
- Gralka, M., Pollak, S., & Cordero, O. X. (2023). Genome content predicts the carbon catabolic preferences of heterotrophic bacteria. *Nature Microbiology*. <https://doi.org/10.1038/s41564-023-01458-z>
- Grossart, H.-P., Kjørboe, T., Tang, K., & Ploug, H. (2003). Bacterial Colonization of Particles: Growth and Interactions. *Applied and Environmental Microbiology*, 69(6), 3500–3509. <https://doi.org/10.1128/AEM.69.6.3500-3509.2003>

- Grossart, H.-P., Levold, F., Allgaier, M., Simon, M., & Brinkhoff, T. (2005). Marine diatom species harbour distinct bacterial communities. *Environmental Microbiology*, 7(6), 860–873. <https://doi.org/10.1111/j.1462-2920.2005.00759.x>
- Gügi, B., Le Costaouec, T., Burel, C., Lerouge, P., Helbert, W., & Bardor, M. (2015). Diatom-Specific Oligosaccharide and Polysaccharide Structures Help to Unravel Biosynthetic Capabilities in Diatoms. *Marine Drugs*, 13(9), 5993–6018. <https://doi.org/10.3390/md13095993>
- Guillard, R. R. L., & Hargraves, P. E. (1993). *Stichochrysis immobilis* is a diatom, not a chrysophyte. *Phycologia*, 32, 234–236.
- Huang, G., Vidal-Melgosa, S., Sichert, A., Becker, S., Fang, Y., Niggemann, J., Iversen, M. H., Cao, Y., & Hehemann, J.-H. (2021). Secretion of sulfated fucans by diatoms may contribute to marine aggregate formation. *Limnology and Oceanography*, 66(10), 3768–3782. <https://doi.org/10.1002/lno.11917>
- Huelsmann, M., Schubert, O. T., & Ackermann, M. (2024). A framework for understanding collective microbiome metabolism. *Nature Microbiology*, 9(12), 3097–3109. <https://doi.org/10.1038/s41564-024-01850-3>
- Julou, T., Mora, T., Guillon, L., Croquette, V., Schalk, I. J., Bensimon, D., & Desprat, N. (2013). Cell–cell contacts confine public goods diffusion inside *Pseudomonas aeruginosa* clonal microcolonies. *Proceedings of the National Academy of Sciences of the United States of America*, 110, 12577–12582. <https://doi.org/10.1073/pnas.1301428110>
- Kaczmarek, I., Ehrman, J. M., Bates, S. S., Green, D. H., Léger, C., & Harris, J. (2005). Diversity and distribution of epibiotic bacteria on *Pseudo-nitzschia* multiseres (Bacillariophyceae) in culture, and comparison with those on diatoms in native seawater. *Harmful Algae*, 4, 725–741. <https://doi.org/10.1016/j.hal.2004.10.001>
- Kaya, M., Mujtaba, M., Ehrlich, H., Salaberria, A. M., Baran, T., Amemiya, C. T., Galli, L., R. Akyuz, Sargin, I., & Labidi, J. (2017). On chemistry of γ -chitin. *Carbohydrate Polymers*, 176, 177–186. <https://doi.org/10.1016/j.carbpol.2017.08.076>
- Kloareg, B., & Quatrano, R. S. (1988). Structure of the cell walls of marine algae and ecophysiological functions of the matrix polysaccharides. *Oceanography and Marine Biology: An Annual Review*, 26, 259–315.
- Krüger, K., Chafee, M., Ben Francis, T., Glavina del Rio, T., Becher, D., Schweder, T., Amann, R. I., & Teeling, H. (2019). In marine Bacteroidetes the bulk of glycan degradation during algae blooms is mediated by few clades using a restricted set of genes. *The ISME Journal*, 13, 2800–2816.

- LeCleir, G. R., DeBruyn, J. M., Maas, E. W., Boyd, P. W., & Wilhelm, S. W. (2014). Temporal changes in particle-associated microbial communities after interception by nonlethal sediment traps. *FEMS Microbiology Ecology*, *87*(1), 153–163. <https://doi.org/10.1111/1574-6941.12213>
- Li, F., Burger, A., Eppley, J. M., Poff, K. E., Karl, D. M., & DeLong, E. F. (2023). Planktonic microbial signatures of sinking particle export in the open ocean's interior. *Nature Communications*, *14*(1), 7177. <https://doi.org/10.1038/s41467-023-42909-9>
- Mestre, M., Ruiz-González, C., Logares, R., Duarte, C. M., Gasol, J. M., & Sala, M. M. (2018). Sinking particles promote vertical connectivity in the ocean microbiome. *Proceedings of the National Academy of Sciences*, *115*(29). <https://doi.org/10.1073/pnas.1802470115>
- Momeni, B., Waite, A. J., & Shou, W. (2013). Spatial self-organization favors heterotypic cooperation over cheating. *eLife*, *2*, e00960. <https://doi.org/10.7554/eLife.00960>
- Myklesstad, S. (1974). Production of carbohydrates by marine planktonic diatoms. I. Comparison of nine different species in culture. *Journal of Experimental Marine Biology and Ecology*, *15*(3), 261–274. [https://doi.org/10.1016/0022-0981\(74\)90049-5](https://doi.org/10.1016/0022-0981(74)90049-5)
- Nadell, C. D., Drescher, K., & Foster, K. R. (2016). Spatial structure, cooperation and competition in biofilms. *Nature Reviews Microbiology*, *14*(9), 589–600. <https://doi.org/10.1038/nrmicro.2016.84>
- Nguyen, T. T. H., Zakem, E. J., Ebrahimi, A., Schwartzman, J., Caglar, T., Amarnath, K., Alcolombri, U., Peaudecerf, F. J., Hwa, T., Stocker, R., Cordero, O. X., & Levine, N. M. (2022). Microbes contribute to setting the ocean carbon flux by altering the fate of sinking particulates. *Nature Communications*, *13*(1), 1657. <https://doi.org/10.1038/s41467-022-29297-2>
- Noinaj, N., Guillier, M., Barnard, T. J., & Buchanan, S. K. (2010). TonB-dependent transporters: Regulation, structure, and function. *Annual Review of Microbiology*, *64*. <https://doi.org/10.1146/annurev.micro.112408.134247>
- Olofsson, M., Ferrer-González, F. X., Uchimiya, M., Schreier, J. E., Holderman, N. R., Smith, C. B., Edison, A. S., & Moran, M. A. (2022). Growth-stage-related shifts in diatom endometabolome composition set the stage for bacterial heterotrophy. *ISME Communications*, *2*(1), 28. <https://doi.org/10.1038/s43705-022-00116-5>
- Pelve, E. A., Fontanez, K. M., & DeLong, E. F. (2017). Bacterial Succession on Sinking Particles in the Ocean's Interior. *Frontiers in Microbiology*, *8*, 2269. <https://doi.org/10.3389/fmicb.2017.02269>

- Pontrelli, S., Szabo, R., Pollak, S., Schwartzman, J., Ledezma-Tejeda, D., Cordero, O. X., & Sauer, U. (2022). Metabolic cross-feeding structures the assembly of polysaccharide degrading communities. *Science Advances*, 8(8), eabk3076. <https://doi.org/10.1126/sciadv.abk3076>
- Rao, D., Webb, J. S., Holmström, C., Case, R., Low, A., Steinberg, P., & Kjelleberg, S. (2007). Low Densities of Epiphytic Bacteria from the Marine Alga *Ulva australis* Inhibit Settlement of Fouling Organisms. *Applied and Environmental Microbiology*, 73(24), 7844–7852. <https://doi.org/10.1128/AEM.01543-07>
- Reintjes, G., Arnosti, C., Fuchs, B. M., & Amann, R. (2017). An alternative polysaccharide uptake mechanism of marine bacteria. *The ISME Journal*, 11(7), 1640–1650. <https://doi.org/10.1038/ismej.2017.26>
- Rooney-Varga, J. N., Giewat, M. W., Savin, M. C., Sood, S., LeGresley, M., & Martin, J. L. (2005). Links between phytoplankton and bacterial community dynamics in a coastal marine environment. *Microbial Ecology*, 49, 163–175.
- Roth Rosenberg, D., Haber, M., Goldford, J., Lalzar, M., Aharonovich, D., Al-Ashhab, A., Lehahn, Y., Segrè, D., Steindler, L., & Sher, D. (2021). Particle-associated and free-living bacterial communities in an oligotrophic sea are affected by different environmental factors. *Environmental Microbiology*, 23(8), 4295–4308. <https://doi.org/10.1111/1462-2920.15611>
- Sampaio, A., Silva, V., Poeta, P., & Aonofriesei, F. (2022). *Vibrio* spp.: Life Strategies, Ecology, and Risks in a Changing Environment. *Diversity*, 14(2), 97. <https://doi.org/10.3390/d14020097>
- Sapp, M., Schwaderer, A. S., Wiltshire, K. H., Hoppe, H.-G., Gerdts, G., & Wichels, A. (2007). Species-specific bacterial communities in the phycosphere of microalgae? *Microbial Ecology*, 53, 683–699.
- Sapp, M., Wichels, A., & Gerdts, G. (2007). Impacts of cultivation of marine diatoms on the associated bacterial community. *Applied and Environmental Microbiology*, 73, 3117–3120.
- Sapp, M., Wichels, A., Wiltshire, K. H., & Gerdts, G. (2007). Bacterial community dynamics during the winter-spring transition in the North Sea. *FEMS Microbiology Ecology*, 59, 622–637.
- Shanks, A. L., & Edmondson, E. W. (1989). Laboratory-made artificial marine snow: A biological model of the real thing. *Marine Biology*, 101(4), 463–470. <https://doi.org/10.1007/BF00541648>
- Sonnenburg, E. D., Zheng, H., Joglekar, P., Higginbottom, S. K., Firbank, S. J., Bolam, D. N., & Sonnenburg, J. L. (2010). Specificity of polysaccharide use in intestinal bacteroides species determines diet-induced microbiota alterations. *Cell*, 141, 1241–1252. <https://doi.org/10.1016/j.cell.2010.05.005>

- Stam, M., Lelièvre, P., Hoebeke, M., Corre, E., Barbeyron, T., & Michel, G. (2023). Sulfatlas, the sulfatase database: State of the art and new developments. *Nucleic Acids Research*, *51*, D647–D653. <https://doi.org/10.1093/nar/gkac977>
- Takemura, A. F., Chien, D. M., & Polz, M. F. (2014). Associations and dynamics of Vibrionaceae in the environment, from the genus to the population level. *Frontiers in Microbiology*, *5*. <https://doi.org/10.3389/fmicb.2014.00038>
- Teeling, H., Fuchs, B. M., Becher, D., Klockow, C., Gardebrecht, A., Bennis, C. M., Kassabgy, M., Huang, S., Mann, A. J., Waldmann, J., Weber, M., Klindworth, A., Otto, A., Lange, J., Bernhardt, J., Reinsch, C., Hecker, M., Peplies, J., Bockelmann, F. D., ... Amann, R. (2012). Substrate-Controlled Succession of Marine Bacterioplankton Populations Induced by a Phytoplankton Bloom. *Science*, *336*(6081), 608–611. <https://doi.org/10.1126/science.1218344>
- Teeling, H., Fuchs, B. M., Bennis, C. M., Krüger, K., Chafee, M., Kappelmann, L., Reintjes, G., Waldmann, J., Quast, C., Glöckner, F. O., Lucas, J., Wichels, A., Gerdt, G., Wiltshire, K. H., & Amann, R. I. (2016). Recurring patterns in bacterioplankton dynamics during coastal spring algae blooms. *eLife*, *5*, e11888. <https://doi.org/10.7554/eLife.11888>
- Tesson, B., Masse, S., Laurent, G., Maquet, J., Livage, J., Martin-Jézéquel, V., & Coradin, T. (2008). Contribution of multi-nuclear solid state NMR to the characterization of the *Thalassiosira pseudonana* diatom cell wall. *Analytical and Bioanalytical Chemistry*, *390*(7), 1889–1898. <https://doi.org/10.1007/s00216-008-1908-0>
- Thornton, D., C. O. (2002). Diatom aggregation in the sea: Mechanisms and ecological implications. *European Journal of Phycology*, *37*(2), 149–161.
- Valencia, B., Stukel, M. R., Allen, A. E., McCrow, J. P., Rabines, A., & Landry, M. R. (2022). Microbial communities associated with sinking particles across an environmental gradient from coastal upwelling to the oligotrophic ocean. *Deep Sea Research Part I: Oceanographic Research Papers*, *179*, 103668. <https://doi.org/10.1016/j.dsr.2021.103668>
- Vidal-Melgosa, S., Sichert, A., Francis, T. B., Bartosik, D., Niggemann, J., Wichels, A., Willats, W. G. T., Fuchs, B. M., Teeling, H., Becher, D., Schweder, T., Amann, R., & Hehemann, J.-H. (2021). Diatom fucan polysaccharide precipitates carbon during algal blooms. *Nature Communications*, *12*(1), 1150. <https://doi.org/10.1038/s41467-021-21009-6>
- Waterkeyn, L., & Bienfait, A. (1987). Localization and function of (1,3)-glucans (callose and chrysolaminarin) in *Pinnularia* genus (Diatoms). *Cellule*, *74*, 199–226.

Zheng, J., Ge, Q., Yan, Y., Zhang, X., Huang, L., & Yin, Y. (2023). dbCAN3: Automated carbohydrate-active enzyme and substrate annotation. *Nucleic Acids Research*, 51(W1), W115–W121. <https://doi.org/10.1093/nar/gkad328>

Chapter 7

Concluding remarks

Throughout this thesis, I have demonstrated through analysis of pure microbial cultures and environmental samples that the hydrogen isotope compositions of amino acids may provide a highly useful, quantitative tracer of microbial metabolism in the environment. Most available tools provide only snapshots of microbial activity at the time of sampling; in contrast, $\delta^2\text{H}_{\text{AA}}$ analysis enables quantitative reconstruction of the history of organic matter processing by microbes prior to sampling (as exemplified in Chapter 5), which is particularly invaluable for understanding how microbial activity is both contributing and responding to environmental changes. We chose marine POM as our target application here, but the potential applications of $\delta^2\text{H}_{\text{AA}}$ analysis are much farther reaching, and will undoubtedly span diverse fields beyond marine geochemistry in the future.

In order for $\delta^2\text{H}_{\text{AA}}$ analysis to be most successfully applied to environmental samples, some understanding of the environmental context is needed prior to sampling. For example, knowledge of the likely metabolisms present will inform what $\delta^2\text{H}_{\text{AA}}$ signals are expected, and will guide construction of experiments and the complementary measurements needed to accurately interpret the microbial processes occurring. Such complementary measurements could include the suite of meta-omics tools to identify key players in the environmental locale (metagenomics) and obtain further insight into the kinds of metabolisms occurring (metatranscriptomics and metaproteomics). $\delta^2\text{H}_{\text{AA}}$ analysis could then provide quantitative information about how the microbial community, through its collective metabolism, shaped the geochemistry of the environmental locale over time. One particularly excit-

ing future analytical prospect is the coupling of proteomics with tandem $\delta^2\text{H}_{\text{AA}}$ analysis as described by Gharibi et al. (2022). This approach could help directly link quantitative metabolic information gained from $\delta^2\text{H}_{\text{AA}}$ analysis to the host organisms responsible for the metabolic activity in order to specifically interrogate *who is doing what* in the environment. In this way, amino acid $\delta^2\text{H}$ analysis may provide a better proxy for modern microbial metabolism than lipid $\delta^2\text{H}$ analysis, although both tools are generally complementary.

Additionally ideal for $\delta^2\text{H}_{\text{AA}}$ analysis are environments where microbial communities or processes are relatively simplistic—i.e., where only a few metabolisms are present, or where one microbial process with a distinct isotopic signal is dominant. My thesis has built toward distinguishing photoautotrophic versus heterotrophic biomass in environmental samples, but microbial metabolisms are incredibly diverse. Exploration of the $\delta^2\text{H}_{\text{AA}}$ signals of other metabolisms will likely inform other exciting applications of this isotopic tool. Toward these endeavors, the $\delta^2\text{H}_{\text{AA}}$ signatures of diverse microbial metabolisms, as well as the controls on these signals, should be explored through experimental studies that build in complexity: from pure cultures, to synthetic communities, to simple and well-constrained environmental communities. This pipeline will provide some quality control on interpretations drawn from $\delta^2\text{H}_{\text{AA}}$ data.

Finally, a major outstanding challenge of $\delta^2\text{H}_{\text{AA}}$ applications is the lack of international amino acid standards with known hydrogen isotope ratios. These reference materials await development until researchers can control for the exchangeable hydrogen in amino acids (discussed in Chapters 2 and 3). In Chapter 3, we introduced one potential approach to isolate the isotope ratios of carbon-bound hydrogen in amino acids. However, our approach requires validation with reference materials in which the carbon-bound hydrogen has been independently characterized. Until such materials are developed, making $\delta^2\text{H}_{\text{AA}}$ measurements that are accurate,

precise, and reproducible across laboratories will remain a challenge. Nevertheless, it is clear that $\delta^2\text{H}_{\text{AA}}$ analysis offers exciting, powerful potential to quantitatively trace microbial processes in the environment. This tool meets a timely need for approaches to monitor the metabolic responses of microbial communities to perturbations amid a time of unprecedented environmental change.

References

- Gharibi, H., Chernobrovkin, A. L., Saei, A. A., Zhang, X., Gaetani, M., Makarov, A. A., & Zubarev, R. A. (2022). Proteomics-compatible Fourier transform isotopic ratio mass spectrometry of polypeptides. *Analytical Chemistry*, *94*, 15048–15056. <https://doi.org/10.1021/acs.analchem.2c03119>

Appendices

Appendix A

Supplementary material for Chapter 2

A.1 Mechanisms of amino acid loss during hydrolysis

Here we provide mechanistic details of amino acid loss during hydrolysis and known fractionations with each residue. This information expands upon our discussion in the main text, providing insight into the atomic sites and isotope system(s) that may fractionate. In several sections, we highlight additional strategies for protection that were not presented in the main text. Amino acid recoveries from proteins visualized in Figure 2.3 (main text) are presented in Supplemental Table A.1.

A.1.1 Aliphatic amino acids

The bonds between pairs of aliphatic amino acids – especially those involving valine, leucine, and isoleucine – are known to be quite stable due to both steric hinderance caused by aliphatic side chains and lack of heteroatoms, which otherwise facilitate peptide bond cleavage (Whitfield, 1963). In addition, glycine-glycine bonds have been observed to remain intact after 500h of heating between 100 and 160°C in unbuffered aqueous solution (Silfer et al., 1992), presumably due to the reversible cyclization of glycine (Supplemental Figure A.1). It is unclear how significant this mechanism may be under conventional (acidic) hydrolysis. As glycine is a common amino acid in protein secondary structures (β turns and transmem-

brane helices; Javadpour et al., 1999), diglycine bonds may be prevalent in natural peptides. In spite of this potential loss mechanism, glycine yields can exceed 100% (due to contamination from fingerprints or reagents; Ozols, 1990).

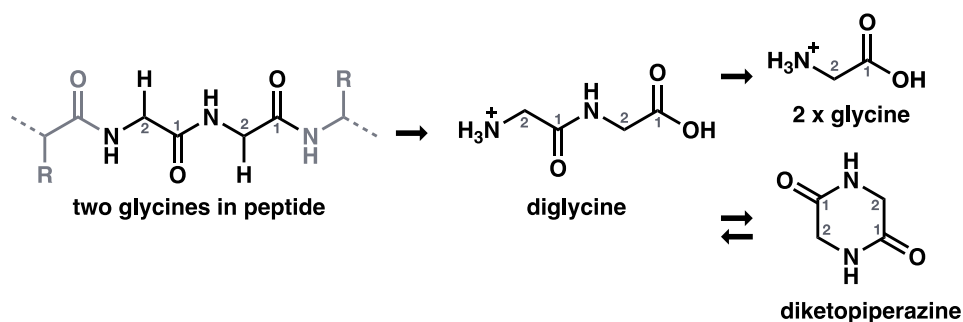


Figure A.1. Reversible cyclization of glycine to diketopiperazine. This competing reaction likely limits the yield of free glycine from acid hydrolysis of proteins. Figure adapted from Silfer et al. (1992).

A.1.2 Acidic and amidic amino acids

During hydrolysis, asparagine and glutamine are quantitatively deamidated to aspartic acid and glutamic acid, respectively (Supplemental Figure A.2). Under aqueous, acidic conditions, deamidation proceeds via an S_N2 reaction (Wright, 1991) at the amide C (C-4 for asparagine, C-5 for glutamine), beginning within a few minutes (R. L. Hill, 1965) and completing within one hour (Hunt, 1985). Quantification of amidic amino acids can be achieved by chemically modifying the amide into inert moieties (e.g., by reaction with bis(1,1-trifluoroacetoxy)iodobenzene; Kuhn et al., 1996), but these techniques have not been adapted for isotopic analyses. Acidic amino acids are stable under conventional acid hydrolysis conditions.

Carbon isotope fractionation of asx and glx during hydrolysis appears minimal ($\leq 1.2\text{‰}$) for standard amino acids and synthetic polypeptides (Demmelmair & Schmidt, 1993; Jim et al., 2003; Metges & Daenzer, 2000). In contrast, H isotope

Esters of serine and threonine can form with organic acids and inorganic oxyanions (Supplemental Figure A.4) throughout the acid hydrolysis procedure and at the drying stage (Davidson, 2003). For example, esters may form with sulfate, which is common in samples of marine origin, and also can be released from connective tissue proteoglycans during acid hydrolysis (Hunt, 1985). The quantitative significance of ester formation for yields from different protein sources has not been documented, however.

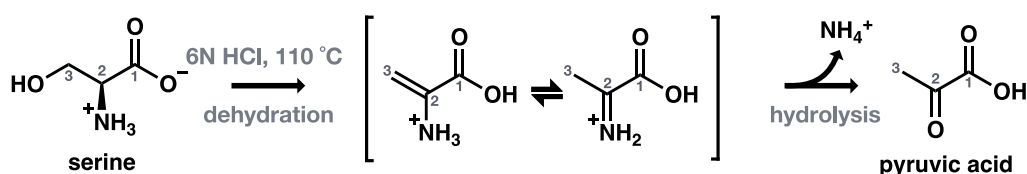


Figure A.3. Proposed mechanism for dehydration of serine to pyruvic acid. Threonine (not shown) loses its hydroxyl group and is converted to α -ketobutyric acid via the same dehydration mechanism. The acid-labile hydroxylic amino acids are progressively destroyed, leading to the stoichiometric release of ammonium. Mechanism depicted is based on descriptions in Hunt (1985) and Lamp et al. (2018).

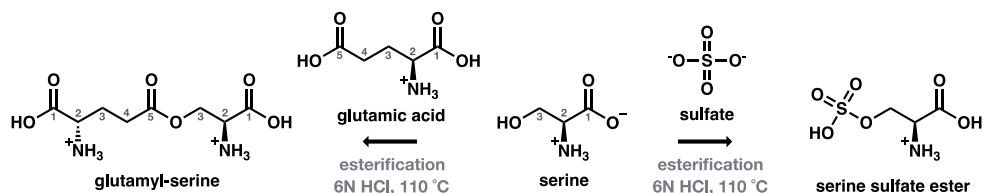


Figure A.4. Esterification of serine during acid hydrolysis. Serine and threonine (not pictured) can form esters with organic acids and inorganic oxyanions from the original protein source. These reactions are thought to occur primarily during evaporation following acid hydrolysis, as described in Hunt (1985) and Davidson (2003).

Despite variable yields, experiments with synthetic serine polypeptides suggest minimal accompanying C isotope fractionation (Jim et al., 2003). Further, pure standards of serine and threonine were only 0.3 and 0.5‰ more ^{13}C -depleted after

hydrolytic conditions, respectively (Metges & Daenzer, 2000). We predict that any isotope fractionation accompanying dehydration and esterification in more complex samples should impact the $\delta^{13}\text{C}$ value of the C-3 position. Deuterated hydrolysis experiments demonstrated H exchange with aqueous media is insignificant for serine and threonine (Fogel et al., 2016).

A.1.4 Aromatic amino acids

Losses of tyrosine are variable and are potentially associated with oxidative halogenation at C-6 and/or C-8 sites by trace HCl contaminants Cl_2 and Br_2 (Supplemental Figure A.5; Sanger and Thompson, 1963), reaction with aspartic acid (Roach & Gehrke, 1970), and esterification with sulfate (Hunt, 1985). Although mechanisms of tyrosine halogenation are not reported, chloro- and bromotyrosines have been observed (Sanger & Thompson, 1963).

Recovery of tryptophan from hydrolysis is especially difficult and has been studied extensively. Tryptophan progressively degrades during acid hydrolysis, with recoveries decreasing from 55 to 11% between 24 and 120h of hydrolysis (Mondino & Bongiovanni, 1970). Two mechanisms have been proposed to account for tryptophan losses in the presence of S-containing compounds: (1) reaction with cystine, the dimer of cysteine (Supplemental Figure A.6; Nakai and Ohta, 1976), and (2) oxidation by organic sulfoxides like dimethyl sulfoxide (DMSO; Supplemental Figure A.7; Lee, 1991; Savige and Fontana, 1980). Evidence for these mechanisms stems from measurements of both the product, β -3-oxindolylalanine, and intermediate, tryptathionine (Nakai & Ohta, 1976; Ohta & Nakai, 1978). Methionine sulfoxide has similar functionality as DMSO (Supplemental Figure A.7) and may account for additional tryptophan losses (Hunt, 1985). Serine and threonine are thought to release ammonia during hydrolysis and simultaneously produce α -keto

acids (Supplemental Figure A.3), which have strong affinities for tryptophan, further complicating recoveries (Gruen, 1973). The details of these mechanisms are not elaborated upon in the literature. The use of mercaptoethanesulfonic acid, *p*-toluenesulfonic acid, or methanesulfonic acid instead of HCl during hydrolysis result in higher tryptophan yields from purified proteins, but recoveries are still affected by carbohydrate content (Hunt, 1985; Rutherford & Gilani, 2009). Use of these additives is beneficial when ion exchange chromatography follows hydrolysis, as these acids can be neutralized rather than evaporated (Penke et al., 1974). Thioglycolic acid (Davidson, 2003; Hunt, 1985) and β -mercaptoethanol (Blake & Li, 1968; Ng et al., 1987) also protect tryptophan from oxidation during acid hydrolysis, significantly increasing recovery, perhaps due to the high reactivity of these reagents with free Cl_2 (Ohta et al., 1981). Overall, conventional hydrolysis is not recommended for tryptophan, and vapor hydrolysis seems most promising. If conventional hydrolysis must be used, care should be taken to ensure conditions are kept anoxic, hydrolysis duration is <24 h, and carbohydrates and S-containing compounds are removed (Rutherford & Gilani, 2009). However, depending on the particular sample being analyzed, the latter two are not always feasible, in which case additives may be necessary.

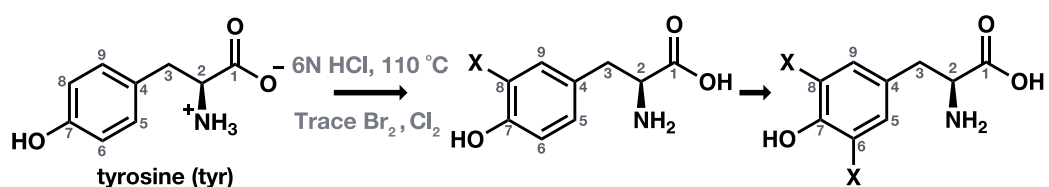


Figure A.5. Trace amounts of Br_2 or Cl_2 in HCl can halogenate tyrosine at the C-6 and/or C-8 position (Sanger & Thompson, 1963).

Hydrolysis does not appear to alter $\delta^{13}\text{C}$ values of tyrosine standards (Metges & Daenzer, 2000) nor phenylalanine standards or synthetic polypeptides (Demmel-

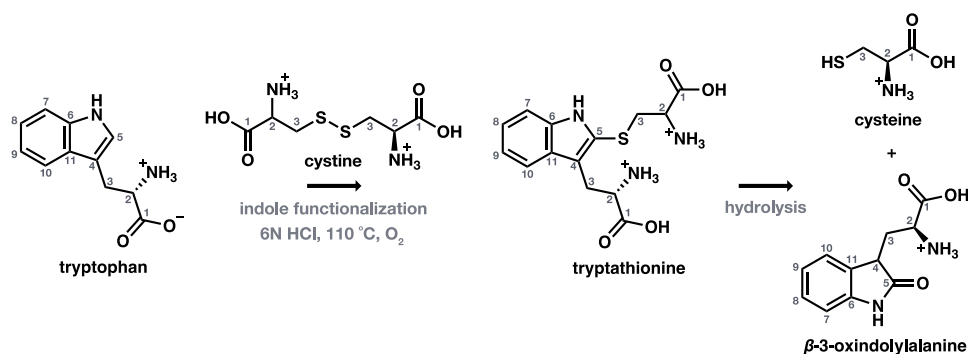


Figure A.6. Degradation of tryptophan during acid hydrolysis in the presence of O_2 and cystine. The indole attacks the disulfide bond of cystine, leading to release of one cysteine molecule and formation of β -3-oxindolylalanine. Mechanism depicted is based on evidence by Nakai and Ohta (1976) and Ohta et al. (1981).

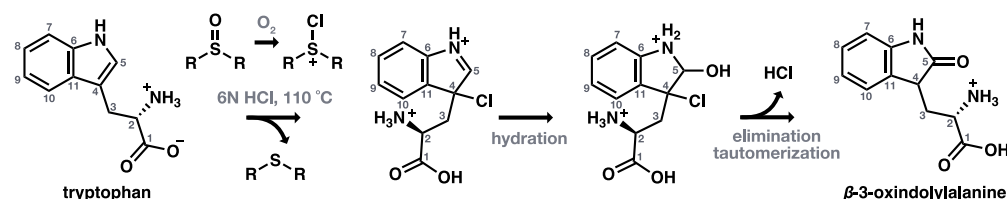


Figure A.7. Degradation of tryptophan during acid hydrolysis in the presence of O_2 and a sulfoxide compound (e.g., dimethyl sulfoxide (DMSO) or methionine sulfoxide). The sulfoxide may react with Cl_2 to form a chlorinated sulfoxide. The Cl atom can then attack the C-4 position of tryptophan. After hydration of the C-5 position, elimination of Cl, and tautomerization of the molecule, β -3-oxindolylalanine is formed. Mechanism proposed by Savige and Fontana (1980).

mair & Schmidt, 1993; Jim et al., 2003; Metges & Daenzer, 2000). Further, H exchange between phenylalanine and the aqueous media is insignificant during hydrolysis (Fogel et al., 2016). For tyrosine, H exchange is known to occur at the C-3 site (J. Hill & Leach, 1964). No C or H isotope fractionation data is yet available for tryptophan during hydrolysis due to its low yields.

A.1.5 S-containing amino acids

Cysteine and methionine suffer significant losses during hydrolysis due to oxidative degradation (Supplemental Figure A.8). Cysteine and its dimer cystine have other published loss mechanisms, but these appear minimal compared to oxidation (Hunt, 1985). One such mechanism is condensation of cysteine with decomposition products of carbohydrates and proteins (such as formaldehyde and pyruvic acid), which condense with cysteine's thiol (Supplemental Figure A.9). The S atoms in the condensation products may attack intramolecular C sites to form thiazolidine rings (Hunt, 1985). As discussed in previous sections, cystine and methionine sulfoxide are also susceptible to loss via formation of C-S bonds with tryptophan (Supplemental Figures A.6 and A.7) and tyrosine.

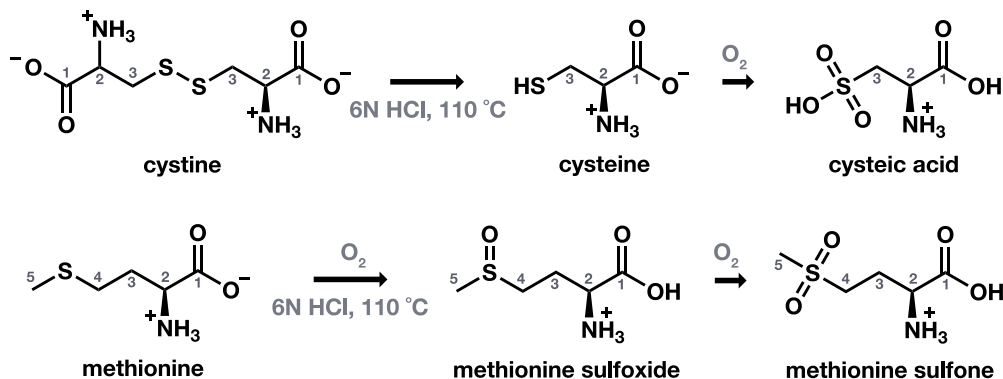


Figure A.8. Progressive oxidation of the S-containing amino acids. Under oxic conditions, cysteine's disulfide bond and cysteine's thiol group can react with O₂ to form a sulfonic acid. Similarly, methionine's thioether can be oxidized to a sulfoxide or sulfone. The ³⁴S normal KIE associated with oxidation of cysteine is estimated to be 1.015 (Phillips et al., 2021).

Although S isotope effects are expressed during incomplete oxidation (Phillips et al., 2021), C, N, and H in cysteine should not be subjected to primary isotope effects. In support of this, Metges and Daenzer (2000) found no significant C

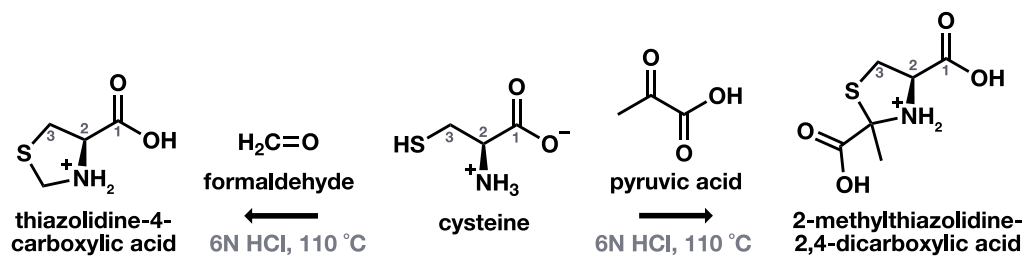


Figure A.9. Condensation reactions of cysteine with formaldehyde and pyruvic acid, forming ring structures after nucleophilic attack and proton transfer of sulfhydryl groups.

isotope fractionation for an unprotected methionine standard analyzed before and after hydrolysis. N isotope ratios of methionine isolated from terrestrial and aquatic organisms using conventional hydrolysis have also been characterized (Ishikawa et al., 2018).

Table A.1. Percentage recovery of amino acids from standards and proteins hydrolyzed under conventional acid hydrolysis conditions (6N HCl, 110°C, 20–24h, anoxic conditions). Abbreviations are spelled out in Figure 2.2 in the main text.

| Group | Amino acid | AA STD 1 ^a | AA STD 2 ^b | RNASE ^b | CYT C ^c | TMV ^c | BSA ^d | LYZ ^d | TRX ^d | IFN A ^d |
|----------------|------------|-----------------------|-----------------------|--------------------|--------------------|------------------|------------------|------------------|------------------|--------------------|
| Basic | Arg | 100 | 100 | 100 | 90 | 94 | 98 | 98 | 100 | 98 |
| | His | 100 | 98 | 100 | 100 | - | 97 | 100 | 100 | 97 |
| | Lys | 99 | 99 | 100 | 100 | 100 | 100 | 87 | 100 | 98 |
| Aliphatic | Ala | 100 | 99 | 100 | 100 | 100 | 100 | 100 | 100 | 100 |
| | Gly | 99 | 94 | 100 | 100 | 98 | 100 | 98 | 99 | 98 |
| | Leu | 100 | 100 | 100 | 99 | 93 | 100 | 99 | 100 | 99 |
| | Ile | 100 | 98 | 66 | 74 | 63 | 99 | 92 | 98 | 91 |
| | Pro | 100 | - | - | 100 | 100 | - | 95 | 100 | 100 |
| | Val | 100 | 98 | 100 | 73 | 69 | 93 | 93 | 100 | 89 |
| Acidic/ Amidic | Glx | 100 | 97 | 100 | 100 | 98 | 100 | 100 | 100 | 99 |
| | Asx | 100 | 96 | 100 | 100 | 100 | 99 | 99 | 100 | 99 |
| Hydroxylic | Ser | 95 | 92 | 93 | 100 | 98 | 83 | 84 | 90 | 84 |
| | Thr | 98 | 95 | 100 | 93 | 94 | 88 | 90 | 99 | 92 |
| Aromatic | Phe | 100 | 97 | 100 | 85 | 94 | 100 | 97 | 100 | 96 |
| | Trp | 55 | - | - | 19 | 48 | 0 | 0 | 0 | 0 |
| | Tyr | 100 | 71 | 83 | 94 | 91 | 98 | 97 | 100 | 98 |
| S-containing | Cys | 65 | 75 | 75 | - | - | 0 | 0 | 0 | 0 |
| | Met | 100 | 98 | 100 | 94 | - | 100 | 100 | 60 | 100 |

^a Mondino and Bongiovanni (1970)

^b Keutmann and Potts (1969)

^c Matsubara and Sasaki (1969)

^d Manneberg et al. (1995)

Table A.2. Yields and N isotope fractionations ($\Delta^{15}\text{N} = \delta^{15}\text{N}_{after} - \delta^{15}\text{N}_{before}$) of amino acids following cation exchange column desalting with Dowex 50WX8 resin, 100–200 or 200–400 mesh size.

| Amino acid group | Amino acid ^a | Yield of amino acid standard | | | | $\Delta^{15}\text{N}$ (‰) |
|------------------|-------------------------|------------------------------|--------------|--------------------------|----------------------|---------------------------|
| | | Moore and Stein (1951) | Cheng (1975) | Amelung and Zhang (2001) | Takano et al. (2010) | Takano et al. (2010) |
| Aliphatic | ala | 100 | 100 | 95 | 84 | 0.1 |
| | gly | 99 | 89 | | 91 | 0.1 |
| | leu | 100 | 100 | 100 | 96 | -0.3 |
| | ile | 100 | 100 | 100 | 100 | -0.1 |
| | pro | 100 | | 96 | 90 | 0.2 |
| | val | 100 | 98 | 99 | 100 | -0.1 |
| Basic | arg | 71 | 96 | | | |
| | his | 70 | 95 | | | |
| | lys | 82 | 94 | 91 | | |
| Acidic | glu | 97 | 100 | 88 | 100 | 0.0 |
| | asp | 100 | 95 | 93 | 100 | 0.1 |
| Hydroxylic | ser | 100 | 96 | 99 | 100 | 0.2 |
| | thr | 100 | 87 | 88 | 100 | |
| Aromatic | phe | 98 | 97 | 97 | 100 | 0.0 |
| | tyr | 100 | | 91 | | |
| Sulfur | met | 96 | | 86 | 91 | -0.1 |

Tryptophan and cysteine have not been investigated.

a

A.2 Data correction, isotope effect quantification, and error propagation for derivatives

The C isotope composition of the exogenous atoms can be determined via mass balance—i.e. by measuring the isotope ratio of a pure amino acid standard before and after derivatization and then employing the following equation (Rieley, 1994):

$$n_{da}F_{da} = n_aF_a + n_dF_d \quad (\text{A.1})$$

where n is the number of C atoms, F is the isotope mole fraction (and can be converted to δ values – see Section 2.1.1 in main text), and subscripts a , da , and d represent the pure amino acid, derivatized amino acid, and derivative atoms, respectively. This relationship is used to solve for F_d , which is the composition of the added derivative atoms, encompassing both the actual C isotope composition of the derivatizing reagent(s) and any fractionation that may occur during the reaction. Unique F_d values must be determined for each amino acid, as isotope effects are reaction- and compound-specific. As long as the reagent is present in excess and the same bottles of reagents and reaction conditions are used, (1) any isotope effect occurring within the reagent will be expressed in a reproducible manner and (2) amino acids will be maximally converted to derivatives, minimizing expression of isotope effects within the amino acids (Docherty et al., 2001). If the reagent is exhausted, F_d must be determined for the new derivatizing reagent to account for the (potentially) different derivative atom $\delta^{13}\text{C}$ values.

Nitrogen is rarely added during GC derivatization of amino acids (Figure 2.5), but N atoms in amino acids participate in the derivatization reaction. Isotope effects should not be expressed when derivatization is quantitative (theoretically achieved

when reagent is present in excess); however, N isotope fractionation has been observed for many derivatization reactions (Hofmann et al., 2003; Walsh et al., 2014), likely due to non-quantitative yield. N isotope fractionation should thus be monitored during method development and addressed using Supplemental Eqns. A.1 or A.2.

For H isotope analyses, F_d must be determined independently (i.e., not using Supplemental Equation A.1 because exchangeable H atoms are included in F_a). F_d can be measured directly by elemental analysis (EA)-IRMS provided the derivatizing reagent does not possess exchangeable H atoms and H isotope effects are not expressed during the reaction. Alternatively, F_d can be obtained indirectly through derivatization of a compound with known isotopic composition in which the exchangeable H has been removed. For example, the carboxylate salt form of phthalic acid with a known $\delta^2\text{H}$ value can be derivatized with methanol, then measured by GC-IRMS to back out the $\delta^2\text{H}$ value of the methyl group H in methanol (Valentine et al., 2004). With the independently constrained F_d , $\delta^2\text{H}$ values of amino acids in a sample can be determined using Supplemental Equation A.1. Note that this equation is exact; when there are large differences between δ values ($>50\text{‰}$), as is often the case for H isotopes, the approximation inherent in using δ values for such mass balance calculations becomes significant. For C isotope analyses, F values in Supplemental Equation A.1 can be approximated as δ values (Supplemental Equation A.2).

$$n_{da}\delta_{da} = n_a\delta_a + n_d\delta_d \quad (\text{A.2})$$

Supplemental Eqns. A.1 and A.2 are sufficient to find the C or H isotope compositions of amino acids in natural samples. In some cases (e.g., when choosing between derivatization reactions) it is helpful to quantify the fractionation. The

whole molecule C or N isotope fractionation associated with derivatization can be described as $\varepsilon_{meas/pred}$ (Supplemental Equation A.3).

$$\varepsilon_{meas/pred} = (\alpha_{meas/pred} - 1) \times 10^3 \quad (\text{A.3})$$

Where $\alpha_{meas/pred}$ is the ratio of measured versus predicted isotope ratios (R_{meas}/R_{pred}) of a derivatized amino acid standard. R_{pred} is the isotope ratio converted from δ_{da} in Supplemental Equation A.2 when an offline measurement of pure derivatizing reagent (δ_d) is obtained. To calculate the position-specific fractionation factor ($\alpha_{meas/pred}^*$, i.e., the approximate isotope effect; Table 2.1 in main text) for a single derivatization reaction, Supplemental Equation A.3 can be rearranged, multiplied by the total number of C or N atoms in the derivatized amino acid (n_{da}) and divided by the number of derivative groups added by the reagent of interest (x ; Corr et al., 2007b; Silfer et al., 1991).

$$\alpha_{meas/pred}^* = 1 + \frac{\varepsilon_{meas/pred} n_{da}}{10^3 x} \quad (\text{A.4})$$

For δ_a values found using Supplemental Equation A.2, and assuming errors in δ_d and δ_{da} are uncorrelated, the overall analytical uncertainty in δ_a can be calculated according to Supplemental Equation A.5, where σ is the uncertainty associated with each isotopic measurement (and $\pm 1\sigma$ encompasses a 68% confidence interval), and n is number of analyte atoms of interest (Rieley, 1994).

$$\sigma_a^2 = \sigma_d^2 \left(\frac{n_d}{n_a} \right)^2 + \sigma_{da}^2 \left(\frac{n_{da}}{n_a} \right)^2 \quad (\text{A.5})$$

Supplemental Equation A.5 is only valid for a pure amino acid where the stoichiometry is perfectly known. For a measurement of multiple analytes (e.g., two

co-eluting amino acids), uncertainty in the amounts (n values) would also need to be included. When the isotopic composition of the derivatizing reagent is directly measured, the uncertainty on the measurement (σ_d) is inserted into Supplemental Equation A.5. When δ_d is calculated from the mass balance between a derivatized standard (δ_{ds}) and standard (δ_s) using Supplemental Equation A.2, σ_d will be the result of propagated uncertainties on δ_s and δ_{ds} measurements. Supplemental Equation A.5 then expands to the following equation (Corr et al., 2007a, 2007b; Rieley, 1994):

$$\sigma_a^2 = \sigma_s^2 \left(\frac{n_s}{n_a} \right)^2 + \sigma_{ds}^2 \left(\frac{n_{ds}}{n_a} \right)^2 + \sigma_{da}^2 \left(\frac{n_{da}}{n_a} \right)^2 \quad (\text{A.6})$$

Note that in Supplemental Eqns. A.5 and A.6, analytical uncertainty for the isotopic composition of the (non-derivatized) amino acid, σ_a^2 , increases strongly with the number of atoms added by the derivative group(s). Therefore, derivative groups contributing large numbers of C, H, and N atoms (Table 2.1) are less optimal for isotope analysis.

A.3 Other IRMS configurations

A variety of additional promising IRMS configurations have been developed and applied to amino acid isotope analysis but are not yet widely available. “Moving-wire” (Sessions et al., 2005) or “spooling wire micro-combustion IRMS” (SWiM-IRMS; Eek et al., 2007) is a bulk measurement technique similar to an EA in that it offers no online separation, but with an improved ability to subtract background CO₂ as a continuous signal. These systems have been used to measure $\delta^{13}\text{C}$ values of pre-purified amino acids and whole proteins, achieving sensitivity and precision on par with GC-IRMS (Table 2.3; Mohr et al., 2014; Sessions et al., 2005). Liquid

samples are deposited on a Ni wire which is passed through a combustion furnace to produce CO₂, which in turn is dried and directed into an IRMS through an open split. Additionally, Zhang et al. (2021) proposed a new analytical strategy for measuring $\delta^{15}\text{N}$ values of amino acids using purge-and-trap continuous-flow IRMS (PT-CF-IRMS). Underivatized amino acids are separated by IC (see Section 2.6.3) and chemically converted to nitrous oxide offline. Cryogenic concentration, purification, and measurement of N₂O (instead of the combustion product, N₂) are carried out using the IRMS system. The method achieves 0.3-0.7‰ precisions with <15 nmol N (similar to GC-IRMS and optimized EA-IRMS; Table 2.3) and may be more convenient in laboratories already analyzing $\delta^{15}\text{N}$ values of N₂O by PT-CF-IRMS.

A.4 Additional details about PSIA of amino acids by high-resolution mass spectrometry

Constraining position-specific isotopic differences in amino acids may be accomplished via comparison of two or more amino acid fragments ions in a mass spectrometer. These measurements require that the spectrometer have sufficient mass resolution to distinguish fragments containing substitutions by ¹³C, ²H, ¹⁵N, ³³S, ³⁴S, ¹⁷O, and ¹⁸O, as well as ¹H adducts formed during ionization. In practice, this requires a mass resolution of $\sim 60,000$ ($m/\Delta m$, where m is mass and Δm is a peak's full width at half maximum) for relatively easily isolated isobars (¹⁵N, ³³S), up to $\sim 250,000$ for challenging separations such as ¹⁷O from ¹³C, at m/z of ~ 100 -200 corresponding to the major fragments and molecular ions of derivatized amino acids. Orbitrap mass analyzers, in particular, are commonly integrated into platforms that include a quadrupole for mass isolation and an ion trap for additional,

collisional fragmentation if needed.

A.5 ^1H Isotopic NMR for PSIA of amino acids

An alternative NMR approach for position-specific $^{13}\text{C}/^{12}\text{C}$ analysis was recently applied to amino acid standards using ^1H NMR (Rasmussen & Hoffman, 2020). This technique characterizes C atoms covalently bonded to H atoms by using peaks within the proton (^1H) NMR spectra and exploiting the amplitudes and shapes of the central ($^1\text{H}-^{12}\text{C}$) and satellite ($\text{H}-^{13}\text{C}$) peaks. This ^1H NMR approach has at least two advantages over direct ^{13}C NMR, while achieving similar precisions ($\sim 1\%$; Table 2.3) and accuracies: (1) it uses more commonly available equipment, and (2) it is more sensitive ($\sim 0.05\text{--}0.3$ mmol analyte; Table 2.3), with potential for further improvements through an ultrahigh field NMR spectrometer (Hoffman & Rasmussen, 2019). One drawback of this strategy is that not all C positions in amino acids are visible.

References

- Blake, J., & Li, C. H. (1968). The solid phase synthesis of methionylglutamyl-histidylphenylalanylarginyltryptophylglycine. *Journal of the Am. Chem. Soc.*, *90*(21), 5882–5884.
- Corr, L. T., Berstan, R., & Evershed, R. P. (2007a). Development of *N*-acetyl methyl ester derivatives for the determination of $\delta^{13}\text{C}$ values of amino acids using gas chromatography-combustion-isotope ratio mass spectrometry. *Analytical Chemistry*, *79*(23), 9082–9090. <https://doi.org/10.1021/ac071223b>
- Corr, L. T., Berstan, R., & Evershed, R. P. (2007b). Optimisation of derivatization procedures for the determination of $\delta^{13}\text{C}$ values of amino acids by gas chromatography-combustion-isotope ratio mass spectrometry. *Rapid Communications in Mass Spectrometry*, *21*, 3759–3771. <https://doi.org/10.1002/rcm.3252>

- Davidson, I. (2003). Hydrolysis of samples for amino acid analysis. In *Methods in Molecular Biology* (pp. 111–122, Vol. 211). <https://doi.org/10.1385/1-59259-342-9:111>
- Demmelair, H., & Schmidt, H.-L. (1993). Precise $\delta^{13}\text{C}$ -determination in the range of natural abundance on amino acids from protein hydrolysates by gas chromatography-isotope ratio mass spectrometry. *Isotopenpraxis Isotopes in Environmental and Health Studies*, 29(3), 237–250. <https://doi.org/10.1080/00211919308046690>
- Docherty, G., Jones, V., & Evershed, R. P. (2001). Practical and theoretical considerations in the gas chromatography-combustion-isotope ratio mass spectrometry $\delta^{13}\text{C}$ analysis of small polyfunctional compounds. *Rapid Communications in Mass Spectrometry*, 15, 730–738. <https://doi.org/10.1002/rcm.270>
- Eek, K., Sessions, A., & Lies, D. (2007). Carbon-isotopic analysis of microbial cells sorted by flow cytometry. *Geobiology*, 5, 85–95.
- Fogel, M. L., Griffin, P. L., & Newsome, S. D. (2016). Hydrogen isotopes in individual amino acids reflect differentiated pools of hydrogen from food and water in *Escherichia coli*. *Proceedings of the National Academy of Sciences*, 113(32), E4648–E4653. <https://doi.org/10.1073/pnas.1525703113>
- Gruen, L. C. (1973). Effect of other amino acids on recovery of tryptophan following acid hydrolysis. *Australian Journal of Biological Sciences*, 26, 287–290. <https://doi.org/10.1071/B19730287>
- Hill, J., & Leach, S. J. (1964). Hydrogen exchange at carbon-hydrogen sites during acid or alkaline treatment of proteins. *Biochemistry*, 3(12), 1814–1818. <https://doi.org/10.1021/bi00900a003>
- Hill, R. L. (1965). Hydrolysis of proteins. *Advances in Protein Chemistry*, 20, 37–107. [https://doi.org/https://doi.org/10.1016/S0065-3233\(08\)60388-5](https://doi.org/https://doi.org/10.1016/S0065-3233(08)60388-5)
- Hoffman, D. W., & Rasmussen, C. (2019). Position-specific carbon stable isotope ratios by proton NMR spectroscopy. *Analytical Chemistry*, 91(24), 15661–15669. <https://doi.org/10.1021/acs.analchem.9b03776>
- Hofmann, D., Gehre, M., & Jung, K. (2003). Sample preparation techniques for the determination of natural $^{15}\text{N}/^{14}\text{N}$ variations in amino acids by gas chromatography-combustion-isotope ratio mass spectrometry (GC-C-IRMS). *Isotopes in Environmental and Health Studies*, 39, 233–244.
- Hunt, S. (1985). Degradation of amino acids accompanying *in vitro* protein hydrolysis. In G. C. Barrett (Ed.), *Chemistry and Biochemistry of the Amino Acids* (pp. 376–398). Springer Netherlands. https://doi.org/10.1007/978-94-009-4832-7_12

- Ishikawa, N., Chikaraishi, Y., Takano, Y., Sasaki, Y., Takizawa, Y., Tsuchiya, M., Tayasu, I., Nagata, T., & Ohkouchi, N. (2018). A new analytical method for determination of the nitrogen isotopic composition of methionine: its application to aquatic ecosystems with mixed resources. *Limnology and Oceanography*, *16*, 607–620.
- Javadpour, M. M., Eilers, M., Groesbeek, M., & Smith, S. O. (1999). Helix packing in polytopic membrane proteins: Role of glycine in transmembrane helix association. *Biophysical Journal*, *77*(3), 1609–1618. [https://doi.org/10.1016/S0006-3495\(99\)77009-8](https://doi.org/10.1016/S0006-3495(99)77009-8)
- Jim, S., Jones, V., Copley, M. S., Ambrose, S. H., & Evershed, R. P. (2003). Effects of hydrolysis on the $\delta^{13}\text{C}$ values of individual amino acids derived from polypeptides and proteins. *Rapid Communications in Mass Spectrometry*, *17*(20), 2283–2289. <https://doi.org/10.1002/rcm.1177>
- Keutmann, H. T., & Potts, J. T. (1969). Improved recovery of methionine after acid hydrolysis using mercaptoethanol. *Analytical Biochemistry*, *29*, 175–185.
- Kuhn, K. S., Stehle, P., & Fürst, P. (1996). Quantitative analyses of glutamine in peptides and proteins. *Journal of Agricultural and Food Chemistry*, *44*(7), 1808–1811. <https://doi.org/10.1021/jf950511i>
- Lamp, A., Kaltschmitt, M., & Lüdtko, O. (2018). Improved HPLC-method for estimation and correction of amino acid losses during hydrolysis of unknown samples. *Analytical Biochemistry*, *543*, 140–145. <https://doi.org/10.1016/j.ab.2017.12.009>
- Lee, T. V. (1991). Oxidation adjacent to oxygen of alcohols by other methods. In Trost, B. M., Fleming, I., Ley, S. V. (Ed.), *Comprehensive Organic Synthesis* (pp. 305–327). Elsevier Ltd. <https://doi.org/10.1016/b978-0-08-052349-1.00192-x>
- Manneberg, M., Lahm, H.-W., & Fountoulakis, M. (1995). Quantification of cysteine residues following oxidation to cysteic acid in the presence of sodium azide. *Analytical Biochemistry*, *231*, 349–353.
- Matsubara, H., & Sasaki, R. M. (1969). High recovery of tryptophan from acid hydrolysates of proteins. *Biochemical and Biophysical Research Communications*, *35*(2), 175–181. [https://doi.org/10.1016/0006-291X\(69\)90263-0](https://doi.org/10.1016/0006-291X(69)90263-0)
- Metges, C. C., & Daenzer, M. (2000). ^{13}C gas chromatography-combustion isotope ratio mass spectrometry analysis of *N*-pivaloyl amino acid esters of tissue and plasma samples. *Analytical Biochemistry*, *278*(2), 156–164. <https://doi.org/10.1006/abio.1999.4426>
- Mohr, W., Tang, T., Sattin, S. R., Bovee, R. J., & Pearson, A. (2014). Protein stable isotope fingerprinting: Multidimensional protein chromatography coupled to stable isotope-ratio mass spectrometry. *Analytical Chemistry*, *86*(17), 8514–8520. <https://doi.org/10.1021/ac502494b>

- Mondino, A., & Bongiovanni, G. (1970). An experimental study of amino acid degradation under open flask hydrolytic conditions. *Journal of Chromatography*, 52, 405–413.
- Moore, S., & Stein, W. H. (1963). Chromatographic determination of amino acids by the use of automatic recording equipment. *Methods in Enzymology*, 6(100), 819–831. [https://doi.org/10.1016/0076-6879\(63\)06257-1](https://doi.org/10.1016/0076-6879(63)06257-1)
- Nakai, T., & Ohta, T. (1976). β -3-oxindolylalanine: the main intermediate in tryptophan degradation occurring in acid hydrolysis of protein. *Biochimica et Biophysica Acta*, 420, 258–264.
- Ng, L. T., Pascaud, A., & Pascaud, M. (1987). Hydrochloric acid hydrolysis of proteins and determination of tryptophan by reversed-phase high-performance liquid chromatography. *Analytical Biochemistry*, 167(1), 47–52. [https://doi.org/10.1016/0003-2697\(87\)90132-1](https://doi.org/10.1016/0003-2697(87)90132-1)
- Ohta, T., & Nakai, T. (1978). The reaction of tryptophan with cystine during acid hydrolysis of proteins. *Biochimica et Biophysica Acta*, 533, 440–445.
- Ohta, T., Suzuki, S., Todo, M., & Kurechi, T. (1981). The decomposition of tryptophan in acid solutions: specific effect of hydrochloric acid. *Chemical Pharmaceutical Bulletin*, 29(6), 1767–1771. <http://www.mendeley.com/research/geology-volcanic-history-eruptive-style-yakedake-volcano-group-central-japan/>
- Ozols, J. (1990). Amino acid analysis. *Methods in Enzymology*, 182(100), 587–601. [https://doi.org/10.1016/0076-6879\(90\)82046-5](https://doi.org/10.1016/0076-6879(90)82046-5)
- Penke, B., Ferenczi, R., & Kovács, K. (1974). A new acid hydrolysis method for determining tryptophan in peptides and proteins. *Analytical Biochemistry*, 60(1), 45–50. [https://doi.org/10.1016/0003-2697\(74\)90129-8](https://doi.org/10.1016/0003-2697(74)90129-8)
- Phillips, A., Wu, F., & Sessions, A. (2021). Compound-specific sulfur isotope analysis of cysteine and methionine via preparatory liquid chromatography and elemental analyzer isotope-ratio mass spectrometry. *Rapid Communications in Mass Spectrometry*.
- Rasmussen, C., & Hoffman, D. W. (2020). Intramolecular distribution of $^{13}\text{C}/^{12}\text{C}$ isotopes in amino acids of diverse origins. *Amino Acids*, 52, 955–964. <https://doi.org/10.1016/j.cossms.2010.07.001>
- Rees, M. W. (1946). The estimation of threonine and serine in proteins. *Biochemical Journal*, 40(5-6), 632–640. <https://doi.org/10.1042/bj0400632>
- Rieley, G. (1994). Derivatization of organic compounds prior to gas chromatographic-combustion-isotope ratio mass spectrometric analysis: identification of isotope fractionation processes. *Analyst*, 119, 915–919.
- Roach, D., & Gehrke, C. W. (1970). The hydrolysis of proteins. *Journal of Chromatography*, 52, 393–404.

- Rutherford, S. M., & Gilani, G. S. (2009). Amino acid analysis. *Current Protocols in Protein Science*, 58, 11.9.1–11.9.37. <https://doi.org/10.1002/0471140864.ps1109s58>
- Samuel, D., & Silver, B. L. (1963). Elimination reactions and hydrolysis of serine phosphate. *Journal of the Chemical Society*, 289–296.
- Sanger, F., & Thompson, E. O. (1963). Halogenation of tyrosine during acid hydrolysis. *Biochimica et Biophysica Acta*, 71(100), 468–471. [https://doi.org/10.1016/0006-3002\(63\)91108-9](https://doi.org/10.1016/0006-3002(63)91108-9)
- Savage, W. E., & Fontana, A. (1980). Oxidation of tryptophan to oxindolylalanine by dimethyl sulfoxide-hydrochloric acid. *International Journal of Peptide and Protein Research*, 15(100), 285–297. [https://doi.org/10.1016/0076-6879\(77\)47044-7](https://doi.org/10.1016/0076-6879(77)47044-7)
- Sessions, A. L., Sylva, S. P., & Hayes, J. M. (2005). Moving-wire device for carbon isotopic analyses of nanogram quantities of nonvolatile organic carbon. *Analytical Chemistry*, 77(20), 6519–6527. <https://doi.org/10.1021/ac051251z>
- Silfer, J. A., Engel, M. H., & Macko, S. A. (1992). Kinetic fractionation of stable carbon and nitrogen isotopes during peptide bond hydrolysis: experimental evidence and geochemical implications. *Chemical Geology*, 101(3-4), 211–221. [https://doi.org/10.1016/0009-2541\(92\)90003-N](https://doi.org/10.1016/0009-2541(92)90003-N)
- Silfer, J. A., Engel, M. H., Macko, S. A., & Jumeau, E. J. (1991). Stable carbon isotope analysis of amino acid enantiomers by conventional isotope ratio mass spectrometry and combined gas chromatography/isotope ratio mass spectrometry. *Analytical Chemistry*, 63(4), 370–374. <https://doi.org/10.1021/ac00004a014>
- Tsugita, A., Uchida, T., Mewes, H. W., & Ataka, T. (1987). A rapid vapor-phase acid (hydrochloric acid and trifluoroacetic acid) hydrolysis of peptide and protein. *Journal of Biochemistry*, 102, 1593–1597. <https://academic.oup.com/jb/article-abstract/102/6/1593/818176>
- Valentine, D., Sessions, A., Tyler, S., & Chidthaisong, A. (2004). Hydrogen isotope fractionation during H₂/CO₂ acetogenesis: hydrogen utilization efficiency and the origin of lipid-bound hydrogen. *Geobiology*, 2, 179–188.
- Walsh, R. G., He, S., & Yarnes, C. T. (2014). Compound-specific $\delta^{13}\text{C}$ and $\delta^{15}\text{N}$ analysis of amino acids: a rapid, chloroformate-based method for ecological studies. *Rapid Communications in Mass Spectrometry*, 28(1), 96–108. <https://doi.org/10.1002/rcm.6761>
- Whitfield, A. (1963). Steric factors in the chemistry of polypeptides, poly- α -amino acids and proteins. *Science*, 142, 577–579.

- Wright, H. T. (1991). Nonenzymatic deamidation of asparaginy and glutaminy residues in proteins. *Critical Reviews in Biochemistry and Molecular Biology*, 26(1), 1–52.
- Zhang, L., Lee, W.-m., Kreider-Mueller, A., Kuhnel, E., Baca, J., Ji, C., & Altabet, M. (2021). High-precision measurement of phenylalanine and glutamic acid $\delta^{15}\text{N}$ by coupling ion-exchange chromatography and purge-and-trap continuous-flow isotope ratio mass spectrometry. *Rapid Communications in Mass Spectrometry*, 35, e9085.

Appendix B

Supplementary material for Chapter 3

B.1 Rationale for amino acids targeted

The five amino acids investigated in this study (proline, phenylalanine, leucine, valine, and isoleucine) were selected because their hydrogen isotope compositions are among the most reliable to interpret based on preparatory and analytical considerations. These amino acids do not degrade during hydrolysis, even in the presence of oxygen (Table B.4; Silverman et al., 2022), nor do they experience hydrogen exchange with aqueous medium during hydrolysis or derivatization (Figures B.9 and B.10). Moreover, they exhibit consistent baseline chromatographic separation, and their high abundances in cells and great ionization efficiencies result in relatively intense chromatographic peaks that can be measured with reasonable precision (Figure B.1; Table B.2).

Of the remaining 15 common biological amino acids, some remain isotopically faithful through preparation, while others may not be possible to target for $\delta^2\text{H}$ analysis. A thorough review of the preparatory and analytical considerations for isotopic analysis of each amino acid is provided in Silverman et al. (2022) and briefly summarized here in the context of our methodological approach. Lysine is stable during hydrolysis and derivatizes sufficiently to an MOC methyl ester, thus is a promising target for future $\delta^2\text{H}$ analyses. Alanine and glycine are also stable during hydrolysis but co-elute on a ZB-5ms column when derivatized as MOC methyl esters; however, these amino acids can be separated when using different derivatization reactions and/or column stationary phases (e.g., Corr et al.,

2007; Walsh et al., 2014). Asparagine and glutamine quantitatively deamidate to aspartic acid and glutamic acid during hydrolysis (Wright, 1991), while the acidic amino acids and tyrosine experience moderate to significant hydrogen exchange with aqueous medium (Figure B.9; Hill and Leach, 1964), so the $\delta^2\text{H}$ values of these amino acids should be interpreted with caution. The peak shape of threonine was often problematic in our analyses (Figure B.1), potentially related to incomplete derivatization of threonine's hydroxyl group and its consequent interaction with the column stationary phase (Hušek, 1991). Histidine and serine have relatively low reaction yields when derivatized to MOC esters (Walsh et al., 2014), but the former amino acid is sometimes still accessible for analysis. Arginine is difficult to derivatize with the majority of common GC-based derivatization reactions (Silverman et al., 2022). Cysteine and methionine experience extensive oxidic degradation during hydrolysis (Phillips et al., 2021), although the mechanism of loss suggests that their hydrogen isotope ratios may not be affected (Silverman et al., 2022), which was corroborated for methionine by hydrolysis tests in this study (Table B.4). Tryptophan also degrades extensively during hydrolysis and is difficult to recover for most applications.

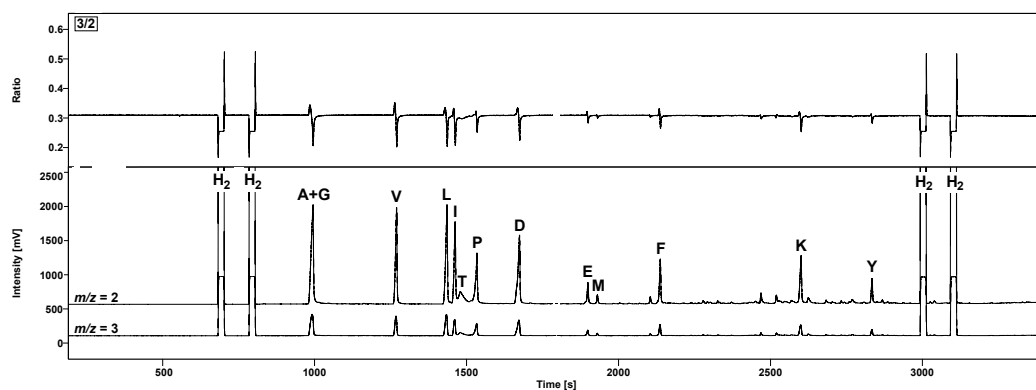


Figure B.1. Typical chromatogram and isotope ratio trace from GC/P/IRMS analysis of amino acids from microbial biomass. The conventional single-letter amino acid codes are used to label peaks. H_2 reference gas with a known isotopic composition was used to calibrate amino acid hydrogen isotope ratios.

Table B.1. Estimated net carbon fluxes of wildtype organisms and *E. coli* mutants grown on glucose, reproduced from Wijker et al. (2019). Fluxes represent reaction rates of enzymatic conversion, in $\text{mmol h}^{-1} \text{g}^{-1}$ biomass.

| Reaction | Wildtype organisms | | | | |
|--|--------------------|----------------|--------------------|-----------------------|-----------------------|
| | <i>B. subtilis</i> | <i>E. coli</i> | <i>E. meliloti</i> | <i>P. fluorescens</i> | <i>R. radiobacter</i> |
| GLU + ATP → G6P | 6.65 ± 0.09 | 8.30 ± 0.10 | 3.64 ± 0.01 | 0.48 ± 0.03 | 3.88 ± 0.02 |
| GLU → GLO | - | - | - | 4.48 ± 0.09 | - |
| GLO + ATP → 6PG | - | - | - | 3.89 ± 0.09 | - |
| GLO → 2KG → 6PG + NADPH | - | - | - | 0.58 ± 0.05 | - |
| G6P → 6PG + NADPH | 2.10 ± 0.07 | 2.40 ± 0.09 | 3.63 ± 0.02 | 0.89 ± 0.06 | 3.86 ± 0.02 |
| 6PG → Ru5P + CO ₂ + NADPH | 2.10 ± 0.07 | 1.72 ± 0.11 | 0.37 ± 0.20 | 0.38 ± 0.03 | 0.41 ± 0.18 |
| G6P → F6P | 4.36 ± 0.09 | 5.87 ± 0.12 | 0.00 ± 0.02 | -0.43 ± 0.03 | 0.00 ± 0.02 |
| 6PG → GAP + PYR | 0.00 ± 0.00 | 0.69 ± 0.12 | 3.26 ± 0.20 | 4.99 ± 0.10 | 3.45 ± 0.18 |
| F6P + ATP → 2 GAP | 5.55 ± 0.08 | 6.68 ± 0.13 | 0.04 ± 0.12 | -0.35 ± 0.02 | 0.06 ± 0.11 |
| X5P + R5P → S7P + GAP | 0.68 ± 0.02 | 0.55 ± 0.04 | 0.07 ± 0.07 | 0.11 ± 0.01 | 0.09 ± 0.06 |
| X5P + E4P → F6P + GAP | 0.51 ± 0.02 | 0.31 ± 0.04 | 0.00 ± 0.06 | 0.00 ± 0.01 | 0.00 ± 0.05 |
| S7P + GAP → E4P + F6P | 0.68 ± 0.02 | 0.55 ± 0.04 | 0.07 ± 0.07 | 0.11 ± 0.01 | 0.09 ± 0.06 |
| GAP → PGA + ATP + NADH | 11.51 ± 0.17 | 14.29 ± 0.21 | 3.31 ± 0.11 | 4.26 ± 0.09 | 3.52 ± 0.10 |
| PGA → PEP | 10.96 ± 0.17 | 13.40 ± 0.22 | 1.46 ± 0.08 | 3.72 ± 0.10 | 1.93 ± 0.08 |
| PEP → PYR + ATP | 11.95 ± 0.25 | 9.07 ± 0.76 | 0.63 ± 0.07 | 3.40 ± 0.11 | 1.20 ± 0.07 |
| PYR → AcCoA + CO ₂ + NADH | 8.19 ± 0.16 | 9.61 ± 0.29 | 2.56 ± 0.26 | 6.00 ± 0.23 | 2.89 ± 0.25 |
| OAA + AcCoA → ICT | 1.39 ± 0.15 | 2.80 ± 0.33 | 2.01 ± 0.29 | 5.18 ± 0.24 | 2.16 ± 0.29 |
| ICT → αKG + CO ₂ + NADPH | 1.39 ± 0.15 | 2.80 ± 0.33 | 2.01 ± 0.29 | 5.18 ± 0.24 | 2.16 ± 0.29 |
| αKG → FUM + CO ₂ + 1.5 ATP + 2 NADH | 0.90 ± 0.15 | 1.89 ± 0.35 | 1.75 ± 0.32 | 4.62 ± 0.26 | 1.81 ± 0.31 |
| FUM → MAL | 0.90 ± 0.15 | 1.89 ± 0.35 | 1.75 ± 0.32 | 4.62 ± 0.26 | 1.81 ± 0.31 |
| MAL → OAA + NADH | 0.66 ± 0.06 | 0.00 ± 0.58 | 1.60 ± 0.31 | 1.80 ± 0.10 | 1.71 ± 0.31 |
| MAL → PYR + CO ₂ + NADPH | 0.24 ± 0.12 | 1.89 ± 0.91 | 0.15 ± 0.05 | 2.82 ± 0.20 | 0.11 ± 0.06 |
| OAA + ATP → PEP + CO ₂ | 1.35 ± 0.14 | 0.48 ± 0.14 | 0.00 ± 0.01 | - | 0.00 ± 0.02 |
| PEP + CO ₂ → OAA | - | 4.28 ± 0.85 | - | - | - |
| PYR + ATP + CO ₂ → OAA | 2.82 ± 0.19 | - | 0.72 ± 0.11 | 4.99 ± 0.21 | 0.88 ± 0.11 |
| OAA → PYR + CO ₂ | - | - | - | 1.02 ± 0.13 | - |
| AcCoA → Acetate + ATP | 6.19 ± 0.09 | 5.39 ± 0.10 | - | - | - |
| NADH → NADPH | 0.72 ± 0.21 | 2.67 ± 0.98 | - | - | - |
| NADPH → NADH | - | - | 1.39 ± 0.36 | 0.42 ± 0.32 | 0.38 ± 0.34 |
| Respiration | 11.75 ± 0.10 | 15.42 ± 0.73 | 5.85 ± 0.58 | 12.4 ± 0.51 | 6.31 ± 0.56 |

| Reaction | <i>E. coli</i> mutant organisms | | | | |
|--|---------------------------------|-------------|--------------|--------------|--------------|
| | JW1841 | JW3985 | PntAB | UdhA | UdhA-PntAB |
| GLU + ATP → G6P | 7.97 ± 0.10 | 4.86 ± 0.10 | 7.10 ± 0.10 | 10.38 ± 0.10 | 7.16 ± 0.10 |
| GLU → GLO | - | - | - | - | - |
| GLO + ATP → 6PG | - | - | - | - | - |
| GLO → 2KG → 6PG + NADPH | - | - | - | - | - |
| G6P → 6PG + NADPH | 0.77 ± 0.10 | 4.83 ± 0.10 | 2.75 ± 0.08 | 2.70 ± 0.12 | 3.10 ± 0.08 |
| 6PG → Ru5P + CO ₂ + NADPH | 0.53 ± 0.10 | 3.05 ± 0.11 | 2.03 ± 0.09 | 1.86 ± 0.14 | 2.52 ± 0.10 |
| G6P → F6P | 7.18 ± 0.14 | 0.02 ± 0.04 | 4.33 ± 0.1 | 7.64 ± 0.14 | 4.03 ± 0.09 |
| 6PG → GAP + PYR | 0.24 ± 0.13 | 1.78 ± 0.09 | 0.71 ± 0.1 | 0.84 ± 0.16 | 0.58 ± 0.10 |
| F6P + ATP → 2 GAP | 7.33 ± 0.15 | 1.92 ± 0.07 | 5.42 ± 0.11 | 8.53 ± 0.15 | 5.46 ± 0.11 |
| X5P + R5P → S7P + GAP | 0.17 ± 0.03 | 1.01 ± 0.03 | 0.66 ± 0.03 | 0.60 ± 0.05 | 0.83 ± 0.03 |
| X5P + E4P → F6P + GAP | 0.01 ± 0.04 | 0.90 ± 0.04 | 0.45 ± 0.03 | 0.34 ± 0.05 | 0.63 ± 0.03 |
| S7P + GAP → E4P + F6P | 0.17 ± 0.03 | 1.01 ± 0.04 | 0.66 ± 0.03 | 0.60 ± 0.05 | 0.82 ± 0.03 |
| GAP → PGA + ATP + NADH | 14.88 ± 0.23 | 6.49 ± 0.15 | 11.96 ± 0.21 | 18.16 ± 0.23 | 12.10 ± 0.20 |
| PGA → PEP | 14.31 ± 0.24 | 6.11 ± 0.16 | 11.10 ± 0.21 | 17.20 ± 0.24 | 11.40 ± 0.21 |
| PEP → PYR + ATP | 9.81 ± 0.86 | 1.18 ± 0.45 | 7.71 ± 2.32 | 11.48 ± 0.85 | 8.44 ± 1.04 |
| PYR → AcCoA + CO ₂ + NADH | 11.57 ± 0.30 | 5.96 ± 0.30 | 6.53 ± 0.30 | 12.99 ± 0.29 | 8.36 ± 0.29 |
| OAA + AcCoA → ICT | 3.50 ± 0.34 | 4.28 ± 0.34 | 1.86 ± 0.34 | 4.02 ± 0.33 | 1.75 ± 0.33 |
| ICT → αKG + CO ₂ + NADPH | 3.50 ± 0.34 | 4.28 ± 0.34 | 1.86 ± 0.34 | 4.02 ± 0.33 | 1.75 ± 0.33 |
| αKG → FUM + CO ₂ + 1.5 ATP + 2 NADH | 2.88 ± 0.36 | 3.88 ± 0.36 | 0.71 ± 0.36 | 2.98 ± 0.36 | 1.01 ± 0.36 |
| FUM → MAL | 2.88 ± 0.36 | 3.88 ± 0.36 | 0.71 ± 0.36 | 2.98 ± 0.36 | 1.01 ± 0.36 |
| MAL → OAA + NADH | 0.00 ± 0.68 | 0.00 ± 0.27 | 0.00 ± 2.14 | 0.00 ± 0.67 | 0.00 ± 0.85 |
| MAL → PYR + CO ₂ + NADPH | 2.88 ± 1.00 | 3.88 ± 0.56 | 0.71 ± 2.49 | 2.98 ± 0.98 | 1.01 ± 1.19 |
| OAA + ATP → PEP + CO ₂ | 2.48 ± 0.20 | 0.19 ± 0.07 | 0.67 ± 0.12 | 1.00 ± 0.19 | 0.53 ± 0.12 |
| PEP + CO ₂ → OAA | 6.64 ± 0.95 | 4.90 ± 0.50 | 3.59 ± 2.44 | 6.15 ± 0.93 | 3.08 ± 1.14 |
| PYR + ATP + CO ₂ → OAA | - | - | - | - | - |
| OAA → PYR + CO ₂ | - | - | - | - | - |
| AcCoA → Acetate + ATP | 7.16 ± 0.10 | 1.09 ± 0.10 | 3.15 ± 0.10 | 7.40 ± 0.10 | 5.50 ± 0.10 |
| NADH → NADPH | 1.21 ± 1.07 | - | 0.54 ± 2.52 | 1.44 ± 1.06 | - |
| NADPH → NADH | - | 7.97 ± 0.67 | - | - | 0.02 ± 1.25 |
| Respiration | 17.92 ± 0.75 | 12.3 ± 0.72 | 10.77 ± 0.73 | 20.71 ± 0.73 | 12.21 ± 0.73 |

- indicates an absent reaction

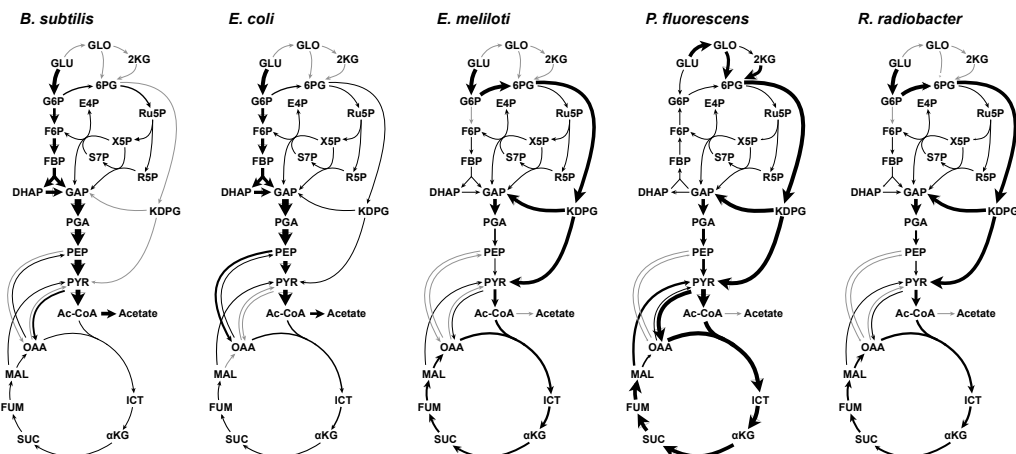


Figure B.3. Visual summary of ^{13}C -based metabolic fluxes in wildtype organisms grown on glucose. Sizes of arrows in flux maps scale with relative flux magnitudes (normalized to organism-specific glucose uptake rates). Flux data is summarized in Table B.1.

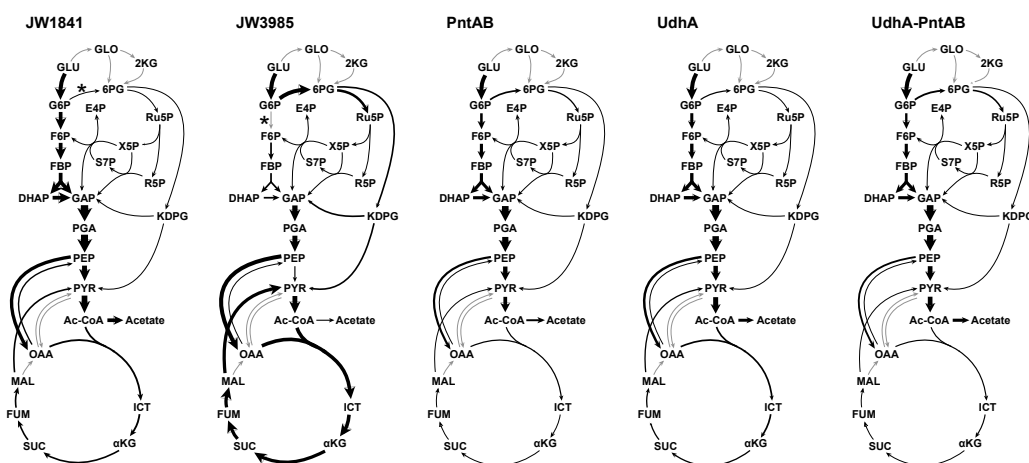


Figure B.4. Visual summary of ^{13}C -based metabolic fluxes in *E. coli* mutant organisms grown on glucose lacking certain dehydrogenase or transhydrogenase genes (glucose 6-phosphate dehydrogenase was deleted in JW1841, phosphoglucose isomerase in JW3985, membrane- bound transhydrogenase in PntAB, soluble transhydrogenase in UdhA, and both transhydrogenases in UdhA-PntAB). The * marks deleted genes in JW1841 and JW3985. Sizes of arrows in flux maps scale with relative flux magnitudes (normalized to organism-specific glucose uptake rates). Flux data is summarized in Table B.1.

B.3 Amino acid $\delta^2\text{H}$ values

Table B.2. Growth rates and measured $\delta^2\text{H}$ values of amino acids (AA), substrates (s), and culture media (w) for each growth condition. Amino acids included are those whose isotopic compositions are discussed in the main text.

| Culture | Substrate | Rep. ¹ | μ (h ⁻¹) ² | $\delta^2\text{H}_s$ (‰) ³ | $\delta^2\text{H}_w \pm \sigma$ (‰) | $\delta^2\text{H}_{\text{AA}} \pm \sigma$ (‰) | | | | | |
|---------------------------|-----------------------|-------------------|---------------------------------------|---------------------------------------|-------------------------------------|---|---------------|-----------|-----------|------------|-----------|
| | | | | | | Proline | Phenylalanine | Leucine | Valine | Isoleucine | |
| Wildtype organisms | | | | | | | | | | | |
| <i>B. subtilis</i> | glucose | 1 | 0.38 | - | -90 ± 0 | -96 ± 2 | -134 ± 5 | -181 ± 3 | -200 ± 4 | -289 ± 2 | |
| | glucose | 2 | - | -60 | -87 ± 0 | -116 ± 2 | -105 ± 16 | -166 ± 9 | -192 ± 10 | -295 ± 9 | |
| | pyruvate | 1 | 0.13 | -12 | -86 ± 0 | 40 ± 2 | -127 ± 6 | -111 ± 3 | -109 ± 7 | -202 ± 6 | |
| | pyruvate | 2 | 0.11 | -12 | -86 ± 0 | 34 ± 2 | -108 ± 7 | -110 ± 3 | -103 ± 10 | -198 ± 8 | |
| | succinate | 1 | 0.09 | -97 | -88 ± 0 | 211 ± 4 | -81 ± 3 | -76 ± 3 | -69 ± 4 | -175 ± 3 | |
| | succinate | 2 | 0.08 | -97 | -88 ± 0 | 113 ± 8 | -120 ± 5 | -70 ± 6 | -70 ± 4 | -193 ± 10 | |
| <i>E. coli</i> | acetate | 1 | - | -76 | -91 ± 1 | 44 ± 5 | -47 ± 3 | -121 ± 2 | -129 ± 3 | -271 ± 8 | |
| | glucose | 1 | 0.57 | - | -88 ± 1 | -90 ± 3 | -88 ± 4 | -213 ± 5 | -243 ± 7 | -392 ± 1 | |
| | glucose | 2 | 0.58 | -60 | -80 ± 0 | -147 ± 2 | -123 ± 2 | -244 ± 4 | -295 ± 1 | -397 ± 7 | |
| | pyruvate | 1 | - | -12 | -91 ± 1 | -27 ± 10 | -102 ± 5 | -165 ± 6 | -175 ± 7 | -325 ± 4 | |
| <i>E. meliloti</i> | acetate | 1 | - | -76 | -76 ± 1 | -4 ± 2 | -12 ± 2 | -93 ± 1 | -175 ± 1 | -193 ± 2 | |
| | acetate | 2 | - | -76 | -76 ± 1 | -6 ± 10 | 1 ± 6 | -88 ± 2 | -174 ± 13 | -199 ± 10 | |
| | fructose | 1 | - | -22 | -85 ± 1 | -123 ± 8 | -78 ± 4 | -222 ± 5 | -324 ± 18 | -284 ± 14 | |
| | fructose | 2 | - | -22 | -85 ± 1 | -120 ± 6 | -67 ± 15 | -218 ± 3 | -321 ± 4 | -282 ± 13 | |
| | glucose | 1 | 0.17 | - | -76 ± 1 | -109 ± 3 | -83 ± 4 | -237 ± 1 | -356 ± 3 | -291 ± 2 | |
| | glucose | 2 | - | -60 | -83 ± 1 | -135 ± 23 | -64 ± 7 | -227 ± 11 | -357 ± 14 | -307 ± 17 | |
| | pyruvate | 1 | - | -12 | -77 ± 0 | -28 ± 4 | -50 ± 10 | -80 ± 3 | -156 ± 11 | -157 ± 4 | |
| | pyruvate | 2 | - | -12 | -77 ± 0 | -36 ± 9 | -51 ± 3 | -86 ± 2 | -153 ± 5 | -157 ± 5 | |
| | succinate | 1 | - | -97 | -83 ± 0 | -60 ± 2 | -54 ± 4 | -87 ± 2 | -166 ± 11 | -165 ± 5 | |
| | succinate | 2 | - | -97 | -83 ± 0 | -32 ± 6 | -44 ± 3 | -81 ± 8 | -154 ± 8 | -155 ± 5 | |
| <i>P. fluorescens</i> | acetate | 1 | - | -76 | -87 ± 0 | 15 ± 3 | 166 ± 7 | -73 ± 2 | -111 ± 3 | -30 ± 2 | |
| | acetate | 2 | - | -76 | -87 ± 1 | 35 ± 9 | 178 ± 11 | -55 ± 3 | -96 ± 5 | -61 ± 10 | |
| | citrate | 1 | 0.52 | - | -88 ± 0 | -65 ± 12 | 43 ± 9 | -92 ± 6 | -136 ± 11 | -192 ± 7 | |
| | citrate | 2 | 0.53 | - | -88 ± 0 | -66 ± 13 | 23 ± 17 | -102 ± 10 | -144 ± 10 | -177 ± 8 | |
| | fructose | 1 | 0.28 | -22 | -87 ± 0 | -70 ± 5 | -40 ± 10 | -195 ± 2 | -269 ± 5 | -299 ± 6 | |
| | fructose | 2 | 0.28 | -22 | -87 ± 0 | -54 ± 8 | -43 ± 3 | -198 ± 3 | -269 ± 7 | -307 ± 8 | |
| | glucose | 1 | 0.31 | - | -82 ± 0 | -90 ± 4 | -103 ± 6 | -227 ± 3 | -308 ± 4 | -287 ± 1 | |
| | glucose | 2 | - | -60 | -88 ± 1 | -77 ± 2 | -53 ± 1 | -225 ± 14 | -321 ± 28 | -252 ± 3 | |
| | pyruvate | 1 | 0.38 | -12 | -87 ± 0 | -6 ± 3 | -38 ± 7 | -136 ± 4 | -185 ± 9 | -182 ± 9 | |
| | pyruvate | 2 | 0.42 | -12 | -87 ± 0 | 9 ± 5 | -31 ± 3 | -126 ± 3 | -170 ± 10 | -171 ± 4 | |
| | succinate | 1 | 0.46 | -97 | -86 ± 0 | 84 ± 4 | 39 ± 9 | -72 ± 3 | -104 ± 10 | -72 ± 3 | |
| | succinate | 2 | 0.45 | -97 | -86 ± 0 | 77 ± 3 | 46 ± 11 | -75 ± 8 | -113 ± 8 | -81 ± 2 | |
| | <i>R. radiobacter</i> | acetate | 1 | - | -76 | -89 ± 1 | 29 ± 3 | 14 ± 3 | -115 ± 1 | -183 ± 4 | -232 ± 1 |
| | | acetate | 2 | - | -76 | -89 ± 1 | 19 ± 6 | 22 ± 11 | -117 ± 3 | -178 ± 21 | -214 ± 11 |
| fructose | | 1 | - | -22 | -88 ± 1 | -87 ± 11 | -14 ± 18 | -242 ± 2 | -327 ± 14 | -318 ± 10 | |
| fructose | | 2 | - | -22 | -88 ± 1 | -86 ± 11 | -32 ± 10 | -250 ± 2 | -337 ± 7 | -309 ± 12 | |
| glucose | | 1 | 0.3 | - | -82 ± 1 | -72 ± 3 | -40 ± 3 | -246 ± 1 | -338 ± 1 | -318 ± 2 | |
| glucose | | 2 | - | -60 | -90 ± 0 | -92 ± 3 | -33 ± 7 | -242 ± 12 | -353 ± 10 | -340 ± 1 | |
| pyruvate | | 1 | - | -12 | -87 ± 1 | -10 ± 5 | -15 ± 4 | -128 ± 4 | -183 ± 3 | -209 ± 4 | |
| pyruvate | | 2 | - | -12 | -88 ± 1 | 3 ± 2 | -26 ± 6 | -131 ± 6 | -185 ± 13 | -209 ± 4 | |
| succinate | | 1 | - | -97 | -85 ± 0 | -48 ± 6 | -41 ± 11 | -118 ± 9 | -174 ± 13 | -219 ± 9 | |
| succinate | | 2 | - | -97 | -87 ± 0 | -13 ± 4 | -45 ± 8 | -119 ± 10 | -170 ± 10 | -216 ± 9 | |

| <i>E. coli</i> knockout mutants | | | | | | | | | | |
|--|---------|---|------|-----|---------|-----------|-----------|-----------|-----------|-----------|
| JW1841 | glucose | 1 | 0.34 | - | -84 ± 2 | -108 ± 3 | -84 ± 3 | -219 ± 4 | -252 ± 5 | -384 ± 2 |
| JW3985 | glucose | 1 | 0.24 | - | -85 ± 1 | -78 ± 3 | -75 ± 3 | -224 ± 2 | -246 ± 6 | -378 ± 2 |
| PntAB | glucose | 1 | 0.33 | - | -74 ± 1 | -69 ± 5 | -63 ± 3 | -201 ± 3 | -238 ± 3 | -363 ± 4 |
| UdhA | glucose | 1 | 0.58 | - | -90 ± 2 | -103 ± 4 | -91 ± 4 | -220 ± 1 | -256 ± 2 | -389 ± 1 |
| UdhA-PntAB | glucose | 1 | 0.42 | - | -90 ± 2 | -92 ± 8 | -72 ± 6 | -212 ± 1 | -247 ± 7 | -378 ± 1 |
| Growth water experiments | | | | | | | | | | |
| <i>B. subtilis</i> | glucose | 2 | - | -60 | -87 ± 0 | -116 ± 2 | -105 ± 16 | -166 ± 9 | -192 ± 10 | -295 ± 9 |
| | | 1 | - | -60 | 194 ± 1 | 55 ± 6 | 12 ± 6 | -37 ± 6 | -94 ± 7 | -173 ± 3 |
| | | 1 | - | -60 | 448 ± 1 | 224 ± 23 | 76 ± 10 | 99 ± 10 | 7 ± 21 | -68 ± 4 |
| | | 1 | - | -60 | 618 ± 1 | 329 ± 6 | 127 ± 2 | 173 ± 1 | 74 ± 11 | 23 ± 6 |
| | | 1 | - | -60 | 911 ± 0 | 497 ± 1 | 226 ± 3 | 296 ± 2 | 159 ± 1 | 152 ± 28 |
| <i>E. coli</i> | glucose | 2 | 0.58 | -60 | -80 ± 0 | -147 ± 2 | -123 ± 2 | -244 ± 4 | -295 ± 1 | -397 ± 7 |
| | | 1 | 0.59 | -60 | 128 ± 0 | -11 ± 8 | -28 ± 1 | -142 ± 7 | -218 ± 2 | -318 ± 2 |
| | | 1 | 0.60 | -60 | 337 ± 0 | 104 ± 8 | 35 ± 2 | -65 ± 8 | -132 ± 8 | -232 ± 2 |
| | | 1 | 0.59 | -60 | 545 ± 0 | 244 ± 3 | 101 ± 2 | 42 ± 3 | -71 ± 4 | -151 ± 8 |
| <i>E. meliloti</i> | glucose | 2 | - | -60 | -83 ± 1 | -135 ± 23 | -64 ± 7 | -227 ± 11 | -357 ± 14 | -307 ± 17 |
| | | 1 | - | -60 | 111 ± 2 | 10 ± 12 | -7 ± 5 | -133 ± 6 | -289 ± 17 | -207 ± 8 |
| | | 1 | - | -60 | 248 ± 1 | 111 ± 3 | 46 ± 6 | -48 ± 8 | -233 ± 20 | -117 ± 17 |
| | | 1 | - | -60 | 405 ± 1 | 246 ± 12 | 106 ± 14 | 36 ± 5 | -168 ± 1 | -62 ± 5 |
| | | 1 | - | -60 | 544 ± 1 | 337 ± 12 | 146 ± 8 | 121 ± 8 | -103 ± 21 | 36 ± 24 |
| <i>P. fluorescens</i> | glucose | 2 | - | -60 | -88 ± 1 | -77 ± 2 | -53 ± 1 | -225 ± 14 | -321 ± 28 | -252 ± 3 |
| | | 1 | - | -60 | 319 ± 1 | 268 ± 15 | 102 ± 9 | 27 ± 16 | -103 ± 22 | -21 ± 2 |
| | | 1 | - | -60 | 643 ± 1 | 521 ± 14 | 297 ± 14 | 244 ± 3 | 84 ± 9 | 198 ± 11 |
| <i>R. radiobacter</i> | glucose | 1 | - | -60 | 868 ± 1 | 654 ± 5 | 367 ± 11 | 375 ± 4 | 223 ± 3 | 326 ± 5 |
| | | 2 | - | -60 | -90 ± 0 | -92 ± 3 | -33 ± 7 | -242 ± 12 | -353 ± 10 | -340 ± 1 |
| | | 1 | - | -60 | 100 ± 1 | 50 ± 6 | 42 ± 3 | -151 ± 9 | -293 ± 11 | -247 ± 11 |
| | | 1 | - | -60 | 253 ± 0 | 165 ± 8 | 92 ± 2 | -67 ± 12 | -231 ± 15 | -179 ± 12 |
| | | 1 | - | -60 | 497 ± 0 | 279 ± 5 | 151 ± 5 | 11 ± 6 | -170 ± 5 | -118 ± 10 |
| | | 1 | - | -60 | 632 ± 2 | 391 ± 3 | 243 ± 11 | 87 ± 2 | -117 ± 3 | -39 ± 22 |

¹Biological replicates are designated as 1 and 2. Data for the most ²H-depleted growth water condition for each organism are included as the second glucose replicate within the 'Wildtype organisms' conditions. Note that *E. coli* was cultured on glucose in two different experiments, so these cultures are not biological replicates (see Section 3.2.1 in the main text).

²Blank entries (-) indicate growth rate was not measured.

³Entries with isotopic compositions are the same substrates used and measured by Zhang et al. (2009). Uncertainties are likely <20%. Blank entries (-) indicate substrate isotopic composition was not measured.

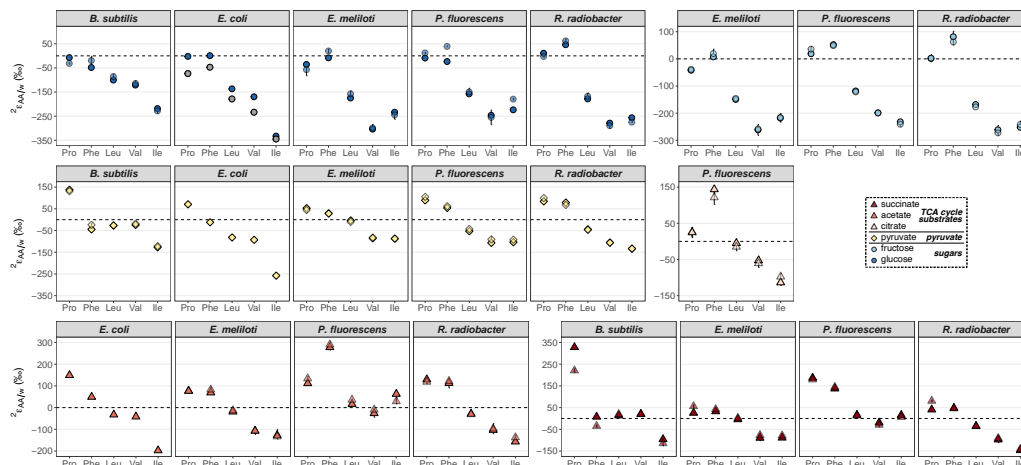


Figure B.5. $^2\text{H}/^1\text{H}$ fractionations between amino acids and water in from biological replicates of wildtype organisms grown on different carbon substrates. Data for replicate 1 are denoted with opaque symbols, and with transparent symbols for replicate 2. Error bars indicate the propagated uncertainties ($\pm 1\sigma$) from the amino acid, derivative, and water $\delta^2\text{H}$ measurements, and in most cases are smaller than symbols. Note that *E. coli* was cultured on glucose in two different experiments, and the amino acids were derivatized via different reaction conditions, so these cultures are not biological replicates and are distinguished as blue (culture 1) and gray (culture 2) symbols (see Section 3.2.1 in the main text for details).

Table B.3. $\delta^2\text{H}$ values of amino acids (AA) that were not discussed in the main text. See Table B.2 for growth rates and $\delta^2\text{H}$ values of substrates and water in each culture.

| Culture | Substrate | Rep. ¹ | $\delta^2\text{H}_w \pm \sigma$ (‰) | $\delta^2\text{H}_{\text{AA}} \pm \sigma$ (‰) ² | | | | | | |
|---------------------------|-----------|-------------------|-------------------------------------|--|------------------------------|-----------------------------|-----------|------------|-----------|-----------|
| | | | | Alanine + Glycine | Aspartic acid (+ Asparagine) | Glutamic acid (+ Glutamine) | Lysine | Methionine | Threonine | Tyrosine |
| Wildtype organisms | | | | | | | | | | |
| <i>B. subtilis</i> | glucose | 1 | -90 ± 0 | -177 ± 9 | -52 ± 29 | -45 ± 5 | - | -136 ± 3 | - | - |
| | glucose | 2 | -87 ± 0 | -178 ± 43 | -62 ± 5 | -49 ± 2 | -126 ± 28 | 23 | - | - |
| | pyruvate | 1 | -86 ± 0 | -111 ± 10 | -6 ± 27 | 23 ± 24 | -77 ± 18 | -100 ± 46 | - | -85 ± 38 |
| | pyruvate | 2 | -86 ± 0 | -104 ± 7 | -15 ± 31 | 14 ± 8 | -73 ± 8 | - | - | -65 ± 25 |
| | succinate | 1 | -88 ± 0 | -56 ± 9 | 72 ± 9 | 22 ± 8 | - | -54 ± 6 | -24 ± 22 | - |
| | succinate | 2 | -88 ± 0 | -91 ± 11 | -1 ± 14 | -39 ± 24 | -69 ± 13 | - | - | -48 ± 42 |
| <i>E. coli</i> | acetate | 1 | -91 ± 1 | -146 ± 7 | 41 ± 10 | 8 ± 3 | - | -10 ± 1 | - | - |
| | glucose | 1 | -88 ± 1 | -237 ± 5 | -41 ± 9 | -48 ± 18 | -143 ± 4 | -157 ± 15 | -267 | -104 ± 13 |
| | glucose | 2 | -80 ± 0 | -394 ± 6 | -198 ± 9 | - | - | - | - | - |
| <i>E. meliloti</i> | pyruvate | 1 | -91 ± 1 | -172 ± 7 | -36 ± 16 | -25 ± 30 | -100 ± 8 | -101 ± 45 | -112 | -123 ± 17 |
| | acetate | 1 | -76 ± 1 | -128 ± 44 | 51 ± 5 | 25 ± 8 | -25 ± 3 | 40 ± 18 | 53 ± 64 | - |
| | acetate | 2 | -76 ± 1 | -133 ± 39 | 60 ± 16 | 24 ± 25 | -29 ± 11 | 11 ± 28 | 212 ± 118 | - |
| | fructose | 1 | -85 ± 1 | -225 ± 69 | -12 ± 6 | -44 ± 3 | -109 ± 12 | -40 ± 8 | - | - |
| | fructose | 2 | -85 ± 1 | -238 ± 69 | -22 ± 17 | -55 ± 10 | -106 ± 25 | - | -99 | - |
| | glucose | 1 | -76 ± 1 | -240 ± 15 | -6 ± 7 | -44 ± 8 | - | - | 13 ± 4 | - |
| | glucose | 2 | -83 ± 1 | -237 ± 43 | -31 ± 10 | -24 ± 10 | -117 ± 16 | -28 ± 10 | - | - |
| | pyruvate | 1 | -77 ± 0 | -108 ± 6 | 4 ± 5 | -9 ± 15 | -55 ± 8 | -64 ± 47 | - | -73 ± 43 |
| | pyruvate | 2 | -77 ± 0 | -106 ± 7 | -8 ± 11 | 9 ± 46 | -60 ± 12 | -76 ± 55 | -82 | -52 ± 17 |
| | succinate | 1 | -83 ± 0 | -139 ± 8 | 2 ± 11 | -31 ± 23 | -68 ± 4 | -96 ± 21 | - | -73 ± 13 |
| <i>P. fluorescens</i> | succinate | 2 | -83 ± 0 | -131 ± 18 | -6 ± 22 | -5 ± 39 | -71 ± 9 | - | - | -48 ± 30 |
| | acetate | 1 | -87 ± 0 | -176 ± 3 | 46 ± 11 | 13 ± 14 | 114 ± 5 | 250 ± 31 | - | - |
| | acetate | 2 | -87 ± 1 | -176 ± 50 | 34 ± 17 | 13 ± 14 | 114 ± 7 | 211 ± 42 | - | - |
| | citrate | 1 | -88 ± 0 | -213 ± 51 | 73 ± 4 | 4 ± 14 | 1 ± 11 | 95 ± 3 | - | - |
| | citrate | 2 | -88 ± 0 | -213 ± 65 | 63 ± 5 | -13 ± 7 | -3 ± 11 | - | - | - |
| | fructose | 1 | -87 ± 0 | -290 ± 75 | -24 ± 6 | -13 ± 5 | -41 ± 18 | 6 ± 8 | 94 | - |
| | fructose | 2 | -87 ± 0 | -290 ± 83 | -18 ± 14 | -32 ± 20 | -52 ± 8 | - | - | - |
| | glucose | 1 | -82 ± 0 | -257 ± 4 | -57 ± 3 | -28 ± 17 | - | - | - | - |
| | glucose | 2 | -88 ± 1 | -281 ± 39 | -55 ± 20 | -41 ± 3 | -61 ± 20 | 38 ± 20 | - | - |
| | pyruvate | 1 | -87 ± 0 | -233 ± 9 | -13 ± 29 | -7 ± 20 | -11 ± 16 | - | - | -35 ± 18 |
| <i>R. radiobacter</i> | pyruvate | 2 | -87 ± 0 | -230 ± 10 | 20 ± 19 | -17 ± 23 | -2 ± 13 | - | - | -59 ± 28 |
| | succinate | 1 | -86 ± 0 | -195 ± 7 | 19 ± 23 | 8 ± 35 | 64 ± 4 | 136 ± 84 | - | -2 ± 14 |
| | succinate | 2 | -86 ± 0 | -201 ± 7 | 11 ± 24 | 21 ± 38 | 38 ± 11 | - | - | -3 ± 13 |
| | acetate | 1 | -89 ± 1 | -145 ± 16 | 41 ± 6 | 49 ± 3 | -47 ± 21 | -13 ± 4 | -72 ± 7 | - |
| | acetate | 2 | -89 ± 1 | -141 ± 36 | 55 ± 4 | 37 ± 36 | -51 ± 17 | 45 ± 29 | 110 ± 58 | - |
| | fructose | 1 | -88 ± 1 | -222 ± 44 | -40 ± 6 | -19 ± 15 | -105 ± 11 | -45 ± 33 | 112 ± 72 | - |
| | fructose | 2 | -88 ± 1 | -224 ± 35 | -51 ± 11 | -26 ± 20 | -130 ± 6 | -63 ± 70 | -58 ± 97 | - |
| | glucose | 1 | -82 ± 1 | -225 ± 8 | -60 ± 5 | -29 ± 12 | - | - | -119 ± 7 | - |
| | glucose | 2 | -90 ± 0 | -143 ± 14 | -13 ± 21 | 69 ± 8 | -39 ± 2 | 56 ± 5 | - | - |
| | pyruvate | 1 | -87 ± 1 | -139 ± 16 | -45 ± 4 | -22 ± 58 | -72 ± 7 | -15 ± 39 | 253 | -75 ± 9 |
| | pyruvate | 2 | -88 ± 1 | -152 ± 16 | -25 ± 18 | 19 ± 10 | -63 ± 20 | - | - | -30 ± 50 |
| | succinate | 1 | -85 ± 0 | -159 ± 17 | -18 ± 33 | -3 ± 60 | -71 ± 14 | -56 ± 45 | - | -64 ± 14 |
| | succinate | 2 | -87 ± 0 | -156 ± 11 | -22 ± 18 | 34 ± 25 | -86 ± 5 | -45 ± 7 | - | -56 ± 40 |

| <i>E. coli</i> knockout mutants | | | | | | | | | | |
|--|---------|---|---------|-----------|----------|----------|-----------|-----------|-----------|---|
| JW1841 | glucose | 1 | -84 ± 2 | -232 ± 9 | -45 ± 10 | -49 ± 8 | - | - | - | - |
| JW3985 | glucose | 1 | -85 ± 1 | -244 ± 11 | -44 ± 6 | -52 ± 7 | - | - | - | - |
| PntAB | glucose | 1 | -74 ± 1 | -196 ± 12 | -53 ± 6 | -20 ± 7 | - | -127 | -147 ± 47 | - |
| UdhA | glucose | 1 | -90 ± 2 | -237 ± 5 | -55 ± 4 | -51 ± 6 | - | - | -216 | - |
| UdhA-PntAB | glucose | 1 | -90 ± 2 | -223 ± 6 | -62 ± 3 | -51 ± 10 | - | -150 ± 13 | -162 ± 28 | - |
| Growth water experiments | | | | | | | | | | |
| <i>B. subtilis</i> | glucose | 2 | -87 ± 0 | -178 ± 43 | -62 ± 5 | -49 ± 2 | -126 ± 28 | 23 | - | - |
| | | 1 | 194 ± 1 | -25 ± 66 | 67 ± 14 | 82 ± 13 | -14 ± 5 | 9 ± 40 | - | - |
| | | 1 | 448 ± 1 | 80 ± 96 | 138 ± 3 | 217 ± 15 | 103 ± 7 | 177 ± 37 | - | - |
| | | 1 | 618 ± 1 | 116 ± 133 | 204 ± 19 | 228 ± 16 | 191 ± 2 | - | - | - |
| | | 1 | 911 ± 0 | 244 ± 91 | 301 ± 7 | 393 ± 17 | 317 ± 7 | 338 ± 37 | - | - |
| <i>E. coli</i> | glucose | 2 | -80 ± 0 | -394 ± 6 | -198 ± 9 | - | - | - | - | - |
| | | 1 | 128 ± 0 | -272 ± 6 | -90 ± 3 | - | - | - | - | - |
| | | 1 | 337 ± 0 | -141 ± 10 | 15 ± 6 | - | - | - | - | - |
| | | 1 | 545 ± 0 | -21 ± 3 | 94 ± 8 | - | - | - | - | - |
| <i>E. meliloti</i> | glucose | 2 | -83 ± 1 | -237 ± 43 | -31 ± 10 | -24 ± 10 | -117 ± 16 | -28 ± 10 | - | - |
| | | 1 | 111 ± 2 | -130 ± 30 | 27 ± 15 | 56 ± 32 | -21 ± 8 | 67 ± 11 | 219 ± 187 | - |
| | | 1 | 248 ± 1 | -50 ± 44 | 100 ± 8 | 127 ± 25 | 71 ± 13 | 150 ± 26 | 361 | - |
| | | 1 | 405 ± 1 | 46 ± 48 | 163 ± 3 | 172 ± 12 | 129 ± 1 | 210 ± 28 | 307 | - |
| | | 1 | 544 ± 1 | 86 ± 74 | 219 ± 34 | 255 ± 12 | 228 ± 5 | 295 ± 44 | - | - |
| <i>P. fluorescens</i> | glucose | 2 | -88 ± 1 | -281 ± 39 | -55 ± 20 | -41 ± 3 | -61 ± 20 | 38 ± 20 | - | - |
| | | 1 | 319 ± 1 | -70 ± 47 | 103 ± 49 | 136 ± 11 | 169 ± 8 | 261 ± 32 | - | - |
| | | 1 | 643 ± 1 | 117 ± 75 | 209 ± 45 | 337 ± 51 | 397 ± 9 | 444 ± 2 | - | - |
| | | 1 | 868 ± 1 | 234 ± 204 | 354 ± 36 | 427 ± 9 | 436 ± 24 | - | - | - |
| <i>R. radiobacter</i> | glucose | 2 | -90 ± 0 | -143 ± 14 | -13 ± 21 | 69 ± 8 | -39 ± 2 | 56 ± 5 | - | - |
| | | 1 | 100 ± 1 | -73 ± 38 | 68 ± 11 | 143 ± 24 | 33 ± 5 | 81 ± 35 | 103 | - |
| | | 1 | 253 ± 0 | -3 ± 56 | 108 ± 32 | 201 ± 21 | 115 ± 3 | - | - | - |
| | | 1 | 497 ± 0 | 110 ± 82 | 159 ± 11 | 278 ± 10 | 180 ± 4 | 279 ± 12 | 674 ± 3 | - |
| | | 1 | 632 ± 2 | -178 ± 43 | -62 ± 5 | -49 ± 2 | -126 ± 28 | 23 | - | - |

¹Biological replicates are designated as 1 and 2. Data for the most ²H-depleted growth water condition for each organism are included as the second glucose replicate within the 'Wildtype organisms' conditions. Note that *E. coli* was cultured on glucose in two different experiments, so these cultures are not biological replicates (see Section 3.2.1 in the main text).

² $\delta^2\text{H}_{\text{AA}}$ values for which no errors are reported were measured in only one of three analytical replicates.

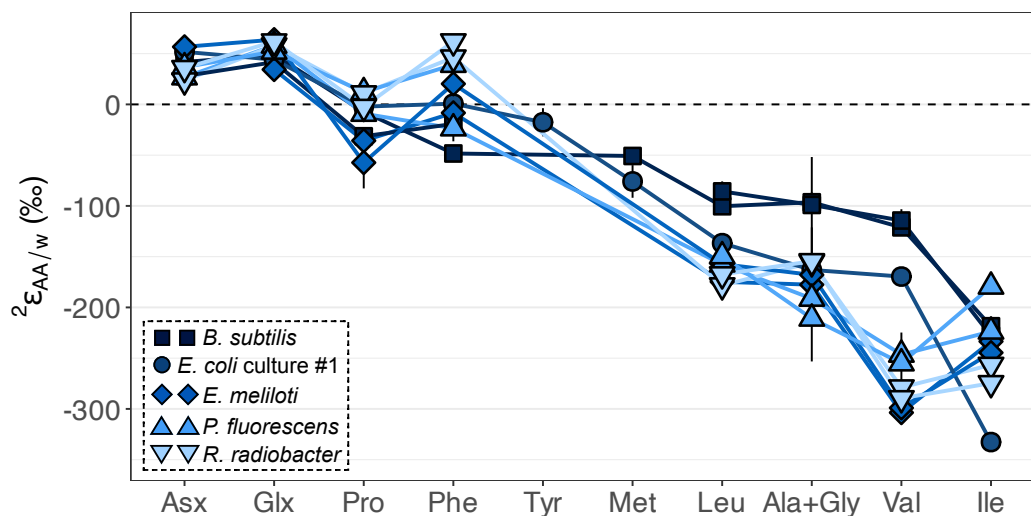


Figure B.6. Summary of $^2\text{H}/^1\text{H}$ fractionations between amino acids and water in replicate cultures of wildtype organisms grown on glucose (except for *E. coli*, for which only data from culture 1 is plotted). Error bars indicate the propagated uncertainties ($\pm 1\sigma$) from the amino acid, derivative, and water $\delta^2\text{H}$ measurements. One $\delta^2\text{H}$ value is given for alanine + glycine because these amino acids co-elute on a ZB-5ms column when derivatized as MOC methyl esters (Figure B.1).

B.4 Error associated with improper $\delta^2\text{H}$ corrections for N-bound hydrogen in amino acids

Amine-, hydroxyl-, and carboxyl-bound hydrogen atoms rapidly exchange with water so do not contribute isotopic information about 'native' (i.e., non-exchangeable, carbon-bound) hydrogen. Derivatization of these functional groups removes all but one exchangeable hydrogen atom, which remains on the amine group and can dilute or obscure native $\delta^2\text{H}_{\text{AA}}$ values. Contribution by this remaining N-bound hydrogen to measured $\delta^2\text{H}_{\text{AA}}$ values must therefore be corrected (in addition to corrections for exogenous hydrogen from derivative reagents). Here, we calculate possible errors (α_{error}) arising from improper correction for the amine hydrogen in two scenarios, with results for a range of $\delta^2\text{H}_{\text{AA}}$ values and equilibrium fractiona-

tions between NH-containing compounds and water (Bigeleisen, 1965; Englander & Poulsen, 1969) visualized in Figure B.7:

Scenario 1: Measured $\delta^2\text{H}_{\text{AA}}$ values are corrected for the derivative hydrogen, but not for the amine-bound hydrogen, thus $F_{\text{CH+NH}}$ is reported:

$$F_{\text{tot}} = X_{\text{CH}}F_{\text{CH}} + X_{\text{NH}}F_{\text{NH}} + X_{\text{dH}}F_{\text{dH}} \quad (\text{B.1})$$

$$\text{where } R_{\text{NH}} = R_w \alpha_{\text{NH/w}}$$

$$F_{\text{CH+NH}} = (F_{\text{tot}} - X_{\text{dH}}F_{\text{dH}})/(X_{\text{CH}} + X_{\text{NH}})$$

$$\alpha_{\text{error}} = R_{\text{CH+NH}}/R_{\text{CH}}$$

where F and X are the respective mole fractions of ^2H in, and hydrogen from, the component in the derivatized amino acid represented by the subscript: C-bound hydrogen (CH); N-bound hydrogen (NH); derivative hydrogen (dH); combined C-bound and N-bound hydrogen (CH+NH); and total hydrogen, including CH, NH, and dH (tot). R is the $^2\text{H}/^1\text{H}$ ratio (R_w is that of water), and $\alpha_{\text{NH/w}}$ is the equilibrium fractionation between the N-bound hydrogen and water. Conversion between F and R is achieved via $F = R/(1 + R)$ and $R = F/(1 - F)$. In general, F_{CH} is the parameter to isolate when correcting $\delta^2\text{H}_{\text{AA}}$ values because it exclusively encompasses non-exchangeable, carbon-bound hydrogen. However, in Scenario 1, $F_{\text{CH+NH}}$ is reported because F_{NH} is not accounted for.

Scenario 2: A correction is applied with the erroneous approximation that $F_{\text{NH}} = F_w$ (i.e., the isotope composition of the N-bound hydrogen equals that of water):

$$F_{CH.corr} = (F_{tot} - X_{NH}F_w - X_{dH}F_{dH})/X_{CH} \quad (B.2)$$

$$\alpha_{error} = R_{CH.corr}/R_{CH.actual}$$

where $R_{CH.corr}$ and $R_{CH.actual}$ are the erroneously corrected and actual isotope compositions of carbon-bound hydrogen in amino acids, respectively.

As shown in Figure B.7, errors associated with lack of or improper correction for the exchangeable, amine-bound hydrogen may be substantial, even when F_{NH} is approximated as F_w . Magnitudes of errors primarily depend on $\alpha_{NH/w}$ and X_{NH} (i.e., amino acids like glycine with the least number of carbon-bound hydrogen atoms are most affected). The difference between F_{CH} and F_w contributes to additional errors in reported δ^2H_{AA} values, although the size of the effect depends on whether an attempt is made to correct for the amine-bound hydrogen. Notably, F_{NH} is included as a distinct parameter in Eqns. B.1 and B.2 for illustration of errors; in reality, we cannot isolate F_{NH} without knowledge of $\alpha_{NH/w}$ values for the derivatized forms of each amino acid. In our correction scheme used in this study, we measure $F_{NH} + F_{dH}$ (where dH represents hydrogen from methyl chloroformate, MCF) as a single parameter (F_{MCF+NH} ; see Section 3.2.5 in the main text).

Proline is the only amino acid in which no amine-bound hydrogen remains after derivatization. In theory, this would allow proline δ^2H values to be reported without correction for exchangeable hydrogen if the isotopic compositions of the derivative reagents are measured independently (hence no errors in proline δ^2H values arise when this correction is not applied in our theoretical calculations; Figure B.7). In our study, some error accompanies reported proline δ^2H values, as we cannot isolate F_{NH} from F_{MCF+NH} in our measurement (see Section 3.2.5 in the main text). Thus, δ^2H values for proline had to be corrected for the combined value of

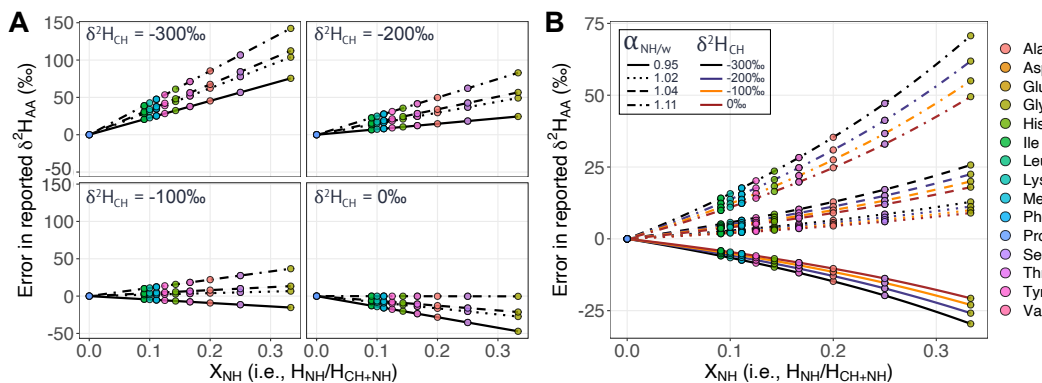


Figure B.7. Theoretical errors in reported $\delta^2\text{H}_{\text{AA}}$ values when **(A)** no correction for the isotopic contribution by amine-bound hydrogen (F_{NH}) is made (Equation B.1), or **(B)** when a correction is made with the erroneous assumption that F_{NH} is equivalent to the isotopic composition of water (F_w ; Equation B.2). Equilibrium fractionations between amine-bound and water hydrogen ($\alpha_{\text{NH}/w}$) have yet to be determined for amino acids, so we use $\alpha_{\text{NH}/w}$ values reported in the literature for a variety of NH-containing compounds: 1.02 (acetamide), 1.04 (formamide), and 1.11 (aniline; Bigeleisen, 1965); and 1.095 (peptide group; calculated as 1/2 the magnitude of $^3\text{H}/^1\text{H}$ fractionation reported in Englander and Poulsen, 1969). Errors are calculated for a range of representative isotope ratios of carbon-bound hydrogen in amino acids ($\delta^2\text{H}_{\text{CH}} = -300$ to 0‰), where $\delta^2\text{H}_w = -100\text{‰}$ and $\delta^2\text{H}_{\text{dH}}$ is assumed to already be subtracted from measured amino acid isotope ratios. Note that only one set of results for amino acids with identical X_{NH} values is displayed.

$F_{\text{MCF}+\text{NH}}$ using the mass balance equation

$$F_{\text{CH.corr}} = (F_{\text{tot}} - 0.23F_{\text{MeOH}} - 0.23F_{\text{MCF}+\text{NH}})/0.54 \quad (\text{B.3})$$

$$\alpha_{\text{error}} = R_{\text{CH.corr}}/R_{\text{CH.actual}}$$

where F_{tot} is the measured isotopic composition of derivatized proline (i.e., including the derivative MeOH and MCF hydrogen, but not including amine-bound hydrogen). Calculations across a range of representative $\delta^2\text{H}_{\text{Pro}}$, $\delta^2\text{H}_{\text{MCF}}$, and $\alpha_{\text{NH}/w}$ values demonstrate that errors in reported proline $\delta^2\text{H}$ values (resulting

from this extraneous derivative correction) are likely no more than 20‰ (Figure B.8).

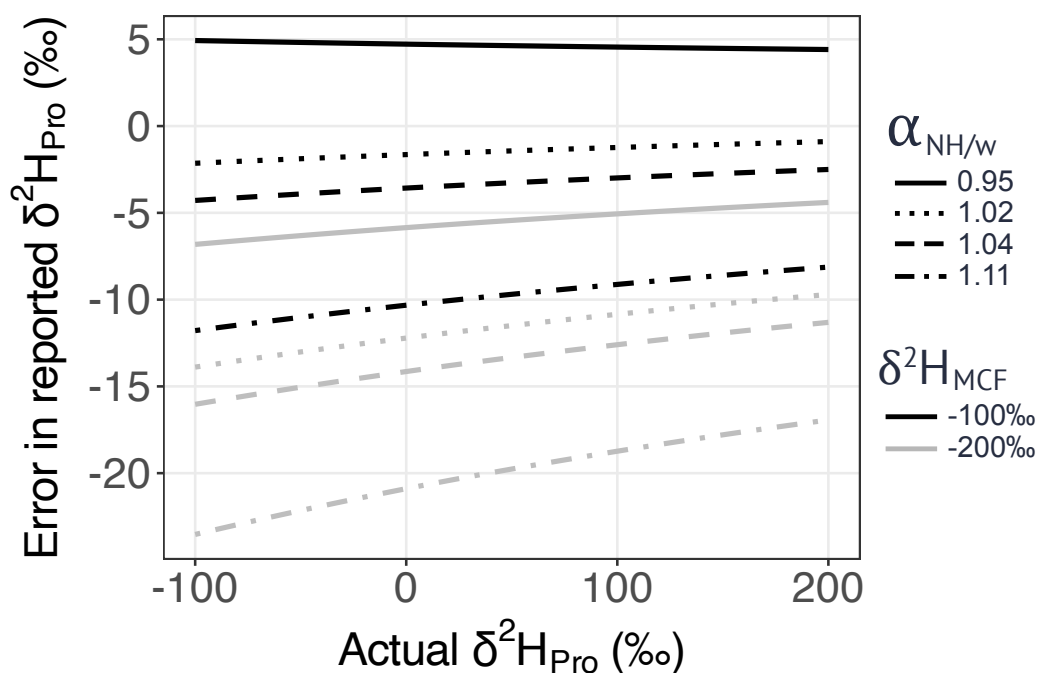


Figure B.8. Theoretical errors in reported $\delta^2\text{H}$ values for proline when our derivative correction is applied (see Equation B.3 and Section 3.2.5 in the main text), as no amine-bound hydrogen remains in proline after derivatization. Errors are calculated for a range of representative isotopic compositions of proline ('actual' $\delta^2\text{H}_{\text{Pro}} = -100$ to $+200$ ‰ for carbon-bound hydrogen in proline), where $\delta^2\text{H}_{\text{MCF}} = -150$ or -50 ‰, $\delta^2\text{H}_{\text{MeOH}}$ and $\delta^2\text{H}_{\text{w}} = -100$ ‰, and $\alpha_{\text{NH/w}}$ values used are those reported in the literature for a variety of NH-containing compounds: 1.02 (acetamide), 1.04 (formamide), and 1.11 (aniline; Bigeleisen, 1965); and 1.095 (peptide group; calculated as 1/2 the magnitude of $^3\text{H}/^1\text{H}$ fractionation reported in Englander and Poulsen, 1969).

B.5 Hydrolysis and derivatization tests

Table B.4. $\delta^2\text{H}$ values and standard deviations (from duplicate or triplicate analyses) of amino acids from bovine serum albumin hydrolyzed under different conditions.

| Amino acid | Replicate | Control ¹ | Oxic ² | 105°C ³ | 20h ⁴ | 48h ⁵ |
|------------|-----------|----------------------|-------------------|--------------------|------------------|------------------|
| Ala+Gly | 1 | -131 ± 2 | -132 ± 2 | -129 ± 1 | -128 ± 1 | -127 ± 2 |
| Ala+Gly | 2 | -129 ± 2 | -127 ± 0 | -128 ± 2 | -129 ± 2 | -128 ± 1 |
| Asx | 1 | -139 ± 2 | -143 ± 0 | -132 ± 2 | -136 ± 2 | -141 ± 1 |
| Asx | 2 | -136 ± 2 | -138 ± 0 | -131 ± 2 | -133 ± 1 | -141 ± 2 |
| Glx | 1 | -110 ± 3 | -115 ± 5 | -98 ± 2 | -104 ± 3 | -111 ± 2 |
| Glx | 2 | -107 ± 3 | -107 ± 1 | -104 ± 1 | -107 ± 2 | -108 ± 1 |
| Ile | 1 | -235 ± 1 | -235 ± 5 | -240 ± 4 | -238 ± 5 | -237 ± 9 |
| Ile | 2 | -233 ± 3 | -232 ± 4 | -235 ± 4 | -235 ± 0 | -238 ± 10 |
| Leu | 1 | -182 ± 1 | -180 ± 3 | -179 ± 0 | -181 ± 1 | -179 ± 3 |
| Leu | 2 | -181 ± 1 | -179 ± 0 | -180 ± 1 | -180 ± 1 | -180 ± 1 |
| Lys | 1 | -167 ± 4 | -171 ± 0 | -165 ± 0 | -170 ± 5 | -171 ± 3 |
| Lys | 2 | -166 ± 2 | -167 ± 1 | -168 ± 2 | -171 ± 4 | -170 ± 4 |
| Met | 1 | -133 ± 11 | -145 ± 11 | -139 ± 11 | -144 ± 10 | -136 ± 8 |
| Met | 2 | -140 ± 13 | -136 ± 0 | -148 ± 10 | -134 ± 9 | -141 ± 8 |
| Phe | 1 | -134 ± 2 | -132 ± 1 | -129 ± 1 | -130 ± 1 | -130 ± 1 |
| Phe | 2 | -131 ± 2 | -130 ± 0 | -131 ± 1 | -129 ± 0 | -129 ± 2 |
| Pro | 1 | 16 ± 2 | 4 ± 2 | 12 ± 2 | 11 ± 1 | 6 ± 3 |
| Pro | 2 | 12 ± 2 | 2 ± 1 | 7 ± 1 | 8 ± 1 | 6 ± 2 |
| Tyr | 1 | -131 ± 3 | -130 ± 1 | -124 ± 4 | -128 ± 1 | -126 ± 2 |
| Tyr | 2 | -127 ± 4 | -126 ± 1 | -127 ± 2 | -129 ± 2 | -127 ± 1 |
| Val | 1 | -165 ± 2 | -164 ± 4 | -160 ± 2 | -162 ± 4 | -163 ± 2 |
| Val | 2 | -163 ± 3 | -159 ± 2 | -159 ± 3 | -160 ± 2 | -164 ± 1 |

¹Anoxic hydrolysis in 6N HCl for 24h at 110°C.

²⁻⁵Identical conditions as used in control, except for one variable altered in each treatment:

²Samples were not sparged with N₂ prior to sealing sample vials for hydrolysis (i.e., O₂ was present during hydrolysis).

³Samples were hydrolyzed at 105°C.

⁴Samples were hydrolyzed for 20h.

⁵Samples were hydrolyzed for 48h.

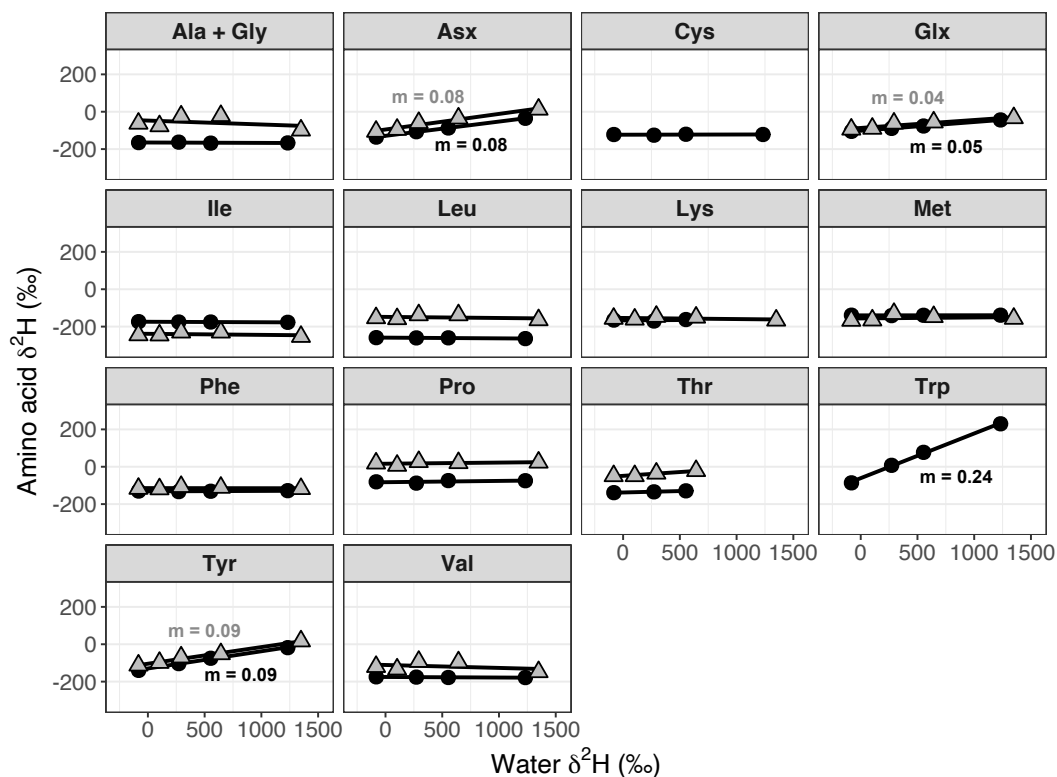


Figure B.9. Effect of hydrolysis on amino acid $\delta^2\text{H}$ values from BSA (gray triangles) and a mixture of pure standards (black circles). Amino acids were hydrolyzed in 6N HCl at 110°C for 24h. The acid was prepared with different $\delta^2\text{H}$ values to test for hydrogen exchange during hydrolysis. Slopes (m) ≥ 0.02 are annotated in gray for BSA and black for the standard mixture.

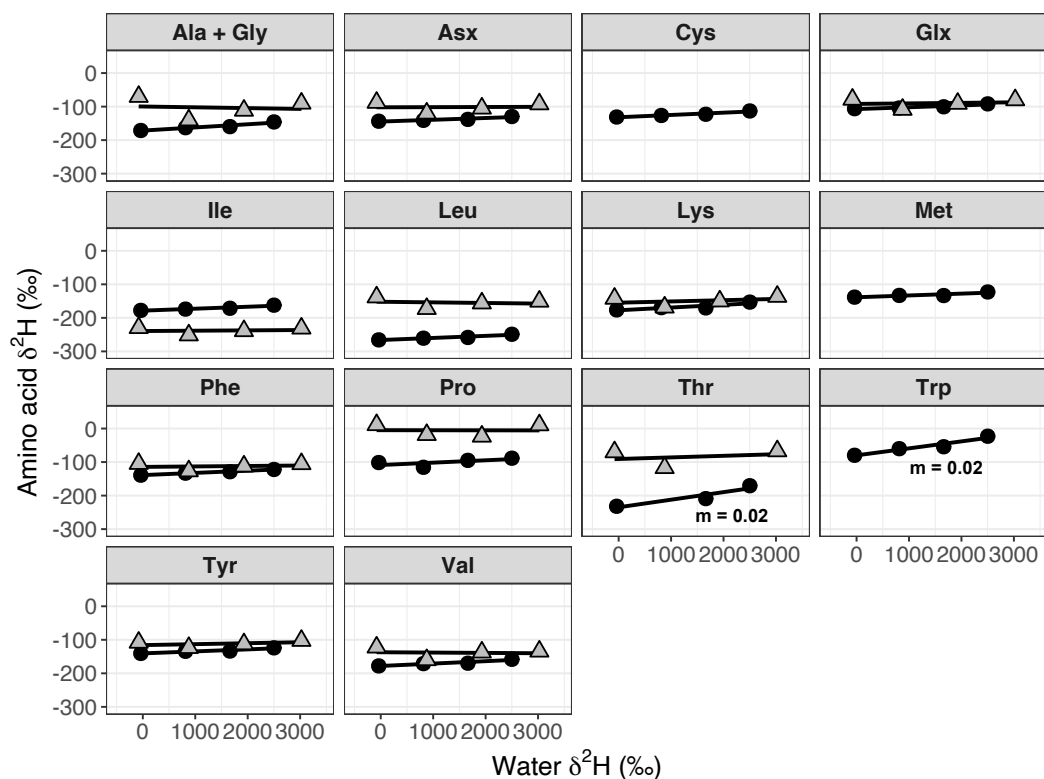


Figure B.10. Effect of derivatization on amino acid $\delta^2\text{H}$ values from BSA (gray triangles) and a mixture of pure standards (black circles). Amino acids were derivatized to MOC esters with 7:2:3 v/v/v anhydrous MeOH, pyridine, and MCF in 0.1N HCl at room temperature. The solvent was prepared with different $\delta^2\text{H}$ values to test for hydrogen exchange during derivatization. Slopes (m) ≥ 0.02 are annotated in gray for BSA and black for the standard mixture.

B.6 Controls on variations in ${}^2\varepsilon_{AA/w}$ values

B.6.1 Water fraction factors

Hydrogen in amino acids ultimately originates from two external sources: organic substrates and water. The hydrogen isotope composition of each amino acid can therefore be conceptualized as the weighted contributions of these sources according to the mass balance equation

$$R_{AA} = X_w \alpha_{AA/w} R_w + (1 - X_w) \alpha_{AA/s} R_s \quad (\text{B.4})$$

where R_{AA} , R_w , and R_s denote the non-exchangeable hydrogen isotope ratios of the amino acid, water, and substrate, respectively; X_w is the mole fraction of water-derived hydrogen in an amino acid; and $\alpha_{AA/w}$ and $\alpha_{AA/s}$ are the net isotopic fractionations associated with hydrogen uptake and incorporation from water and the substrate, respectively (although note that treatment of $\alpha_{AA/w}$ and $\alpha_{AA/s}$ as distinct is often an artificial simplification – see Zhang et al., 2009). Without additional constraints on the system, a unique solution for the three unknown parameters (X_w , $\alpha_{AA/w}$, and $\alpha_{AA/s}$) is not possible (Sessions & Hayes, 2005). However, the combined effect of $X_w \cdot \alpha_{AA/w}$ (termed the ‘water fraction factor’ after Kopf, 2014) can be obtained from the slope of the regression between R_{AA} and R_w , with values resulting from culturing experiments in which the $\delta^2\text{H}$ value of an organism’s growth water is manipulated (Figure B.11A). Water fraction factors provide an additional means to compare physiological differences across organisms, and when combined with ${}^2\varepsilon_{AA/w}$ data, can help constrain some of the control by

X_w versus $\alpha_{AA/w}$ on ${}^2\varepsilon_{AA/w}$ values.

Wildtype organisms showed similar patterns of water fraction factors (Figures B.11B; Table B.5), implying similar net amino acid/water fractionations for a given amino acid. Water fraction factors in *E. coli* are comparable to those calculated from similar published growth water experiments (Table B.5; Fogel et al., 2016), demonstrating that organisms yield reproducible amino acid/water fractionations when grown under similar conditions. For a given amino acid in *B. subtilis*, *E. coli*, and *R. radiobacter*, water fraction factors are approximately within error, suggesting that differences in corresponding $\delta^2\text{H}_{AA}$ values in these organisms are likely not driven by differences in $\alpha_{AA/w}$ or X_w , but rather may be attributed to variations in the isotopic composition of hydrogen from organic precursors or in the isotope fractionations imparted during post-synthesis reactions. In contrast, the generally higher but similar ordering of water fraction factors in *E. meliloti* and *P. fluorescens* imply potential differences in X_w at the level of central metabolites (e.g., pyruvate), which in turn may reflect the variations in relative fluxes through central metabolic pathways, as well as different extents of organic hydrogen equilibration with water in pools of central metabolites. Some of the variation across organisms may be driven by different intracellular water isotope ratios, which can be distinct from the growth medium when cellular growth rates are high (Kreuzer-Martin et al., 2006), although the extent to which this effect was relevant in our cultures is unclear.

The overall pattern of water fraction factors generally followed that of ${}^2\varepsilon_{AA/w}$ values (Figure B.6A), with the exception of phenylalanine, which had notably low water fraction factors yet high $\delta^2\text{H}$ values. This difference is puzzling given that the small phenylalanine/water fractionations in each substrate condition (Figure 3.6) support a high X_w and large $\alpha_{AA/w}$ (i.e., small net fractionation), yet together these would yield high water fraction factors. This discrepancy could not be resolved here.

Proline had the highest water fraction factors, which, coupled with its high $\delta^2\text{H}$ values and potentially high fraction of water-derived hydrogen (Figure B.16), can likely be explained by both a large X_w and large $\alpha_{\text{AA}/w}$ (i.e., small fractionation). In turn, a large $\alpha_{\text{AA}/w}$ can be explained in part by ^2H -enrichment of water-derived hydrogen from acetyl-CoA by citrate synthase (Section 3.4.1.1 in main text), which would increase the apparent $\alpha_{\text{AA}/w}$ value toward or beyond unity. The ordering of water fraction factors for leucine, isoleucine, and valine is consistent across organisms and matches that of $^2\varepsilon_{\text{AA}/w}$ values in *E. meliloti*, *P. fluorescens*, and *R. radiobacter*, suggesting a strong control by the water-derived fraction of hydrogen in these amino acids on their overall isotopic compositions.

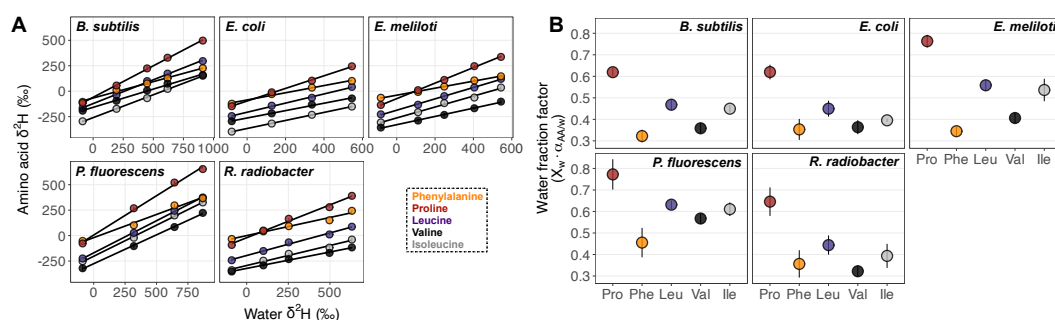


Figure B.11. Influence of media $\delta^2\text{H}$ on amino acid $\delta^2\text{H}$ values in wildtype organisms grown on glucose. **(A)** Regressions of $\delta^2\text{H}$ values of amino acids versus media water. Error bars indicate the propagated uncertainties ($\pm 1\sigma$) from the amino acid, derivative, and water measurements, and are smaller than symbols. **(B)** Summary of water fraction factors (i.e., slopes from regressions in A). Error bars are 95% confidence intervals of the coefficients from the linear regression fit. Slopes and 95% confidence intervals are summarized in Table B.5. Note that the *E. coli* cultures were grown at a different time, and amino acids were derivatized following a different reaction procedure, compared to the cultures of the other four organisms (see Sections 3.2.1 and 3.2.2 in the main text). We do not expect these differences to affect the interpretations drawn from this data.

Table B.5. Summary of slopes and 95% confidence intervals calculated from regressions of amino acid versus water $\delta^2\text{H}$ values for wildtype organisms grown on glucose (Figure B.11).

| Organism | Study | Proline | Phenylalanine | Leucine | Valine |
|-----------------------|--------------------|------------------|----------------------|------------------|------------------|
| <i>B. subtilis</i> | This study | 0.62 ± 0.018 | 0.32 ± 0.030 | 0.47 ± 0.025 | 0.36 ± 0.024 |
| <i>E. coli</i> | This study | 0.62 ± 0.017 | 0.35 ± 0.025 | 0.45 ± 0.019 | 0.36 ± 0.017 |
| <i>E. coli</i> | Fogel et al., 2016 | 0.56 ± 0.025 | 0.24 ± 0.077 | 0.44 ± 0.009 | 0.37 ± 0.023 |
| <i>E. meliloti</i> | This study | 0.76 ± 0.029 | 0.34 ± 0.022 | 0.56 ± 0.026 | 0.41 ± 0.025 |
| <i>P. fluorescens</i> | This study | 0.77 ± 0.071 | 0.46 ± 0.068 | 0.63 ± 0.020 | 0.57 ± 0.024 |
| <i>R. radiobacter</i> | This study | 0.65 ± 0.066 | 0.36 ± 0.064 | 0.44 ± 0.045 | 0.32 ± 0.026 |

B.6.2 Pyruvate hydrogen

Pyruvate occupies a crucial node in central metabolism and contributes hydrogen to all amino acids either directly (the case for leucine, valine, and isoleucine), or indirectly (through α -ketoglutarate for proline when pyruvate hydrogen is routed through the TCA cycle, and through PEP for phenylalanine when flux is gluconeogenic). The altered metabolic programming in organisms grown on different substrates undoubtedly alters the hydrogen isotope composition of pyruvate, which likely contributes to some of the observed shifts in all $\delta^2\text{H}_{\text{AA}}$ values. To explore this control, we estimated the fraction of 'pyruvate-related' hydrogen in each amino acid (i.e., the fraction of hydrogen directly derived from pyruvate or derived from a metabolite whose hydrogen exchanges with that of pyruvate). For leucine, valine, and isoleucine, pyruvate hydrogen is directly incorporated (Figures B.2 and B.18-B.19), thus pyruvate-related hydrogen fractions are 60, 75, and 30%, respectively in these amino acids. Pyruvate hydrogen is routed into proline via acetyl-CoA during pyruvate and succinate metabolism (Gerosa et al., 2015); estimates of 29% pyruvate hydrogen in proline are included for these conditions based on hydrogen accounting (Figures B.2 and B.16). Upon growth on acetate, pyruvate hydrogen is not technically routed into proline (e.g., Dolan et al., 2020; Gerosa et al., 2015); nevertheless, substantial shifts in the $\delta^2\text{H}$ value of acetyl-CoA from glucose to acetate metabolism likely occurred, as evidenced by proline's significantly higher $\delta^2\text{H}$ values. Thus, the fraction of acetyl-CoA-derived hydrogen in proline during acetate metabolism (29%) is additionally included in the pyruvate-related fraction of proline hydrogen. PEP hydrogen, which is incorporated into phenylalanine, is directly related to pyruvate hydrogen through pyruvate kinase or PEP synthetase activity (which interconvert PEP and pyruvate). However, this relationship is impeded when PEP is predominantly synthesized through PEP carboxykinase, or

pyruvate through KDPG aldolase (Figure B.3), which occurs when different central metabolic pathways are activated (Dolan et al., 2020; Gerosa et al., 2015). Because exact determination of the relationship between PEP and pyruvate hydrogen in each substrate growth condition is difficult, an estimate of 50% relatedness was used here, which equates to 19% pyruvate-related hydrogen in phenylalanine when accounting for the fact that 38% of hydrogen in phenylalanine is PEP-derived. Plotting these pyruvate-related hydrogen fractions against shifts in $\delta^2\text{H}_{\text{AA}}$ values in wildtype organisms grown on glucose versus on acetate, pyruvate, or succinate reveals that changes in the isotope composition of pyruvate-related hydrogen alone explains 15–52% of the variation in $\delta^2\text{H}_{\text{AA}}$ values (Figure B.12).

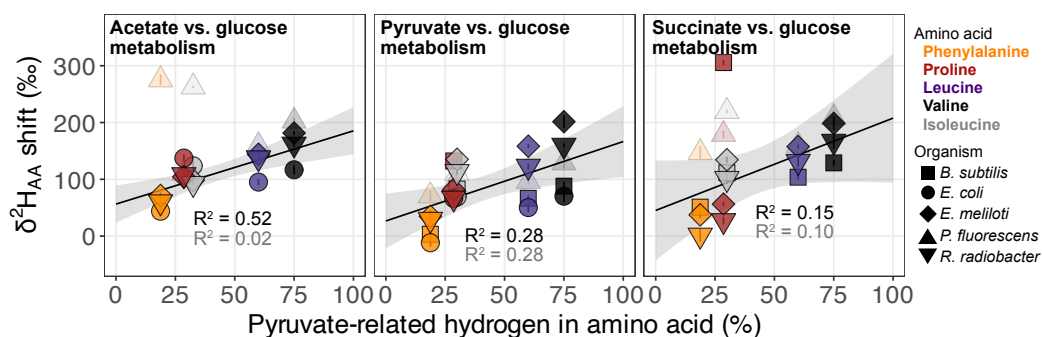


Figure B.12. Regressions of pyruvate-derived hydrogen in amino acids versus shifts in $\delta^2\text{H}_{\text{AA}}$ values in wildtype organisms grown on glucose versus on acetate, pyruvate, and succinate. $\delta^2\text{H}_{\text{AA}}$ shifts were calculated as the difference in $\delta^2\text{H}$ value of a given amino acid between the two conditions compared in each panel. Error bars on individual data points indicate the propagated uncertainties ($\pm 1\sigma$) from each pair of $\delta^2\text{H}_{\text{AA}}$ values measured and are smaller than symbols. Data are shown for one biological replicate. The shaded gray region indicates the 95% confidence interval of the coefficients from the linear regression fit. Adjusted R^2 values for regressions are shown when *P. fluorescens* data (transparent symbols) are excluded (black) versus included (gray).

B.6.3 NADPH hydrogen

For amino acids that derive hydrogen from NADPH, regression analysis shows that 61% of $\delta^2\text{H}_{\text{AA}}$ shifts from glucose to acetate metabolism, and 34% of shifts from

glucose to pyruvate metabolism, may be explained when only considering the proportion of NADPH-derived hydrogen in each amino acid (Figure B.13). Significant deviations in proline $\delta^2\text{H}$ values in organisms grown on succinate impedes interpretation of NADPH's influence on $\delta^2\text{H}_{\text{AA}}$ values during succinate metabolism. As the isotopic compositions of leucine and valine are not impacted by NADPH but vary significantly across substrate conditions, contributions by pyruvate must be additionally accounted for to capture the major variations in all amino acid $\delta^2\text{H}$ values (Figure 3.7B; Supplementary Section B.6.2).

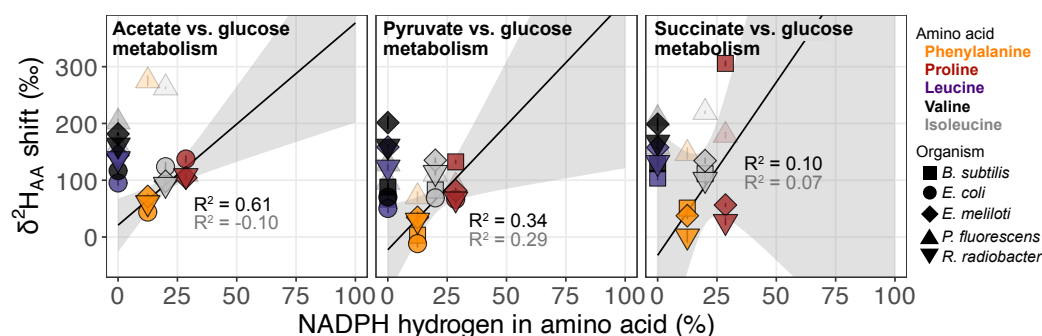


Figure B.13. Regressions of NADPH-derived hydrogen in amino acids versus shifts in $\delta^2\text{H}_{\text{AA}}$ values in wildtype organisms grown on glucose versus on acetate, pyruvate, and succinate. $\delta^2\text{H}_{\text{AA}}$ shifts were calculated as the difference in $\delta^2\text{H}$ value of a given amino acid between the two conditions compared in each panel. Error bars on individual data points indicate the propagated uncertainties ($\pm 1\sigma$) from each pair of $\delta^2\text{H}_{\text{AA}}$ values measured and are smaller than symbols. Data are shown for one biological replicate. The shaded gray region indicates the 95% confidence interval of the coefficients from the linear regression fit. Adjusted R^2 values for regressions are shown when *P. fluorescens* data (transparent symbols) are excluded (black) versus included (gray). Regressions displayed only include amino acids that inherit hydrogen from NADPH (i.e., phenylalanine, proline, and isoleucine); when all amino acids are included, adjusted R^2 values are ~ 0 with or without *P. fluorescens* data.

Variations in $\delta^2\text{H}_{\text{AA}}$ values due to NADPH may be further interrogated through $\delta^2\text{H}$ shifts in proline, whose hydrogen sources and proportions (29% from NAD(P)H, 29% from acetyl-CoA, and 42% from water; Figures B.2 and B.16) are invariant regardless of the catabolic pathway activated. Upon growth on different substrates

relative to growth on glucose, changes in the isotopic composition of proline beyond those due to shifts in acetyl-CoA $\delta^2\text{H}$ are presumably related to changes in the $\delta^2\text{H}$ value of NADPH (thus are referred to here as “NADPH-driven ^2H -enrichment,” or $\Delta^2 H_{NADPH}$), as the water-derived fraction is assumed to be isotopically invariant. We can estimate $\Delta^2 H_{NADPH}$ of proline across growth conditions by subtracting the relative contribution of acetyl-CoA $\delta^2\text{H}$ variations ($\Delta^2 H_{AcCoA}$) from total shifts in proline $\delta^2\text{H}$ values ($\Delta^2 H_{Pro}$):

$$\Delta^2 H_{NADPH} = 7\Delta^2 H_{Pro}/2 - \Delta^2 H_{AcCoA} \quad (\text{B.5})$$

In turn, $\Delta^2 H_{AcCoA}$ can be estimated based on assumptions about how hydrogen is routed through the catabolic pathways. During glucose, pyruvate, and succinate metabolism, the majority of acetyl-CoA is produced from pyruvate via pyruvate dehydrogenase (Gerosa et al., 2015). The methyl group of pyruvate remains intact during this conversion, so the hydrogen isotope composition of the acetyl-CoA methyl group is presumed to be identical to that of cellular pyruvate (Figure 3.8). Thus, $\Delta^2 H_{AcCoA}$ from glucose to pyruvate or succinate metabolism can be determined based on shifts in cellular pyruvate $\delta^2\text{H}$ ($\Delta^2 H_{Pyr}$; Equation B.6), which, in turn, can be calculated through shifts in leucine or valine $\delta^2\text{H}$ ($\Delta^2 H_{Leu}$ or $\Delta^2 H_{Val}$), as leucine and valine only inherit hydrogen from pyruvate and water (Equation B.7; Figures B.2 and B.18; Table B.6), and the water-derived fraction is presumed to be isotopically invariant.

$$\Delta^2 H_{AcCoA} = \Delta^2 H_{Pyr} \quad (\text{B.6})$$

$$\Delta^2 H_{Pyr} = 10\Delta^2 H_{Leu}/6 \quad (\text{B.7})$$

$$\Delta^2 H_{Pyr} = 8\Delta^2 H_{Val}/6$$

During acetate metabolism, pyruvate hydrogen does not route into proline (Figure 3.8; Dolan et al., 2020; Gerosa et al., 2015), so acetyl-CoA $\delta^2\text{H}$ shifts could not be directly calculated through $\Delta^2 H_{Leu}$ or $\Delta^2 H_{Val}$. Instead, cellular acetyl-CoA $\delta^2\text{H}$ values during acetate and glucose metabolism were estimated individually. The hydrogen isotope composition of acetyl-CoA produced during acetate metabolism ($\delta^2 H_{AcCoA.Ace}$) was approximated as equal to that of the acetate substrate (Equation B.8; $\delta^2 H_{Ace} = -76 \pm 20\%$, measured by Zhang et al., 2009). The isotopic composition of acetyl-CoA produced during glucose metabolism ($\delta^2 H_{AcCoA.Glu}$) was assumed to be equal to that of intracellular pyruvate ($\Delta^2 H_{Pyr.Glu}$; Equation B.9; Figure 3.8). In turn, $\delta^2 H_{Pyr.Glu}$ was estimated based on intracellular pyruvate $\delta^2\text{H}$ shifts from glucose to pyruvate metabolism (Equation B.10), which were calculated through shifts in leucine and valine $\delta^2\text{H}$ values (Equation B.7), with the assumption that during pyruvate metabolism, the isotopic composition of intracellular pyruvate ($\delta^2 H_{Pyr.Pyr}$) is equal to that of the substrate pyruvate (Equation B.11; where $\delta^2 H_{Pyr} = -12 \pm 20\%$, as measured by Zhang et al., 2009). Estimated shifts in the hydrogen isotope composition of intracellular acetyl-CoA from glucose to acetate metabolism were subtracted from measured shifts in proline $\delta^2\text{H}$ values in order to estimate the contribution of NADPH to ^2H -enrichment of proline (Equation B.5). Results of these calculations are shown in Figure 3.7C and Table B.6, and are discussed in Section 3.4.2.1.2 in the main text.

$$\delta^2 H_{AcCoA.Ace} = \delta^2 H_{Ace} \quad (\text{B.8})$$

$$\delta^2 H_{AcCoA.Glu} = \delta^2 H_{Pyr.Glu} \quad (\text{B.9})$$

$$\delta^2 H_{Pyr.Glu} = \delta^2 H_{Pyr} - (\delta^2 H_{Pyr.Pyr} - \delta^2 H_{Pyr.Glu}) \quad (\text{B.10})$$

$$\delta^2 H_{Pyr.Pyr} = \delta^2 H_{Pyr} \quad (\text{B.11})$$

Table B.6. Estimated isotopic compositions of and shifts in intracellular metabolite pools presented in Supplementary Section B.6.2.

| Organism | Condition 2 ¹ | Pyruvate $\delta^2\text{H}$ shift ($\Delta^2\text{H}_{\text{Pyr}}$) ² | Intracellular pyruvate $\delta^2\text{H}$ in glucose cond ³ | NADPH-driven ^2H -enrichment in proline ($\Delta^2\text{H}_{\text{NADPH}}$) ⁴ |
|-----------------------|--------------------------|---|---|--|
| <i>B. subtilis</i> | pyruvate | 114 ± 6 | -126 ± 15 | 99 ± 7 |
| | succinate | 172 ± 5 | | 256 ± 7 |
| <i>E. coli</i> | acetate | 157 ± 7 | -101 ± 17 | 130 ± 27 |
| | pyruvate | 87 ± 10 | | 41 ± 15 |
| <i>E. meliloti</i> | acetate | 241 ± 3 | -278 ± 16 | 46 ± 26 |
| | fructose | 48 ± 13 | | -19 ± 16 |
| | pyruvate | 266 ± 8 | | 5 ± 9 |
| | succinate | 264 ± 8 | | -20 ± 9 |
| <i>P. fluorescens</i> | acetate | 268 ± 5 | -178 ± 16 | 81 ± 26 |
| | citrate | 236 ± 9 | | 8 ± 9 |
| | fructose | 61 ± 5 | | 42 ± 10 |
| | pyruvate | 166 ± 8 | | 100 ± 10 |
| | succinate | 272 ± 8 | | |
| <i>R. radiobacter</i> | acetate | 223 ± 4 | -221 ± 15 | 66 ± 25 |
| | fructose | 20 ± 10 | | -14 ± 15 |
| | pyruvate | 209 ± 5 | | 6 ± 7 |
| | succinate | 221 ± 11 | | -37 ± 13 |

¹Condition 1 = glucose metabolism.

²Estimated average pyruvate $\delta^2\text{H}$ shift from glucose metabolism to growth condition 2, computed from two independent estimates calculated using $\delta^2\text{H}$ shifts in leucine and valine (Equation B.7) in replicate 1 cultures, with $\Delta^2\text{H}_{\text{Leu}}$ and $\Delta^2\text{H}_{\text{Val}}$ adjusted for differences in growth medium $\delta^2\text{H}$. Errors indicate propagated uncertainties ($\pm 1\sigma$) in leucine, valine, and growth medium $\delta^2\text{H}$ values in each pair of conditions.

³ $\delta^2\text{H}$ value of intracellular pyruvate produced during glucose metabolism, estimated for each organism as $-12\text{‰} - [\text{pyruvate } \delta^2\text{H} \text{ shift from the glucose to pyruvate condition; Equation B.10}]$. This calculation assumes that during pyruvate metabolism, the $\delta^2\text{H}$ value of intracellular pyruvate is equivalent to that of the substrate pyruvate (-12‰ ; Zhang et al., 2009). Errors indicate propagated uncertainties ($\pm 1\sigma$) in the measured pyruvate $\delta^2\text{H}$ value ($\sim 20\text{‰}$; Zhang et al., 2009) and in the estimated pyruvate $\delta^2\text{H}$ shifts (see footnote 2).

⁴Estimated ^2H -enrichment in proline caused by NADPH. See Supplementary Section B.6.3 for calculation details. Errors indicate propagated uncertainties ($\pm 1\sigma$) in measured proline, pyruvate, and/or acetate $\delta^2\text{H}$ values, as well as estimated pyruvate $\delta^2\text{H}$ shifts (see footnote 2).

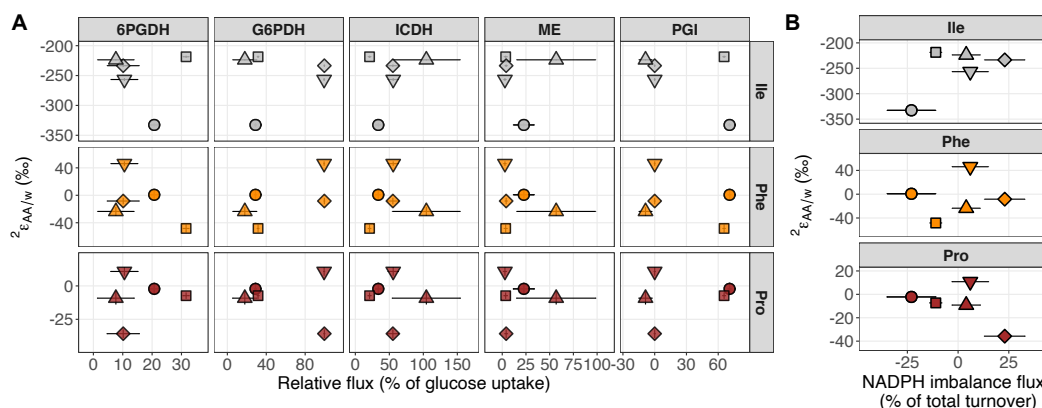


Figure B.14. Lack of correlations between amino acid/water fractionations and NADPH metabolism in wildtype organisms grown on glucose. **(A)** ${}^2\epsilon_{AA/w}$ values for amino acids that inherit NADPH hydrogen versus relative carbon flux (i.e., normalized to glucose uptake rates) through NADPH-relevant enzymes. **(B)** ${}^2\epsilon_{AA/w}$ values versus NADPH imbalance flux, calculated for these organisms in Wijker et al. (2019) as the difference between all NADPH-producing and -consuming fluxes. Error bars represent $\pm 1\sigma$. Only data from replicate 1 cultures are plotted. Enzyme abbreviations: 6PGDH, 6-phosphogluconate dehydrogenase; G6PDH, glucose-6-phosphate dehydrogenase; ICDH, isocitrate dehydrogenase; ME, malic enzyme; PGI, phosphoglucose isomerase.

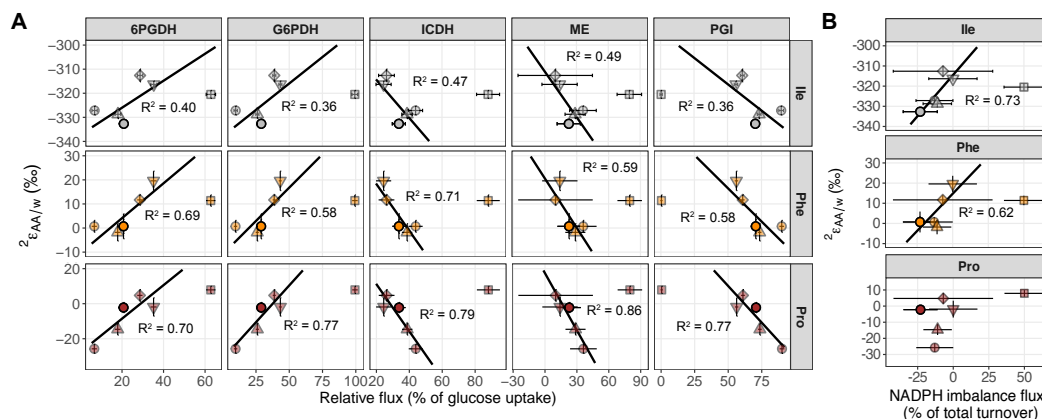


Figure B.15. Correlations between amino acid/water fractionations and NADPH metabolism in *E. coli* wildtype and mutant organisms grown on glucose. **(A)** ${}^2\epsilon_{AA/w}$ values for amino acids that inherit NADPH hydrogen versus relative carbon flux (i.e., normalized to glucose uptake rates) through NADPH-relevant enzymes. **(B)** ${}^2\epsilon_{AA/w}$ values versus NADPH imbalance flux, calculated for these organisms in Wijker et al. (2019) as the difference between all NADPH-producing and -consuming fluxes. JW3985 was excluded from all regression analyses because in most cases it was a significant outlier for unclear reasons. Moderate to weak correlations were observed for all comparisons, except for proline $\delta^2\text{H}$ versus NADPH imbalance flux, which for unknown reasons did not appear to correlate. Error bars represent $\pm 1\sigma$. Enzyme abbreviations: 6PGDH, 6-phosphogluconate dehydrogenase; G6PDH, glucose-6-phosphate dehydrogenase; ICDH, isocitrate dehydrogenase; ME, malic enzyme; PGI, phosphoglucose isomerase.

B.7 Biosynthetic pathways

B.7.1 Proline biosynthesis

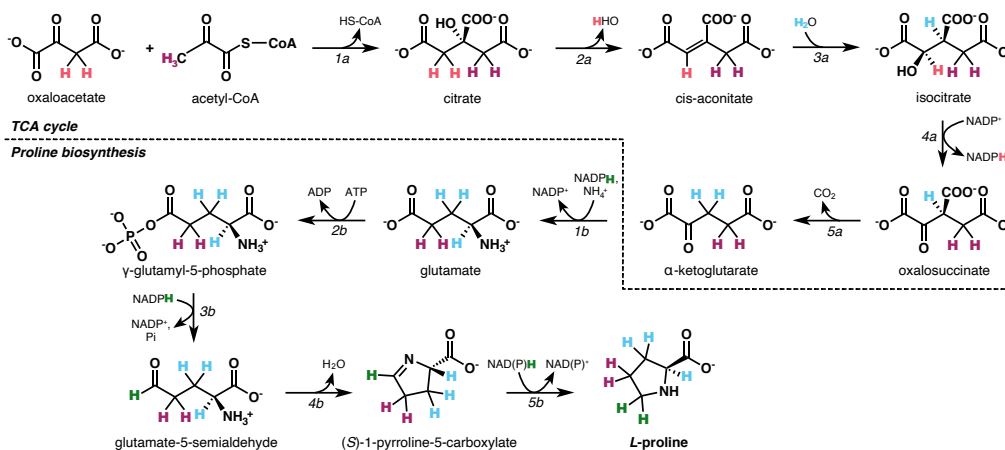


Figure B.16. General biosynthetic pathway of proline with colors representing tracked hydrogen sources (red for OAA, purple for acetyl-CoA, light blue for water, green for NADPH). As summarized in Section 3.4.1.1 in the main text, aconitase and isocitrate dehydrogenase stereospecifically remove the oxaloacetate-derived hydrogen from citrate and isocitrate, respectively (Csonka & Fraenkel, 1977; Lowenstein, 1967; Ochs & Talele, 2020; Smith & York, 1970), resulting in exclusive retention of acetyl-CoA hydrogen in proline. The hydrogen atom transferred from NADPH in step 1b likely equilibrates with water due to PLP-dependent enzyme reactions that target the α -hydrogen position in amino acids (Csonka & Fraenkel, 1977; Eliot & Kirsch, 2004), as well as relative acidity of α -hydrogen positions; thus, this NADPH-derived hydrogen is not propagated to proline in our schematic. Acidity of hydrogen in aldehyde positions may result in additional loss of NADPH hydrogen transferred in step 3b, although tritium labeling experiments support retention of this hydrogen through synthesis of proline (Csonka & Fraenkel, 1977). Enzymes: 1a, citrate synthase; 2-3a, aconitase; 4-5a, isocitrate dehydrogenase; 1b, glutamate dehydrogenase; 2b, glutamate-5-kinase; 3b, γ -glutamyl phosphate reductase; 4b, spontaneous cyclization; 5b, 1-pyrroline-5-carboxylate reductase. See Figure B.20 for distribution of isozymes across organisms investigated in this study.

B.7.2 Phenylalanine biosynthesis

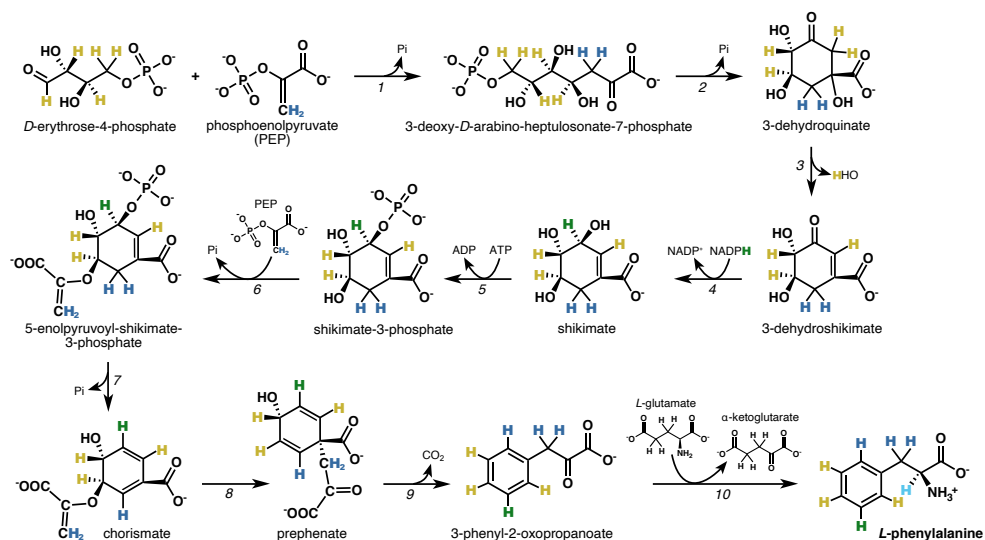


Figure B.17. General biosynthetic pathway of phenylalanine with colors representing tracked hydrogen sources (yellow for erythrose-4-phosphate, dark blue for PEP, green for NADPH, light blue for water). During step 6, hydrogen in the incoming PEP substrate may be ²H-enriched during its condensation with shikimate-3-phosphate, as the methylene group of PEP is transiently converted to a methyl group in the enzyme-bound intermediate, then deprotonated with an accompanying normal KIE (Grimshaw et al., 1982). This hydrogen atom eventually becomes the C₃ hydrogen in phenylalanine. Although steps 3 and 7 result in abstraction of one proton from a pair, these reactions likely do not contribute to phenylalanine's ²H-enrichment due to their stereospecificity (Bornemann et al., 2000; Onderka & Floss, 1969; Turner et al., 1975; Vaz, 1980). PLP-dependent enzyme reactions equilibrate the α-hydrogen in amino acids with solvent (Eliot & Kirsch, 2004). Enzymes: 1, 3-deoxy-7-phosphoheptulonate synthase; 2, 3-dehydroquinate synthase; 3, 3-dehydroquinate dehydratase; 4, shikimate dehydrogenase; 5, shikimate kinase; 6, 3-phosphoshikimate 1-carboxyvinyltransferase; 7, chorismate synthase; 8, chorismate mutase; 9, prephenate dehydratase; 10, phenylalanine transaminase/ aromatic aminotransferase. See Figure B.20 for distribution of isozymes across organisms investigated in this study.

B.7.3 Leucine and valine biosynthesis

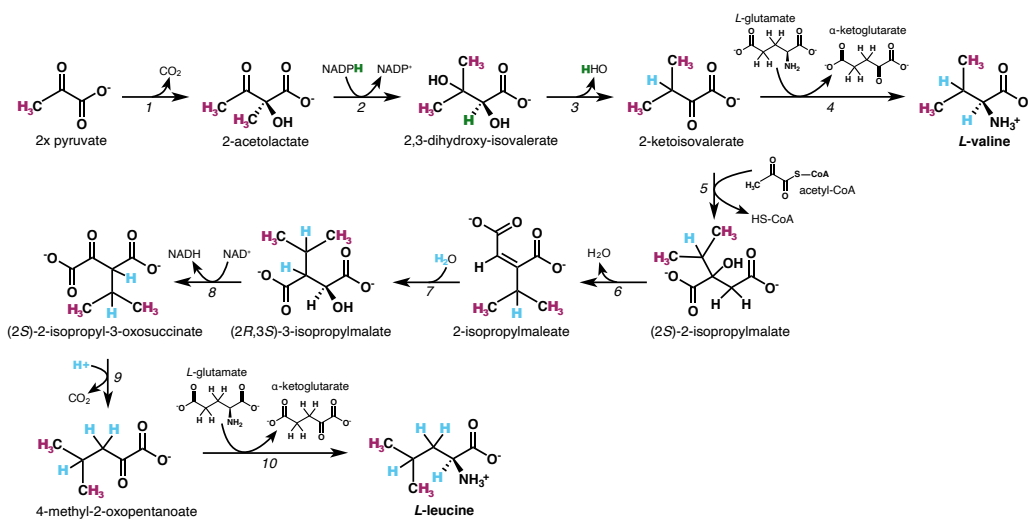


Figure B.18. General biosynthetic pathways of leucine and valine with colors representing tracked hydrogen sources (purple for pyruvate, green for NADPH, light blue for water). PLP-dependent enzyme reactions equilibrate the α -hydrogen in amino acids with solvent (Eliot & Kirsch, 2004). Enzymes: 1, acetolactate synthase; 2, ketol-acid reductoisomerase; 3, dihydroxy-acid dehydratase; 4, valine transaminase/ branched-chain amino acid aminotransferase; 5, 2-isopropylmalate synthase; 6-7, 3-isopropylmalate dehydratase; 8, 3-isopropylmalate dehydrogenase; 9, spontaneous rearrangement; 10, leucine aminotransferase/ branched-chain amino acid aminotransferase. See Figure B.20 for distribution of isozymes across organisms investigated in this study.

B.7.4 Isoleucine biosynthesis

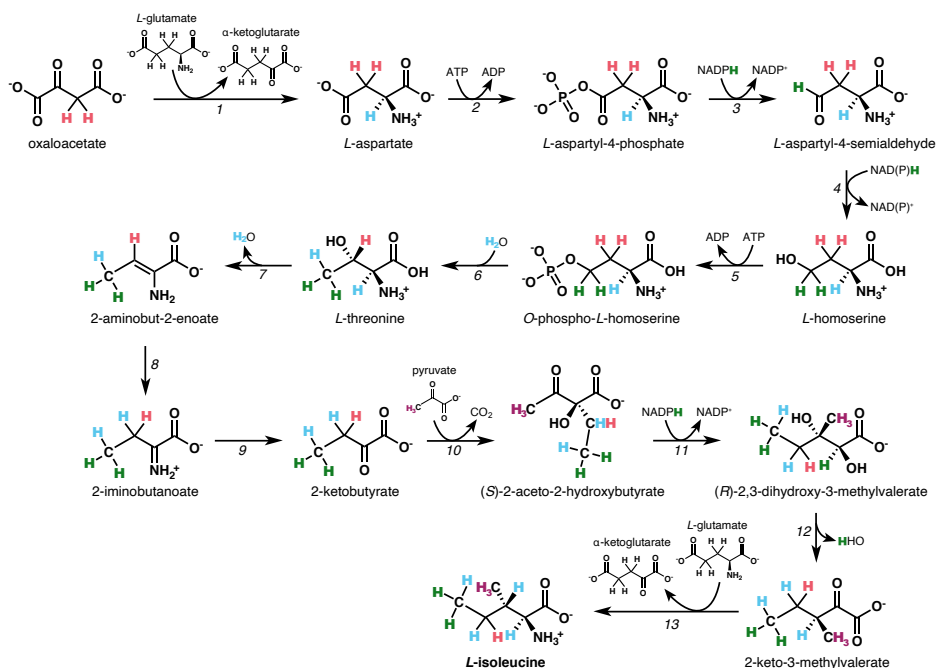


Figure B.19. General biosynthetic pathway of isoleucine with colors representing tracked hydrogen sources (red for oxaloacetate, light blue for water, green for NADPH, purple for pyruvate). The hydrogen atom transferred from NADPH in step 3 may equilibrate with water due to its acidity in an aldehyde position, but is shown as retained through isoleucine synthesis here. Threonine synthase (step 6) stereospecifically abstracts the *pro-R* hydrogen from phosphohomoserine (Omi et al., 2003); in turn, this *pro-R* hydrogen originates from fumarate (while the *pro-S* hydrogen is water-derived) when oxaloacetate is synthesized through fumarase and malate dehydrogenase activity (Gawron & Fondy, 1959). The methylene hydrogen in oxaloacetate and aspartyl-4-semialdehyde may equilibrate with water through keto-enol tautomerizations (Bruice & Bruice, 1978; Kosicki, 1962), although the extents of these equilibrations depend on the rates of subsequent transformation reactions (e.g., the rate of aspartyl-4-semialdehyde conversion to homoserine). PLP-dependent enzyme reactions equilibrate the α -hydrogen in amino acids with solvent (Eliot & Kirsch, 2004). Enzymes: 1, aspartate transaminase; 2, aspartate kinase; 3, aspartate semialdehyde dehydrogenase; 4, homoserine dehydrogenase; 5, homoserine kinase; 6, threonine synthase; 7, threonine deaminase; 8-9, spontaneous rearrangement; 10, acetoacetylase; 11, ketol-acid reductoisomerase; 12, dihydroxyacid dehydratase; 13, isoleucine transaminase/ branched-chain amino acid aminotransferase. See Figure B.20 for distribution of isozymes across organisms investigated in this study.

B.7.5 Distribution of amino acid biosynthetic enzymes across organisms

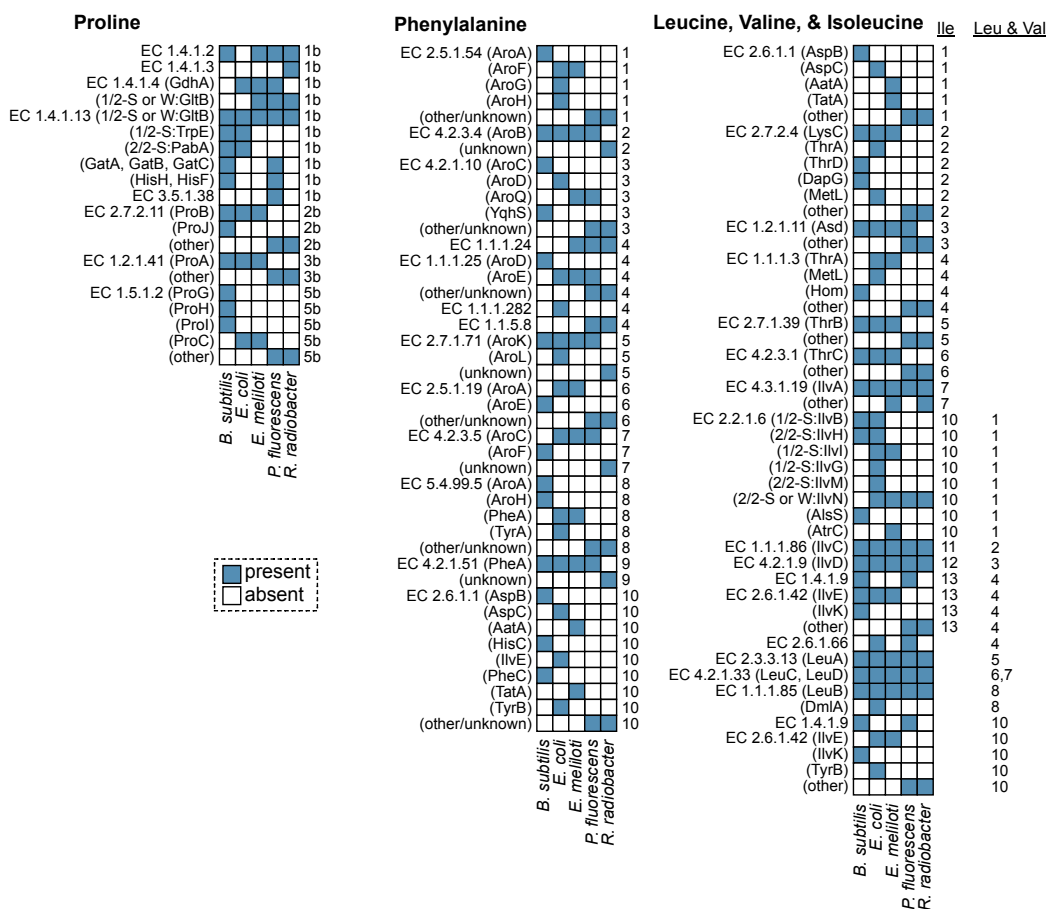


Figure B.20. Distribution of enzymes in amino acid biosynthetic pathways across organisms investigated in this study. Reactions are denoted by their EC numbers (bold text), with numbers to the right of each grid row denoting the step in the biosynthetic pathway (Figures B.16-B.19) where the enzyme is found. Leucine, valine, and isoleucine have overlapping biosynthetic pathways, so are displayed as one set of grids, with numbers to the right additionally denoting steps corresponding to leucine + valine versus isoleucine pathways. Proteins are annotated in parentheses as single or multi-subunit complexes. All proteins corresponding with a given reaction are listed in the grid block next to or under their respective EC number. The presence/absence of each enzyme in each organism was determined using a combination of BsubCyc, EcoCyc (Keseler et al., 2021), BioCyc (Karp et al., 2019), and KEGG pathway (Kanehisa et al., 2016) databases. For *E. meliloti* and *R. radiobacter*, reference genomes used in BioCyc were '*Sinorhizobium meliloti* 1021 reference genome' and '*Agrobacterium fabrum* C58 reference genome,' respectively. (Caption continued on next page).

Figure B.20. (cont.) Organism databases referenced for KEGG pathway searches were 'Bacillus subtilis subsp. subtilis 168 [bsu],' 'Escherichia coli K-12 MG1655 [eco],' 'Sinorhizobium meliloti 1021 [sme],' and 'Agrobacterium fabrum [atu]' for *B. subtilis*, *E. coli*, *E. meliloti* (formerly *S. meliloti*), and *R. radiobacter* (syn. *Agrobacterium fabrum*). For *P. fluorescens*, no BioCyc or KEGG pathway database included a strain sufficiently genetically similar to our strain (average nucleotide identity cutoff score >95%), so KEGG Orthologs were assigned to GenBank protein sequences in *P. fluorescens* strain 2-79 (BioSample: SAMN03278127) using KofamKOALA (Aramaki et al., 2020), and enzymes were identified using KEGG pathway maps.

References

- Aramaki, T., Blanc-Mathieu, R., Endo, H., Ohkubo, K., Kanehisa, M., Goto, S., & Ogata, H. (2020). KofamKOALA: KEGG Ortholog assignment based on profile HMM and adaptive score threshold. *Bioinformatics*, *36*, 2251–2252.
- Bigeleisen, J. (1965). Chemistry of Isotopes. *Science*, *147*(3657), 463–471. <https://doi.org/10.2172/4014119>
- Bornemann, S., Theoclitou, M.-E., Brune, M., Webb, M. R., Thorneley, R. N., & Abell, C. (2000). A secondary β deuterium kinetic isotope effect in the chorismate synthase reaction. *Bioorganic Chemistry*, *28*(4), 191–204. <https://doi.org/10.1006/bioo.2000.1174>
- Bruice, P. Y., & Bruice, T. C. (1978). Lack of concertedness in the catalysis of the enolization of oxaloacetic acid by general acids and bases. Formation of a carbinolamine intermediate in the tertiary amine catalyzed enolization reaction. *Journal of the American Chemical Society*, *100*(15), 4793–4801. <https://doi.org/10.1021/ja00483a027>
- Corr, L. T., Berstan, R., & Evershed, R. P. (2007). Optimisation of derivatisation procedures for the determination of $\delta^{13}\text{C}$ values of amino acids by gas chromatography/combustion/isotope ratio mass spectrometry. *Rapid Communications in Mass Spectrometry*, *21*(23), 3759–3771. <https://doi.org/10.1002/rcm.3252>
- Csonka, L. N., & Fraenkel, D. G. (1977). Pathways of NADPH formation in *Escherichia coli*. *The Journal of Biological Chemistry*, *252*, 3382–3391.
- Dolan, S. K., Kohlstedt, M., Trigg, S., Ramirez, P. V., Kaminski, C. F., Wittmann, C., & Welch, M. (2020). Contextual flexibility in *Pseudomonas aeruginosa* central carbon metabolism during growth in single carbon sources. *American Society for Microbiology*, *11*(2), e02684–19. <https://doi.org/https://doi.org/10.1128/mBio.02684-19>
- Eliot, A. C., & Kirsch, J. F. (2004). Pyridoxal Phosphate Enzymes: Mechanistic, Structural, and Evolutionary Considerations. *Annual Review of Biochemistry*, *73*(1), 383–415. <https://doi.org/10.1146/annurev.biochem.73.011303.074021>
- Englander, S. W., & Poulsen, A. (1969). Hydrogen-tritium exchange of the random chain polypeptide. *Biopolymers*, *7*, 379–393.
- Fogel, M. L., Griffin, P. L., & Newsome, S. D. (2016). Hydrogen isotopes in individual amino acids reflect differentiated pools of hydrogen from food and water in *Escherichia coli*. *Proceedings of the National Academy of Sciences*, *113*(32), E4648–E4653. <https://doi.org/10.1073/pnas.1525703113>

- Gawron, O., & Fondy, T. P. (1959). Stereochemistry of the fumarase and aspartase catalyzed reactions and of the krebs cycle from fumaric acid to *d*-isocitric acid. *Journal of the American Chemical Society*, *81*, 6333–6334.
- Gerosa, L., Haverkorn van Rijsewijk, B. R., Christodoulou, D., Kochanowski, K., Schmidt, T. S., Noor, E., & Sauer, U. (2015). Pseudo-transition analysis identifies the key regulators of dynamic metabolic adaptations from steady-state data. *Cell Systems*, *1*(4), 270–282. <https://doi.org/10.1016/j.cels.2015.09.008>
- Grimshaw, C., Sogo, S., & Knowles, J. (1982). The fate of the hydrogens of phosphoenolpyruvate in the reaction catalyzed by 5-enolpyruvylshikimate-3-phosphate synthase. Isotope effects and isotope exchange. *Journal of Biological Chemistry*, *257*(2), 596–598. [https://doi.org/10.1016/S0021-9258\(19\)68232-3](https://doi.org/10.1016/S0021-9258(19)68232-3)
- Hill, J., & Leach, S. J. (1964). Hydrogen exchange at carbon-hydrogen sites during acid or alkaline treatment of proteins. *Biochemistry*, *3*(12), 1814–1818. <https://doi.org/10.1021/bi00900a003>
- Hušek, P. (1991). Rapid derivatization and gas chromatographic determination of amino acids. *Journal of Chromatography A*, *552*, 289–299. [https://doi.org/10.1016/S0021-9673\(01\)95945-X](https://doi.org/10.1016/S0021-9673(01)95945-X)
- Kanehisa, M., Y., S., Kawashima, M., Furumichi, M., & Tanabe, M. (2016). KEGG as a reference resource for gene and protein annotation. *Nucleic Acids Research*, *44*, D457–D462.
- Karp, P. D., Billington, R., Caspi, R., Fulcher, C. A., Latendresse, M., Kothari, A., Keseler, I. M., Krummenacker, M., Midford, P. E., Ong, Q., Ong, W. K., Paley, S. M., & Subhraveti, P. (2019). The BioCyc collection of microbial genomes and metabolic pathways. *Briefings in Bioinformatics*, *20*, 1085–1093.
- Keseler, I. M., Gama-Castro, S., Mackie, A., Billington, R., Billington, R., Caspi, R., Kothari, A., Krummenacker, M., Midford, P., Muñoz-Rascado, L., Ong, W., Paley, S., Santos-Zavaleta, A., Subhraveti, P., Terrafria, V., Wolfe, A., Collado-Vides, J., Paulsen, I., & Karp, P. D. (2021). The EcoCyc database in 2021. *Frontiers in Microbiology*, *12*, 711077.
- Kopf, S. H. (2014). *From lakes to lungs: Assessing microbial activity in diverse environments* [Doctoral dissertation, California Institute of Technology].
- Kosicki, G. W. (1962). Isotope rate effects in the enolization of oxalacetic acid. *Canadian Journal of Chemistry*, *40*(7), 1280–1284. <https://doi.org/10.1139/v62-196>
- Kreuzer-Martin, H. W., Lott, M. J., Ehleringer, J. R., & Hegg, E. L. (2006). Metabolic Processes Account for the Majority of the Intracellular Water in Log-Phase *Escherichia coli* Cells As Revealed by Hydrogen Isotopes. *Biochemistry*, *45*(45), 13622–13630. <https://doi.org/10.1021/bi0609164>

- Lowenstein, J. M. (1967). The tricarboxylic acid cycle. In D. M. Greenberg (Ed.), *Metabolic Pathways* (pp. 146–270, Vol. 1). Academic Press.
- Ochs, R. S., & Talele, T. T. (2020). Revisiting prochirality. *Biochimie*, *170*, 65–72. <https://doi.org/10.1016/j.biochi.2019.12.009>
- Omi, R., Goto, M., Miyahara, I., Mizuguchi, H., Hayashi, H., Kagamiyama, H., & Hirotsu, K. (2003). Crystal structures of threonine synthase from *Thermus thermophilus* HB8. *The Journal of Biological Chemistry*, *278*, 46035–46045.
- Onderka, D. K., & Floss, H. G. (1969). Steric course of the chorismate synthetase reaction and the 3-deoxy-D-arabino-heptulosonate 7-phosphate (DAHP) synthetase reaction. *Journal of the American Chemical Society*, *91*(21), 5894–5896. <https://doi.org/10.1021/ja01049a046>
- Phillips, A. A., Wu, F., & Sessions, A. L. (2021). Sulfur isotope analysis of cysteine and methionine via preparatory liquid chromatography and elemental analyzer isotope ratio mass spectrometry. *Rapid Communications in Mass Spectrometry*, *35*, e9007. <https://doi.org/10.1002/rcm.9007>
- Sessions, A. L., & Hayes, J. M. (2005). Calculation of hydrogen isotopic fractionations in biogeochemical systems. *Geochimica et Cosmochimica Acta*, *69*(3), 593–597. <https://doi.org/10.1016/j.gca.2004.08.005>
- Silverman, S. N., Phillips, A. A., Weiss, G. M., Wilkes, E. B., Eiler, J. M., & Sessions, A. L. (2022). Practical considerations for amino acid isotope analysis. *Organic Geochemistry*, *164*, 104345. <https://doi.org/10.1016/j.orggeochem.2021.104345>
- Smith, W. G., & York, J. L. (1970). Stereochemistry of the citric acid cycle. *Journal of Chemical Education*, *47*(8), 588. <https://doi.org/10.1021/ed047p588>
- Turner, M. J., Smith, B. W., & Haslam, E. (1975). The Shikimate Pathway. Part IV. The Stereochemistry of the 3-Dehydroquinate Dehydratase Reaction and Observations on 3-Dehydroquinate Synthetase. *Journal of the Chemical Society, Perkin Transactions 1*, *1*, 52–55.
- Vaz, A. D. N. (1980). *Studies on the enzymatic cis dehydration of 3-dehydroquinic acid catalyzed by Escherichia coli 3-dehydroquinate dehydratase* [Doctoral dissertation, Tulane University].
- Walsh, R. G., He, S., & Yarnes, C. T. (2014). Compound-specific $\delta^{13}\text{C}$ and $\delta^{15}\text{N}$ analysis of amino acids: A rapid, chloroformate-based method for ecological studies. *Rapid Communications in Mass Spectrometry*, *28*(1), 96–108. <https://doi.org/10.1002/rcm.6761>
- Wijker, R. S., Sessions, A. L., Fuhrer, T., & Phan, M. (2019). $^2\text{H}/^1\text{H}$ variation in microbial lipids is controlled by NADPH metabolism. *Proceedings of the National Academy of Sciences*, *116*(25), 12173–12182.

- Wright, H. T. (1991). Nonenzymatic deamidation of asparaginy and glutaminy residues in proteins. *Critical Reviews in Biochemistry and Molecular Biology*, 26(1), 1–52.
- Zhang, X., Gillespie, A. L., & Sessions, A. L. (2009). Large D/H variations in bacterial lipids reflect central metabolic pathways. *Proceedings of the National Academy of Sciences*, 106(31), 12580–12586. <https://doi.org/10.1073/pnas.0903030106>

Appendix C

Supplementary material for Chapter 4

C.1 Consistency standards

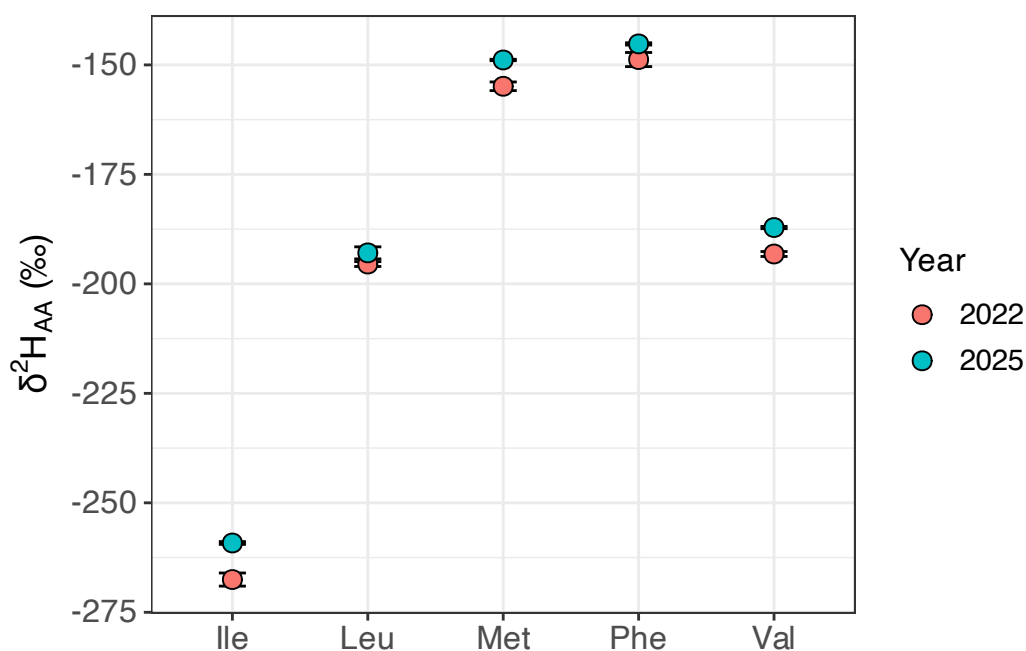


Figure C.1. Summary of measured $\delta^2\text{H}$ values of amino acid standards injected throughout sample analyses carried out in 2022 and 2025 to monitor analytical consistency and ensure cross-experimental data comparability. $\delta^2\text{H}_{\text{AA}}$ values were within 10‰.

C.2 Peak size corrections

Small compound peak areas measured via GC/IRMS can introduce problematic artefacts in $\delta^2\text{H}$ measurements. For the same amino acid standard injected in decreasing amounts, measured $\delta^2\text{H}$ appear to artificially increase (Figure C.2). The

origin of this effect is unknown, but may be related to isotopic memory effects (i.e., adsorption of hydrogen to the pyrolysis reactor surface), which increase with decreasing analyte abundance (Wang & Sessions, 2008). Alternatively, smaller peaks sample greater relative proportions of the conceptual chromatography baseline, which may lead to artificial ^2H -enrichment, although in theory baseline corrections should resolve these effects. Regardless, this 'amount effect' is often avoided by ensuring that samples are injected with sufficiently high concentrations to ensure peaks areas fall in the linear range of $\delta^2\text{H}$ versus peak size regressions. However, with amino acids analyses, this problem can be difficult to avoid due to the substantial differences in peak size distributions across a single chromatogram (driven by differences in amino acid abundances and number of hydrogen atoms). Sample injection volumes must be optimized to balance the need to maximize peak areas of less abundant compounds (e.g., Glx, Met; Figure B.1), while avoiding overloading the column with the more abundant compounds (e.g., Leu, Ile; Figure B.1), which can otherwise contribute to poor chromatography (e.g., lack of baseline resolution) and reduced isotopic measurement accuracy. These considerations must be further balanced with considerations of measurement time. Optimal baseline separation of all amino acids in a single run is achieved in ~ 70 min on a 30m column, and individual samples are injected in at least triplicate for estimation of isotopic precision. When time is not an issue, a best practice solution is to make repeat injections of the same sample at multiple concentrations for optimal measurement of each individual amino acid. However, this approach is not feasible when instrument time is limited; thus, we endeavored to determine whether a suitable strategy could be developed to correct $\delta^2\text{H}_{\text{AA}}$ values for peak size effects. A suite of amino acid standards was injected at different concentrations to generate a regression of reported $\delta^2\text{H}_{\text{AA}}$ value versus mass-3 peak amplitudes (Figure C.2). Although the actual $\delta^2\text{H}_{\text{AA}}$ values of each standard have not been externally cali-

brated (as amino acid standards for hydrogen isotope measurements have yet to be developed - see Section 2.7.4), we specifically use these standards to calibrate and correct for the effect of peak size on measured $\delta^2\text{H}_{\text{AA}}$ values, rather than for offset corrections, which are achieved with FAME standards (e.g., Section 4.2.2). $\delta^2\text{H}_{\text{AA}}$ values generally fall within a linear range above 250mV mass-3 peak amplitudes (Figure C.2A). Normalizing mass-3 amplitudes of individual amino acid peaks to the average mass-3 amplitude of the hydrogen reference gas peaks injected during the given analysis enables comparison of relative peak amplitudes across sample runs with different hydrogen reference gas amplitudes. In this framework, the linear range of $\delta^2\text{H}_{\text{AA}}$ values is above relative mass-3 amplitudes of 0.25 (Figure C.2B).

To correct for peak size effects, we treated the contributing source (referred to here as the baseline for simplicity, although we note that the actual source of this effect is unknown) as a blank contaminant and solved for its fixed 'isotopic composition' (F_{base}) and 'amount' (conceptual peak amplitude A_{base} representing moles H) contribution to measured amino acid isotopic compositions (F_{tot}) via mass balance. Starting with the standard formula for blank correction via isotopic mass balance (Hayes, 2002):

$$A_{\text{tot}}F_{\text{tot}} = A_{\text{AA}}F_{\text{AA}} + A_{\text{base}}F_{\text{base}} \quad (\text{C.1})$$

where A_{tot} is the mass-3 amplitude of the measured amino acid peak relative to that of the hydrogen reference gas (and $A_{\text{tot}} = A_{\text{AA}} + A_{\text{base}}$), and F_{AA} is the theoretical isotopic composition of the amino acid without baseline contribution. Substituting $A_{\text{AA}} = A_{\text{tot}} - A_{\text{base}}$ and rearranging Equation C.1 yields

$$F_{\text{tot}} = F_{\text{AA}} - \frac{A_{\text{base}}(F_{\text{AA}} - F_{\text{base}})}{A_{\text{tot}}} \quad (\text{C.2})$$

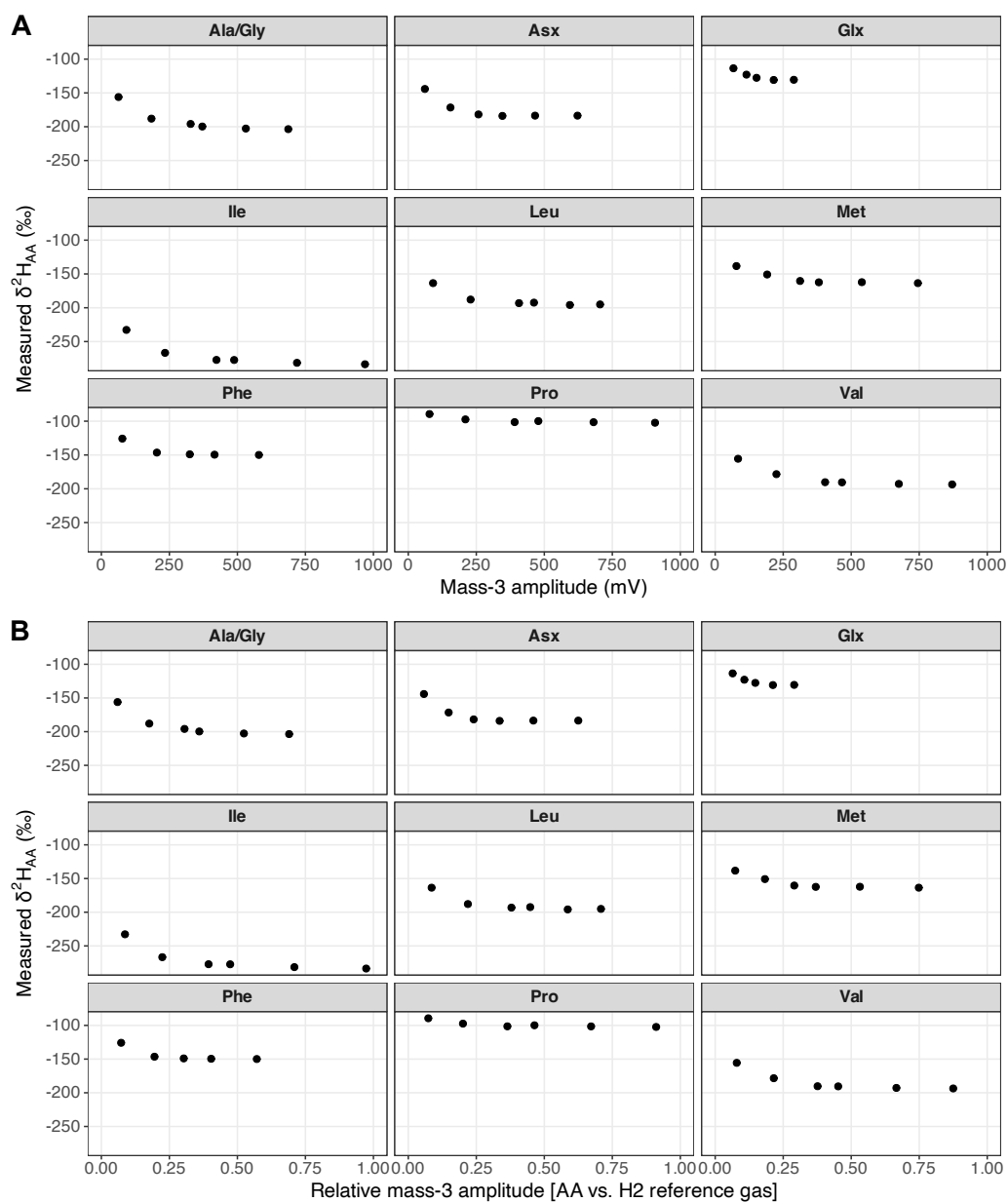


Figure C.2. Effect of peak size on measured $\delta^2\text{H}$ values amino acid standards, plotted with peak size represented by the mass-3 amplitude (**A**) and by the mass-3 amplitude normalized to that of the hydrogen reference gas peaks within the given analysis (**B**).

Eqn C.2 is formulated as a linear regression ($y = mx + b$), where $m = -A_{base}(F_{AA} - F_{base})$, $x = 1/A_{tot}$, and $b = F_{AA}$. Recasting Figure C.2B by plotting the amino acid isotopic compositions (in F notation) against $1/A_{tot}$ yields linear regressions for all amino acids (Figure C.3; all R^2 values ≥ 0.975). Calibration data for all

amino acids were pooled, and F_{base} and A_{base} were simultaneously constrained via a numerical optimization model minimizing the residual sum of squares between the predicted and observed F_{tot} in Equation C.2. The model converged on values for F_{base} (0.00014618, or $\delta^2\text{H} = -61.4\text{‰}$) and A_{base} (0.021), which yielded predicted F_{tot} values in excellent agreement with data (Figure C.4A), and a root-mean-square error of 2.55‰ of the residuals between actual F_{AA} values (y-intercepts of regressions; Equation C.2; Figure C.3) and predicted F_{AA} values (i.e., measured F_{AA} values at each amplitude corrected for baseline contributions using Equation C.3, which is Equation C.2 rearranged to isolate F_{AA}). During each round of sample analysis, the same set of calibration curve standards was run, and new F_{base} and A_{base} parameters were obtained to correct $\delta^2\text{H}_{AA}$ data for peak size effects based on the instrument conditions at the time of analysis.

$$F_{AA} = \frac{F_{tot} - (A_{base}F_{base})/A_{tot}}{1 - A_{base}/A_{tot}} \quad (\text{C.3})$$

In our dataset of all phytoplankton amino acids measured (917 total peaks), 272 sample peaks had relative mass-3 amplitudes of 0.05-0.25, falling within both the range requiring peak size corrections and that captured by our calibration standards (Figures C.2 and C.5). 53 peaks were below the range captured by our calibration standards (i.e., relative mass-3 amplitudes ≤ 0.05), so were excluded from analysis. Amplitude-dependent corrections were applied to all phytoplankton data for consistency, leading to up to 80‰ adjustments in $\delta^2\text{H}_{AA}$ values (Figure C.6).

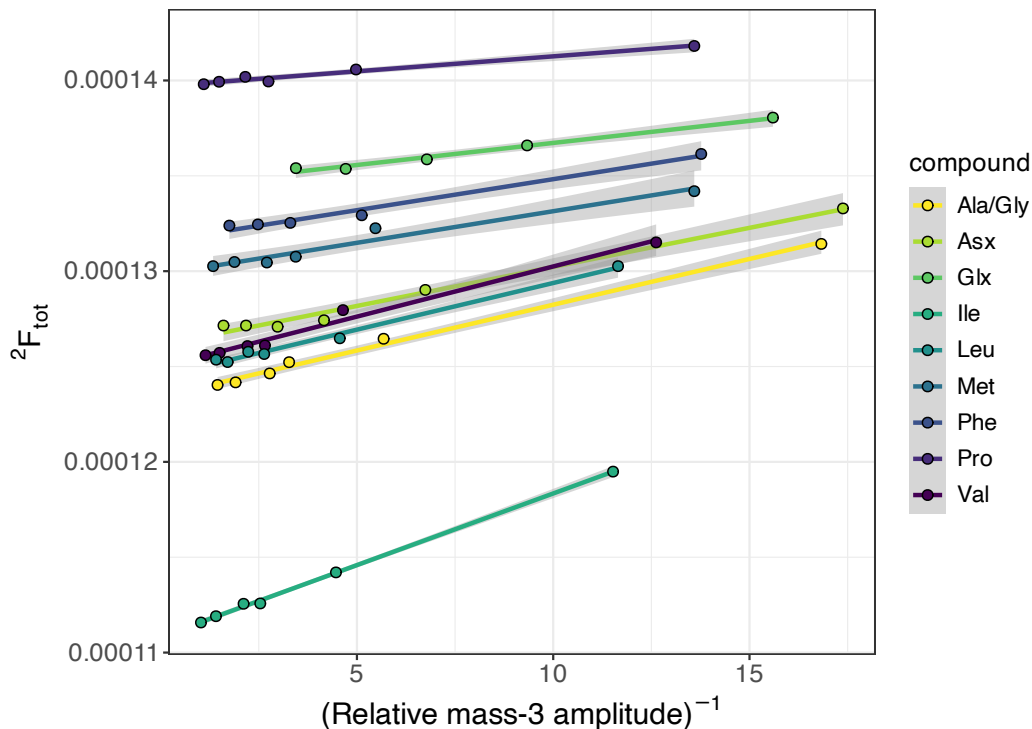


Figure C.3. Linear regressions of standard amino acid isotopic compositions (in F notation) versus the inverse of the mass-3 amplitudes (relative to hydrogen reference gas peak amplitudes, and normalized to the relative number of hydrogen atoms in each amino acid). R^2 values for all linear regressions ≥ 0.975 .

C.3 Phytoplankton $^2\text{H}/^1\text{H}$ fractionations

The normality of distributions of phytoplankton and bacteria amino acid $^2\text{H}/^1\text{H}$ fractionations was assessed via a Shapiro-Wilk statistical test. Most distributions were found to significantly deviate from normal (Figures C.7 and C.8). As such, the non-parametric Mann-Whitney U test was chosen to assess differences between distributions of $^2\varepsilon_{\text{AA/w}}$ values among pairs of organism subgroups. In most pairwise comparisons, distributions were found to be significantly different (Tables C.1 and C.2).

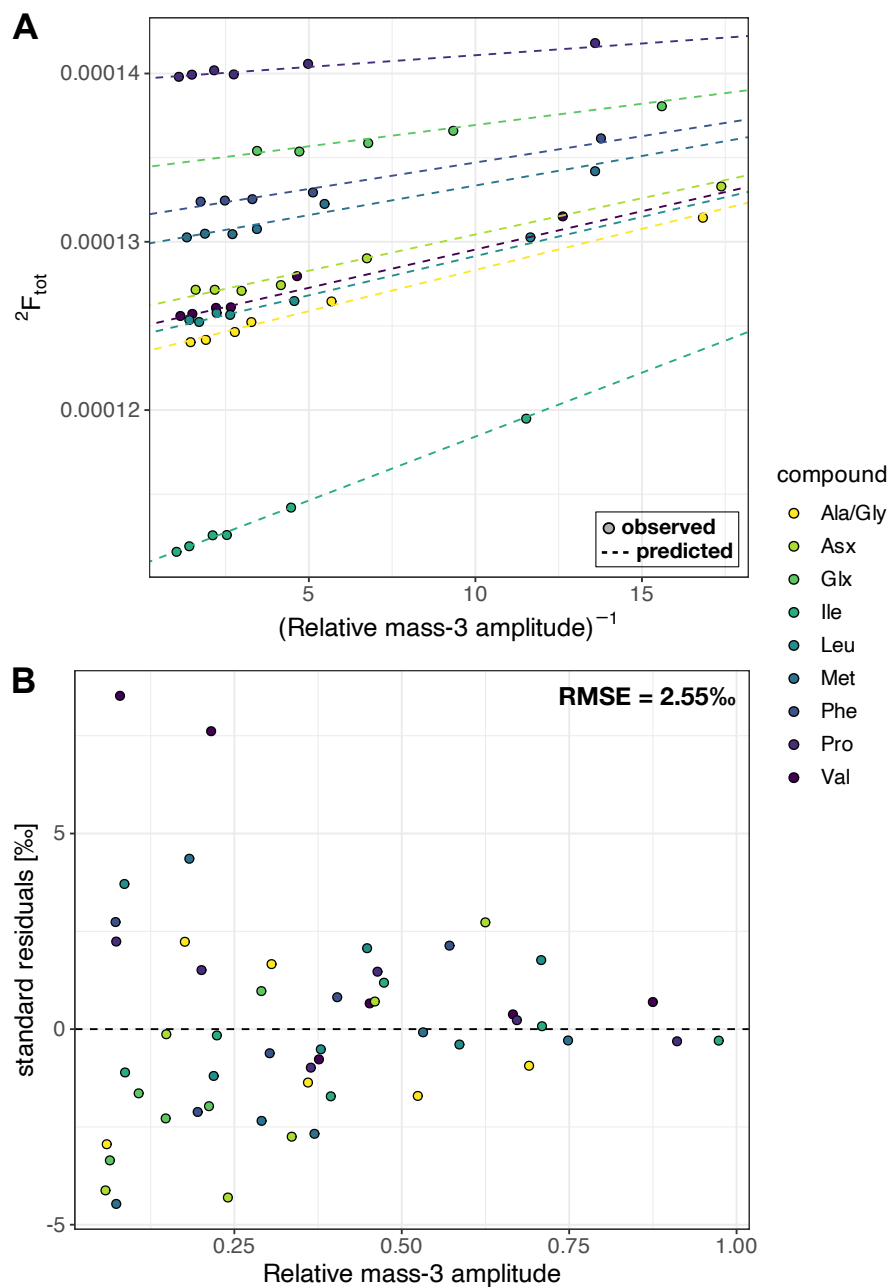


Figure C.4. Results from residual sum of squares model to correct amino acid isotope data for peak size effects. **(A)** Observed F_{tot} values (points), and those predicted using Equation C.2 (dashed lines). **(B)** Residuals of the calibration standards corrected using Equation C.3. All results are plotted against the normalized relative mass-3 amplitudes (see Figure C.3 caption for details).

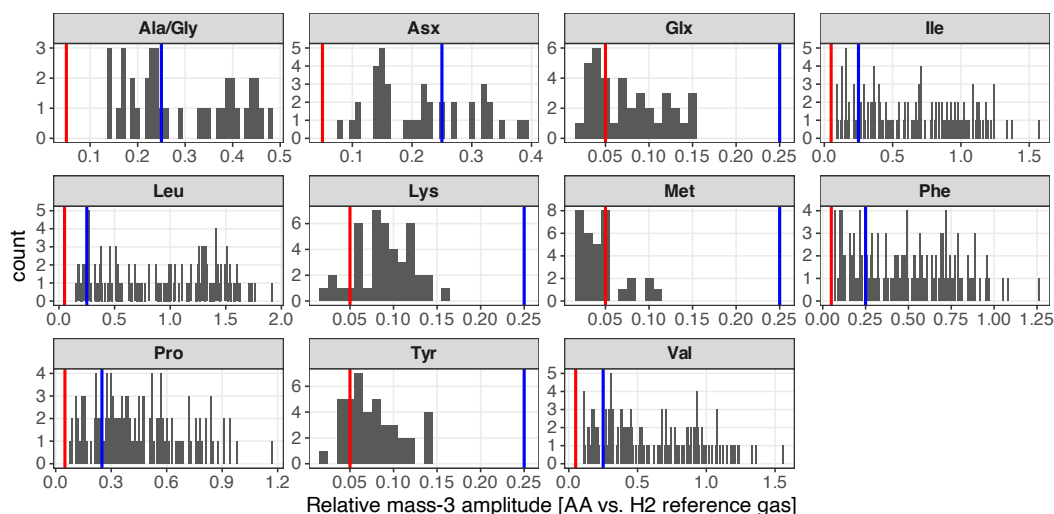


Figure C.5. Distribution of relative mass-3 peak amplitudes of all phytoplankton biomass samples measured in this study. The majority of peak amplitudes fell within the linear range of measured $\delta^2\text{H}$ values (above 0.25 relative amplitude; blue line). Relative peak amplitudes below 0.25 needed $\delta^2\text{H}$ corrections for peak size effects, while those smaller than 0.05 (red line) fell outside the calibration range and were excluded from analysis.

Table C.1. Summary of pairwise comparisons of differences between phytoplankton subgroup ${}^2\varepsilon_{\text{AA}/w}$ distributions (data from Figure 4.2) as determined from the non-parametric Mann-Whitney U test. Asterisks denote statistically significant differences in distributions, with p-values < 0.001 (***), $0.001 < \text{p-value} < 0.01$ (**), $0.01 < \text{p-value} < 0.05$ (*), and p-value > 0.05 (-). Blank entries indicate the pairwise statistical test was not performed due to lack of sufficient data within the corresponding subgroups.

| | coccolithophore versus cyanobacteria | coccolithophore versus diatoms | cyanobacteria versus diatoms |
|---------|---|-----------------------------------|---------------------------------|
| Ala/Gly | *** | *** | ** |
| Asx | - | ** | ** |
| Glx | | | *** |
| Ile | - | - | *** |
| Leu | *** | *** | - |
| Lys | *** | *** | *** |
| Phe | *** | - | *** |
| Pro | - | - | - |
| Tyr | *** | ** | *** |
| Val | *** | *** | *** |

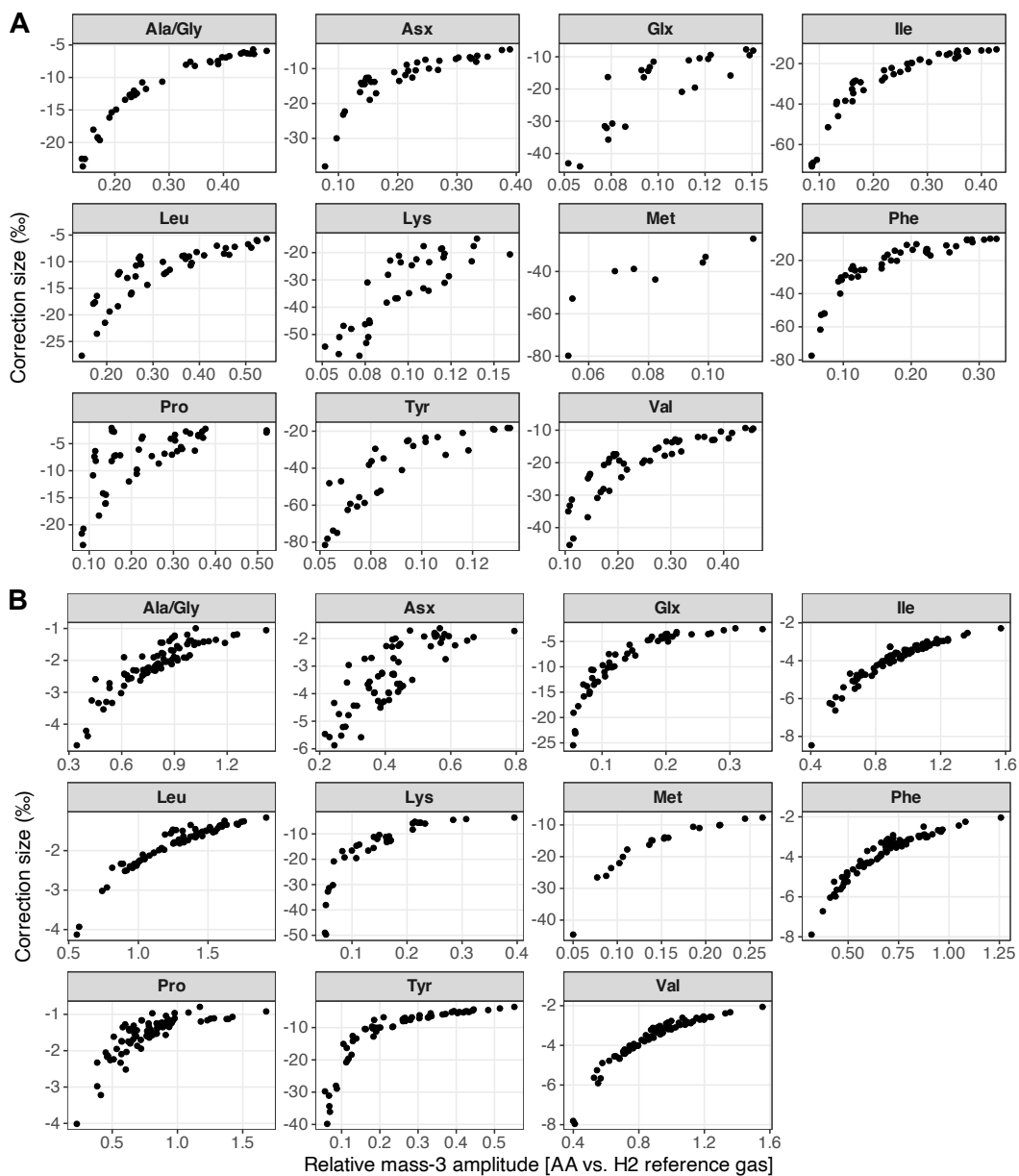


Figure C.6. Peak size-dependent $\delta^2\text{H}_{\text{AA}}$ corrections applied to phytoplankton biomass from control and salinity experiments (**A**) and from irradiance experiments (**B**).

C.4 *E. huxleyi* $^2\text{H}/^1\text{H}$ fractionations in response to salinity

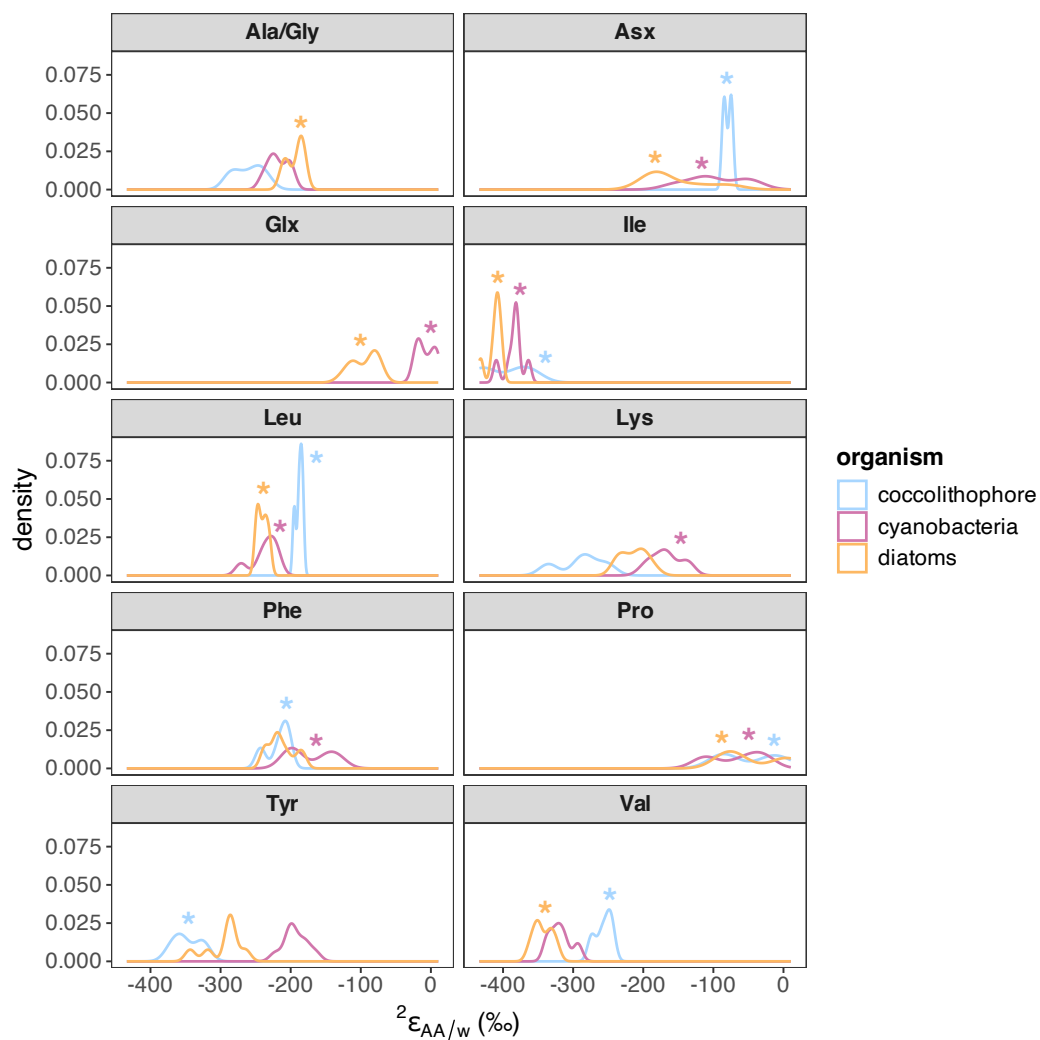


Figure C.7. Comparison of phytoplankton amino acid $^2\text{H}/^1\text{H}$ fractionations, with data from Figure 4.2 visualized here as density curves. Asterisk symbols (*) denote distributions that significantly deviate from normality (p -value < 0.05), as determined from a Shapiro-Wilk statistical test.

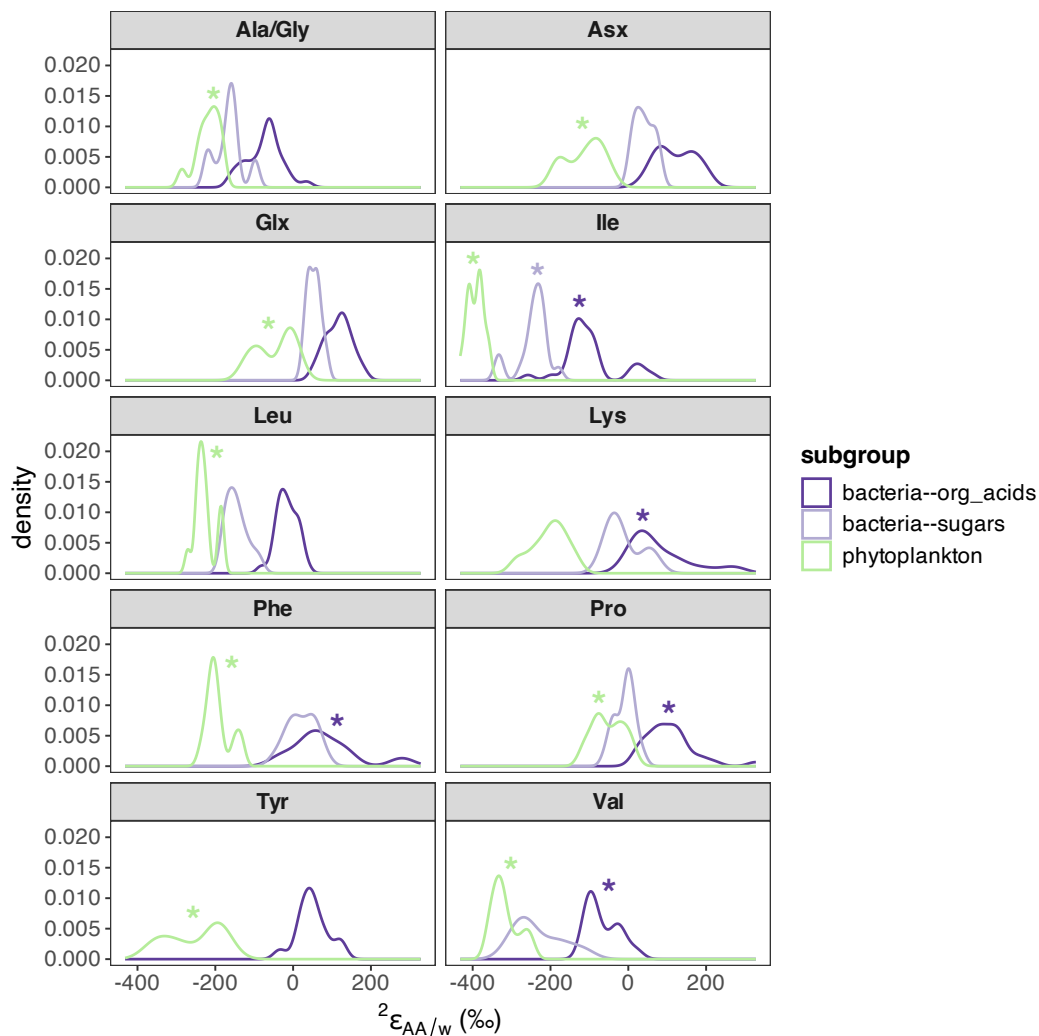


Figure C.8. Comparison of bacteria and phytoplankton amino acid $^2\text{H}/^1\text{H}$ fractionations, with data from Figure 4.3 and visualized here as density curves. Data on bacteria are grouped according to the type of carbon substrate fed to the bacteria (organic acid versus sugar) and are from Silverman et al. (2024). Asterisk symbols (*) denote distributions that significantly deviate from normality (p -value < 0.05), as determined from a Shapiro-Wilk statistical test.

Table C.2. Summary of pairwise comparisons of differences between phytoplankton and bacteria ${}^2\varepsilon_{AA/w}$ distributions (data from Figure 4.3) as determined from the non-parametric Mann-Whitney U test. Asterisks denote statistically significant differences in distributions, with p-values < 0.001 (***), $0.001 < \text{p-value} < 0.01$ (**), $0.01 < \text{p-value} < 0.05$ (*), and p-value > 0.05 (-). Blank entries indicate the pairwise statistical test was not performed due to lack of sufficient data within the corresponding subgroups.

| | bacteria on org. acids versus bacteria on sugars | bacteria on org. acids versus phytoplankton | bacteria on sugars versus phytoplankton |
|---------|---|--|--|
| Ala/Gly | *** | *** | *** |
| Asx | *** | *** | *** |
| Glx | *** | *** | *** |
| Ile | *** | *** | *** |
| Leu | *** | *** | *** |
| Lys | *** | *** | *** |
| Phe | ** | *** | *** |
| Pro | *** | *** | *** |
| Tyr | | *** | |
| Val | *** | *** | *** |

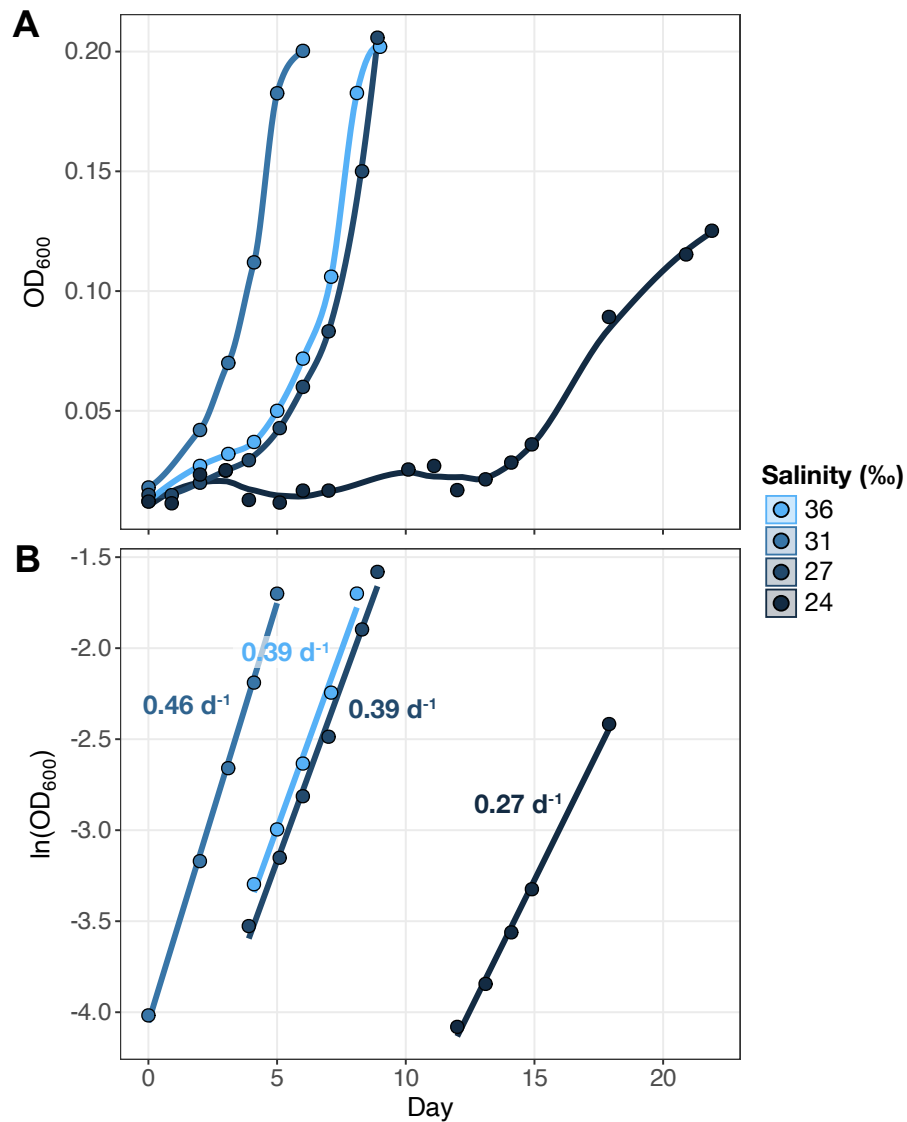


Figure C.9. Growth of *E. huxleyi* in media with different salinities, plotted as full growth curves measured via OD_{600} (A) and as the linear portions of the growth curves in logarithmic space (B). Growth rates calculated from OD_{600} measurements are shown next to each corresponding growth curve.

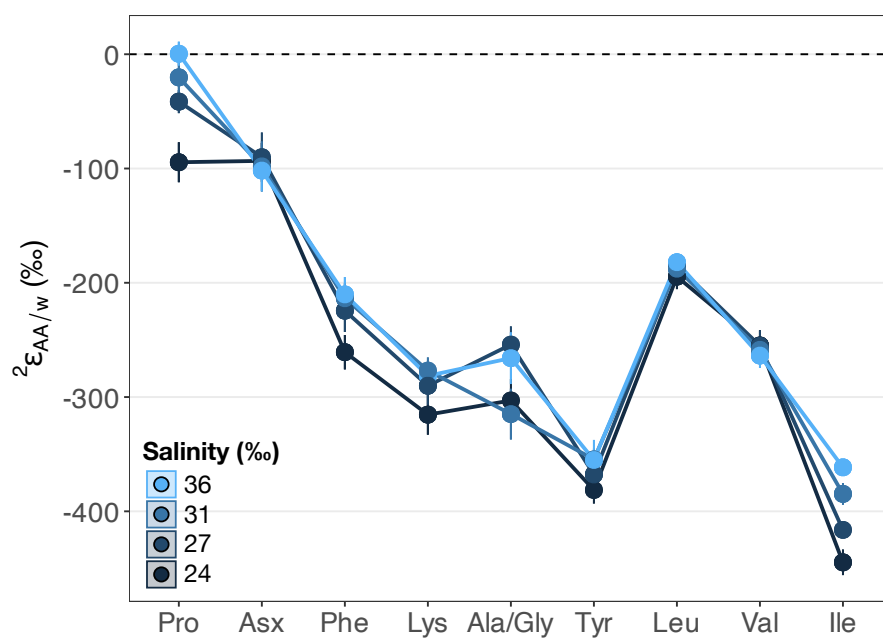


Figure C.10. Amino acid/water $^2\text{H}/^1\text{H}$ fractionations in *E. huxleyi* grown in media with different salinities.

C.5 Diatom $^2\text{H}/^1\text{H}$ fractionations in response to irradiance

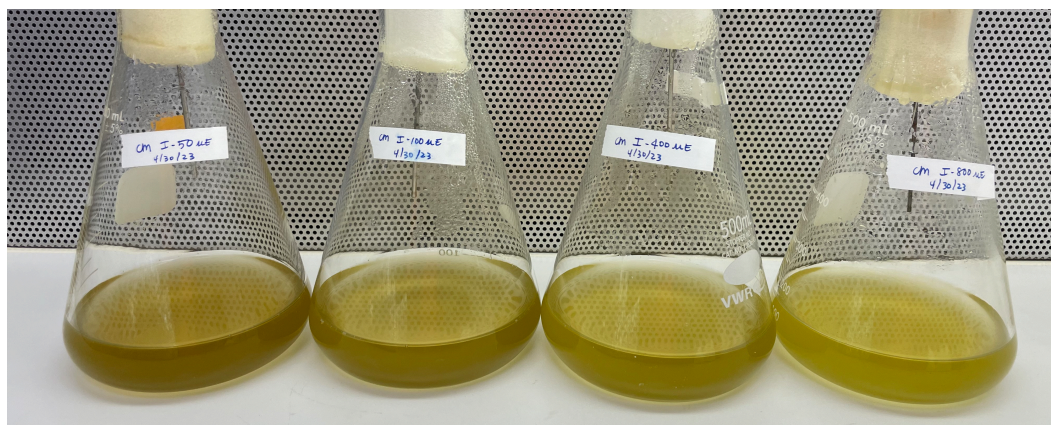


Figure C.11. *C. muelleri* cultures grown under varying light intensities.

Table C.3. Growth rates of diatoms grown under different light intensities, measured from the logarithmic OD_{750} data shown in Figure C.12B.

| Species | Irradiance ($\mu\text{mol s}^{-1} \text{m}^{-2}$) | μ (d^{-1}) |
|----------------------|--|------------------------------|
| <i>C. muelleri</i> | 50 | 1.04 |
| | 100 | 1.49 |
| | 400 | 1.55 |
| | 800 | 1.60 |
| <i>T. pseudonana</i> | 50 | 0.88 |
| | 100 | 1.04 |
| | 400 | 1.45 |
| | 800 | 1.46 |

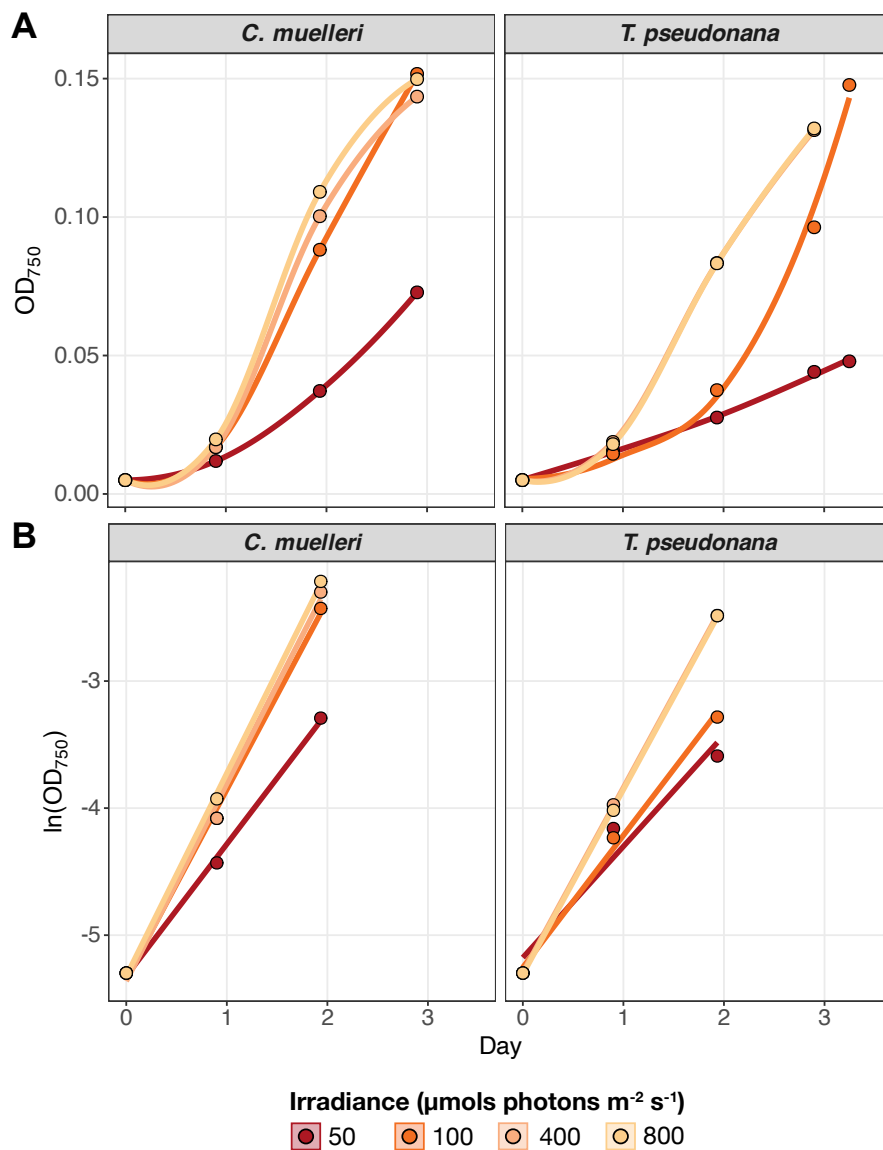


Figure C.12. Growth of diatoms under varying light intensities, plotted as full growth curves measured via OD₇₅₀ (**A**) and as the linear portions of the growth curves in logarithmic space (**B**). Growth rates calculated from OD₇₅₀ measurements are summarized in Table C.3.

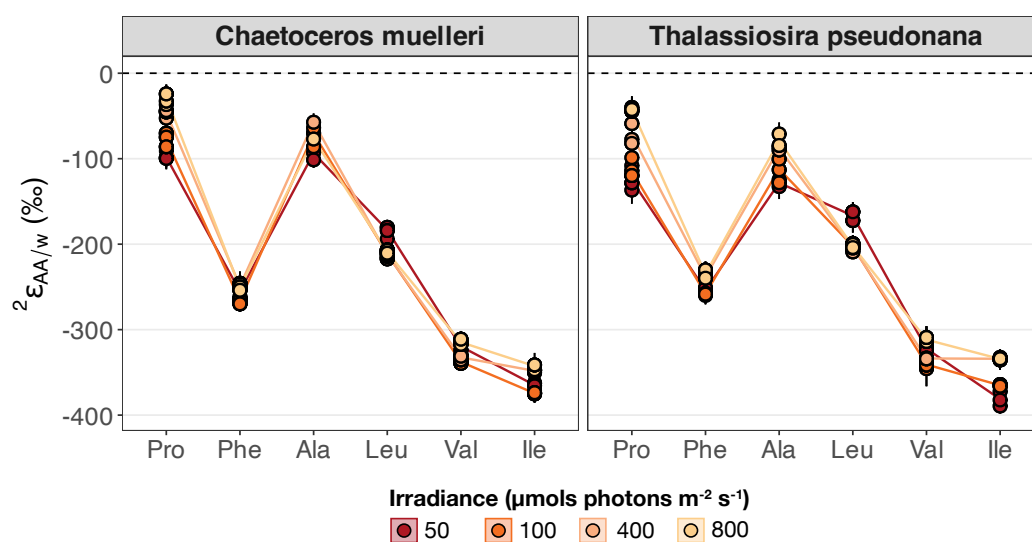


Figure C.13. Amino acid/water $^2\text{H}/^1\text{H}$ fractionations in *C. muelleri* and *T. pseudonana* grown under different irradiances. Data from biological triplicates are displayed, except in cases where amino acid $\delta^2\text{H}$ values were not reliably measurable due to chromatography issues. Lines are plotted through the average of each set of culture replicates. Note that, unlike most of our GC/IRMS analyses which used a ZB-5ms column (on which alanine + glycine co-elute), here we were able to isolate alanine using a DB-XLB column.

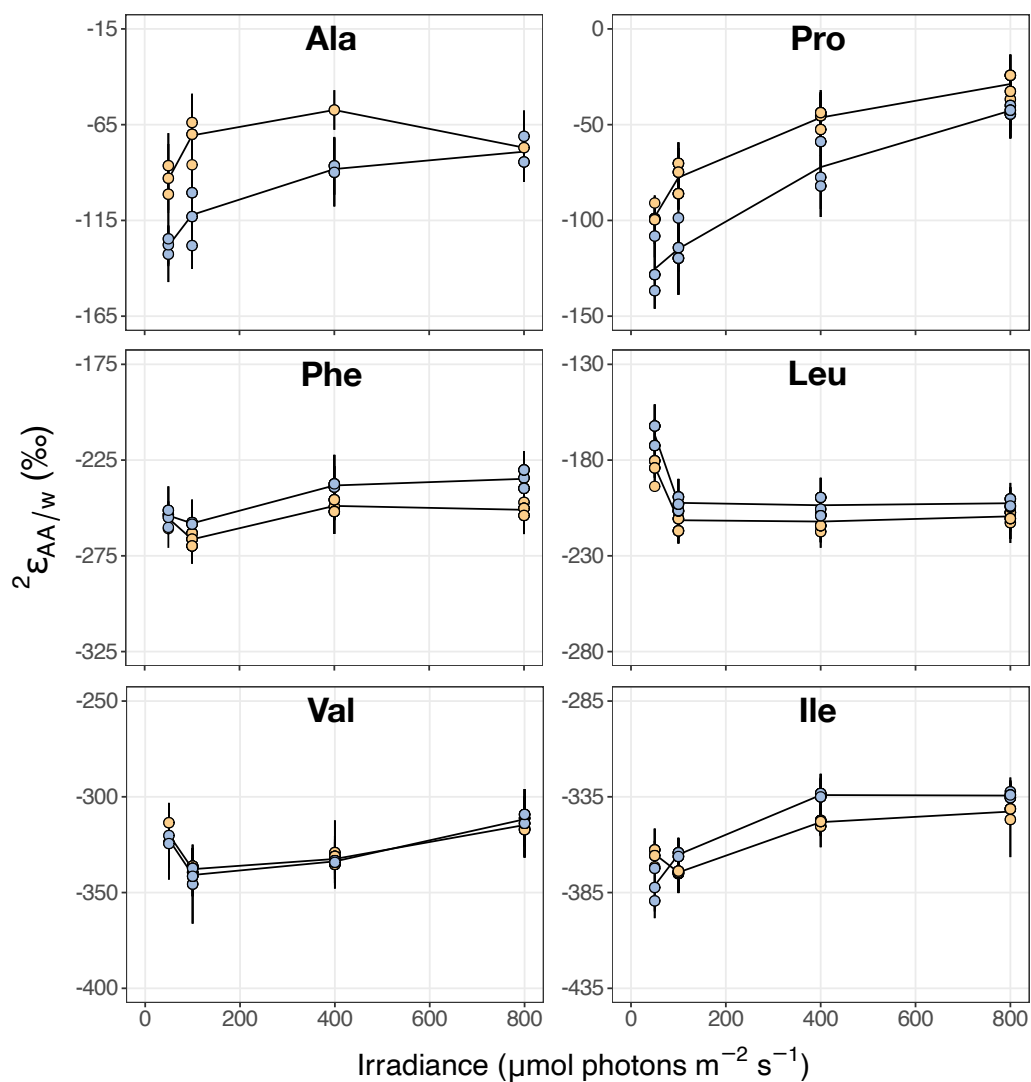


Figure C.14. Amino acid/water $^2\text{H}/^1\text{H}$ fractionations in *C. muelleri* (orange) and *T. pseudonana* (blue) grown under different irradiances, including $I=50\mu\text{mol photons m}^{-2} \text{s}^{-1}$. Data from biological triplicates are displayed, except in cases where amino acid $\delta^2\text{H}$ values were not reliably measurable due to chromatography issues. Lines are plotted through the average of each set of culture replicates. See the note in the Figure C.13 caption about isolating alanine.

References

- Hayes, J. M. (2002). Practice and Principles of Isotopic Measurements in Organic Geochemistry. *Society*, (August).
- Silverman, S. N., Wijker, R. S., & Sessions, A. L. (2024). Biosynthetic and catabolic pathways control amino acid $\delta^2\text{H}$ values in aerobic heterotrophs. *Frontiers in Microbiology*, *15*, 1–20. <https://doi.org/10.3389/fmicb.2024.1338486>
- Wang, Y., & Sessions, A. L. (2008). Memory Effects in Compound-Specific D/H Analysis by Gas Chromatography/Pyrolysis/Isotope-Ratio Mass Spectrometry. *Analytical Chemistry*, *80*(23), 9162–9170. <https://doi.org/10.1021/ac801170v>

Appendix D

Supplementary material for Chapter 6

Table D.1. Particulate amino acid concentrations from Station ALOHA used to calculate lower bound estimates of POM turnover. Concentrations were measured by H. Close (unpublished data)^a. Those measured at PAP-SO are reported in Yanuskiewicz et al. (unpublished).

| Site | Particle size | Depth | Concentration (nmol L ⁻¹) | | | | | |
|------------|---------------|-------|---------------------------------------|------|------|------|------|------|
| | | | Asx | Ile | Leu | Lys | Phe | Val |
| Sta. ALOHA | 0.7–53 μm | 25 m | 1.00 | 0.08 | 0.30 | 0.75 | 0.09 | 0.17 |
| Sta. ALOHA | 0.7–53 μm | 75 m | 9.18 | 0.61 | 2.49 | 5.99 | 1.06 | 1.23 |
| Sta. ALOHA | 0.7–53 μm | 275 m | 0.94 | 0.06 | 0.19 | 0.48 | 0.12 | 0.11 |

^a Amino acids at Station ALOHA were quantified for slightly different size fractions and depths than those for which POM- $\delta^2\text{H}_{\text{AA}}$ values are reported in this study.

Table D.2. Estimated contributions of heterotrophic biomass to POM based on Bayesian mixing model results.

| Site | Particle size | Depth | Mean heterotrophic biomass (%) ^a | | | | | |
|------------|---------------|-------|---|-----|-----|-----|-----|-----|
| | | | Asx | Ile | Leu | Lys | Phe | Val |
| Sta. ALOHA | 3–53 μm | 25 m | 23 | 24 | 24 | 17 | 13 | 55 |
| Sta. ALOHA | 3–53 μm | 72 m | 13 | 22 | 24 | 16 | 11 | 53 |
| Sta. ALOHA | 3–53 μm | 296 m | - | 88 | 79 | 30 | 42 | 88 |
| PAP-SO | >51 μm | 30 m | 26 | 54 | 52 | 16 | 11 | 56 |
| PAP-SO | >51 μm | 50 m | 19 | 45 | 49 | 15 | 9 | 50 |
| PAP-SO | >51 μm | 340 m | 52 | 70 | 65 | 25 | 18 | 67 |

^a Contributions of photoautotrophic biomass can be estimated as 100 - (% heterotrophic biomass).

^b - denotes $\delta^2\text{H}_{\text{AA}}$ data was not sufficient to enable mixing estimation.

References

- Yanusiewicz, E. A., Wojtal, P. K., Shea, C. H., Benitez-Nelson, C. R., Buesseler, K., Estapa, M., Roca-Mart, M., Popp, B. N., & Close, H. G. (unpublished). *Organic indicators for the alteration of exported phytodetritus during the North Atlantic spring bloom, Part I: Nitrogen isotopic patterns of amino acids.*

Appendix E

Supplementary material for Chapter 6

Table E.1. Isolation details for bacterial strains used in particle colonization experiments.

| Strain | Hydrogel polymer | Source |
|--------|------------------|---------------------|
| 3D05 | chitin | Datta et al. (2016) |
| C1M14 | carageenan | Enke et al. (2019) |
| 6B07 | chitin | Datta et al. (2016) |
| A2M03 | agarose | Enke et al. (2019) |
| C3M10 | carageenan | Enke et al. (2019) |
| A3M17 | agarose | Enke et al. (2019) |
| 1A01 | chitin | Datta et al. (2016) |
| C3R12 | carageenan | Enke et al. (2019) |



Figure E.1. Image of *T. pseudonana* aggregates.

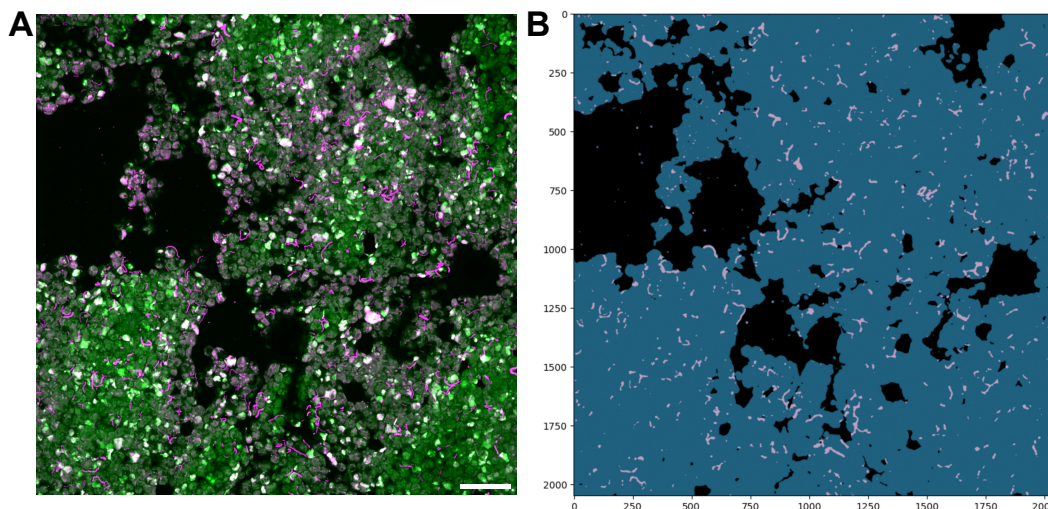


Figure E.2. Example image segmentation performed for particle-attached bacteria cells. **(A)** Maximum intensity project of 3D05 (pink cells) attached to *T. pseudonana* aggregate (green). **(B)** Results of final segmentation of bacteria cells (pink), particle (blue), and background (black). Segmented images were denoised (median filter using 5×5 px² windows), and cell masks were filtered using a minimum threshold of $0.2 \mu\text{m}^2$ to produce the final segmented images.

References

- Datta, M. S., Sliwerska, E., Gore, J., Polz, M. F., & Cordero, O. X. (2016). Microbial interactions lead to rapid micro-scale successions on model marine particles. *Nature Communications*, 7(1), 11965. <https://doi.org/10.1038/ncomms11965>
- Enke, T. N., Datta, M. S., Schwartzman, J., Cermak, N., Schmitz, D., Barrere, J., Pascual-García, A., & Cordero, O. X. (2019). Modular Assembly of Polysaccharide-Degrading Marine Microbial Communities. *Current Biology*, 29(9), 1528–1535.e6. <https://doi.org/10.1016/j.cub.2019.03.047>

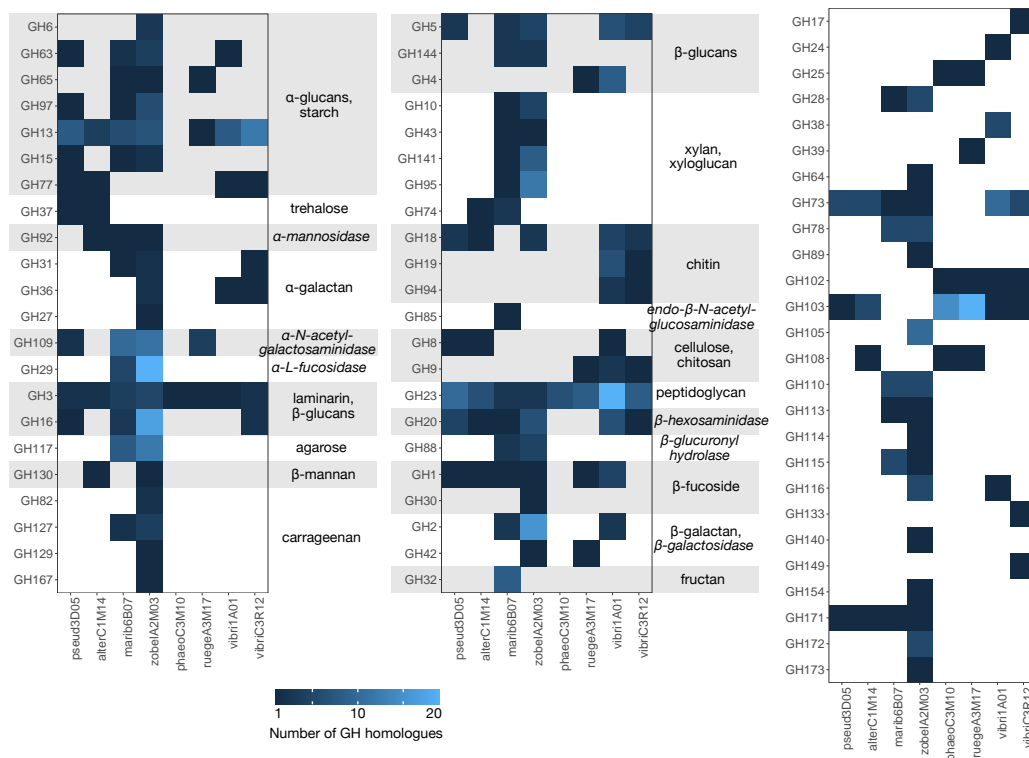


Figure E.3. Heatmap showing the number of homologues of glycoside hydrolase (GH) family CAZymes within each strain. CAZyme families are grouped based on the target substrate(s) of homologues within each family. In cases where the target substrate has not been experimentally characterized, the name of the CAZyme is included instead (denoted in italics). GH family CAZymes in the right-most column have not yet been experimentally characterized.

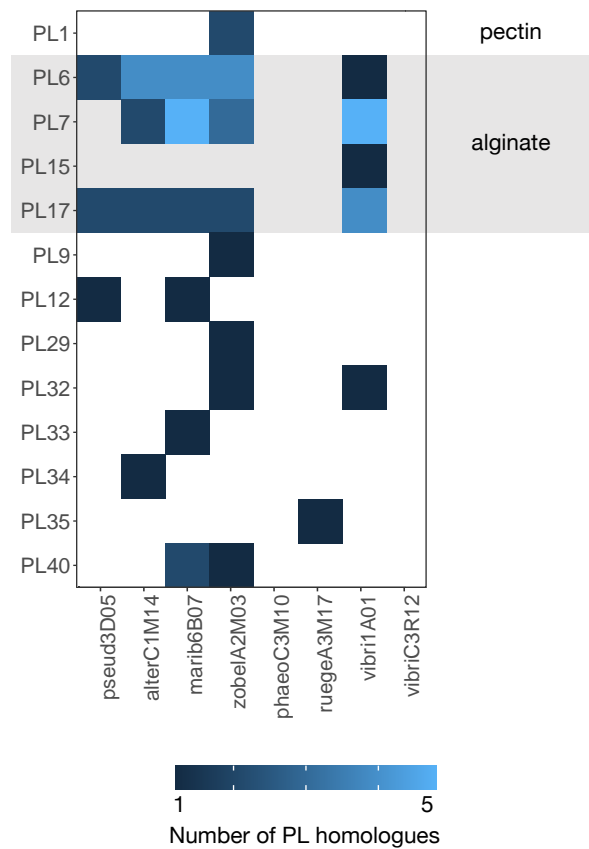


Figure E.4. Heatmap showing the number of homologues of polysaccharide lyase (PL) family CAZymes within each strain. CAZyme families are grouped based on the target substrate (pectin or alginate) of homologues within each family. Those without substrate annotations have not yet been experimentally characterized.

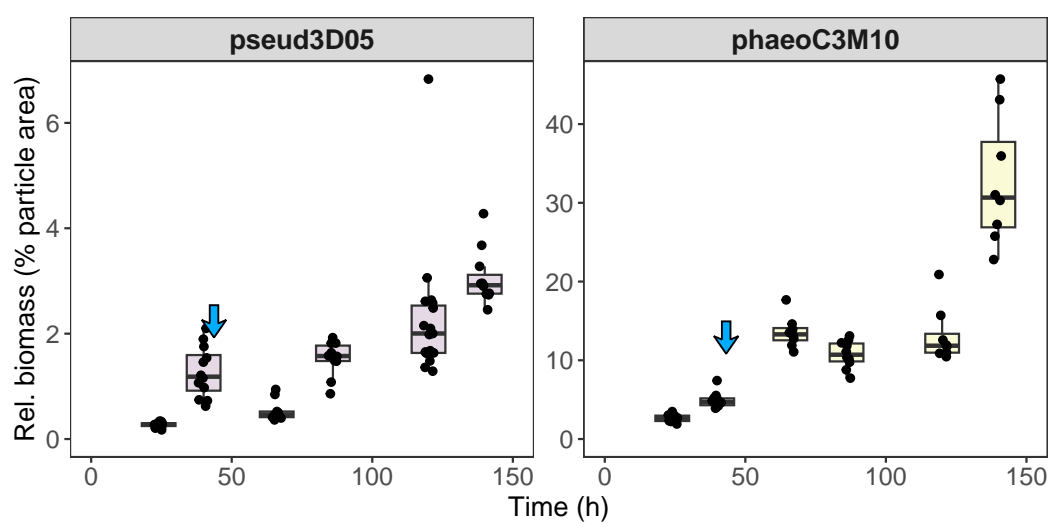


Figure E.5. Increase in relative biomass of pseud3D05 and phaeoC3M10 (each strain in monoculture) on *T. pseudonana* aggregates after 42h of continuous colonization followed by washing of unattached cells and 98h of continued growth on particles. Relative abundances are quantified as the percent of particle surface area occupied by the biomass of each strain. The blue arrow in each panel denotes the point when cells were washed.

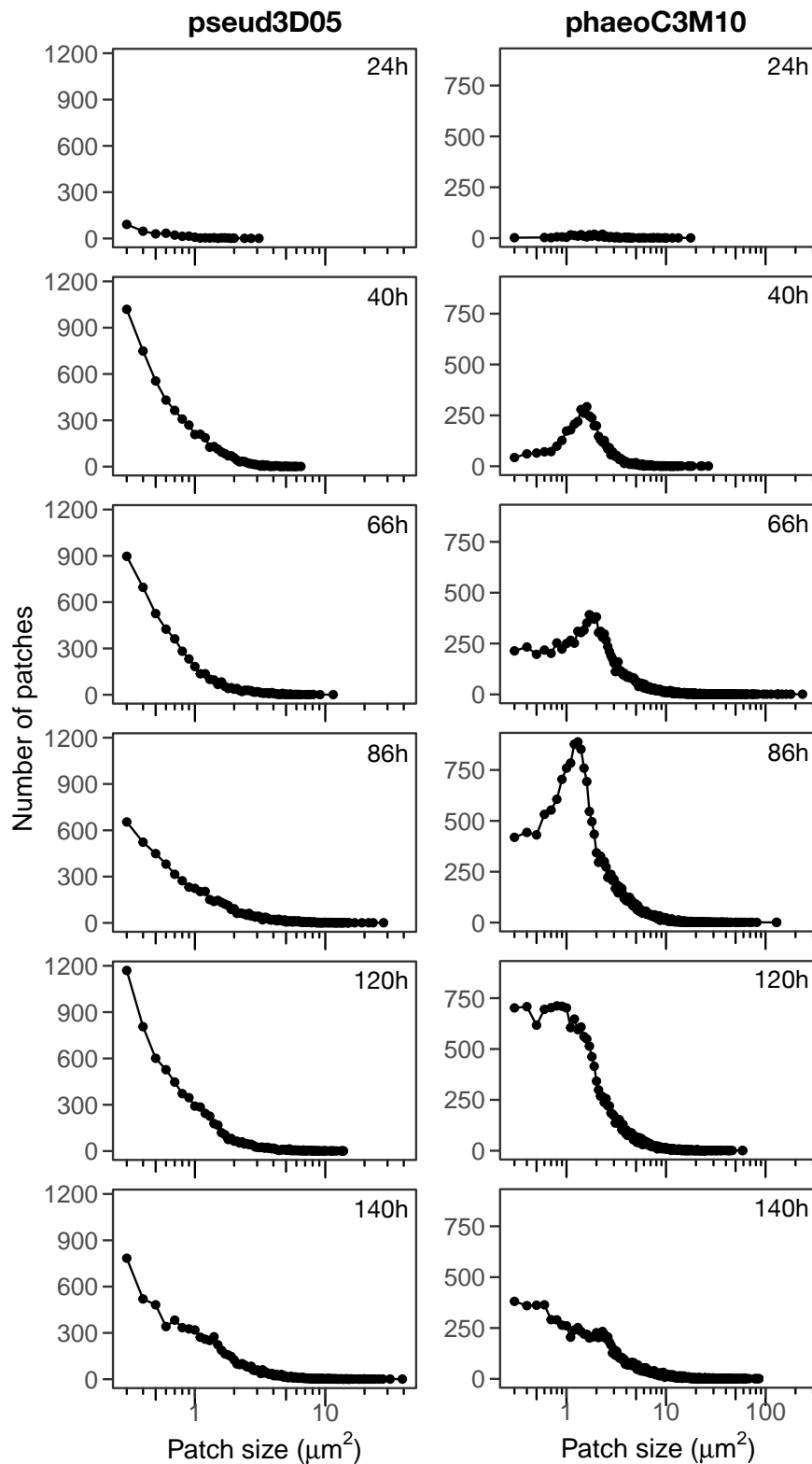


Figure E.6. Distribution of pseud3D05 and phaeoC3M10 cell patches on *T. pseudonana* aggregates over time in monoculture colonization experiments. A cell patch is defined as all cells within 0.5 μm from one another, and include isolated single cells. Distributions were compiled using data from 10 randomly sampled particles to facilitate comparisons across experiments.